



Health

- ▶ Coffee
- ▶ Cooking Tips
- ▶ Recipes & Food and Drink
- ▶ Wine & Spirits
- ▶ Elder Care
- ▶ Babies & Toddler
- ▶ Pregnancy
- ▶ Acne
- ▶ Aerobics & Cardio
- ▶ Alternative Medicine
- ▶ Beauty Tips
- ▶ Depression
- ▶ Diabetes
- ▶ Exercise & Fitness
- ▶ Hair Loss
- ▶ Medicine
- ▶ Meditation
- ▶ Muscle Building & Bodybuilding
- ▶ Nutrition
- ▶ Nutritional Supplements
- ▶ Weight Loss
- ▶ Yoga
- ▶ Martial Arts
- ▶ Finding Happiness
- ▶ Inspirational
- ▶ Breast Cancer
- ▶ Mesothelioma & Cancer
- ▶ Fitness Equipment
- ▶ Nutritional Supplements
- ▶ Weight Loss



Internet

- ▶ Affiliate Revenue
- ▶ Blogging, RSS & Feeds
- ▶ Domain Name
- ▶ E-Book
- ▶ E-commerce
- ▶ Email Marketing
- ▶ Ezine Marketing
- ▶ Ezine Publishing
- ▶ Forums & Boards
- ▶ Internet Marketing
- ▶ Online Auction
- ▶ Search Engine Optimization
- ▶ Spam Blocking
- ▶ Streaming Audio & Online
- Music**
- ▶ Traffic Building
- ▶ Video Streaming
- ▶ Web Design
- ▶ Web Development
- ▶ Web Hosting
- ▶ Web Site Promotion
- ▶ Broadband Internet
- ▶ VOIP
- ▶ Computer Hardware
- ▶ Data Recovery & Backup
- ▶ Internet Security
- ▶ Software



Business

- ▶ Advertising
- ▶ Branding
- ▶ Business Management
- ▶ Business Ethics
- ▶ Careers, Jobs & Employment
- ▶ Customer Service
- ▶ Marketing
- ▶ Networking
- ▶ Network Marketing
- ▶ Pay-Per-Click Advertising
- ▶ Presentation
- ▶ Public Relations
- ▶ Sales
- ▶ Sales Management
- ▶ Sales Telemarketing
- ▶ Sales Training
- ▶ Small Business
- ▶ Strategic Planning
- ▶ Entrepreneur
- ▶ Negotiation Tips
- ▶ Team Building
- ▶ Top Quick Tips
- ▶ Book Marketing
- ▶ Leadership
- ▶ Positive Attitude Tips
- ▶ Goal Setting
- ▶ Innovation
- ▶ Success
- ▶ Time Management
- ▶ Public Speaking
- ▶ Get Organized - Organization



Finances

- ▶ Credit
- ▶ Currency Trading
- ▶ Debt Consolidation
- ▶ Debt Relief
- ▶ Loan
- ▶ Insurance
- ▶ Investing
- ▶ Mortgage Refinance
- ▶ Personal Finance
- ▶ Real Estate
- ▶ Taxes
- ▶ Stocks & Mutual Fund
- ▶ Structured Settlements
- ▶ Leases & Leasing
- ▶ Wealth Building
- ▶ Home Security



Entertainment

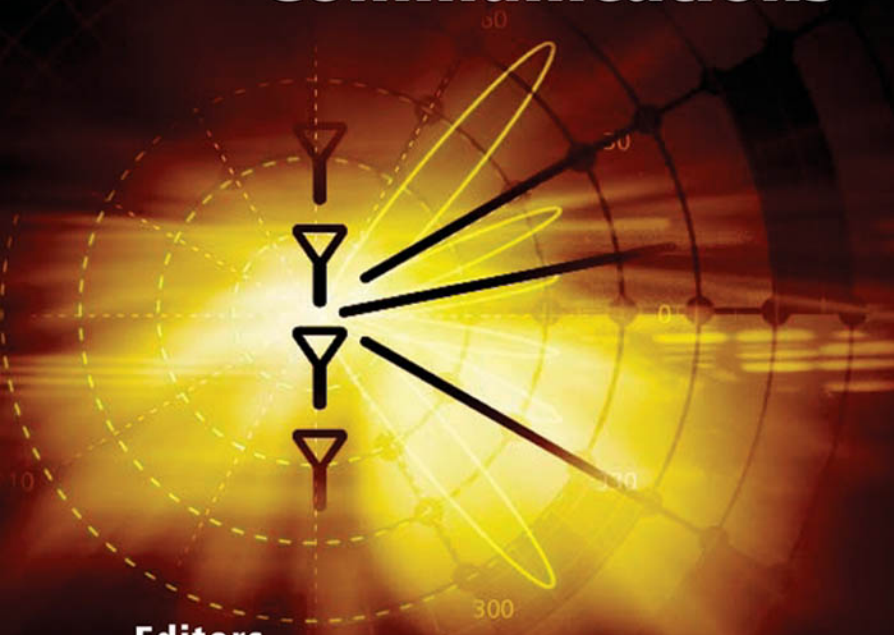
- ▶ Mobile & Cell Phone
- ▶ Video Conferencing
- ▶ Satellite TV
- ▶ Dating
- ▶ Relationships
- ▶ Game
- ▶ Casino & Gambling
- ▶ Humor & Entertainment
- ▶ Music & MP3
- ▶ Photography
- ▶ Golf
- ▶ Attraction
- ▶ Motorcycle
- ▶ Fashion & Style
- ▶ Crafts & Hobbies
- ▶ Home Improvement
- ▶ Interior Design & Decorating
- ▶ Landscaping & Gardening
- ▶ Pets
- ▶ Marriage & Wedding
- ▶ Holiday
- ▶ Fishing
- ▶ Aviation & Flying
- ▶ Cruising & Sailing
- ▶ Outdoors
- ▶ Vacation Rental



Education

- ▶ Book Reviews
- ▶ College & University
- ▶ Psychology
- ▶ Science Articles
- ▶ Religion
- ▶ Personal Technology
- ▶ Humanities
- ▶ Language
- ▶ Philosophy
- ▶ Poetry
- ▶ Book Reviews
- ▶ Medicine
- ▶ Coaching
- ▶ Creativity
- ▶ Dealing with Grief & Loss
- ▶ Motivation
- ▶ Spirituality
- ▶ Stress Management
- ▶ Article Writing
- ▶ Writing
- ▶ Political
- ▶ Copywriting
- ▶ Parenting
- ▶ Divorce

Space-Time Processing for MIMO Communications



Editors

A.B. Gershman and N.D. Sidiropoulos

 WILEY

Space-Time Processing for MIMO Communications

Edited by

A. B. Gershman

McMaster University, Canada

and University of Duisburg-Essen, Germany

N. D. Sidiropoulos

Technical University of Crete, Greece



John Wiley & Sons, Ltd

Space-Time Processing for MIMO Communications

Space-Time Processing for MIMO Communications

Edited by

A. B. Gershman

McMaster University, Canada

and University of Duisburg-Essen, Germany

N. D. Sidiropoulos

Technical University of Crete, Greece



John Wiley & Sons, Ltd

Copyright © 2005

John Wiley & Sons Ltd, The Atrium, Southern Gate, Chichester,
West Sussex PO19 8SQ, England

Telephone (+44) 1243 779777

Email (for orders and customer service enquiries): cs-books@wiley.co.uk
Visit our Home Page on www.wiley.com

All Rights Reserved. No part of this publication may be reproduced, stored in a retrieval system or transmitted in any form or by any means, electronic, mechanical, photocopying, recording, scanning or otherwise, except under the terms of the Copyright, Designs and Patents Act 1988 or under the terms of a licence issued by the Copyright Licensing Agency Ltd, 90 Tottenham Court Road, London W1T 4LP, UK, without the permission in writing of the Publisher. Requests to the Publisher should be addressed to the Permissions Department, John Wiley & Sons Ltd, The Atrium, Southern Gate, Chichester, West Sussex PO19 8SQ, England, or emailed to permreq@wiley.co.uk, or faxed to (+44) 1243 770620.

Designations used by companies to distinguish their products are often claimed as trademarks. All brand names and product names used in this book are trade names, service marks, trademarks or registered trademarks of their respective owners. The Publisher is not associated with any product or vendor mentioned in this book.

This publication is designed to provide accurate and authoritative information in regard to the subject matter covered. It is sold on the understanding that the Publisher is not engaged in rendering professional services. If professional advice or other expert assistance is required, the services of a competent professional should be sought.

Other Wiley Editorial Offices

John Wiley & Sons Inc., 111 River Street, Hoboken, NJ 07030, USA

Jossey-Bass, 989 Market Street, San Francisco, CA 94103-1741, USA

Wiley-VCH Verlag GmbH, Boschstr. 12, D-69469 Weinheim, Germany

John Wiley & Sons Australia Ltd, 33 Park Road, Milton, Queensland 4064, Australia

John Wiley & Sons (Asia) Pte Ltd, 2 Clementi Loop #02-01, Jin Xing Distripark, Singapore 129809

John Wiley & Sons Canada Ltd, 22 Worcester Road, Etobicoke, Ontario, Canada M9W 1L1

Wiley also publishes its books in a variety of electronic formats. Some content that appears in print may not be available in electronic books.

British Library Cataloguing in Publication Data

A catalogue record for this book is available from the British Library

ISBN-13 978-0-470-01002-0 (HB)

ISBN-10 0-470-01002-9 (HB)

Typeset in 10/12pt Times by Laserwords Private Limited, Chennai, India
Printed and bound in Great Britain by Antony Rowe Ltd, Chippenham, Wiltshire.
This book is printed on acid-free paper responsibly manufactured from sustainable forestry
in which at least two trees are planted for each one used for paper production.

Contents

List of Contributors	xi
Preface	xiii
Acknowledgements	xvii
1 MIMO Wireless Channel Modeling and Experimental Characterization	1
<i>Michael A. Jensen and Jon W. Wallace</i>	
1.1 Introduction	1
1.1.1 MIMO system model	2
1.1.2 Channel normalization	4
1.2 MIMO Channel Measurement	5
1.2.1 Measurement system	6
1.2.2 Channel matrix characteristics	8
1.2.3 Multipath estimation	11
1.3 MIMO Channel Models	13
1.3.1 Random matrix models	13
1.3.2 Geometric discrete scattering models	19
1.3.3 Statistical cluster models	20
1.3.4 Deterministic ray tracing	24
1.4 The Impact of Antennas on MIMO Performance	24
1.4.1 Spatial diversity	25
1.4.2 Pattern (angle and polarization) diversity	26
1.4.3 Mutual coupling and receiver network modeling	28
References	35
2 Multidimensional Harmonic Retrieval with Applications in MIMO Wireless Channel Sounding	41
<i>Xiangqian Liu, Nikos D. Sidiropoulos, and Tao Jiang</i>	
2.1 Introduction	41
2.2 Harmonic Retrieval Data Model	43
2.2.1 2-D harmonic retrieval model	43
2.2.2 N -D harmonic retrieval model	44
2.2.3 Khatri–Rao product of Vandermonde matrices	45

2.3	Identifiability of Multidimensional Harmonic Retrieval	46
2.3.1	Deterministic ID of N -D harmonic retrieval	47
2.3.2	Stochastic ID of 2-D harmonic retrieval	48
2.3.3	Stochastic ID of N -D harmonic retrieval	51
2.4	Multidimensional Harmonic Retrieval Algorithms	53
2.4.1	2-D MDF	54
2.4.2	N -D MDF	54
2.4.3	N -D unitary ESPRIT	55
2.4.4	N -D MUSIC	57
2.4.5	N -D RARE	58
2.4.6	Summary	58
2.5	Numerical Examples	59
2.5.1	2-D harmonic retrieval (simulated data)	59
2.5.2	3-D harmonic retrieval (simulated data)	61
2.6	Multidimensional Harmonic Retrieval for MIMO Channel Estimation	61
2.6.1	Parametric channel modeling	62
2.6.2	MIMO channel sounding	65
2.6.3	Examples of 3-D MDF applied to measurement data	66
2.7	Concluding Remarks	70
	References	73
3	Certain Computations Involving Complex Gaussian Matrices with Applications to the Performance Analysis of MIMO Systems	77
	<i>Ming Kang, Lin Yang, and Mohamed-Slim Alouini</i>	
3.1	Introduction	77
3.2	Performance Measures of Multiple Antenna Systems	78
3.2.1	Noise-limited MIMO fading channels	78
3.2.2	MIMO channels in the presence of cochannel interference	80
3.2.3	MIMO beamforming	83
3.3	Some Mathematical Preliminaries	85
3.4	General Calculations with MIMO Applications	87
3.4.1	Main result	90
3.4.2	Application to noise-limited MIMO systems	92
3.4.3	Applications to MIMO channels in the presence of interference	97
3.5	Summary	101
	References	102
4	Recent Advances in Orthogonal Space-Time Block Coding	105
	<i>Mohammad Gharavi-Alkhansari, Alex B. Gershman, and Shahram Shahbazpanahi</i>	
4.1	Introduction	105
4.2	Notations and Acronyms	106
4.3	Mathematical Preliminaries	106
4.4	MIMO System Model and OSTBC Background	108

4.5	Constellation Space Invariance and Equivalent Array-Processing-Type MIMO Model	111
4.6	Coherent ML Decoding	115
4.7	Exact Symbol Error Probability Analysis of Coherent ML Decoder	119
4.7.1	Probability of error for a separable input constellation	119
4.7.2	Probability of error for a nonseparable input constellation	128
4.8	Optimality Properties of OSTBCs	133
4.8.1	Sufficient conditions for optimal space-time codes with dimension-constrained constellations	135
4.8.2	Optimality of OSTBCs for dimension-constrained constellations	140
4.8.3	Optimality of OSTBCs for small-size constellations	141
4.8.4	Optimality of OSTBCs among LD codes with the same number of complex variables	144
4.9	Blind Decoding of OSTBCs	145
4.9.1	Signal model and its properties	146
4.9.2	Blind channel estimation	147
4.9.3	Relationship to the blind ML estimator	153
4.9.4	Numerical examples	154
4.10	Multiaccess MIMO Receivers for OSTBCs	157
4.10.1	Multiaccess MIMO model	158
4.10.2	Minimum variance receivers	159
4.10.3	Numerical examples	161
4.11	Conclusions	163
	References	163
5	Trace-Orthogonal Full Diversity Cyclotomic Space-Time Codes	169
	<i>Jian-Kang Zhang, Jing Liu, and Kon Max Wong</i>	
5.1	Introduction	169
5.2	Channel Model with Linear Dispersion Codes	172
5.3	Good Structures for LD Codes: Trace Orthogonality	174
5.3.1	An information-theoretic viewpoint	174
5.3.2	A detection error viewpoint	177
5.4	Trace-orthogonal LD Codes	182
5.4.1	Trace orthogonality	182
5.4.2	Optimality of trace-orthogonal LD codes from a linear MMSE receiver viewpoint	183
5.5	Construction of Trace Orthogonal LD Codes	187
5.6	Design of Full Diversity LD Codes	192
5.6.1	Some basic definitions and results in algebraic number theory	192
5.6.2	Design of full diversity LD codes	194
5.7	Design of Full Diversity Linear Space-time Block Codes for $N < M$	197
5.8	Design Examples and Simulations	200
5.9	Conclusion	204
	References	205

6 Linear and Dirty-Paper Techniques for the Multiuser MIMO Downlink	209
<i>Christian B. Peel, Quentin H. Spencer, A. Lee Swindlehurst, Martin Haardt, and Bertrand M. Hochwald</i>	
6.1 Introduction	209
6.1.1 Problem overview	209
6.1.2 Literature survey	210
6.1.3 Chapter organization	212
6.2 Background and Notation	212
6.2.1 Capacity	213
6.2.2 Dirty-paper coding	215
6.2.3 Discussion	216
6.3 Single Antenna Receivers	217
6.3.1 Channel inversion	217
6.3.2 Regularized channel inversion	218
6.3.3 Sphere encoding	219
6.3.4 Computationally efficient precoding	223
6.3.5 Power control	226
6.4 Multiple Antenna Receivers	227
6.4.1 Channel block diagonalization	227
6.4.2 Combined block diagonalization and MMSE THP precoding	228
6.4.3 Coordinated Tx/Rx beamforming	231
6.5 Open Problems	234
6.5.1 Coding and capacity	234
6.5.2 Partial or imperfect CSI	234
6.5.3 Scheduling	235
6.5.4 Resource allocation	235
6.6 Summary	236
References	236
7 Antenna Subset Selection in MIMO Communication Systems	245
<i>Alexei Gorokhov, Dhananjay A. Gore, and Arogyaswami J. Paulraj</i>	
7.1 Introduction	245
7.1.1 Signal and channel model	246
7.2 SIMO/MISO Selection	247
7.2.1 Maximum ratio combining	247
7.2.2 Antenna selection	248
7.2.3 MRC versus antenna selection: performance comparison	248
7.3 MIMO Selection	251
7.3.1 Antenna selection for practical space-time processing	251
7.3.2 Antenna selection to maximize Shannon capacity	251
7.4 Diversity and Multiplexing with MIMO Antenna Selection	254
7.4.1 Diversity versus multiplexing	254
7.4.2 Transmit/receive antenna selection	255
7.4.3 Diversity and multiplexing: numerical example	259

CONTENTS	ix
----------	----

7.5	Receive Antenna Selection Algorithms	259
7.5.1	Incremental and decremental selection	260
7.5.2	Numerical study	262
7.6	Antenna Selection in MIMO Wireless LAN Systems	262
7.7	Summary	265
	References	266
8	Convex Optimization Theory Applied to Joint Transmitter-Receiver Design in MIMO Channels	269
	<i>Daniel Pérez Palomar, Antonio Pascual-Iserte, John M. Cioffi, and Miguel Angel Lagunas</i>	
8.1	Introduction	269
8.2	Convex Optimization Theory	271
8.2.1	Definitions and classes of convex problems	271
8.2.2	Reformulating a problem in convex form	273
8.2.3	Lagrange duality theory and KKT optimality conditions	274
8.2.4	Efficient numerical algorithms to solve convex problems	275
8.2.5	Applications in signal processing and communications	277
8.3	System Model and Preliminaries	281
8.3.1	Signal model	281
8.3.2	Measures of quality	282
8.3.3	Optimum linear receiver	283
8.4	Beamforming Design for MIMO Channels: A Convex Optimization Approach	284
8.4.1	Problem formulation	285
8.4.2	Optimal design with independent QoS constraints	287
8.4.3	Optimal design with a global QoS constraint	289
8.4.4	Extension to multicarrier systems	295
8.4.5	Numerical results	296
8.5	An Application to Robust Transmitter Design in MIMO Channels	298
8.5.1	Introduction and state-of-the-art	298
8.5.2	A generic formulation of robust approaches	300
8.5.3	Problem formulation	301
8.5.4	Reformulating the problem in a simplified convex form	304
8.5.5	Convex uncertainty regions	307
8.5.6	Numerical results	308
8.6	Summary	311
	References	313
9	MIMO Communications with Partial Channel State Information	319
	<i>Shengli Zhou and Georgios B. Giannakis</i>	
9.1	Introduction	319
9.2	Partial CSI Models	319
9.2.1	Statistical models	320
9.2.2	Finite-rate feedback model	322

9.3	Capacity-Optimal Designs	323
9.3.1	Capacity optimization with statistical CSI	324
9.3.2	Capacity optimization with finite-rate feedback	329
9.4	Error Performance Oriented Designs	331
9.4.1	Combining orthogonal STBC with linear precoding	331
9.4.2	Finite-rate one-dimensional beamforming	341
9.4.3	Further results	345
9.5	Adaptive Modulation with Partial CSI	347
9.5.1	Adaptive modulation based on 2D coder-beamformer	347
9.5.2	Adaptive modulation/beamforming with finite-rate feedback	350
9.5.3	Other combinations	352
9.6	Conclusions	352
Appendix	352
References	353
Index		357

List of Contributors

- **Mohamed-Slim Alouini**
University of Minnesota, Minneapolis, MN, USA
- **John M. Cioffi**
Stanford University, Stanford, CA, USA
- **Alex B. Gershman**
McMaster University, Hamilton, ON, Canada
and
University of Duisburg-Essen, Duisburg, Germany
- **Mohammad Gharavi-Alkhansari**
University of Duisburg-Essen, Duisburg, Germany
- **Georgios B. Giannakis**
University of Minnesota, Minneapolis, MN, USA
- **Dhananjay A. Gore**
Qualcomm Inc., San Diego, CA, USA
- **Alexei Gorokhov**
Qualcomm Inc., San Diego, CA, USA
- **Martin Haardt**
Ilmenau University of Technology, Ilmenau, Germany
- **Bertrand M. Hochwald**
Lucent Technologies (Bell Laboratories), Murray Hill, NJ, USA
- **Michael A. Jensen**
Brigham Young University, Provo, UT, USA
- **Tao Jiang**
Royal Institute of Technology (KTH), Stockholm, Sweden
- **Ming Kang**
University of Minnesota, Minneapolis, MN, USA

- ***Miguel Angel Lagunas***
Technical University of Catalonia, Barcelona, Spain
and
Telecommunications Technological Center of Catalonia, Barcelona, Spain
- ***Jing Liu***
McMaster University, Hamilton, ON, Canada
- ***Xiangqian Liu***
University of Louisville, Louisville, KY, USA
- ***Daniel Pérez Palomar***
Princeton University, Princeton, NJ, USA
- ***Antonio Pascual-Iserte***
Technical University of Catalonia, Barcelona, Spain
- ***Arogyaswami J. Paulraj***
Stanford University, Stanford, CA, USA
- ***Christian B. Peel***
Swiss Federal Institute of Technology, Zürich, Switzerland
- ***Shahram Shahbazpanahi***
McMaster University, Hamilton, ON, Canada
- ***Nikos D. Sidiropoulos***
Technical University of Crete, Crete, Greece
- ***Quentin H. Spencer***
Distribution Control Systems Inc., Hazelwood, MO, USA
- ***A. Lee Swindlehurst***
Brigham Young University, Provo, UT, USA
- ***Jon W. Wallace***
Brigham Young University, Provo, UT, USA
- ***Kon Max Wong***
McMaster University, Hamilton, ON, Canada
- ***Lin Yang***
University of Minnesota, Minneapolis, MN, USA
- ***Jian-Kang Zhang***
McMaster University, Hamilton, ON, Canada
- ***Shengli Zhou***
University of Connecticut, Storrs, CT, USA

Preface

Driven by the desire to boost the quality of service of wireless systems closer to that afforded by wireline systems, space-time processing for multiple-input multiple-output (MIMO) wireless communications research has drawn remarkable interest in recent years. Exciting theoretical advances, complemented by rapid transition of research results to industry products and services, have created a vibrant and growing area that is already established by all counts. This offers a good opportunity to reflect on key developments in the area during the past decade and also outline emerging trends.

Space-time processing for MIMO communications is a broad area, owing in part to the underlying convergence of information theory, communications, and signal processing research that brought it to fruition. Among its constituent topics, space-time coding has played a prominent role, and is well summarized in recent graduate texts. Several other topics, however, are also important in order to grasp the bigger picture in space-time processing. These include MIMO wireless channel characterization, modeling, and validation; model-based performance analysis; spatial multiplexing; and joint transceiver design using channel state information (CSI). Our aim in embarking on this edited book project was twofold: (i) present a concise, balanced, and timely introduction to the broad area of space-time processing for MIMO communications; (ii) outline emerging trends, particularly in terms of spatial multiplexing and joint transceiver optimization. In this regard, we were fortunate to be able to solicit excellent contributions from some of the world's leading experts in the respective subjects.

This book is aimed at the advanced level, and is suitable for graduate students, researchers, and practicing engineers. The material can be used for an advanced special topics graduate course in MIMO communications, but the book can also be used for independent study, for example, an introduction for graduate students who wish to conduct research in the area. Practicing engineers will appreciate the up-to-date tutorial exposition to timely topics. Several technologies reviewed here are already incorporated in commercial systems.

This book is organized in three intertwined thematic areas: *MIMO channel measurement, modeling, and performance analysis* (Chapters 1-3); *space-time coding* (Chapters 4-5); *spatial multiplexing and transmitter design with full or partial CSI* (Chapters 6-9). A threaded overview of the individual chapter contributions follows.

MIMO wireless channel modeling and characterization: Chapter 1, by Jensen and Wallace, begins with a derivation of pertinent MIMO wireless channel models, starting from first principles and taking into account the directional characteristics of antenna elements. The channel sounding process is then described for a specific narrowband MIMO system operating at 2.45 GHz and three representative indoor propagation scenarios. Useful

plots of channel magnitude, phase, and capacity distributions are provided. This part of the chapter will be especially useful for practicing engineers interested in channel sounding. The chapter then discusses common simplified random matrix models of the MIMO wireless channel and their statistical properties. Going beyond the commonly assumed Rayleigh model, the chapter also explores geometric discrete scattering models and statistical cluster models, including an extension of the well-known Saleh–Valenzuela model. A comparison of capacity distributions obtained from measured versus model-based synthesized channels is included, and the impact of angle, polarization, and mutual coupling on channel capacity is illustrated.

Under certain scenarios, the discrete parametric MIMO channel models in Chapter 1 reduce to multidimensional harmonic mixture models, a core subject in signal processing research. Chapter 2, by Liu, Sidiropoulos, and Jiang, provides a concise overview of recent advances in multidimensional harmonic retrieval theory and algorithms, with application to MIMO channel parameter estimation from measured data. The chapter begins with a review of the state of art in terms of associated parameter identifiability results. Identifiability is a prerequisite for meaningful estimation but is often far from enough for accurate estimation. Interestingly, in this case the authors show that identifiability considerations also yield good estimation algorithms as a side-benefit. The chapter continues with a review of several competitive multidimensional harmonic mixture parameter estimation algorithms. Selected algorithms are then compared, first using simulated mixture data, then using measured data. The measured data are taken from two channel sounding campaigns: an outdoor urban environment and an outdoor suburban environment. Discussion of the associated channel sounding setup and process is also included. Chapters 1 and 2 complement each other nicely: the first is focused on modeling and characterization, the second on parameter estimation for a special but important class of MIMO channel models. The discussion of indoor channel models and measurements in Chapter 1 is complemented by the discussion of outdoor channel models and measurements in Chapter 2.

Performance analysis: Parsimonious MIMO channel models facilitate system design, for they enable preliminary performance assessment via simulation. Simulation helps in identifying promising designs for further consideration, thus cutting down research and development cycles and associated costs. Still, realistic MIMO simulations are time-consuming, especially because the target transmit-receive architectures typically entail nontrivial processing. For this reason, closed-form performance analysis of MIMO communication over simplified but realistic channel models is of paramount importance. In Chapter 3, Kang, Yang, and Alouini take us on a tour of MIMO performance analysis. They expose us to key tools that, perhaps surprisingly, permeate the subject matter. In particular, they show that many pertinent performance metrics, such as information rate and outage probability, are closely related to the distribution of eigenvalues of certain Hermitian matrices, derived from complex Gaussian matrices. The key is in reducing seemingly complicated multidimensional integrals to simpler closed forms, expressed in terms of special functions. These forms are often amenable to further manipulation, which directly reveals the effect of individual system parameters on the overall performance.

Space-time coding: Among the many types of space-time codes, the class of orthogonal space-time block codes (OSTBCs) is special in many ways. It includes the celebrated 2×1 Alamouti code, which was instrumental in the development of the area, and quickly made it all the way to standards and actual systems. Orthogonal space-time block codes have

numerous desirable properties, not the least of which is simple linear optimal decoding. Chapter 4, by Gharavi-Alkhansari, Gershman, and Shahbazpanahi, covers both basic and advanced aspects of OSTBCs, with notable breadth and timeliness. The exposition is built around certain key properties of OSTBCs. For example, the fact that OSTBCs yield an orthogonal equivalent mixing matrix irrespective of the MIMO channel matrix (so long as the latter is not identically zero) enables a remarkably general performance analysis, even for nonseparable constellations. The chapter also covers important recent developments in the area, such as blind channel estimation for OSTBC-coded systems, and multiuser interference mitigation in the same context.

OSTBCs have numerous desirable features, but other linear space-time block codes may be preferable if the goal is to maximize the information rate. Early designs of the latter kind were based on maximizing ergodic capacity. Since diversity was not explicitly accounted for in those designs, the resulting codes could not guarantee full diversity. More recently, specific examples of full-rate, full-diversity designs appeared in the literature, based on number theory. Still, a general systematic design methodology was missing. Chapter 5, by Zhang, Liu, and Wong, makes important steps in this direction, using cyclotomic field theory. The development is based on exploring the structural properties of good codes, leading to the identification of *trace-orthogonality* as the central structure. Trace-orthogonal linear block codes are proven to be optimal from a linear MMSE receiver viewpoint, and several examples of specific trace-orthogonal code designs are provided and compared to the pertinent state of the art.

Spatial multiplexing for the multiuser MIMO downlink: Multiple antennas can also be used for *spatial multiplexing*: that is, the simultaneous transmission of multiple streams, separated via transmit or receive ‘beams’. The uplink scenario, wherein a base station employs multiple receive antennas and beamforming to separate transmissions from the different mobiles, has been thoroughly studied in the array processing literature. More recently, transmit beamforming/precoding for multiuser downlink transmission is drawing increasing attention. This scenario corresponds to a nondegraded Gaussian broadcast channel, and, until very recently, this was unchartered territory for information theorists. Interestingly, the aforementioned multiuser multiantenna downlink scenario is quite different, and, at the same time, closely tied, via duality, to the corresponding uplink scenario. In Chapter 6, Peel, Spencer, Swindlehurst, Haardt, and Hochwald deliver a concise overview of recent developments in this exciting area. The authors present linear and nonlinear precoding approaches. Simple regularized channel inversion precoding is shown to perform well in many cases. Attaining sum capacity turns out to require so-called *Dirty-Paper* coding, also known as *Costa* coding, which is nonlinear and often complex to implement. As an interesting alternative, the authors propose *Sphere Precoding*, an interesting application of the Sphere Decoding algorithm on the transmitter’s end instead of the receiver’s end, as is usual. Generalizations to multiple-antenna receivers are also considered, including joint transmit–receive beamforming.

Antenna selection: While multiple antennas help in improving performance, there are situations wherein it pays to work with a properly selected subset of the available antennas. Each ‘live’ antenna requires a separate down-conversion chain, and it often makes better sense to employ a few down-conversion chains along with a cross-bar switch to choose from the available elements. In Chapter 7, Gorokhov, Gore, and Paulraj summarize the state of the art in MIMO antenna selection research. They consider the impact of antenna selection

on capacity and diversity and establish a nice relationship between spatial multiplexing and diversity gains. The authors also present effective greedy incremental selection algorithms that work by either pruning or augmenting the list of selected antennas, one element at a time. Interestingly, these greedy algorithms can yield almost-optimal selection results, as the authors illustrate by simulation.

Joint transmitter–receiver design based on convex optimization: When channel state information (CSI) is available at both ends of the MIMO communication link, joint transmit and receive beamforming optimization is possible. In many cases, the resulting optimization problems appear difficult if not intractable to solve. Fortunately, however, they can often be transformed to convex optimization problems, and thus efficiently solved via modern numerical interior-point methods. Sometimes, the solution can even be put in closed form, taking advantage of Karush–Kuhn–Tucker conditions. In Chapter 8, Palomar, Pascual–Iserte, Cioffi, and Lagunas take us on a fascinating tour of modern convex optimization theory and algorithms, with applications in MIMO communications. Examples include robust single-user receive-beamforming, multiuser beamforming, and optimal (e.g., minimum BER) linear MIMO transceiver design under various pertinent quality of service constraints. Practical aspects such as imperfect CSI and quantization errors are also considered. The breadth of this chapter is remarkable. In our opinion, the chapter can serve as an excellent concise introduction to modern convex optimization and its applications to array signal processing and communications. In this context, the message is that it is important to know what can be done with convex optimization today, for clever reformulation may turn one’s seemingly difficult problem into a convex one – at which point most of the work has already been done.

MIMO communications with partial CSI at the transmitter: Transmitter optimization based on CSI has well-documented advantages. While it is often reasonable to assume that the receiver can acquire accurate CSI, assuming that the same holds on the transmitter’s end can be very unrealistic for mobile wireless links. In between perfect CSI and no CSI lies the pragmatic case of partial CSI: the case wherein the transmitter only has a coarse estimate of the actual channel. This coarse estimate can be in the form of a quantization index, denoting the region where the channel vector (as measured at the receiver) falls; or in the form of a noisy channel estimate, whose difference from the actual channel is treated as a random vector. The former corresponds to finite-rate feedback, while the latter can also model analog feedback. In Chapter 9, Zhou and Giannakis treat both cases, from two basic viewpoints: optimizing average capacity, and minimizing symbol error rate. They show that, with partial CSI, antenna correlation can in fact increase capacity. With finite-rate feedback, joint optimization of the channel quantization codebook and the selection of transmission mode for each of the quantized channel states is needed for capacity optimization. Interestingly, a generalization of the Lloyd–Max vector quantization algorithm can be used for this purpose. With CSI at the transmitter, it becomes possible to improve the performance of OSTBCs by combining them with linear precoding and adjusting the linear precoder according to CSI. Chapter 9 includes symbol error rate minimization strategies for linearly precoded OSTBC systems, along with numerous extensions of the above ideas to incorporate, for example, adaptive modulation and beamforming.

Alex B. Gershman & Nikos D. Sidiropoulos

Acknowledgements

We would like to express our sincere thanks to Dr. Mohammad Gharavi-Alkhansari, who compiled the individual chapter contributions into the final book draft that was delivered to the publisher. Dr. Gharavi-Alkhansari spared no effort to ensure consistency, uniformity, and attention to detail – by no means an easy task.

We would also like to acknowledge the help of our contacts at John Wiley & Sons Ltd: Sarah Hinton, Mark Hammond, and Graham Woodward.

We owe a great deal to our families – it would have been impossible to maintain our spirit and work habits without their continuous love and support – thank you.

Last but not least, we would like to thank our contributing authors. We were fortunate to be able to bring such distinguished researchers aboard this project. Their high-quality contributions make this book worthwhile.

– Alex B. Gershman & Nikos D. Sidiropoulos

1

MIMO Wireless Channel Modeling and Experimental Characterization

Michael A. Jensen and Jon W. Wallace

1.1 Introduction

While coding and signal processing are key elements to successful implementation of a MIMO system, the communication channel represents a major component that determines system performance. A considerable volume of work has been performed to characterize communication channels for general wireless applications. However, because MIMO systems operate at an unprecedented level of complexity to exploit the channel space-time resources, a new level of understanding of the channel space-time characteristics is required to assess the potential performance of practical multiantenna links.

This chapter will focus on experimental measurements and models aimed at characterizing the MIMO channel spatio-temporal properties. Generally, we will define this channel to include the electromagnetic propagation, antennas, and transmit/receive radio circuitry, although different measurement and modeling techniques may include all or only part of this set. When evaluating the results of these modeling and measurement campaigns, much of the discussion will focus on the pertinent properties of the propagation environment. However, an examination of the topic of MIMO channels would be incomplete without some discussion of the impact of antenna element properties – such as directivity, polarization, and mutual coupling – antenna array configuration, and radio frequency (RF) architecture on communication behavior. Therefore, we will highlight techniques for including these channel aspects in MIMO system characterization and will

show examples that demonstrate the impact that different design features can have on system performance.

1.1.1 MIMO system model

Figure 1.1 depicts a generic MIMO system that will serve as a reference for defining the MIMO communication channel. For this discussion and throughout this chapter, boldface uppercase and lowercase letters will represent matrices (matrix \mathbf{H} with m th element H_{mn}) and column vectors (vector \mathbf{h} with m th element h_m), respectively. A stream of $Q \times 1$ vector input symbols $\mathbf{b}^{(k)}$, where k is a time index, are fed into a space-time encoder, generating a stream of $N_T \times 1$ complex vectors $\mathbf{x}^{(k)}$, where N_T represents the number of transmit antennas. Pulse shaping filters transform each element of the vector to create a $N_T \times 1$ time-domain signal vector $\mathbf{x}(t)$, which is up-converted to a suitable transmission carrier (RF, microwave, optical, acoustic). The resulting signal vector $\mathbf{x}_A(t)$ drives the transmit transducer array (antennas, lasers, speakers), which in turn radiates energy into the propagation environment.

The function $h_P(t, \tau, \theta_R, \phi_R, \theta_T, \phi_T)$ represents the impulse response relating field radiated by the transmit array to the field incident on the receive array. The dependence on time t suggests that this impulse response is time variant because of motion of scatterers within the propagation environment or motion of the transmitter and receiver. The variable τ represents the time delay relative to the excitation time t . We assume a finite impulse response, so that $h_P(t, \tau, \theta_R, \phi_R, \theta_T, \phi_T) = 0$ for $\tau > \tau_0$. We also assume that $h_P(t, \tau, \theta_R, \phi_R, \theta_T, \phi_T)$ remains constant over a time interval (in t) of duration τ_0 so that over a single transmission, the physical channel can be treated as a linear, time-invariant system.

Assume now that the input signal $\mathbf{x}_A(t)$ creates the field $x_P(t, \theta_T, \phi_T)$ radiated from the transmit array, where (θ_T, ϕ_T) denote the elevation and azimuthal angles taken with respect to the coordinate frame of the transmit array. At the receive array, the field distribution $y_P(t, \theta_R, \phi_R)$, where (θ_R, ϕ_R) represent angles referenced to the receive array coordinate frame, and can be expressed as the convolution

$$y_P(t, \theta_R, \phi_R) = \int_0^{2\pi} \int_0^\pi \int_{-\infty}^{\infty} h_P(t, \tau, \theta_R, \phi_R, \theta_T, \phi_T) x_P(t - \tau, \theta_T, \phi_T) \sin \theta_T d\tau d\theta_T d\phi_T \quad (1.1)$$

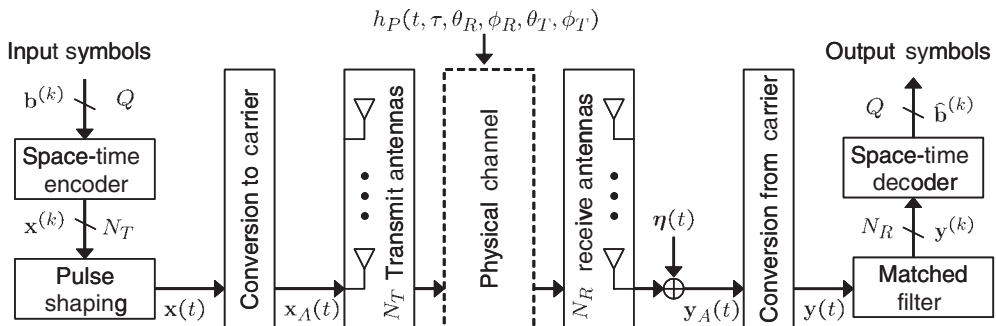


Figure 1.1 A generic MIMO communication system.

The N_R -element receive array then samples this field and generates the $N_R \times 1$ signal vector $\mathbf{y}'_A(t)$ at the array terminals. Noise in the system is typically generated in the physical propagation channel (interference) and the receiver front-end electronics (thermal noise). To simplify the discussion, we will lump all additive noise into a single contribution represented by the $N_R \times 1$ vector $\boldsymbol{\eta}(t)$ that is injected at the receive antenna terminals. The resulting signal plus noise vector $\mathbf{y}_A(t)$ is then downconverted to produce the $N_R \times 1$ baseband output vector $\mathbf{y}(t)$. Finally, $\mathbf{y}(t)$ is passed through a matched filter whose output is sampled once per symbol to produce $\mathbf{y}^{(k)}$, after which the space-time decoder produces estimates $\hat{\mathbf{b}}^{(k)}$ of the originally transmitted symbols.

This chapter focuses on the characteristics of the channel, although the specific definition of this channel can vary depending on the goal of the analysis. For example, in some cases we wish to focus on the physical channel impulse response and use it to generate a channel matrix relating the signals $\mathbf{x}_A(t)$ and $\mathbf{y}_A(t)$. A common assumption will be that all scattering in the propagation channel is in the far field and that a discrete number of propagation “paths” connects the transmit and receive arrays. Under this assumption, the physical channel response for L paths may be written as

$$h_P(t, \tau, \theta_R, \phi_R, \theta_T, \phi_T) = \sum_{\ell=1}^L A_\ell \delta(\tau - \tau_\ell) \delta(\theta_T - \theta_{T,\ell}) \\ \times \delta(\phi_T - \phi_{T,\ell}) \delta(\theta_R - \theta_{R,\ell}) \delta(\phi_R - \phi_{R,\ell}), \quad (1.2)$$

where A_ℓ is the gain of the ℓ th path with angle of departure (AOD) $(\theta_{T,\ell}, \phi_{T,\ell})$, angle of arrival (AOA) $(\theta_{R,\ell}, \phi_{R,\ell})$, and time of arrival (TOA) τ_ℓ . The term $\delta(\cdot)$ represents the Dirac delta function. The time variation of the channel is included by making the parameters of the multipaths ($L, A_\ell, \tau_\ell, \theta_{T,\ell}, \dots$) time dependent. To use this response to relate $\mathbf{x}_A(t)$ to $\mathbf{y}_A(t)$, it is easier to proceed in the frequency domain. We take the Fourier transform of the relevant signals to obtain $\tilde{\mathbf{x}}_A(\omega)$, $\tilde{\mathbf{y}}_A(\omega)$, and $\tilde{\boldsymbol{\eta}}(\omega)$, and take the Fourier transform of h_P with respect to the delay variable τ to obtain $\tilde{h}_P(t, \omega, \theta_R, \phi_R, \theta_T, \phi_T)$ where ω is the radian frequency. Assuming single-polarization array elements, the frequency domain radiation patterns of the n th transmit and m th receive array elements are $e_{T,n}(\omega, \theta_T, \phi_T)$ and $e_{R,m}(\omega, \theta_R, \phi_R)$, respectively. We must convolve these patterns with \tilde{h}_P in the angular coordinates to obtain

$$\tilde{\mathbf{y}}_A(\omega) = \mathbf{H}_P(\omega) \tilde{\mathbf{x}}_A(\omega) + \tilde{\boldsymbol{\eta}}(\omega) \quad (1.3)$$

where

$$H_{P,mn}(\omega) = \sum_{\ell=1}^L \beta_\ell e_{R,m}(\omega, \theta_R, \ell, \phi_R, \ell) e_{T,n}(\omega, \theta_T, \ell, \phi_T, \ell) \quad (1.4)$$

and $\beta_\ell = A_\ell \exp\{-j\omega\tau_\ell\}$ is the complex gain of the ℓ th path. $\mathbf{H}_P(\omega)$ is referred to as the *channel transfer matrix* or simply *channel matrix*. Although this representation is usually inconvenient for closed-form analysis of space-time code behavior, it explicitly uses the antenna properties in constructing the channel matrix, and therefore facilitates examination of a variety of antenna configurations for a single physical propagation channel. Also, because it is based on the physical channel impulse response, it is appropriate for wideband or *frequency selective* channels for which the elements of $\mathbf{H}_P(\omega)$ vary significantly over the bandwidth of interest.

While the physical channel model in (1.3) is useful for certain cases, in most signal-processing analyses the channel is taken to relate the input to the pulse shaping block $\mathbf{x}^{(k)}$ to the output of the matched filter $\mathbf{y}^{(k)}$. This model is typically used for cases where the frequency domain channel transfer function remains approximately constant over the bandwidth of the transmitted waveform, often referred to as the *frequency nonselective* or *flat fading* scenario. In this case, the frequency domain transfer functions can be treated as complex constants that simply scale the complex input symbols. We can therefore write the input/output relationship as

$$\mathbf{y}^{(k)} = \mathbf{H}^{(k)}\mathbf{x}^{(k)} + \boldsymbol{\eta}^{(k)} \quad (1.5)$$

where $\boldsymbol{\eta}^{(k)}$ denotes the noise that has passed through the receiver and has been sampled at the matched-filter output. The term $\mathbf{H}^{(k)}$ represents the channel matrix for the k th transmitted symbol, with the superscript explicitly indicating that the channel can change over time. Throughout this chapter, we will sometimes drop this superscript for convenience. We emphasize here that $\mathbf{H}^{(k)}$ is based on the value of $\mathbf{H}_P(\omega)$ evaluated at the carrier frequency but includes the additional effects of the transmit and receive electronics. This model forms the basis of the random matrix models covered in Section 1.3.1 and is very convenient for closed-form analysis. The main drawbacks of this approach are the modeling inaccuracy, the difficulty of specifying $\mathbf{H}^{(k)}$ for all systems of practical interest, and the fact that it does not lend itself to the description of frequency selective channels.

The discussion thus far has ignored certain aspects of the MIMO system that may be important in some applications. For example, realistic microwave components will experience complicated interactions due to coupling and noise, factors that may be treated with advanced network models as detailed in Section 1.4.3. The effects of non-ideal matched filters and sampling may also be of interest, which can be analyzed with the appropriate level of modeling detail [1].

1.1.2 Channel normalization

Consider the channel model in (1.5) where the noise $\boldsymbol{\eta}^{(k)}$ is assumed to be a random vector with zero-mean complex normal entries and covariance $\sigma_\eta^2 \mathbf{I}$, where \mathbf{I} is the identity matrix. The average noise power in each receiver is therefore given by the variance σ_η^2 of the complex random variables. The signal power averaged in time as well as over all receive ports is given as

$$P_R = \frac{1}{N_R} \mathbb{E} \left\{ \mathbf{x}^{(k)H} \mathbf{H}^{(k)H} \mathbf{H}^{(k)} \mathbf{x}^{(k)} \right\} = \frac{1}{N_R} \text{Tr} \left(\mathbb{E} \left\{ \mathbf{x}^{(k)} \mathbf{x}^{(k)H} \right\} \mathbb{E} \left\{ \mathbf{H}^{(k)H} \mathbf{H}^{(k)} \right\} \right), \quad (1.6)$$

where $\mathbb{E} \{ \cdot \}$ denotes expectation, $\{ \cdot \}^H$ represents a matrix conjugate transpose and $\text{Tr}(\cdot)$ is a matrix trace. We have used the statistical independence of the signal $\mathbf{x}^{(k)}$ and channel matrix $\mathbf{H}^{(k)}$ to manipulate this expression. If the transmitter divides the total transmit power P_T equally across statistically independent streams on the multiple antennas, $\mathbb{E} \{ \mathbf{x}^{(k)} \mathbf{x}^{(k)H} \} = (P_T / N_T) \mathbf{I}$. If the expectation $\mathbb{E} \{ \mathbf{H}^{(k)H} \mathbf{H}^{(k)} \}$ is approximated using a sample mean over a series $1 \leq k \leq K$, the average received signal power is

$$P_R = \frac{P_T}{N_T N_R K} \sum_{k=1}^K \|\mathbf{H}^{(k)}\|_F^2, \quad (1.7)$$

where $\|\cdot\|_F$ is the Frobenius norm. The signal-to-noise ratio (SNR) averaged in time as well as over all receive ports is therefore

$$\text{SNR} = \frac{P_T}{\sigma_\eta^2} \underbrace{\frac{1}{N_T N_R K} \sum_{k=1}^K \|\mathbf{H}^{(k)}\|_F^2}_{\Upsilon}. \quad (1.8)$$

We recognize that Υ represents the average of the power gains between each pair of transmit and receive antennas. The resulting SNR is equivalent to what would be obtained if the power were transmitted between a single pair of antennas with channel power gain Υ . We therefore refer to (1.8) as the **single-input single-output** (SISO) SNR.

When performing simulations and analyses using channel matrices obtained from measurements or models, it is often useful to be able to properly scale $\mathbf{H}^{(k)}$ to achieve a specified average SNR. We therefore define a new set of channel matrices $\mathbf{H}_0^{(k)} = \Psi \mathbf{H}^{(k)}$, where Ψ is a normalizing constant. To achieve a given average SNR, Ψ should be chosen according to

$$\Psi^2 = \text{SNR} \frac{\sigma_\eta^2}{P_T} \frac{N_T N_R K}{\sum_{k=1}^K \|\mathbf{H}^{(k)}\|_F^2}. \quad (1.9)$$

If $K = 1$, this implies that each individual channel matrix is normalized to have the specified SNR. If $K > 1$, the average SNR over the group of K matrices will be as specified, although the SNR for each individual matrix will fluctuate about this mean value. This allows investigation of the relative variations in received signal strength over an ensemble of measurements or simulations.

1.2 MIMO Channel Measurement

The most direct way to gain an understanding of the MIMO wireless channel is to experimentally measure the $N_R \times N_T$ channel matrix \mathbf{H} . These measurements include the effects of the RF subsystems and the antennas, and therefore the results are dependent on the array configurations used. A variety of such measurements have been reported [2–11], and results obtained include channel capacity, signal correlation structure (in space, frequency, and time), channel matrix rank, path loss, delay spread, and a variety of other quantities. *True array* systems, where all antennas operate simultaneously, most closely model real-world MIMO communication, and can accommodate channels that vary in time. However, the implementation of such a system comes at significant cost and complexity because of the requirement of multiple parallel transmit and receive electronic subsystems.

Other measurement systems are based on either *switched array* or *virtual array* architectures. Switched array designs use a single transmitter and single receiver, sequentially connecting all array elements to the electronics using high-speed switches [12, 13]. Switching times for such systems are necessarily low (2 μ s to 100 ms) to allow the measurement over all antenna pairs to be completed before the channel changes. Virtual array architectures use precision displacement (or rotation) of a single antenna element rather than a set of fixed antennas connected via switches [14–16]. Although this method has the advantage of eliminating mutual coupling, a complete channel matrix measurement often takes several

seconds or minutes. Therefore, such a technique is appropriate for fixed indoor measurement campaigns when the channel remains constant for relatively long periods.

In this section, we will provide details regarding a true array system for direct transfer matrix measurement and illustrate MIMO performance for representative propagation environments. While the approach taken here is not unique, particularly with regard to the modulation constellation used and specific system architecture, the system shown is representative of typical platforms used in MIMO channel probing. Following the discussion of the system, we will discuss additional processing that can be accomplished using MIMO system measurements to allow estimation of the physical multipath characteristics associated with the propagation channel.

1.2.1 Measurement system

The platform detailed here, as depicted in Figure 1.2, uses a narrowband MIMO communications system operating at a center frequency of 2.45 GHz. Up to 16 unique binary sequences are constructed using a shift-generator employing a maximal length sequence polynomial [17] and then output using a digital pattern generator ($\pm 5V$). The sequences are individually multiplied by a common microwave local oscillator (LO) signal to generate binary phase shift keyed (BPSK) waveforms that are amplified and fed to one of the N_T transmit antennas. The signal on each of the $N_R \leq 16$ receive antennas is amplified, down-converted to an intermediate frequency (IF), filtered, and sampled on a 16-channel 1.25 Msample/s analog-to-digital (A/D) conversion card for storage and postprocessing. The system is calibrated before each measurement to remove the effects of unequal complex gains in the electronics.

Once the IF data is collected, postprocessing is used to perform carrier and symbol timing recovery and code synchronization. To locate the start of the codes, the signal from one of the N_R receive antennas is correlated with a baseband representation of one of the transmit codes. A Fast Fourier Transform (FFT) of this result produces a peak at the IF when the selected transmit code is aligned with the same code in the receive signal. The search for this alignment is simplified by using shortened correlating codes and coarse steps at the beginning of the process and adaptively reducing the step size and switching to full-length codes as the search converges. Additionally, if the specified code is weakly represented in the received signal chosen, the maximum correlation may not occur at code alignment. The

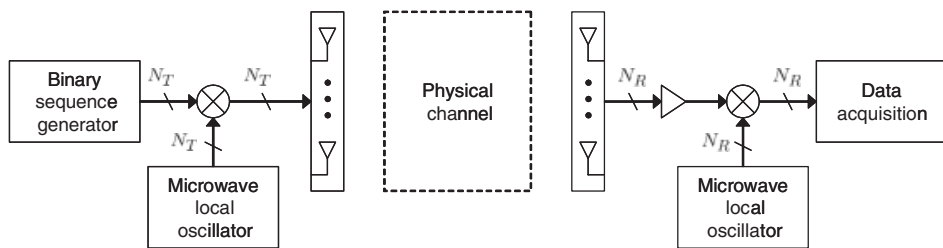


Figure 1.2 High level system diagram of the narrowband wireless MIMO measurement system.

procedure therefore searches over all combinations of receive channel and code to ensure accurate code synchronization.

The IF is approximately given by the frequency at which the peak in the FFT occurs. This frequency estimate is refined using a simple optimization that maximizes the magnitude of the Discrete Time Fourier Transform (DTFT) of the known aligned code multiplied by the receive signal (despread signal). Subsequently, the waveform generated by moving a window along the despread signal is correlated against a complex sinusoid at the IF, and the phase of the result is taken as the carrier phase at the center of the recovery window. A moving average filter is finally used to smooth this phase estimate.

With the carrier and timing recovery performed, the channel transfer matrix can be extracted from the data using a maximum likelihood (ML) channel inversion technique. Let A_{mn} and ϕ_{mn} represent the amplitude and phase, respectively, of the signal from transmit antenna n as observed on receive antenna m . Therefore, the estimate of the mn th element of the transfer matrix is $\hat{H}_{mn} = A_{mn}e^{j\phi_{mn}} = H_{mn}^R + jH_{mn}^I$, where H_{mn}^R and H_{mn}^I represent the real and imaginary parts of \hat{H}_{mn} , respectively. If $f_n^{(k)}$ represents the k th sample of the code from the n th transmit antenna, the discrete signal at the port of the m th receive antenna is given as

$$y_m^{(k)} = \sum_{n=1}^{N_T} A_{mn} f_n^{(k)} \cos(\varpi_0 k + \phi^{(k)}) + \eta_m^{(k)} \quad (1.10)$$

where ϖ_0 is the discrete (recovered) carrier frequency, $\phi^{(k)}$ is the randomly varying carrier phase, and $\eta_m^{(k)}$ represents the discrete noise sample that is assumed to be spectrally white with a zero-mean Gaussian amplitude distribution.

We now consider a sequence of $k_2 - k_1 + 1$ samples, which is the length of the code multiplied by the number of samples per symbol. If $\hat{y}_m^{(k)}$ represents the observed signal, then the ML estimate of the channel transfer function results from finding the values of \hat{H}_{mn} that minimize

$$T_m = \sum_{k=k_1}^{k_2} \left| \hat{y}_m^{(k)} - \sum_{n=1}^{N_T} \left\{ H_{mn}^R \cos(\varpi_0 k + \phi^{(k)}) - H_{mn}^I \sin(\varpi_0 k + \phi^{(k)}) \right\} f_n^{(k)} \right|^2. \quad (1.11)$$

Taking the derivative of T_m with respect to both H_{ms}^R and H_{ms}^I , $1 \leq s \leq N_T$, and setting the result to zero produces the equations

$$2 \sum_{k=k_1}^{k_2} \hat{y}_m^{(k)} f_s^{(k)} \cos(\varpi_0 k + \phi^{(k)}) = \sum_{k=k_1}^{k_2} \sum_{n=1}^{N_T} f_n^{(k)} f_s^{(k)} \left\{ H_{mn}^R (1 + \alpha_k) - H_{mn}^I \beta_k \right\} \quad (1.12)$$

$$2 \sum_{k=k_1}^{k_2} \hat{y}_m^{(k)} f_s^{(k)} \sin(\varpi_0 k + \phi^{(k)}) = \sum_{k=k_1}^{k_2} \sum_{n=1}^{N_T} f_n^{(k)} f_s^{(k)} \left\{ H_{mn}^I (1 - \alpha_k) - H_{mn}^R \beta_k \right\} \quad (1.13)$$

where $1 \leq m \leq N_R$, $\alpha_k = \cos[2(\varpi_0 k + \phi^{(k)})]$ and $\beta_k = \sin[2(\varpi_0 k + \phi^{(k)})]$. For a given value of m , these equations form a linear system that can be solved for the unknown coefficients H_{mn}^R and H_{mn}^I .

1.2.2 Channel matrix characteristics

Measurements were taken in a building constructed with cinder-block partition walls and steel-reinforced concrete structural walls and containing classrooms, laboratories, and several small offices. Data were collected using 1000-bit binary codes at a chip rate of 12.5 kbps, producing one channel matrix estimate every 80 ms (representing the average channel response over the code length). Because channel changes occur on the timescales of relatively slow physical motion (people moving, doors closing, etc.), this sample interval is adequate for the indoor environment under investigation. For all measurements, the SISO SNR is set to 20 dB and, unless explicitly stated, is computed for $K = 1$ in (1.9).

The three different measurement scenarios considered here are listed in the table below. In this list, “Room A” and “Room B” are central labs separated by a hallway (designated as “Hall”), while “Many Rooms” indicates that the receiver was placed at several locations in different rooms. The arrays were all linear with the element type and spacing as indicated in the table, where λ represents the free-space wavelength of the excitation. Multiple 10-second data records (200–700) were taken for each scenario.

Name ($N_R \times N_T$)	Transmitter location	Receiver location	Antenna elements	Spacing
4 × 4-V	Room A	Many rooms	4 vertical monopoles	$\lambda/2$
4 × 4-VH	Hall	Room B	2 dual-polarization patches	$\lambda/2$
10 × 10-V	Many rooms	Many rooms	10 vertical monopoles	$\lambda/4$

For the data collected, the marginal probability density functions (PDF) for the magnitude and phase of the elements of \mathbf{H} can be estimated using the histograms

$$p_{\text{mag}}[x] = \frac{1}{K N_R N_T \Delta x} \text{HIST}_{K, N_R, N_T}(|H_{mn}^{(k)}|, \Delta x) \quad (1.14)$$

$$p_{\text{pha}}[x] = \frac{1}{K N_R N_T \Delta x} \text{HIST}_{K, N_R, N_T}(\angle H_{mn}^{(k)}, \Delta x) \quad (1.15)$$

where $\text{HIST}(f, \Delta x)$ represents a histogram of the function f with bins of size Δx and K is the number of transfer matrix samples. These histograms are computed by treating each combination of matrix sample, transmit antenna, and receive antenna as an observation. Figure 1.3 shows the empirical PDFs for sets 4 × 4-V (subplots (a) and (b)) and 10 × 10-V (subplots (c) and (d)). The fitting curves for magnitude and phase are the Rayleigh PDF with a variance of 0.5 and the uniform distribution on $[-\pi, \pi]$, respectively. The agreement between the analytical and empirical PDFs is excellent.

The timescale of channel variation is an important consideration since this indicates the frequency with which channel estimation (and perhaps channel feedback) must occur to maintain reliable communication. To assess this temporal variability, we can examine the temporal autocorrelation function for each element of the transfer matrix. Assuming the channel matrix elements are zero mean, the average autocorrelation is given as

$$X_\ell = \mathbb{E} \left\{ H_{mn}^{(k)} H_{mn}^{*(k+\ell)} \right\} \quad (1.16)$$

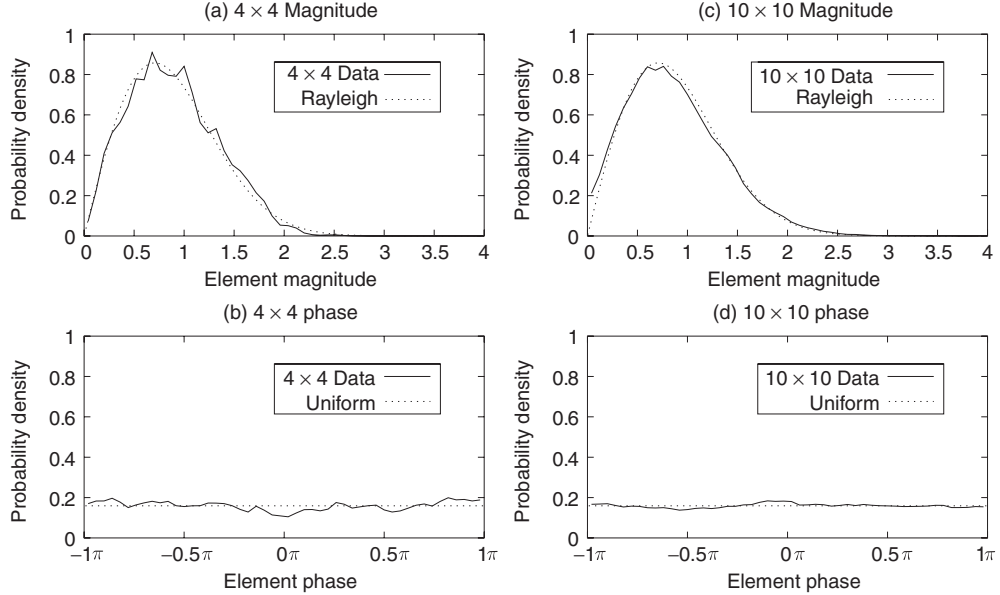


Figure 1.3 Empirical PDFs for the magnitude and phase of the 4×4 \mathbf{H} matrix elements compared with Rayleigh and uniform PDFs, respectively.

where ℓ is a sample shift, $\{\cdot\}^*$ denotes complex conjugate, and the expectation is approximated as a sample mean over all combinations of transmit antenna (n), receive antenna (m), and starting time sample (k). The temporal correlation coefficient is then given by $\rho_\ell = X_\ell / X_0$. Figure 1.4 plots the magnitude of ρ_ℓ over a period of 5 seconds for the two different 4×4 data sets. For all measurements, the correlation remains relatively high, indicating that the channel remains relatively stationary in time. The more dramatic decrease in ρ_ℓ for set 4x4-VH is likely a consequence of the fact that this data was taken during the day when activity was high, while the data for set 4x4-V was taken while activity was low.

The correlation between the signals on the antennas is another important indicator of performance since lower signal correlation tends to produce higher average channel capacity. We assume that the correlation functions at transmit and receive antennas are shift-invariant, and we therefore treat all pairs of antennas with the same spacing as independent observations. This allows us to define the transmit and receive correlation functions

$$R_{T,q} = \frac{1}{N_R N_q} \sum_{n=1}^{N_q} \sum_{m=1}^{N_R} \text{E} \left\{ H_{mn} H_{m,n+q}^* \right\} \quad (1.17)$$

$$R_{R,p} = \frac{1}{N_T N_p} \sum_{n=1}^{N_T} \sum_{m=1}^{N_p} \text{E} \left\{ H_{mn} H_{m+p,n}^* \right\}. \quad (1.18)$$

where N_q (N_p) represents the number of unique pairs of transmit (receive) antennas separated by the distance $q \Delta z$ ($p \Delta z$), where Δz represents the antenna element spacing. For the

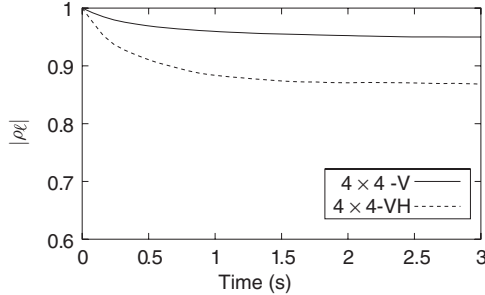


Figure 1.4 Temporal correlation coefficient over a 5-second interval for the two 4×4 data sets.

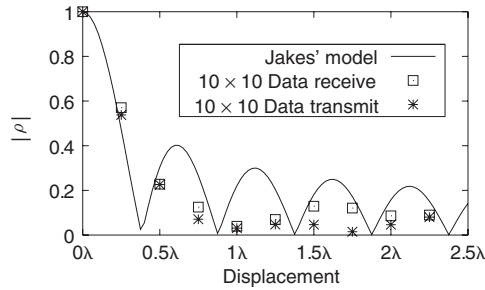


Figure 1.5 Magnitude of the shift-invariant transmit and receive spatial correlation coefficients compared with Jakes' model.

measured data, the expectation is replaced by an average over all time samples. The transmit and receive correlation coefficients are then constructed using $\rho_{T,q} = R_{T,q}/R_{T,0}$ and $\rho_{R,p} = R_{R,p}/R_{R,0}$, respectively. Figure 1.5 shows the shift-invariant spatial transmit and receive correlation coefficient computed from the 10×10 data versus antenna separation $p\Delta z$ and $q\Delta z$. For comparison, results obtained from Jakes' model [18], where an assumed uniform distribution on multipath arrival angles leads to $R_{R,s} = R_{T,s} = J_0(2\pi s\Delta z/\lambda)$ with $J_0(\cdot)$ the Bessel function of order zero, are also included. These results show that for antenna spacings where measurements were performed, Jakes' model predicts the trends observed in the data.

Finally, we examine the channel capacities associated with the measured channel matrices. Capacities are computed using the water-filling solution [19], which provides the upper bound on data throughput across the channel under the condition that the transmitter is aware of the channel matrix \mathbf{H} . For this study, we consider transmit and receive arrays each confined to a 2.25λ aperture and consisting of 2, 4, and 10 equally spaced monopoles. Figure 1.6 shows the complementary cumulative distribution functions (CCDF) of capacity for these scenarios. Also, Monte Carlo simulations were performed to obtain capacity CCDFs for channel matrices whose elements are independent, identically distributed (i.i.d.)

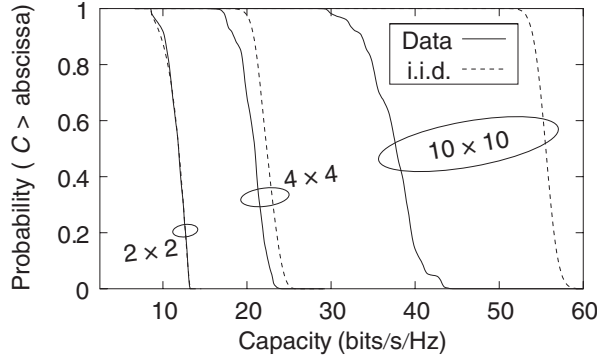


Figure 1.6 Complementary cumulative distribution functions of capacity for transmit/receive arrays of increasing number of elements. The array length is 2.25λ for all cases.

zero-mean complex Gaussian random variables, as outlined in Section 1.3.1. The agreement between the measured and modeled 2×2 channels is excellent because of the very wide separation of the antennas (2.25λ). However, as the array size increases, the simulated capacity continues to grow while the measured capacity *per antenna* decreases because of higher correlation between adjacent elements.

The capacity results of Figure 1.6 neglect differences in received SNR among the different channel measurements since each channel matrix realization is independently normalized to achieve the 20 dB average SISO SNR. To examine the impact of this effect more closely, the 10×10 linear arrays of monopoles with $\lambda/4$ element separation were deployed in a number of different locations. Figure 1.7 shows the different locations, where each arrow points from transmit to receive location. The top number in the circle on each arrow represents the capacity obtained when the measured channel matrix is independently normalized to achieve 20 dB SISO SNR ($K = 1$ in (1.9)). The second number (in italics) represents the capacity obtained when the normalization is applied over *all* \mathbf{H} matrices considered in the study. Often, when the separation between transmit and receive is large ($E \rightarrow C$, for example), the capacity degradation observed when propagation loss is included is significant. In other cases (such as $G \rightarrow D$), the capacity computed with propagation loss included actually increases because of the high SNR resulting from the small separation between transmit and receive.

1.2.3 Multipath estimation

Another philosophy regarding MIMO channel characterization is to directly describe the properties of the physical multipath propagation channel, independent of the measurement antennas. Most such system-independent representations use the double-directional channel concept [20, 21] in which the AOD, AOA, TOA, and complex gain of each multipath component are specified. Once this information is known, the performance of arbitrary antennas and array configurations placed in the propagation channel may be analyzed by creating a channel transfer function from the measured channel response as in (1.4).

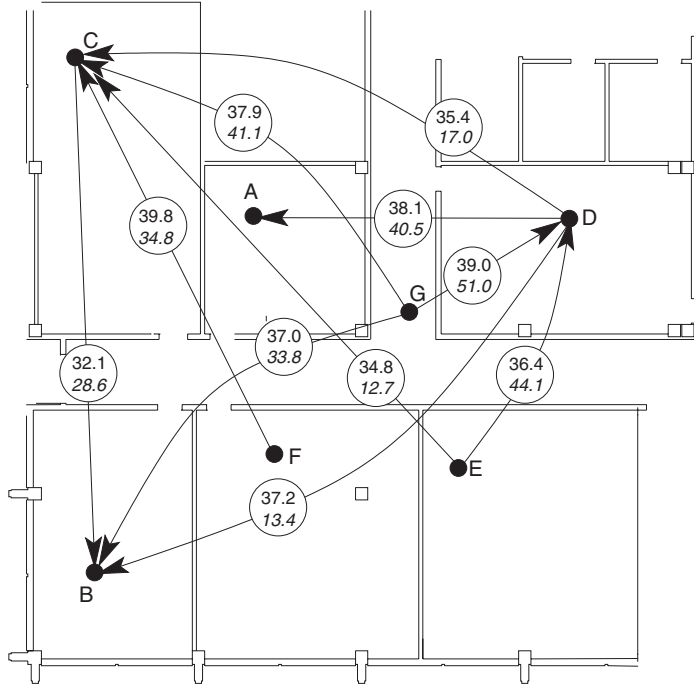


Figure 1.7 Study showing the impact of including the effects of propagation loss in computing the capacity. Arrows are drawn from transmit to receive positions. The top and bottom number in each circle give capacity without and with propagation loss, respectively.

Conceptually, the simplest method for measuring the physical channel response is to use two steerable (manually or electronically) high-gain antennas. For each fixed position of the transmit beam, the receive beam is rotated through 360° , thus mapping out the physical channel response as a function of azimuth angle at the transmit and receive antenna locations [22, 23]. Typically, broad probing bandwidths are used to allow resolution of the multipath plane waves in time as well as angle. The resolution of this system is proportional to the antenna aperture (for directional estimation) and the bandwidth (for delay estimation). Unfortunately, because of the long time required to rotate the antennas, the use of such a measurement arrangement is limited to channels that are highly stationary.

To avoid the difficulties with steered-antenna systems, it is more common and convenient to use the same measurement architecture as is used to directly measure the channel transfer matrix (Figure 1.2). However, attempting to extract more detailed information about the propagation environment requires a much higher level of postprocessing. Assuming far-field scattering, we begin with relationship (1.4), where the radiation patterns for the antennas are known. Our goal is then to estimate the number of arrivals L , the directions of departure ($\theta_{T,\ell}, \phi_{T,\ell}$) and arrival ($\theta_{R,\ell}, \phi_{R,\ell}$), and times of arrival τ_ℓ . Theoretically, this information could be obtained by applying an optimal ML estimator. However, since many practical scenarios will have tens to hundreds of multipath components, this method quickly becomes computationally intractable.

On the other hand, subspace parametric estimators like ESPRIT provide an efficient method of obtaining the multipath parameters without the need for computationally expensive search algorithms. The resolution of such methods is not limited by the size of the array aperture, as long as the number of antenna elements is larger than the number of multipaths. These estimators usually require knowledge about the number of multipath components, which can be obtained by a simple “Scree” plot or minimum description length criterion [24–26].

While this double-directional channel characterization is very powerful, there are several basic problems inherent to this type of channel estimation. First, the narrowband assumption in the signal space model precludes the direct use of wideband data. Thus, angles and times of arrival must be estimated independently, possibly leading to suboptimal parameter estimation. Second, in their original form, parametric methods such as ESPRIT only estimate directions of arrival and departure separately, and therefore the estimator does not pair these parameters to achieve an optimal fit to the data. This problem can be overcome by either applying alternating conventional beamforming and parametric estimation [20] or by applying advanced joint diagonalization methods [27, 28]. Third, in cases where there is near-field or diffuse scattering [21, 29] the parametric plane-wave model is incorrect, leading to inaccurate estimation results. However, in cases where these problems are not severe, the wealth of information obtained from these estimation procedures gives deep insight into the behavior of MIMO channels and allows development of powerful channel models that accurately capture the physics of the propagation environment.

1.3 MIMO Channel Models

Direct channel measurements provide definitive information regarding the potential performance of MIMO wireless systems. However, owing to the cost and complexity of conducting such measurement campaigns, it is important to have channel models available that accurately capture the key behaviors observed in the experimental data [30–33, 1]. Modeling of SISO and MIMO wireless systems has also been addressed extensively by several working groups as part of European COST Actions (COST-231 [34], COST-259 [21], and COST-273), whose goal is to develop and standardize propagation models.

When accurate, these models facilitate performance assessment of potential space-time coding approaches in realistic propagation environments. There are a variety of different approaches used for modeling the MIMO wireless channel. This section outlines several of the most widely used techniques and discusses their relative complexity and accuracy tradeoffs.

1.3.1 Random matrix models

Perhaps the simplest strategy for modeling the MIMO channel uses the relationship (1.5), where the effects of antennas, the physical channel, and matched filtering have been lumped into a single matrix $\mathbf{H}^{(k)}$. Throughout this section, the superscript (k) will be dropped for simplicity. The simple linear relationship allows for convenient closed-form analysis, at the expense of possibly reduced modeling accuracy. Also, any model developed with this method will likely depend on assumptions made about the specific antenna types and

array configurations, a limitation that is overcome by the more advanced path-based models presented in Section 1.3.3.

The multivariate complex normal distribution

The multivariate complex normal (MCN) distribution has been used extensively in early as well as recent MIMO channel modeling efforts, because of simplicity and compatibility with single-antenna Rayleigh fading. In fact, the measured data in Figure 1.3 shows that the channel matrix elements have magnitude and phase distributions that fit well to Rayleigh and uniform distributions, respectively, indicating that these matrix entries can be treated as complex normal random variables.

From a modeling perspective, the elements of the channel matrix \mathbf{H} are stacked into a vector \mathbf{h} , whose statistics are governed by the MCN distribution. The PDF of an MCN distribution may be defined as

$$f(\mathbf{h}) = \frac{1}{\pi^N \det\{\mathbf{R}\}} \exp[-(\mathbf{h} - \boldsymbol{\mu})^H \mathbf{R}^{-1} (\mathbf{h} - \boldsymbol{\mu})], \quad (1.19)$$

where

$$\mathbf{R} = \mathbb{E} \left\{ (\mathbf{h} - \boldsymbol{\mu})(\mathbf{h} - \boldsymbol{\mu})^H \right\} \quad (1.20)$$

is the (non-singular) covariance matrix of \mathbf{h} , N is the dimensionality of \mathbf{R} , $\boldsymbol{\mu}$ is the mean of \mathbf{h} , and $\det\{\cdot\}$ is a determinant. In the special case where the covariance \mathbf{R} is singular, the distribution is better defined in terms of the characteristic function. This distribution models the case of Rayleigh fading when the mean channel vector $\boldsymbol{\mu}$ is set to zero. If $\boldsymbol{\mu}$ is nonzero, a non-fading or line-of-sight component is included and the resulting channel matrix describes a Rician fading environment.

Covariance matrices and simplifying assumptions

The zero mean MCN distribution is completely characterized by the covariance matrix \mathbf{R} in (1.20). For this discussion, it will be convenient to represent the covariance as a tensor indexed by four (rather than two) indices according to

$$R_{mn,pq} = \mathbb{E} \left\{ H_{mn} H_{pq}^* \right\}. \quad (1.21)$$

This form is equivalent to (1.20), since m and n combine and p and q combine to form row and column indices, respectively, of \mathbf{R} .

While defining the full covariance matrix \mathbf{R} presents no difficulty conceptually, as the number of antennas grows, the number of covariance matrix elements can become prohibitive from a modeling standpoint. Therefore, the simplifying assumptions of *separability* and *shift invariance* can be applied to reduce the number of parameters in the MCN model.

Separability assumes that the full covariance matrix may be written as a product of transmit covariance (\mathbf{R}_T) and receive covariance (\mathbf{R}_R) or

$$R_{mn,pq} = R_{R,mp} R_{T,nq}, \quad (1.22)$$

where \mathbf{R}_T and \mathbf{R}_R are defined in (1.17) and (1.18). When this assumption is valid, the transmit and receive covariance matrices can be computed from the full covariance matrix as

$$R_{T,nq} = \frac{1}{\alpha} \sum_{m=1}^{N_R} R_{mn,mq} \quad (1.23)$$

$$R_{R,mp} = \frac{1}{\beta} \sum_{n=1}^{N_T} R_{mn,pn}, \quad (1.24)$$

where α and β are chosen such that

$$\alpha\beta = \sum_{k_1=1}^{N_R} \sum_{k_2=1}^{N_T} R_{k_1 k_2, k_1 k_2}. \quad (1.25)$$

In the case where \mathbf{R} is a correlation coefficient matrix, we may choose $\alpha = N_R$ and $\beta = N_T$. The separability assumption is commonly known as the *Kronecker model* in recent literature, since we may write

$$\mathbf{R} = \mathbf{R}_T \otimes \mathbf{R}_R, \quad (1.26)$$

$$\mathbf{R}_T = \frac{1}{\alpha} \mathbb{E} \left\{ \mathbf{H}^H \mathbf{H} \right\}^T, \quad (1.27)$$

$$\mathbf{R}_R = \frac{1}{\beta} \mathbb{E} \left\{ \mathbf{H} \mathbf{H}^H \right\}, \quad (1.28)$$

$$\alpha\beta = \text{Tr}(\mathbf{R}) = \mathbb{E} \left\{ \|\mathbf{H}\|_F^2 \right\}, \quad (1.29)$$

where $\{\cdot\}^T$ is a matrix transpose. The separable Kronecker model appeared in early MIMO modeling work [31, 35, 7] and has demonstrated good agreement for systems with relatively few antennas (2 or 3). However, for systems with a large number of antennas, the Kronecker relationship becomes an artificial constraint that leads to modeling inaccuracy [36, 37].

Shift invariance assumes that the covariance matrix is only a function of antenna separation and not absolute antenna location [24]. The relationship between the full covariance and shift-invariant covariance \mathbf{R}^S is

$$R_{mn,pq} = R_{m-p, n-q}^S. \quad (1.30)$$

For example, shift invariance is valid for the case of far-field scattering for linear antenna arrays with identical, uniformly spaced elements.

Computer generation

Computer generation of a zero mean MCN vector for a specified covariance matrix \mathbf{R} is performed by generating a vector \mathbf{a} of i.i.d. complex normal elements with unit variance. The transformation

$$\mathbf{y} = \boldsymbol{\Sigma} \boldsymbol{\Lambda}^{1/2} \mathbf{a} \quad (1.31)$$

produces a new complex normal vector with the proper covariance, where $\boldsymbol{\Sigma}$ and $\boldsymbol{\Lambda}$ are the matrix of eigenvectors and the diagonal matrix of eigenvalues of \mathbf{R} , respectively.

For the case of the Kronecker model, applying this method to construct \mathbf{H} results in

$$\mathbf{H} = \mathbf{R}_R^{1/2} \mathbf{H}_{\text{IID}} \mathbf{R}_T^{1/2 T}, \quad (1.32)$$

where \mathbf{H}_{IID} is an $N_R \times N_T$ matrix of i.i.d. complex normal elements.

Complex and power envelope correlation

The *complex correlation* in (1.20) is the preferred way to specify the covariance of the complex normal channel matrix. However, for cases in which only power information is available, a *power envelope correlation* may be constructed. Let $\mathbf{R}_P = E\{(|\mathbf{h}|^2 - \mu_P)(|\mathbf{h}|^2 - \mu_P)^T\}$, where $\mu_P = E\{|\mathbf{h}|^2\}$, and $|\cdot|^2$ is an element-wise squaring of the magnitude. Interestingly, for a zero-mean MCN distribution with covariance \mathbf{R} , the power correlation matrix is simply $\mathbf{R}_P = |\mathbf{R}|^2$. This can be seen by considering a bivariate complex normal vector $[a_1 \ a_2]^T$ with covariance matrix

$$\mathbf{R} = \begin{bmatrix} R_{11} & R_{R,12} - jR_{I,12} \\ R_{R,12} + jR_{I,12} & R_{22} \end{bmatrix}, \quad (1.33)$$

where all $R_{\{\cdot\}}$ are real scalars, and subscripts R and I correspond to real and imaginary parts, respectively. Letting $u_m = \text{Re}\{a_m\}$ and $v_m = \text{Im}\{a_m\}$, the complex normal distribution may also be represented by the 4-variate real Gaussian vector $[u_1 \ u_2 \ v_1 \ v_2]^T$ with covariance matrix

$$\mathbf{R}' = \frac{1}{2} \left[\begin{array}{cc|cc} R_{11} & R_{R,12} & 0 & R_{I,12} \\ R_{R,12} & R_{22} & -R_{I,12} & 0 \\ \hline 0 & -R_{I,12} & R_{11} & R_{R,12} \\ R_{I,12} & 0 & R_{R,12} & R_{22} \end{array} \right]. \quad (1.34)$$

The power correlation of the m th and n th elements of the complex normal vector is

$$\begin{aligned} R_{P,mn} &= E\{|a_m|^2 |a_n|^2\} - E\{|a_m|^2\} E\{|a_n|^2\} \\ &= E\{(u_m^2 + v_m^2)(u_n^2 + v_n^2)\} - 4 E\{u_m^2\} E\{u_n^2\} \\ &= 4E^2\{u_m u_n\} + 4E^2\{u_m v_n\}, \end{aligned} \quad (1.35)$$

where the structure of (1.34) was used in conjunction with the identity

$$E\{A^2 B^2\} = E\{A^2\} E\{B^2\} + 2E^2\{AB\}. \quad (1.36)$$

This identity is true for real zero-mean Gaussian random variables A and B and is easily derived from tabulated multidimensional normal distribution moment integrals [38]. The magnitude squared of the complex envelope correlation is

$$\begin{aligned} |R_{mn}|^2 &= |E\{u_m u_n\} + E\{v_m v_n\} + j(-E\{u_m v_n\} + E\{v_m u_n\})|^2 \\ &= 4E^2\{u_m u_n\} + 4E^2\{u_m v_n\}, \end{aligned} \quad (1.37)$$

and therefore, $\mathbf{R}_P = |\mathbf{R}|^2$. Thus, for a given power correlation \mathbf{R}_P , we usually have a family of compatible complex envelope correlations. For simplicity, we may let $\mathbf{R} = \sqrt{\mathbf{R}_P}$,

where $\sqrt{\cdot}$ is element-wise square root, to obtain the complex-normal covariance matrix for a specified power correlation. However, care must be taken, since $\sqrt{\mathbf{R}_P}$ is not guaranteed to be positive semi definite. Although this method is convenient, for many scenarios it can lead to very high modeling error since only power correlations are required [39].

Covariance models

Research in the area of random matrix channel modeling has proposed many possible methods for defining the covariance matrix \mathbf{R} . Early MIMO studies assumed an i.i.d. MCN distribution for the channel matrix ($\mathbf{R} = \mathbf{I}$) resulting in high channel capacity [40]. This model is appropriate when the multipath scattering is sufficiently rich and the spacing between antenna elements is large. However, for most realistic scenarios the i.i.d. MCN model is overly optimistic, motivating the search for more detailed specification of the covariance.

Although only approximate, closed-form expressions for covariance are most convenient for analysis. Perhaps the most obvious expression for covariance is that obtained by extending Jakes' model [18] to the multiantenna case as was performed in generating Figure 1.5. Assuming shift invariance and separability of the covariance, we may write

$$R_{mn,pq} = J_0(2\pi \|\mathbf{x}_{R,m} - \mathbf{x}_{R,p}\|) J_0(2\pi \|\mathbf{x}_{T,n} - \mathbf{x}_{T,q}\|), \quad (1.38)$$

where $\mathbf{x}_{P,m}$, $P \in \{T, R\}$ is the vectorial location of the m th transmit or receive antenna in wavelengths and $\|\cdot\|$ is the vector Euclidean norm. Alternatively, let r_T and r_R represent the real transmit and receive correlation, respectively, for signals on antennas that are immediately adjacent to each other. We can then assume the separable correlation function is exponential, or

$$R_{mn,pq} = r_R^{-|m-p|} r_T^{-|n-q|}. \quad (1.39)$$

This model builds on our intuition that correlation should decrease with increasing antenna spacing. Assuming only correlation at the receiver so that

$$R_{mn,pq} = r_R^{-|m-p|} \delta_{nq}, \quad (1.40)$$

where δ_{mp} is the Kronecker delta, bounds for channel capacity may be computed in closed form, leading to the observation that increasing r_R is effectively equivalent to decreasing SNR [41]. The exponential correlation model has also been proposed for urban measurements [5].

Other methods for computing covariance involve the use of the path-based models in Section 1.3.3 and direct measurement. When path-based models assume that the path gains, given by β_ℓ in (1.4), are described by complex normal statistics, the resulting channel matrix is MCN. Even when the statistics of the path gains are not complex normal, the statistics of the channel matrix may tend to the MCN from the central limit theorem if there are enough paths. In either case, the covariance for a specific environment may be computed directly from the known paths and antenna properties. On the other hand, direct measurement provides an exact site-specific snapshot of the covariance [42, 43, 14], assuming that movement during the measurement is sufficiently small to achieve stationary statistics. This approach potentially reduces a large set of channel matrix measurements into a smaller set

of covariance matrices. When the Kronecker assumption holds, the number of parameters may be further reduced.

Modifications have been proposed to extend the simpler models outlined above to account for dual polarization and time-variation. For example, given existing models for single-polarization channels, a new dual-polarized channel matrix can be constructed as [44]

$$\mathbf{H} = \begin{bmatrix} \mathbf{H}_{VV} & \sqrt{X}\mathbf{H}_{VH} \\ \sqrt{X}\mathbf{H}_{HV} & \mathbf{H}_{HH} \end{bmatrix}, \quad (1.41)$$

where the subchannels H_{QP} are single-polarization MIMO channels that describe propagation from polarization P to polarization Q, and X represents the ratio of the power scattered into the orthogonal polarization to the power that remains in the originally transmitted polarization. This very simple model assumes that the various single-polarization subchannels are independent, an assumption that is often true in practical scenarios. The model may also be extended to account for the case where the single-polarization subchannels are correlated [45]. Another example modification includes the effect of time variation in the i.i.d. complex normal model by writing [46]

$$\mathbf{H}^{(r+t)} = \sqrt{\alpha_t} \mathbf{H}^{(r)} + \sqrt{1 - \alpha_t} \mathbf{W}^{(r+t)}, \quad (1.42)$$

where $\mathbf{H}^{(t)}$ is the channel matrix at the t th time step, $\mathbf{W}^{(t)}$ is an i.i.d. MCN-distributed matrix at each time step, and α_t is a real number between 0 and 1 that controls the channel stationarity. For example, for $\alpha_t = 1$, the channel is time-invariant, and for $\alpha_t = 0$, the channel is completely random.

Unconventional random matrix models

Although most random matrix models have focused on the MCN distribution for the elements of the channel matrix, here we highlight two interesting exceptions. In order to describe rank-deficient channels with low transmit/receive correlation (i.e., the *keyhole* or *pinhole* channel [47]), random channel matrices of the form [48]

$$\mathbf{H} = \mathbf{R}_R^{1/2} \mathbf{H}_{\text{IID},1} \mathbf{R}_S^{1/2} \mathbf{H}_{\text{IID},2} \mathbf{R}_T^{1/2 \ T} \quad (1.43)$$

have been proposed, where \mathbf{R}_T and \mathbf{R}_R represent the separable transmit and receive covariances present in the Kronecker model, $\mathbf{H}_{\text{IID},1}$ and $\mathbf{H}_{\text{IID},2}$ are $N_R \times S$ and $S \times N_T$ matrices containing i.i.d. complex normal elements, \mathbf{R}_S is the so-called scatterer correlation matrix, and the dimensionality S corresponds roughly to the number of scatterers. Although heuristic in nature, this model has the advantage of separating local correlation at the transmit and receive and global correlation because of long-range scattering mechanisms, thus allowing adequate modeling of rank-deficient channels.

Another very interesting random matrix modeling approach involves allowing the number of transmit and receive antennas as well as the scatterers to become infinite, while setting finite ratios for transmit to receive antennas and transmit antennas to scatterers [42, 49]. Under certain simplifying assumptions, closed-form expressions may be obtained for the singular values of the channel matrix as the matrix dimension tends to infinity. Therefore, for systems with many antennas, this model provides insight into the overall behavior of the eigenmodes for MIMO systems.

1.3.2 Geometric discrete scattering models

By appealing more directly to the environment propagation physics, we can obtain channel models that provide MIMO performance estimates which closely match measured observations. Typically, this is accomplished by determining the AOD, AOA, TOA (generally used only for frequency selective analyses), and complex channel gain (attenuation and phase shift) of the electromagnetic plane waves linking the transmit and receive antennas. Once these propagation parameters are determined, the transfer matrix can be constructed using (1.4).

Perhaps the simplest models based on this concept place scatterers within the propagation environment, assigning a complex electromagnetic scattering cross-section to each one. The cross-section is generally assigned randomly on the basis of predetermined statistical distributions. The scatterer placement can also be assigned randomly, although often some deterministic structure is used in scatterer placement in an effort to match a specific type of propagation environment or even to represent site-specific obstacles. Simple geometrical optics is then used to track the propagation of the waves through the environment, and the time/space parameters are recorded for each path for use in constructing the transfer matrix. Except in the case of the two-ring model discussed below, it is common to only consider waves that reflect from a single scatterer (single bounce models).

One commonly used discrete scattering model is based on the assumption that scatterers surrounding the transmitter and receiver control the AOD and AOA respectively. Therefore, two circular rings are “drawn” with centers at the transmit and receive locations and whose radii represent the average distance between each communication node and their respective scatterers. The scatterers are then placed randomly on these rings. Comparison with experimental measurements has revealed that when determining the propagation of a wave through this simulated environment, each transmit and receive scatterer participates in the propagation of only one wave (transmit and receive scatterers are randomly paired). The scenario is depicted in Figure 1.8. These *two-ring* models are very simple to generate and provide flexibility in modeling different environments through adaptation of the scattering ring radii and scatterer distributions along the ring. For example, in something like a forested environment the scatterers might be placed according to a uniform distribution in angle around the ring. In contrast, in an indoor environment a few groups of closely spaced scatterers might be used to mimic the “clustered” multipath behavior frequently observed.

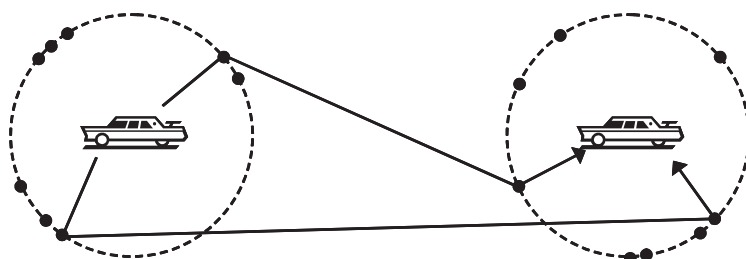


Figure 1.8 Geometry of a typical two-ring discrete scattering model showing some representative scattering paths.

Another practical method for choosing scatterer placement is to draw a set of ellipses with varying focal lengths whose foci correspond to the transmit and receive positions. Scatterers are then placed according to a predetermined scheme on these ellipses, and only single reflections are considered. In this model, all waves bouncing off scatterers located on the same ellipse will have the same propagation time delay, leading to the designation of *constant delay ellipses*. The spacing of the ellipses should be determined according to the arrival time resolution desired from the model, which would typically correspond to the inverse of the frequency bandwidth of the communication signal. With the spacing so determined, the number of rings should be chosen to provide the proper average delay spread associated with the propagation environment of interest.

In addition to their relative simplicity, these models have two interesting features. First, once the scattering environment has been realized using an appropriate mechanism, one or both of the communication nodes can move within the environment to simulate mobility. Second, with certain statistical scatterer distributions, convenient, closed-form statistical distributions can be found for delay spread, angular spread, and spatial correlation [50–52].

1.3.3 Statistical cluster models

Statistical cluster models directly specify distributions on the multipath AOD/AOA, TOA, and complex amplitude. Most current models are based on initial work by Turin, *et al.* [53] who observed that multipath components can be grouped into clusters that decay exponentially with increasing delay time. Intuitively, a single cluster of arrivals might correspond to a single scattering object and the arrivals within the cluster arise because of smaller object features. Later work applied the model to indoor scenarios [54] and added directional information [44, 22, 55, 56]. Statistical descriptions of the multipath arrival parameters can be obtained from measurements or from ray-tracing simulations [57]. Provided that the underlying statistical distributions are properly specified, these models can offer highly accurate channel representations (in a statistical sense). As a result, in this section we will detail one implementation of such a model that extends the well-known Saleh-Valenzuela model of [54] to include AOA/AOD in addition to TOA and multipath amplitude. This model will be referred to as the *Saleh-Valenzuela Model with Angle* or simply *SVA model*.

The SVA model is based on the experimentally observed phenomenon that multipath arrivals appear at the receiver in clusters in both space and time. We will refer to arrivals within a cluster as *rays*, and will restrict our discussion to the horizontal plane for simplicity ($\theta_T = \theta_R = \pi/2$). If we assume we have L clusters with K rays per cluster, then the directional channel impulse response of (1.2) can be written as

$$h_P(\tau, \phi_R, \phi_T) = \frac{1}{\sqrt{LK}} \sum_{\ell=0}^{L-1} \sum_{k=0}^{K-1} \beta_{k\ell} \delta(\tau - T_\ell - \tau_{k\ell}) \\ \times \delta(\phi_T - \Phi_{T,\ell} - \phi_{T,k\ell}) \delta(\phi_R - \Phi_{R,\ell} - \phi_{R,k\ell}) \quad (1.44)$$

where we have removed the time dependence, and the summation now explicitly reveals the concept of clusters (index ℓ) and rays within the cluster (index k). The parameters T_ℓ , $\Phi_{T,\ell}$, and $\Phi_{R,\ell}$ represent the initial arrival time, mean departure angle, and mean arrival angle, respectively, of the ℓ th cluster. Also, in this context, the k th ray arrival time $\tau_{k\ell}$, departure

angle $\phi_{T,k\ell}$, and arrival angle $\phi_{R,k\ell}$ are taken with respect to the mean time/angle values for the ℓ th cluster.

It is conventional to specify the cluster and ray parameters as random variables that obey a predefined statistical distribution. We must first identify the times of arrivals of the multipath components. One common description defines the PDF of the cluster arrival time T_ℓ conditioned on the value of the prior cluster arrival time as

$$p(T_\ell|T_{\ell-1}) = \Lambda_T e^{-\Lambda_T(T_\ell - T_{\ell-1})}, T_\ell > T_{\ell-1}, T_0 > 0 \quad (1.45)$$

where Λ_T is a parameter that controls the cluster arrival rate for the environment of interest. Similarly, the arrival time for the k th ray in the ℓ th cluster obeys the conditional PDF

$$p(\tau_{k\ell}|\tau_{k-1,\ell}) = \lambda_\tau e^{-\lambda_\tau(\tau_{k\ell} - \tau_{k-1,\ell})}, \tau_{k\ell} > \tau_{k-1,\ell}, \tau_{0\ell} > 0 \quad (1.46)$$

where λ_τ controls the ray arrival rate.

With the arrival times defined, we focus on the complex gain $\beta_{k\ell}$. This gain has a magnitude that is Rayleigh distributed, with the expected power (or variance) satisfying

$$\mathbb{E}\left\{|\beta_{k\ell}|^2\right\} = \mathbb{E}\left\{|\beta_{00}|^2\right\} e^{-T_\ell/\Gamma_T} e^{-\tau_{k\ell}/\gamma_\tau}, \quad (1.47)$$

which makes the amplitudes of the clusters as well as the amplitudes of the rays within the clusters decay exponentially with the time constants Γ_T and γ_τ , respectively. The phase of the complex gain is assumed uniformly distributed on $[0, 2\pi]$.

Finally, the angles of departure and arrival must be specified. For indoor and dense urban areas where scattering tends to come from all directions, the cluster departure and arrival angles can be modeled as uniformly distributed random variables on $[0, 2\pi]$. On the basis of measured data taken in [22], a two-sided Laplacian distribution is assumed for the ray AOA/AOD distribution with PDF given by

$$p(\phi_P) = \frac{1}{\sqrt{2}\sigma_{P,\phi}} \exp\left(-\left|\sqrt{2}\phi_P/\sigma_{P,\phi}\right|\right) \quad (1.48)$$

where $P \in \{T, R\}$ and $\sigma_{P,\phi}$ is the standard deviation of angle in radians. Other distributions, such as a simple Gaussian, can also be used to describe this parameter.

When using the model for narrowband implementation (the maximum multipath delay is much shorter than a symbol duration), the system cannot temporally resolve all of the arrivals within each cluster. The rays within a cluster all appear to arrive at the same time, and therefore we can simplify the model by letting the average ray power in each cluster remain constant rather than decaying exponentially. This implies that λ_τ and γ_τ are not important for model implementation. Similarly, we can arbitrarily set $\Lambda_T = 1$, since the narrowband assumption already specifies that the system cannot resolve the clusters temporally, making the absolute value of T_ℓ unimportant. Under this narrowband approximation, we will use the terminology SVA(Γ_T, σ_ϕ) to denote the SVA model with constant average ray power and unit cluster arrival rate and where $\sigma_\phi = \sigma_{R,\phi} = \sigma_{T,\phi}$.

With all of the parameters and distributions of the SVA model specified, a statistical realization of a propagation channel can be generated. The transfer matrix for this channel realization may then be constructed directly by computing (1.4) for the antennas of interest. When statistics of the channel behavior are desired, an ensemble of realizations must be created and a new channel matrix created for each realization. Statistics can then be constructed concerning the transfer matrix (matrix element distributions, spatial

correlation) or concerning the performance of the MIMO system using the transfer matrix (capacity).

Comparison of model and data

In [22], high-resolution AOA measurements were performed on the same floor of the same building the transfer matrix measurements summarized in Section 1.2.2 were taken. Although the AOA measurements were at a higher frequency (≈ 7 GHz), the extracted parameters serve as a logical starting point. The key parameters discovered during that study are $\sigma_\phi = 26^\circ$, $\Gamma_T = 2$, $\Lambda_T = 1$. For simulation, transmit and receive cluster arrival angles are assumed to be uniform on $[0, 2\pi]$ radians. The data below is compared to two measured data sets: (i) the data from a 4×4 system using vertically polarized patch antennas with $\lambda/2$ element separation, and (ii) the data from set 10 \times 10-V discussed in Section 1.2. For the monopole array used in the 10 \times 10 measurements, the radiation pattern of the m th monopole is specified as

$$e_{P,m}(\phi_P) = \exp\{jk_0(x_{P,m} \cos \phi_P + y_{P,m} \sin \phi_P)\}, \quad (1.49)$$

where $P \in \{T, R\}$, $k_0 = 2\pi/\lambda$ is the free-space wavenumber, and $(x_{P,m}, y_{P,m})$ is the location of the m th antenna referenced to the appropriate array coordinate frame. For the patch array used in the 4×4 measurements, the radiation patterns were obtained using an electromagnetic solver. In all model simulations, 10^5 channels are used (100 cluster configurations with 1000 channels each).

Figure 1.9 compares CCDFs of capacity (obtained using the water-filling algorithm) for channel matrices obtained by measurement and by Monte Carlo simulations of the SVA model. The fit between the measured and modeled channels is very good, implying that the SVA model is able to capture the important mechanisms that contribute to the channel capacity. Additional work has shown that the SVA model not only captures the capacity behavior but also accurately models pairwise joint statistics of the channel transfer matrix [44]. These results suggest that from a statistical perspective, models such as the SVA model detailed here can accurately represent physical propagation channels.

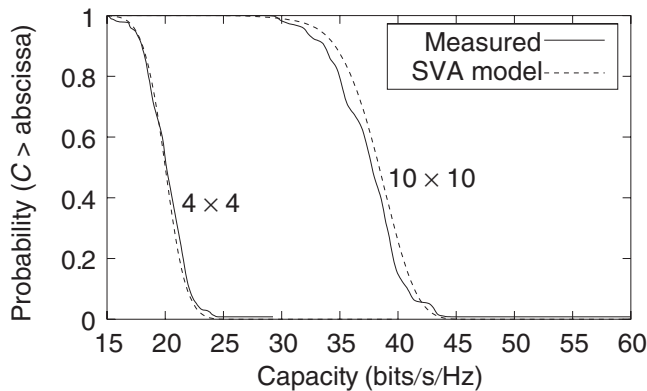


Figure 1.9 Comparison of capacity CCDFs for measured data and SVA model simulations for 4×4 and 10×10 MIMO systems.

Comparison with random matrix models

Figure 1.10 plots capacity CCDFs for channel matrices obtained from the SVA model with parameters $\Gamma_T = 2$, $\sigma_\phi = 26^\circ$, and uniform cluster AOA/AOD. Results for matrices drawn from the MCN with the covariance \mathbf{R} computed directly from the measured data are also shown. Both sets of data use linear arrays of monopoles, with the 4×4 and 8×8 configurations using antenna element spacings of $\lambda/2$ and $\lambda/4$, respectively.

For the 4×4 results, use of the complex correlation provides a somewhat optimistic estimate of the capacity, while the power correlation works surprisingly well, given that this approach neglects phase information in the covariance. However, for the 8×8 channels, the addition of antennas and reduction in antenna spacing amplifies the deficiencies associated with the random matrix models, leading to significant discrepancies in the results produced by both techniques. In particular, neglecting phase information by using the power correlation technique creates significant error in the results.

Other model considerations

A variety of other extensions to statistical path-based models such as the SVA model outlined here are possible. For example, the SVA model as presented above is valid only for a single polarization. For dual polarizations, it has been found that generating a different SVA model realization for each different polarization works effectively [44]. Also, if movement of one of the nodes is to be considered, the path configuration should evolve. This is commonly handled through statistically determining “death” of clusters and “birth” of new ones [57]. Finally, some studies have used cluster models to describe the impact of distant scatterers with discrete scattering models to represent the effect of local scatterers [58, 59].

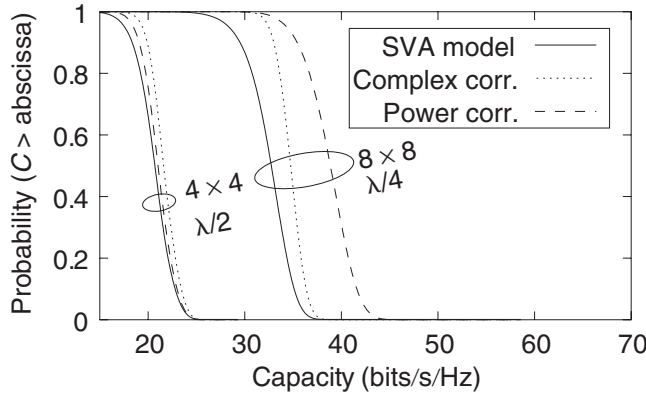


Figure 1.10 Capacity CCDFs for the 4×4 channels with $\lambda/2$ interelement spacing and 8×8 channels with $\lambda/4$ interelement spacing. Results are shown for the SVA model and MCN model with complex and power covariances obtained directly from experimental observations.

1.3.4 Deterministic ray tracing

Deterministic site-specific modeling begins by creating a two- or three-dimensional computer model of a propagation environment. The response of the model to electromagnetic excitation may then be obtained through computational techniques. Such models can also provide statistical channel information by applying Monte Carlo analysis on many random transmit/receive locations and/or model geometries.

Ray tracing [60–64] has emerged as the most popular technique for the analysis of site-specific scenarios, due to its ability to analyze very large structures with reasonable computational resources. The technique is based on geometrical optics, often supplemented by diffraction theory to enhance accuracy in shadowed regions. Recent studies have further combined ray tracing with full-wave electromagnetic solvers to model objects with features that are comparable to the illumination wavelength [65, 66].

Ray-tracing techniques have demonstrated reasonable accuracy in predicting large-scale path loss variation, with error standard deviations of 3–7 dB being reported. However, preliminary comparisons of ray-tracing predictions with measurements indicate that the simulations tend to underestimate MIMO channel capacity [67], likely due more to oversimplification of the geometrical scenario representation than failure of the electromagnetic simulation approach. Other recent work [68] shows promising agreement in AOAs of measured and simulated microcells. In this case, the results can be combined with a random distribution for phase [68–71] to create a complete model. Further work is needed to identify how much model detail is required to correctly represent the channel.

Ray-tracing simulations have been used to study MIMO channel characteristics such as spatial-signature variation with small-scale movement [72], capacity variation with array location and antenna spacing [73, 74], and angular clustering of multipath arrivals [75]. Ray-tracing studies have also led to the development of simpler statistical models such as those described in Section 1.3.3.

1.4 The Impact of Antennas on MIMO Performance

The propagation environment plays a dominant role in determining the capacity of the MIMO channel. However, robust MIMO performance depends also on proper implementation of the antenna system. To see this, consider two receive antennas with vector field patterns $\mathbf{e}_1(\theta, \phi)$ and $\mathbf{e}_2(\theta, \phi)$ and placed at the coordinates $(-d/2, 0, 0)$ and $(d/2, 0, 0)$ in Cartesian space. A set of L plane waves, with the ℓ th plane wave characterized by complex strength E_ℓ , arrival angles (θ_ℓ, ϕ_ℓ) , and electric field polarization $\hat{\mathbf{e}}_\ell$, impinges on the antenna array. The signals received by the two antennas are given as

$$\begin{aligned} s_1 &= \sum_{\ell=1}^L E_\ell [\mathbf{e}_1(\theta_\ell, \phi_\ell) \cdot \hat{\mathbf{e}}_\ell] e^{-j(\pi d/\lambda) \sin \theta_\ell \cos \phi_\ell} \\ s_2 &= \sum_{\ell=1}^L E_\ell [\mathbf{e}_2(\theta_\ell, \phi_\ell) \cdot \hat{\mathbf{e}}_\ell] e^{j(\pi d/\lambda) \sin \theta_\ell \cos \phi_\ell}, \end{aligned} \quad (1.50)$$

where λ is the free-space wavelength. For the MIMO system to work effectively, the signals s_1 and s_2 must be unique, despite the fact that both antennas observe the same set of plane

waves, which can be accomplished when each antenna provides a unique weighting to each of the plane waves. Equation (1.50) reveals that this can occur in three different ways:

1. On the basis of the different antenna element positions, each antenna places a unique phase on each multipath component based on its arrival angles. This is traditional *spatial diversity*.
2. If the radiation patterns $\mathbf{e}_1(\theta, \phi)$ and $\mathbf{e}_2(\theta, \phi)$ are different, then each multipath will be weighted differently by the two antennas. When the antennas share the same polarization but have different magnitude and phase responses in different directions, this is traditional *angle diversity*.
3. If in case 2 the two antennas have different polarizations, the dot product will lead to a unique weighting of each multipath component. This is traditional *polarization diversity*.

It is noteworthy that both angle and polarization diversity are subsets of the more inclusive *pattern diversity*, which simply implies that the two antenna radiation patterns (magnitude, phase, and polarization) differ to create the unique multipath weighting.

Many of the measurement and modeling approaches outlined above, particularly those based on the multipath wave parameters, provide a provision for including these antenna properties into the formulation of the channel matrix. In fact, direct measurement of the channel matrix inherently includes all antenna properties, although the direct channel matrix models typically do not. This section uses some of these appropriate measurement and modeling techniques to demonstrate the performance impact of antenna properties on MIMO system performance. Such a discussion must include the impact of antenna mutual coupling both on the antenna radiation/reception properties and the power collection capabilities of the antenna when interfaced to the RF subsystem. Therefore, an extension of the modeling approaches is presented that accurately accounts for mutual coupling as well as amplifier noise on MIMO system performance.

1.4.1 Spatial diversity

It is important to emphasize that the transfer matrix \mathbf{H} in (1.5) depends not only on the propagation environment but also on the array configurations. The question becomes which array topology is best in terms of maximizing capacity (perhaps in an average sense over a variety of propagation channels) or minimizing symbol error rates. This is difficult to answer definitively, since the optimal array shape depends on the site-specific propagation characteristics. One rule of thumb is to place antennas as far apart as possible to reduce the correlation between the received signals.

There has been one notable study where several different array types were explored for both the base station and the mobile unit in an outdoor environment [76]. The base station antennas included single and dual polarization array and multibeam structures. The arrays on the mobile were constructed from monopoles to achieve spatial, angle, and/or polarization diversity. All of the array configurations provided very similar performance, with the exception of the multibeam base station antennas, which resulted in a 40–50% reduction in measured capacity since generally only one of the beams pointed in the direction

of the mobile. These results suggest that average capacity is relatively insensitive to array configuration provided the signal correlation is adequately low.

1.4.2 Pattern (angle and polarization) diversity

If the radiation patterns of the antenna elements are *orthogonal* when integrated over the range of multipath arrival angles, the goal of having the antenna apply a unique weighting to the incident multipath waves is optimally achieved [77]. For now neglecting the pattern polarization, this can be accomplished with proper element design to achieve the appropriate angular distribution of field strength. For example, one suggested approach for realizing such a situation involves the use of a single multimode antenna where the patterns for different modes exhibit high orthogonality (low correlation) [78]. However, in such a case it is important to use modes that not only provide the high orthogonality required but also all properly direct their energy in angular regions where multipath power is the highest. Failure to do so can reduce the effective received signal power so severely that the benefit gained by pattern orthogonality can be outweighed by the loss in SNR due to poor excitation/reception within the environment of interest [79].

A more common application of pattern diversity is the use of antennas with different polarizations. This is an intriguing concept, since polarization allows pattern orthogonality that can increase communication capacity even when no multipath is present. Therefore, when implementing MIMO systems, use of different polarizations can enable MIMO performance to remain high even when a mobile subscriber moves into a region where the multipath richness is low. However, proper implementation of polarization diversity for MIMO systems requires understanding of the physics involved.

To begin this analysis, consider the case of infinitesimal electric and magnetic current elements (dipoles) radiating into free space. For a three-dimensional coordinate frame, we may orient each of the two current types in the \hat{x} , \hat{y} , and \hat{z} directions. Each of these six possible currents will create a unique vector far-field radiation pattern given by

Current orientation	Pattern: electric current	Pattern: magnetic current
\hat{x}	$\mathbf{e}_1 = -\hat{\theta} \cos \theta \cos \phi + \hat{\phi} \sin \phi$	$\mathbf{e}_4 = \hat{\theta} \sin \phi + \hat{\phi} \cos \theta \cos \phi$
\hat{y}	$\mathbf{e}_2 = -\hat{\theta} \cos \theta \sin \phi - \hat{\phi} \cos \phi$	$\mathbf{e}_5 = -\hat{\theta} \cos \phi + \hat{\phi} \cos \theta \sin \phi$
\hat{z}	$\mathbf{e}_3 = \hat{\theta} \sin \theta$	$\mathbf{e}_6 = -\hat{\phi} \sin \theta$

These results make it very clear that polarization diversity *cannot* be completely independent of angle diversity, since the angular distribution of power is dependent on the orientation (polarization) of the radiating current.

Now, consider all six possible infinitesimal dipoles located at the same point in space and receiving an incident multipath field. Assuming that on average, the power in the multipath field is uniformly distributed in angle over a solid angle sector $\Delta\Omega = (\Delta\theta, \Delta\phi)$ and equally represents both polarizations, we can express the elements of the covariance matrix of the signals received by the six antennas as [80]

$$R_{pq} = \int_{\Delta\Omega} \mathbf{e}_p(\Omega) \cdot \mathbf{e}_q^*(\Omega) d\Omega. \quad (1.51)$$

We then define the eigenvalues of the matrix \mathbf{R} as $\hat{\lambda}_p$, $1 \leq p \leq 6$. If all eigenvalues are equal and nonzero, this implies that six spatial degrees of freedom are created by the antenna

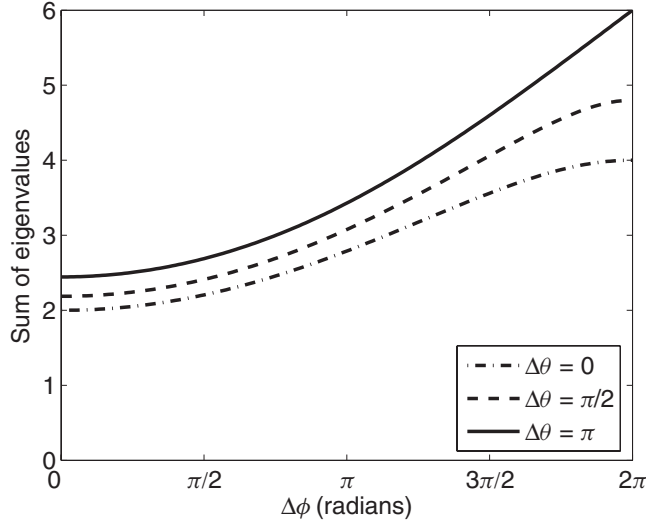


Figure 1.11 Normalized sum of the eigenvalues of the correlation matrix versus incident field angle spread parameters assuming ideal point sensors.

structure. From a MIMO perspective, this would mean the creation of six independent spatial communication channels. To assess this number of communication channels, we will use the parameter

$$\kappa = \frac{1}{\hat{\lambda}_{\max}} \sum_{p=1}^6 \hat{\lambda}_p, \quad (1.52)$$

where $\hat{\lambda}_{\max}$ represents the maximum eigenvalue. The quantity κ can assume values in the range $1 \leq \kappa \leq 6$, and gives some indication of the number of spatial degrees of freedom available in the channel.

Figure 1.11 plots κ versus angular spread parameter $\Delta\phi$ for three different values of $\Delta\theta$. As can be seen, for a single propagation path ($\Delta\theta = \Delta\phi = 0$), only two channels exist corresponding to the two possible polarizations of the incident plane wave. As the angle spread increases, κ increases to a maximum value of six, indicating the availability of six independent communication modes [81]. Because observed elevation spread in indoor and urban environments is relatively small, the curve for $\Delta\theta = 0$ is particularly interesting. Most noteworthy for this case is the fact that if full azimuthal spread is considered, the correlation matrix becomes diagonal, indicating six independent channels. These channels, however, are not all equally “good” since the power received by the \hat{z} oriented sensors is twice as large as the power received by the other sensors [18].

From a practical standpoint, constructing a multipolarized antenna that can achieve the performance suggested in Figure 1.11 is problematic. Using half-wavelength dipoles and full-wavelength loops leads to strong mutual coupling and nonideal pattern characteristics that can reduce the number of independent channels. One interesting geometry is a cube consisting of dipole antennas to obtain a high degree of polarization diversity in a compact

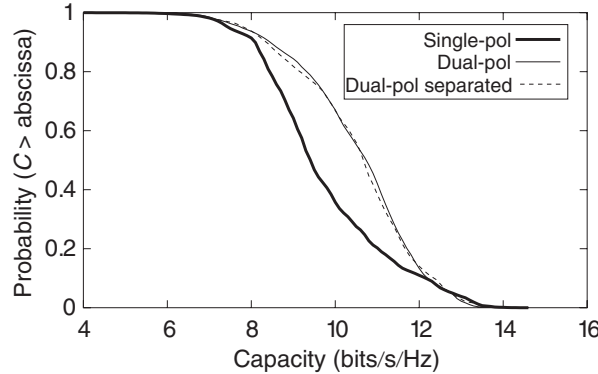


Figure 1.12 CCDFs for 2×2 channels employing different types of polarization/spatial separation with realistic normalization.

form [82]. It is, however, much more common to simply construct antennas with two polarizations and use a combination of polarization and spatial diversity to achieve MIMO capacity. The linear patch arrays employed in the measurements outlined in Section 1.2 consist of four dual-polarization elements separated by a half-wavelength, and therefore allow some assessment of the performance achievable with practical geometries. In this study, four transmit/receive channels (set 4×4 -VH) were used to excite both vertical and horizontal polarizations on two $\lambda/2$ separated patches on each side of the link. By looking at the appropriate submatrices of \mathbf{H} , the capacity can be compared for three different 2×2 subchannels: (i) Two elements with the same polarization (vertical or horizontal) but separated by $\lambda/2$, (ii) Two elements that have orthogonal polarization and are co-located, and (iii) Two elements that have both orthogonal polarization and are separated by $\lambda/2$.

When considering the effect of polarization, it is important to keep in mind that if the vertical polarization is transmitted, the received power in the horizontal polarization will typically be 3–10 dB lower than the power received in the horizontal polarization. A similar statement can be made for transmission of the horizontal polarization. This suggests that entries in the channel matrix corresponding to reception on a different polarization than the transmission will tend to be weaker than those entries corresponding to transmission and reception on the same polarization. When normalizing the channel matrix, therefore, the normalization constant is set to achieve an average SISO SNR of 20 dB for the copolarized matrix elements only. Figure 1.12 depicts the CCDFs resulting from the measured data. As can be seen, using polarization diversity tends to increase capacity over what is possible using spatial separation alone. It is also interesting that combining spatial separation and polarization does not increase the capacity over what is possible with polarization alone for this scenario.

1.4.3 Mutual coupling and receiver network modeling

In many compact devices, the antenna elements must be closely spaced, and the resulting antenna mutual coupling can impact communication performance. Evaluating the effect of

this coupling is often approached by examining how the altered radiation patterns change the signal correlation [77] and using this correlation to derive the system capacity [83–85]. When applying this technique, however, it is important to understand that there are two different physical phenomena that impact these radiation patterns:

1. When an open-circuited (coupled) antenna is placed near an antenna connected to a generator, the electromagnetic boundary conditions are changed, leading to a change in the radiation behavior. However, because the coupled antenna is open-circuited, the impact on the pattern of the driven element is often relatively minor for most practical configurations.
2. The open-circuit voltage V_c induced at the coupled antenna terminals is related to the current I_d in the driven element according to $V_c = Z_m I_d$, where Z_m is the mutual impedance. If the coupled antenna is now terminated with a load, the induced voltage will create a current in the coupled antenna that depends on the termination impedance. Therefore, the effective radiation pattern will be the superposition of the driven element pattern and the coupled element pattern weighted by this induced current. The composite pattern therefore depends on the load attached to the coupled element.

Item 2 makes it clear that ambiguity exists in defining the pattern to use in standard correlation analysis. Furthermore, since the composite pattern is a linear combination of the individual element patterns, compensation for the impact of this effect can theoretically be achieved through proper signal combination after reception, and therefore any analysis conducted in this manner only represents the performance achievable for the specific load configuration used in the computations. In this section, we present an extension to the channel modeling approaches discussed in this chapter that rigorously incorporates the electromagnetic coupling and accurately models the receiver subsystem in terms of impedance characteristics and thermal noise properties.

MIMO network model

Figure 1.13 shows a block diagram of the system model, which includes all major channel components between the coupled transmit antennas and terminated receive amplifiers, used in this analysis. We use scattering parameters (S-parameters) referenced to a real impedance Z_0 [86] to describe the network signal flow wherein the forward and reverse traveling waves are denoted as \mathbf{a} and \mathbf{b} , respectively. The various specific traveling wave vectors, S-parameter matrices (symbol \mathbf{S}), and reflection coefficient matrices (symbol $\mathbf{\Gamma}$) appearing in Figure 1.13 will be identified in the following derivation.

The signal \mathbf{a}_T excites the transmit array consisting of N_T mutually coupled antenna elements characterized by an S-matrix \mathbf{S}_{TT} . The net power flowing into the network is $\|\mathbf{a}_T\|^2 - \|\mathbf{b}_T\|^2$, which, for lossless antennas, equals the instantaneous radiated transmit power P_T^{inst} . Since $\mathbf{b}_T = \mathbf{S}_{TT} \mathbf{a}_T$, we have

$$P_T^{\text{inst}} = \mathbf{a}_T^H \underbrace{(\mathbf{I} - \mathbf{S}_{TT}^H \mathbf{S}_{TT})}_{\mathbf{A}} \mathbf{a}_T. \quad (1.53)$$

For zero mean signals, the average radiated power is given by

$$P_T = \text{E} \left\{ P_T^{\text{inst}} \right\} = \text{Tr}(\mathbf{R}_a \mathbf{A}), \quad (1.54)$$

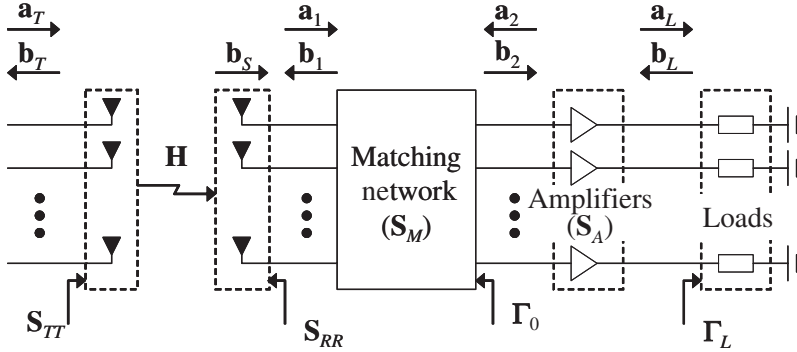


Figure 1.13 Block diagram of the MIMO system of Subsection 1.4.3 including mutually coupled arrays, propagation channel, matching network, receiver amplifiers, and loads.

where $\mathbf{R}_a = \mathbb{E}\{\mathbf{a}_T \mathbf{a}_T^H\}$. We emphasize that in traditional analysis of MIMO systems, the total power is taken as $\text{Tr}(\mathbf{R}_a)$. Eq. (1.54) therefore illustrates one way in which antenna coupling impacts the system analysis.

The radiation pattern for the q th element of the transmit array for a unit driving current and all other elements in the array terminated in an open circuit is denoted as $\mathbf{e}_{T,q}(\theta_T, \phi_T)$, where (θ_T, ϕ_T) represent the angular spherical coordinates referenced to the transmit array origin. The two elements of the column vector represent the $\hat{\theta}$ and $\hat{\phi}$ polarizations. The total transmitted field is then

$$\mathbf{e}_T(\theta_T, \phi_T) = \sum_{q=1}^{N_T} \mathbf{e}_{T,q}(\theta_T, \phi_T) i_{T,q} = \mathbf{E}_T(\theta_T, \phi_T) \mathbf{i}_T, \quad (1.55)$$

where $i_{T,q}$, the q th element of \mathbf{i}_T , is the excitation current on the q th antenna and $\mathbf{e}_{T,q}(\theta_T, \phi_T)$ is the q th column of the $2 \times N_T$ matrix $\mathbf{E}_T(\theta_T, \phi_T)$.

We now represent the radiation pattern of the p th coupled receive element ($1 \leq p \leq N_R$) referenced to the receiver coordinate origin as $\mathbf{e}_{R,p}(\theta_R, \phi_R)$. Using a path-based propagation model, the open circuit voltage on the p th receive element is (see (1.4))

$$v_{R,p} = \underbrace{\sum_{q=1}^{N_T} \sum_{\ell=1}^L \mathbf{e}_{R,p}^T(\theta_R, \phi_R, \ell) \beta_\ell \mathbf{e}_{T,q}(\theta_T, \phi_T, \ell) i_{T,q}}_{2Z_0 H_{P,pq}}, \quad (1.56)$$

where the term $2Z_0$ is isolated for later convenience. The vector of received open-circuit voltages at the antenna terminals is then

$$\mathbf{v}_R = 2Z_0 \mathbf{H}_P \mathbf{i}_T. \quad (1.57)$$

We emphasize that \mathbf{H}_P represents the channel matrix derived from the physical channel impulse response as discussed in several sections of this chapter. The analysis that follows demonstrates how this model can be extended to include other effects present in the electronic subsystems.

The signal \mathbf{b}_S represents the traveling wave delivered by the receive antenna terminals to a set of independent loads of resistance Z_0 (so that $\mathbf{b}_1 = \mathbf{0}$). If a general termination is attached to the array, the composite array output signal is

$$\mathbf{a}_1 = \mathbf{b}_S + \mathbf{S}_{RR}\mathbf{b}_1. \quad (1.58)$$

For an open-circuit termination ($\mathbf{a}_1 = \mathbf{b}_1$), this becomes $\mathbf{b}_S = (\mathbf{I} - \mathbf{S}_{RR})\mathbf{a}_1$. We can also express the voltage at the open-circuit antenna terminals using $\mathbf{v}_R = Z_0^{1/2}(\mathbf{a}_1 + \mathbf{b}_1) = 2Z_0^{1/2}\mathbf{a}_1$. Using these results in (1.57) and recognizing that the transmit current is $\mathbf{i}_T = Z_0^{-1/2}(\mathbf{a}_T - \mathbf{b}_T) = Z_0^{-1/2}(\mathbf{I} - \mathbf{S}_{TT})\mathbf{a}_T$, we obtain

$$\mathbf{b}_S = \underbrace{(\mathbf{I} - \mathbf{S}_{RR}) \mathbf{H}_P (\mathbf{I} - \mathbf{S}_{TT})}_{\mathbf{S}_{RT}} \mathbf{a}_T. \quad (1.59)$$

The multiport matching network is described by the block S-parameter matrix

$$\mathbf{S}_M = \begin{bmatrix} \mathbf{S}_{11} & \mathbf{S}_{12} \\ \mathbf{S}_{21} & \mathbf{S}_{22} \end{bmatrix}, \quad (1.60)$$

where 1 and 2 refer to input and output ports, respectively. With this notation, network analysis shows that the signal \mathbf{b}_2 at the matching network output is

$$\mathbf{b}_2 = \mathbf{S}_{21}(\mathbf{I} - \mathbf{S}_{RR}\mathbf{S}_{11})^{-1}\mathbf{b}_S + \underbrace{\left[\mathbf{S}_{22} + \mathbf{S}_{21}(\mathbf{I} - \mathbf{S}_{RR}\mathbf{S}_{11})^{-1}\mathbf{S}_{RR}\mathbf{S}_{12} \right]}_{\Gamma_0} \mathbf{a}_2 \quad (1.61)$$

where Γ_0 represents the reflection coefficient at the matching network output as shown in Figure 1.13.

The p th noisy amplifier injects forward and reverse traveling noise waves $a_{\eta,p}$ and $b_{\eta,p}$, respectively, at the amplifier input. The amplifier signal-plus-noise output waves are of the form [87]

$$\mathbf{a}_2 = \mathbf{S}_{A,11}\mathbf{b}_2 + \mathbf{S}_{A,12}\mathbf{b}_L - \mathbf{S}_{A,11}\mathbf{a}_{\eta} + \mathbf{b}_{\eta} \quad (1.62)$$

$$\mathbf{a}_L = \mathbf{S}_{A,21}\mathbf{b}_2 + \mathbf{S}_{A,22}\mathbf{b}_L - \mathbf{S}_{A,21}\mathbf{a}_{\eta}, \quad (1.63)$$

where the subscript ‘A’ denotes the S-parameters of the amplifiers. Using additional network analysis with these expressions and (1.61) leads to the vector of voltages across the amplifier terminations (characterized by the reflection coefficient matrix Γ_L) given by

$$\mathbf{v}_L = \mathbf{Q}[\mathbf{G}\mathbf{S}_{RT} \mathbf{a}_T + \Gamma_0 \mathbf{b}_{\eta} - \mathbf{a}_{\eta}]. \quad (1.64)$$

where

$$\mathbf{G} = \mathbf{S}_{21}(\mathbf{I} - \mathbf{S}_{RR}\mathbf{S}_{11})^{-1} \quad (1.65)$$

$$\mathbf{Q} = Z_0^{1/2}(\mathbf{I} + \Gamma_L) \left[(\mathbf{I} - \Gamma_0 \mathbf{S}_{A,11}) \mathbf{S}_{A,21}^{-1} (\mathbf{I} - \mathbf{S}_{A,22} \Gamma_L) - \Gamma_0 \mathbf{S}_{A,12} \Gamma_L \right]^{-1}. \quad (1.66)$$

Matching network specification

Practical amplifier design involves specifying an amplifier performance goal and synthesizing the source and load terminations that achieve this goal. Signal amplifiers are typically designed to provide minimum noise figure, optimal power gain, or some compromise between the two [88]. Our task is to define a desired value of Γ_0 , which is the source termination seen by the amplifier, and use this value to determine the \mathbf{S}_M for the matching network.

If the matching network is constrained to be lossless, the problem of determining \mathbf{S}_M for a given Γ_0 can be solved. Let $\Gamma_0 = \mathbf{U}_0 \Lambda_0^{1/2} \mathbf{V}_0^H$ represent the singular value decomposition (SVD) of Γ_0 , where \mathbf{U}_0 and \mathbf{V}_0 are unitary matrices of singular vectors and $\Lambda_0^{1/2}$ is a diagonal matrix of real singular values. Similarly, let $\mathbf{S}_{RR} = \mathbf{U}_{RR} \Lambda_{RR}^{1/2} \mathbf{V}_{RR}^H$ be the SVD of \mathbf{S}_{RR} . The matrix \mathbf{S}_M can be written using the block matrix product

$$\mathbf{S}_M = \begin{bmatrix} \mathbf{V}_{RR} & \mathbf{0} \\ \mathbf{0} & \mathbf{U}_0 \end{bmatrix} \begin{bmatrix} \Lambda_{11}^{1/2} & j(\mathbf{I} - \Lambda_{11})^{1/2} \\ j(\mathbf{I} - \Lambda_{11})^{1/2} & \Lambda_{11}^{1/2} \end{bmatrix} \begin{bmatrix} \mathbf{U}_{RR} & \mathbf{0} \\ \mathbf{0} & \mathbf{V}_0 \end{bmatrix}^H. \quad (1.67)$$

We assume uncoupled amplifiers ($\mathbf{S}_{A,ij}$ and Γ_L are diagonal), so that typical design goals are achieved for diagonal Γ_0 . If Γ_{opt} and Γ_{MS} represent the (scalar) source reflection coefficient for achieving amplifier minimum noise figure and maximum power gain [88], respectively, then achieving the these goals are accomplished by setting $\Gamma_0 = \Gamma_{opt} \mathbf{I}$ and $\Gamma_0 = \Gamma_{MS} \mathbf{I}$. Since MIMO capacity depends on SNR, we expect a design for minimum noise figure to outperform one for maximum power gain.

To achieve diagonal Γ_0 , the matching network must be coupled to “undo” the coupling created by the antenna, and it therefore acts as an *array combining network* as well as an impedance transforming network. This is an important observation, since the linear combination of the signals in the matching network is performed *before* injection of the noise by the amplifiers. In fact, it has been shown that if the matching network produces diagonal Γ_0 , the capacity of a MIMO system with mutually coupled antennas can be greater than the capacity obtained when uncoupled antennas are assumed. This observation will be reinforced by the example later in this section.

Finally, while optimal matching networks must be coupled, practically speaking it is easier to design an uncoupled network. We assume that the coupled antenna impedance can be represented using only the diagonal elements of the full impedance matrix \mathbf{Z}_{RR} to obtain $\bar{\mathbf{Z}}_{RR}$ and compute a diagonal $\bar{\mathbf{S}}_{RR}$ with elements $\bar{S}_{RR,ii} = (\bar{Z}_{RR,ii} - Z_0)/(\bar{Z}_{RR,ii} + Z_0)$. This value of $\bar{\mathbf{S}}_{RR}$ is then used in place of \mathbf{S}_{RR} in (1.67). However, when analyzing the performance of this *self-impedance* match, the nondiagonal form of \mathbf{S}_{RR} must be used in (1.64).

Coupled system capacity

Computing the capacity for the MIMO signal relationship in (1.64) requires that we formulate the covariance of \mathbf{v}_L assuming the input signal \mathbf{a}_T and noise are drawn from zero-mean complex Gaussian distributions. Using the statistical properties of the noise vectors \mathbf{a}_η and \mathbf{b}_η [87] and assuming that the noise in each amplifier is statistically uncorrelated with that

of all other amplifiers, we can express the covariance as

$$\mathbf{R}_L = \mathbb{E} \left\{ \mathbf{v}_L \mathbf{v}_L^H \right\} = \mathbf{Q} \left[\mathbf{G} \mathbf{S}_{RT} \mathbf{R}_a \mathbf{S}_{RT}^H \mathbf{G}^H + \mathbf{R}_\eta \right] \mathbf{Q}^H \quad (1.68)$$

$$\begin{aligned} \mathbf{R}_\eta &= \mathbb{E} \left\{ (\mathbf{\Gamma}_0 \mathbf{b}_\eta - \mathbf{a}_\eta) (\mathbf{\Gamma}_0 \mathbf{b}_\eta - \mathbf{a}_\eta)^H \right\} \\ &= k_B B \underbrace{\left(T_\alpha \mathbf{I} + T_\beta \mathbf{\Gamma}_0 \mathbf{\Gamma}_0^H - T_\Gamma \mathbf{\Gamma}_0 - T_\Gamma^* \mathbf{\Gamma}_0^H \right)}_{T_\alpha \mathbf{R}_{\eta o}} \end{aligned} \quad (1.69)$$

where k_B is the Boltzmann constant and B is the system noise power bandwidth. The effective noise temperatures (T_α , T_β , $T_\Gamma = T_\gamma e^{j\phi_\gamma}$), which can be determined from the amplifier noise characteristics [87], are assumed identical for all amplifiers.

The capacity for the system in (1.64) can now be determined by finding the covariance \mathbf{R}_a that maximizes the mutual information expression

$$I(\mathbf{v}_L, \mathbf{a}_T) = \log_2 \frac{\det \left\{ \mathbf{G} \mathbf{S}_{RT} \mathbf{R}_a \mathbf{S}_{RT}^H \mathbf{G}^H + \mathbf{R}_\eta \right\}}{\det \left\{ \mathbf{R}_\eta \right\}}. \quad (1.70)$$

Computing the eigenvalue decomposition $\mathbf{R}_{\eta o} = \boldsymbol{\xi}_\eta \boldsymbol{\Lambda}_\eta \boldsymbol{\xi}_\eta^H$ where $\boldsymbol{\xi}_\eta$ is unitary, the mutual information expression becomes

$$I(\mathbf{v}_L, \mathbf{a}_T) = \log_2 \det \left\{ \frac{\mathbf{Y} \mathbf{R}_T \mathbf{Y}^H}{k_B B T_\alpha} + \mathbf{I} \right\}, \quad (1.71)$$

where $\mathbf{Y} = \boldsymbol{\Lambda}_\eta^{-1/2} \boldsymbol{\xi}_\eta^H \mathbf{G} \mathbf{S}_{RT}$. The capacity results when the transmit covariance matrix \mathbf{R}_a is specified according to the water-filling solution, with the total transmit power limited according to $\text{Tr}(\mathbf{R}_a \mathbf{A}) \leq P_T$ as derived in (1.54). Because this power constraint is a departure from the typical constraint $\text{Tr}(\mathbf{R}_a) \leq P_T$, the water-filling procedure must be modified, as detailed in [89, 90].

Computational example

To demonstrate application of the analysis framework and to illustrate the impact of antenna coupling and amplifier matching on MIMO system capacity, we use a model problem consisting of two half-wave dipoles at transmit and receive. The coupled dipoles, which have a wire radius of 0.01λ , are characterized using the finite-difference time-domain method [91]. We use a bipolar junction transistor that for $Z_0 = 50 \Omega$ has noise and S-parameters

$$\begin{aligned} \mathbf{S}_{11} &= 0.552 \angle 169^\circ & \mathbf{S}_{12} &= 0.049 \angle 23^\circ \\ \mathbf{S}_{21} &= 1.681 \angle 26^\circ & \mathbf{S}_{22} &= 0.839 \angle -67^\circ \\ F_{min} &= 2.5 \text{ dB} & \Gamma_{opt} &= 0.475 \angle 166^\circ \\ R_n &= 3.5 \text{ Ohms}, \end{aligned} \quad (1.72)$$

where F_{min} , Γ_{opt} , and R_n represent the minimum noise figure, optimal source termination for noise figure, and effective noise resistance respectively. These parameters are converted to the effective noise temperatures T_α , T_β , and T_Γ using standard techniques.

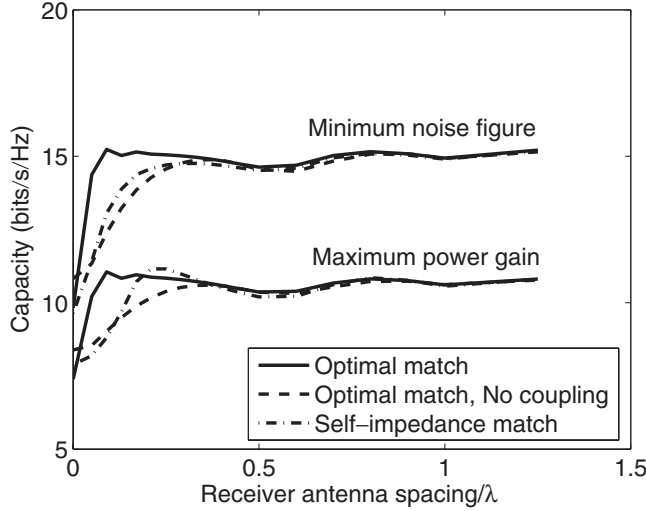


Figure 1.14 Average capacity as a function of receive dipole separation with mutual coupling (optimal and self-impedance match) as well as without mutual coupling. Matching for both minimum noise figure and maximum power gain are considered.

We use 5000 realizations of the SVA model to create a set of transfer matrices \mathbf{H}_P as in (1.56). For each realization, we place single dipoles in the transmit and receive spaces and create a lossless receive matching network with $S_{11} = S_{RR}^*$ so that $\Gamma_0 = 0$ (all terms are scalars). We then can simplify the SISO SNR as

$$\text{SNR} = \frac{|S_{RT}|^2}{1 - |S_{RR}|^2} \frac{P_T}{k_B T_\alpha}. \quad (1.73)$$

This SNR value is then averaged in space by moving each dipole in 0.1λ steps over a linear range of 1.5λ . For a given transmit power, the value of $k_B T_\alpha$ can be computed to achieve an average SISO SNR (20 dB in this work) for the channel realization.

We next construct the matching network to achieve the specified design goal for each transmit/receive dipole spacing, as outlined in Section 1.4.3. For each configuration, we compute the capacity averaged over the 5000 channel matrices with the corresponding noise power levels $k_B T_\alpha$. The transmit array spacing is fixed at 0.5λ for all computations.

Figure 1.14 plots the capacity as a function of receive dipole spacing for matching networks that achieve minimum noise figure and maximum amplifier gain. Results for a coupled match and a simpler self-impedance match as well as for no receiver coupling are included. We first observe that the match achieving minimum amplifier noise figure (noise figure of $F = F_{min} = 2.5$ dB) produces notably higher capacity than the match providing maximum power transfer, which generates a much higher noise figure of $F = 7.2$ dB. This result is intuitive, since ultimately capacity depends on SNR as opposed to absolute signal strength. We also observe that for close antenna spacings with high coupling, the shortcomings of the self-impedance match are evident. However, once the spacing reaches approximately $d = \lambda/4$, this match provides near optimal performance. Finally, Figure 1.14

indicates that for small antenna spacings, coupled dipoles can have a higher capacity than uncoupled ones. This possibility was discussed in Section 1.4.3.

References

- [1] C. Xiao, J. Wu, S.-Y. Leong, Y. R. Zheng, and K. B. Letaief, “A discrete-time model for spatio-temporally correlated MIMO WSSUS multipath channels,” in *Proc. 2003 IEEE Wireless Commun. Network. Conf.*, vol. 1, New Orleans, LA, Mar. 16-20, 2003, pp. 354–358.
- [2] D. P. McNamara, M. A. Beach, P. N. Fletcher, and P. Karlsson, “Capacity variation of indoor multiple–input multiple–output channels,” *Electron. Lett.*, vol. 36, pp. 2037–2038, Nov. 2000.
- [3] J. W. Wallace, M. A. Jensen, A. L. Swindlehurst, and B. D. Jeffs, “Experimental characterization of the MIMO wireless channel: Data acquisition and analysis,” *IEEE Trans. Wireless Commun.*, vol. 2, pp. 335–343, Mar. 2003.
- [4] M. Lienard, P. Degauque, J. Baudet, and D. Degardin, “Investigation on MIMO channels in subway tunnels,” *IEEE J. Sel. Areas Commun.*, vol. 21, pp. 332–339, Apr. 2003.
- [5] D. Chizhik, J. Ling, P. W. Wolniansky, R. A. Valenzuela, N. Costa, and K. Huber, “Multiple–input–multiple–output measurements and modeling in Manhattan,” *IEEE J. Sel. Areas Commun.*, vol. 21, pp. 321–331, Apr. 2003.
- [6] C. C. Martin, J. H. Winters, H. H. Zeng, N. R. Sollenberger, and A. Dixit, “Multiple–input multiple–output (MIMO) radio channel measurements and experimental implementation for EDGE,” in *Conf. Rec. 34th Asilomar Conf. Signals Syst. Comput.*, vol. 1, Pacific Grove, CA, Oct. 29 – Nov. 1, 2000, pp. 738–742.
- [7] K. Yu, M. Bengtsson, B. Ottersten, D. McNamara, P. Karlsson, and M. Beach, “Second order statistics of NLOS indoor MIMO channels based on 5.2 GHz measurements,” in *Proc. 2001 IEEE Glob. Telecomm. Conf.*, vol. 1, San Antonio, TX, Nov. 25-29, 2001, pp. 156–160.
- [8] J. Medbo and J.-E. Berg, “Simple and accurate path loss modeling at 5 GHz in indoor environments with corridors,” in *Proc. 2000 IEEE 52nd Veh. Technol. Conf.*, vol. 1, Boston, MA, Sep. 24-28, 2000, pp. 30–36.
- [9] V. Erceg, P. Soma, D. S. Baum, and A. J. Paulraj, “Capacity obtained from multiple–input multiple – output channel measurements in fixed wireless environments at 2.5 GHz,” in *Proc. 2002 IEEE Intl. Conf. Commun.*, vol. 1, New York, Apr. 28- May 2, 2002, pp. 396–400.
- [10] M. D. Batariere, T. K. Blankenship, J. F. Kepler, T. P. Krauss, I. Lisica, S. Mukthavaram, J. W. Porter, T. A. Thomas, and F. W. Vook, “Wideband MIMO mobile impulse response measurements at 3.7 GHz,” in *Proc. 2002 IEEE 55th Veh. Technol. Conf.*, vol. 1, Birmingham, AL, May 6-9, 2002, pp. 26–30.
- [11] J. P. Kermoal, L. Schumacher, P. E. Mogensen, and K. I. Pedersen, “Experimental investigation of correlation properties of MIMO radio channels for indoor picocell scenarios,” in *Proc. 2000 IEEE 52nd Veh. Technol. Conf.*, vol. 1, Boston, MA, Sep. 24-28, 2000, pp. 14–21.
- [12] A. F. Molisch, M. Steinbauer, M. Toeltsch, E. Bonek, and R. S. Thoma, “Measurement of the capacity of MIMO systems in frequency-selective channels,” in *Proc. 2001 IEEE 53rd Veh. Technol. Conf.*, vol. 1, Rhodes, Greece, May 6-9, 2001, pp. 204–208.
- [13] A. F. Molisch, M. Steinbauer, M. Toeltsch, E. Bonek, and R. S. Thoma, “Capacity of MIMO systems based on measured wireless channels,” *IEEE J. Sel. Areas Commun.*, vol. 20, pp. 561–569, Apr. 2002.
- [14] M. Herdin, H. Özcelik, H. Hofstetter, and E. Bonek, “Variation of measured indoor MIMO capacity with receive direction and position at 5.2 GHz,” *Electron. Lett.*, vol. 38, pp. 1283–1285, Oct. 10, 2002.

- [15] J. Medbo and J.-E. Berg, "Spatio-temporal channel characteristics at 5 GHz in a typical office environment," in *Proc. 2001 IEEE 54th Veh. Technol. Conf.*, vol. 3, Atlantic City, NJ, Oct. 7-11, 2001, pp. 1256–1260.
- [16] D. Kim, M. A. Ingram, and W. W. Smith, "Small-scale fading for an indoor wireless channel with modulated backscatter," in *Proc. 2001 IEEE 54th Veh. Technol. Conf.*, Atlantic City, NJ, Oct. 7-11, 2001, pp. 1616–1620.
- [17] T. Hellesteth and P. V. Kumar, "Pseudonoise sequences," in *The Mobile Communications Handbook*, J. D. Gibson, Ed. CRC Press, 1999, ch. 8.
- [18] W. C. Jakes, *Microwave Mobile Communications*. IEEE Press, 1993.
- [19] G. G. Raleigh and J. M. Cioffi, "Spatio-temporal coding for wireless communication," *IEEE Trans. Commun.*, vol. 46, pp. 357–366, Mar. 1998.
- [20] M. Steinbauer, A. F. Molisch, and E. Bonek, "The double-directional radio channel," *IEEE Antennas Propag. Mag.*, vol. 43, pp. 51–63, Aug. 2001.
- [21] L. M. Correia, *Wireless Flexible Personalised Communications*. John Wiley & Sons, 2001.
- [22] Q. H. Spencer, B. D. Jeffs, M. A. Jensen, and A. L. Swindlehurst, "Modeling the statistical time and angle of arrival characteristics of an indoor multipath channel," *IEEE J. Sel. Areas Commun.*, vol. 18, pp. 347–360, Mar. 2000.
- [23] B. D. Jeffs, E. Pyper, and B. Hunter, "A wireless MIMO channel probing approach for arbitrary antenna arrays," in *Proc. 2001 IEEE Intl. Conf. Acoust. Speech Signal Process.*, vol. 4, Salt Lake City, UT, May 7-11, 2001, pp. 2493–2496.
- [24] R. Roy and T. Kailath, "ESPRIT – estimation of signal parameters via rotational invariance techniques," *IEEE Trans. Acoust. Speech Signal Process.*, vol. 37, pp. 984–995, Jul. 1989.
- [25] J. Fuhl, J.-P. Rossi, and E. Bonek, "Highresolution 3-D direction-of-arrival determination for urban mobile radio," *IEEE Trans. Antennas Propag.*, vol. 45, pp. 672–682, Apr. 1997.
- [26] H. Krim and M. Viberg, "Two decades of array signal processing research: The parametric approach," *IEEE Signal Process. Mag.*, vol. 13, pp. 67–94, Jul. 1996.
- [27] M. Haardt and J. A. Nossek, "Simultaneous Schur decomposition of several nonsymmetric matrices to achieve automatic pairing in multidimensional harmonic retrieval problems," *IEEE Trans. Signal Process.*, vol. 46, pp. 161–169, Jan. 1998.
- [28] A.-J. van der Veen and A. Paulraj, "An analytical constant modulus algorithm," *IEEE Trans. Signal Process.*, vol. 44, pp. 1136–1155, May 1996.
- [29] I. De Coster, E. Van Lil, B. G. Loureiro, P. Delmotte, and A. Van de Capelle, "Validation measurements for the Fresnel approximation of the PO model," in *Proc. 28th. Eur. Microw. Conf.*, vol. 1, Amsterdam, The Netherlands, Oct. 5-9, 1998, pp. 463–468.
- [30] R. B. Ertel, P. Cardieri, K. W. Sowerby, T. S. Rappaport, and J. H. Reed, "Overview of spatial channel models for antenna array communication systems," *IEEE Pers. Commun.*, vol. 5, pp. 10–22, Feb. 1998.
- [31] K. I. Pedersen, J. B. Andersen, J. P. Kermoal, and P. Mogensen, "A stochastic multiple-input-multiple-output radio channel model for evaluation of space-time coding algorithms," in *Proc. 2000 IEEE 52nd Veh. Technol. Conf.*, vol. 2, Boston, MA, Sep. 24-28, 2000, pp. 893–897.
- [32] A. M. Sayeed, "Modeling and capacity of realistic spatial MIMO channels," in *Proc. 2001 IEEE Intl. Conf. Acoust. Speech Signal Process.*, vol. 4, Salt Lake City, UT, May 7-11, 2001, pp. 2489–2492.
- [33] D. Gesbert, H. Bölskei, D. A. Gore, and A. J. Paulraj, "Outdoor MIMO wireless channels: Models and performance prediction," *IEEE Trans. Commun.*, vol. 50, pp. 1926–1934, Dec. 2002.
- [34] D. J. Cichon and T. Kurner, "Propagation prediction models," in *COST 231 Final Rep.*, 1995, available online at <http://www.lx.it.pt/cost231/>.

- [35] J. W. Wallace and M. A. Jensen, "Characteristics of measured 4x4 and 10x10 MIMO wireless channel data at 2.4-GHz," in *Proc. 2001 IEEE Antennas Propag. Soc. Intl. Symp.*, vol. 3, Boston, MA, Jul. 8-13, 2001, pp. 96–99.
- [36] H. Özcelik, M. Herdin, W. Weichselberger, J. Wallace, and E. Bonek, "Deficiencies of 'Kronecker' MIMO radio channel model," *Electron. Lett.*, vol. 39, pp. 1209–1210, Aug. 7, 2003.
- [37] T. Svantesson and J. W. Wallace, "Tests for assessing multivariate normality and the covariance structure of MIMO data," in *Proc. 2003 IEEE Intl. Conf. Acoust. Speech Signal Process.*, vol. 4, Hong Kong, Apr. 6-10, 2003, pp. 656–659.
- [38] D. Zwillinger, Ed., *Standard Mathematical 's and Formulae*, 30th ed. CRC Press, 1996.
- [39] J. Wallace, H. Özcelik, M. Herdin, E. Bonek, and M. Jensen, "Power and complex envelope correlation for modeling measured indoor MIMO channels: A beamforming evaluation," in *Proc. 2003 IEEE 58th Veh. Technol. Conf.*, vol. 1, Orlando, FL, Oct. 6-9, 2003, pp. 363–367.
- [40] G. J. Foschini and M. J. Gans, "On limits of wireless communications in a fading environment when using multiple antennas," *Wireless Pers. Commun.*, vol. 6, pp. 311–335, Mar. 1998.
- [41] S. Loyka and A. Kouki, "The impact of correlation on multi-antenna system performance: Correlation matrix approach," in *Proc. 2001 IEEE 54th Veh. Technol. Conf.*, vol. 2, Atlantic City, NJ, Oct. 7-11, 2001, pp. 533–537.
- [42] K. Yu, M. Bengtsson, B. Ottersten, D. McNamara, P. Karlsson, and M. Beach, "A wideband statistical model for NLOS indoor MIMO channels," in *Proc. 2002 IEEE 55th Veh. Technol. Conf.*, vol. 1, Birmingham, AL, May 6-9, 2002, pp. 370–374.
- [43] J. P. Kermoal, L. Schumacher, K. I. Pedersen, P. E. Mogensen, and F. Frederiksen, "A stochastic MIMO radio channel model with experimental validation," *IEEE J. Sel. Areas Commun.*, vol. 20, pp. 1211–1226, Aug. 2002.
- [44] J. W. Wallace and M. A. Jensen, "Modeling the indoor MIMO wireless channel," *IEEE Trans. Antennas Propag.*, vol. 50, pp. 591–599, May 2002.
- [45] J. Kermoal, L. Schumacher, F. Frederiksen, and P. Mogensen, "Polarization diversity in MIMO radio channels: Experimental validation of a stochastic model and performance assessment," in *Proc. 2001 IEEE 54th Veh. Technol. Conf.*, vol. 1, Atlantic City, NJ, Oct. 7-11, 2001, pp. 22–26.
- [46] C. B. Peel and A. L. Swindlehurst, "Effective SNR for space-time modulation over a time-varying Rician channel," *IEEE Trans. Commun.*, vol. 52, pp. 17–23, Jan. 2004.
- [47] D. Chizhik, G. J. Foschini, M. J. Gans, and R. A. Valenzuela, "Keyholes, correlations, and capacities of multielement transmit and receive antennas," *IEEE Trans. Wireless Commun.*, vol. 2, pp. 361–368, Apr. 2002.
- [48] D. Gesbert, H. Bölcskei, D. A. Gore, and A. J. Paulraj, "Performance evaluation for scattering MIMO channel models," in *Conf. Rec. 34th Asilomar Conf. Signals Syst. Comput.*, vol. 1, Pacific Grove, CA, Oct. 29 - Nov. 1, 2000, pp. 738–742.
- [49] D. W. Bliss, K. W. Forsythe, and A. F. Yegulalp, "MIMO communication capacity using infinite dimension random matrix eigenvalue distributions," in *Conf. Rec. 35th Asilomar Conf. Signals Syst. Comput.*, vol. 2, Pacific Grove, CA, Nov. 4-7, 2001, pp. 969–974.
- [50] R. B. Ertel and J. H. Reed, "Angle and time of arrival statistics for circular and elliptical scattering models," *IEEE J. Sel. Areas Commun.*, vol. 17, pp. 1829–1840, Nov. 1999.
- [51] A. Abdi and M. Kaveh, "A space-time correlation model for multielement antenna systems in mobile fading channels," *IEEE J. Sel. Areas Commun.*, vol. 20, pp. 550–560, Apr. 2002.
- [52] O. Nørklit and J. B. Andersen, "Diffuse channel model and experimental results for array antennas in mobile environments," *IEEE Trans. Antennas Propag.*, vol. 46, pp. 834–840, Jun. 1998.
- [53] G. L. Turin, F. D. Clapp, T. L. Johnston, B. F. Stephen, and D. Lavry, "A statistical model of urban multipath propagation," *IEEE Trans. Veh. Technol.*, vol. VT-21, pp. 1–9, Feb. 1972.

- [54] A. A. M. Saleh and R. A. Valenzuela, "A statistical model for indoor multipath propagation," *IEEE J. Sel. Areas Commun.*, vol. SAC-5, pp. 128–137, Feb. 1987.
- [55] A. F. Molisch, "A generic model for MIMO wireless propagation channels," in *Proc. 2002 IEEE Intl. Conf. Commun.*, vol. 1, New York, Apr. 28 - May 2, 2002, pp. 277–282.
- [56] C.-C. Chong, C.-M. Tan, D. I. Laurenson, S. McLaughlin, M. A. Beach, and A. R. Nix, "A new statistical wideband spatio-temporal channel model for 5-GHz band WLAN systems," *IEEE J. Sel. Areas Commun.*, vol. 21, pp. 139–150, Feb. 2003.
- [57] T. Zwick, C. Fischer, D. Didascalou, and W. Wiesbeck, "A stochastic spatial channel model based on wave-propagation modeling," *IEEE J. Sel. Areas Commun.*, vol. 18, pp. 6–15, Jan. 2000.
- [58] J. Fuhl, A. F. Molisch, and E. Bonek, "Unified channel model for mobile radio systems with smart antennas," *IEE Proc. Radar Sonar Navigation*, vol. 145, pp. 32–41, Feb. 1998.
- [59] M. Stege, J. Jelitto, M. Bronzel, and G. Fettweis, "A multiple input-multiple output channel model for simulation of Tx- and Rx-diversity wireless systems," in *Proc. 2000 IEEE 52nd Veh. Technol. Conf.*, vol. 2, Boston, MA, Sep. 24-28, 2000, pp. 833–839.
- [60] T. Kurner, D. J. Cichon, and W. Wiesbeck, "Concepts and results for 3D digital terrain-based wave propagation models: An overview," *IEEE J. Sel. Areas Commun.*, vol. 11, pp. 1002–1012, Sep. 1993.
- [61] H. L. Bertoni, W. Honcharenko, L. R. Macel, and H. H. Xia, "UHF propagation prediction for wireless personal communications," *Proc. IEEE*, vol. 82, pp. 1333–1359, Sep. 1994.
- [62] S. Y. Seidel and T. S. Rappaport, "Site-specific propagation prediction for wireless in-building personal communication system design," *IEEE Trans. Veh. Technol.*, vol. 43, pp. 879–891, Nov. 1994.
- [63] G. E. Athanasiadou, A. R. Nix, and J. P. McGeehan, "A microcellular ray-tracing propagation model and evaluation of its narrow-band and wide-band predictions," *IEEE J. Sel. Areas Commun.*, vol. 18, pp. 322–335, Mar. 2000.
- [64] M. F. Iskander and Z. Yun, "Propagation prediction models for wireless communication systems," *IEEE Trans. Microw. Theory Tech.*, vol. 50, pp. 662–673, Mar 2002.
- [65] Y. Wang, S. Safavi-Naeini, and S. K. Chaudhuri, "A hybrid technique based on combining ray tracing and FDTD methods for site-specific modeling of indoor radio wave propagation," *IEEE Trans. Antennas Propag.*, vol. 48, pp. 743–754, May 2000.
- [66] Z. Zhang, R. Sorensen, Z. Yun, M. F. Iskander, and J. F. Harvey, "A ray-tracing approach for indoor/outdoor propagation through window structures," *IEEE Trans. Antennas Propag.*, vol. 50, pp. 742–748, May 2002.
- [67] A. L. Swindlehurst, G. German, J. Wallace, and M. Jensen, "Experimental measurements of capacity for MIMO indoor wireless channels," in *IEEE Third Workshop Signal Process. Adv. Wireless Commun. 2001. (SPAWC '01)*, Taoyuan, Taiwan, R.O.C. Mar. 2001, pp. 30–33.
- [68] H. Zhu, J. Takada, and T. Kobayashi, "The verification of a deterministic spatio-temporal channel modeling approach by applying a deconvolution technique in the measurement," in *Proc. 2001 IEEE 53rd Veh. Technol. Conf.*, vol. 1, Rhodes, Greece, May 6-9, 2001, pp. 362–366.
- [69] A. Muller, "Monte-carlo multipath simulation of ray tracing channel models," in *Proc. 1994 IEEE Global Telecomm. Conf.*, vol. 3, San Francisco, CA, Nov. 11 - Dec. 2, 1994, pp. 1446–1450.
- [70] R. A. Valenzuela, "Ray tracing prediction of indoor radio propagation," in *Proc. 1994 IEEE 5th Intl. Symp. Pers. Indoor Mobile Radio Commun.*, vol. 1, The Hague, The Netherlands, Sep. 18-23, 1994, pp. 140–144.
- [71] P. Marques, J. Fernandes, and J. Neves, "Complex impulse response modeling for wideband channels," in *Proc. 1998 IEEE Spring Veh. Technol. Conf.*, vol. 2, Ottawa, Ontario, Canada, May 18-21, 1998, pp. 702–706.

- [72] K. R. Dandekar, A. Arredondo, G. Xu, and H. Ling, "Using ray tracing to study urban vector channel propagation characteristics," in *Proc. 1999 IEEE Spring Veh. Technol. Conf.*, vol. 1, Houston, TX, May 16-20, 1999, pp. 381–385.
- [73] C.-N. Chuah, D. N. C. Tse, J. M. Kahn, and R. A. Valenzuela, "Capacity scaling in MIMO wireless systems under correlated fading," *IEEE Trans. Inf. Theory*, vol. 48, pp. 637–650, Mar. 2002.
- [74] F. Tila, P. R. Shepherd, and S. R. Pennock, "Theoretical capacity evaluation of indoor micro- and macro-MIMO systems at 5 GHz using site specific ray tracing," *Electron. Lett.*, vol. 39, pp. 471–472, Mar. 6 2003.
- [75] J.-H. Jo, M. A. Ingram, and N. Jayant, "Angle clustering in indoor space-time channels based on ray tracing," in *Proc. 2001 IEEE 54th Veh. Technol. Conf.*, vol. 4, Atlantic City, NJ, Oct. 7-11, 2001, pp. 2067–2071.
- [76] C. Martin, J. Winters, and N. Sollenberger, "MIMO radio channel measurements: Performance comparison of antenna configurations," in *Proc. 2001 IEEE 54th Veh. Technol. Conf.*, vol. 2, Atlantic City, NJ, Oct. 7-11, 2001, pp. 1225–1229.
- [77] R. G. Vaughan and J. B. Andersen, "Antenna diversity in mobile communications," *IEEE Trans. Veh. Technol.*, vol. VT-36, pp. 147–172, Nov. 1987.
- [78] T. Svantesson, "Correlation and channel capacity of MIMO systems employing multimode antennas," *IEEE Trans. Veh. Technol.*, vol. 51, pp. 1304–1312, Nov. 2002.
- [79] C. Waldschmidt, T. Fugen, and W. Wiesbeck, "Spiral and dipole antennas for indoor MIMO-systems," *IEEE Antennas Wireless Propag. Lett.*, vol. 1, no. 1, pp. 176–178, 2002.
- [80] T. Svantesson, M. A. Jensen, and J. W. Wallace, "Analysis of electromagnetic field polarizations in multi-antenna systems," *IEEE Trans. Wireless Commun.*, vol. 3, pp. 641–646, Mar. 2004.
- [81] R. A. Andrews, P. P. Mitra, and R. deCarvalho, "Tripling the capacity of wireless communications using electromagnetic polarization," *Nature*, vol. 409, pp. 316–318, Jan. 2001.
- [82] J. B. Andersen and B. N. Getu, "The MIMO cube - a compact MIMO antenna," in *Proc. 5th Intl. Symp. Wireless Pers. Multimedia Commun.*, vol. 1, Honolulu, HI, Oct. 27-30, 2002, pp. 112–114.
- [83] T. Svantesson and A. Ranheim, "Mutual coupling effects on the capacity of multielement antenna systems," in *Proc. 2001 IEEE Intl. Conf. Acoust. Speech Signal Process.*, vol. 4, Salt Lake City, UT, May 7-11, 2001, pp. 2485–2488.
- [84] C. Waldschmidt, J. v. Hagen, and W. Wiesbeck, "Influence and modeling of mutual coupling in MIMO and diversity systems," in *Proc. 2002 IEEE Antennas Propag. Soc. Intl. Symp.*, vol. 3, San Antonio, TX, Jun. 16-21, 2002, pp. 190–193.
- [85] B. Clerckx, D. Vanhoenacker-Janvier, C. Oestges, and L. Vandendorpe, "Mutual coupling effects on the channel capacity and the space-time processing of MIMO communication systems," in *Proc. 2003 IEEE Intl. Conf. Commun.*, vol. 4, Anchorage, AK, May 11-15, 2003, pp. 2638–2642.
- [86] D. M. Pozar, *Microwave Engineering*. John Wiley & Sons, 1998.
- [87] J. Engberg and T. Larsen, *Noise Theory of Linear and Nonlinear Circuits*. John Wiley & Sons, 1995.
- [88] G. Gonzalez, *Microwave Transistor Amplifiers*. Prentice-Hall, 1997.
- [89] J. W. Wallace and M. A. Jensen, "Mutual coupling in MIMO wireless systems: A rigorous network theory analysis," *IEEE Trans. Wireless Commun.*, vol. 3, pp. 1317–1325, Jul. 2004.
- [90] J. W. Wallace and M. A. Jensen, "The capacity of MIMO wireless systems with mutual coupling," in *Proc. 2002 IEEE 56th Veh. Technol. Conf.*, vol. 2, Vancouver, British Columbia, Canada, Sep. 24-28, 2002, pp. 696–700.
- [91] A. Taflove and S. C. Hagness, *Computational Electrodynamics: The Finite-Difference Time-Domain Method*, 2nd ed. Artech House, Boston, 2000.

2

Multidimensional Harmonic Retrieval with Applications in MIMO Wireless Channel Sounding

Xiangqian Liu, Nikos D. Sidiropoulos, and Tao Jiang

2.1 Introduction

Multiple-Input Multiple-Output (MIMO) wireless systems employing transmit and receive antenna arrays have emerged as an important enabling technology for boosting system performance in terms of spectrum efficiency, user capacity, data rate, and quality of service (QoS). Various MIMO wireless techniques, such as the BLAST system [5], and space-time coding [35], have been proposed and drawn much attention lately. In practice, attaining the benefits predicted by information theory requires parsimonious modeling and accurate estimation of the MIMO wireless channel. Good channel models and associated channel estimation enable fading mitigation and diversity combining at the receiver, and/or transmit optimization when channel information is fed back to the transmitters. In addition, good models are also useful to service providers for infrastructure layout and service provisioning purposes.

To this end, numerous spatial wireless channel models have been developed (see [4] for an overview) in an effort to predict the effects of the actual wireless channel without directly measuring it. On one hand, these models must adequately capture the complicated electromagnetic propagation environment resulting from reflection, scattering, diffraction

and shadowing. On the other hand, these models must be simple enough to allow system designers to assess the performance of various transmission modalities over different propagation scenarios, without the need for time-consuming measurement campaigns.

A parsimonious yet often realistic channel model is the so-called double-directional (DD) MIMO model [29] (see also [12, 42]). This model parameterizes the MIMO channel in terms of a finite number of paths, each characterized by its direction-of-departure (DOD), direction-of-arrival (DOA), time-delay of arrival, Doppler shift, and path loss. DOD and DOA are generally parameterized by azimuth and elevation angles, but azimuth-only parameterization is also common. The parameters of the model are usually fitted from measurements collected in channel sounding campaigns. Under certain conditions, joint estimation of several multipath signal parameters (e.g., azimuth, elevation, delay, Doppler shift) gives rise to a multidimensional harmonic retrieval (HR) problem. The dimensionality depends on the assumptions about mobility, transmit–receive array geometry, and other system parameters. Furthermore, several related signal parameter estimation problems, for example, [18, 41] also reduce to multidimensional HR.

A plethora of multidimensional HR techniques have been developed, ranging from non-parametric Fourier-based methods to modern parametric methods that are not bound by the Fourier resolution limit. In the high signal-to-noise ratio (SNR) regime, parametric methods work well with only a limited number of samples. Multidimensional HR theory has advanced in recent years, due in part to the discovery of close links to multiway analysis [11, 15, 26]. While progress has been primarily in terms of identifiability, these theoretical results have subsequently guided the development of effective high-resolution algebraic identification algorithms for 2-D and N -D HR [18, 16, 19].

This chapter reviews recent developments in multidimensional HR theory and algorithms, with applications in MIMO wireless channel sounding. This chapter is structured as follows. Section 2.2 presents the multidimensional HR problem, including some preliminaries. Section 2.3 presents associated identifiability results and proofs. Section 2.4 reviews high-resolution algebraic identification algorithms for 2-D and N -D HR. The emphasis is on recent algebraic algorithms, which provide good performance at moderate complexity. Performance is assessed by means of simulation in Section 2.5. Section 2.6 explains the DD-MIMO channel model and the channel sounding process, followed by examples of application of multidimensional HR to real channel sounder data, provided courtesy of www.channelsounder.com and *ftw.* of Vienna. This chapter concludes with a summary and overview of pertinent open research problems.

Some notational conventions that will be used in this chapter:

$\mathbf{A}^T, \mathbf{A}^*, \mathbf{A}^H$	the transpose, complex conjugate, and conjugate transpose of \mathbf{A} ;
\mathbf{A}^\dagger	the pseudoinverse of \mathbf{A} ;
\mathbf{a}_i	the i th column of \mathbf{A} ;
$\mathbf{A}(i, f)$	the (i, f) th element of $\mathbf{A} \in \mathbb{C}^{I \times F}$;
$\mathbf{D}_i(\mathbf{A})$	a diagonal matrix constructed from the i th row of \mathbf{A} ;
$\mathbf{A}^{(m)}$	a submatrix of \mathbf{A} that is formed by its first m rows;
$\mathbf{X}(:, k : m)$	a submatrix of \mathbf{X} consisting of its k th to m th columns;
$\mathbf{X}(k : m, :)$	a submatrix of \mathbf{X} consisting of its k th to m th rows;

- $\mathbf{A} \otimes \mathbf{B}$ the Kronecker product of \mathbf{A} and \mathbf{B} ;
 $\mathbf{A} \odot \mathbf{B}$ the Khatri–Rao (column-wise Kronecker) product of $\mathbf{A} \in \mathbb{C}^{I \times F}$ and $\mathbf{B} \in \mathbb{C}^{J \times F}$, i.e., $\mathbf{A} \odot \mathbf{B} = [\mathbf{a}_1 \otimes \mathbf{b}_1, \mathbf{a}_2 \otimes \mathbf{b}_2, \dots, \mathbf{a}_F \otimes \mathbf{b}_F]$.

2.2 Harmonic Retrieval Data Model

2.2.1 2-D harmonic retrieval model

The (noiseless) 2-D HR problem can be stated as follows: Given a mixture of F 2-D exponentials

$$x_{k,l} = \sum_{f=1}^F c_f e^{j\omega_f(k-1)} e^{j\nu_f(l-1)}, \quad (2.1)$$

for $k = 1, \dots, K$ and $l = 1, \dots, L$, where $\omega_f, \nu_f \in \Pi$, and the set $\Pi := (-\pi, \pi]$, find the parameter triples (ω_f, ν_f, c_f) , for $f = 1, \dots, F$. Here, (ω_f, ν_f) contains the two frequencies associated with the f th 2-D harmonic, and c_f stands for the corresponding complex amplitude. In practice, noisy data $\tilde{x}_{k,l} = x_{k,l} + n_{k,l}$ will be available, in which case the problem becomes one of estimating (ω_f, ν_f, c_f) , $f = 1, \dots, F$. The noiseless model is appropriate for the study of identifiability issues. The model in (2.1) is also referred to as an undamped or constant modulus 2-D harmonic mixture. For HR in the case of damped harmonics, interested readers are referred to [11].

Given (2.1), define $\mathbf{X} \in \mathbb{C}^{K \times L}$ with $\mathbf{X}(k, l) = x_{k,l}$, $\mathbf{A} \in \mathbb{C}^{K \times F}$ with $\mathbf{A}(k, f) = e^{j\omega_f(k-1)}$, $\mathbf{B} \in \mathbb{C}^{L \times F}$ with $\mathbf{B}(l, f) = e^{j\nu_f(l-1)}$, and a diagonal matrix $\mathbf{C} \in \mathbb{C}^{F \times F}$ with $\mathbf{C}(f, f) = c_f$. Then the 2-D harmonic mixture in (2.1) can be written in matrix form

$$\mathbf{X} = \mathbf{ACB}^T. \quad (2.2)$$

Notice that \mathbf{A} and \mathbf{B} are Vandermonde matrices, for example,

$$\mathbf{A} = \begin{pmatrix} 1 & 1 & \dots & 1 \\ e^{j\omega_1} & e^{j\omega_2} & \dots & e^{j\omega_F} \\ e^{j2\omega_1} & e^{j2\omega_2} & \dots & e^{j2\omega_F} \\ \vdots & & & \\ e^{j(K-1)\omega_1} & e^{j(K-1)\omega_2} & \dots & e^{j(K-1)\omega_F} \end{pmatrix}.$$

An important property of Vandermonde matrices is their shift-invariance. For example, let us define two selection matrices

$$\mathbf{J}_1 = [\mathbf{I}_{K-1} \quad \mathbf{0}_{(K-1) \times 1}], \quad \mathbf{J}_2 = [\mathbf{0}_{(K-1) \times 1} \quad \mathbf{I}_{K-1}],$$

where \mathbf{I}_{K-1} is a $(K-1) \times (K-1)$ identity matrix. Then

$$\mathbf{J}_2 \mathbf{A} = \mathbf{J}_1 \mathbf{A} \Phi,$$

where Φ is a diagonal matrix with $e^{j\omega_f}$'s, the generators of \mathbf{A} , on its diagonal. Many algebraic algorithms for signal parameter estimation are based on this shift invariance property, among which, ESPRIT is probably the most widely known one [22, 34, 33]. The

property will be further explored in the development of model identifiability results and HR algorithms later on.

Equation (2.1) can also be written in vector form. For example, let

$$\mathbf{y} = \begin{bmatrix} \mathbf{x}_1 \\ \mathbf{x}_2 \\ \vdots \\ \mathbf{x}_L \end{bmatrix} : KL \times 1$$

then it can be verified that

$$\mathbf{y} = (\mathbf{B} \odot \mathbf{A})\mathbf{c}, \quad (2.3)$$

where $\mathbf{c} = [c_1, c_2, \dots, c_F]^T$. This representation will be used in the development of the multidimensional unitary ESPRIT and the N -D MUSIC algorithm in Section 2.4.

2.2.2 N -D harmonic retrieval model

Generalizing the data model to the multidimensional case, the N -D HR problem can be stated as follows. Given a sum of F N -D exponentials

$$x_{i_1, \dots, i_N} = \sum_{f=1}^F c_f \prod_{n=1}^N e^{j\omega_{f,n}(i_n - 1)}, \quad (2.4)$$

for $i_n = 1, \dots, I_n \geq 2$, and $n = 1, \dots, N$, find $(\omega_{f,1}, \dots, \omega_{f,N}, c_f)$, for $f = 1, \dots, F$. Upon defining $\mathbf{A}_n \in \mathbb{C}^{I_n \times F}$ with $\mathbf{A}_n(i_n, f) = e^{j\omega_{f,n}(i_n - 1)}$, for $n = 1, \dots, N$, many matrix representations of (2.4) are possible, for example,

$$\begin{aligned} \mathbf{X}_{I_2 \dots I_N \times I_1} &= (\mathbf{A}_N \odot \dots \odot \mathbf{A}_2) \mathbf{C} \mathbf{A}_1^T, \\ &\vdots \\ \mathbf{X}_{I_1 \dots I_{N-1} \times I_N} &= (\mathbf{A}_{N-1} \odot \dots \odot \mathbf{A}_1) \mathbf{C} \mathbf{A}_N^T. \end{aligned} \quad (2.5)$$

The subscript of $\mathbf{X}_{I_1 \dots I_{N-1} \times I_N}$ means that the matrix is of size $(I_1 \dots I_{N-1}) \times I_N$, and also that the I_1 -index (I_1 goes first in the product $I_1 \dots I_{N-1}$) runs fastest and the I_{N-1} -index runs slowest along the rows of $\mathbf{X}_{I_1 \dots I_{N-1} \times I_N}$, respectively. Notice that \mathbf{A}_n , $n = 1, \dots, N$ are all Vandermonde matrices. Similar to the 2-D case, vectorizing $\mathbf{X}_{I_1 \dots I_{N-1} \times I_N}$ along its columns results in

$$\mathbf{y} = (\mathbf{A}_N \odot \mathbf{A}_{N-1} \odot \dots \odot \mathbf{A}_1)\mathbf{c}. \quad (2.6)$$

It is clear that through row rearrangement, (2.6) can also be transformed to

$$\mathbf{P}\mathbf{y} = (\mathbf{A}_1 \odot \mathbf{A}_2 \odot \dots \odot \mathbf{A}_N)\mathbf{c} = \tilde{\mathbf{A}}\mathbf{c}, \quad (2.7)$$

where $\tilde{\mathbf{A}} = \mathbf{A}_1 \odot \mathbf{A}_2 \odot \dots \odot \mathbf{A}_N$, and \mathbf{P} is a row-permutation matrix. Equations (2.6) and (2.7) are equivalent from the viewpoint of estimation of N -D harmonics. Multiple snapshots of the harmonic mixture can be obtained if \mathbf{c} varies as a function of, for example, time, while harmonic frequencies are kept the same. Our discussion will be focused on HR from a single snapshot. If multiple snapshots are available, one can process the data correlation matrix $\mathbf{R} = E[\mathbf{y}\mathbf{y}^H]$ (in practice, a sample estimate thereof) instead of the data matrix \mathbf{X} .

2.2.3 Khatri–Rao product of Vandermonde matrices

It can be clearly seen from the above that the Khatri–Rao product of Vandermonde matrices plays a key role in the HR context. In the following, we present a result regarding the rank of a Khatri–Rao product of multiple Vandermonde matrices. The result is crucial for the analysis of model identifiability in Section 2.3.

To establish full rank of the Khatri–Rao product of multiple Vandermonde matrices, we will need the following Lemma.

Lemma 2.2.1 *Consider an analytic function $h(\mathbf{x})$ of several complex variables $\mathbf{x} = [x_1, \dots, x_n]^T \in \mathbb{C}^n$. If h is nontrivial in the sense that there exists $\mathbf{x}_0 \in \mathbb{C}^n$ such that $h(\mathbf{x}_0) \neq 0$, then the zero set of $h(\mathbf{x})$*

$$\mathcal{Z} := \{\mathbf{x} \in \mathbb{C}^n | h(\mathbf{x}) = 0\}$$

is of measure (Lebesgue measure in \mathbb{C}^n) zero.

Proof. See, for example, [11] and [32]. □

Theorem 2.2.2 *(Almost surely (a.s.) full rank of Khatri–Rao product of two Vandermonde matrices) For a pair of Vandermonde matrices $\mathbf{A} \in \mathbb{C}^{K \times F}$ and $\mathbf{B} \in \mathbb{C}^{L \times F}$, $\mathbf{A} \odot \mathbf{B}$ is a.s. full rank, that is,*

$$r_{\mathbf{A} \odot \mathbf{B}} = \min(KL, F), \quad (2.8)$$

provided that the $2F$ generators of \mathbf{A} and \mathbf{B} are drawn from a distribution that is continuous with respect to the Lebesgue measure in \mathbb{C}^{2F} .

Proof. We will prove for the $KL = F$ case, since if $KL < F$ or $KL > F$, it suffices to prove that the result holds for the corresponding column-reduced or row-reduced square submatrix.

When $KL = F$, full rank of $\mathbf{A} \odot \mathbf{B}$ can be established by showing that the determinant of $\mathbf{A} \odot \mathbf{B}$ is nonzero. Suppose $\{\alpha_f\}$ and $\{\beta_f\}$ are the generators of \mathbf{A} and \mathbf{B} , respectively. Define

$$H(\alpha_1, \dots, \alpha_F, \beta_1, \dots, \beta_F) = \det(\mathbf{A} \odot \mathbf{B}).$$

H is a polynomial in variables $\{\alpha_f\}$ and $\{\beta_f\}$, hence is analytic in \mathbb{C}^{2F} . According to Lemma 2.2.1, to prove Theorem 2.2.2, it suffices to show that H is nontrivial. This requires a “generic” example that works for any K , L , and F , which can be constructed as follows. For any given K , L , F with $2 \leq K < F$, $2 \leq L < F$, and $KL = F$, choose the generators such that

$$\alpha_f = e^{j2L\pi(f-1)/F}, \quad \beta_f = e^{j2\pi(f-1)/F},$$

for $f = 1, \dots, F$. It can be verified that with this choice of generators, $\mathbf{A} \odot \mathbf{B}$ is a Vandermonde matrix with generators equally spaced on the unit circle, and hence is full rank. This shows that H is a nontrivial polynomial in \mathbb{C}^{2F} . Invoking Lemma 2.2.1, H is nonzero almost everywhere, except for a measure zero subset of \mathbb{C}^{2F} . □

Theorem 2.2.2 says that $r_{\mathbf{A} \odot \mathbf{B}} = \min(KL, F)$ is an event whose probability is 1, if the generators are drawn from a jointly continuous distribution. Theorem 2.2.2 can be generalized to Khatri–Rao products of N Vandermonde matrices, as stated in the following.

Theorem 2.2.3 (*a.s. full rank of Khatri–Rao product of N Vandermonde matrices*) Given N Vandermonde matrices $\mathbf{A}_n \in \mathbb{C}^{I_n \times F}$ for $n = 1, \dots, N \geq 2$, the Khatri–Rao product $\mathbf{A}_1 \odot \dots \odot \mathbf{A}_N$ is a.s. full rank, that is,

$$r_{\mathbf{A}_1 \odot \dots \odot \mathbf{A}_N} = \min \left(\prod_{n=1}^N I_n, F \right), \quad (2.9)$$

provided that the distribution used to draw the NF generators for \mathbf{A}_n , $n = 1, \dots, N$, is continuous with respect to the Lebesgue measure in \mathbb{C}^{NF} .

Proof. The general case can be reduced to the case when $\prod_{n=1}^N I_n = F$. The proof is similar to that of Theorem 2.2.2. Define

$$H(\alpha_{1,1}, \dots, \alpha_{1,F}, \dots, \alpha_{N,1}, \dots, \alpha_{N,F}) = \det(\mathbf{A}_1 \odot \dots \odot \mathbf{A}_N),$$

where $\{\alpha_{n,f}\}$ is the f th generator of \mathbf{A}_n . H is a polynomial of NF variables, thus is analytic in \mathbb{C}^{NF} . If the generators are chosen such that

$$\alpha_{n,f} = \exp \left(j2\pi \prod_{k=1}^{n-1} I_k \frac{f-1}{F} \right),$$

for $n = 1, \dots, N$ and $f = 1, \dots, F$, then it can be verified that $\mathbf{A}_1 \odot \dots \odot \mathbf{A}_N$ is a Vandermonde matrix with generators equally spaced on the unit circle, hence is full rank. Therefore, H is nontrivial. Invoking Lemma 2.2.1, (2.9) follows. \square

2.3 Identifiability of Multidimensional Harmonic Retrieval

An important issue with parametric methods is to determine the maximum number of harmonics that can be resolved for a given sample size in the noiseless case; another is to determine the sample size needed to meet performance specifications in the noisy case.

Determining the maximum number of resolvable harmonics is a parameter identifiability (ID) problem. Identifiability-imposed bounds on sample size are often not the issue in time series analysis (though sometimes time-variations may dictate such a bound) because samples are collected along the temporal dimension, and performance considerations dictate many more samples than what is needed for identifiability [30]. The maximum number of resolvable harmonics is of importance in situations in which data samples along the harmonic mode come at a premium, for example, in spatial sampling for DOA estimation using an antenna array, in which case one can meet performance requirements with few spatial samples but many temporal samples. As another example, in timing and frequency estimation of multiple frequency hopped signals, sometimes only a few temporal samples in each system-wide dwell are available in a heavily loaded system [17, 18].

The identifiability problem for constant-modulus 1-D harmonics is well understood [2, 21, 32]; see also [25] for the damped case. The situation is considerably more complicated (and interesting) for multidimensional harmonics, especially in higher dimensions. Most of

the work to date on this subject has been focused on the 2-D case, but some treatments of higher-dimensional cases are also available. The results can be classified to deterministic ones, which place conditions on the frequencies but do not rely on distributional assumptions (e.g., [14, 25, 40]); and stochastic ones, which postulate a distribution from which the harmonic components are drawn and in turn guarantee identifiability with probability 1 [11, 15]. For example, [14] considers one possible formulation of the 2-D HR problem wherein the frequencies are assumed to occur at the intersections of certain unknown grid lines in the 2-D frequency domain, and provides sufficient conditions for identifiability. In the case of a single realization of the 2-D harmonic mixture, the conditions in [14] require that one has sufficiently many samples in each dimension as required by the 1-D identifiability result. Recently, stronger identifiability results have been obtained in both the deterministic sense [25] and the stochastic sense [11, 15]. In the following, we present these recent results, with emphasis on stochastic ID, which provides the most relaxed generic identifiability bound to date. Because of the constructive nature of the associated proof, we will also obtain an algebraic multidimensional HR algorithm, called the multidimensional folding (MDF) algorithm [15], as a by-product. One of the advantages of MDF is that it does not impose any additional conditions to uniquely recover the sought parameters in the noiseless case.

2.3.1 Deterministic ID of N -D harmonic retrieval

A generalization of Carathéodory's uniqueness condition in [2] to the N -D case has been derived in [25]. The result in [25] deals with possibly damped harmonics in each dimension; in the case of constant modulus harmonics, it specializes as follows.

Theorem 2.3.1 (*Deterministic identifiability of N -D HR*) *Given a sum of F N -D exponentials*

$$x_{i_1, \dots, i_N} = \sum_{f=1}^F c_f \prod_{n=1}^N e^{j\omega_{f,n}(i_n - 1)}, \quad (2.10)$$

for $i_n = 1, \dots, I_n \geq 2$, $n = 1, \dots, N$, with $c_f \in \mathbb{C}$ and $\omega_{f,n} \in \Pi$ such that $\omega_{f_1,n} \neq \omega_{f_2,n}$, $\forall f_1 \neq f_2$ and all n , if

$$\sum_{n=1}^N I_n \geq 2F + N - 1, \quad (2.11)$$

then there exist unique $(\{\omega_{f,n}\}_{n=1}^N, c_f)$, $f = 1, \dots, F$ that give rise to x_{i_1, \dots, i_N} .

Proof. See [25]. □

Theorem 2.3.1 indicates that the identifiability bound depends on the *sum* of sample sizes along the N dimensions. In the 2-D case, the ID result is illustrated in Figure 2.1. A total of $(K + L - 1)/2$ harmonics are deterministically identifiable, where K is the number of samples along one dimension, and L likewise for the other dimension. The result is deterministic in the sense that no stochastic assumptions are needed, aside from the requirement that the frequencies along each dimension are distinct. However, the sufficient condition improves with the *sum* of I_n 's, whereas the total sample size grows with the *product* of I_n 's. This indicates that significantly stronger results may be possible, and leads to the following stochastic identifiability results.

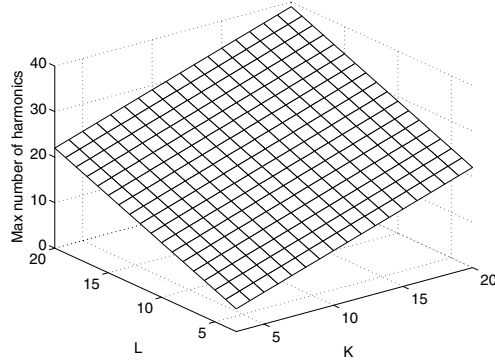


Figure 2.1 Deterministic ID: maximum number of retrievable harmonics in the 2-D case.

2.3.2 Stochastic ID of 2-D harmonic retrieval

Theorem 2.3.2 (*Stochastic identifiability of 2-D HR*) Given a sum of F 2-D undamped exponentials

$$x_{k,l} = \sum_{f=1}^F c_f e^{j\omega_f(k-1)} e^{j\nu_f(l-1)}, \quad (2.12)$$

for $k = 1, \dots, K \geq 3$, and $l = 1, \dots, L \geq 3$, the parameter triples (ω_f, ν_f, c_f) , $f = 1, \dots, F$ are $P_{\mathcal{L}}(\Pi^{2F})$ -a.s. unique, provided that

$$F \leq \left\lceil \frac{K}{2} \right\rceil \left\lceil \frac{L}{2} \right\rceil, \quad (2.13)$$

where $P_{\mathcal{L}}(\Pi^{2F})$ is the distribution used to draw the $2F$ frequencies (ω_f, ν_f) , $f = 1, \dots, F$, assumed continuous with respect to the Lebesgue measure in Π^{2F} .

Proof. Equation (2.12) can be written in matrix form as in (2.2). Note that both \mathbf{A} and \mathbf{B} are Vandermonde matrices with exponential generators. The idea is to explore the inherent shift-invariance property of these two matrices. Define L_1 matrices, \mathbf{X}_{l_1} , each of size $K \times L_2$ such that

$$\mathbf{X}_{l_1} = \mathbf{X}(:, l_1 : (L_2 + l_1 - 1)), \quad l_1 = 1, \dots, L_1,$$

where L_1 is known as the smoothing factor, and $L_1 + L_2 = L + 1$. It is easy to verify that

$$\mathbf{X}_{l_1} = \mathbf{ACD}_{l_1}(\mathbf{B}) \mathbf{B}_2^T, \quad l_1 = 1, \dots, L_1, \quad (2.14)$$

where $\mathbf{B}_2 = \mathbf{B}^{(L_2)}$, that is, the first L_2 rows of \mathbf{B} . Therefore,

$$\bar{\mathbf{X}}_{KL_1 \times L_2} = \begin{bmatrix} \mathbf{X}_1 \\ \mathbf{X}_2 \\ \vdots \\ \mathbf{X}_{L_1} \end{bmatrix} = \begin{bmatrix} \mathbf{ACD}_1(\mathbf{B}) \\ \mathbf{ACD}_2(\mathbf{B}) \\ \vdots \\ \mathbf{ACD}_{L_1}(\mathbf{B}) \end{bmatrix} \mathbf{B}_2^T = (\mathbf{B}_1 \odot \mathbf{A}) \mathbf{C} \mathbf{B}_2^T, \quad (2.15)$$

where $\mathbf{B}_1 = \mathbf{B}^{(L_1)}$, that is, the first L_1 rows of \mathbf{B} . The third equation in (2.15) can be easily checked using the definition of the Khatri–Rao product. Similarly, we can perform smoothing along the other dimension. Define K_2 matrices, $\bar{\mathbf{X}}_{k_2}$, each of size $K_1 L_1 \times L_2$ such that

$$\bar{\mathbf{X}}_{k_2} = \begin{bmatrix} \mathbf{X}_1(k_2 : K_1 + k_2 - 1, :) \\ \mathbf{X}_2(k_2 : K_1 + k_2 - 1, :) \\ \vdots \\ \mathbf{X}_{L_1}(k_2 : K_1 + k_2 - 1, :) \end{bmatrix}, \quad k_2 = 1, \dots, K_2.$$

Define $\mathbf{A}_1 = \mathbf{A}^{(K_1)}$ and $\mathbf{A}_2 = \mathbf{A}^{(K_2)}$. It can be verified that

$$\bar{\mathbf{X}}_{k_2} = (\mathbf{B}_1 \odot \mathbf{A}_1) \mathbf{D}_{k_2}(\mathbf{A}) \mathbf{C} \mathbf{B}_2^T, \quad k_2 = 1, \dots, K_2. \quad (2.16)$$

Thus

$$\hat{\mathbf{X}} := [\bar{\mathbf{X}}_1 \ \bar{\mathbf{X}}_2 \ \cdots \ \bar{\mathbf{X}}_{K_2}] = (\mathbf{B}_1 \odot \mathbf{A}_1) \mathbf{C} (\mathbf{A}_2 \odot \mathbf{B}_2)^T. \quad (2.17)$$

The order of $\mathbf{B}_1 \odot \mathbf{A}_1$ in (2.17) can be changed by simple permutation of the rows of $\hat{\mathbf{X}}$. In particular, defining a permutation matrix

$$\mathbf{J} = [\mathbf{I}_{L_1} \otimes \mathbf{e}_1 \ \mathbf{I}_{L_1} \otimes \mathbf{e}_2 \ \cdots \ \mathbf{I}_{L_1} \otimes \mathbf{e}_{K_1}]^T,$$

where \mathbf{e}_{k_1} is the k_1 -th column of \mathbf{I}_{K_1} , we then have

$$\tilde{\mathbf{X}} := \mathbf{J} \hat{\mathbf{X}} = (\mathbf{A}_1 \odot \mathbf{B}_1) \mathbf{C} (\mathbf{A}_2 \odot \mathbf{B}_2)^T := \mathbf{G} \mathbf{C} \mathbf{H}^T, \quad (2.18)$$

where

$$\mathbf{G} = \mathbf{A}_1 \odot \mathbf{B}_1, \quad \mathbf{H} = \mathbf{A}_2 \odot \mathbf{B}_2. \quad (2.19)$$

This is important because under the premise of Theorem 2.2.2, \mathbf{G} and \mathbf{H} are a.s. full column rank if $K_1 L_1 \geq F$ and $K_2 L_2 \geq F$, and consequently $\tilde{\mathbf{X}}$ is of rank F .

To further increase the data size, we can use the “forward-backward averaging¹” technique. It can be verified that

$$\mathbf{Y} := \boldsymbol{\Pi}_K \mathbf{X}^* \boldsymbol{\Pi}_L = \mathbf{A} \tilde{\mathbf{C}} \mathbf{B}^T, \quad (2.20)$$

where $\boldsymbol{\Pi}_p$ is a permutation matrix with ones on its main antidiagonal, that is,

$$\boldsymbol{\Pi}_p = \begin{bmatrix} & & & 1 \\ & & 1 & \\ & \dots & & \\ 1 & & & \end{bmatrix} \in \mathbb{R}^{p \times p}. \quad (2.21)$$

and

$$\tilde{\mathbf{C}} = \text{diag}(\tilde{c}_1, \dots, \tilde{c}_F),$$

¹Similar to the well-known “forward-backward averaging” trick used in the context of 1-D HR (see, for example, [31], pp.165–167). In the context of multidimensional HR, this trick has been used by Haardt [8] in a similar fashion.

with $\tilde{c}_f := c_f^* e^{-j\omega_f(K-1)-j\nu_f(L-1)}$. This means that by conjugation and folding of the lower-left quadrant, we obtain another harmonic mixture with the same harmonics as \mathbf{X} , but different proportions. Following the same procedure as in the construction of $\tilde{\mathbf{X}}$ from \mathbf{X} , we can construct a matrix $\tilde{\mathbf{Y}} \in \mathbb{C}^{K_1 L_1 \times K_2 L_2}$ from \mathbf{Y} , such that

$$\tilde{\mathbf{Y}} = \mathbf{G}\tilde{\mathbf{C}}\mathbf{H}^T. \quad (2.22)$$

Invoking Theorem 2.2.2, if $K_1 L_1 \geq F$ and $K_2 L_2 \geq F$, then both \mathbf{G} and \mathbf{H} in (2.19) and (2.22) are a.s. full column rank. Hence $\tilde{\mathbf{X}}$ and $\tilde{\mathbf{Y}}$ are of rank F , and the singular value decomposition (SVD) of the stacked data yields

$$\begin{bmatrix} \tilde{\mathbf{X}} \\ \tilde{\mathbf{Y}} \end{bmatrix} = \begin{bmatrix} \mathbf{GC} \\ \mathbf{G}\tilde{\mathbf{C}} \end{bmatrix} \mathbf{H}^T = \mathbf{U}_{2K_1 L_1 \times F} \boldsymbol{\Sigma}_{F \times F} \mathbf{V}_{K_2 L_2 \times F}^H,$$

where \mathbf{U} has F columns that together span the column space of $[\tilde{\mathbf{X}}^T \ \tilde{\mathbf{Y}}^T]^T$. Since the same space is spanned by the columns of $[(\mathbf{GC})^T \ (\mathbf{G}\tilde{\mathbf{C}})^T]^T$, there exists an $F \times F$ non-singular matrix \mathbf{T} such that

$$\mathbf{U} = \begin{bmatrix} \mathbf{U}_1 \\ \mathbf{U}_2 \end{bmatrix} = \begin{bmatrix} \mathbf{GC} \\ \mathbf{G}\tilde{\mathbf{C}} \end{bmatrix} \mathbf{T}. \quad (2.23)$$

It then follows that

$$\mathbf{U}_1^\dagger \mathbf{U}_2 = \mathbf{T}^{-1} \mathbf{C}^{-1} \tilde{\mathbf{C}} \mathbf{T}, \quad (2.24)$$

which is an eigenvalue decomposition (EVD) problem. \mathbf{T}^{-1} contains the eigenvectors of $\mathbf{U}_1^\dagger \mathbf{U}_2$ (scaled to unit norm). Notice that the eigenvectors in (2.24) can be reordered and scaled arbitrarily. Therefore,

$$\mathbf{U}_1 \mathbf{T}^{-1} = \mathbf{G} \mathbf{C} \boldsymbol{\Lambda} \boldsymbol{\Delta}, \quad [(\mathbf{U} \mathbf{T}^{-1})^\dagger \tilde{\mathbf{X}}]^T = \mathbf{H} \boldsymbol{\Lambda}^{-1} \boldsymbol{\Delta}, \quad (2.25)$$

where $\boldsymbol{\Delta}$ is a permutation matrix and $\boldsymbol{\Lambda}$ is a non-singular diagonal column scaling matrix, which carry over from the solution of the eigenvalue problem. In (2.25), we have used the fact that $(\boldsymbol{\Delta}^{-1})^T = \boldsymbol{\Delta}$. The permutation is not an issue here, however, because ω_f and ν_f appear in the same column of $\mathbf{G} \mathbf{C} \boldsymbol{\Lambda} \boldsymbol{\Delta}$ (albeit not necessarily in column f , because of the arbitrary permutation) and are thus automatically paired; and arbitrary nonzero column scaling is immaterial, because the sought frequencies can be obtained by dividing suitably chosen elements of the aforementioned column. After the 2-D frequencies are obtained, the associated complex amplitudes can be obtained by solving (2.3).

Therefore, we have shown that the parameter triples (ω_f, ν_f, c_f) , $f = 1, \dots, F$, can be uniquely recovered a.s., provided there exist positive integers K_1, K_2, L_1, L_2 such that

$$K_1 L_1 \geq F, \quad K_2 L_2 \geq F, \quad (2.26)$$

subject to the constraint that $K_1 + K_2 = K + 1$ and $L_1 + L_2 = L + 1$. If the integers are chosen such that

$$\begin{cases} \text{if } K \text{ is odd, pick } K_1 = K_2 = \frac{K+1}{2}, \\ \text{if } K \text{ is even, pick } K_1 = \frac{K}{2}, \ K_2 = \frac{K+2}{2}, \end{cases} \quad (2.27)$$

and similarly for L_1 and L_2 , then the constraint is satisfied. Once we pick four integers following the rules in (2.27), condition (2.13) assures that Inequality (2.26) holds for those particular integers. This completes the proof. \square

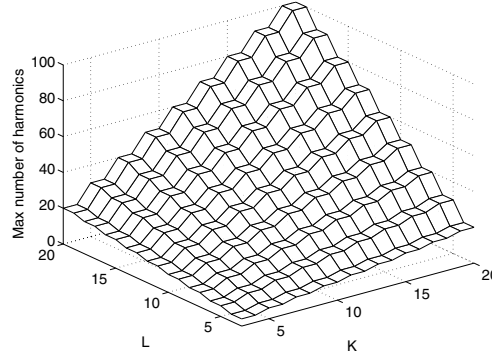


Figure 2.2 Stochastic ID: maximum number of retrievable harmonics in the 2-D case.

The stochastic ID result for 2-D HR is illustrated in Figure 2.2, which shows significant improvement in the number of harmonics that can be uniquely recovered, relative to the deterministic ID result illustrated in Figure 2.1.

2.3.3 Stochastic ID of N -D harmonic retrieval

The previous theorem can be generalized to the N -D case. The result is as follows.

Theorem 2.3.3 (*Stochastic identifiability of N -D HR*) *Given a sum of F N -D undamped exponentials*

$$x_{i_1, \dots, i_N} = \sum_{f=1}^F c_f \prod_{n=1}^N e^{j\omega_{f,n}(i_n-1)}, \quad (2.28)$$

for $i_n = 1, \dots, I_n \geq 3$, $n = 1, \dots, N$, if

$$F \leq \prod_{n=1}^N \left\lceil \frac{I_n}{2} \right\rceil, \quad (2.29)$$

and the distribution used to draw the NF frequencies $(\omega_{f,1}, \dots, \omega_{f,N})$, for $f = 1, \dots, F$, denoted by $P_{\mathcal{L}}(\Pi^{NF})$, is continuous with respect to Lebesgue measure in Π^{NF} , then the parameter $(N+1)$ -tuples $(\omega_{f,1}, \dots, \omega_{f,N}, c_f)$, $f = 1, \dots, F$, are $P_{\mathcal{L}}(\Pi^{NF})$ -a.s. unique.

Proof. A proof utilizing the theory of low-rank three-way array decomposition is given in [11]. Here, we give a constructive algebraic proof similar to the proof of Theorem 2.3.2.

Given (2.28), recall that one of its matrix representations may be written as

$$\mathbf{X}_{I_2 \cdots I_N \times I_1} = (\mathbf{A}_N \odot \cdots \odot \mathbf{A}_2) \mathbf{C} \mathbf{A}_1^T. \quad (2.30)$$

Using the same smoothing and matrix permutation techniques from which we obtained (2.18) from (2.2), except that now the smoothing is done along each of the N -dimensions instead of two dimensions, we can obtain

$$\tilde{\mathbf{X}} = \left(\mathbf{A}_1^{(I_{1,1})} \odot \cdots \odot \mathbf{A}_N^{(I_{N,1})} \right) \mathbf{C} \left(\mathbf{A}_1^{(I_{1,2})} \odot \cdots \odot \mathbf{A}_N^{(I_{N,2})} \right)^T := \mathbf{G} \mathbf{C} \mathbf{H}^T, \quad (2.31)$$

where $I_{n,1} + I_{n,2} = I_n + 1$, $n = 1, \dots, N$. (It can be shown that N -D smoothing can be implemented equivalently using (2.44) to form $\tilde{\mathbf{X}}$.) Similarly, from

$$\mathbf{Y} := \boldsymbol{\Pi}_{I_2 \dots I_N} \mathbf{X}^* \boldsymbol{\Pi}_{I_1},$$

where the permutation matrix $\boldsymbol{\Pi}_p$ is defined in (2.21), we can obtain

$$\tilde{\mathbf{Y}} = \left(\mathbf{A}_1^{(I_{1,1})} \odot \dots \odot \mathbf{A}_N^{(I_{N,1})} \right) \tilde{\mathbf{C}} \left(\mathbf{A}_1^{(I_{1,2})} \odot \dots \odot \mathbf{A}_N^{(I_{N,2})} \right)^T := \mathbf{G} \tilde{\mathbf{C}} \mathbf{H}^T, \quad (2.32)$$

where $\tilde{\mathbf{C}} = \text{diag}(\tilde{c}_1, \dots, \tilde{c}_F)$, and

$$\tilde{c}_f := c_f^* \exp \left(-j \sum_{n=1}^N \omega_{f,n} (I_n - 1) \right).$$

(It can also be shown that equivalently $\tilde{\mathbf{Y}}$ may be formed from \mathbf{X} using (2.45).)

Invoking Theorem 2.2.3, if $\prod_{n=1}^N I_{n,1} \geq F$ and $\prod_{n=1}^N I_{n,2} \geq F$, then both \mathbf{G} and \mathbf{H} in (2.31) and (2.32) are a.s. full column rank. Hence, $\tilde{\mathbf{X}}$ and $\tilde{\mathbf{Y}}$ are of rank F . Let $I_1 = \prod I_{n,1}$ and $I_2 = \prod I_{n,2}$, then the SVD of the stacked data yields

$$\begin{bmatrix} \tilde{\mathbf{X}} \\ \tilde{\mathbf{Y}} \end{bmatrix} = \begin{bmatrix} \mathbf{G} \mathbf{C} \\ \mathbf{G} \tilde{\mathbf{C}} \end{bmatrix} \mathbf{H}^T = \mathbf{U}_{2I_1 \times F} \boldsymbol{\Sigma}_{F \times F} \mathbf{V}_{I_2 \times F}^H, \quad (2.33)$$

where \mathbf{U} has F columns that together span the column space of $[\tilde{\mathbf{X}}^T \ \tilde{\mathbf{Y}}^T]^T$. Since the same space is spanned by the columns of $[(\mathbf{G} \mathbf{C})^T \ (\mathbf{G} \tilde{\mathbf{C}})^T]^T$, there exists an $F \times F$ non-singular matrix \mathbf{T} such that

$$\mathbf{U} = \begin{bmatrix} \mathbf{U}_1 \\ \mathbf{U}_2 \end{bmatrix} = \begin{bmatrix} \mathbf{G} \mathbf{C} \\ \mathbf{G} \tilde{\mathbf{C}} \end{bmatrix} \mathbf{T}. \quad (2.34)$$

It then follows that

$$\mathbf{U}_1^\dagger \mathbf{U}_2 = \mathbf{T}^{-1} \mathbf{C}^{-1} \tilde{\mathbf{C}} \mathbf{T}, \quad (2.35)$$

which is an EVD problem. \mathbf{T}^{-1} contains the eigenvectors of $\mathbf{U}_1^\dagger \mathbf{U}_2$ (scaled to unit norm). Similar to the 2-D case, we have

$$\mathbf{U}_1 \mathbf{T}^{-1} = \mathbf{G} \mathbf{C} \boldsymbol{\Lambda} \boldsymbol{\Delta}, \quad [(\mathbf{U} \mathbf{T}^{-1})^\dagger \tilde{\mathbf{X}}]^T = \mathbf{H} \boldsymbol{\Lambda}^{-1} \boldsymbol{\Delta}, \quad (2.36)$$

The N -D harmonics $\{\omega_{f,n}\}_{n=1}^N$, $f = 1, \dots, F$, can be retrieved from $\mathbf{G} \mathbf{C} \boldsymbol{\Lambda} \boldsymbol{\Delta}$ and/or $\mathbf{H} \boldsymbol{\Lambda}^{-1} \boldsymbol{\Delta}$ accordingly. After the N -D frequencies are obtained, the associated complex amplitudes can be obtained by solving (2.7).

Hence, we have shown that the N -D harmonics can be uniquely recovered a.s., provided there exist positive integers $I_{n,1}$ and $I_{n,2}$, for $n = 1, \dots, N$, such that

$$\prod_{n=1}^N I_{n,1} \geq F, \quad \prod_{n=1}^N I_{n,2} \geq F, \quad (2.37)$$

subject to the constraint that

$$I_{n,1} + I_{n,2} = I_n + 1, \quad \text{for } n = 1, \dots, N. \quad (2.38)$$

If the integers are chosen such that

$$\begin{cases} \text{if } I_n \text{ is odd, pick } I_{n,1} = I_{n,2} = (I_n + 1)/2, \\ \text{if } I_n \text{ is even, pick } I_{n,1} = I_n/2, I_{n,2} = (I_n + 2)/2, \end{cases} \quad (2.39)$$

then condition (2.38) is satisfied. Once we pick four integers following the rules in (2.39), condition (2.29) assures that inequality (2.37) holds for those particular integers. This completes the proof. \square

Remark 1 *In most applications, having two or more identical frequencies along one dimension is a zero probability event. However, in certain applications, common frequencies along particular dimensions are a modeling assumption. Hence, it is of interest to study identifiability of HR subject to common frequency constraints. The identifiability can be analyzed by the tools developed herein, but a case-by-case approach may be more appropriate since a unified treatment does not seem to be possible. Further discussions on this topic can be found in [11], where one case of 2-D HR with common frequencies is illustrated analytically and the identifiability condition is shown to be unaffected for this example.*

2.4 Multidimensional Harmonic Retrieval Algorithms

A variety of multidimensional HR techniques are available in the literature. These range from nonparametric multidimensional Fourier transform based methods (e.g., peak-picking the multidimensional periodogram) to modern high-resolution parametric methods [3, 10, 8, 14, 13, 20]. In the high SNR regime, parametric methods generally work well with only a limited number of samples. Each method has advantages and disadvantages in terms of identifiability, estimation performance, and computational complexity.

Clearly, a “verbatim” copy of the steps in the constructive proof of the identifiability result in the previous section yields an algebraic multidimensional HR algorithm, which attains the associated model identifiability bound in (2.29). Perhaps more interestingly, the aforementioned algorithm (dubbed MDF for *multidimensional folding*²) exhibits good performance, as will be illustrated later by means of simulation. The MDF algorithm remains close to the Cramér-Rao Bound (CRB) at moderate to high SNR, and small rank relative to identifiability conditions. Furthermore, the MDF is able to resolve harmonic parameters when there are identical frequencies along one dimension [11, 16].

In the following, we describe the 2-D MDF and N -D MDF algorithms. Numerical examples are provided in Section 2.5 with simulated data, as well as in Section 2.6 with the application to MIMO channel sounding measurement data. In order to provide better perspective, we also review three other N -D HR algorithms: the multidimensional unitary ESPRIT algorithm [8], the N -D MUSIC algorithm, and the rank reduction estimator (RARE) [20]. A summary note is provided at the end of this section.

²The multidimensional smoothing steps embedded in MDF can be visualized as first expanding the N -D data to a higher-dimensional structure, then folding back this structure into a matrix.

2.4.1 2-D MDF

Given noisy data \mathbf{X} of size $K \times L$ with typical element

$$x_{k,l} = \sum_{f=1}^F c_f e^{j\omega_f(k-1)} e^{j\nu_f(l-1)} + n_{k,l}, \quad (2.40)$$

where $n_{k,l}$ is white circularly symmetric Gaussian noise with variance σ^2 , the 2-D MDF algorithm to estimate (ω_f, ν_f, c_f) , $f = 1, \dots, F$, is given as follows.

1. Form $\tilde{\mathbf{X}}$ and $\tilde{\mathbf{Y}}$ from \mathbf{X} by 2-D (forward-backward) smoothing as described in (2.15), (2.18), (2.20), and (2.22). The integers K_1 , K_2 , L_1 , and L_2 should be chosen according to (2.27). It can be shown that equivalently, $\tilde{\mathbf{X}}$ and $\tilde{\mathbf{Y}}$ may also be formed from \mathbf{X} using

$$\tilde{x}_{u,v} = x_{k_1+k_2-1, l_1+l_2-1}, \quad (2.41)$$

$$\tilde{y}_{u,v} = x_{K-(k_1+k_2-1)+1, L-(l_1+l_2-1)+1}^*, \quad (2.42)$$

where

$$u = (k_1 - 1)L_1 + l_1, \quad v = (k_2 - 1)L_2 + l_2,$$

for $k_i = 1, \dots, K_i$, and $l_i = 1, \dots, L_i$, with $i = 1, 2$.

2. Compute the F principal left singular vectors (i.e., \mathbf{U}) of $[\tilde{\mathbf{X}}^T \tilde{\mathbf{Y}}^T]^T$. Partition \mathbf{U} into two equal-sized matrices \mathbf{U}_1 and \mathbf{U}_2 as in (2.23).
3. Compute the eigenvectors of $\mathbf{U}_1^\dagger \mathbf{U}_2$, which yield \mathbf{T}^{-1} as in (2.24).
4. Estimate the 2-D frequencies, (ω_f, ν_f) , from (2.25). After the 2-D frequencies are obtained, the associated complex amplitudes, c_f , can be obtained by solving a simple linear least squares problem as in (2.3). (ω_f, ν_f, c_f) are paired up automatically without extra association needed. Note that the rich structure of the Khatri–Rao product of Vandermonde matrices can be exploited to average point estimates of (ω_f, ν_f) . For example, the first row of \mathbf{G} is $[e^{j\nu_1}, \dots, e^{j\nu_F}]$, and the ratio of the second row and the first row of \mathbf{G} is also $[e^{j\nu_1}, \dots, e^{j\nu_F}]$, and so on, thus average may be used.

2.4.2 N-D MDF

Given noisy observation \mathbf{X} of size $I_1 \times I_2 \times \dots \times I_N$ with typical element

$$x_{i_1, \dots, i_N} = \sum_{f=1}^F c_f \prod_{n=1}^N e^{j\omega_{f,n}(i_n-1)} + n_{i_1, \dots, i_N}, \quad (2.43)$$

the N -D MDF algorithm to estimate $(\omega_{f,1}, \dots, \omega_{f,N}, c_f)$, $f = 1, \dots, F$, is given as follows.

1. Form $\tilde{\mathbf{X}}$ and $\tilde{\mathbf{Y}}$ from \mathbf{X} by N -D (forward-backward) smoothing as described in (2.31) and (2.32). The integers $I_{n,1}$ and $I_{n,2}$ should be chosen according to (2.39). Equivalently, $\tilde{\mathbf{X}}$ and $\tilde{\mathbf{Y}}$ can also be formed from \mathbf{X} using

$$\tilde{x}_{u,v} = x_{i_{1,1}+i_{1,2}-1, i_{2,1}+i_{2,2}-1, \dots, i_{N,1}+i_{N,2}-1}, \quad (2.44)$$

$$\tilde{y}_{u,v} = x^*_{I_1-(i_{1,1}+i_{1,2}-1)+1, I_2-(i_{2,1}+i_{2,2}-1)+1, \dots, I_N-(i_{N,1}+i_{N,2}-1)+1} \quad (2.45)$$

where

$$\begin{aligned} u &= ((\dots + i_{N-2,1} + 1)I_{N-1,1} + i_{N-1,1} - 1)I_{N,1} + i_{N,1}, \\ v &= ((\dots + i_{N-2,2} + 1)I_{N-1,2} + i_{N-1,2} - 1)I_{N,2} + i_{N,2}, \end{aligned}$$

for $i_{n,1} = 1, \dots, I_{n,1}$, and $i_{n,2} = 1, \dots, I_{n,2}$, with $n = 1, \dots, N$.

2. Compute the F principal left singular vectors (i.e., \mathbf{U}) of $[\tilde{\mathbf{X}}^T \tilde{\mathbf{Y}}^T]^T$. Partition \mathbf{U} into two equal-sized matrices \mathbf{U}_1 and \mathbf{U}_2 as in (2.34).
3. Compute the eigenvectors of $\mathbf{U}_1^\dagger \mathbf{U}_2$, which yield \mathbf{T}^{-1} as in (2.35).
4. Estimate the N -D frequencies, $(\omega_{f,1}, \dots, \omega_{f,N})$, from (2.36). After the N -D frequencies are obtained, the associated complex amplitudes, c_f , can be obtained by solving the linear system in (2.7). Averaging can be utilized because of the rich structure of the Khatri–Rao product of multiple Vandermonde matrices. $(\omega_{f,1}, \dots, \omega_{f,N}, c_f)$ are paired up automatically.

2.4.3 N -D unitary ESPRIT

Two-dimensional unitary ESPRIT was proposed in [41], and later it was extended to multiple dimensions in [8]. Our discussion of N -D unitary ESPRIT is closer to that of [8]. The N -D unitary ESPRIT is derived in the context of multiple data snapshots, that is, see (2.7),

$$\mathbf{y}_p = \tilde{\mathbf{A}}\mathbf{c}_p + \mathbf{n}, \quad p = 1, \dots, P. \quad (2.46)$$

For the p th snapshot, the amplitude vector is \mathbf{c}_p . When P snapshots are available, the data matrix can be written as

$$\mathbf{Y} = [\mathbf{y}_1 \cdots \mathbf{y}_P] = \tilde{\mathbf{A}}\mathbf{C}, \quad (2.47)$$

where the $F \times P$ matrix $\mathbf{C} = [\mathbf{c}_1 \cdots \mathbf{c}_P]$. Let $I = \prod_{n=1}^N I_n$, and define N pairs of selection matrices of size $m_n \times I$, that are centro-symmetric with respect to one another, that is,

$$\mathbf{J}_{(n)1} = \boldsymbol{\Pi}_{m_n} \mathbf{J}_{(n)2} \boldsymbol{\Pi}_I, \quad (2.48)$$

where the exchange matrix $\boldsymbol{\Pi}_p$ has been defined in (2.21), and the index m_n is defined as

$$m_n := I - \prod_{k=1, k \neq n}^N I_k = I \left(1 - \frac{1}{I_n}\right), \quad 1 \leq n \leq N. \quad (2.49)$$

Taking into account the structure of $\tilde{\mathbf{A}}$, the desired $m_n \times I$ dimensional selection matrices can be constructed as

$$\mathbf{J}_{(n)2} = \mathbf{I}_{\prod_{k=n+1}^N I_k} \otimes \mathbf{J}_2^{(I_n)} \otimes \mathbf{I}_{\prod_{k=1}^{n-1} I_k}, \quad (2.50)$$

where

$$\mathbf{J}_2^{(I_n)} = [\mathbf{0}_{(I_n-1) \times 1} \ \mathbf{I}_{I_n-1}], \quad 1 \leq n \leq N. \quad (2.51)$$

Since $\tilde{\mathbf{A}}$ is a multiple Khatri–Rao product of Vandermonde matrices (see (2.7)), the following invariance properties are satisfied.

$$\mathbf{J}_{(n)1} \tilde{\mathbf{A}} \Phi_n = \mathbf{J}_{(n)2} \tilde{\mathbf{A}}, \quad 1 \leq n \leq N, \quad (2.52)$$

where the diagonal matrix $\Phi_n = \text{diag}[e^{j\omega_{1,n}}, \dots, e^{j\omega_{F,n}}]$ contains the phase factors in the n -th dimension.

To implement unitary ESPRIT, we need to build a real model based on (2.52). Define left Π -real matrices $\mathbf{Q} \in \mathbb{C}^{I \times I}$ satisfying $\Pi_I \mathbf{Q}^* = \mathbf{Q}$ [8]. The unitary left Π -real matrices for odd and even sizes can be constructed as

$$\mathbf{Q}_{2q+1} = \frac{1}{\sqrt{2}} \begin{bmatrix} \mathbf{I}_q & \mathbf{0} & j\mathbf{I}_q \\ \mathbf{0}^T & \sqrt{2} & \mathbf{0}^T \\ \mathbf{\Pi}_q & \mathbf{0} & -j\mathbf{\Pi}_q \end{bmatrix}, \quad \mathbf{Q}_{2q} = \frac{1}{\sqrt{2}} \begin{bmatrix} \mathbf{I}_q & j\mathbf{I}_q \\ \mathbf{\Pi}_q & -j\mathbf{\Pi}_q \end{bmatrix}. \quad (2.53)$$

Further define the transformed steering matrix as $\Psi = \mathbf{Q}_I^H \tilde{\mathbf{A}}$. On the basis of the invariance properties in (2.52) and the definition of left Π -real matrix, we have

$$\mathbf{K}_{(n)1} \Psi \Omega_n = \mathbf{K}_{(n)2} \Psi, \quad (2.54)$$

where the transformed selection matrices are given by

$$\begin{aligned} \mathbf{K}_{(n)1} &= 2\Re\{\mathbf{Q}_{m_n}^H \mathbf{J}_{(n)2} \mathbf{Q}_I\}, \\ \mathbf{K}_{(n)2} &= 2\mathcal{I}\{\mathbf{Q}_{m_n}^H \mathbf{J}_{(n)2} \mathbf{Q}_I\}, \end{aligned} \quad (2.55)$$

and the real diagonal matrix Ω_n is

$$\Omega_n = \text{diag}[\tan(\omega_{1,n}/2), \dots, \tan(\omega_{F,n}/2)], \quad 1 \leq n \leq N. \quad (2.56)$$

Transforming the complex-valued data matrix \mathbf{Y} into a real-valued matrix, the following forward-backward averaging can be carried out

$$\tilde{\mathbf{Y}} = \mathbf{Q}_I^H [\mathbf{Y} \ \mathbf{\Pi}_I \mathbf{Y}^* \mathbf{\Pi}_P] \mathbf{Q}_{2P}. \quad (2.57)$$

One can then perform real-valued SVD of $\tilde{\mathbf{Y}}$ or real-valued EVD of $\tilde{\mathbf{Y}} \tilde{\mathbf{Y}}^H$ to obtain the F dominant left singular vectors \mathbf{U}_s . If \mathbf{C} has full rank F , then \mathbf{U}_s and Ψ span the same subspace. Thus, one can obtain [c.f. (2.54)]:

$$\mathbf{K}_{(n)1} \mathbf{U}_s \Gamma_n \approx \mathbf{K}_{(n)2} \mathbf{U}_s, \quad (2.58)$$

where $\Gamma_n = \mathbf{T} \Omega_n \mathbf{T}^{-1}$, and \mathbf{T} is a non-singular matrix satisfying $\Psi \approx \mathbf{U}_s \mathbf{T}$. The diagonal elements of Ω_n yield estimates of the harmonic frequencies in the n -th dimension.

The resulting N sets of frequency estimates need to be associated to form N -D harmonics. One way is to determine an approximation of the set of common eigenvectors from one of the Γ_n , which is obviously not the best solution, since the choice is arbitrary and may result in discarding information contained in the other $N - 1$ dimensions. To address this issue, a simultaneous Schur decomposition approach was developed in [8] to jointly diagonalize the N matrices Γ_n 's and thereby achieve automatic pairing. Finally, we note that if only a single harmonic mixture (snapshot) is available, the data matrix \mathbf{Y} can be replaced by the N -D smoothed $\tilde{\mathbf{X}}$ in (2.31).

2.4.4 N -D MUSIC

Spectral algorithms such as MUSIC can also be applied for multidimensional spectrum estimation ([1, 24], see also [38], Chapter 9 and references therein). Given the data model in (2.46), the correlation matrix of \mathbf{y}_p is $\mathbf{R} = E[\mathbf{y}_p \mathbf{y}_p^H]$. Assuming that $E[\mathbf{c}_p \mathbf{c}_p^H]$ has full rank F , and collecting $P > \prod_{n=1}^N I_n$ snapshots, we have the finite sample estimate of the covariance matrix

$$\hat{\mathbf{R}} = \frac{1}{P} \sum_{p=1}^P \mathbf{y}_p \mathbf{y}_p^H. \quad (2.59)$$

Performing EVD of $\hat{\mathbf{R}}$, we can split the eigenvectors into a signal subspace of dimension F and a null (noise) subspace of dimension $I - F$ (recall that $I = \prod_{n=1}^N I_n$)

$$\hat{\mathbf{R}} = \mathbf{U}_s \boldsymbol{\Lambda}_s \mathbf{U}_s^H + \mathbf{U}_n \boldsymbol{\Lambda}_n \mathbf{U}_n^H, \quad (2.60)$$

where \mathbf{U}_s spans the signal subspace, \mathbf{U}_n spans the noise subspace, and diagonal matrices $\boldsymbol{\Lambda}_s$ and $\boldsymbol{\Lambda}_n$ contain the corresponding eigenvalues.

Following the N -D spectral MUSIC approach, multidimensional HR can be accomplished by finding the F minima of the following cost function.

$$J(\boldsymbol{\omega}) = \mathbf{a}^H(\boldsymbol{\omega}) \mathbf{U}_n \mathbf{U}_n^H \mathbf{a}(\boldsymbol{\omega}), \quad (2.61)$$

or equivalently in terms of the signal eigenvectors,

$$J(\boldsymbol{\omega}) = \mathbf{a}^H(\boldsymbol{\omega}) (\mathbf{I} - \mathbf{U}_s \mathbf{U}_s^H) \mathbf{a}(\boldsymbol{\omega}), \quad (2.62)$$

over all possible $\boldsymbol{\omega} = [\omega_1, \dots, \omega_N]^T$, where $\mathbf{a}(\boldsymbol{\omega})$ is the Kronecker product of Vandermonde vectors, that is,

$$\mathbf{a}(\boldsymbol{\omega}) = \mathbf{a}_1(\omega_1) \otimes \mathbf{a}_2(\omega_2) \otimes \cdots \otimes \mathbf{a}_N(\omega_N), \quad (2.63)$$

with

$$\mathbf{a}_n(\omega_n) = [1 \ e^{j\omega_n} \ e^{j2\omega_n} \ \dots \ e^{j(I_n-1)\omega_n}]^T. \quad (2.64)$$

To find the minima of (2.62), searching jointly over N -D space by MUSIC is too complex. A reasonable alternative is to implement 1-D algorithms such as root MUSIC to generate estimates of harmonics in individual dimensions, and then use (2.61) or (2.62) to associate the N frequency estimates corresponding to each of the F multidimensional harmonic components ([38], Chapter 9).

In order to implement the 1-D algorithm for the n th dimension, the sample covariance matrices can be computed for each corresponding data block, then they can be averaged over the remaining $N - 1$ dimensions to obtain

$$\hat{\mathbf{R}}_n = \frac{1}{\prod_{m=1, m \neq n}^N I_m} \sum_{i_1=1}^{I_1} \cdots \sum_{i_m=1, m \neq n}^{I_m} \cdots \sum_{i_N=1}^{I_N} \hat{\mathbf{R}}_{i_1, \dots, i_m, \dots, i_N, n}. \quad (2.65)$$

Root MUSIC can be applied with $\hat{\mathbf{R}}_n$ to find preliminary estimates of $(\omega_{1,n}, \omega_{2,n}, \dots, \omega_{F,n})$, and similarly for the other dimensions. The next step is to associate the estimates. One approach is to evaluate (2.62) by exhausting all possible combinations of individual 1-D estimates, and choose the F combinations that yield the smallest values. A second approach is to use F points in the N -D grid as the initial value for a localized gradient algorithm to find the minima of (2.62). The second approach has poorer performance than the first one ([38], Chapter 9).

2.4.5 N -D RARE

In N -D MUSIC, we can implement root MUSIC with the covariance matrix $\hat{\mathbf{R}}_n$ in the n th dimension, for $n = 1, \dots, N$. Another way to decouple the N -D MUSIC parameter estimation problem to individual dimensions is the rank reduction estimator (RARE) method [20]. Instead of searching over the N -D manifold in (2.63), a relaxed optimization problem can be solved by searching over the so-called RARE manifold in each individual dimension. For example, to estimate the harmonics in the first dimension, $(\omega_{1,1}, \omega_{2,1}, \dots, \omega_{F,1})$, the RARE method determines the F minima of (2.62) over

$$\mathbf{a}(\boldsymbol{\omega}) = (\mathbf{a}_1(\omega_1) \otimes \mathbf{I}_{r_1}) \mathbf{b}_1, \quad (2.66)$$

where \mathbf{b}_1 is an arbitrary nonzero vector, $\mathbf{a}_n(\omega_n)$ is defined as in (2.64), and $r_1 = \prod_{n=2}^N I_n$. It is shown in [20] that searching over the RARE manifold is equivalent to finding the F roots of

$$\det \left\{ \mathbf{U}_s^H (\mathbf{I} - \mathbf{T}_1 (\mathbf{T}_1^H \mathbf{T}_1)^{-1} \mathbf{T}_1^H) \mathbf{U}_s \right\} = 0, \quad (2.67)$$

where $\mathbf{T}_1 = \mathbf{a}_1(\omega_1) \otimes \mathbf{I}_{r_1}$.

The harmonic parameters in other dimensions can be estimated similarly. Notice that one can rearrange $\tilde{\mathbf{A}}$ in (2.7) according to (2.5). Thus, the estimation problems for the different dimensions become decoupled.

After estimates for the individual dimensions have been obtained, the association can be done by exhaustive search as described in Section 2.4.4, albeit at high computational complexity when the number of dimensions or the number of harmonics is large. An association method with reduced complexity is presented in [20]. If only a single snapshot is available, a suitable subspace can be extracted directly from (2.33).

2.4.6 Summary

We have described four high-resolution multidimensional HR algorithms: the N -D MDF, unitary ESPRIT, MUSIC, and RARE. The N -D MDF and unitary ESPRIT exploit the

structure of the signal subspace, but in different ways (MDF is explicitly optimized from an identifiability viewpoint). One advantage of MDF is that the N frequency parameters corresponding to the individual dimensions of a given multidimensional harmonic component are associated automatically once the eigenvalue problem is solved. The other three multidimensional HR algorithms generally require an extra association step, which can be both complex and fallible. For example, multidimensional unitary ESPRIT [8] entails a simultaneous Schur decomposition (joint diagonalization) step to attain automatic pairing. While this step improves performance, joint diagonalization algorithms are less efficient than EVD.

If one implements the N -D MUSIC by N -D grid search, no association step is needed, but fine N -D grid search is very complex. Alternatively, 1-D search can be implemented in individual dimensions of the N -D MUSIC spectrum and exhaustive search can then be used for association of the 1-D results. The N -D RARE offers an alternative way to decouple the N -D MUSIC parameter estimation problem to individual dimensions, and a parameter association step is still required.

In terms of estimation performance measured by root mean square error (RMSE), it is shown in [20] that 3-D RARE outperforms 3-D unitary ESPRIT. The numerical examples of the next section demonstrate that the MDF algorithm surpasses some existing ESPRIT-like algorithms and offers comparable performance as that of RARE.

2.5 Numerical Examples

In this section, we present some numerical examples of multidimensional HR. We evaluate various 2-D and 3-D HR algorithms using simulated data, and compare their RMSE estimation performance to the corresponding CRB on standard deviation. The application of multidimensional HR algorithms on channel sounding measurement data is discussed in Section 2.6.

2.5.1 2-D harmonic retrieval (simulated data)

Here we compare the performance of 2-D MDF with that of the matrix enhancement and matrix pencil (MEMP) algorithm [10] and the 2-D ESPRIT-based joint angle and frequency Estimation (JAFE) algorithm [13]. Unlike 2-D MDF, neither MEMP nor JAFE can generally achieve the identifiability bound in Theorem 2.3.2. While identifiability potential *per se* does not imply anything about performance, MDF aims to work with an eigenvalue problem that is as “overdetermined” as possible. Intuitively, this should also yield good performance. This intuition is tested in the sequel.

We consider the recovery of three 2-D frequencies from a single snapshot comprising 20×20 noisy data samples. Throughout this section, SNR is defined as (c.f., (2.40))

$$\text{SNR} = 10 \log_{10} \frac{\|\mathbf{X} - \mathbf{N}\|_F^2}{KL\sigma^2},$$

where $\|\cdot\|_F$ stands for the Frobenius norm, and \mathbf{N} is the noise matrix.

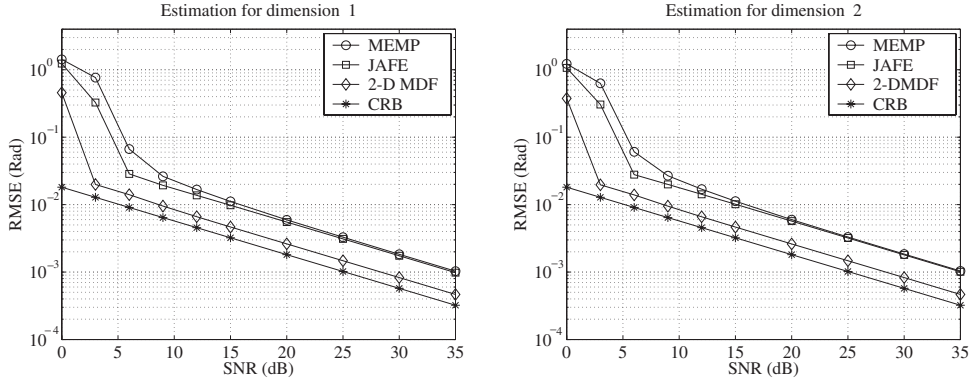


Figure 2.3 Performance comparison of the MDF, MEMP, and JAFE algorithms. Frequencies are distinct in each dimension.

In the first experiment, we test a case where frequencies are distinct in each dimension. The three frequency pairs are chosen as follows

$$\begin{aligned} f = 1 : \quad (\omega_1, v_1) &= (0.42\pi, 0.60\pi), \\ f = 2 : \quad (\omega_2, v_2) &= (0.46\pi, 0.52\pi), \\ f = 3 : \quad (\omega_3, v_3) &= (0.38\pi, 0.56\pi). \end{aligned}$$

Notice that the three 2-D frequencies are too close to each other to be separated by 2-D FFT since the resolution limit for a 20×20 data set is 0.1π . In Figure 2.3, we plot the RMSE of MDF, MEMP, and JAFE for frequency estimation in each dimension. The results for dimension 1 are averaged over ω_1 , ω_2 , and ω_3 , and similarly for dimension 2. The associated CRB on standard deviation is also plotted. The smoothing parameters of MEMP and JAFE were chosen according to [10] and [13], respectively. For JAFE, the optimal choice of parameters depends on whether one optimizes variance along one or the other dimension. The difference is small, so smoothing parameters were set halfway between for balance considerations.

It is seen from Figure 2.3 that the MDF algorithm offers about 5dB SNR advantage over the MEMP and JAFE algorithms, and stays close to CRB for a wide range of SNR, due to the fact that it better exploits model structure.

In the second experiment, we test a case when there are *identical* frequencies along both dimensions. The three frequency pairs are given by

$$\begin{aligned} f = 1 : \quad (\omega_1, v_1) &= (0.52\pi, 0.48\pi), \\ f = 2 : \quad (\omega_2, v_2) &= (0.48\pi, 0.48\pi), \\ f = 3 : \quad (\omega_3, v_3) &= (0.48\pi, 0.44\pi). \end{aligned}$$

Figure 2.4 illustrates the performance comparison of the MDF, MEMP and JAFE algorithms. Again, the MDF algorithm offers about 6–8 dB SNR advantage over the MEMP and JAFE algorithms.

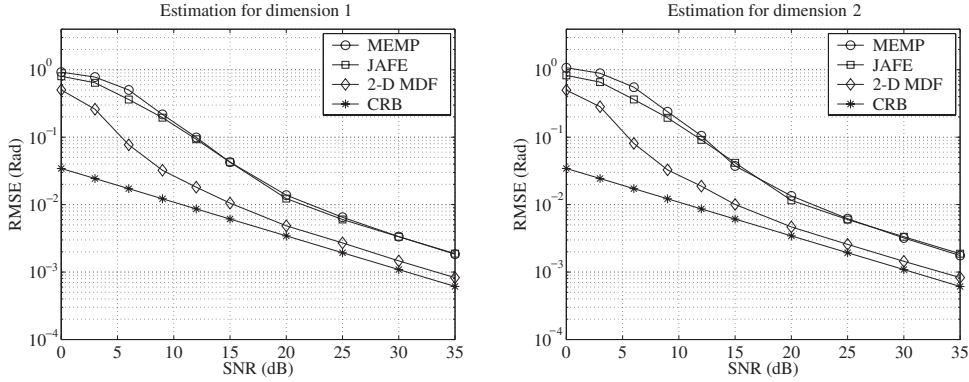


Figure 2.4 Performance comparison of the MDF, MEMP, and JAFE algorithms. Identical frequencies exist in both dimensions.

2.5.2 3-D harmonic retrieval (simulated data)

In this experiment, we compare the 3-D MDF and 3-D RARE algorithms. We apply 3-D MDF and 3-D RARE to estimate three sets of 3-D frequencies from noisy observations of size $6 \times 6 \times 6$. The 3-D frequencies are as follows:

$$\begin{aligned} f = 1 : (\omega_{1,1}, \omega_{1,2}, \omega_{1,3}) &= (0.550\pi, 0.719\pi, 0.906\pi), \\ f = 2 : (\omega_{2,1}, \omega_{2,2}, \omega_{2,3}) &= (0.410\pi, 0.777\pi, 0.276\pi), \\ f = 3 : (\omega_{3,1}, \omega_{3,2}, \omega_{3,3}) &= (0.340\pi, 0.906\pi, 0.358\pi). \end{aligned}$$

For 3-D MDF, the associated parameters are chosen such that $I_{1,1} = I_{2,1} = I_{3,1} = 3$ and $I_{1,2} = I_{2,2} = I_{3,2} = 4$. Figure 2.5 depicts the RMSE of both algorithms for the three individual dimensions. For example, the RMSE results for dimension 2 are obtained by averaging over $\omega_{1,2}$, $\omega_{2,2}$, $\omega_{3,3}$. The RMSE results averaged over all dimensions are also shown.

Figure 2.5 shows that the 3-D MDF and 3-D RARE algorithms provide comparable results in this case. Compared to MDF, a disadvantage of RARE is the need for a separate postprocessing step to associate the parameter estimates in the individual dimensions. Exhaustive search over all associations is used in the simulations. The computational complexity of this association step can be significant if the number of superimposed multidimensional harmonic components and/or the number of dimensions is large.

2.6 Multidimensional Harmonic Retrieval for MIMO Channel Estimation

General techniques of multidimensional HR have a broad range of signal processing and communications applications such as radar [9, 14], passive range-angle localization [28], and

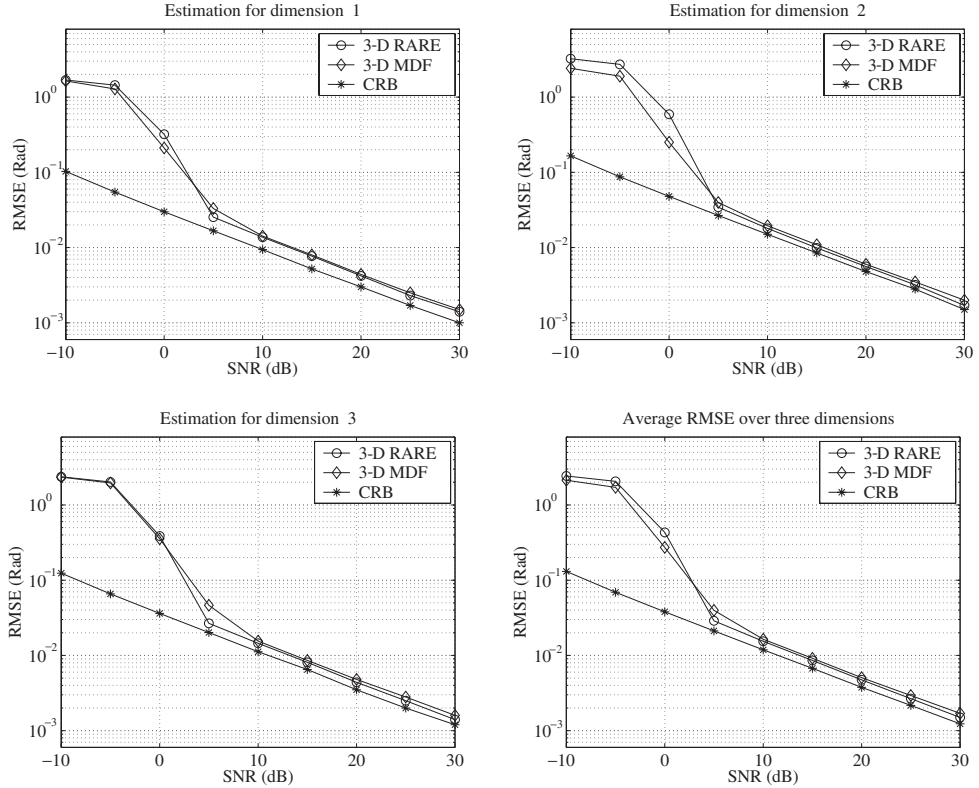


Figure 2.5 RMSE of 3-D MDF and 3-D RARE versus SNR.

wireless channel parameter estimation from sounding data [7, 20, 29, 36]. In this section, we focus on the application of multidimensional HR to parametric channel estimation from MIMO sounding measurements. We will first develop the parametric channel model, then introduce the measurement mechanism, and finally present numerical results.

2.6.1 Parametric channel modeling

Multipath propagation is a key characteristic of radio channels, due to the presence of scatterers in the propagation environment. Multipath not only causes delay spread and thus frequency selectivity at higher data rates but also fading due to incoherent combining even at lower rates. In addition to frequency-selective fading, cellular systems have to cope with time-selective fading due to mobility-induced Doppler shifts.

High rate wireless communication can be achieved by MIMO radio channel access based on dual antenna arrays at both the mobile station (MS) and the base station (BS). When antenna arrays are employed on either end of the radio link, the directional characteristics of the propagation environment assume a more prominent role. For example, if there are preferred transmit directions (due to the presence of dominant scatterers), it makes a lot of

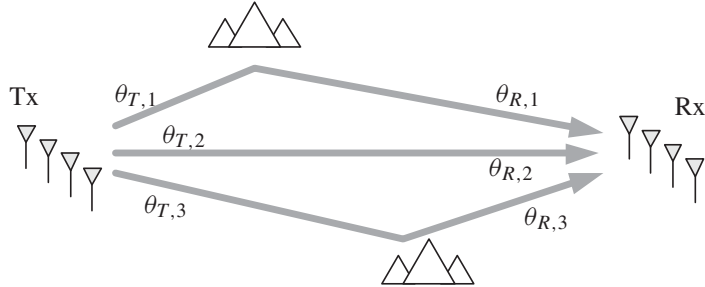


Figure 2.6 Illustration of DD MIMO wireless channels.

sense to tune the transmission along these directions by means of transmit beamforming. It is clear that appropriate spatio-temporal MIMO channel models and model fitting procedures are indispensable tools for the design and performance evaluation of MIMO space-time adaptive links, as well as for service provisioning and infrastructure deployment for cellular radio access systems.

In order to be useful, channel models have to be reasonably realistic on one hand, and parsimonious on the other hand. Parsimony is needed both for simplicity and for effective model fitting. Among the various MIMO radio channel models proposed to date, the DD model [29] appears to strike a good compromise between these two objectives. The premise of the DD-MIMO channel model is that the propagation environment is characterized by a few dominant paths. Each path is parameterized by its direction of departure from the transmitter antenna array, direction of arrival at the receiver antenna array, time-varying complex path loss (incorporating Doppler variation), and delay. An important point is that these paths are *common for all pairs of transmit-receive antenna element*. This assumption is well-justified in practice. When the signal bandwidth is narrow relative to the carrier frequency³, then the channel between any particular (transmit,receive) pair of antenna elements is the superposition of signals from the same dominant paths, except for the introduction of transmit and receive path weights due to displacement-induced phase shifts that depend on the path's departure and arrival directions.

An illustration of the DD MIMO wireless channels is shown in Figure 2.6. Let there be a total of K paths. We will adopt the following notation.

- $\theta_{T,k}$: direction of departure (DOD) of the k th path;
- $\theta_{R,k}$: direction of arrival (DOA) of the k th path;
- τ_k : time delay (lag) of the k th path;
- α_k : Doppler shift frequency for the k th path;
- r_k : complex path loss (including phase shift) of the k th path.

³This assumption is usually justified even for relatively broadband wireless systems.

We will assume that the channel's time-variation is solely due to Doppler shift within the measurement interval; path parameters (including Doppler frequencies) are assumed to be constant within the aforementioned interval. Then, the time-varying impulse response between transmit antenna element m_T and receive antenna element m_R can be written as

$$g(t, \tau, m_R, m_T) = \sum_{k=1}^K r_k e^{j2\pi\alpha_k t} \delta(\tau - \tau_k) e^{j\langle p_R, \theta_{R,k} \rangle} e^{j\langle p_T, \theta_{T,k} \rangle}, \quad (2.68)$$

where p_R denotes the displacement of receive element m_R relative to the reference receive element, $\langle p_R, \theta_{R,k} \rangle$ denotes the projection of this displacement onto the direction of arrival of the k th path, and similarly for p_T , m_T , and $\langle p_T, \theta_{T,k} \rangle$. Taking Fourier transform along the delay (lag) variable τ , assuming an M_R -element receive uniform linear array (ULA) and M_T -element transmit ULA, and uniformly sampling in the time domain with M_t samples, and in the frequency domain with M_f samples, we obtain

$$G(m_t, m_f, m_R, m_T) = \sum_{k=1}^K r_k e^{j2\pi(\alpha_k m_t + \tau_k m_f + \frac{1}{\lambda} d_R m_R \cos \theta_{R,k} + \frac{1}{\lambda} d_T m_T \cos \theta_{T,k})}, \quad (2.69)$$

for $m_t = 0, \dots, M_t - 1$, $m_f = 0, \dots, M_f - 1$, $m_R = 0, \dots, M_R - 1$, and $m_T = 0, \dots, M_T - 1$, where d_R and d_T are the antenna spacing of the receive ULA and the transmit ULA, respectively.

Equation (2.69) shows that channel parameter estimation may be considered as a 4-D HR problem. By fixing a particular dimension, a lower-dimensional HR problem is obtained. For example, if the transmit array geometry does not bring harmonic structure, then we can fix m_t and solve the estimation problem by 3-D HR, while the estimation of DOD can be achieved afterward by other means such as 1-D spectral fitting.

We now generalize the above discussion. In so doing, it is convenient to think of the DD-MIMO channel as being characterized by a four-dimensional (Doppler shift, delay, DOA, DOD) distribution, namely

$$h(\alpha, \tau, \theta_R, \theta_T) = \sum_{k=1}^K r_k \delta(\alpha - \alpha_k) \delta(\tau - \tau_k) \delta(\theta_R - \theta_{R,k}) \delta(\theta_T - \theta_{T,k}). \quad (2.70)$$

Taking Fourier transform along α , τ , θ_R , θ_T , the distribution $h(\alpha, \tau, \theta_R, \theta_T)$ is transformed to the dimensions of time t , frequency f , receive antenna aperture p_R , and transmit antenna aperture p_T , respectively, resulting in the following DD MIMO channel response

$$H(t, f, p_R, p_T) = \sum_{k=1}^K r_k e^{j2\pi\alpha_k t} e^{j2\pi f \tau_k} e^{j\langle p_R, \theta_{R,k} \rangle} e^{j\langle p_T, \theta_{T,k} \rangle}, \quad (2.71)$$

where in the 1-D array case, we have

$$\langle p, \theta \rangle = \frac{2\pi}{\lambda} p_x \cos(\theta), \quad (2.72)$$

where p_x is the displacement in the x -direction. For an M -element, uniform linear array (ULA) with baseline separation d as shown in Figure 2.7, (2.72) can be further written as

$$\langle p_m, \theta \rangle = \frac{2\pi}{\lambda} m d \cos(\theta), \quad m = 0, \dots, M - 1.$$

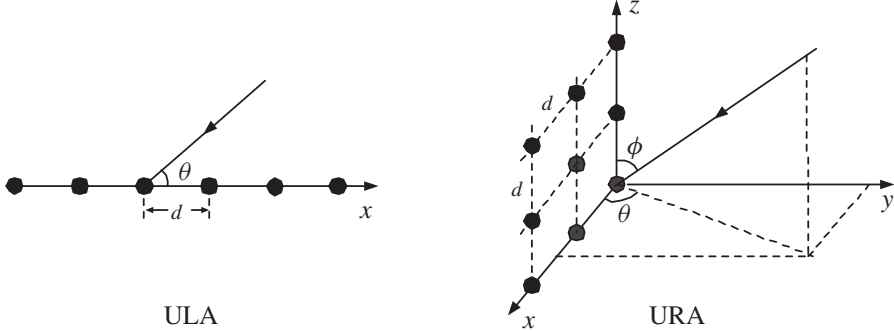


Figure 2.7 Uniform linear array and uniform rectangular array.

Notice that (2.69) can be obtained by plugging the above equation into (2.71), and uniformly sampling in the time and frequency domains.

If 2-D antenna arrays are used, both azimuth and elevation angles may be retrieved. A uniform rectangular array (URA) is shown in Figure 2.7, where θ is azimuth angle and ϕ is elevation angle. In this case, $\langle p, (\theta, \phi) \rangle$ can be written as

$$\langle p, (\theta, \phi) \rangle = \frac{2\pi}{\lambda} [p_x \quad p_y \quad p_z] \begin{bmatrix} \sin \phi \cos \theta \\ \sin \phi \sin \theta \\ \cos \phi \end{bmatrix}. \quad (2.73)$$

Plugging (2.73) into (2.71), a six-dimensional HR problem is then obtained ($p_y = 0$).

2.6.2 MIMO channel sounding

A broadband real-time MIMO channel sounder can measure the time-varying channel in time, frequency, and spatial domains. Propagation parameters, such as delay, Doppler shift, DOA, and DOD, can be estimated from the channel sounding measurement data, which is the discrete counterpart of $H(t, f, p_R, p_T)$ plus noise.

Recently there has been a growing interest in wireless channel sounding, and various measurement campaigns have been conducted [29, 36, 37, 39, 42]. We take the often-used channel sounder RUSK-ATM, manufactured by MEDAV, as an example to explain the mechanism of channel sounding [36]. The RUSK-ATM consists of a mobile transmitter (Tx) and a fixed receiver (Rx), which act as the MS and BS, respectively. It operates at 5.2 GHz and allows real-time measurements of the complex channel impulse response with a bandwidth of 120 MHz. The measurement process relies on periodic multifrequency excitation, real-time sampling, and correlation processing. The resulting $H(t, f, P_R, P_T)$ is obtained by deconvolving the received data in the frequency domain with the known transmitted signal. The excitation period ranges from $t_p = 0.8 \mu s$ to $t_p = 25.6 \mu s$, corresponding to the anticipated maximum channel excess delay.

Fast multiplexing is employed both at the transmit and at the receive antenna array, in order to enable MIMO measurement with only a single RF processing chain at the Tx and Rx ends of the link. Timing and carrier synchronization between Tx and Rx are

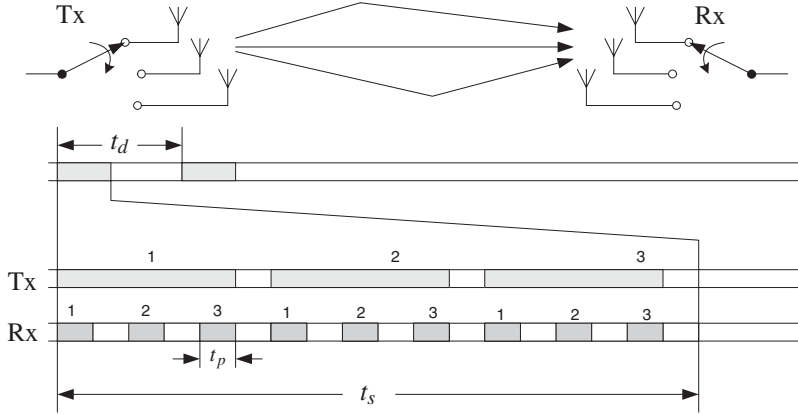


Figure 2.8 Antenna switching in MIMO channel sounding.

attained using well-adjusted Rubidium frequency references. Phase coherence between Tx and Rx can be achieved via a separate optical fiber link. The switching scheme for 3 transmit antennas and 3 receive antennas is shown in Figure 2.8. Switching is synchronized to the signal period t_p . After data acquisition for each Rx antenna, one t_p cycle is used for antenna switching. t_p is usually much longer than the travel time of the wave across the antenna aperture⁴, thus additional compensation is required to make valid array snapshots. In RUSK, this is done by using interpolation filters in multiplexed channels for correct phase alignment.

In Figure 2.8, t_s denotes the time-duration of a complete cycle of transmit–receive measurements comprising a measurement snapshot, and t_d is the snapshot period. The channel’s delay profile (equivalently, frequency response) is measured over the t_p time scale. With $t_p = 3.2 \mu\text{s}$, a complete MIMO snapshot will take $t_s = 2t_p M_T M_R = 57.6 \mu\text{s}$ to acquire if three transmit antennas and three receive antennas are used. Time-variation due to Doppler shift is captured over the much longer baseline $t_d > t_s$. For example, if MIMO snapshots are taken every 20 ms, then the maximum resolvable Doppler shift is 25 Hz.

2.6.3 Examples of 3-D MDF applied to measurement data

Measured data in urban environment

The measured data used for this test was obtained from a MIMO channel sounding campaign conducted at the campus of Ilmenau Technical University in an urban environment [23]. Measurements were taken using the vector channel sounder RUSK-ATM operating at a carrier frequency of 5.2 GHz. The transmitted signal power was 27 dBm and its bandwidth was 120 MHz. At the transmitter (the mobile station), an omnidirectional 16 element uniform circular array (UCA) was used, with interelement spacing of 0.38λ , mounted at a height of

⁴The travel time is equal to the ratio of the aperture length and the light speed. For the problem considered here, it is around a nanosecond.

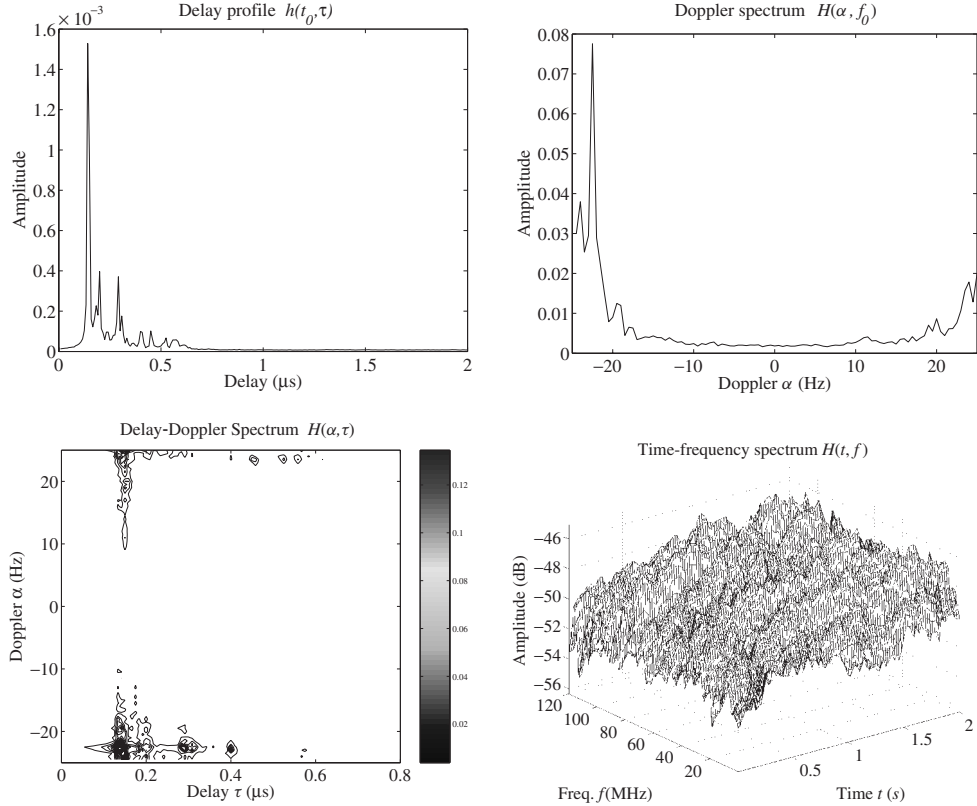


Figure 2.9 Spatially averaged channel impulse response in an urban environment.

1.2 m above ground level. At the receiver, an 8-element ULA with interelement spacing 0.49λ was mounted at height 1.2 m as well.

The receive array looks into a passage leading to a large courtyard where the mobile station is placed. The courtyard is completely enclosed by a building of height about 15 m. The mobile station is moving at about 5 km/h, which corresponds to a maximum Doppler shift of 24 Hz. MIMO sounding snapshots were taken every $t_d = 20$ ms, which corresponds to a maximum resolvable Doppler spread of 25 Hz. The data used here cover a time period of 2 s, during which the mobile station moved about 2.7 m. Various descriptions of the channel impulse response can be obtained by Fourier transform along time t and/or delay τ , as shown in Figure 2.9. The delay profile is obtained by averaging over all transmit and receive antennas in a single snapshot ($t = t_0$). The Doppler spectrum is averaged over all transmit and receive antennas for a single frequency ($f = f_0$). The delay-Doppler spectrum and time-frequency spectrum are spatially averaged over all transmit and receive antennas.

Assuming a 3-D mixture model with three harmonic components for $H(t, f, p_R, p_T)$ with a fixed p_T , we apply 3-D MDF to jointly estimate path delay, DOA, and Doppler shift, as well as complex path amplitude while fixing a transmit antenna. The number

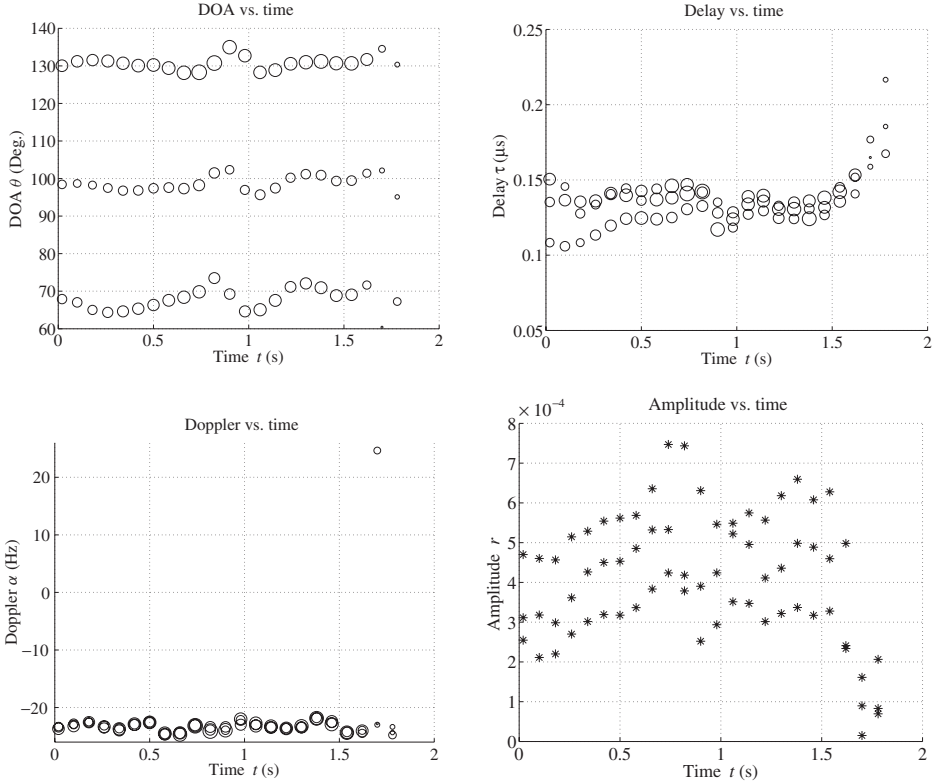


Figure 2.10 Results of 3-D MDF applied to measurement data for urban environment: parameters of three dominant paths as functions of time (snapshots).

of samples in the time domain is 10 (measurement snapshots). Multipath parameters are assumed to be approximately constant during this period. The number of samples in the frequency domain is 30. Hence, 3-D MDF is applied directly to a data block of size $10 \times 30 \times 8$. DOD is not estimated via HR because a UCA is used at the transmitter, rendering the DOD dimension nonharmonic. Results of 3-D MDF estimation are shown in Figures 2.10 and 2.11. The diameter of the buttons reflects the relative amplitude of the corresponding multipath components. Figure 2.10 depicts the evolution of multipath parameters for the three dominant paths as functions of time (we shift the 10-snapshot window along the time domain). Figure 2.11 illustrates the association of the parameters for a fixed 10-snapshot data segment, for all possible combinations of delay, DOA, and Doppler shift.

Practical antenna arrays suffer from various impairments, such as mechanical or electrical manufacturing tolerances, antenna element coupling, and phase mismatch in antenna feeding. These imperfections can have a negative impact on the performance of parametric estimation algorithms, such as MDF or any other of the aforementioned algorithms. To address this problem, an antenna calibration procedure is usually necessary, for example, see [27]. In calibration, the antenna array response is measured in a tightly controlled environment, and

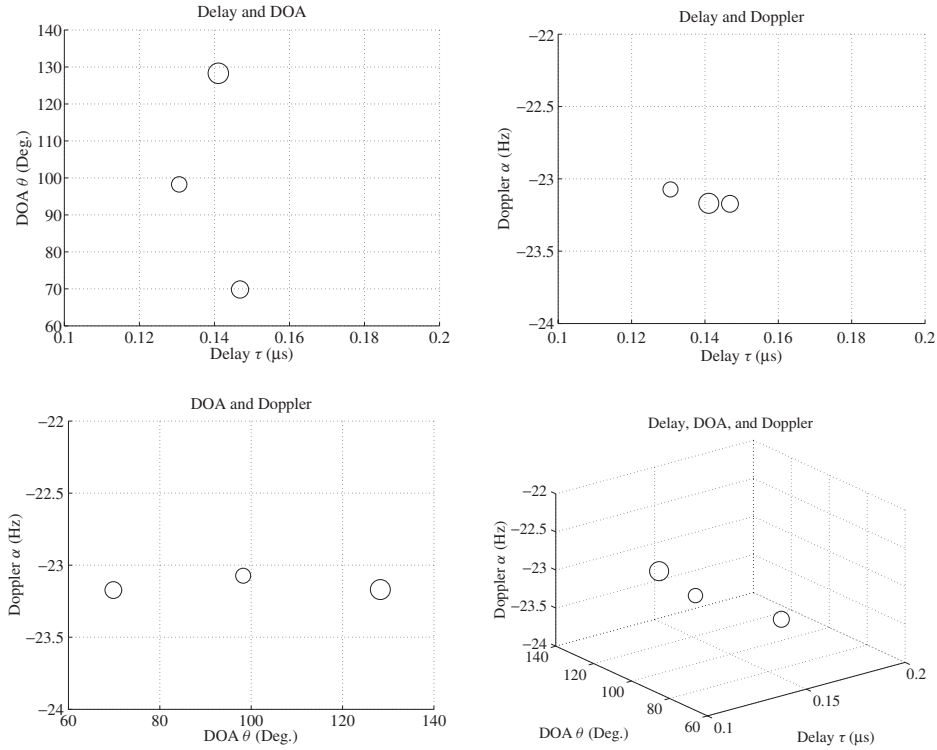


Figure 2.11 Results of 3-D MDF applied to measurement data for urban environment and a fixed 10-snapshot time segment.

a suitable calibration matrix is designed to compensate for the impairments. Calibration can help improve the quality of parameter estimates (e.g., [20, 36]), but the associated information is not publicly available for the datasets considered here.

Measured data in suburban environment

Another set of MIMO measurement data is now tested. The measurement campaign took place at a suburban area of a small town north of Vienna [6]. In this case, the channel sounder RUSK-ATM was operating at a carrier frequency of 2 GHz with an output power of 2 Watts and a transmitted signal bandwidth of 120 MHz. At the mobile station, an omnidirectional 15-element UCA was used, with interelement spacing of 0.43λ , mounted on a small trolley at a height of 1.5 m above ground. An 8-element ULA with half wavelength spacing was used at the receiver. To simulate a typical base station position, the receiver was lifted up at a height of about 20 m above ground, much higher than anything in the surroundings. Therefore, line-of-sight propagation is highly likely. The MS is moving at about 3 km/h to 6 km/h.

MIMO sounding snapshots were taken every $t_d = 21$ ms. The sample data used here cover a time period of about 5 s. Again, various coarse descriptions of the spatially averaged

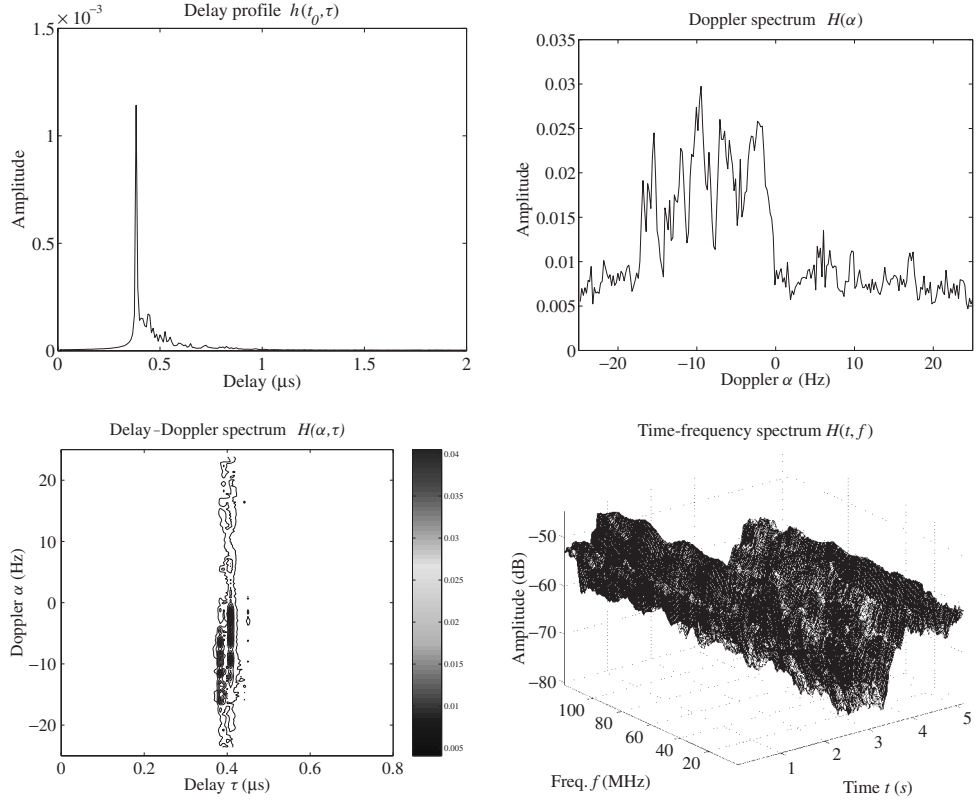


Figure 2.12 Spatially averaged channel impulse response in a suburban environment.

channel impulse response can be obtained by Fourier transform along time t and/or delay τ dimensions, as shown in Figure 2.12.

We apply 3-D MDF to data segments each of duration 0.21 s, for a fixed transmit antenna. Again, the goal is to jointly estimate delay, DOA, Doppler shift, and the corresponding complex amplitude for each path. Figures 2.13 and 2.14 show the estimation results.

2.7 Concluding Remarks

This chapter has reviewed multidimensional HR and its application to multipath parameter estimation in MIMO wireless channel sounding. On the theory side, emphasis has been placed on model identifiability analysis. An algebraic algorithm stemming from a constructive proof of the main identifiability result provides a good alternative to other multidimensional HR algorithms reviewed in this chapter.

Theorem 2.3.3 offers the most relaxed identifiability conditions to date for multidimensional HR. However, fundamental questions remain: Are there even better bounds to be found? Is it possible to establish sufficient and necessary conditions on the identifiability

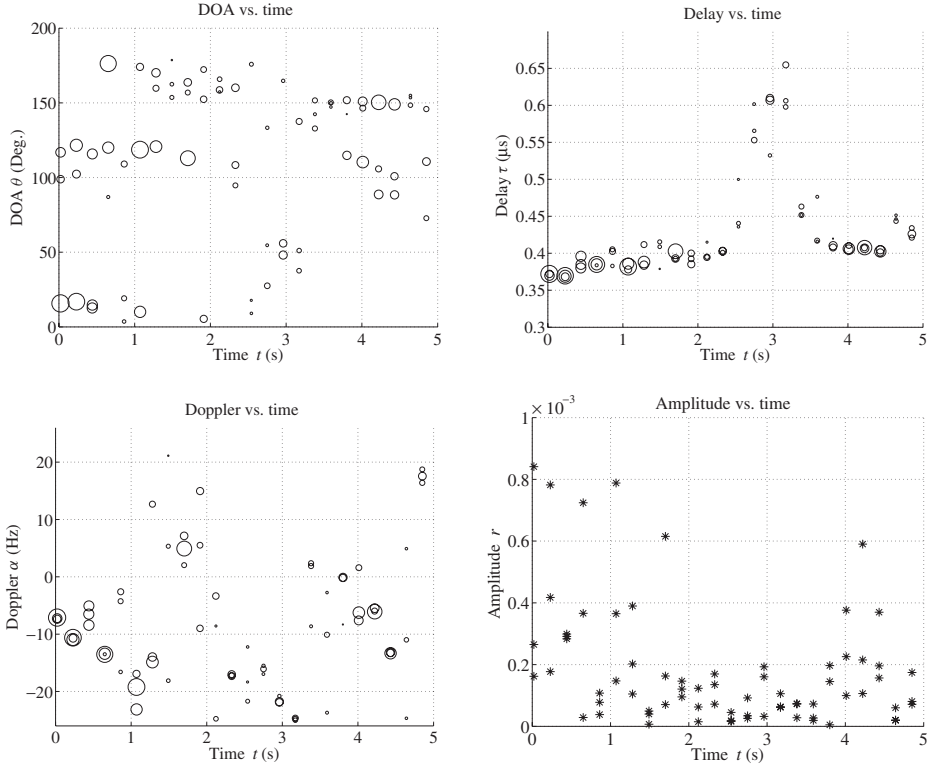


Figure 2.13 Results of 3-D MDF applied to measurement data for suburban environment: parameters of three dominant paths as functions of time (snapshots).

bound? In addition, since the identifiability results in Theorem 2.3.3 were derived for a single snapshot of harmonic mixture, it would be interesting to see how these results change when multiple snapshots are considered, which is a topic under investigation.

In the 2-D case, we note that there are KL equations versus $3F$ unknowns in (2.1), while the bound in Theorem 2.3.2 is approximately $KL/4$. This indicates that stronger identifiability results for 2-D HR may be possible, but will not add substantially to the existing result. The situation may be different in higher dimensions because the bound in Theorem 2.3.3, while still proportional to the total sample size, includes a $1/2^N$ penalty factor – thus being further away from equations-versus-unknowns considerations. While counting “degrees of freedom” can be misleading in the context of nonlinear equations, this still indicates that better results may be possible.

In the constructive proof of Theorem 2.3.2, the data matrix \mathbf{X} given in (2.2) is smoothed along both dimensions to obtain matrix $\tilde{\mathbf{X}} = \mathbf{G}\mathbf{C}\mathbf{H}^T$ in such a way that \mathbf{G} and \mathbf{H} are Khatri–Rao products of two Vandermonde matrices with generators being the harmonics. To derive a stronger identifiability condition, one may wonder if it is possible to optimize the above smoothing procedure to achieve even better bounds. Notice that the Khatri–Rao product of two Vandermonde matrices can be extended to a Khatri–Rao product of three

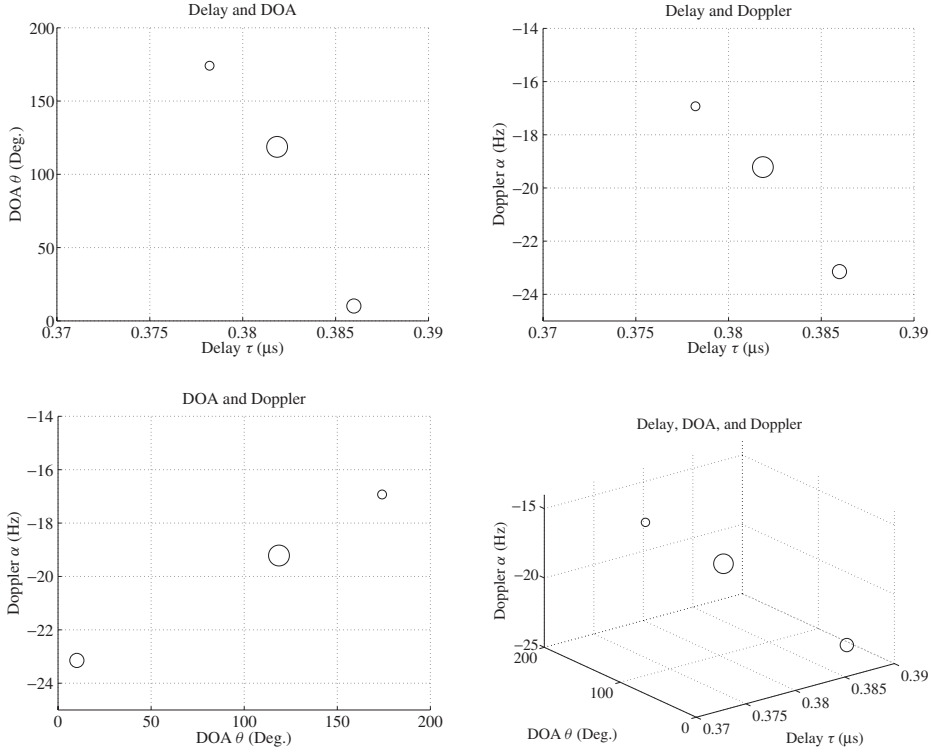


Figure 2.14 Results of 3-D MDF applied to measurement data for suburban environment and a fixed 10-snapshot time segment.

or more Vandermonde matrices by data smoothing. For example, given $\mathbf{G} = \mathbf{A} \odot \mathbf{B}$, where \mathbf{A} is Vandermonde of size $I \times F$ and \mathbf{B} is Vandermonde of size $J \times F$, a matrix $\tilde{\mathbf{G}} = \mathbf{B}_1 \odot \mathbf{A} \odot \mathbf{B}_2$ can be obtained by smoothing along the row dimension of \mathbf{G} , where \mathbf{B}_1 and \mathbf{B}_2 are submatrices of \mathbf{B} consisting of its first J_1 and J_2 rows, respectively, and $J_1 + J_2 = J - 1$. The size of $\tilde{\mathbf{G}}$ is now $I J_1 J_2 \times F$, which is larger than $I J \times F$, the size of \mathbf{G} . However, linear dependent rows may be introduced into $\tilde{\mathbf{G}}$ during this process, hence its full rank becomes an issue. Notice that this is equivalent to extending a two-way data set to a three-way array, then folding back to a large two-way array, and the process can go on to N -way arrays folded back to a two-way array recursively. How to optimize the dimension extension for given I and J , or in general, for given I_n 's in the case of N -D HR, is still an open question.

Acknowledgments

This chapter draws upon research supported by the U.S. Army Research Office under grant DAAD19-03-1-0228 and the Collaborative Technology Alliance for Communications and Networks sponsored by the U.S. Army Research Laboratory under Cooperative Agreement

DAAD19-01-2-0011. Channel sounder measurement data used in this chapter are provided courtesy of MEDAV, Germany (<http://www.channelsounder.de>), and *ftw.*, Vienna, Austria (<http://www.ftw.at/MIMO/Measurements>). X. Liu would like to acknowledge Prof. X. Ma for insightful discussions with her on the material presented in this chapter and beyond.

References

- [1] G. Bienvenu and L. Kopp, "Adaptivity to background noise spatial coherence for high resolution passive methods," in *Proceedings of the IEEE International Conference on Acoustics, Speech, and Signal Processing*, Denver, CO, pp. 307–310, Apr. 1980.
- [2] C. Carathéodory and L. Fejér, "Über den Zusammenhang der Extremen von harmonischen Funktionen mit ihren Koeffizienten und über den Picard-Landauschen Satz," *Rend. Circolo Matematico Palermo*, vol. 32, pp. 218–239, 1911.
- [3] M. P. Clark and L. L. Scharf, "Two-dimensional modal analysis based on maximum likelihood," *IEEE Trans. Signal Process.*, vol. 42, no. 6, pp. 1443–1452, Jun. 1994.
- [4] R. B. Ertel, P. Cardieri, K.W. Sowerby, T. S. Rappaport, and J. H. Reed, "Overview of spatial channel models for antenna array communication systems," *IEEE Pers. Commun.*, vol. 5, pp. 10–22, Feb. 1998.
- [5] G. J. Foschini, "Layered space-time architectures for wireless communications in a fading environment," *Bell Labs Tech. J.*, pp. 41–59, 1996.
- [6] *ftw.*'s MIMO measurements, online documentation and selected data sets are available for download at <http://www.ftw.at/MIMO/Measurements>, 2004.
- [7] M. Haardt, C. Brunner, and J. H. Nossek, "Efficient high-resolution 3-D channel sounding," in *Proceedings of the IEEE Vehicular Technology Conference*, vol. 1, pp. 164–168, May 1998.
- [8] M. Haardt and J. A. Nossek, "Simultaneous Schur decomposition of several nonsymmetric matrices to achieve automatic pairing in multidimensional harmonic retrieval problems," *IEEE Trans. Signal Process.*, vol. 46, no. 1, pp. 161–169, Jan. 1998.
- [9] Y. Hua, "High resolution imaging of continuously moving object using stepped frequency radar," *Signal Process.*, vol. 35, no. 1, pp. 33–40, Jan. 1994.
- [10] Y. Hua, "Estimating two-dimensional frequencies by matrix enhancement and matrix pencil," *IEEE Trans. Signal Process.*, vol. 40, no. 9, pp. 2267–2280, Sep. 1992.
- [11] T. Jiang, N. D. Sidiropoulos, and J. M. F. ten Berge, "Almost-sure identifiability of multidimensional harmonic retrieval," *IEEE Trans. Signal Process.*, vol. 49, no. 9, pp. 1849–1859, Sep. 2001.
- [12] K. Kalliola, H. Laitinen, P. Vainikainen, M. Toeltsch, J. Laurila, and E. Bonek, "3-D double-directional radio channel characterization for urban macrocellular applications," *IEEE Trans. Antennas Propag.*, vol. 51, no. 11, pp. 3122–3133, Nov. 2003.
- [13] A. N. Lemma, A.-J. van der Veen, and E. F. Deprettere, "Analysis of ESPRIT based joint angle-frequency estimation," in *Proceedings of the IEEE International Conference on Acoustics, Speech, and Signal Processing*, vol. 5, Istanbul, Turkey, pp. 3053–3056, Jun. 2000.
- [14] J. Li, P. Stoica, and D. Zheng, "An efficient algorithm for two-dimensional frequency estimation," *Multidim. Syst. Signal Process.*, vol. 7, no. 2, pp. 151–178, Apr. 1996.
- [15] X. Liu and N. D. Sidiropoulos, "Almost sure identifiability of multidimensional constant modulus harmonic retrieval," *IEEE Trans. Signal Process.*, vol. 50, no. 9, pp. 2366–2368, Sep. 2002.
- [16] X. Liu and N. D. Sidiropoulos, "On constant modulus multidimensional harmonic retrieval," in *Proceedings of the IEEE International Conference on Acoustics, Speech, and Signal Processing*, vol. 3, Orlando, FL, pp. 2977–2980, May 2002.

- [17] X. Liu, N. D. Sidiropoulos, and A. Swami, “Code-blind reception of frequency hopped signals over multipath fading channels,” in *Proceedings of the IEEE International Conference on Acoustics, Speech, and Signal Processing*, vol. IV, Hongkong, China, pp. 592–595, Apr. 2003.
- [18] X. Liu, N. D. Sidiropoulos, and A. Swami, “Blind high resolution localization and tracking of multiple frequency hopped signals,” *IEEE Trans. Signal Process.*, vol. 50, no. 4, pp. 889–901, Apr. 2002.
- [19] K. N. Mokios, N. D. Sidiropoulos, M. Pesavento, and C. F. Mecklenbräuker, “On 3-D harmonic retrieval for wireless channel sounding,” in *Proceedings of the International Conference on Acoustics, Speech, and Signal Processing*, vol. II, Montreal, Quebec, Canada, pp. 89–92, May 2004.
- [20] M. Pesavento, C. F. Mecklenbräuker, and J. F. Böhme, “Multidimensional rank reduction estimator for parametric MIMO channel models,” *EURASIP J. Appl. Signal Process.*, vol. 2004, no. 9, pp. 1354–1363, 2004.
- [21] V. F. Pisarenko, “The retrieval of harmonics from a covariance function,” *Geophys. J. R. Astron. Soc.*, vol. 33, pp. 347–366, 1973.
- [22] R. Roy and T. Kailath, “ESPRIT-estimation of signal parameters via rotational invariance techniques,” *IEEE Trans. Acoust. Speech Signal Process.*, vol. 37, no. 7, pp. 984–995, July 1989.
- [23] RUSK channel sounding measurements, online documentation and selected data sets from various measurement campaigns are available for download at <http://www.channelsounder.de>, 2004.
- [24] R. O. Schmidt, “Multiple emitter location and signal parameter estimation,” in *Proceedings of the RADC Spectral Estimation Workshop*, Rome, NY, pp. 243–258, 1983.
- [25] N. D. Sidiropoulos, “Generalizing Carathéodory’s uniqueness of harmonic parameterization to N dimensions,” *IEEE Trans. Inf. Theory*, vol. 47, no. 4, pp. 1687–1690, May 2001.
- [26] N. D. Sidiropoulos and R. Bro, “On the uniqueness of multilinear decomposition of N-way arrays,” *J. Chemometr.*, vol. 14, no. 3, pp. 229–239, May 2000.
- [27] G. Sommerkorn, D. Hampicke, R. Klukas, A. Richter, A. Schneider, and R. Thomä, “Uniform rectangular antenna array design and calibration issues for 2-D ESPRIT application,” in *Proceedings of the 4th European Personal Mobile Communications Conference (EPMCC’01)*, Vienna, Austria, Feb. 2001.
- [28] D. Starer and A. Nehorai, “Passive localization of near-field sources by path following,” *IEEE Trans. Signal Process.*, vol. 42, no. 3, pp. 677–680, Mar. 1994.
- [29] M. Steinbauer, A. F. Molisch, and E. Bonek, “The double-directional radio channel,” *IEEE Antennas Propag. Mag.*, vol. 43, no. 4, pp. 51–63, Aug. 2003.
- [30] P. Stoica and A. Nehorai, “MUSIC, maximum likelihood, and Cramér-Rao bound,” *IEEE Trans. Acoust. Speech Signal Process.*, vol. 37, no. 5, pp. 720–741, May 1989.
- [31] P. Stoica and R. L. Moses, *Introduction to Spectral Analysis*. Upper Saddle River, NJ: Prentice-Hall, 1997.
- [32] P. Stoica and T. Söderström, “Parameter identifiability problem in signal processing,” *Proc. Inst. Elect. Eng. F–Radar Sonar Navigat.*, vol. 141, pp. 133–136, 1994.
- [33] A. Swindlehurst and T. Kailath, “Algorithms for azimuth/elevation direction finding using regular array geometries,” *IEEE Trans. Aerosp. Electron. Syst.*, vol. 29, no. 1, pp. 145–156, Jan. 1993.
- [34] A. Swindlehurst, B. Ottersten, R. Roy, and T. Kailath, “Multiple invariance ESPRIT,” *IEEE Trans. Signal Process.*, vol. 40, no. 4, pp. 868–881, Apr. 1992.
- [35] V. Tarokh, N. Sheshadri, and A. R. Calderbank, “Space-time codes for high data rate wireless communications: performance criterion and code construction,” *IEEE Trans. Inf. Theory*, vol. 44, no. 3, pp. 744–765, Mar. 1998.

- [36] R. S. Thomä, D. Hampicke, A. Richter, G. Sommerkorn, A. Schneider, U. Trautwein, and W. Wirnitzer, "Identification of time-variant directional mobile radio channels," *IEEE Trans. Instrum. Meas.*, vol. 49, no. 2, pp. 357–364, Apr. 2000.
- [37] P. Truffer and P. E. Leuthold, "Wide-band channel sounding at 24 GHz based on a novel fiber-optic synchronization concept," *IEEE Trans. Microw. Theory Tech.*, vol. 49, no. 4, pp. 692–700, Apr. 2001.
- [38] H. L. Van Trees, *Optimum Array Processing (Detection, Estimation, and Modulation Theory, Part IV)*. New York: Wiley, 2002.
- [39] P. F. Wilson, P. B. Papazian, M. G. Cotton, Y. Lo, and S. C. Bundy, "Simultaneous wide-band four-antenna wireless channel-sounding measurements at 1920 MHz in a suburban environment," *IEEE Trans. Veh. Tech.*, vol. 50, no. 1, 67–78, Jan. 2001.
- [40] H. Yang and Y. Hua, "On rank of block Hankel matrix for 2-D frequency detection and estimation," *IEEE Trans. Signal Process.*, vol. 44, no. 4, pp. 1046–1048, Apr. 1996.
- [41] M. D. Zoltowski, M. Haardt, and C. P. Mathews, "Closed-form 2-D angle estimation with rectangular arrays in element space or beamspace via unitary ESPRIT," *IEEE Trans. Signal Process.*, vol. 44, pp. 316–328, Feb. 1996.
- [42] T. Zwick, D. Hampicke, A. Richter, G. Sommerkorn, R. Thomä, and W. Wiesbeck, "A novel antenna concept for double-directional channel measurements," *IEEE Trans. Veh. Tech.*, vol. 53, no. 2, pp. 527–537, Mar. 2004.

3

Certain Computations Involving Complex Gaussian Matrices with Applications to the Performance Analysis of MIMO Systems

Ming Kang, Lin Yang, and Mohamed-Slim Alouini

3.1 Introduction

Multiple antenna systems, also known as *multiple-input-multiple-output* (MIMO) systems, have been widely accepted as a promising technology for high data-rate communications [1–3]. Performance measures of MIMO systems, such as the channel mutual information rate, the outage probability, the channel capacity, and/or the MIMO diversity combining performance, are closely related to the distribution of the eigenvalues of certain Hermitian matrices derived from complex Gaussian matrices. The complex Gaussian matrix is of particular interest because channel coefficients of wireless fading channels are often modeled as complex Gaussian processes because of constructive and/or destructive additions of signal copies arriving at the receiver from different paths. Previous work studying the performance of MIMO systems often assumed that the number of antennas is large and as such used an asymptotic study as an indication to the actual system performance. The techniques for such asymptotic studies are well developed and have been successfully used for the performance of large code-division-multiple-access (CDMA) systems.

On the other hand, practical wireless systems can afford often no more than a handful of antennas because of cost, size, and complexity limitations. For such MIMO systems with

a finite number of antennas, the analytical techniques are relatively less well known. In this chapter, we first illustrate by some examples that many times the statistical performance analysis of MIMO systems falls into a similar calculation problem. We then compile and develop techniques involved in such calculations. We show by further examples how other seemingly irrelevant problems can be solved by this technique if we properly adjust the integrand function and the integration regions. Finally, some extensions to the techniques are given for more complicated scenarios in which multiple and possibly correlated cochannel interferers exist.

These expressions can be useful in two ways. First, most of them are in terms of special functions built in well-known software packages such as Mathematica, Matlab, and Maple. Therefore, they can be used to calculate exact results to generate performance curves without resorting to time-consuming Monte Carlo simulations. Second, although the expressions are in a seemingly complicated determinant form, they can often be further manipulated to investigate the effect of system parameters on the performance. This is often done by relating performance measures of more complicated MIMO channels to those of independent and identically distributed Rayleigh channels. For example, as will be shown in the body of this chapter, the outage probability of MIMO beamforming over Rician channels is lower bounded by that over Rayleigh channels multiplied by $e^{-\text{tr}(\mathbf{M}\mathbf{M}^H)/\sigma^2}$, where tr is the trace operator, \mathbf{M} is the channel mean matrix, and σ^2 is the variance of channel coefficients. It is further shown that the same relationship is true between the mutual information moment-generating function of MIMO Rician channels and that of the MIMO Rayleigh channels. We believe that further manipulations on the presented exact results can lead to some other interesting approximations.

The remainder of this chapter is organized as follows. Section 3.2 describes MIMO fading channel models and presents some important transmission schemes for MIMO systems as well as their performance measures. Section 3.3 briefly reviews preliminary concepts and definitions of multivariate statistical distributions. Section 3.4 provides the mathematical formulation and detailed calculations. Finally, Section 3.5 ends the chapter with a brief summary and some concluding remarks.

3.2 Performance Measures of Multiple Antenna Systems

3.2.1 Noise-limited MIMO fading channels

System and channel models

A MIMO channel with T transmit antennas and R receive antennas can be modeled by

$$\mathbf{y} = \mathbf{Hx} + \mathbf{n}, \quad (3.1)$$

where $\mathbf{y} \in \mathbb{C}^R$ (\mathbb{C}^R denotes the vector space containing all $R \times 1$ complex vectors) is the output, $\mathbf{x} \in \mathbb{C}^T$ the input vector with the power constraint

$$\text{tr} \left(E \left(\mathbf{x} \mathbf{x}^H \right) \right) \leq \Omega, \quad (3.2)$$

where the superscript H stands for the conjugate transpose operator, $E(\cdot)$ the expectation, $\mathbf{H} \in \mathbb{C}^{R \times T}$ the channel matrix with the entry at the i th row and the j th column, $\{\mathbf{H}\}_{i,j}$,

being the complex channel coefficient between the j th transmit antenna and the i th receive antenna, and $\mathbf{n} \in \mathbb{C}^R$ is the additive complex Gaussian noise vector with zero mean and covariance matrix $\sigma_n^2 \mathbf{I}_R$, where \mathbf{I}_R denotes the $R \times R$ identity matrix.

In this chapter, we consider MIMO channels that are subject to frequency-flat fading. Therefore, \mathbf{H} is a random matrix that is often assumed to be complex Gaussian, that is, its probability density function (PDF) is given by

$$\pi^{-RT} |\Sigma_R|^{-T} |\Sigma_T|^{-R} \exp\left(-\text{tr}\left(\Sigma_R^{-1}(\mathbf{H} - \mathbf{M}) \Sigma_T^{-1}(\mathbf{H} - \mathbf{M})^H\right)\right), \quad (3.3)$$

where $|\cdot|$ denotes the determinant and $(\cdot)^{-1}$ is the matrix inversion.

Some common fading scenarios include:

- *Rayleigh* fading is often used to model non-line-of-sight (NLOS) scattering channels. For Rayleigh MIMO channels, the channel matrix \mathbf{H} is of zero mean, that is, $\mathbf{M} = \mathbf{0}$ in (3.3).
- When there is a line-of-sight path between the transmitter and receiver, the channel matrix \mathbf{H} has nonzero mean matrix, that is, $\mathbf{M} \neq \mathbf{0}$. Such channels are said to be *Rician* faded.
- Fading correlation often arises when there is no enough spatial separation between antennas and/or lack of scattering. It was pointed out that for GHz communication systems, the antenna decorrelation distance can range from a few centimeters in a rich scattering environment to several hundred meters in a lack-scattering environment [4]. In (3.3), the correlation is of the particular form of $\Sigma_R \otimes \Sigma_T$, where \otimes stands for the Kronecker product [5]. Note that the Kronecker-product covariance model is shown by experimental tests to be a good model for MIMO channels with a small number of antennas [6] but not as accurate for larger antenna arrays [7]. Σ_R can be viewed as the covariance matrix among receive antennas and Σ_T the covariance matrix among transmit antennas. We say the fading channels are fully (spatially) correlated when both Σ_R and Σ_T are nonidentity Hermitian positive semidefinite matrices. The channel is said to be semicorrelated when one of the two covariance matrices is an identity matrix. When both of them are identity matrices, the channel is (spatially) uncorrelated (and therefore independent for Gaussian matrices).

Mutual information

If the receiver knows the channel realization, the mutual information (MI) between the input and the output under the transmission power constraint $\text{tr}(E(\mathbf{x}\mathbf{x}^H)) \leq \Omega$ is maximized when \mathbf{x} is of zero mean circularly symmetric complex Gaussian vector with the optimum choice of covariance matrix \mathbf{Q} and the MI is then given by [3]

$$\mathcal{I} = \log_2 \det\left(\mathbf{I}_R + \frac{1}{\sigma_n^2} \mathbf{H} \mathbf{Q} \mathbf{H}^H\right) \text{ bps/Hz.} \quad (3.4)$$

When the channels are independent and identically distributed (i.i.d.) Rayleigh faded, that is, the channel matrix \mathbf{H} has i.i.d. entries from the complex Gaussian distribution with zero

mean and variance σ^2 , and if the channel realization is unknown at the transmitter, the optimum choice of $\mathbf{Q} = \frac{\Omega}{T}\mathbf{I}_T$, and the resulting MI is therefore [3]

$$\begin{aligned}\mathcal{I} &= \log_2 \det \left(\mathbf{I}_R + \frac{\Omega}{T\sigma_n^2} \mathbf{H}\mathbf{H}^H \right) \\ &= \sum_{i=1}^{\min(T, R)} \log_2 (1 + \rho\phi_i) \text{ bps/Hz},\end{aligned}\quad (3.5)$$

where $\rho = \frac{\Omega}{T\sigma_n^2}$, ϕ_i , $i = 1, \dots, s = \min(T, R)$, are the nonzero eigenvalues of the Hermitian matrix $\mathbf{H}\mathbf{H}^H$. We further define at this point $t = \max(T, R)$ for future use. This equal power transmission of multiple complex Gaussian data streams is also referred to as the equal power transmission scheme. It was shown that this equal power transmission is a robust transmission scheme for the correlated or Rician fading channels in the sense that it maximizes the worst-case capacity [8–10].

Interesting performance measures include the average MI and the distribution function of MI. The average MI is primarily used to describe ergodic channels, that is, all channel realizations will be taken during each channel use. On the other hand, nonergodic channels (i.e., the channel is randomly drawn but remains fixed for the whole channel use) often use the cumulative distribution function (CDF) of the MI (i.e., the MI outage probability) to indicate the probability that the channel fails to support a given rate threshold. Exact expressions for the CDF of MI are difficult to derive, even for the simplest case of the i.i.d. Rayleigh faded MIMO channels. The mean MI for the i.i.d. Rayleigh case was obtained by Telatar in [3] but it is difficult to extend the result to more complicated fading scenarios. Instead, we can first derive the moment generating function (MGF) of the MI defined by

$$\begin{aligned}\mathcal{M}_{\mathcal{I}}(\tau) &= E_{\mathbf{H}} \left(e^{\tau\mathcal{I}} \right) = \int_{0 < \phi_1 < \dots < \phi_s < \infty} \prod_{k=1}^s (1 + \rho\phi_k)^{\tau/\ln(2)} \\ &\quad \times f_{\phi_1, \dots, \phi_s}(\phi_1, \dots, \phi_s) d\phi_1 \dots d\phi_s,\end{aligned}\quad (3.6)$$

where $\phi_1 < \dots < \phi_s$ are the ordered nonzero eigenvalues of the Hermitian matrix $\mathbf{H}\mathbf{H}^H$ and $f_{\phi_1, \dots, \phi_s}(\phi_1, \dots, \phi_s)$ is their joint PDF. The reason is that all the moments can be obtained in a straightforward manner once the MGF is obtained. It is also possible to obtain the CDF by the numerical evaluation of the inverse Fourier transform.

3.2.2 MIMO channels in the presence of cochannel interference

System and channel models

In a MIMO channel with T antennas at the transmitter, R antennas at the receiver and L interfering users each equipped with T_i transmit antenna elements, $i = 1, \dots, L$, the $R \times 1$ vector at the desired user's receiver can be modeled as

$$\mathbf{y} = \mathbf{H}_D \mathbf{x}_D + \sum_{i=1}^L \sqrt{\Omega_i} \mathbf{H}_i \mathbf{x}_i + \mathbf{n}, \quad (3.7)$$

where $\mathbf{H}_D: R \times T$ and $\mathbf{x}_D: T \times 1$ are the normalized channel matrix and the transmitted data vector for the desired user, respectively. Similarly, Ω_i , $\mathbf{H}_i: R \times T_i$, and $\mathbf{x}_i: T_i \times 1$ are the short-term average power, the normalized channel matrix, and the normalized transmitted vectors for the i th cochannel interferer. We further assume that all transmitted symbols are from complex Gaussian code books and as such the interference-plus-noise $\sum_{i=1}^L \sqrt{\Omega_i} \mathbf{H}_i \mathbf{x}_i + \mathbf{n}$, conditioned on \mathbf{H}_i , $i = 1, \dots, L$, is a complex Gaussian vector with zero mean and covariance matrix

$$\mathbf{B}_I = \sum_{i=1}^L \Omega_i \mathbf{H}_i \mathbf{K}_i \mathbf{H}_i^H + \sigma_n^2 \mathbf{I}_R, \quad (3.8)$$

where $\mathbf{K}_i = E(\mathbf{x}_i \mathbf{x}_i^H)$. Given $\mathbf{K}_D = E(\mathbf{x}_D \mathbf{x}_D^H)$ and the total transmitting power constraint Ω_D , we have $\text{tr}(\mathbf{K}_D) \leq \Omega_D$. Similar to the noise-limited case, we assume that fading is frequency-flat. We further assume that CCI users are subject to Rayleigh fading. The interfering channel matrices \mathbf{H}_i , $i = 1, \dots, L$ are complex Gaussian matrices with zero mean and independent rows, but we allow the columns to be correlated (i.e., the receiver antennas are uncorrelated but the transmitter antennas are possibly correlated).

To simplify the interference component in (3.7), we have now a closer look at \mathbf{B}_I defined in (3.8).

1. Let us assume that \mathbf{H}_i , $i = 1, \dots, L$, are zero mean complex Gaussian matrices with i.i.d. rows, but the columns are possibly correlated with covariance matrix $\mathbf{A}_i: T_i \times T_i$ (semicorrelated Rayleigh faded interferers), then \mathbf{H}_i can be represented as $\mathbf{Z}_i \mathbf{A}_i^{\frac{1}{2}}$, where $\mathbf{Z}_i: R \times T_i$ denotes the complex Gaussian matrix whose entries are i.i.d. $\mathcal{CN}(0, 1)$ (complex Gaussian random variable with zero mean and variance 1). In this case, the term $\mathbf{H}_i \mathbf{K}_i \mathbf{H}_i^H$ in (3.8) can be written as $\mathbf{Z}_i \left(\mathbf{A}_i^{\frac{1}{2}} \mathbf{K}_i \mathbf{A}_i^{\frac{1}{2}} \right) \mathbf{Z}_i^H$, that is, this interferer can be viewed to be subject to i.i.d. Rayleigh fading but with the “effective” signal covariance $\left(\mathbf{A}_i^{\frac{1}{2}} \mathbf{K}_i \mathbf{A}_i^{\frac{1}{2}} \right)$. This means that the correlations among the transmitter antenna elements of each interferer do not change the problem if we properly adjust the \mathbf{K}_i (One exception to this argument is when interferers have perfect channel state information (CSI) at both the transmitter and the receiver and their signals are designed to exploit this CSI, for example, when interferers are transmitting on the basis of the water-filling principle with CSI at both transmitter and receiver. This case is beyond the scope of this work). The same arguments apply to the correlations among different interferers. Therefore, it is sufficient to study the case when \mathbf{H}_i , $i = 1, \dots, L$, are uncorrelated and each has i.i.d. complex Gaussian entries with zero mean and variance 1, even if interferers’ transmit antennas are correlated and/or interferers are correlated.
2. Since \mathbf{K}_i , $i = 1, \dots, L$, are positive semidefinite, we can write $\mathbf{K}_i = \mathbf{U}_i \Lambda_i \mathbf{U}_i^H$, where \mathbf{U}_i is the unitary matrix consisting of the eigenvectors of \mathbf{K}_i and Λ_i the diagonal matrix composed of the corresponding eigenvalues (real and nonnegative). Note that Λ_i is a $T_i \times T_i$ matrix but may have rank $n_i \leq T_i$ depending on the number of independent streams transmitted each time. Because \mathbf{H}_i is invariant under the unitary transformation $\mathbf{H}_i \mathbf{U}_i$ (i.e., they have the same distribution), it is clear that assuming \mathbf{K}_i to be a diagonal matrix does not make us lose any generality. As such, we will assume from now on that \mathbf{K}_i is diagonal.

3. Let this diagonal matrix $\mathbf{K}_i = \text{diag}(K_{i,1}, K_{i,2}, \dots, K_{i,n_i}, 0, \dots)$, then $\Omega_i \mathbf{H}_i \mathbf{K}_i \mathbf{H}_i^H$ can be written as

$$\Omega_i \mathbf{H}_i \mathbf{K}_i \mathbf{H}_i^H = \sum_{l=1}^{n_i} \Omega_i K_{i,l} \mathbf{H}_{i,l} \mathbf{H}_{i,l}^H, \quad (3.9)$$

where $\mathbf{H}_{i,l}$ is the l th column of \mathbf{H}_i . Substituting (3.9) into (3.8), we get

$$\mathbf{B}_I = \sum_{i=1}^L \sum_{l=1}^{n_i} \Omega_i K_{i,l} \mathbf{H}_{i,l} \mathbf{H}_{i,l}^H + \sigma_n^2 \mathbf{I}_R. \quad (3.10)$$

If we let $\sum_{i=1}^L n_i = N_I$, P_m , $m = 1, \dots, N_I$, be the m th smallest $\Omega_i K_{i,l}$ for $i = 1, \dots, L$ and $l = 1, \dots, n_i$, and \mathbf{H}_I to be the $R \times N_I$ matrix whose m th column is the channel vector corresponding to P_m , we can write (3.7) into the matrix form

$$\mathbf{y} = \mathbf{H}_D \mathbf{x}_D + \mathbf{H}_I \mathbf{P}_I^{\frac{1}{2}} \mathbf{x}_I + \mathbf{n} \quad (3.11)$$

where $\mathbf{P}_I = \text{diag}(P_1, P_2, \dots, P_{N_I})$, and \mathbf{B}_I becomes

$$\mathbf{B}_I = \mathbf{H}_I \mathbf{P}_I \mathbf{H}_I^H + \sigma_n^2 \mathbf{I}_R. \quad (3.12)$$

Equation (3.11) provides an equivalent model to (3.7), which can now be viewed as a system with N_I independent interferers with single transmitter antenna, each with short-term average power P_k ($k = 1, \dots, N_I$), and normalized signal $\mathbf{x}_{I,k}$ over channel vector $\mathbf{H}_{I,k}$. However, we should keep in mind that on the basis of the previous arguments, we are in fact including in our analysis the more general case in which there are correlations among interferers' transmitter antenna elements, among different interferers, and among the interfering signals, as well as different numbers of transmit antenna elements and/or transmitting strategies.

We finally assume that there is no centralized mechanism to jointly maximize the total system capacity for both desired user and interferers. This is particularly true when some or all the interferers are from neighboring cells, in which case the transmitter has no control over the transmitting strategies of interferers. Under these conditions, the desired user simply optimizes the capacity of its own link.

Mutual information

When realizations of \mathbf{H}_D and \mathbf{H}_I are known at the receiver, the MI of the desired link is given by [11]

$$\mathcal{I} = \log_2 \left(\det \left(\mathbf{I}_R + \mathbf{H}_D \mathbf{K}_D \mathbf{H}_D^H \mathbf{B}_I^{-1} \right) \right) \text{ bps/Hz.} \quad (3.13)$$

When the transmitter does not have any CSI and as such the scheme of transmitting multiple independent complex Gaussian streams with equal power allocation is used, that is,

$$\mathbf{K}_D = \frac{\Omega}{T} \mathbf{I}_T. \quad (3.14)$$

The MI of the desired link achieved by the equal power transmission scheme is given by

$$\begin{aligned}
\mathcal{I} &= \log_2 \det \left(\mathbf{I}_R + \frac{\Omega_D}{T} \mathbf{H}_D \mathbf{H}_D^H \mathbf{B}_I^{-1} \right) \\
&= \log_2 \det \left(\mathbf{I}_T + \frac{\Omega_D}{T} \mathbf{H}_D^H \mathbf{B}_I^{-1} \mathbf{H}_D \right) \\
&= \log_2 \det \left(\mathbf{I}_T + \frac{\Omega_D}{T} \mathbf{H}_D^H \left(\mathbf{H}_I \mathbf{P}_I \mathbf{H}_I + \sigma_n^2 \mathbf{I}_R \right)^{-1} \mathbf{H}_D \right) \\
&= \log_2 \det \left(\mathbf{I}_T + \frac{\Omega_D}{T} \mathbf{F}_1 \right) \text{ bps/Hz,}
\end{aligned} \tag{3.15}$$

where we define \mathbf{F}_1 as

$$\mathbf{F}_1 = \mathbf{H}_D^H \left(\mathbf{H}_I \mathbf{P}_I \mathbf{H}_I + \sigma_n^2 \mathbf{I}_R \right)^{-1} \mathbf{H}_D. \tag{3.16}$$

3.2.3 MIMO beamforming

Beamforming is another important transmission scheme that exploits the spatial dimensions in MIMO channels. In a noise-limited MIMO channel, the optimum beamforming is the maximal ratio combining (MRC) solution that provides the maximum output signal-to-noise ratio (SNR). In a MIMO channel with interference, the optimum beamforming is the minimum-mean-square-error (MMSE) solution and is also referred to as the *optimum combining* (OC) scheme in that it maximizes the output signal-interference-plus-noise ratio (SINR).

MIMO beamforming in noise-limited channels—MRC

The MIMO MRC is a scheme that maximizes the instantaneous output SNR by jointly choosing optimum transmit weight vector \mathbf{w}_t and receive weight vector \mathbf{w}_r . This maximum instantaneous output SNR lowers the probability of reception error. Specifically, for the MIMO MRC scheme, the input vector \mathbf{x} in (3.1) is $\mathbf{x} = \mathbf{w}_t s$, where s is a scalar complex symbol with normalized power. Now the channel model (3.1) becomes

$$\mathbf{y} = \mathbf{H} \mathbf{w}_t s + \mathbf{n}. \tag{3.17}$$

At the receiver, the received vector \mathbf{y} is linearly combined by the receive weight vector \mathbf{w}_r , that is,

$$\mathbf{w}_r^H \mathbf{y} = \mathbf{w}_r^H \mathbf{H} \mathbf{w}_t s + \mathbf{w}_r^H \mathbf{n}. \tag{3.18}$$

The instantaneous (conditioned on the channel realization) SNR at the receive combiner output is

$$\mu = \frac{\|\mathbf{w}_r^H \mathbf{H} \mathbf{w}_t\|^2 E(ss^H)}{\|\mathbf{w}_r^H\|^2 \sigma_n^2} \tag{3.19}$$

The objective is to maximize μ , given the power constraint $\mathbf{w}_t^H \mathbf{w}_t \leq \Omega$, and the solution is [12]

$$\begin{aligned}\mathbf{w}_t &= \sqrt{\Omega} \mathbf{U} \\ \mathbf{w}_r &= \mathbf{H} \mathbf{U},\end{aligned}\tag{3.20}$$

where \mathbf{U} is the eigenvector associated with the largest eigenvalue of $\mathbf{H}^H \mathbf{H}$. The maximized output SNR is given by [12]

$$\mu = \frac{\Omega}{\sigma_n^2} \lambda_{\max},\tag{3.21}$$

where λ_{\max} is the largest eigenvalue of $\mathbf{H} \mathbf{H}^H$, or, equivalently, that of $\mathbf{H}^H \mathbf{H}$.

MIMO beamforming in the presence of interference–OC

Similar to the MIMO MRC scheme, the beamforming transmission in the presence of interference is also of interest [13]. The objective is to maximize the output SINR by jointly choosing the optimum weight vector \mathbf{w}_t and \mathbf{w}_r . The argument for the optimum combining weights is similar to that for the MIMO MRC scheme. The weight vectors are shown to be given by [13]

$$\begin{aligned}\mathbf{w}_t &= \sqrt{\Omega_D} \mathbf{U}_{\max} \\ \mathbf{w}_r &= \alpha \mathbf{R}^{-1} \mathbf{H}_D \mathbf{w}_t\end{aligned}\tag{3.22}$$

where α is a constant that does not affect the output SINR and \mathbf{U}_{\max} ($\|\mathbf{U}_{\max}\| = 1$) denotes the eigenvector corresponding to the largest eigenvalue of the quadratic form and the maximum SINR is given by

$$\mu_{\text{SINR}} = \Omega_D \lambda_{\max},\tag{3.23}$$

where λ_{\max} is the largest eigenvalue of the matrix \mathbf{F}_1 defined in (3.16).

Before dealing directly with the general case when \mathbf{P}_I is of any Hermitian positive semidefinite matrix and $\sigma_n^2 > 0$, we first consider a simplified problem by making the two following assumptions.

- The system is interference limited with high interference to noise ratio (INR) and therefore the effect of thermal noise is neglected. Under this assumption, we have $\sigma_n^2 = 0$ in (3.15) and (3.16).
- We assume that $\mathbf{P}_I = \Omega_I \mathbf{I}_{N_I}$. This assumption is reasonable when interferers are uncorrelated and the receiver adopts power control.

Under these two assumptions, the Hermitian matrix \mathbf{F}_1 in (3.15) and (3.16) becomes

$$\mathbf{F}_2 = \mathbf{H}_D^H \left(\Omega_I \mathbf{H}_I \mathbf{H}_I^H \right)^{-1} \mathbf{H}_D,\tag{3.24}$$

where $N_I \geq R$ is assumed in (3.24) so that $(\mathbf{H}_I \mathbf{H}_I^H)^{-1}$ exists.

Beamforming outage probability

One important performance measure of MIMO beamforming is the outage probability, which is defined as the probability of the output SNR (for MIMO MRC) or SINR (for MIMO optimum combining) falling below a threshold, which is the CDF of the SNR or SINR evaluated at the threshold μ_{th} , that is, the outage probability P_{out} is defined as

$$\begin{aligned} P_{\text{out}} &= \Pr(\mu \leq \mu_{\text{th}}) \\ &= \int_{0 < \phi_1 < \dots < \phi_s < x} f_{\phi_1, \dots, \phi_s}(\phi_1, \dots, \phi_s) d\phi_1 \dots d\phi_s \end{aligned} \quad (3.25)$$

where x is related to μ_{th} by (i) $x = \frac{\mu_{\text{th}}\sigma_n^2}{\Omega}$ for MIMO MRC and (ii) $x = \frac{\mu_{\text{th}}}{\Omega_D}$ for MIMO OC. and $f_{\phi_1, \dots, \phi_s}(\phi_1, \dots, \phi_s)$ is the joint PDF of nonzero eigenvalues of the respective Hermitian matrices.

It is clear that all the above performance analysis problems of MIMO systems are closely related to the joint distributions of eigenvalues of certain Hermitian forms in complex Gaussian matrices. Before looking further at this connection, we first introduce in the following section some basic concepts and techniques of interest used in multivariate statistical analysis dealing with matrix distributions.

3.3 Some Mathematical Preliminaries

1. For complex matrices $\mathbf{A}: m \times m$ and $\mathbf{B}: m \times m$, we say $\mathbf{A} > \mathbf{B}$ if $\mathbf{A} - \mathbf{B}$ is a positive definite matrix. In particular, we denote $\mathbf{A} > \mathbf{0}$ if \mathbf{A} is a positive definite matrix.
2. The complex multivariate gamma function is defined as

$$\begin{aligned} \tilde{\Gamma}_m(a) &= \int_{\mathbf{A}^H = \mathbf{A} > 0} e^{-\text{tr}\mathbf{A}} |\mathbf{A}|^{a-m} d\mathbf{A} \\ &= \pi^{\frac{1}{2}m(m-1)} \prod_{i=1}^m \Gamma(a - i + 1), \end{aligned} \quad (3.26)$$

where $\Gamma(\cdot)$ is the ordinary gamma function defined by [14], Eqn. (8.31.1). The integration region $\mathbf{A} = \mathbf{A}^H > 0$ denotes all $m \times m$ Hermitian positive definite matrices.

3. The hypergeometric function of complex (Hermitian) matrix arguments is a generalization of the ordinary hypergeometric function defined by [14], Eqn. (9.14.1). It is defined as

$$\begin{aligned} {}_p\tilde{F}_q^{(m)}(a_1, \dots, a_p; b_1, \dots, b_q; \mathbf{A}, \mathbf{B}) \\ = \sum_{k=0}^{\infty} \sum_{\kappa} \frac{[a_1]_{\kappa} \dots [a_p]_{\kappa}}{[b_1]_{\kappa} \dots [b_q]_{\kappa}} \frac{C_{\kappa}(\mathbf{A})C_{\kappa}(\mathbf{B})}{C_{\kappa}(\mathbf{I}_m)k!}. \end{aligned} \quad (3.27)$$

In (3.27), $\kappa = (k_1, k_2, \dots, k_m)$ is a partition of the integer k into no more than m parts with $k_1 \geq k_2 \geq \dots \geq k_m \geq 0$ and $k_1 + k_2 + \dots + k_m = k$. The complex multivariate

hypergeometric coefficients $[a]_k$ is defined as

$$[a]_k = \prod_{i=1}^m (a - i + 1)_{k_i}, \quad (3.28)$$

where $(b)_k = b(b+1)\dots(b+k-1)$ is referred to as Pochhammer number. In (3.27), $C_\kappa(\mathbf{A})$ is the *zonal polynomial* of the Hermitian matrix \mathbf{A} and is defined as

$$C_\kappa(\mathbf{A}) = \chi_{[\kappa]}(1)\chi_{[\kappa]}(\mathbf{A}), \quad (3.29)$$

where $\chi_{[\kappa]}(1)$ is given by

$$\chi_{[\kappa]}(1) = k! \prod_{i < j}^{m-1} (k_i - k_j - i + j) / \prod_{i=1}^m (k_i + m - i)! \quad (3.30)$$

and is the dimension of the representation $[\kappa]$ of the symmetric group. $\chi_{[\kappa]}(\mathbf{A})$ in (3.29) is the character of the representation $\{\kappa\}$ of the linear group. Let ϵ_i , $i = 1, \dots, m$ be the *latent roots* (eigenvalues) of \mathbf{A} , then $\chi_{[\kappa]}(\mathbf{A})$ can be written as [15]

$$\chi_{[\kappa]}(\mathbf{A}) = \frac{\left| \binom{\epsilon_i^{k_j+m-j}}{\epsilon_i^{m-j}} \right|}{\left| \binom{\epsilon_i^{m-j}}{\epsilon_i^{m-j}} \right|}. \quad (3.31)$$

The zonal polynomial has the following *reproductive property*

$$\frac{1}{\tilde{\Gamma}_m(a)} \int_{\mathbf{A}^H = \mathbf{A} > \mathbf{0}} e^{-\text{tr}\mathbf{A}} |\mathbf{A}|^{a-m} C_\kappa(\mathbf{AB}) d\mathbf{A} = [a]_k C_\kappa(\mathbf{B}). \quad (3.32)$$

4. The hypergeometric function of complex matrix argument has the following *splitting property*

$${}_p\tilde{F}_q^{(m)}(\mathbf{A}, \mathbf{B}) = \int_{U(m)} {}_p\tilde{F}_q^{(m)}(\mathbf{AUBU}^H) d\mathbf{U}, \quad (3.33)$$

where $U(m)$ is the unitary group (i.e., the group containing all $m \times m$ unitary matrices \mathbf{U}) and $d\mathbf{U}$ is the invariant measure on $U(m)$. This is essentially due to the splitting property of the zonal polynomial given by

$$\int_{U(m)} C_\kappa(\mathbf{AUBU}^H) d\mathbf{U} = \frac{C_\kappa(\mathbf{A})C_\kappa(\mathbf{B})}{C_\kappa(\mathbf{I}_m)}. \quad (3.34)$$

5. \mathbf{X} : $m \times n$ is a complex Gaussian matrix if its PDF is given by

$$\pi^{-mn} |\Sigma|^{-n} |\mathbf{B}|^{-m} \exp \left(-\text{tr} \left(\Sigma^{-1} (\mathbf{X} - \mathbf{M}) \mathbf{B}^{-1} (\mathbf{X} - \mathbf{M})^H \right) \right), \quad (3.35)$$

where $\Sigma : m \times m$ is the covariance matrix of column vectors of \mathbf{X} , $\mathbf{B} : n \times n$ the covariance matrix of row vectors of \mathbf{X} , and $\mathbf{M} : m \times n$ the mean matrix of \mathbf{X} . The

distribution functions of quadratic functions of \mathbf{X} have been of interest in classic multivariate statistics for several decades. Some examples of these quadratic functions include \mathbf{XX}^H and $\mathbf{XX}^H (\mathbf{YY}^H)^{-1}$, where \mathbf{Y} is also a complex Gaussian matrix independent of \mathbf{X} . The distribution functions of these quadratic forms can often be conveniently represented in terms of hypergeometric function of matrix arguments. A good expository of these distribution functions is given in [15]. One of the simplest cases is the *central complex Wishart distribution*. Specifically, let \mathbf{X} be an $m \times n$ complex random matrix whose PDF is in the form of (3.35) with $\mathbf{B} = \mathbf{I}_m$ and $\mathbf{M} = \mathbf{0}$. Then the Hermitian positive definite matrix $\mathbf{A} = \mathbf{XX}^H$ (\mathbf{A}/n is the *sample covariance matrix*) is complex (central) Wishart distributed when $m \leq n$. The PDF of \mathbf{A} is given by [16]

$$\frac{1}{\tilde{\Gamma}_m(n)|\Sigma|^n} e^{-\text{tr}\Sigma^{-1}\mathbf{A}}|\mathbf{A}|^{n-m}. \quad (3.36)$$

Since \mathbf{A} is Hermitian positive definite, its eigenvalues are real and positive. In general, the joint PDF of the eigenvalues of \mathbf{A} can be obtained from the PDF of \mathbf{A} , $f(\mathbf{A})$, by the transformation $\mathbf{A} = \mathbf{UWU}^H$. Considering the example when the PDF of \mathbf{A} is given by (3.36) and denoting its nonzero eigenvalues by $0 < w_1 < w_2 < \dots < w_m$ (since we assume $n \geq m$ for the moment) and defining $\mathbf{W} = \text{diag}(w_1, w_2, \dots, w_m)$, the joint PDF of w_i , $i = 1, \dots, m$, $g(\mathbf{W})$, can be obtained by the transform $\mathbf{A} = \mathbf{UWU}^H$ given in general by

$$\begin{aligned} g(\mathbf{W}) &= \frac{\pi^{m(m-1)}}{\tilde{\Gamma}_m(m)} \prod_{i < j}^m (w_i - w_j)^2 \\ &\times \int_{U(m)} f(\mathbf{U}\mathbf{AU}^H) d\mathbf{U}, \end{aligned} \quad (3.37)$$

where the integral in (3.37) can often be evaluated using the splitting property of the hypergeometric function in matrix argument given by (3.33). When \mathbf{A} is a complex central Wishart matrix whose PDF is given by (3.36), first noting that

$$e^{\text{tr}(\mathbf{B})} = {}_0F_0(\mathbf{B}), \quad (3.38)$$

then applying (3.37) and (3.33) gives the joint PDF of its nonzero eigenvalues as [15]

$$\frac{\pi^{m(m-1)}}{\tilde{\Gamma}_m(n)\tilde{\Gamma}_m(m)|\Sigma|^n} {}_0F_0(-\Sigma^{-1}, \mathbf{W}) \prod_{i=1}^m w_i^{n-m} \prod_{i < j}^m (w_i - w_j)^2 \prod_{i=1}^m dw_i. \quad (3.39)$$

3.4 General Calculations with MIMO Applications

A close look at (3.6) and (3.25) reveals that they both belong to the general problem of evaluating the following integral:

$$\int_D \prod_{i=1}^s g(\phi_i) f_{\phi_1 \dots \phi_s}(\phi_1, \dots, \phi_s) d\phi_1 \dots d\phi_s, \quad (3.40)$$

where the integration region is $D = \{a < \phi_1 < \dots < \phi_s < b\}$, where $0 \leq a < b$, and $g(\phi_i)$ is a function of ϕ_i , $i = 1, \dots, s$, that makes (3.40) integrable. Indeed, many interesting distribution problems fall into this form. For example,

- In (3.6), $D = \{0 < \phi_1 < \dots < \phi_s < \infty\}$ and $g(\phi_i) = (1 + \rho\phi_i)^{\tau/\ln(2)}$.
- In (3.25), $D = \{0 < \phi_1 < \dots < \phi_s < x\}$ and $g(\phi_i) = 1$.
- Letting $D = \{0 < x < \phi_1 < \dots < \phi_s < \infty\}$ and $g(\phi_i) = 1$, we get the complementary CDF (CCDF, or 1-CDF) of the smallest eigenvalue ϕ_1 .
- Letting $D = \{0 < \phi_1 < \dots < \phi_s < \infty\}$ and $g(\phi_i) = e^{j\tau\phi_i}$, we get the characteristic function of the trace. Therefore, the moments of the trace can be obtained in a straightforward fashion by taking derivatives.
- Letting $D = \{0 < \phi_1 < \dots < \phi_s < \infty\}$ and $g(\phi_i) = \phi_i^n$, we get the n th moment of the determinant.

We further assume that the joint PDF of the eigenvalues of interest $f_{\phi_1, \dots, \phi_s}(\phi_1, \dots, \phi_s)$ in (3.40) is in the form of

$$c \prod_{i=1}^s h(\phi_i)_p \tilde{F}_q(\mathbf{a}; \mathbf{b}; \mathbf{A}, \Phi) \prod_{i < j}^s (\phi_i - \phi_j)^2. \quad (3.41)$$

where \mathbf{A} is a Hermitian matrix of system parameters and $\Phi = \text{diag}(\phi_1, \dots, \phi_s)$, c is the normalized constant, $\mathbf{a} = [a_1, a_2, \dots, a_p]$ and $\mathbf{b} = [b_1, b_2, \dots, b_q]$ are the parameter vectors. This particular form is frequently encountered in the calculations related to MIMO fading channels, as the following examples will show it.

- When a MIMO Rician fading channel is independently faded but with nonidentical specular components, the PDF of channel matrix \mathbf{H} is given by

$$\pi^{-RT} (\sigma^{-2RT}) \exp \left(-\frac{1}{\sigma^2} \text{tr} \left(\mathbf{H} - \mathbf{M} \right) \left(\mathbf{H} - \mathbf{M} \right)^H \right). \quad (3.42)$$

When \mathbf{H} is a complex Gaussian matrix whose entries $\{\mathbf{H}\}_{i,j}$ are independent with mean m_{ij} and variance σ^2 , the joint PDF of the s nonzero eigenvalues $0 < \phi_1 < \phi_2 < \dots < \phi_s$ of $\mathbf{H}\mathbf{H}^H$, $f_{\phi_1, \dots, \phi_s}(\phi_1, \dots, \phi_s)$, is given by [15]

$$\begin{aligned} f_{\phi_1, \dots, \phi_s}(\phi_1, \dots, \phi_s) &= c_1 {}_0\tilde{F}_1(t; \Lambda, \Phi) \\ &\times e^{-\text{tr}(\Phi)} \prod_{k=1}^s \phi_k^{t-s} \prod_{i < j}^s (\phi_i - \phi_j)^2, \end{aligned} \quad (3.43)$$

where ${}_0\tilde{F}_1(\cdot; \cdot, \cdot)$ is the hypergeometric function of two matrix arguments with parameters $p = 0$ and $q = 1$ (this particular form is also referred to as the Bessel type of hypergeometric function with two matrix arguments) and

$$c_1 = \frac{e^{-\text{tr}(\Lambda)}}{\prod_{k=1}^s \Gamma(t - k + 1) \Gamma(s - k + 1)}, \quad (3.44)$$

where $\Lambda = \text{diag}(\lambda_1, \dots, \lambda_s)$, where $0 < \lambda_1 < \dots < \lambda_s$ are s nonzero distinct eigenvalues of $\mathbf{M}^H \Sigma^{-1} \mathbf{M}$ (this is often referred to the *noncentrality matrix* and in our case, $\Sigma = \sigma^2 \mathbf{I}_R$).

Equation (3.43) is clearly in the form of (3.41) with $c = c_1$, $h(x) = e^{-x} x^{t-s}$ and the hypergeometric function is ${}_0\tilde{F}_1(t, \Lambda, \Phi)$.

- For correlated Rayleigh MIMO channels, the channel matrix \mathbf{H} has a PDF given by

$$\pi^{-RT} |\Sigma_R|^{-T} |\Sigma_T|^{-R} \exp\left(-\text{tr}\left(\Sigma_R^{-1} \mathbf{H} \Sigma_T^{-1} \mathbf{H}^H\right)\right) \quad (3.45)$$

and the joint PDF of the nonzero eigenvalues of the Hermitian matrix $\mathbf{H}\mathbf{H}^H$ is in the form of

$$\begin{aligned} & \frac{\pi^{s(s-1)}}{\tilde{\Gamma}_s(s) \tilde{\Gamma}_s(t) \det(\Sigma_T)^R \det(\Sigma_R)^T} \prod_{j=1}^s \phi_j^{t-s} \prod_{i < j}^s (\phi_i - \phi_j)^2 \\ & \times {}_0\tilde{F}_0^{(t)(s)}\left(-\Sigma_T^{-1}, \Sigma_R^{-1}, \Phi\right), \end{aligned} \quad (3.46)$$

where

$${}_0\tilde{F}_0^{(t)(s)}\left(-\Sigma_T^{-1}, \Sigma_R^{-1}, \mathbf{W}\right) = \sum_{k=0}^{\infty} \sum_{\kappa} \frac{C_{\kappa}\left(-\Sigma_T^{-1}\right) C_{\kappa}\left(\Sigma_R^{-1}\right) C_{\kappa}(\mathbf{W})}{C_{\kappa}(\mathbf{I}_t) C_{\kappa}(\mathbf{I}_s) k!}. \quad (3.47)$$

Note that in (3.47) the superscript $(t)(s)$ indicates the dimensions of \mathbf{I}_t and \mathbf{I}_s . If either Σ_T or Σ_R in (3.47) is an identity matrix, its zonal polynomial will cancel the one at the denominator and (3.47) reduces to the hypergeometric function in two matrices. Now it can be seen that when either one of Σ_T and Σ_R is an identity matrix, the PDF (3.46) reduces to either [15, 17]

$$\begin{aligned} & \frac{\pi^{s(s-1)}}{\tilde{\Gamma}_s(s) \tilde{\Gamma}_s(t) \det(\Sigma_s)^t} \prod_{j=1}^s \phi_j^{t-s} \prod_{i < j}^s (\phi_i - \phi_j)^2 \\ & \times {}_0\tilde{F}_0^{(s)}\left(-\Sigma_s^{-1}, \Phi\right) \end{aligned} \quad (3.48)$$

if the correlated side has s antennas. We denote this covariance matrix by Σ_s . On the other hand, if the correlated side has t antennas, which we denote by Σ_t , the joint PDF reduces to

$$\begin{aligned} & \frac{\pi^{s(s-1)}}{\tilde{\Gamma}_s(s) \tilde{\Gamma}_s(t) \det(\Sigma_t)^s} \prod_{j=1}^s \phi_j^{t-s} \prod_{i < j}^s (\phi_i - \phi_j)^2 \\ & \times \lim_{\delta_1, \dots, \delta_{(t-s)} \rightarrow 0} {}_0\tilde{F}_0^{(t)}\left(-\Sigma_t^{-1}, \Phi^*\right), \end{aligned} \quad (3.49)$$

where $\Phi^* = \text{diag}(\delta_1, \dots, \delta_{(t-s)}, \phi_1, \dots, \phi_s)$ is an augmented version of Φ by adding $0 < \delta_1 < \dots < \delta_{(t-s)} < \phi_1$.

3.4.1 Main result

In what follows, we first look at the integral

$$\begin{aligned} I &= \int_{D=\{\alpha < \phi_1 < \dots < \phi_n < b\}} \prod_{k=1}^n g(\phi_k) f_{\phi_1, \dots, \phi_n}(\phi_1, \dots, \phi_n) d\phi_1 \dots d\phi_n \\ &= c \int_D \prod_{k=1}^n h(\phi_k) g(\phi_k) {}_p F_q^{(n)}(\mathbf{a}; \mathbf{b}; \Lambda, \Phi) \prod_{i < j}^n (\phi_i - \phi_j)^2 d\phi_1 \dots d\phi_n, \end{aligned} \quad (3.50)$$

where $\Lambda: n \times n$ is Hermitian positive definite with eigenvalues $0 < \lambda_1 < \dots < \lambda_n$ and $\Phi: n \times n$ is Hermitian positive definite with eigenvalues $0 < \phi_1 < \dots < \phi_n$.

The hypergeometric function in two matrix arguments ${}_p F_q^{(n)}(\mathbf{a}; \mathbf{b}; \Lambda, \Phi)$ can be written as the following determinant [18].

$${}_p F_q^{(n)}(\mathbf{a}; \mathbf{b}; \Lambda, \Phi) = c_f \frac{\det({}_p F_q(\mathbf{a} - n + 1, \mathbf{b} - n + 1, \lambda_i \phi_j))}{\det(\lambda_i^{n-j}) \det(\phi_i^{n-j})}, \quad (3.51)$$

where

$$c_f = \frac{\prod_{i=1}^n \Gamma(i) \left(\prod_{j=1}^q (b_j - n + 1)_{(n-i)} \right)}{\prod_{i=1}^n \left(\prod_{j=1}^p (a_j - n + 1)_{(n-i)} \right)},$$

${}_p F_q([a_1, \dots, a_p]; [b_1, \dots, b_q]; x)$ is the ordinary hypergeometric function [14], Eqn. (9.14.1), and $\mathbf{a} - n + 1 = [a_1 - n + 1, a_2 - n + 1, \dots, a_p - n + 1]$ and $\mathbf{b} - n + 1 = [b_1 - n + 1, b_2 - n + 1, \dots, b_q - n + 1]$. The determinant $\det(\lambda_i^{n-j})$ is a Vandermonde determinant and therefore it can be evaluated as

$$\det(\lambda_i^{n-j}) = \prod_{i < j}^n (\lambda_i - \lambda_j). \quad (3.52)$$

and the determinant $\det(\phi_i^{n-j})$ in (3.51) can also be evaluated similarly. Note that the $\det(\phi^{n-j}) = \prod_{i < j} (\phi_i - \phi_j)$ in the denominator is cancelled by the term $\prod_{i < j} (\phi_i - \phi_j)^2$. Therefore, the integral to be evaluated becomes

$$\begin{aligned} I &= \int_D \prod_{k=1}^n g(\phi_k) f_{\phi_1, \dots, \phi_n}(\phi_1, \dots, \phi_n) d\phi_1 \dots d\phi_n \\ &= \frac{c' \doteq c \cdot c_f}{\det(\lambda_i^{n-j})} \int_D \prod_{i=1}^n h(\phi_i) g(\phi_i) \det({}_p F_q(\mathbf{a} - n + 1, \mathbf{b} - n + 1, \lambda_i \phi_j)) \\ &\quad \times \det(\phi_i^{n-j}) d\phi_1 \dots d\phi_n. \end{aligned} \quad (3.53)$$

Using the fact that for square matrices \mathbf{A} and \mathbf{B} , $\det(\mathbf{AB}) = \det(\mathbf{A})\det(\mathbf{B})$, we have

$$\begin{aligned} & \det(pF_q(\mathbf{a} - n + 1, \mathbf{b} - n + 1, \lambda_i \phi_j)) \det(\phi_i^{n-j}) \\ &= \det\left(\sum_{k=1}^n pF_q(\mathbf{a} - n + 1, \mathbf{b} - n + 1, \lambda_i \phi_k) \phi_k^{n-j}\right), \end{aligned} \quad (3.54)$$

that is, each entry of the resulting determinant is a summation of n terms. Since the determinant operator is by definition a multilinear function, we have for 2×1 vectors $\mathbf{a}, \mathbf{b}, \mathbf{c}$, and \mathbf{d} ,

$$\det(\mathbf{a} + \mathbf{b}, \mathbf{c} + \mathbf{d}) = \det(\mathbf{a}, \mathbf{c}) + \det(\mathbf{a}, \mathbf{d}) + \det(\mathbf{b}, \mathbf{c}) + \det(\mathbf{b}, \mathbf{d}).$$

It follows that the above determinant (3.54) can be expanded as the sum of n^n determinants. Specifically, (3.54) becomes

$$\begin{aligned} & \det\left(\sum_{k=1}^n pF_q(\mathbf{a} - n + 1, \mathbf{b} - n + 1, \lambda_i \phi_k) \phi_k^{n-j}\right) \\ &= \sum_{\sigma_1=1}^n \cdots \sum_{\sigma_n=1}^n \det(\mathbf{A}_{\sigma_1, \dots, \sigma_n}), \end{aligned} \quad (3.55)$$

where $\mathbf{A}_{\sigma_1, \dots, \sigma_n}$ is an $n \times n$ matrix whose i th column is the σ_i th term in the summation of the i th column of $\det\left(\sum_{k=1}^n pF_q(\mathbf{a} - n + 1, \mathbf{b} - n + 1, \lambda_i \phi_k) \phi_k^{n-j}\right)$, that is, the entry at the i th row and the j th column is given by

$$\{\mathbf{A}_{\sigma_1, \dots, \sigma_n}\}_{i,j} = pF_q(\mathbf{a} - n + 1, \mathbf{b} - n + 1, \lambda_i \phi_{\sigma_j}) \phi_{\sigma_j}^{n-j} \quad (3.56)$$

Now it can be seen from (3.56) that $\det(\mathbf{A}_{\sigma_1, \dots, \sigma_n}) = 0$ if $\sigma_k = \sigma_l$, for $k \neq l$ because in these cases, the k th column of $\mathbf{A}_{\sigma_1, \dots, \sigma_n}$ will be proportional to its l th column. In other words, survival combinations of $(\sigma_1, \dots, \sigma_n)$ have to be from permutations of $(1, \dots, n)$. Therefore, (3.55) becomes

$$\begin{aligned} & \sum_{(\sigma_1, \dots, \sigma_n)} \det(pF_q(\mathbf{a} - n + 1, \mathbf{b} - n + 1, \lambda_i \phi_{\sigma_j}) \phi_{\sigma_j}^{n-j}) \\ &= \sum_{(\sigma_1, \dots, \sigma_n)} \sum_{(i_1, \dots, i_n)} (-1)^{(i_1, \dots, i_n)} \prod_{j=1}^n pF_q(\mathbf{a} - n + 1, \mathbf{b} - n + 1, \lambda_{i_j} \phi_{\sigma_j}) \\ & \quad \times \phi_{\sigma_j}^{n-j} \\ &= \sum_{(i_1, \dots, i_n)} (-1)^{(i_1, \dots, i_n)} \sum_{(\sigma_1, \dots, \sigma_n)} \prod_{j=1}^n pF_q(\mathbf{a} - n + 1, \mathbf{b} - n + 1, \lambda_{i_j} \phi_{\sigma_j}) \\ & \quad \times \phi_{\sigma_j}^{n-j}, \end{aligned} \quad (3.57)$$

where the first equality of (3.57) is obtained by expanding the determinant and the second one follows from the interchanging of the order of the two summations. In (3.57), $(-1)^{(i_1, i_2, \dots, i_n)}$

is 1 if the permutation (i_1, i_2, \dots, i_n) is even and -1 if the permutation (i_1, i_2, \dots, i_n) is odd (A permutation (i_1, i_2, \dots, i_n) is even if it takes an even number of steps to pass from (i_1, i_2, \dots, i_n) to $(1, 2, \dots, n)$). Finally, substituting (3.57) into (3.50), we get

$$\begin{aligned}
I &= \int_D \prod_{i=1}^n g(\phi_i) f_{\phi_1 \dots \phi_n}(\phi_1, \dots, \phi_n) d\phi_1 \dots d\phi_n \\
&= \frac{c'}{\det(\lambda_i^{n-j})} \sum_{i_1, \dots, i_n} (-1)^{(i_1, \dots, i_n)} \\
&\quad \times \int_D \sum_{(\sigma_1, \dots, \sigma_s)} \prod_{j=1}^n {}_p F_q (\mathbf{a} - n + 1, \mathbf{b} - n + 1, \lambda_{i_j} \phi_{\sigma_j}) \\
&\quad \times \phi_{\sigma_j}^{n-j} d\phi_1 \dots d\phi_n \\
&= \frac{c'}{\det(\lambda_i^{n-j})} \sum_{i_1, \dots, i_n} (-1)^{(i_1, \dots, i_n)} \prod_{j=1}^n \int_a^b h(x) g(x) \\
&\quad \times {}_p F_q (\mathbf{a} - n + 1, \mathbf{b} - n + 1, \lambda_{i_j} x) x^{n-j} dx \\
&= \frac{c'}{\det(\lambda_i^{n-j})} \det \left(\int_a^b h(x) g(x) \right. \\
&\quad \left. \times {}_p F_q (\mathbf{a} - n + 1, \mathbf{b} - n + 1, \lambda_i x) x^{n-j} dx \right). \tag{3.58}
\end{aligned}$$

3.4.2 Application to noise-limited MIMO systems

We now show that some results of Section 3.2 can be quite easily obtained with the help of (3.58). For example, for the Rician case with joint PDF given by (3.43), it can be verified that

$$c' = \frac{e^{-\text{tr}(\Lambda)}}{(\Gamma(t-s+1))^s} \tag{3.59}$$

and the general integral is given in this case by

$$\begin{aligned}
I_{\text{Rician}} &= \frac{c'}{\det(\lambda_i^{s-j})} \\
&\quad \times \det \left(\int_a^b y^{t-i} g(y) e^{-y} {}_0 F_1 (t-s+1; y\lambda_j) dy \right) i, \quad j = 1, \dots, s, \\
&= \frac{c'}{\det(\lambda_i^{s-j})} \det(\Psi_{\text{nc}}),
\end{aligned} \tag{3.60}$$

where the last equality is obtained by defining the $s \times s$ matrix

$$\{\Psi_{\text{nc}}\}_{i,j} = \int_a^b y^{t-i} g(y) e^{-y} {}_0 F_1 (t-s+1; y\lambda_j) dy.$$

Results for cases when $\lambda_i = \lambda_j$ for some $i \neq j$ can be obtained by taking the limit $\lim_{\lambda_i \rightarrow \lambda_j}$. As an example, we consider the i.i.d. Rician fading case, that is, $\{\mathbf{H}\}_{i,j} \sim \mathcal{CN}(\eta, \sigma^2)$ (complex Gaussian random variable with mean μ and variance σ^2), it is easy to see that $\mathbf{M}^H \Sigma^{-1} \mathbf{M}$ has only one nonzero eigenvalue

$$\lambda_s = \frac{st|\eta|^2}{\sigma^2}, \quad (3.61)$$

where $|\cdot|$ is the modulus of a complex number. Therefore, the general integral is simply

$$\lim_{\lambda_{s-1}, \dots, \lambda_1 \rightarrow 0} I_{\text{Rician}}, \quad (3.62)$$

Since this is a $\frac{0}{0}$ type of limit, we apply l'Hôpital rule by taking $(j-1)$ th derivative of the column/row of determinants at the numerator and denominator containing λ_j with respect to λ_j and then setting $\lambda_j = 0$, for $j = 1, \dots, s-1$. After such manipulations, $\det(\lambda_i^{s-j})$ becomes

$$(-1)^{\frac{s(s-1)}{2}} \lambda_s^{s-1} \prod_{i=1}^{s-1} \Gamma(s-i). \quad (3.63)$$

After the manipulations mentioned above, we have

$$\begin{aligned} & \lim_{\lambda_j \rightarrow 0} \frac{d^{j-1}}{d\lambda_j^{j-1}} \det \left(\int_a^b g(y) y^{t-i} e^{-y} {}_0F_1(t-s+1; y\lambda_j) dy \right) \\ &= \frac{1}{\Gamma(t-s+j)} \\ & \quad \times \det \left(\lim_{\lambda_j \rightarrow 0} \int_a^b g(y) y^{t-i+j-1} e^{-y} {}_0F_1(t-s+j; y\lambda_j) dy \right). \end{aligned} \quad (3.64)$$

We need now to show that the order of the limit and the integration in (3.64) is interchangeable. Define a sequence of functions

$$\begin{aligned} h_n(y) &= {}_0F_1 \left(t-s+j; \frac{1}{n}y \right) \bar{g}(y), \\ n &= 1, 2, \dots, \end{aligned} \quad (3.65)$$

where

$$\bar{g}(y) = g(y) y^{t-i+j-1} e^{-y}. \quad (3.66)$$

It is obvious that

$$\lim_{n \rightarrow \infty} h_n(y) = \bar{g}(y), \text{ for all } y > 0, \quad (3.67)$$

and that $|h_n(y)|$ is bounded by

$$|\bar{g}(y) {}_0F_1(t-s+j; y)|. \quad (3.68)$$

Now if

$$\int_a^b |\bar{g}(y)|_0 F_1(t-s+j; y) dy < \infty, \quad (3.69)$$

for choices of $g(y)$ (which is the case for MRC and the MI MGF), by Lebesgue's Dominated Convergence Theorem, we can interchange the order of the limit and the integration in (3.64). Since $\mathbf{M}^H \Sigma^{-1} \mathbf{M}$ now has only one nonzero eigenvalue, we denote it by λ_1 . In summary, we have the general integral for this i.i.d. Rician fading case to be given by

$$I_{\text{iid}} = \frac{e^{-\lambda_1}}{\Gamma(t-s+1)\lambda_1^{s-1}} \frac{\det(\Psi_{\text{iid}})}{\prod_{m=1}^{s-1} \Gamma(t-m)\Gamma(s-m)}, \quad (3.70)$$

where Ψ_{iid} is an $s \times s$ matrix whose entries in the first column are the same as those of Ψ_{nc} defined by (3.60), that is,

$$\{\Psi_{\text{iid}}\}_{i,1} = \{\Psi_{\text{nc}}\}_{i,1}, \quad i = 1, \dots, s \quad (3.71)$$

and the entries from the second column to the s th column are given by

$$\begin{aligned} \{\Psi_{\text{iid}}\}_{i,j} &= \int_a^b g(y) y^{t+s-i-j} e^{-y} dy \\ i &= 1, \dots, s, \quad j = 2, \dots, s. \end{aligned} \quad (3.72)$$

When $E(\mathbf{H}) = \mathbf{0}$, taking the $(s-1)$ th derivative with respect to λ_1 in both numerator (the term $\det(\Psi_{\text{iid}})$) and denominator (the term λ_1^{s-1}) and then setting $\lambda_1 = 0$ give the general integral for the i.i.d. MIMO Rayleigh fading channels as

$$I_{\text{Rayleigh}} = \frac{\det(\Psi_{\text{Rayleigh}})}{\prod_{m=1}^s \Gamma(t-m+1)\Gamma(s-m+1)}, \quad (3.73)$$

where Ψ_{Rayleigh} is an $s \times s$ Hankel matrix function of τ with entries given by

$$\begin{aligned} \{\Psi_{\text{Rayleigh}}\}_{i,j} &= \int_a^b g(y) y^{t+s-i-j} e^{-y} dy \\ i, \quad j &= 1, \dots, s. \end{aligned} \quad (3.74)$$

The MGF of the MI (3.6) can be obtained by letting $a = 0$, $b = \infty$, and $g(y) = (1 + \rho y)^{\tau/\ln(2)}$. The SNR outage probability for the MIMO MRC system over Rician fading channels can also be obtained by letting $a = 0$, $b = x$, and $g(y) = 1$. Related results on this topic include the MGF of the MI with equal power allocation for noniid Rician, i.i.d. Rician MIMO channels [19] and for the i.i.d. Rayleigh MIMO channels in [20, 19, 21]. In addition, the outage probability of MIMO MRC over i.i.d. Rayleigh MIMO channels was derived in [22] and over Rician MIMO channels was obtained in [23, 24].

Scalar hypergeometric functions are built-in functions in well-known software packages such as Matlab, Mathematica, and Maple. Therefore, one can calculate exact results for given system parameters without using time-consuming Monte Carlo simulations. On the other hand, it is more interesting to investigate the effect of system parameters on the system

performance. As an example, we look at how the Rician fading affects the MIMO system performance.

We first take a close look at (3.60) and expand the ${}_0F_1(t - s + 1; y\lambda_j)$ into its series representation, we get

$${}_0F_1(t - s + 1; y\lambda_j) = \sum_{k=0}^{\infty} \frac{(y\lambda_j)^k}{k!(t - s + 1)_k}. \quad (3.75)$$

Therefore, the determinant becomes

$$\begin{aligned} \det(\Phi_{nc}) &= \det \left(\sum_{k=0}^{\infty} \int_a^b y^{t-i} g(y) e^{-y} \frac{(y\lambda_j)^k}{k!(t - s + 1)_k} \right) \\ &= \det \left(\sum_{k=0}^{\infty} \left(\int_a^b y^{t-i+k} g(y) e^{-y} dy \right) \left(\frac{(\lambda_j)^k}{k!(t - s + 1)_k} \right) \right) \\ &\approx \det \left(\sum_{k=0}^{s-1} \left(\int_a^b y^{t-i+k} g(y) e^{-y} dy \right) \left(\frac{(\lambda_j)^k}{k!(t - s + 1)_k} \right) \right) \\ &= \left(\prod_{m=0}^{s-1} \frac{1}{m!(t - s + 1)_m} \right) \\ &\quad \times \det \left(\sum_{k=1}^s \left(\int_a^b y^{t-i+k-1} g(y) e^{-y} dy \right) \left((\lambda_j)^{k-1} \right) \right) \\ &= \left(\prod_{m=0}^{s-1} \frac{1}{m!(t - s + 1)_m} \right) \\ &\quad \times \det \left(\int_a^b y^{t-i+j-1} g(y) e^{-y} dy \right) \det \left(\lambda_j^{i-1} \right), \end{aligned} \quad (3.76)$$

where the last equality follows from the definition of product of matrices and the fact that the determinant of the two matrices is the product of determinants. We then replace j with $s - j + 1$ (i.e., switch the j th column with the $s - j + 1$ th column in a matrix) in the two determinants, and substitute the resulted expression into (3.60). After simplifications, we get

$$I_{\text{Rician}} \approx \frac{e^{-\text{tr}(\Lambda)}}{\prod_{m=1}^s \Gamma(s - m + 1) \Gamma(t - m + 1)} \det \left(\int_a^b y^{t+s-i-j} g(y) e^{-y} dy \right) \quad (3.77)$$

Now comparing (3.77) with (3.73), one immediately recognizes that

$$I_{\text{Rician}} \approx e^{-\text{tr}(\Lambda)} I_{\text{Rayleigh}} \quad (3.78)$$

This approximation is accurate when $s = \min(T, R)$ is large. Specifically, the outage probability of MIMO MRC over Rician channels is asymptotically close to that over Rayleigh channels multiplied by $e^{-\text{tr}(\Lambda)}$. Figure 3.1 verifies the exact expressions with Monte Carlo

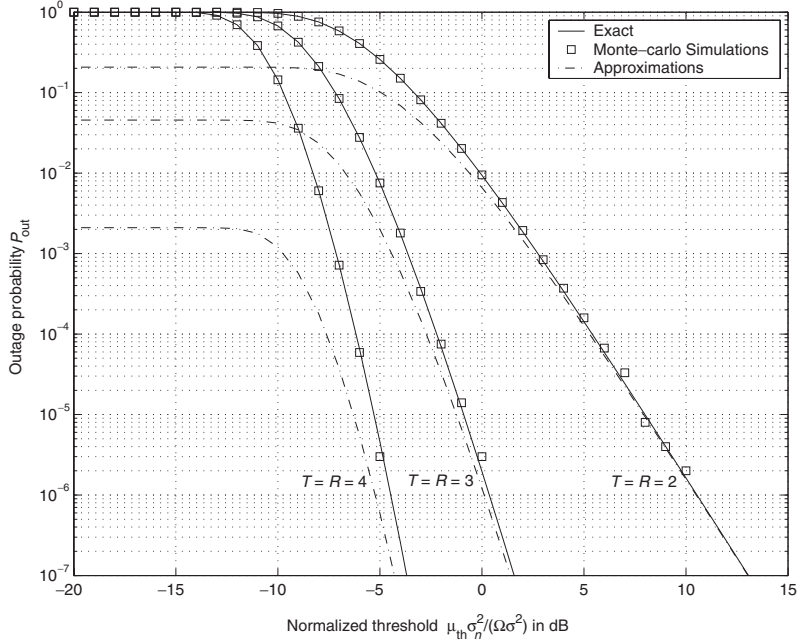


Figure 3.1 Comparison between (i) exact results, (ii) simulations, and (iii) approximations, when $\sigma^2 = \sigma_n^2 = 2$ and $\{\mathbf{M}\}_{i,j} \sim \text{Uniform}(0,1)$.

simulations for the outage probability of MIMO MRC over Rician channels. It also compares the exact results with the approximate relationship given in (3.78). It can be seen that the outage probability is lower bounded by the approximation and this bound is quite tight for high SNR.

Similar calculations for the semicorrelated Rayleigh channels whose channel matrix has the PDF given by (3.48) or (3.49) can also be obtained as we present in what follows.

1. If the nonidentity covariance matrix is an $s \times s$ matrix with distinct eigenvalues $0 < \phi_1 < \dots < \phi_s$, then the integral is given by

$$I_{\text{cor}} = \frac{\det(\Psi_1)}{\det(\mathbf{V}_1) \prod_{i=1}^s \Gamma(t-i+1)}, \quad (3.79)$$

where $P = \frac{\Omega}{\sigma_n^2 T}$ is the transmitting SNR per branch, Ψ_1 is an $s \times s$ matrix with entries given by

$$\{\Psi_1\}_{i,j} = \int_a^b g(y) y^{t-i} e^{-\frac{y}{\phi_j}} dy, \quad (3.80)$$

and \mathbf{V}_1 is an $s \times s$ matrix whose determinant is given by

$$\begin{aligned} \det(\mathbf{V}_1) &= \det\left((-1)^{s-j}\phi_i^{t-s+j}\right) = \left(\prod_{i=1}^s \phi_i^t\right) \\ &\quad \times \prod_{1 \leq l < k \leq s} \left(\frac{1}{\phi_k} - \frac{1}{\phi_l}\right). \end{aligned} \quad (3.81)$$

2. If the nonidentity covariance matrix is a $t \times t$ matrix with distinct eigenvalues $0 < \phi_1 < \dots < \phi_t$, then the integral is given by

$$I_{\text{cor}} = \frac{(-1)^{s(t-s)} \det(\Psi_2)}{\det(\mathbf{V}_2) \prod_{i=1}^s \Gamma(s-i+1)}, \quad (3.82)$$

where Ψ_2 is a $t \times t$ matrix given by

$$\Psi_2 = \begin{pmatrix} \Psi_{2A} \\ \Psi_{2B} \end{pmatrix}, \quad (3.83)$$

where Ψ_{2A} is a $(t-s) \times t$ matrix with entries given by

$$\{\Psi_{2A}\}_{i,j} = \left(\frac{-1}{\phi_j}\right)^{t-s-i}, \quad i = 1, \dots, t-s; j = 1, \dots, t, \quad (3.84)$$

Ψ_{2B} is an $s \times t$ matrix with entries given by

$$\begin{aligned} \{\Psi_{2B}\}_{i,j} &= \int_a^b g(y) y^{s-i} e^{-\frac{y}{\phi_j}} dy, \\ i &= 1, \dots, s; j = 1, \dots, t, \end{aligned} \quad (3.85)$$

The MI MGF can be obtained by setting $a = 0$, $b = \infty$, and $g(y) = (1 + \rho y)^{\tau/\ln(2)}$ [25–27] and the MIMO MRC outage probability can be obtained by setting $a = 0$, $b = x$, and $g(y) = 1$ [25].

Figure 3.2 plots the effect of antenna correlation coefficients on the average MI with equal power transmission. For simplicity, we assume that the fading correlation coefficient between the different antennas is constant and equal to ζ . It can be seen from this figure that a moderate antenna correlation coefficient ζ (i.e., $\zeta \leq 0.5$) does not have significant impact on the average MI.

3.4.3 Applications to MIMO channels in the presence of interference

We first consider the simplified problem in which the Hermitian matrix involved is given by (3.24). When there exists an LOS path for the desired user while interferers are assumed to be subject to purely scattering fading, \mathbf{H}_D is a complex Gaussian matrix with a nonzero mean matrix and \mathbf{H}_I is a complex Gaussian matrix with zero mean. It is also reasonable to assume that the desired signal and interfering signals are independently faded. In such a scenario, $\mathbf{H}_D: R \times T$ and $\mathbf{H}_I: R \times N_I$ are independent matrices whose columns are independent

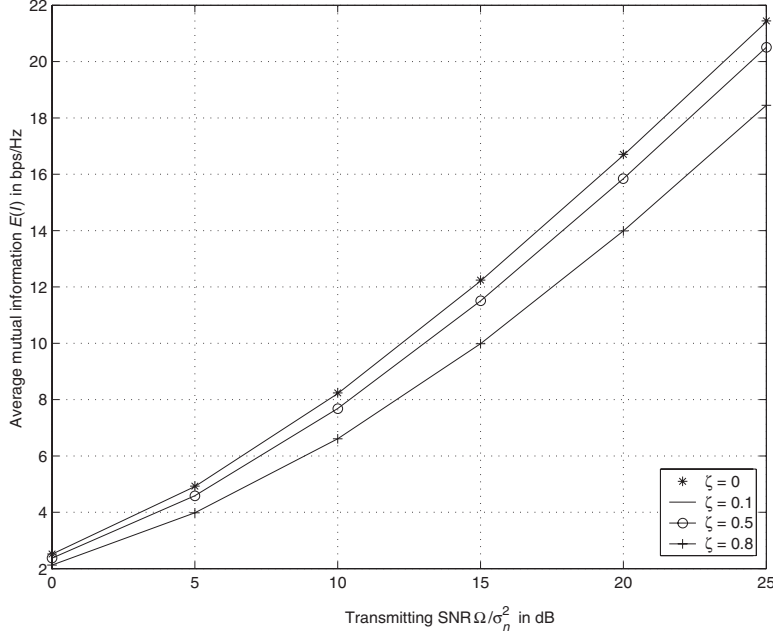


Figure 3.2 Effect of antenna correlation on the average MI when $T = R = 3$ with different fading correlation coefficient ζ (for simplicity, we use a correlation model in which correlation coefficients between different antennas are identically equal to ζ).

complex R -variate Gaussian vectors with covariance matrix $\Sigma = \sigma^2 \mathbf{I}_R$. The mean matrices are $E(\mathbf{H}_D) = \mathbf{M}$ and $E(\mathbf{H}_I) = \mathbf{0}$. Note that in order for $\mathbf{H}_I \mathbf{H}_I^H$ to be invertible, it is required that $N_I \geq R$, which is equivalent to saying that the number of interfering signals is greater than or equal to the number of the desired user's receive antennas. Define $s = \min(T, R)$, $t = \max(T, R)$, and $r = \min(N_I, N_I + T - R)$. If $\mathbf{M}^H \Sigma^{-1} \mathbf{M}$ has s nonzero distinct eigenvalues $0 < \lambda_1 < \lambda_2 < \dots < \lambda_s$, then the joint PDF of the s nonzero eigenvalues $0 < \phi_1 < \phi_2 < \dots < \phi_s$ of \mathbf{F}_2 , $f_{\phi_1, \dots, \phi_s}(\phi_1, \dots, \phi_s)$, is given by [15]

$$f_{\phi_1, \dots, \phi_s}(\phi_1, \dots, \phi_s) = c_2 {}_1\tilde{F}_1 \left(r + s; t; \Lambda, \left(\mathbf{I}_s + \Phi^{-1} \right)^{-1} \right) \\ \times \prod_{k=1}^s \frac{\phi_k^{t-s}}{(1 + \phi_k)^{t+r}} \prod_{i < j}^s (\phi_i - \phi_j)^2, \quad (3.86)$$

where

$$c_2 = e^{-\text{tr}(\Lambda)} \prod_{i=1}^s \frac{\Gamma(r + t - i + 1)}{\Gamma(r - i + 1)\Gamma(t - i + 1)\Gamma(s - i + 1)}, \quad (3.87)$$

where $\Lambda = \text{diag}(\lambda_1, \dots, \lambda_s)$. The PDF given by (3.86) is not exactly in the form of that in (3.50) in that the second matrix parameter is $(\mathbf{I}_s + \Phi^{-1})^{-1}$ rather than Φ . One way to

transform the integral into the form (3.50) is to use the following transformation

$$\psi_i = \frac{\phi_i}{1 + \phi_i}, \quad i = 1, \dots, s.$$

The Jacobian of such transformation is

$$d\phi_1 \dots d\phi_s = \left(\prod_{i=1}^s \frac{1}{1 - \psi_i} \right) d\psi_1 \dots d\psi_s.$$

The integral of interest is given by

$$\begin{aligned} I_{\text{ccil}} &= \int_{a < \phi_1 < \dots < \phi_s < b} \prod_{k=1}^s g(\phi_k) f_{\phi_1, \dots, \phi_s}(\phi_1, \dots, \phi_s) d\phi_1 \dots d\phi_s \\ &= \int_{\frac{a}{1+a} < \psi_1 < \dots < \psi_s < \frac{b}{1+b}} \prod_{k=1}^s g\left(\frac{\psi_k}{1 - \psi_k}\right) f_{\phi_1, \dots, \phi_s}\left(\frac{\psi_1}{1 - \psi_1}, \dots, \frac{\psi_s}{1 - \psi_s}\right) \\ &\quad \times \prod_{k=1}^s \frac{1}{1 - \psi_k} d\psi_1 \dots d\psi_s \end{aligned} \tag{3.88}$$

and

$$\begin{aligned} f_{\phi_1, \dots, \phi_s}\left(\frac{\psi_1}{1 - \psi_1}, \dots, \frac{\psi_s}{1 - \psi_s}\right) \prod_{k=1}^s \frac{1}{1 - \psi_k} \\ = c_{2-1} \tilde{F}_1(r+s; t; \Lambda, \Psi) \\ \times \prod_{k=1}^s \psi_k^{t-s} (1 - \psi_k)^{r+s-1} \prod_{i < j}^s (\psi_i - \psi_j)^2 d\psi_1 \dots d\psi_s, \end{aligned} \tag{3.89}$$

where $\Psi = \text{diag}(\psi_1, \dots, \psi_s)$. Substituting (3.89) into (3.88), we get I_{ccil}

$$\begin{aligned} I_{\text{ccil}} &= \int_{\{\frac{a}{1+a} < \psi_1 < \dots < \psi_s < \frac{b}{1+b}\}} \prod_{k=1}^s g\left(\frac{\psi_k}{1 - \psi_k}\right) c_{2-1} \tilde{F}_1(r+s; t; \Lambda, \Psi) \\ &\quad \times \prod_{k=1}^s \psi_k^{t-s} (1 - \psi_k)^{r+s-1} \prod_{i < j}^s (\psi_i - \psi_j)^2 d\psi_1 \dots d\psi_s. \end{aligned} \tag{3.90}$$

Now (3.90) is in the exactly same form of (3.50) and can be evaluated as

$$\begin{aligned} I_{\text{ccil}} &= \frac{c'}{\det(\lambda_i^{s-j})} \det \left(\int_{\frac{a}{1+a}}^{\frac{b}{1+b}} g\left(\frac{x}{1-x}\right) \right. \\ &\quad \times {}_1F_1(r+t-s+1, t-s+1, \lambda_i x) x^{t-j} (1-x)^{r+s-1} dx \Big) \\ &= \frac{c'}{\det(\lambda_i^{s-j})} \det(\Psi_{\text{ccil}}) \end{aligned} \tag{3.91}$$

$$c' = e^{-\text{tr}(\Lambda)} \prod_{l=1}^s \frac{\Gamma(r+t-s+1)}{\Gamma(t-s+1)\Gamma(r-l+1)}. \quad (3.92)$$

Results for limiting cases when some $\lambda_i = \lambda_j$, for $i \neq j$, or the number of nonzero eigenvalues is less than s , can be obtained by the same procedure as in the noise-limited case. Therefore, we omit here the detailed derivations and directly give the expressions. When \mathbf{M} has η at each entry and $\Sigma = \sigma^2 \mathbf{I}_R$, then $\mathbf{M}^H \Sigma^{-1} \mathbf{M}$ has only single nonzero eigenvalue $\lambda_1 = \frac{st|\eta|^2}{\sigma^2}$. The general integral reduces to

$$\begin{aligned} I_{\text{cc}i2} &= \frac{e^{-\lambda_1}}{\lambda_1^{s-1}} \frac{\Gamma(r+t-s+1)\Gamma(s)\Gamma(t)}{\Gamma(t-s+1)\Gamma(t+r)} \det(\Psi_{\text{cc}i-\text{iid}}) \\ &\times \prod_{k=1}^s \frac{\Gamma(t+r-k+1)}{\Gamma(t-k+1)\Gamma(r-k+1)\Gamma(s-k+1)}, \end{aligned} \quad (3.93)$$

where $\det(\Psi_{\text{cc}i-\text{iid}})$ is an $s \times s$ matrix whose entries in first column are the same as those of $\Psi_{\text{cc}i}$ defined in (3.91), that is,

$$\{\Psi_{\text{cc}i-\text{iid}}\}_{i,1} = \{\Psi_{\text{cc}i}\}_{i,1}, i = 1, \dots, s \quad (3.94)$$

and entries from 2th column to s th column are given by

$$\begin{aligned} \{\Psi_{\text{cc}i-\text{iid}}\}_{i,j} &= \int_{\frac{a}{1+a}}^{\frac{b}{1+b}} g\left(\frac{y}{1-y}\right) y^{t+s-i-j} (1-y)^{r-s+i-1} dy \\ i &= 1, \dots, s, \quad j = 2, \dots, s. \end{aligned} \quad (3.95)$$

When $E(\mathbf{X}) = E(\mathbf{Y}) = \mathbf{0}$, (i.e., both \mathbf{X} and \mathbf{Y} are central), the integral reduces to

$$\begin{aligned} I_{\text{cc}i3} &= \det(\Psi_{\text{cc}i-\text{Rayleigh}}) \\ &\times \prod_{k=1}^s \frac{\Gamma(t+r-k+1)}{\Gamma(t-k+1)\Gamma(r-k+1)\Gamma(s-k+1)}, \end{aligned} \quad (3.96)$$

where $\Psi_{\text{cc}i-\text{Rayleigh}}$ is an $s \times s$ matrix function of $x \in (0, \infty)$ with entries given by

$$\begin{aligned} \{\Psi_{\text{cc}i-\text{Rayleigh}}\}_{i,j} &= \int_{\frac{a}{1+a}}^{\frac{b}{1+b}} g\left(\frac{y}{1-y}\right) y^{t+s-i-j} (1-y)^{r-s+i-1} dy \\ i, j &= 1, \dots, s. \end{aligned} \quad (3.97)$$

Note that (3.96) are applicable to any positive definite covariance matrix Σ because of the fact that in the central case, $\mathbf{X}\mathbf{X}^H (\mathbf{Y}\mathbf{Y}^H)^{-1}$ is invariant under simultaneous transformations of $\Sigma^{-\frac{1}{2}}\mathbf{X}$ and $\Sigma^{-\frac{1}{2}}\mathbf{Y}$.

The MGF of the MI with equal power transmission can be obtained from (3.91) by setting $g\left(\frac{x}{1+x}\right) = \log_2\left(1 + \rho \frac{x}{1+x}\right)$, $\frac{a}{1+a} = 0$, and $\frac{b}{1+b} = 1$. The MIMO optimum combining SINR

outage probability can be obtained from (3.91) by setting $g\left(\frac{x}{1+x}\right) = 1$, $\frac{a}{1+a} = 0$, and $\frac{b}{1+b} = \frac{x}{1+x}$, where $x = \frac{\Omega_L}{\Omega_D} \mu_{\text{th}}$. Most integrals involved in the determinants can be evaluated in close-form expressions, as it was presented in [28] and [29].

Results for some more complicated scenarios can be derived via further manipulations. For example, we can study the integral for the CCI MIMO channels when \mathbf{P}_I is an arbitrary Hermitian positive matrix and $\sigma_n^2 > 0$.

Let $\mathbf{F} = \mathbf{H}_D^H \mathbf{B}_I^{-1} \mathbf{H}_D = \mathbf{H}_D^H (\mathbf{H}_I \mathbf{P}_I \mathbf{H}_I^H + \sigma_n^2 \mathbf{I}_R)^{-1} \mathbf{H}_D$, where $\mathbf{H}_D: R \times T$ and $\mathbf{H}_I: R \times N_I$ are independent complex Gaussian matrices with i.i.d. entries $\sim \mathcal{CN}(0, 1)$. Let \mathbf{P}_I be a Hermitian positive definite matrix. We assume that $\mathbf{P}_I = \text{diag}(P_1, \dots, P_{N_I})$, where $0 < P_1 < P_2 < \dots < P_{N_I}$, is a diagonal matrix without losing any generality. The general integral given by (3.50) can be evaluated by first conditioning on the \mathbf{H}_I and then averaging over \mathbf{H}_I , that is,

$$I = E_{\mathbf{H}_I} (I|_{\mathbf{H}_I}). \quad (3.98)$$

Note that conditioning on \mathbf{H}_I , or equivalently on the nonzero eigenvalues of $\mathbf{H}_I \mathbf{P}_I \mathbf{H}_I^H$, \mathbf{F} is nothing but the noise-limited semicorrelated case and its general integral is given by (3.79) or (3.82), while the joint PDF of the nonzero eigenvalues of $\mathbf{H}_I \mathbf{P}_I \mathbf{H}_I^H$ is given by (3.48) or (3.49). The final results can be derived by following the similar steps, which are given in detail in the journal version of [30].

3.5 Summary

In this chapter, we showed that evaluating several performance measures of MIMO fading channels can be put under a common integration problem. We then presented the techniques for evaluating this integration problem. Examples were given for the performance expressions of several MIMO fading channels as well as MIMO diversity combining schemes. It was shown that several different MIMO performance analysis problems can be readily derived under this framework.

The expressions and the techniques can be useful in two ways. First, they can replace time-consuming Monte Carlo simulations for generating exact performance results for a given set of system parameters. Second, they can be further manipulated and simplified to investigate the effect of system parameters on the performance under certain conditions. For example, we showed that the outage probability of MIMO MRC over Rician fading channels can be approximated by $e^{-\text{tr}(\mathbf{M}\mathbf{M}^H)/\sigma^2}$ multiplied by the outage probability of MIMO MRC over MIMO Rayleigh channels.

Acknowledgment

This work was supported in part by the National Science Foundation grant NO. CCR-983462. The authors are with the Department of Electrical and Computer Engineering, University of Minnesota, Minneapolis. They can be reached at E-mails: <mkang, lyang, alouini> @ece.umn.edu.

References

- [1] J. H. Winters, "On the capacity of radio communications with diversity in a Rayleigh fading environment," *IEEE J. Sel. Area Commun.*, vol. SAC-5, no. 1, pp. 871–878, Jun. 1987.
- [2] G. J. Foschini and M. J. Gans, "On limits of wireless communication in a fading environment when using multiple antennas," *Wireless Pers. Commun.*, vol. 6, no. 3, pp. 311–335, Mar. 1998.
- [3] I. E. Telatar, "Capacity of multi-antenna Gaussian channels," *Eur. Trans. Telecommun.*, vol. 10, no. 6, pp. 585–596, Nov.-Dec. 1999.
- [4] S. A. Jafar, S. Vishwanath, and A. J. Goldsmith, "Channel capacity and beamforming for multiple transmit and receive antennas with covariance feedback," in *Proc. IEEE Int. Conf. Commun. (ICC'2001)*, Helsinki, Finland, Apr. 2001, pp. 2266–2270.
- [5] R. A. Horn and C. R. Johnson, *Matrix Analysis*. Cambridge University Press, 1985.
- [6] K. Yu, M. Bengtsson, B. Ottersten, D. McNamara, P. Karlsson, and M. Beach, "Modeling of wide-band MIMO radio channels based on NLoS indoor measurements," *IEEE Trans. Veh. Tech.*, vol. 53, pp. 655–665, May 2004.
- [7] H. Ozcelik, M. Herdin, W. Weichselberger, J. Wallace, and E. Bonek, "Deficiencies of 'Kronecker' MIMO radio channel model," *Electron. Lett.*, vol. 39, pp. 1209–1210, Aug. 2003.
- [8] D. P. Palomar, J. M. Cioffi, and M. A. Lagunas, "Uniform power allocation in MIMO channels: A game-theoretic approach," *IEEE Trans. Inf. Theory*, vol. 49, pp. 1707–1727, July 2003.
- [9] H. Boche and E. A. Jorswieck, "On the ergodic capacity as a function of the correlation properties in systems with multiple transmit antennas without CSI at the transmitter," *IEEE Trans./ Commun.*, vol. 52, no. 10, pp. 1654–1657, Oct. 2004.
- [10] M. Godavarti, A. O. Hero III, and T. Marzetta, "Min-capacity of a multiple-antenna wireless channel in a static Rician fading environment," in *Proc. IEEE Int. Symp. Inf. Theory (ISIT'2001)*, Washington, DC, June 2001, p. 57.
- [11] R. S. Blum, J. H. Winters, and N. R. Sollenberger, "On the capacity of cellular systems with MIMO," *IEEE Commun. Lett.*, vol. 2, pp. 242–244, Jun. 2002.
- [12] C. H. Tse, K.-W. Yip, and T.-S. Ng, "Performance tradeoffs between maximum ratio transmission and switched-transmit diversity," in *Proc. 11th IEEE Int. Symp. Pers., Indoor Mobile Radio Commun. (PIMRC'2000)*, London, UK, Sept. 2000, pp. 1485–1489.
- [13] K.-K. Wong, R. S. K. Cheng, K. B. Letaief, and R. D. Murch, "Adaptive antennas at the mobile and base stations in an OFDM/TDMA system," *IEEE Trans. Commun.*, vol. 49, no. 1, pp. 195–206, Jan. 2001.
- [14] I. S. Gradshteyn and I. M. Ryzhik, *Table of Integrals, Series, and Products*, 5th ed. Orlando, FL: Academic Press, 1994.
- [15] A. T. James, "Distributions of matrix variates and latent roots derived from normal samples," *Ann. Math. Stat.*, vol. 35, no. 2, pp. 475–501, June 1964.
- [16] N. R. Goodman, "Statistical analysis based on a certain multivariate complex Gaussian distribution (an introduction)," *Ann. Math. Stat.*, vol. 34, no. 1, pp. 152–177, Feb. 1965.
- [17] C. G. Khatri, "On certain distribution problems based on positive definite quadratic functions in normal vectors," *Ann. Math. Stat.*, vol. 37, no. 2, pp. 468–470, Apr. 1966.
- [18] K. I. Gross and D. S. P. Richards, "Total positivity, spherical series, and hypergeometric functions of matrix argument," *J. Approx. Theory*, vol. 59, no. 2, pp. 224–246, 1989.
- [19] M. Kang and M.-S. Alouini, "On the capacity of MIMO Rician channels," in *Proc. 40th Annu. Allerton Conf. Commun., Control, Comput. (Allerton'2002)*, Monticello, IL, Oct. 2002.
- [20] M. Chiani, "Evaluating the capacity distribution of MIMO Rayleigh channels," in *Proc. IEEE Int. Symp. Adv. Wireless Commun. (ISWC'2002)*, Victoria, BC, Canada, Sept. 2002, pp. 3–4.

- [21] Z. Wang and G. B. Giannakis, "Outage mutual information of space-time MIMO channels," in *Proc. 40th Annu. Allerton Conf. Commun., Control Comput. (Allerton'2002), Monticello, IL*, Oct. 2002.
- [22] P. A. Dighe, R. K. Mallik, and S. R. Jamuar, "Analysis of transmit-receive diversity in Rayleigh fading," in *Proc. IEEE Globel Telecom. Conf. (Globecom'2001), San Antonio, TX*, Nov. 2001, pp. 1132–1136.
- [23] M. Kang and M.-S. Alouini, "Performance analysis of MIMO MRC systems over Rician fading channels," in *Proc. IEEE Veh. Tech. Conf. (VTC'2002 Fall)*, Vancouver, Canada, Sept. 2002, pp. 869–873.
- [24] M. Kang and M.-S. Alouini, "Largest eigenvalue of complex Wishart matrices and performance analysis of MIMO MRC systems," *IEEE J. Sel. Areas Commun., Spec. Issue MIMO Syst. Appl. (JSAC-MIMO)*, vol. 21, pp. 418–426, Apr. 2003.
- [25] M. Kang and M. S. Alouini, "Impact of correlation on the capacity of MIMO channels," in *Proc. IEEE Int. Conf. Commun. (ICC'2003), Anchorage, AK*, May 2003, pp. 2623–2627.
- [26] M. Chiani, M. Win, and A. Zanella, "On the capacity of spatially correlated MIMO Rayleigh-fading channels," *IEEE Trans. Inf. Theory, Spec. Issue Space-time Tech.*, vol. 4, pp. 2363–2371, Oct. 2003.
- [27] P. J. Smith, S. Roy, and M. Shafi, "Capacity of MIMO systems with semicorrelated flat fading," *IEEE Trans. Inf. Theory, Spec. Issue Space-time Tech.*, vol. 4, pp. 2781–2788, Oct. 2003.
- [28] M. Kang and M.-S. Alouini, "Quadratic forms in complex Gaussian matrices and performance analysis of MIMO systems with cochannel interference," *IEEE Trans. Wireless Commun.*, vol. 3, pp. 418–431, Mar. 2004.
- [29] M. Kang, L. Yang, and M.-S. Alouini, "Capacity of MIMO Rician channels with multiple correlated Rayleigh cochannel interferers," in *Proc. IEEE Global Telecommun. (GLOBECOM'2003), San Francisco, CA*, Dec. 2003, pp. 1119-1123.
- [30] M. Kang and M.-S. Alouini, "Performance analysis of MIMO systems in presence of cochannel interference and additive Gaussian noise," in *Proc. 37th Annu. Conf. Inf. Sci. Syst. (CISS'2003), Baltimore, MD*, Mar. 2003. Journal version submitted for publication.

4

Recent Advances in Orthogonal Space-Time Block Coding

**Mohammad Gharavi-Alkhansari, Alex B. Gershman,
and Shahram Shahbazpanahi**

4.1 Introduction

Exploiting multiple antennas at the transmitter and the receiver in wireless communication systems has recently been proven to provide substantial benefits in both increasing system capacity and improving its immunity to deep fading in the channel [1, 2]. To take advantage of these benefits, special *space-time coding* techniques are required. A pioneering work in the area of space-time coding for multiple-input multiple-output (MIMO) wireless channels has been done by Tarokh *et al.* in [3], in which two code design criteria have been proposed for flat fading channels with coherent receivers, and high-performance space-time trellis codes have been designed. However, these codes suffer from rather high decoding complexity. In the same year, Alamouti proposed his celebrated space-time block coding (STBC) scheme for two transmit and multiple receive antennas [4]. The maximum likelihood (ML) decoder for Alamouti's code has very low complexity. Inspired by this work, Tarokh *et al.* generalized Alamouti's code to multiple transmit antennas using the theories of orthogonal and amicable designs [5]. The codes developed in [5] are known as orthogonal STBCs (OSTBCs) and are able to provide high performance at very low decoding complexity. Some other designs of OSTBCs have also been recently developed in [6–8].

OSTBCs have a rich and fascinating theory. This theory can be divided into two almost separate parts. The first part deals with how OSTBCs can be designed. This aspect of the OSTBC theory is beyond the scope of our chapter, and interested readers are referred to the relevant literature [5–9]. The second part of this theory deals with the properties of these codes and constitutes the focus of our chapter. Interestingly, the main properties of OSTBCs

can be derived from their simple definition proposed in [5] and are almost independent of the way these codes have been constructed. In this chapter, we provide a background of the theory of OSTBCs and review recent results that are based on their *constellation space invariance* property and similarities between OSTBC models and signal models used in array processing.

The remainder of this chapter is organized as follows. In Section 4.3, we review necessary mathematical concepts. In Section 4.4, a point-to-point MIMO model for flat block fading channels is introduced. In the same section, the concepts of OSTBCs and the coherent ML decoder are reviewed. In Section 4.5, the constellation space invariance property of OSTBCs is derived and discussed in detail. This property forms a basis for the main developments in the chapter. Using this property, an equivalent array-processing-type model of an orthogonally coded MIMO system is developed in the same section. Furthermore, the constellation space invariance property is used in Section 4.6 to develop simple and intuitive formulae for the coherent ML decoder and to explain why symbol-by-symbol ML decoding of OSTBCs is possible. This property is further exploited in Section 4.7 to provide an exact symbol error probability analysis for the coherent ML decoder. In Section 4.8, the optimality properties of OSTBCs are proven and discussed. Section 4.9 presents a blind OSTBC decoder based on the aforementioned equivalent array-processing-type model, and the performance of this technique is compared with that of the popular differential blind decoder. In Section 4.10, the problem of using OSTBCs in multiaccess MIMO systems is considered. In this section, the array-processing-type MIMO model is used to formulate computationally efficient minimum variance (MV) multiuser receivers. Conclusions are drawn in Section 4.11.

4.2 Notations and Acronyms

All of the notations and acronyms are defined at the time of their first appearance in the text.

4.3 Mathematical Preliminaries

In this section, we review some basic mathematical concepts needed for the developments in the following sections. We assume that the reader is familiar with the concepts of vector spaces, inner product spaces, and linear operators.

The set of $I \times J$ complex matrices forms a vector space over the field of real numbers \mathbb{R} . For any $I \times J$ complex matrix \mathbf{A} , we can introduce a real $2IJ \times 1$ column vector $\underline{\mathbf{A}}$ representation built by stacking the real and imaginary parts of all the elements of \mathbf{A} in a single column so that

$$\underline{\mathbf{A}} \triangleq \begin{bmatrix} \text{Re}\{\text{vec}\{\mathbf{A}\}\} \\ \text{Im}\{\text{vec}\{\mathbf{A}\}\} \end{bmatrix}. \quad (4.1)$$

Here, $\text{Re}\{\cdot\}$ and $\text{Im}\{\cdot\}$ denote the real and imaginary parts, respectively, and $\text{vec}\{\cdot\}$ is the vectorization operator stacking all columns of a matrix on top of each other. For any two

$I \times J$ complex matrices \mathbf{A} and \mathbf{B} , let us define the function

$$\begin{aligned}\langle \mathbf{A}, \mathbf{B} \rangle &\triangleq \operatorname{Re} \left\{ \operatorname{tr}(\mathbf{AB}^H) \right\} \\ &= \operatorname{Re} \left\{ \operatorname{tr}(\mathbf{B}^H \mathbf{A}) \right\} \\ &= \operatorname{Re} \left\{ \operatorname{tr}(\mathbf{BA}^H) \right\} \\ &= \operatorname{Re} \left\{ \operatorname{tr}(\mathbf{A}^H \mathbf{B}) \right\} \\ &= \underline{\mathbf{A}}^T \underline{\mathbf{B}}\end{aligned}\tag{4.2}$$

where $\operatorname{tr}\{\cdot\}$, $(\cdot)^H$, and $(\cdot)^T$ denote the trace, Hermitian transpose, and transpose of a matrix, respectively. It is easy to verify that the aforementioned vector space of $I \times J$ complex matrices with the above function $\langle \cdot, \cdot \rangle$ defines a real inner product (vector) space [10] where the word *real* refers to the fact that all the scalars in this linear space and all the values of inner products are real.

In this space, the Frobenius norm, denoted by $\|\cdot\|_F$, is the *natural norm* [10], that is,

$$\|\mathbf{A}\|_F \triangleq \sqrt{\operatorname{tr}(\mathbf{AA}^H)} = \sqrt{\operatorname{tr}(\mathbf{A}^H \mathbf{A})} = \sqrt{\langle \mathbf{A}, \mathbf{A} \rangle}.\tag{4.3}$$

Consider a linear operator $\mathcal{F} : \mathcal{S}_1 \mapsto \mathcal{S}_2$ where \mathcal{S}_1 and \mathcal{S}_2 are any normed vector spaces whose norms we denote by $\|\cdot\|$. We call \mathcal{F} a *similarity* with the scaling factor β if

$$\text{for all } \mathbf{a} \in \mathcal{S}_1, \quad \|\mathcal{F}(\mathbf{a})\| = \beta \|\mathbf{a}\|.$$

The following remarks are in order.

- If \mathcal{S}_1 and \mathcal{S}_2 are real inner product spaces, then

$$\langle \mathcal{F}(\mathbf{a}), \mathcal{F}(\mathbf{b}) \rangle = \beta^2 \langle \mathbf{a}, \mathbf{b} \rangle.\tag{4.4}$$

This can be shown by noting that for any \mathbf{a} and \mathbf{b} in \mathcal{S}_1 , the expression $\|\mathcal{F}(\mathbf{a} + \mathbf{b})\|^2$ can be expanded in the two different forms of

$$\begin{aligned}\|\mathcal{F}(\mathbf{a} + \mathbf{b})\|^2 &= \langle \mathcal{F}(\mathbf{a} + \mathbf{b}), \mathcal{F}(\mathbf{a} + \mathbf{b}) \rangle \\ &= \langle \mathcal{F}(\mathbf{a}) + \mathcal{F}(\mathbf{b}), \mathcal{F}(\mathbf{a}) + \mathcal{F}(\mathbf{b}) \rangle \\ &= \|\mathcal{F}(\mathbf{a})\|^2 + \|\mathcal{F}(\mathbf{b})\|^2 + 2\langle \mathcal{F}(\mathbf{a}), \mathcal{F}(\mathbf{b}) \rangle \\ &= \beta^2 \|\mathbf{a}\|^2 + \beta^2 \|\mathbf{b}\|^2 + 2\langle \mathcal{F}(\mathbf{a}), \mathcal{F}(\mathbf{b}) \rangle\end{aligned}\tag{4.5}$$

and

$$\begin{aligned}\|\mathcal{F}(\mathbf{a} + \mathbf{b})\|^2 &= \beta^2 \|\mathbf{a} + \mathbf{b}\|^2 \\ &= \beta^2 \langle \mathbf{a} + \mathbf{b}, \mathbf{a} + \mathbf{b} \rangle \\ &= \beta^2 \left(\|\mathbf{a}\|^2 + \|\mathbf{b}\|^2 + 2\langle \mathbf{a}, \mathbf{b} \rangle \right).\end{aligned}\tag{4.6}$$

Equating (4.5) and (4.6) gives (4.4).

For any two vectors \mathbf{a} and \mathbf{b} in an inner product space, we can define the angle between \mathbf{a} and \mathbf{b} as

$$\angle(\mathbf{a}, \mathbf{b}) \triangleq \cos^{-1} \frac{\langle \mathbf{a}, \mathbf{b} \rangle}{\|\mathbf{a}\| \|\mathbf{b}\|}.$$

Then (4.4) yields

$$\angle(\mathcal{F}(\mathbf{a}), \mathcal{F}(\mathbf{b})) = \angle(\mathbf{a}, \mathbf{b}).$$

- Since the operator \mathcal{F} is linear and \mathcal{S}_1 is closed under vector addition (subtraction), \mathcal{F} uniformly scales the distances between *any* two points of \mathcal{S}_1 when it maps them to \mathcal{S}_2 , that is,

$$\text{for all } \mathbf{a}, \mathbf{b} \in \mathcal{S}_1, \quad \|\mathcal{F}(\mathbf{a}) - \mathcal{F}(\mathbf{b})\| = \beta \|\mathbf{a} - \mathbf{b}\|.$$

- If $\beta \neq 0$, then it is easy to show that \mathcal{F} is a one-to-one injection operator and the dimensions of \mathcal{S}_1 and $\mathcal{F}(\mathcal{S}_1)$ are the same.
- The vector spaces \mathcal{S}_1 and \mathcal{S}_2 may be subspaces of one larger normed space. In this case, the effect of applying \mathcal{F} to \mathcal{S}_1 is equivalent to a combination of rotation, reflection, or isotropic scaling of \mathcal{S}_1 . However, \mathcal{F} does not skew \mathcal{S}_1 , that is, the scaling of \mathcal{S}_1 is the same in all directions in \mathcal{S}_1 .

4.4 MIMO System Model and OSTBC Background

A MIMO system with N transmit and M receive antennas and flat fading channel is depicted in Figure 4.1. The input–output relationship for such a system can be expressed as

$$\mathbf{y}(t) = \mathbf{x}(t)\mathbf{H} + \mathbf{v}(t) \quad (4.7)$$

where \mathbf{H} is the $N \times M$ complex channel matrix and

$$\begin{aligned} \mathbf{y}(t) &= [y_1(t), y_2(t), \dots, y_M(t)] \\ \mathbf{x}(t) &= [x_1(t), x_2(t), \dots, x_N(t)] \\ \mathbf{v}(t) &= [v_1(t), v_2(t), \dots, v_M(t)] \end{aligned}$$

are the complex row vectors of the received signal, transmitted signal, and noise, respectively. We do not make any assumptions about the distribution of the elements of $\mathbf{v}(t)$ at

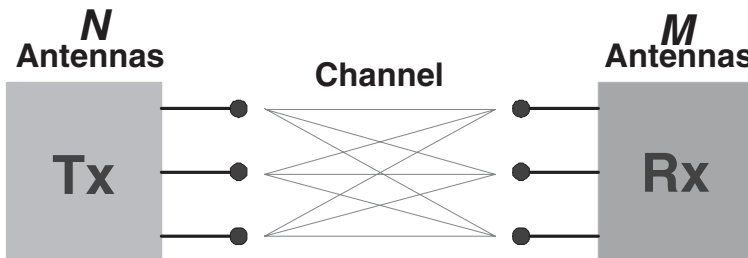


Figure 4.1 MIMO system with flat fading channel.

this point. All necessary assumptions on the noise will be made later in different sections of this chapter.

Let us assume that the channel in (4.7) is used within the block length T at times $t = 1, \dots, T$ and consider the block fading case where \mathbf{H} does not change within a block. Using the notations

$$\mathbf{Y} \triangleq \begin{bmatrix} \mathbf{y}(1) \\ \mathbf{y}(2) \\ \vdots \\ \mathbf{y}(T) \end{bmatrix}, \quad \mathbf{X} \triangleq \begin{bmatrix} \mathbf{x}(1) \\ \mathbf{x}(2) \\ \vdots \\ \mathbf{x}(T) \end{bmatrix}, \quad \mathbf{V} \triangleq \begin{bmatrix} \mathbf{v}(1) \\ \mathbf{v}(2) \\ \vdots \\ \mathbf{v}(T) \end{bmatrix}$$

equation (4.7) can be written as

$$\mathbf{Y} = \mathbf{X}\mathbf{H} + \mathbf{V} \quad (4.8)$$

for any $T \times N$ transmitted signal matrix \mathbf{X} .

Consider a complex symbol vector

$$\mathbf{s} \triangleq [s_1, s_2, \dots, s_K]^T \quad (4.9)$$

and a $T \times N$ complex matrix-valued function

$$\mathcal{G}_c(\mathbf{s}) : \mathbb{C}^{K \times 1} \mapsto \mathbb{C}^{T \times N}.$$

The matrix operator $\mathcal{G}_c(\mathbf{s})$ is called an OSTBC¹ if it satisfies the following two conditions [5].

1. All the entries of $\mathcal{G}_c(\mathbf{s})$ are linear functions of the K entries of \mathbf{s} and their complex conjugates.
2. For all \mathbf{s} in $\mathbb{C}^{K \times 1}$,

$$\mathcal{G}_c^H(\mathbf{s})\mathcal{G}_c(\mathbf{s}) = \|\mathbf{s}\|^2 \mathbf{I}_N \quad (4.10)$$

where \mathbf{I}_N is the $N \times N$ identity matrix and $\|\cdot\|$ denotes the Euclidean norm.

We will refer to s_1, s_2, \dots, s_K as the *complex variables* of an OSTBC, and to \mathbf{s} as the *vector variable* of an OSTBC. The ratio K/T is also called the *rate* of an OSTBC.

The following are three standard examples of OSTBCs [4, 5]:

$$\mathcal{G}_1 \left(\begin{bmatrix} s_1 \\ s_2 \end{bmatrix} \right) = \begin{bmatrix} s_1 & s_2 \\ -s_2^* & s_1^* \end{bmatrix} \quad \text{for } \begin{array}{rcl} K & = & 2 \\ T & = & 2 \\ N & = & 2 \end{array} \quad (4.11)$$

$$\mathcal{G}_2 \left(\begin{bmatrix} s_1 \\ s_2 \\ s_3 \end{bmatrix} \right) = \begin{bmatrix} s_1 & s_2 & \frac{s_3}{\sqrt{2}} \\ -s_2^* & s_1^* & \frac{s_3}{\sqrt{2}} \\ \frac{s_3^*}{\sqrt{2}} & \frac{s_3}{\sqrt{2}} & \frac{-s_1-s_1^*+s_2-s_2^*}{2} \\ \frac{s_3^*}{\sqrt{2}} & -\frac{s_3}{\sqrt{2}} & \frac{s_2+s_2^*+s_1-s_1^*}{2} \end{bmatrix} \quad \text{for } \begin{array}{rcl} K & = & 3 \\ T & = & 4 \\ N & = & 3 \end{array} \quad (4.12)$$

¹The term OSTBC is now commonly used to refer to the type of codes that we discuss in this chapter. However, in the early papers on OSTBCs, beginning with [5], these codes were referred to as STBCs and the term STBC is still occasionally used to refer to these codes in some papers. Like many other papers in the literature, in this chapter, we adopt the convention to reserve the abbreviation “STBC” for a more general class of codes that have a space-time structure, and are applied block by block using a fixed block length.

$$\mathcal{G}_3 \left(\begin{bmatrix} s_1 \\ s_2 \\ s_3 \\ s_4 \end{bmatrix} \right) = \frac{1}{\sqrt{2}} \begin{bmatrix} s_1 & s_2 & s_3 \\ -s_2 & s_1 & -s_4 \\ -s_3 & s_4 & s_1 \\ -s_4 & -s_3 & s_2 \\ s_1^* & s_2^* & s_3^* \\ -s_2^* & s_1^* & -s_4^* \\ -s_3^* & s_4^* & s_1^* \\ -s_4^* & -s_3^* & s_2^* \end{bmatrix} \quad \text{for } \begin{array}{lll} K = 4 \\ T = 8 \\ N = 3 \end{array} \quad (4.13)$$

where $(\cdot)^*$ denotes the complex conjugate. Note that $\mathcal{G}_1(\cdot)$ is the celebrated Alamouti code [4].

From (4.10) it is clear that the columns of $\frac{1}{\|\mathbf{s}\|} \mathcal{G}_c(\mathbf{s})$ are *orthonormal* for any \mathbf{s} in $\mathbb{C}^{K \times 1}$. For any given N , one is interested in designing high-rate (large K/T) and low-delay (small T) OSTBCs. In general, designing such OSTBCs is not an easy task and, currently, only a few design methods are available [4–8]. However, if one or more OSTBCs are given, there are simple rules for generating other OSTBCs from them. Some simple rules include, but are not limited to, premultiplying an OSTBC by any $T \times T$ unitary matrix or removing some of the columns from an OSTBC.

It is evident that OSTBCs do not exist for every combination of the values of K , T , and N . In particular,

- The columns of $\mathcal{G}_c(\mathbf{s})$ are mutually orthogonal, therefore $T \geq N$.
- In [5], it was shown that for all OSTBCs

$$K/T \leq 1 \quad (4.14)$$

with equality holding only for $N = 2$.² The OSTBC $\mathcal{G}_1(\cdot)$ in (4.11) is one such *full-rate* code.

- Any positive integer K can be uniquely written in the form $K = b 2^a$ for some nonnegative integers a and b , where b is odd. The integer a can be uniquely written as $a = 4c + d$ for some integers c and d where $0 \leq d < 4$ and $c \geq 0$. Then, one can define $\zeta(K) \triangleq 8c + 2^d$. In [5], half-rate (i.e., $K/T = 1/2$) OSTBCs have been found for any values of N and K that satisfy $\zeta(K) \geq N$. The OSTBC \mathcal{G}_3 is an example of such a half-rate code.
- In [8], it has been shown that, for a given N , the maximal rate for an OSTBC is $\frac{\lceil N/2 \rceil + 1}{2\lceil N/2 \rceil}$. It has also been shown how OSTBCs with such rate can be constructed for any value of N . The OSTBCs \mathcal{G}_1 and \mathcal{G}_2 are such maximal-rate codes for $N = 2$ and $N = 3$, respectively.

Let us now discuss how an OSTBC-based system with the coherent ML decoder operates. First, a vector \mathbf{s} is drawn from a vector constellation $\tilde{\mathcal{S}}$ of cardinality L . Hence, there are L possibilities in selecting the vector \mathbf{s} , and, if the elements of $\tilde{\mathcal{S}}$ are equi-probable, then any \mathbf{s} contains $\log_2 L$ bits of information.

²This is also true for the trivial case of $N = 1$. Furthermore, for *real* OSTBCs, where the domain of the OSTBC is $\mathbb{R}^{K \times 1}$ rather than $\mathbb{C}^{K \times 1}$, the equality holds only for $N = 2, 4$, and 8 [5].

If $\tilde{\mathcal{S}}$ can be written as

$$\tilde{\mathcal{S}} = \tilde{\mathcal{U}}_1 \times \tilde{\mathcal{U}}_2 \times \cdots \times \tilde{\mathcal{U}}_K \quad (4.15)$$

for some sets $\mathcal{U}_1, \mathcal{U}_2, \dots, \mathcal{U}_K \subset \mathbb{C}$, then we call $\tilde{\mathcal{S}}$ *separable*. We will denote the cardinality of \mathcal{U}_k by I_k , and its elements by $u_{1,k}, u_{2,k}, \dots, u_{I_k,k}$. It is clear that a sufficient condition for $\tilde{\mathcal{S}}$ to be separable is that each information symbol s_k is drawn independently from its own complex constellation $\tilde{\mathcal{U}}_k$. If $\tilde{\mathcal{S}}$ does not satisfy (4.15), we call it *nonseparable*. Separability of a constellation implies a certain orthogonal lattice structure for $\tilde{\mathcal{S}}$ that can simplify decoding as will be discussed in Section 4.6.

In the space-time coding literature, as a rule, it is assumed that all the information symbols s_k are drawn independently from the same complex constellation. This implies a separable constellation $\tilde{\mathcal{S}}$ with $\tilde{\mathcal{U}}_1 = \tilde{\mathcal{U}}_2 = \cdots = \tilde{\mathcal{U}}_K$. However, we consider both the separable and nonseparable constellation cases. For separable constellations, we focus on the general case where $\tilde{\mathcal{U}}_1, \tilde{\mathcal{U}}_2, \dots, \tilde{\mathcal{U}}_K$ may be different, and we do not restrict them to any specific constellation.

The OSTBC is then applied to the complex vector \mathbf{s} where a $T \times N$ matrix \mathbf{X} is built as

$$\mathbf{X} = \mathcal{G}_c(\mathbf{s}) . \quad (4.16)$$

The entries of \mathbf{X} are linear combinations of the elements of \mathbf{s} and their complex conjugates. Thus, the space-time coded signal \mathbf{X} belongs to a constellation $\tilde{\mathcal{X}} \triangleq \{\mathbf{X}_1, \mathbf{X}_2, \dots, \mathbf{X}_L\}$, where $\mathbf{X}_\ell = \mathcal{G}_c(\mathbf{s}_\ell)$, for $\ell = 1, 2, \dots, L$. We consider the case where \mathbf{H} is known at the receiver and the ML decoder is used. In the literature, such a decoder is called the *coherent* ML decoder. Conditioned on \mathbf{H} , the constellation of the received symbols is given by $\tilde{\mathcal{Y}} = \{\mathbf{Y}_1, \mathbf{Y}_2, \dots, \mathbf{Y}_L\}$, where $\mathbf{Y}_\ell = \mathbf{X}_\ell \mathbf{H}$. If all the entries of \mathbf{V} are complex variables whose joint probability density function (pdf) is a decreasing function of $\|\mathbf{V}\|_F$ (this is, in particular, true for i.i.d. (independent identically distributed) zero-mean circular Gaussian entries of \mathbf{V}), then the task of the coherent ML decoder is to find

$$\ell_{\text{opt}} = \underset{\ell \in \{1, \dots, L\}}{\operatorname{argmin}} \|\mathbf{Y} - \mathbf{Y}_\ell\|_F . \quad (4.17)$$

This decoder then uses the obtained index ℓ_{opt} to recover the transmitted bits.

4.5 Constellation Space Invariance and Equivalent Array-Processing-Type MIMO Model

In this section, we consider the constellation space invariance property of OSTBCs [11–14] and develop the vectorized MIMO model [15, 14, 16–18] which has certain similarities to a familiar signal model used in array processing. The developments in this section will form a basis for the next sections of this chapter.

Let us introduce the following inner product spaces.

$$\begin{aligned} \mathcal{S} &\triangleq \mathbb{C}^{K \times 1} \\ \mathcal{X} &\triangleq \mathcal{G}_c(\mathcal{S}) = \{\mathcal{G}_c(\mathbf{s}) \mid \mathbf{s} \in \mathcal{S}\} \\ \mathcal{Y} &\triangleq \mathcal{H}(\mathcal{X}) = \{\mathbf{X}\mathbf{H} \mid \mathbf{X} \in \mathcal{X}\} \end{aligned}$$

with the inner product defined in (4.2). Here,

$$\mathcal{H} : \mathcal{X} \mapsto \mathcal{Y}$$

where for all $\mathbf{X} \in \mathcal{X}$

$$\mathcal{H}(\mathbf{X}) \triangleq \mathbf{X}\mathbf{H}. \quad (4.18)$$

Note that any symbol vector \mathbf{s} prior to OSTBC encoding lies in \mathcal{S} , while the corresponding transmitted matrix \mathbf{X} and received matrix \mathbf{Y} lie in \mathcal{X} and \mathcal{Y} , respectively. It is clear that

$$\begin{aligned} \tilde{\mathcal{S}} &\subset \mathcal{S} = \mathbb{C}^{K \times 1} \\ \tilde{\mathcal{X}} &\subset \mathcal{X} \subset \mathbb{C}^{T \times N} \\ \tilde{\mathcal{Y}} &\subset \mathcal{Y} \subset \mathbb{C}^{T \times M}. \end{aligned}$$

First, let us verify that \mathcal{G}_c is a linear operator from \mathcal{S} to $\mathbb{C}^{T \times N}$. According to the definition of OSTBCs, $\mathcal{G}_c(\mathbf{s})$ is linear in terms of s_k and s_k^* . Therefore, for any OSTBC, $\mathcal{G}_c(\mathbf{s})$ can be written in the form [15]

$$\mathcal{G}_c(\mathbf{s}) = \sum_{k=1}^K (\mathbf{A}_k s_k + \mathbf{B}_k s_k^*) \quad (4.19)$$

where \mathbf{A}_k and \mathbf{B}_k ($k = 1, 2, \dots, K$) are complex $T \times N$ matrices that define the OSTBC matrix \mathcal{G}_c . Using (4.19), we have that

$$\text{for all } \mathbf{a}, \mathbf{b} \in \mathcal{S}, \quad \mathcal{G}_c(\mathbf{a} + \mathbf{b}) = \mathcal{G}_c(\mathbf{a}) + \mathcal{G}_c(\mathbf{b})$$

$$\text{for all } \mathbf{a} \in \mathcal{S}, \text{ and for all } \beta \in \mathbb{R}, \quad \mathcal{G}_c(\beta\mathbf{a}) = \beta\mathcal{G}_c(\mathbf{a})$$

and, therefore, \mathcal{G}_c is a linear operator.

From (4.3), (4.10), and (4.16), we further obtain that \mathcal{G}_c is a similarity with the scaling factor of \sqrt{N} :

$$\text{for all } \mathbf{X} \in \mathcal{X}, \quad \|\mathbf{X}\|_F = \sqrt{\text{tr}(\mathbf{X}^H \mathbf{X})} = \sqrt{N} \|\mathbf{s}\|. \quad (4.20)$$

As \mathcal{S} is a $2K$ -dimensional inner product space and \mathcal{G}_c is a similarity, $\mathcal{X} = \mathcal{G}_c(\mathcal{S})$ is a $2K$ -dimensional subspace of $\mathbb{C}^{T \times N}$.

From the definition (4.18), it is evident that the operator \mathcal{H} is linear. By using (4.3), (4.10), (4.20), and the properties of the trace operator, for all $\mathbf{X} \in \mathcal{X}$ we can write

$$\begin{aligned} \|\mathcal{H}(\mathbf{X})\|_F^2 &= \|\mathbf{X}\mathbf{H}\|_F^2 \\ &= \text{tr}(\mathbf{X}\mathbf{H}\mathbf{H}^H \mathbf{X}^H) \\ &= \text{tr}(\mathbf{X}^H \mathbf{X} \mathbf{H}\mathbf{H}^H) \\ &= \text{tr}(\|\mathbf{s}\|^2 \mathbf{H}\mathbf{H}^H) \\ &= \|\mathbf{H}\|_F^2 \|\mathbf{s}\|^2 \end{aligned}$$

which after substituting $\|\mathbf{s}\|$ from (4.20) yields

$$\|\mathcal{H}(\mathbf{X})\|_F = (1/\sqrt{N}) \|\mathbf{H}\|_F \|\mathbf{X}\|_F. \quad (4.21)$$

Hence, \mathcal{H} is a similarity with a scaling factor of $(1/\sqrt{N})\|\mathbf{H}\|_F$. This means that if $\|\mathbf{H}\|_F \neq 0$, then $\mathcal{H} : \mathcal{X} \mapsto \mathcal{Y}$ is a one-to-one bijection operator and \mathcal{Y} is a $2K$ -dimensional subspace of $\mathbb{C}^{T \times M}$. It is worth noting that if the domain of \mathcal{H} is not restricted to \mathcal{X} in $\mathbb{C}^{T \times N}$, then \mathcal{H} is not a similarity in general. In fact, it is easy to verify that if the domain of \mathcal{H} is the entire $\mathbb{C}^{T \times N}$ rather than \mathcal{X} , then \mathcal{H} is not a similarity unless the columns of \mathbf{H} are orthonormal with equal norms.

Since the operator \mathcal{G}_c is a similarity with the scaling factor \sqrt{N} , the ratio of the distance between any two vectors in \mathcal{X} and the corresponding two vectors in \mathcal{S} is given by the constant \sqrt{N} . Furthermore, since the operator \mathcal{H} is a similarity with the scaling factor $(1/\sqrt{N})\|\mathbf{H}\|_F$, the ratio of the distances between any two vectors in \mathcal{Y} and the corresponding two vectors in \mathcal{X} is given by $(1/\sqrt{N})\|\mathbf{H}\|_F$. Note that the same conclusion is true for the combined operator $\mathcal{H}\mathcal{G}_c$ where the scaling constant becomes equal to $\|\mathbf{H}\|_F$. This mathematical fact implies that *neither the space-time encoder nor the channel will skew the shape of the signal constellation* [11–14, 19]. That is, if we take any set of distinct points in the constellation space of the signal \mathbf{s} and introduce relative distances between these points that are normalized by the minimal distance within this set, then all these relative distances will remain invariant to the effect of the space-time encoder and the MIMO channel independently of the realization of the channel matrix \mathbf{H} . In other words, the OSTBC positions the transmitted signal matrix \mathbf{X} in a certain “magic” subspace that makes the shape of the signal constellation immune to the skewing effect of the channel. Clearly, this remarkable property is valid entirely because of the specific structure of OSTBCs.

Interestingly, the inner product space representation of constellation spaces and operators in these spaces can be interpreted from a different point of view.

Let us introduce a vector basis $\{\mathbf{e}_k, j\mathbf{e}_k\}_{k=1}^K$ for \mathcal{S} where \mathbf{e}_k is the k th column of \mathbf{I}_K and $j \triangleq \sqrt{-1}$. Note that these basis vectors are orthonormal according to the definition (4.2) of the inner product. Furthermore, let us define the matrices

$$\mathbf{C}_k \triangleq \mathcal{G}_c(\mathbf{e}_k) \quad (4.22)$$

$$\mathbf{D}_k \triangleq \mathcal{G}_c(j\mathbf{e}_k) \quad (4.23)$$

for $k = 1, 2, \dots, K$, and the sets

$$\mathcal{B}_{\mathcal{S}} \triangleq \{\mathbf{e}_k, j\mathbf{e}_k\}_{k=1}^K \quad (4.24)$$

$$\mathcal{B}_{\mathcal{X}} \triangleq \{\mathbf{C}_k, \mathbf{D}_k\}_{k=1}^K \quad (4.25)$$

$$\mathcal{B}_{\mathcal{Y}} \triangleq \{\mathbf{C}_k \mathbf{H}, \mathbf{D}_k \mathbf{H}\}_{k=1}^K \quad (4.26)$$

where the members of $\mathcal{B}_{\mathcal{X}}$ and $\mathcal{B}_{\mathcal{Y}}$ are obtained by applying the operators \mathcal{G}_c and \mathcal{H} to the members of $\mathcal{B}_{\mathcal{S}}$ and $\mathcal{B}_{\mathcal{X}}$, respectively. As the members of $\mathcal{B}_{\mathcal{S}}$ are orthonormal and \mathcal{G}_c is a similarity with a scaling factor \sqrt{N} , the members of $\mathcal{B}_{\mathcal{X}}$ are orthogonal with equal norms of

$$\|\mathbf{C}_k\|_F = \|\mathbf{D}_k\|_F = \sqrt{N}. \quad (4.27)$$

Similarly, as \mathcal{H} is a similarity with a scaling factor $1/\sqrt{N}\|\mathbf{H}\|_F$, the members of $\mathcal{B}_{\mathcal{Y}}$ are orthogonal with equal norms of

$$\|\mathbf{C}_k \mathbf{H}\|_F = \|\mathbf{D}_k \mathbf{H}\|_F = \|\mathbf{H}\|_F. \quad (4.28)$$

Table 4.1 Signal constellations and the corresponding inner product spaces in an OSTBC-based MIMO system with block flat fading channel

Stage	Transmitter before encoder	OSTBC encoder	Transmitter after encoder	Channel matrix	Receiver after channel
Signal Space	\mathbf{s}	$\xrightarrow{\mathcal{G}_c}$	\mathbf{X}	$\xrightarrow{\mathcal{H}}$	\mathbf{Y}
Constellation	$\mathbb{C}^{K \times 1}$	—	$\mathbb{C}^{T \times N}$	—	$\mathbb{C}^{T \times M}$
Subspace	$\tilde{\mathcal{S}}$	$\xrightarrow{\mathcal{G}_c}$	$\tilde{\mathcal{X}}$	$\xrightarrow{\mathcal{H}}$	$\tilde{\mathcal{Y}}$
Dimension of subspace	\mathcal{S}	$\xrightarrow{\mathcal{G}_c}$	\mathcal{X}	$\xrightarrow{\mathcal{H}}$	\mathcal{Y}
Orthogonal basis	$2K$	$\xrightarrow{\mathcal{G}_c}$	$2K$	$\xrightarrow{\mathcal{H}}$	$2K$
Orthogonal basis members	$\mathcal{B}_{\mathcal{S}}$	$\xrightarrow{\mathcal{G}_c}$	$\mathcal{B}_{\mathcal{X}}$	$\xrightarrow{\mathcal{H}}$	$\mathcal{B}_{\mathcal{Y}}$
Norm of basis members	$\mathbf{e}_k, j\mathbf{e}_k$	$\xrightarrow{\mathcal{G}_c}$	$\mathbf{C}_k, \mathbf{D}_k$	$\xrightarrow{\mathcal{H}}$	$\mathbf{C}_k \mathbf{H}, \mathbf{D}_k \mathbf{H}$
Scaling factor of operator	1	—	\sqrt{N}	—	$\ \mathbf{H}\ _F$
	—	\sqrt{N}	—	$\frac{1}{\sqrt{N}} \ \mathbf{H}\ _F$	—

Thus, $\mathcal{B}_{\mathcal{S}}$, $\mathcal{B}_{\mathcal{X}}$, and $\mathcal{B}_{\mathcal{Y}}$ constitute orthogonal bases for the inner product spaces \mathcal{S} , \mathcal{X} , and \mathcal{Y} , respectively.

Table 4.1 summarizes the notations used to represent the signals and their corresponding constellations at different stages of an OSTBC-based MIMO system.

It can be readily verified that the effects of the OSTBC and the channel matrix on \mathbf{s} and \mathbf{X} can be represented by multiplication of the matrices

$$\mathbb{G} = [\underline{\mathbf{C}}_1 \ \underline{\mathbf{C}}_2 \ \dots \ \underline{\mathbf{C}}_K \ \underline{\mathbf{D}}_1 \ \underline{\mathbf{D}}_2 \ \dots \ \underline{\mathbf{D}}_K] \quad (4.29)$$

$$\mathbb{H} = \begin{bmatrix} \text{Re}\{\mathbf{H}^T\} \otimes \mathbf{I}_T & -\text{Im}\{\mathbf{H}^T\} \otimes \mathbf{I}_T \\ \text{Im}\{\mathbf{H}^T\} \otimes \mathbf{I}_T & \text{Re}\{\mathbf{H}^T\} \otimes \mathbf{I}_T \end{bmatrix} \quad (4.30)$$

by \mathbf{s} and \mathbf{X} , respectively. Here, \otimes denotes the Kronecker product. Hence

$$\underline{\mathbf{X}} = \mathbb{G}\underline{\mathbf{s}} \quad (4.31)$$

and the vectorized version of (4.8) can be written as

$$\underline{\mathbf{Y}} = \mathbb{H}\mathbb{G}\underline{\mathbf{s}} + \underline{\mathbf{V}}. \quad (4.32)$$

If we use the notation

$$\mathbf{A}(\mathbf{H}) \triangleq \mathbb{H}\mathbb{G} \quad (4.33)$$

then (4.32) can be written as [15, 14, 16–18]

$$\underline{\mathbf{Y}} = \mathbf{A}(\mathbf{H})\underline{\mathbf{s}} + \underline{\mathbf{V}} \quad (4.34)$$

where

$$\mathbf{A}(\mathbf{H}) = [\underline{\mathbf{C}}_1 \mathbf{H} \ \underline{\mathbf{C}}_2 \mathbf{H} \ \dots \ \underline{\mathbf{C}}_K \mathbf{H} \ \underline{\mathbf{D}}_1 \mathbf{H} \ \underline{\mathbf{D}}_2 \mathbf{H} \ \dots \ \underline{\mathbf{D}}_K \mathbf{H}]. \quad (4.35)$$

It is worth noting that in the model (4.32), both the effects of the channel and OSTBC are captured in the matrix $\mathbf{A}(\mathbf{H})$, while all the symbols are contained in the vector $\underline{\mathbf{s}}$. Note that the columns of \mathbb{G} and $\mathbf{A}(\mathbf{H})$ are the members of $\mathcal{B}_{\mathcal{X}}$ and $\mathcal{B}_{\mathcal{Y}}$ after application of the “underline” operator of (4.1), respectively. Thus, (4.27), (4.28), and orthogonality of members of $\mathcal{B}_{\mathcal{X}}$ and $\mathcal{B}_{\mathcal{Y}}$ yield

$$\mathbb{G}^T \mathbb{G} = N \mathbf{I}_{2K} \quad (4.36)$$

$$\mathbf{A}^T(\mathbf{H}) \mathbf{A}(\mathbf{H}) = \|\mathbf{H}\|_F^2 \mathbf{I}_{2K} \quad (4.37)$$

for any OSTBC and any channel matrix \mathbf{H} . This means that $\mathbf{A}(\mathbf{H})$ is a matrix with orthogonal and equal-norm columns regardless of the values of the entries of \mathbf{H} .

A key observation following from (4.34) is that this equivalent MIMO model has a strong similarity to the familiar model used in array processing [20]. Note that in the array processing context, $\underline{\mathbf{Y}}$, $\mathbf{A}(\mathbf{H})$, and $\underline{\mathbf{s}}$ play the roles of the array snapshot vector, signal steering matrix, and the source waveform vector, respectively. However, a strong property that is not satisfied in array processing *almost surely* but holds true for the model (4.34) is that all the columns of the “steering matrix” $\mathbf{A}(\mathbf{H})$ are orthonormal, except for a scaling factor, irrespective of the channel matrix. Furthermore, the model in (4.34) is real valued while the aforementioned array processing model is complex valued. The similarity between these two models will be exploited later in this chapter to develop an incoherent (blind) decoder for OSTBCs in Section 4.9, and to design MV multiuser linear receivers in Section 4.10.

4.6 Coherent ML Decoding

In this section, the constellation space invariance property will be used to show why a low complexity symbol-by-symbol decoding is possible for OSTBCs and to derive simple alternative formulas for the coherent ML decoder [12, 14].

Throughout this section, let us assume that all the entries of the noise matrix \mathbf{V} are i.i.d. zero-mean circular complex Gaussian variables. Given the matrix \mathbf{Y} at the receiver, the ML decoder finds a member of \mathcal{Y} that is closest to \mathbf{Y} . As has been shown in Section 4.5, \mathcal{Y} is located in the subspace \mathcal{Y} . The matrix \mathbf{Y} can be uniquely decomposed into the sum of two components \mathbf{Y}_{\parallel} and \mathbf{Y}_{\perp} , where $\mathbf{Y}_{\parallel} \in \mathcal{Y}$ is the projection of \mathbf{Y} onto \mathcal{Y} and \mathbf{Y}_{\perp} is orthogonal to \mathcal{Y} . Note that the concepts of “projection” of matrix \mathbf{Y} onto \mathcal{Y} , and that of orthogonality of the matrix \mathbf{Y}_{\perp} with respect to \mathcal{Y} , are meaningful because of the inner product definition (4.2). Hence, $\mathbf{Y} = \mathbf{Y}_{\parallel} + \mathbf{Y}_{\perp}$ and the task of the ML decoder is to find

$$\begin{aligned} \ell_{\text{opt}} &= \underset{\ell \in \{1, \dots, L\}}{\operatorname{argmin}} \| \mathbf{Y} - \mathbf{Y}_{\ell} \|_F^2 \\ &= \underset{\ell \in \{1, \dots, L\}}{\operatorname{argmin}} \| \mathbf{Y}_{\perp} + \mathbf{Y}_{\parallel} - \mathbf{Y}_{\ell} \|_F^2. \end{aligned} \quad (4.38)$$

Noting that \mathbf{Y}_{\parallel} and \mathbf{Y}_{ℓ} are in \mathcal{Y} , and \mathbf{Y}_{\perp} is orthogonal to \mathcal{Y} , (4.38) can be written as

$$\ell_{\text{opt}} = \underset{\ell \in \{1, \dots, L\}}{\operatorname{argmin}} \left(\| \mathbf{Y}_{\perp} \|_F^2 + \| \mathbf{Y}_{\parallel} - \mathbf{Y}_{\ell} \|_F^2 \right). \quad (4.39)$$

In (4.39), the term $\| \mathbf{Y}_{\perp} \|_F^2$ is independent of ℓ and can be ignored in the minimization, which means that the component \mathbf{Y}_{\perp} does not contain any signal information and does not

affect the output of the coherent ML decoder. Thus, (4.39) yields

$$\ell_{\text{opt}} = \underset{\ell \in \{1, \dots, L\}}{\operatorname{argmin}} \| \mathbf{Y}_{\parallel} - \mathbf{Y}_{\ell} \|_F$$

and the ML decoder finds a member of $\tilde{\mathcal{V}}$ that is closest to \mathbf{Y}_{\parallel} . As \mathcal{HG}_c is a similarity and a bijection from \mathcal{S} to \mathcal{Y} , this problem is equivalent to finding the member of $\tilde{\mathcal{S}}$ that is closest to

$$\mathbf{s}_{\parallel} \triangleq (\mathcal{HG}_c)^{-1}(\mathbf{Y}_{\parallel})$$

where $\mathbf{s}_{\parallel} \in \mathcal{S}$.

If the constellation $\tilde{\mathcal{S}}$ is separable, then because of its orthogonal lattice structure, each component s_k of \mathbf{s}_{\parallel} can be quantized independently to the closest member of \mathcal{U}_k . Hence, the symbol-by-symbol decoding of \mathbf{Y} is equivalent to the optimal ML decoding, when $\tilde{\mathcal{S}}$ is separable. Note that if $\tilde{\mathcal{S}}$ is nonseparable, then symbol-by-symbol decoding is not ML optimal.

The constellation space invariance property can also be used to obtain alternative, conceptually simple expressions for the coherent ML decoder.

Making use of the basis $\mathcal{B}_{\mathcal{S}}$ defined in (4.24) and denoting the elements of \mathbf{s}_{\parallel} by $s_{\parallel 1}, s_{\parallel 2}, \dots, s_{\parallel K}$, we have

$$\operatorname{Re}\{s_{\parallel k}\} = \langle \mathbf{s}_{\parallel}, \mathbf{e}_k \rangle, \quad \operatorname{Im}\{s_{\parallel k}\} = \langle \mathbf{s}_{\parallel}, j\mathbf{e}_k \rangle. \quad (4.40)$$

Using equations (4.4) and (4.40) yields

$$\begin{aligned} \operatorname{Re}\{s_{\parallel k}\} &= \frac{1}{\|\mathbf{H}\|_F^2} \langle \mathcal{HG}_c(\mathbf{s}_{\parallel}), \mathcal{HG}_c(\mathbf{e}_k) \rangle \\ &= \frac{1}{\|\mathbf{H}\|_F^2} \langle \mathbf{Y}_{\parallel}, \mathcal{HG}_c(\mathbf{e}_k) \rangle \\ &= \frac{1}{\|\mathbf{H}\|_F^2} \langle \mathbf{Y}, \mathcal{HG}_c(\mathbf{e}_k) \rangle \\ &= \frac{1}{\|\mathbf{H}\|_F^2} \langle \mathbf{Y}, \mathbf{C}_k \mathbf{H} \rangle \end{aligned} \quad (4.41)$$

which is the algebraic magnitude of the projection of \mathbf{Y} onto the basis vector $\mathbf{C}_k \mathbf{H}$ in $\mathcal{B}_{\mathcal{Y}}$. Similarly, we have

$$\operatorname{Im}\{s_{\parallel k}\} = \frac{1}{\|\mathbf{H}\|_F^2} \langle \mathcal{HG}_c(\mathbf{s}_{\parallel}), \mathcal{HG}_c(j\mathbf{e}_k) \rangle = \frac{1}{\|\mathbf{H}\|_F^2} \langle \mathbf{Y}, \mathbf{D}_k \mathbf{H} \rangle \quad (4.42)$$

which is the algebraic magnitude of the projection of \mathbf{Y} onto the basis vector $\mathbf{D}_k \mathbf{H}$ in $\mathcal{B}_{\mathcal{Y}}$. This means that, in order to find the real and imaginary parts of $s_{\parallel k}$, one needs to compute the projection of $\mathbf{s}_{\parallel k}$ on the basis vectors \mathbf{e}_k and $j\mathbf{e}_k$. As \mathcal{HG} is a similarity and does not affect the angles between the vectors, we can equivalently apply \mathcal{HG} to $\mathbf{s}_{\parallel k}$, \mathbf{e}_k , and $j\mathbf{e}_k$, compute the projection of $\mathcal{HG}(\mathbf{s}_{\parallel k})$ onto $\mathcal{HG}(\mathbf{e}_k)$ and $\mathcal{HG}(j\mathbf{e}_k)$, respectively, and divide the result by the square of the scaling factor of \mathcal{HG} .

Equations (4.41) and (4.42) represent alternative decoding formulae that are written in a much simpler and intuitively clearer form than the expressions given in [5], equation (7).

The exact equivalence of the decoding equations of [5] and equations (4.41) and (4.42) is readily verifiable.

Using the matrices \mathbb{G} and \mathbb{H} , we can rewrite the decoding equation in the simple alternative form

$$\underline{\mathbf{s}}_{\parallel} = \frac{1}{\|\mathbf{H}\|_F^2} (\mathbb{H}\mathbb{G})^T \underline{\mathbf{Y}}. \quad (4.43)$$

From the definition (4.33), we have

$$\frac{1}{\|\mathbf{H}\|_F^2} (\mathbb{H}\mathbb{G})^T = \frac{1}{\|\mathbf{H}\|_F^2} \mathbf{A}^T(\mathbf{H})$$

and, according to (4.37), we obtain

$$\mathbf{A}^\dagger(\mathbf{H}) = \frac{1}{\|\mathbf{H}\|_F^2} \mathbf{A}^T(\mathbf{H})$$

where $(\cdot)^\dagger$ denotes pseudoinverse. Thus, (4.43) can be rewritten as

$$\underline{\mathbf{s}}_{\parallel} = \frac{1}{\|\mathbf{H}\|_F^2} \mathbf{A}^T(\mathbf{H}) \underline{\mathbf{Y}} \quad (4.44)$$

$$= \mathbf{A}^\dagger(\mathbf{H}) \underline{\mathbf{Y}}. \quad (4.45)$$

Equation (4.45) implies that decoding can be done by multiplying the vectorized received signal $\underline{\mathbf{Y}}$ by the matrix $\mathbf{A}^\dagger(\mathbf{H})$. Therefore, the coherent ML decoder can be equivalently interpreted as a matched filter (MF), decorrelator receiver, or zeroforcing (ZF) receiver.

By substituting (4.45) in (4.32) and taking into account (4.37), we obtain the following relationship between \mathbf{s} and $\underline{\mathbf{s}}_{\parallel}$

$$\underline{\mathbf{s}}_{\parallel} = \underline{\mathbf{s}} + \mathbf{A}^\dagger(\mathbf{H}) \underline{\mathbf{V}}. \quad (4.46)$$

Because of (4.37), we have

$$\mathbf{A}^\dagger(\mathbf{H}) (\mathbf{A}^\dagger(\mathbf{H}))^T = \frac{1}{\|\mathbf{H}\|_F^2} \mathbf{I}_{2K}. \quad (4.47)$$

If the elements of $\underline{\mathbf{V}}$ are i.i.d. Gaussian with the variance σ^2 per element, then because of (4.47), the elements of $\mathbf{A}^\dagger(\mathbf{H}) \underline{\mathbf{V}}$ are i.i.d. Gaussian with the variance $\sigma^2/\|\mathbf{H}\|_F^2$ per element. Let us define the operator $\text{mat}(\cdot)$ to be the inverse of the underline operator of (4.1), that is, for any given I and J and any $2IJ \times 1$ real vector \mathbf{z} , let us use the notation

$$\underset{I,J}{\text{mat}}(\mathbf{z}) \triangleq \mathbf{Z}$$

when $\mathbf{z} = \underline{\mathbf{Z}}$. Then, using the notation

$$\begin{aligned} \xi &\triangleq \underset{K,1}{\text{mat}} \left(\mathbf{A}^\dagger(\mathbf{H}) \underline{\mathbf{V}} \right) \\ &= [\mathbf{I}_K \quad j\mathbf{I}_K] \mathbf{A}^\dagger(\mathbf{H}) \underline{\mathbf{V}} \end{aligned}$$

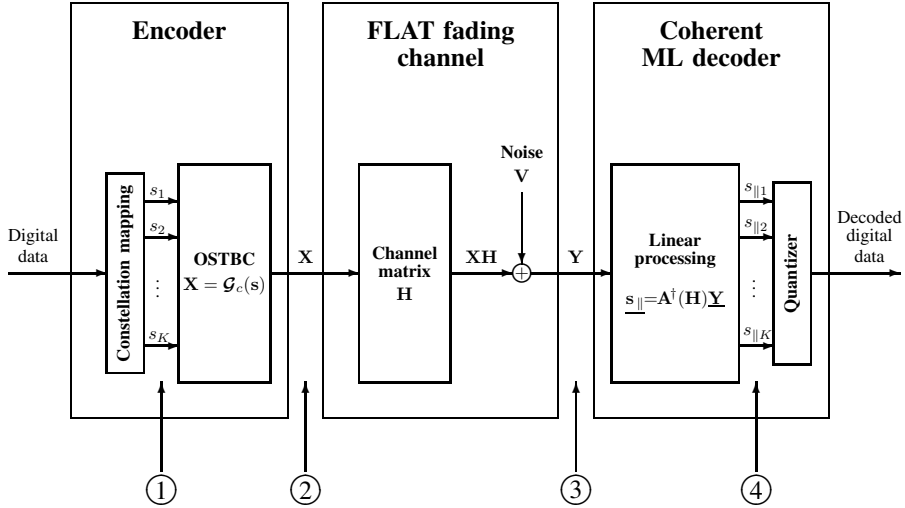


Figure 4.2 Different stages of an OSTBC-based MIMO system with block flat fading channel. According to the constellation space invariance property, for any \mathbf{H} , the shape of the signal constellation is the same at points 1, 2, 3, and 4.

equation (4.46) can be rewritten as

$$\underline{\mathbf{s}}_{\parallel} = \underline{\mathbf{s}} + \underline{\xi} \quad (4.48)$$

or, alternatively,

$$\underline{\mathbf{s}}_{\parallel} = \mathbf{s} + \underline{\xi} \quad (4.49)$$

where the elements of $\underline{\xi}$ are i.i.d. circularly symmetric Gaussian complex random variables with the variance $\sigma^2/\|\mathbf{H}\|_F^2$ per real dimension and these elements are independent of \mathbf{s} .

Equation (4.49) shows that the constellation for $\underline{\mathbf{s}}_{\parallel}$ is the same as the constellation $\tilde{\mathcal{S}}$ for \mathbf{s} . This is another form of the OSTBC constellation space invariance property stated in Section 4.5.

Figure 4.2 shows the different stages of an OSTBC-based MIMO system with flat block fading channel. The constellation space invariance property implies that for any \mathbf{H} , the shape of the constellation is the same at the points 1, 2, 3, and 4 of this figure.

Equation (4.49) can be interpreted as the input–output relationship of K parallel single-input single-output (SISO) additive white Gaussian noise (AWGN) channels. This means that in Figure 4.2, the part of the system from point 1 to point 4 is equivalent to K parallel SISO AWGN channels with inputs s_k and outputs $s_{\parallel k}$, $k = 1, 2, \dots, K$. Thus, the net effect of the OSTBC encoder, the channel, and the linear processing of the ML decoder on complex symbols s_1, s_2, \dots, s_K is that of the addition of the elements of $\underline{\xi}$ as noise. This property, which we will refer to as the *SISO equivalence* property of OSTBCs, has been discovered for a few specific OSTBCs in [21] and has been generalized to the case of arbitrary OSTBCs in [22] and [23].

Note that the constellation space invariance property is more general than the parallel SISO equivalence property. Indeed, the constellation space invariance is solely a property of

the OSTBC itself, that is, it is not related to the type of decoder used and the pdf of noise. This is in contrast to the parallel SISO equivalence of OSTBCs where such an invariance has been established between the points 1 and 4 of Figure 4.2 only, and requires the noise to be i.i.d. Gaussian and the linear processing to be of a specific type. That is, the parallel SISO equivalence is a direct corollary of the constellation space invariance but not vice versa.

4.7 Exact Symbol Error Probability Analysis of Coherent ML Decoder

Recently, several attempts to analyze the error probability of OSTBCs have been made for the coherent receiver where the channel state information (CSI) is known at the decoder [6, 24–27]. However, the results of these papers are limited by the case of uncorrelated Rayleigh fading channel. Moreover, the error probability analysis in [6, 24–27] is either approximate or is further limited by assuming some specific class of input signal constellations.

An interesting attempt at OSTBC error probability analysis in the correlated channel case has been recently made in [28]. However, the analysis of [28] is limited only to the Rayleigh channel case and the pairwise error probability. Additionally, the authors of [28] have limited their consideration to a particular channel model that assumes a particular Kronecker product structure for the channel correlation matrix [29].

In this section, we will use the constellation space invariance property to develop an exact error probability analysis of OSTBCs that is valid for the general cases of arbitrary separable/nonseparable input symbol constellations, arbitrarily correlated or uncorrelated channel matrix elements, and both the Rayleigh and Rician channels [13, 30, 19, 31, 32].

We begin our analysis by noting that (4.49) implies that the analysis of the probability of error at the output of the ML decoder can be done by using the input constellation $\tilde{\mathcal{S}}$ instead of the receiver constellation $\tilde{\mathcal{Y}}$ while “correcting” the standard deviation of the AWGN by the factor of $1/\|\mathbf{H}\|_F$. In other words, to compute the exact symbol error probability in the MIMO case, we can *ignore* the effect of the OSTBC and the channel matrix and use an equivalent model with the original input constellation $\tilde{\mathcal{S}}$ and a properly *rescaled* noise variance.

4.7.1 Probability of error for a separable input constellation

Probability of error for a given channel realization

For a given (fixed) \mathbf{H} , the probability of erroneous ML detection of the k th symbol s_k can be written as [19]

$$\begin{aligned} P(\mathcal{E}_k) &= \frac{1}{I_k} \sum_{i=1}^{I_k} \left(1 - \iint_{R_{i,k}} p_{X,Y}(x - \operatorname{Re}\{u_{i,k}\}, y - \operatorname{Im}\{u_{i,k}\}) dx dy \right) \\ &= 1 - \frac{1}{I_k} \sum_{i=1}^{I_k} \iint_{R_{i,k}} p_{X,Y}(x - \operatorname{Re}\{u_{i,k}\}, y - \operatorname{Im}\{u_{i,k}\}) dx dy \end{aligned} \quad (4.50)$$

where $R_{i,k}$ is the optimal decision region [33] for $u_{i,k}$ (which is independent of the channel and the OSTBC) and $p_{X,Y}(x, y)$ is the pdf of the two-dimensional Gaussian noise with the variance $\sigma^2/\|\mathbf{H}\|_F^2$ per real dimension:

$$p_{X,Y}(x, y) = \frac{\|\mathbf{H}\|_F^2}{2\pi\sigma^2} \exp\left(-\frac{\|\mathbf{H}\|_F^2}{2\sigma^2}(x^2 + y^2)\right). \quad (4.51)$$

Inserting (4.51) into (4.50) yields

$$\begin{aligned} P(\mathcal{E}_k) &= 1 - \frac{1}{I_k} \sum_{i=1}^{I_k} \iint_{R_{i,k}} \frac{\|\mathbf{H}\|_F^2}{2\pi\sigma^2} \\ &\quad \times \exp\left(-\frac{\|\mathbf{H}\|_F^2}{2\sigma^2} ((x - \operatorname{Re}\{u_{i,k}\})^2 + (y - \operatorname{Im}\{u_{i,k}\})^2)\right) dx dy. \end{aligned} \quad (4.52)$$

We note that $P(\mathcal{E}_k)$ can be easily computed for any complex constellation whose probability of error is known for the SISO AWGN channel.

A noteworthy observation is that if N , M , $\|\mathbf{H}\|_F$, and the set of constellations $\{\tilde{\mathcal{U}}_k\}$ are fixed, then the error probability depends neither on the particular choice of the OSTBC nor on the individual entries of \mathbf{H} . Moreover, the error probabilities are the same for \mathbf{H} and \mathbf{H}^T , which implies a certain transmitter-receiver *reciprocity* in MIMO systems with OSTBCs.

Probability of error averaged over channel realizations

In the case of random \mathbf{H} , let us denote $\|\mathbf{H}\|_F^2$ by Z and its pdf by $p_Z(z)$. Then, the probability of error averaged over realizations of \mathbf{H} becomes [19]

$$\begin{aligned} P(\mathcal{E}_k) &= \int_0^\infty P(\mathcal{E}_k|z) p_Z(z) dz \\ &= \int_0^\infty (1 - \frac{1}{I_k} \sum_{i=1}^{I_k} \iint_{R_{i,k}} p_{X,Y|Z}(x - \operatorname{Re}\{u_{i,k}\}, y - \operatorname{Im}\{u_{i,k}\}|z) dx dy) p_Z(z) dz \\ &= 1 - \frac{1}{I_k} \sum_{i=1}^{I_k} \iint_{R_{i,k}} p_{X,Y}(x - \operatorname{Re}\{u_{i,k}\}, y - \operatorname{Im}\{u_{i,k}\}) dx dy \end{aligned} \quad (4.53)$$

where

$$p_{X,Y|Z}(x, y|z) = \frac{z}{2\pi\sigma^2} \exp\left(-z\frac{x^2 + y^2}{2\sigma^2}\right) \quad (4.54)$$

and

$$\begin{aligned} p_{X,Y}(x, y) &= \int_0^\infty p_{X,Y|Z}(x, y|z) p_Z(z) dz \\ &= \int_0^\infty \frac{z}{2\pi\sigma^2} \exp\left(-z\frac{x^2 + y^2}{2\sigma^2}\right) p_Z(z) dz. \end{aligned} \quad (4.55)$$

In the Rician fading channel case, if the real and the imaginary parts of the entries of \mathbf{H} are independent Gaussian random variables with (possibly) nonzero means and the same variance, then Z has a noncentral χ^2 distribution with $2MN$ degrees of freedom [34]. Denoting the standard deviation of real and imaginary parts of each element of \mathbf{H} by ρ , the pdf of Z becomes [34]

$$p_Z(z) = \frac{z^{MN-1} \exp(-z/2\rho^2 - \lambda/2)}{\rho^{2MN} 2^{MN}} \sum_{k=0}^{\infty} \frac{(\lambda z)^k}{\rho^{2k} 2^{2k} k! \Gamma(k + MN)} \quad (4.56)$$

where $\Gamma(\cdot)$ denotes the gamma function,

$$\lambda = \|\mathbb{E}\{\mathbf{H}\}\|_F^2 / \rho^2 \quad (4.57)$$

is the noncentrality parameter of the distribution, and $\mathbb{E}\{\cdot\}$ denotes the statistical expectation. The mean of the noncentral χ^2 distribution (4.56) is given by

$$\mu(\lambda, 2MN, \rho) \triangleq \mathbb{E}\{Z\} = \rho^2(\lambda + 2MN). \quad (4.58)$$

Substituting (4.56) into (4.55) and using (4.58), we obtain after straightforward manipulations that [19]

$$p_{X,Y}(x, y) = \frac{\frac{\rho^2}{\sigma^2} \left(\frac{\lambda/2}{\frac{\rho^2}{\sigma^2}(x^2+y^2)+1} + MN \right) \exp \left(-\frac{\lambda}{2} \left(1 - \frac{1}{\frac{\rho^2}{\sigma^2}(x^2+y^2)+1} \right) \right)}{\pi \left(\frac{\rho^2}{\sigma^2}(x^2+y^2)+1 \right)^{MN+1}}. \quad (4.59)$$

Now, $P(\mathcal{E}_k)$ can be obtained by inserting (4.59) into (4.53). This yields

$$P(\mathcal{E}_k) = 1 - \frac{1}{I_k} \sum_{i=1}^{I_k} \iint_{R_{i,k}} \frac{\frac{\rho^2}{\sigma^2} \left(\frac{\lambda/2}{C(x,y,u_{i,k})} + MN \right) \exp \left(-\frac{\lambda}{2} \left(1 - \frac{1}{C(x,y,u_{i,k})} \right) \right)}{\pi C^{MN+1}(x, y, u_{i,k})} dx dy \quad (4.60)$$

where

$$C(x, y, u_{i,k}) = \frac{\rho^2}{\sigma^2} \left((x - \operatorname{Re}\{u_{i,k}\})^2 + (y - \operatorname{Im}\{u_{i,k}\})^2 \right) + 1.$$

Figure 4.3 shows the symbol error rates (SERs) obtained via simulations (as a scatter plot) and by theoretical evaluation using (4.60). In this figure, SERs are displayed versus MN where we assume that all symbol constellations are 16-QAM (quadrature amplitude modulation) with the minimal distance $2/3$, $\sigma^2 = 1$, and all products MN are generated for $1 \leq M, N \leq 6$. To obtain each point of this plot, independent realizations of a random Rician fading channel with the parameters $\rho = 1$ and $\lambda = 10$ have been generated.

In the Rayleigh channel case, $p_{X,Y}(x, y)$ can be found by setting $\lambda = 0$ in (4.59):

$$p_{X,Y}(x, y) = \frac{\frac{\rho^2}{\sigma^2} MN}{\pi \left(\frac{\rho^2}{\sigma^2}(x^2+y^2)+1 \right)^{MN+1}}. \quad (4.61)$$

Interestingly, if all parameters except M and N are fixed, the dependence of $p_{X,Y}(x, y)$ on M and N in equations (4.59) and (4.61) is through the term MN . The same conclusion

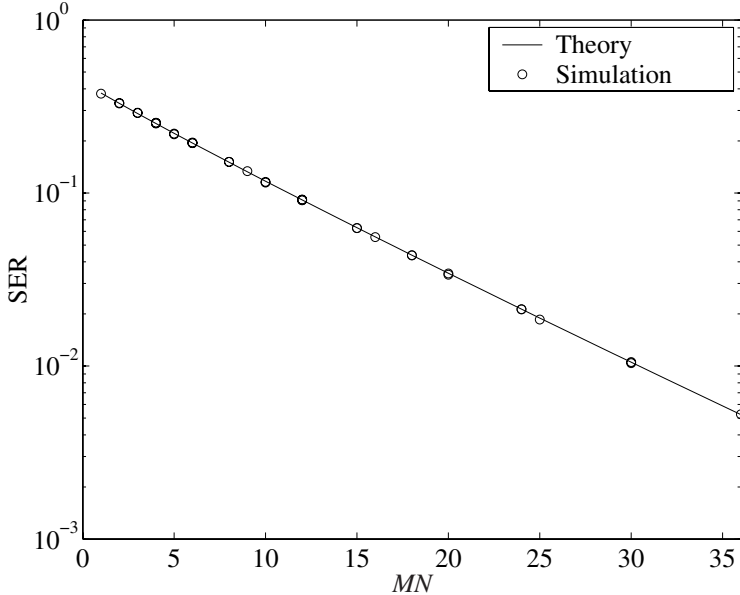


Figure 4.3 Theoretical and simulated SERs versus MN in the random Rician fading channel case.

holds true concerning the dependence of $P(\mathcal{E}_k)$ on the parameters M and N . This means that when MN is fixed, any variations of M and N do not alter the error probability and that the role of M and N in the error probability is symmetric. This fact further illustrates the aforementioned transmitter-receiver reciprocity property.

Another important observation is that if an OSTBC is transmitted over both the Rician or Rayleigh fading channels, then the error probabilities can be computed in the same way as for the SISO AWGN channel with the only difference that the two-dimensional Gaussian pdf in the probability of error integrals has to be replaced by the equivalent pdf's of (4.59) or (4.61), respectively.

It may be useful to rewrite (4.59) and (4.60) in terms of the average Rician parameter (ARP) of the channel and the average signal-to-noise ratio (SNR). Let us denote the (i, j) th element of \mathbf{H} by $H_{i,j}$, the Rician parameter of $H_{i,j}$ by $\alpha_{i,j} \triangleq |E\{H_{i,j}\}|^2/(2\rho^2)$, and the ARP of the elements of \mathbf{H} by $\bar{\alpha} \triangleq \frac{1}{MN} \sum_{i,j} \alpha_{i,j}$. Then, (4.57) yields

$$\lambda = 2 \sum_{i,j} \alpha_{i,j} = 2MN\bar{\alpha}. \quad (4.62)$$

Let us denote the instantaneous SNR in (4.49) by $\gamma(\mathbf{H})$, and the average SNR by $\bar{\gamma}$. Then, (4.49) yields

$$\gamma(\mathbf{H}) \triangleq \frac{E\{\|\mathbf{s}\|^2\}}{E\{\|\boldsymbol{\xi}\|^2\}} = \frac{KE_s}{K \frac{2\sigma^2}{\|\mathbf{H}\|_F^2}} = \frac{\|\mathbf{H}\|_F^2 E_s}{2\sigma^2} \quad (4.63)$$

where $E_s \triangleq \text{E}\{\|\mathbf{s}\|^2\}/K$ is the average energy of the constellations. Thus

$$\begin{aligned} \bar{\gamma} &\triangleq \text{E}\{\gamma(\mathbf{H})\} = \frac{\text{E}\{\|\mathbf{H}\|_F^2\}E_s}{2\sigma^2} = \frac{\text{E}\{Z\}E_s}{2\sigma^2} \\ &= \frac{\rho^2(\lambda + 2MN)E_s}{2\sigma^2} = \frac{\rho^2 MN(\bar{\alpha} + 1)E_s}{\sigma^2} \end{aligned} \quad (4.64)$$

where (4.64) is due to (4.58) and (4.62). Hence, (4.64) yields

$$\frac{\rho^2}{\sigma^2} = \frac{\bar{\gamma}}{E_s MN(\bar{\alpha} + 1)}. \quad (4.65)$$

Also, let us normalize the constellations $\tilde{\mathcal{U}}_k$ using contraction by a factor $\sqrt{E_s}$. Let

$$\begin{aligned} \tilde{X} &\triangleq X/\sqrt{E_s} \\ \tilde{Y} &\triangleq Y/\sqrt{E_s} \\ \tilde{u}_{i,k} &\triangleq u_{i,k}/\sqrt{E_s} \end{aligned}$$

and let $\tilde{R}_{i,k}$ denote the optimal decision regions after contraction. Then, it can be readily shown [19] that (4.59) and (4.60) yield

$$\begin{aligned} p_{\tilde{X}, \tilde{Y}}(\tilde{x}, \tilde{y}) &= \\ &\frac{\frac{\bar{\gamma}}{\bar{\alpha}+1} \left(\frac{\bar{\alpha}}{\frac{\bar{\gamma}}{MN(\bar{\alpha}+1)}(\tilde{x}^2+\tilde{y}^2)+1} + 1 \right) \exp \left(-MN\bar{\alpha} \left(1 - \frac{1}{\frac{\bar{\gamma}}{MN(\bar{\alpha}+1)}(\tilde{x}^2+\tilde{y}^2)+1} \right) \right)}{\pi \left(\frac{\bar{\gamma}}{MN(\bar{\alpha}+1)}(\tilde{x}^2+\tilde{y}^2)+1 \right)^{MN+1}} \end{aligned} \quad (4.66)$$

and

$$P(\mathcal{E}_k) = 1 - \frac{1}{I_k} \sum_{i=1}^{I_k} \iint_{\tilde{R}_{i,k}} \frac{\frac{\bar{\gamma}}{\bar{\alpha}+1} \left(\frac{\bar{\alpha}}{\tilde{C}(\tilde{x}, \tilde{y}, \tilde{u}_{i,k})} + 1 \right) \exp \left(-MN\bar{\alpha} \left(1 - \frac{1}{\tilde{C}(\tilde{x}, \tilde{y}, \tilde{u}_{i,k})} \right) \right)}{\pi \tilde{C}^{MN+1}(\tilde{x}, \tilde{y}, \tilde{u}_{i,k})} d\tilde{x} d\tilde{y}$$

respectively, where

$$\tilde{C}(\tilde{x}, \tilde{y}, \tilde{u}_{i,k}) \triangleq \frac{\bar{\gamma}}{MN(\bar{\alpha}+1)} \left((\tilde{x} - \text{Re}\{\tilde{u}_{i,k}\})^2 + (\tilde{y} - \text{Im}\{\tilde{u}_{i,k}\})^2 \right) + 1.$$

For the Rayleigh case, (4.61) gives

$$p_{\tilde{X}, \tilde{Y}}(\tilde{x}, \tilde{y}) = \frac{\bar{\gamma}}{\pi \left(\frac{\bar{\gamma}}{MN}(\tilde{x}^2+\tilde{y}^2)+1 \right)^{MN+1}}.$$

To illustrate the effect of the ARP on the effective pdf of the noise for a Rician fading channel, Figure 4.4 displays the one-dimensional slice of $p_{\tilde{X}, \tilde{Y}}(\tilde{x}, \tilde{y})$ evaluated using (4.66) at $\tilde{y} = 0$ for different values of $\bar{\alpha}$. In this figure, it is assumed that $MN = 6$ and $\bar{\gamma} = 20$ dB. This figure shows that increasing the ARP of the channel coefficients increases the concentration

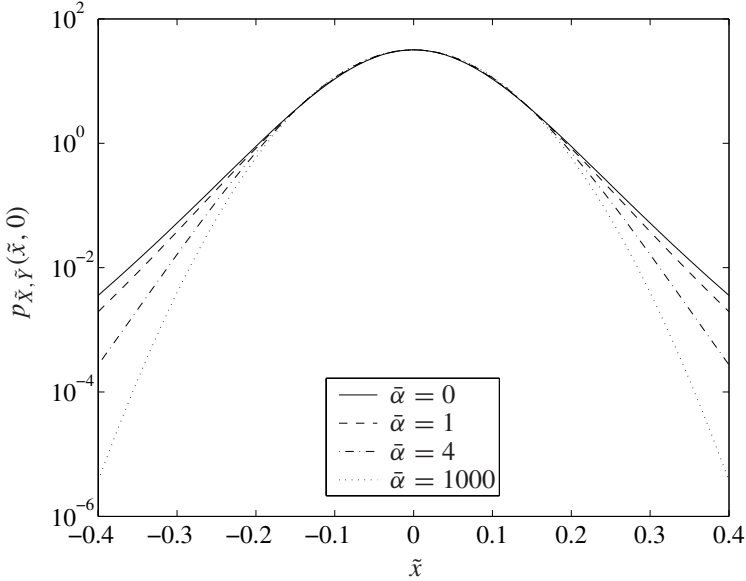


Figure 4.4 One slice of the effective pdf of the noise $p_{\tilde{X}, \tilde{Y}}(\tilde{x}, 0)$ for a Rician channel with different values of ARP $\bar{\alpha}$.

of the effective pdf of the noise around the origin, which results in a decreased SER for *any* constellation.

In the case when the elements of \mathbf{H} are correlated Gaussian random variables, the pdf of Z does not have a closed form [35], Chapter 29, and the above technique for computing the probability of error cannot be applied. Therefore, to compute $P(\mathcal{E}_k)$ explicitly in the correlated channel case, let us adopt the approach of [31, 32], which uses a moment generating function (MGF) based technique. It should be noted that MGF-related approaches have previously found numerous applications to error probability analysis of fading SISO and single-input multiple-output (SIMO) channels [36].

Using the notation

$$\phi \triangleq \frac{1}{2\pi\sigma^2}, \quad \psi \triangleq -\frac{x^2 + y^2}{2\sigma^2} \quad (4.67)$$

equation (4.55) can be written as

$$p_{X,Y}(x, y) = \phi \int_0^\infty z e^{\psi z} p_Z(z) dz. \quad (4.68)$$

Denoting the MGF of Z as $M(t)$, and its derivative as $M'(t)$, we have [32]

$$\begin{aligned} M(t) &\triangleq \text{E}\{e^{Zt}\} = \int_0^\infty e^{zt} p_Z(z) dz \\ M'(t) &= \text{E}\{Z e^{Zt}\} = \int_0^\infty z e^{zt} p_Z(z) dz. \end{aligned} \quad (4.69)$$

Using (4.69), equation (4.68) can be written as

$$p_{X,Y}(x, y) = \phi M'(\psi). \quad (4.70)$$

Fortunately, simple closed-form expressions can be obtained for the MGF of Z as described below.

The covariance matrix of $\underline{\mathbf{H}}$ can be defined as

$$\mathbf{C} \triangleq \mathbb{E}\{(\underline{\mathbf{H}} - \mathbb{E}\{\underline{\mathbf{H}}\})(\underline{\mathbf{H}} - \mathbb{E}\{\underline{\mathbf{H}}\})^T\}.$$

The eigendecomposition of \mathbf{C} can be written as

$$\mathbf{C} = \mathbf{U} \Lambda_{\mathbf{C}} \mathbf{U}^T \quad (4.71)$$

where $\Lambda_{\mathbf{C}} = \text{diag}\{\rho_1^2, \dots, \rho_{2MN}^2\}$ is the diagonal matrix of the eigenvalues ρ_i^2 (for $i = 1, 2, \dots, 2MN$) of \mathbf{C} , and \mathbf{U} is the $2MN \times 2MN$ real unitary matrix of the corresponding eigenvectors of \mathbf{C} . Note that the matrix \mathbf{C} is symmetric and positive semidefinite and, therefore, all its eigenvalues are nonnegative. If we use the notation [32]

$$\tilde{\underline{\mathbf{H}}} \triangleq \mathbf{U}^T \underline{\mathbf{H}} \triangleq [W_1, W_2, \dots, W_{2MN}]^T$$

then it can be easily shown that W_i ($i = 1, 2, \dots, 2MN$) are all independent Gaussian random variables with the variances ρ_i^2 ($i = 1, 2, \dots, 2MN$), respectively. Denoting the mean of W_i by μ_i , we have

$$[\mu_1, \mu_2, \dots, \mu_{2MN}]^T = \mathbf{U}^T \mathbb{E}\{\underline{\mathbf{H}}\}. \quad (4.72)$$

It is clear that

$$Z = \|\mathbf{H}\|_F^2 = \|\underline{\mathbf{H}}\|^2 = \|\tilde{\underline{\mathbf{H}}}\|^2 = \sum_{i=1}^{2MN} W_i^2.$$

As all W_i^2 are independent, the MGF of Z is the product of the MGFs of W_i^2 . The random variables W_i^2 have a noncentral χ^2 distribution with one degree of freedom whose MGF is known to be [35]

$$(1 - 2t\rho_i^2)^{-1/2} \exp\left(\frac{t\mu_i^2}{1 - 2t\rho_i^2}\right).$$

Therefore, the MGF of Z and its derivative become [31]

$$M(t) = \prod_{i=1}^{2MN} \left((1 - 2t\rho_i^2)^{-1/2} \exp\left(\frac{t\mu_i^2}{1 - 2t\rho_i^2}\right) \right) \quad (4.73)$$

$$\begin{aligned} M'(t) &= \left(\sum_{i=1}^{2MN} \frac{\rho_i^2 (1 - 2t\rho_i^2) + \mu_i^2}{(1 - 2t\rho_i^2)^2} \right) \\ &\quad \times \left(\prod_{i=1}^{2MN} \left((1 - 2t\rho_i^2)^{-1/2} \exp\left(\frac{t\mu_i^2}{1 - 2t\rho_i^2}\right) \right) \right) \end{aligned} \quad (4.74)$$

respectively. Substituting (4.67) and (4.74) into (4.70) yields [31]

$$p_{X,Y}(x, y) = \frac{1}{2\pi} \left(\sum_{i=1}^{2MN} \frac{\frac{\rho_i^2}{\sigma^2} \left(\frac{\rho_i^2}{\sigma^2} (x^2 + y^2) + 1 \right) + \frac{\mu_i^2}{\sigma^2}}{\left(\frac{\rho_i^2}{\sigma^2} (x^2 + y^2) + 1 \right)^2} \right) \\ \times \prod_{i=1}^{2MN} \left(\left(\frac{\rho_i^2}{\sigma^2} (x^2 + y^2) + 1 \right)^{-1/2} \exp \left(-\frac{\frac{\mu_i^2}{2\sigma^2} (x^2 + y^2)}{\frac{\rho_i^2}{\sigma^2} (x^2 + y^2) + 1} \right) \right). \quad (4.75)$$

Equations (4.53) and (4.75) express the probability of error in the case of an arbitrary correlated Rician channel in a closed form. According to (4.71), the channel correlation properties are determined in (4.75) by the values of ρ_i^2 ($i = 1, \dots, 2MN$). In particular, if $\rho_1^2 = \rho_2^2 = \dots = \rho_{2MN}^2 \triangleq \rho^2$, then the channel is uncorrelated with the covariance matrix $\mathbf{C} = \rho^2 \mathbf{I}_{2MN}$.

The transmitter-receiver reciprocity can again be observed from (4.53) and (4.75). Indeed, if the parameter MN is fixed, then the symbol error probability does not depend on specific values of M and N . Also, if MN and the input constellations $\{\tilde{\mathcal{U}}_k\}_{k=1}^K$ are all fixed, then the symbol error probability is independent of the particular choice of OSTBC.

In the special case of an uncorrelated channel, equation (4.75) reduces to (4.59), and in the case of a correlated Rayleigh fading channel, we have $\mu_i = 0$ ($i = 1, 2, \dots, 2MN$), and (4.75) can be simplified to [31]

$$p_{X,Y}(x, y) = \frac{1}{2\pi} \left(\sum_{i=1}^{2MN} \frac{\frac{\rho_i^2}{\sigma^2}}{\frac{\rho_i^2}{\sigma^2} (x^2 + y^2) + 1} \right) \prod_{i=1}^{2MN} \left(\frac{\rho_i^2}{\sigma^2} (x^2 + y^2) + 1 \right)^{-1/2}. \quad (4.76)$$

Let us now compare the theoretical results of (4.75) and (4.76) with simulations. To illustrate the effect of the channel correlation on the effective pdf of the noise for a Rayleigh channel, Figure 4.5 shows the one-dimensional slice of $p_{X,Y}(x, y)$ evaluated using (4.76) and by simulations at $y = 0$ for different correlation levels. In this figure, we assumed $M = N = 4$, $\sigma^2 = 1$,

$$\rho_i^2 = \begin{cases} \eta/\kappa, & i = 1, \dots, \kappa \\ 0, & i = \kappa + 1, \dots, 2MN \end{cases}$$

and $\eta = 5$. Here, κ is the rank of \mathbf{C} and the parameter η characterizes the strength of the channel. Low values of κ correspond to high channel correlations (in this case, the channel covariance matrix is low rank), whereas higher values of this parameter correspond to low channel correlations (so that at the maximal value of κ , $\kappa_{\max} = 2MN = 32$, the channel becomes uncorrelated). The simulation points in Figure 4.5 are obtained using the half-rate code of [5] and the quadrature phase shift keying (QPSK) input constellation with the minimum distance of $\sqrt{2}$. This figure demonstrates that increasing the correlation of the channel enhances the tails of the effective pdf of the noise, while making the central part of this pdf narrower. This gives a qualitative explanation why channel correlation leads to higher SERs.

Figure 4.6 displays the SER versus the correlation (in terms of κ) for the same example as before and for different values of η . It can be seen from this figure that the SER reduces as the channel becomes less correlated. This effect is especially strong at large values of η .

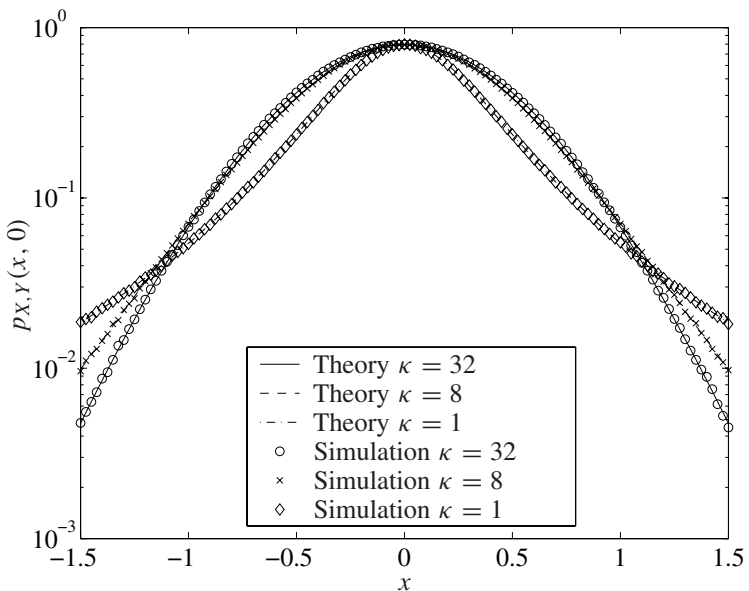


Figure 4.5 $p_{X,Y}(x, 0)$ for different values of κ in the Rayleigh fading channel case. Smaller κ 's correspond to higher channel correlations.

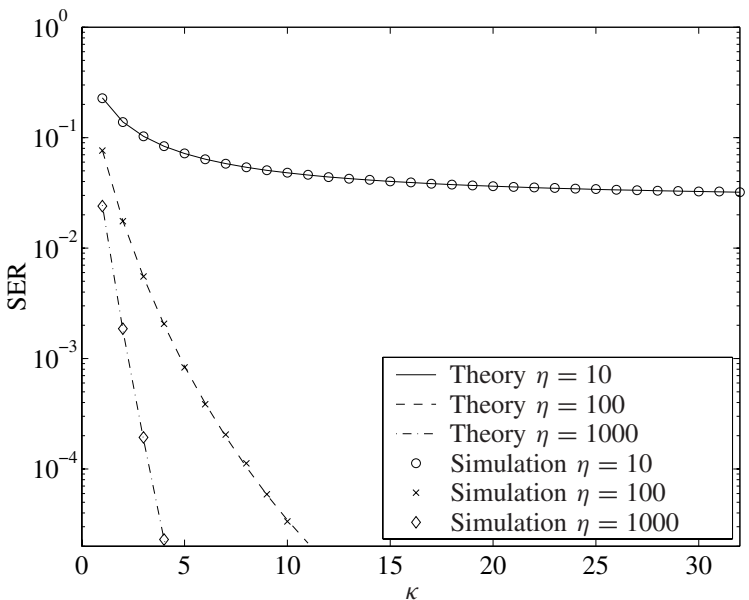


Figure 4.6 SER versus channel correlation (in terms of κ) for different values of η in the Rayleigh fading channel case.

In the Rician channel case, the channel matrix can be represented as a sum of the line-of-sight (LOS) and non-line-of-sight (NLOS) components

$$\mathbf{H} = \mathbf{H}_{\text{LOS}} + \mathbf{H}_{\text{NLOS}}$$

where $\mathbf{H}_{\text{LOS}} \triangleq \mathbb{E}\{\mathbf{H}\}$ and $\mathbf{H}_{\text{NLOS}} \triangleq \mathbf{H} - \mathbf{H}_{\text{LOS}}$. A commonly used, although quite specific, model for correlated Rician fading channels [37, 29, 9] assumes independent transmit and receive correlation matrices. According to this model

$$\mathbf{H}_{\text{NLOS}} = \mathbf{R}_T^{1/2} \mathbf{H}_w \mathbf{R}_R^{1/2}$$

where \mathbf{R}_R is the $M \times M$ correlation matrix of the receive antennas, \mathbf{R}_T is the $N \times N$ correlation matrix of the transmit antennas, and \mathbf{H}_w is a complex $N \times M$ matrix whose elements are zero-mean i.i.d. complex Gaussian random variables.

In the next example, we use this particular channel model. We consider the case of $M = N = 2$ and model \mathbf{H} as [32]

$$\mathbf{H} = c_{\text{LOS}} \begin{bmatrix} 1 & 1 \\ 1 & 1 \end{bmatrix} + c_{\text{NLOS}} \begin{bmatrix} 1 & \zeta_T \\ \zeta_T & 1 \end{bmatrix}^{1/2} \mathbf{H}_w \begin{bmatrix} 1 & \zeta_R \\ \zeta_R & 1 \end{bmatrix}^{1/2}$$

where the constants c_{LOS}^2 and c_{NLOS}^2 characterize the powers of the LOS and NLOS components of \mathbf{H} and jointly determine the SNR and the power ratio α of these components. Here, the parameters ζ_R and ζ_T characterize the receive and transmit correlations, respectively. In this example, Alamouti's code with the QPSK input constellation is used.

Figure 4.7 shows theoretical curves for SER versus α for different values of ζ_T and ζ_R at SNR=10 dB. This figure demonstrates that if the power ratio between the LOS and NLOS components is fixed, then increasing the correlation of the NLOS part of the channel increases the SER. This effect is similar to that observed from Figure 4.6 in the Rayleigh channel case (where there is no LOS component). However, it can be seen from this figure that SER is not always a monotonic function of α . In particular, SER can be seen to reach its maximum at a value of α that depends on ζ_T and ζ_R , and, for large values of α , SER is a decreasing function of α . As α tends to infinity, the difference between SERs corresponding to different values of ζ_T and ζ_R vanishes because, when α tends to infinity, the role of the NLOS component of the channel vanishes, and so does the effect of ζ_T and ζ_R .

Figure 4.8 shows the SER versus SNR for different values of ζ_T and ζ_R in the case $\alpha = 1$. This figure shows again that increasing ζ_T and ζ_R increases SER for all the SNR values tested.

Figure 4.9 displays the SER versus SNR for different values of α in the case $\zeta_T = \zeta_R = 0.5$. Similarly to Figure 4.7, the latter figure shows that for $\zeta_T = \zeta_R = 0.5$ and for medium to high SNRs, SER first increases and then decreases as a function of α .

4.7.2 Probability of error for a nonseparable input constellation

In space-time coding, it is possible to use constellations with dimensions higher than two (e.g., using orthogonal, biorthogonal, simplex, or other multidimensional constellations [34]). By using appropriate multidimensional constellations, better performance can be achieved at the cost of higher implementation complexity, see [38] and the next section. This can also be the case, for example, when the digital symbols are coded before being mapped to complex

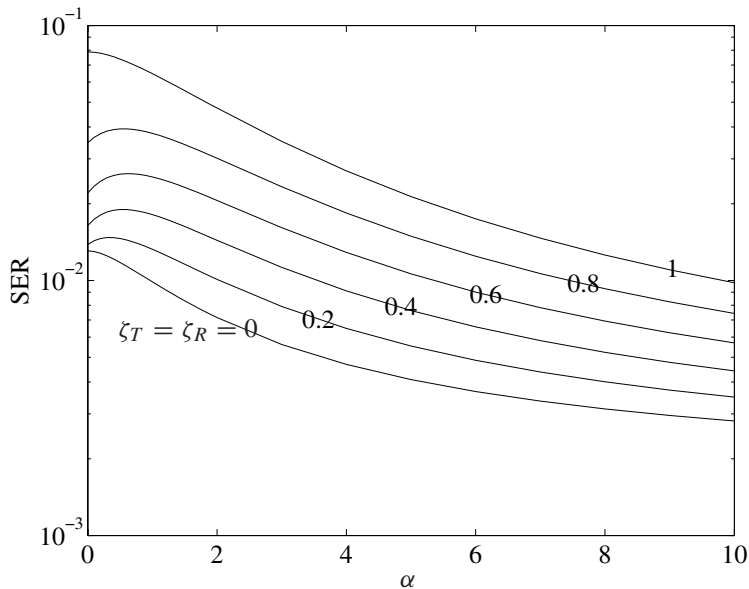


Figure 4.7 Theoretical curves for SER versus α for different values of ζ_T and ζ_R , and fixed SNR = 10 dB in the Rician fading channel case.

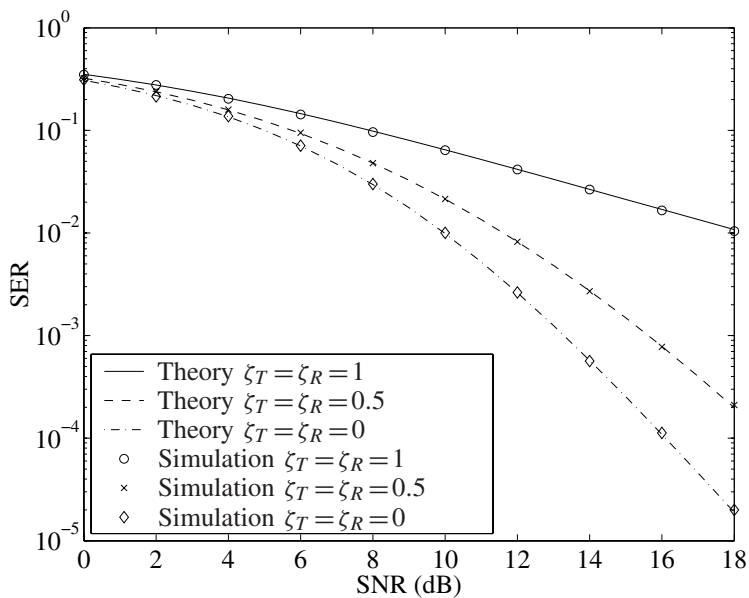


Figure 4.8 SER versus SNR for different values of ζ_T and ζ_R , and fixed $\alpha = 1$ in the Rician fading channel case.

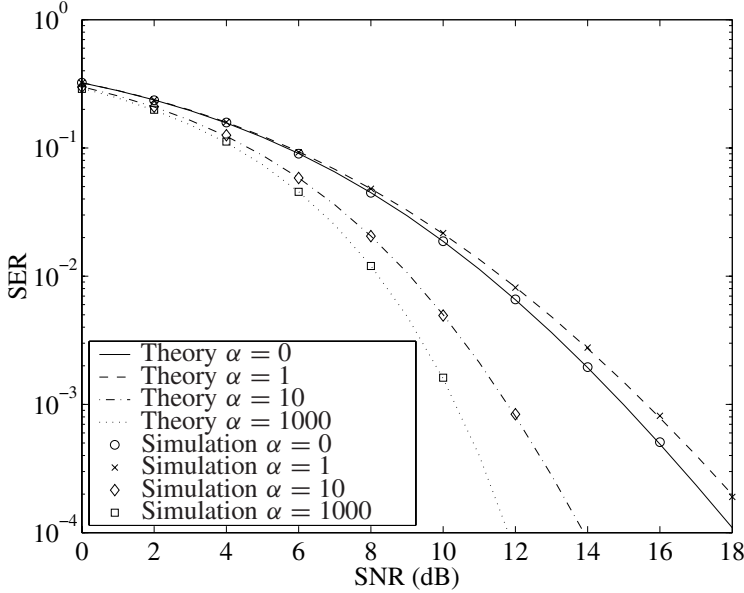


Figure 4.9 SER versus SNR for different values of α and fixed $\zeta_T = \zeta_R = 0.5$ in the Rician fading channel case.

symbols. In such cases, each information symbol s_k is not drawn independently from its own constellation but the K symbols are coded jointly. Then, the input constellation $\tilde{\mathcal{S}}$ is not restricted to (4.15), and the optimal ML decoding is no longer equivalent to symbol-by-symbol decoding.

Let us denote the event of erroneous detection of \mathbf{s} by \mathcal{E} , and the optimal $2K$ -dimensional decision region corresponding to $\underline{\mathbf{s}}_\ell$ by R_ℓ . Then, we obtain that the probability of error for a given channel realization can be expressed as [19]

$$P(\mathcal{E}) = 1 - \frac{1}{L} \sum_{\ell=1}^L \int_{R_\ell} \cdots \int \frac{\|\mathbf{H}\|_F^{2K}}{(2\pi\sigma^2)^K} \exp\left(-\frac{\|\mathbf{H}\|_F^2}{2\sigma^2} \|\underline{\mathbf{s}} - \underline{\mathbf{s}}_\ell\|^2\right) d\underline{\mathbf{s}}. \quad (4.77)$$

where L is defined on page 110. The probability of error averaged over channel realizations becomes [19]

$$P(\mathcal{E}) = 1 - \frac{1}{L} \sum_{\ell=1}^L \int_{R_\ell} \cdots \int p_{\mathbf{u}}(\underline{\mathbf{s}} - \underline{\mathbf{s}}_\ell) d\underline{\mathbf{s}} \quad (4.78)$$

where

$$p_{\mathbf{u}}(\mathbf{u}) = \int_0^\infty \frac{z^K}{(2\pi\sigma^2)^K} \exp\left(-z \frac{\|\mathbf{u}\|^2}{2\sigma^2}\right) p_Z(z) dz. \quad (4.79)$$

The function $p_{\mathbf{u}}(\mathbf{u})$ is the effective pdf of the $2K$ -dimensional noise, that is, the pdf of the Gaussian noise averaged over all possible variances σ^2/Z .

In the Rician fading channel case, substituting (4.56) in (4.79), after straightforward manipulations we have [19]

$$p_{\mathbf{u}}(\mathbf{u}) = \frac{\left(\frac{\rho^2}{\sigma^2}\right)^K \mu'_K \left(\frac{\lambda}{\frac{\rho^2}{\sigma^2} \|\mathbf{u}\|^2 + 1}, 2MN, 1\right) \exp\left(-\frac{\lambda}{2} \left(1 - \frac{1}{\frac{\rho^2}{\sigma^2} \|\mathbf{u}\|^2 + 1}\right)\right)}{(2\pi)^K \left(\frac{\rho^2}{\sigma^2} \|\mathbf{u}\|^2 + 1\right)^{MN+K}} \quad (4.80)$$

where

$$\mu'_K(\lambda, r, \rho) \triangleq \mathbb{E}\left\{Z^K\right\} = \int_0^\infty z^K p_Z(z) dz \quad (4.81)$$

is the K th raw moment of Z .

Simple expressions exist for μ'_K when K is small [39]

$$\begin{aligned} \mu'_1(\lambda, r, 1) &= r + \lambda \\ \mu'_2(\lambda, r, 1) &= r^2 + 2r(\lambda + 1) + \lambda(\lambda + 4) \\ \mu'_3(\lambda, r, 1) &= r^3 + 3r^2(\lambda + 2) + \lambda(\lambda^2 + 12\lambda + 24) + r(3\lambda^2 + 18\lambda + 8). \end{aligned}$$

For an arbitrary value of K , μ'_K can be written as

$$\mu'_K(\lambda, r, 1) = \frac{2^K e^{-\lambda/2} \Gamma\left(K + \frac{1}{2}r\right)}{\Gamma(\frac{1}{2}r)} {}_1F_1\left(K + \frac{1}{2}r, \frac{1}{2}r, \frac{1}{2}\lambda\right) \quad (4.82)$$

where ${}_1F_1$ is a hypergeometric function.

Substituting (4.82) in (4.80) gives [19]

$$p_{\mathbf{u}}(\mathbf{u}) = \frac{\left(\frac{\rho^2}{\sigma^2}\right)^K \frac{\Gamma(K+MN)}{\Gamma(MN)} {}_1F_1\left(K + MN, MN, \frac{\lambda/2}{\frac{\rho^2}{\sigma^2} \|\mathbf{u}\|^2 + 1}\right) \exp\left(-\frac{\lambda}{2}\right)}{\pi^K \left(\frac{\rho^2}{\sigma^2} \|\mathbf{u}\|^2 + 1\right)^{MN+K}}. \quad (4.83)$$

Now, $P(\mathcal{E}_k)$ can be obtained by substituting (4.83) in (4.78).

For Rayleigh channels, (4.83) can be simplified to

$$p_{\mathbf{u}}(\mathbf{u}) = \frac{\left(\frac{\rho^2}{\sigma^2}\right)^K \frac{\Gamma(MN+K)}{\Gamma(MN)}}{\pi^K \left(\frac{\rho^2}{\sigma^2} \|\mathbf{u}\|^2 + 1\right)^{MN+K}}. \quad (4.84)$$

Equations (4.78) and (4.83) can be alternatively expressed in the form [19]

$$P(\mathcal{E}) = 1 - \frac{1}{L} \sum_{\ell=1}^L \int \cdots \int_{\tilde{R}_\ell} p_{\tilde{\mathbf{u}}}(\tilde{\mathbf{s}} - \tilde{\mathbf{s}}_\ell) d\tilde{\mathbf{s}} \quad (4.85)$$

$$p_{\tilde{\mathbf{u}}}(\tilde{\mathbf{u}}) = \frac{\left(\frac{\bar{\gamma}}{MN(\bar{\alpha}+1)}\right)^K \frac{\Gamma(K+MN)}{\Gamma(MN)} {}_1F_1\left(K + MN, MN, \frac{MN\bar{\alpha}}{\frac{\bar{\gamma}}{MN(\bar{\alpha}+1)} \|\tilde{\mathbf{u}}\|^2 + 1}\right) \exp(-MN\bar{\alpha})}{\pi^K \left(\frac{\bar{\gamma}}{MN(\bar{\alpha}+1)} \|\tilde{\mathbf{u}}\|^2 + 1\right)^{MN+K}}$$

where $\tilde{\mathbf{s}}_\ell \triangleq \underline{\mathbf{s}}_\ell / \sqrt{E_s}$, $\tilde{\mathbf{u}} \triangleq \mathbf{u} / \sqrt{E_s}$ and \tilde{R}_ℓ are obtained by contraction of R_ℓ by a factor of $\sqrt{E_s}$. In the Rayleigh channel case, (4.84) becomes

$$p_{\tilde{\mathbf{u}}}(\tilde{\mathbf{u}}) = \frac{\left(\frac{\bar{\gamma}}{MN(\bar{\alpha}+1)}\right)^K \frac{\Gamma(MN+K)}{\Gamma(MN)}}{\pi^K \left(\frac{\bar{\gamma}}{MN(\bar{\alpha}+1)} \|\tilde{\mathbf{u}}\|^2 + 1\right)^{MN+K}}. \quad (4.86)$$

Figure 4.10 displays block error rates (BLERs) versus $\bar{\gamma}$ for $M = N = K = 2$. These BLERs are obtained via simulations and by means of theoretical evaluation using (4.85) and (4.86) for the four-dimensional simplex constellation [34]. Note that the slope of this curve at large average SNRs agrees with the diversity order [3] of $MN = 4$.

When the elements of \mathbf{H} are *correlated* Gaussian random variables, the pdf of Z again does not have a closed form, and the earlier technique cannot be applied. Therefore, following [32], the MGF approach will be used again to compute the probability of error.

Using the notation

$$\phi_K \triangleq \frac{1}{(2\pi\sigma^2)^K}, \quad \psi_K \triangleq -\frac{\|\mathbf{u}\|^2}{2\sigma^2}$$

equation (4.79) can be written as [31]

$$p_{\mathbf{u}}(\mathbf{u}) = \phi_K \int_0^\infty z^K \exp(\psi_K z) p_Z(z) dz. \quad (4.87)$$

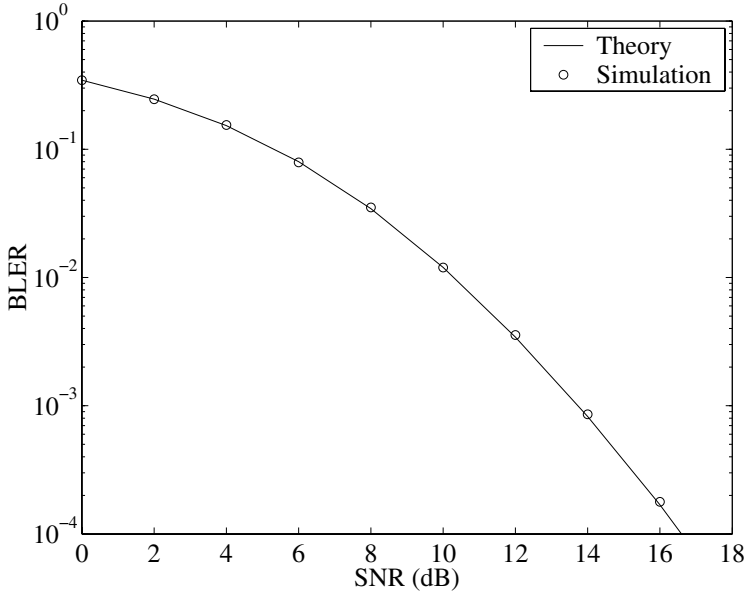


Figure 4.10 Theoretical and simulated BLERs versus $\bar{\gamma}$ in the random Rayleigh case for the four-dimensional simplex constellation.

We note that

$$M^{(K)}(t) = \mathbb{E} \left\{ Z^K e^{Zt} \right\} = \int_0^\infty z^K e^{zt} p_Z(z) dz \quad (4.88)$$

where $M^{(K)}(t)$ denotes the K th derivative of $M(t)$ with respect to t . Using (4.87) and (4.88) yields

$$\begin{aligned} p_{\mathbf{u}}(\mathbf{u}) &= \phi_K M^{(K)}(\psi_K) \\ &= \frac{1}{(2\pi\sigma^2)^K} \left[\frac{d^K}{dt^K} \left(\prod_{i=1}^{2MN} \left(1 - 2t\rho_i^2 \right)^{-1/2} \exp \left(\frac{t\mu_i^2}{1 - 2t\rho_i^2} \right) \right) \right]_{t=-\frac{\|\mathbf{u}\|^2}{2\sigma^2}}. \end{aligned} \quad (4.89)$$

This expression can easily be computed symbolically for any value of K .

In the special case of $\rho_1 = \rho_2 = \dots = \rho_{2MN} = \rho$, (4.89) becomes

$$p_{\mathbf{u}}(\mathbf{u}) = \frac{1}{(2\pi\sigma^2)^K} \left[\frac{d^K}{dt^K} \left((1 - 2t\rho^2)^{-MN} \exp \left(\frac{t\rho^2\lambda}{1 - 2t\rho^2} \right) \right) \right]_{t=-\frac{\|\mathbf{u}\|^2}{2\sigma^2}}. \quad (4.90)$$

For the case of $\lambda = 0$ with equal ρ_i (uncorrelated Rayleigh fading channel), (4.90) can be simplified to

$$\begin{aligned} p_{\mathbf{u}}(\mathbf{u}) &= \frac{1}{(2\pi\sigma^2)^K} \left[\frac{d^K}{dt^K} \left((1 - 2t\rho^2)^{-MN} \right) \right]_{t=-\frac{\|\mathbf{u}\|^2}{2\sigma^2}} \\ &= \frac{1}{(2\pi\sigma^2)^K} \left[\frac{d^{K-1}}{dt^{K-1}} \left((MN)(2\rho^2) (1 - 2t\rho^2)^{-MN-1} \right) \right]_{t=-\frac{\|\mathbf{u}\|^2}{2\sigma^2}} \\ &= \frac{1}{(2\pi\sigma^2)^K} \left[\frac{d^{K-2}}{dt^{K-2}} \left((MN)(MN+1)(2\rho^2)^2 (1 - 2t\rho^2)^{-MN-2} \right) \right]_{t=-\frac{\|\mathbf{u}\|^2}{2\sigma^2}} \\ &= \frac{1}{(2\pi\sigma^2)^K} \left[\frac{(MN+K-1)!}{(MN-1)!} (2\rho^2)^K (1 - 2t\rho^2)^{-MN-K} \right]_{t=-\frac{\|\mathbf{u}\|^2}{2\sigma^2}} \\ &= \frac{\left(\frac{\rho^2}{\sigma^2} \right)^K \frac{\Gamma(MN+K)}{\Gamma(MN)}}{\pi^K \left(\frac{\rho^2}{\sigma^2} \|\mathbf{u}\|^2 + 1 \right)^{MN+K}} \end{aligned}$$

which is the same as (4.84).

4.8 Optimality Properties of OSTBCs

In this section, we prove two strong optimality properties of OSTBCs [40]. To do this, we first consider the problem of optimal space-time constellations. Note that for MIMO systems with Rayleigh flat fading, the problem of finding optimal constellations in the sense of minimizing the average error probability of the ML decoder under average power constraint is an open issue of great interest.

In [24] and [41], it has been shown that OSTBCs are optimal *among linear unitary codes*, with optimality in the sense of minimizing the union bound of the error probability under the *equal* power constraint. In [42–44], as a general design guideline, it has been proposed that for MIMO systems that use STBCs, the constellation should be designed so that for any pair of constellation matrices, the singular values of the code differences are equal.³ Such a design has been demonstrated to minimize the pairwise error probability when the distances of the constellation points are given [44]. Even though OSTBCs perfectly satisfy the equal-singular-value property, it has been shown in [15] that at high rates the error probabilities of certain OSTBCs are higher than those of linear dispersion (LD) codes of the same dimensions and constellation sizes, whereas the singular values of the LD codes are *not* equal. The results of [15] give an indication that OSTBCs are not necessarily optimal for all constellation sizes. The reasons for these seemingly contradictory results can be recognized by noting that the distances between the members of the constellation play a role in the pairwise error probability [44]. More specifically, under an average power constraint, the objective of maximizing the distances for all pairs and that of making the singular values equal for all pairs are, in general, conflicting. Intuitively, it may be expected that the optimal solution is somewhere in between where each of these two objectives is partially met, and finding the optimal solution requires a sort of joint optimization.

In this section, we give a solution to this problem for the case of small constellation sizes and show the answer to be OSTBCs [40]. That is, we obtain optimal STBCs in the sense of minimizing the exact average pairwise error probability under the *average energy constraint*. In contrast to [24] and [41], this optimal solution will be developed for the set of *all* possible space-time constellations (rather than the set of unitary constellations) for a fixed block length T and under a power constraint that is milder than that used in [24] and [41]. Also, in contrast to [42–44], the optimality of the resulting codes for the whole constellation rather than for a particular pair of constellation points will be shown. In fact, we will show that for small-size constellations, OSTBCs are optimal among all possible block codes [40]. This result will be proven for constellation sizes up to $2K + 1$ where K is the number of the OSTBC complex variables. In particular, it will be clarified that, if the constellation size is not larger than $2K + 1$, then the objectives of maximizing the distances for all constellation pairs and of making the singular values equal for all these pairs are not conflicting and can be achieved *independently*. For the case of small-size constellations, this seems to be the strongest-sense optimality result proven for OSTBCs so far. Additionally, it will be demonstrated that the optimal multi-dimensional OSTBC constellations form a regular simplex if the number of receivers is large [40].

Since this proof of optimality of OSTBCs is valid only in the small-size constellation case, it does not contradict the result of [15] where suboptimality of OSTBCs is shown for certain large-size constellations.

Furthermore, it will be proven that for any constellation of any size, OSTBCs are optimal among all LD codes of the same dimensions and with the same number K of complex variables (substreams) [40]. This result will illustrate that using optimized LD codes instead

³For any matrix \mathbf{Z} , the singular values of \mathbf{Z} can be defined as the square root of the eigenvalues of $\mathbf{Z}\mathbf{Z}^H$, that is, the singular values are positive by definition.

of OSTBCs can bring some advantages only when no OSTBC exists with the same values of K , T , and N .

Interested readers are referred to [40] for further details.

4.8.1 Sufficient conditions for optimal space-time codes with dimension-constrained constellations

In this subsection, we formulate sufficient conditions for optimality of dimension-constrained space-time constellations in the sense of minimizing average pairwise error probability under the average power constraint. The main result of this subsection is Theorem 4.8.4, which will be used later to prove optimality results for OSTBCs.

Let us consider a MIMO system whose input-output relationship is given by (4.8). Let us assume in this section that the entries of \mathbf{H} and \mathbf{V} are i.i.d. zero-mean complex circular Gaussian random variables with variance 0.5 and σ^2 per real dimension, respectively. As before, \mathbf{X} belongs to the constellation $\tilde{\mathcal{X}} \triangleq \{\mathbf{X}_1, \mathbf{X}_2, \dots, \mathbf{X}_L\}$. We do not restrict $\tilde{\mathcal{X}}$ to have any particular structure such as the rectangular lattice one.

Similarly to the previous sections, we consider the case where \mathbf{H} is known at the receiver and the coherent ML decoder is used. Recall that, conditioned on \mathbf{H} , the constellation of the received symbols is given by $\tilde{\mathcal{Y}} = \{\mathbf{Y}_1, \mathbf{Y}_2, \dots, \mathbf{Y}_L\}$, where $\mathbf{Y}_\ell = \mathbf{X}_\ell \mathbf{H}$.

For a given channel matrix realization \mathbf{H} , let $P(\mathbf{X}_i \rightarrow \mathbf{X}_\ell | \mathbf{H})$ denote the pairwise error probability of the coherent ML decoder for \mathbf{X}_i and \mathbf{X}_ℓ , $i \neq \ell$. Furthermore, let $P(\mathbf{X}_i \rightarrow \mathbf{X}_\ell)$ denote the pairwise error probability that is averaged over all realizations of \mathbf{H} . Then,

$$P(\mathbf{X}_i \rightarrow \mathbf{X}_\ell) = E_{\mathbf{H}} \{ P(\mathbf{X}_i \rightarrow \mathbf{X}_\ell | \mathbf{H}) \}$$

where $E_{\mathbf{H}} \{\cdot\}$ denotes the expectation with respect to \mathbf{H} .

Let us denote the union bound of the error probability by U , that is,

$$U \triangleq \frac{1}{L} \sum_i \sum_{\substack{\ell \\ \ell \neq i}} P(\mathbf{X}_i \rightarrow \mathbf{X}_\ell) \quad (4.91)$$

$$= \frac{1}{L} \sum_i \sum_{\substack{\ell \\ \ell \neq i}} E_{\mathbf{H}} \{ P(\mathbf{X}_i \rightarrow \mathbf{X}_\ell | \mathbf{H}) \}$$

$$= \frac{1}{L} \sum_i \sum_{\substack{\ell \\ \ell \neq i}} E_{\mathbf{H}} \left\{ Q \left(\frac{\|\mathbf{X}_i \mathbf{H} - \mathbf{X}_\ell \mathbf{H}\|_F}{2\sigma} \right) \right\} \quad (4.92)$$

where

$$\text{for all } x \in \mathbb{R}, \quad Q(x) \triangleq \frac{1}{\sqrt{2\pi}} \int_x^\infty e^{-\beta^2/2} d\beta.$$

Using Craig's formula for the Q function [45]

$$Q(x) = \frac{1}{\pi} \int_0^{\frac{\pi}{2}} \exp \left(-\frac{x^2}{2 \sin^2 \theta} \right) d\theta$$

equation (4.92) yields [46, 44]

$$\begin{aligned} U &= \frac{1}{\pi L} \sum_i \sum_{\substack{\ell \\ \ell \neq i}} \mathbb{E}_{\mathbf{H}} \left\{ \int_0^{\frac{\pi}{2}} \exp \left(-\frac{1}{8\sigma^2 \sin^2 \theta} \|\mathbf{X}_i \mathbf{H} - \mathbf{X}_\ell \mathbf{H}\|_F^2 \right) d\theta \right\} \\ &= \frac{1}{\pi L} \sum_i \sum_{\substack{\ell \\ \ell \neq i}} \int_0^{\frac{\pi}{2}} \mathbb{E}_{\mathbf{H}} \left\{ \exp \left(-\frac{1}{8\sigma^2 \sin^2 \theta} \|\mathbf{X}_i \mathbf{H} - \mathbf{X}_\ell \mathbf{H}\|_F^2 \right) \right\} d\theta. \end{aligned} \quad (4.93)$$

It can be shown [3] that for any $\beta \in \mathbb{R}$,

$$\mathbb{E}_{\mathbf{H}} \left\{ \exp \left(-\beta \|\mathbf{X}_i - \mathbf{X}_\ell\|_F^2 \right) \right\} = \left(\prod_{r=1}^R (1 + \beta \lambda_r) \right)^{-M} \quad (4.94)$$

where

$$R \triangleq \min(T, N)$$

and $\lambda_1, \lambda_2, \dots, \lambda_R$ are the squared singular values of $\mathbf{X}_i - \mathbf{X}_\ell$. Inserting (4.94) into (4.93) with $\beta = 1/(8\sigma^2 \sin^2 \theta)$ yields [40]

$$U = \frac{1}{\pi L} \sum_i \sum_{\substack{\ell \\ \ell \neq i}} \int_0^{\frac{\pi}{2}} \left(\prod_{r=1}^R \left(1 + \frac{1}{8\sigma^2 \sin^2 \theta} \lambda_r \right) \right)^{-M} d\theta. \quad (4.95)$$

Defining

$$\varphi(\theta, \sigma, \mathbf{X}_i - \mathbf{X}_\ell) \triangleq \frac{\sqrt{\prod_{r=1}^R \left(1 + \frac{1}{8\sigma^2 \sin^2 \theta} \lambda_r \right)}}{\frac{1}{R} \sum_{r=1}^R \left(1 + \frac{1}{8\sigma^2 \sin^2 \theta} \lambda_r \right)} \quad (4.96)$$

it is easy to prove that

$$0 < \varphi(\theta, \sigma, \mathbf{X}_i - \mathbf{X}_\ell) \leq 1$$

where equality holds if and only if $\lambda_1 = \lambda_2 = \dots = \lambda_R$. Using the notation of (4.96), equation (4.95) can be written as [40]

$$U = \frac{1}{\pi L} \sum_i \sum_{\substack{\ell \\ \ell \neq i}} \int_0^{\frac{\pi}{2}} (\varphi(\theta, \sigma, \mathbf{X}_i - \mathbf{X}_\ell))^{-RM} \left(1 + \frac{1}{8\sigma^2 \sin^2 \theta} \frac{\|\mathbf{X}_i - \mathbf{X}_\ell\|_F^2}{R} \right)^{-RM} d\theta. \quad (4.97)$$

We now would like to find a constellation that minimizes (4.97), that is, to solve the following optimization problem [40]

$$\min_{\tilde{\mathcal{X}}} \frac{1}{\pi L} \sum_i \sum_{\substack{\ell \\ \ell \neq i}} \int_0^{\frac{\pi}{2}} (\varphi(\theta, \sigma, \mathbf{X}_i - \mathbf{X}_\ell))^{-RM} \left(1 + \frac{1}{8\sigma^2 \sin^2 \theta} \frac{\|\mathbf{X}_i - \mathbf{X}_\ell\|_F^2}{R} \right)^{-RM} d\theta \quad (4.98)$$

subject to the average power constraint

$$\frac{1}{L} \sum_{\ell=1}^L \|\mathbf{X}_\ell\|_F^2 = E_X \quad (4.99)$$

where E_X , σ , and L are given, whereas $\|\mathbf{X}_i - \mathbf{X}_\ell\|_F^2$ and $\varphi(\theta, \sigma, \mathbf{X}_i - \mathbf{X}_\ell)$ depend on the pairs in $\tilde{\mathcal{X}}$.

Using (4.1), the minimization problem of (4.98) can be rewritten as

$$\min_{\tilde{\mathcal{X}}} \frac{1}{\pi L} \sum_i \sum_{\substack{\ell \\ \ell \neq i}} \int_0^{\frac{\pi}{2}} (\varphi(\theta, \sigma, \mathbf{X}_i - \mathbf{X}_\ell))^{-RM} \left(1 + \frac{1}{8\sigma^2 \sin^2 \theta} \frac{\|\underline{\mathbf{X}}_i - \underline{\mathbf{X}}_\ell\|^2}{R} \right)^{-RM} d\theta. \quad (4.100)$$

Let us denote the optimal constellation by $\tilde{\mathcal{X}}^{\text{opt}}$, and its elements by $\mathbf{X}_\ell^{\text{opt}}$, where $1 \leq \ell \leq L$. Furthermore, let us use the notation

$$\underline{\mathcal{X}}^{\text{opt}} \triangleq \{\underline{\mathbf{X}}_1^{\text{opt}}, \underline{\mathbf{X}}_2^{\text{opt}}, \dots, \underline{\mathbf{X}}_L^{\text{opt}}\} \subset \mathbb{R}^{2NT \times 1}.$$

Also, for any $D \in \{1, 2, \dots, 2NT\}$, let us use $\tilde{\mathcal{X}}_D^{\text{opt}}$ to denote the constellation that minimizes (4.98) subject to (4.99) and subject to the additional constraint that the set of vectorized members of $\tilde{\mathcal{X}}^{\text{opt}}$, denoted by $\underline{\mathcal{X}}_D^{\text{opt}}$, is located in a D -dimensional hyperplane in $\mathbb{R}^{2NT \times 1}$. Clearly, $\underline{\mathcal{X}}_{2NT}^{\text{opt}} = \underline{\mathcal{X}}^{\text{opt}}$. Hence, simply by letting $D = 2NT$, all the results obtained for $\tilde{\mathcal{X}}_D^{\text{opt}}$ in the rest of this section are equally valid for $\tilde{\mathcal{X}}^{\text{opt}}$.

Theorem 4.8.1 *The sum of the elements in $\tilde{\mathcal{X}}_D^{\text{opt}}$ is $\mathbf{0}$.*

This theorem can be proven by showing that if the sum of the elements in $\tilde{\mathcal{X}}_D^{\text{opt}}$ is not $\mathbf{0}$, then the error probability can be reduced by shifting the mean of the constellation to $\mathbf{0}$, followed by the proper scaling of the constellation. This proof is similar to that for SISO AWGN channels [33], page 248. For a complete proof of this theorem, see [40].

Theorem 4.8.2 *Any hyperplane in $\mathbb{R}^{2NT \times 1}$ that contains the members of $\underline{\mathcal{X}}_D^{\text{opt}}$ also includes the origin.*

Proof. According to Theorem 4.8.1, the average of the points in $\underline{\mathcal{X}}_D^{\text{opt}}$ is zero. It is clear that if any L points are located in a hyperplane, then so is their average. Therefore, the zero vector is also located in this hyperplane. \square

From Theorem 4.8.2, it can be concluded that the elements of $\underline{\mathcal{X}}_D^{\text{opt}}$ are located in a D -dimensional subspace of $\mathbb{R}^{2NT \times 1}$.

In what follows, we will call a matrix *semiunitary* if it is full rank and all its nonzero singular values are equal to 1. This implies that a matrix \mathbf{Z} is semiunitary if and only if $\mathbf{Z}^H \mathbf{Z} = \mathbf{I}$ or $\mathbf{Z} \mathbf{Z}^H = \mathbf{I}$. We also call a matrix \mathbf{Z} a multiple of a semiunitary matrix (MSUM) if $\mathbf{Z}^H \mathbf{Z} = \beta \mathbf{I}$ or $\mathbf{Z} \mathbf{Z}^H = \beta \mathbf{I}$ for some nonnegative $\beta \in \mathbb{R}$.

Theorem 4.8.3 *If $L = 2$, then for any $D \in \{1, 2, \dots, 2NT\}$, and any semiunitary matrix \mathbf{Z} , the constellation $\{\sqrt{E_X/R} \mathbf{Z}, -\sqrt{E_X/R} \mathbf{Z}\}$ is $\tilde{\mathcal{X}}_D^{\text{opt}}$ and $\tilde{\mathcal{X}}^{\text{opt}}$.*

Proof. When $L = 2$, let us denote the members of $\tilde{\mathcal{X}}_D^{\text{opt}}$ by \mathbf{X}_1 and \mathbf{X}_2 . Because of Theorem 4.8.1, $\mathbf{X}_1 + \mathbf{X}_2 = \mathbf{0}$. Thus, an optimal constellation can be written as $\tilde{\mathcal{X}}_D^{\text{opt}} = \{\mathbf{F}, -\mathbf{F}\}$ for some $T \times N$ matrix \mathbf{F} . Then, (4.99) yields

$$\|\mathbf{F}\|_F = \sqrt{E_X} \quad (4.101)$$

and (4.97) reduces to

$$U = \frac{1}{\pi} \int_0^{\frac{\pi}{2}} (\varphi(\theta, \sigma, 2\mathbf{F}))^{-RM} \left(1 + \frac{E_X}{2\sigma^2 \sin^2 \theta} \frac{1}{R} \right)^{-RM} d\theta. \quad (4.102)$$

Noting that $\varphi(\theta, \sigma, \mathbf{X}_i - \mathbf{X}_\ell) \leq 1$, we have that, if \mathbf{F} has R equal to nonzero singular values, then it sets φ to 1 and therefore minimizes (4.102), and any other \mathbf{F} gives a larger U . This result and (4.101) yield $\mathbf{F} = \sqrt{\frac{E_X}{R}} \mathbf{Z}$ for some semiunitary matrix \mathbf{Z} . \square

Note that the constellation proposed in Theorem 4.8.3 corresponds to antipodal signaling with MSUM signals.

Any D -dimensional subspace \mathcal{D} of $\mathbb{R}^{2NT \times 1}$ can be represented by a $2NT \times D$ matrix \mathbf{Q} where columns of \mathbf{Q} make an orthogonal basis for \mathcal{D} . Then, there is a one-to-one correspondence between the elements \mathbf{x} in \mathcal{D} and elements \mathbf{v} in $\mathbb{R}^{D \times 1}$, which can be written as

$$\mathbf{x} = \mathbf{Q}\mathbf{v} \quad (4.103)$$

where

$$\mathbf{x} \in \mathcal{D} \subset \mathbb{R}^{2NT \times 1}, \quad \mathbf{Q} \in \mathbb{R}^{2NT \times D}, \quad \mathbf{v} \in \mathbb{R}^{D \times 1}$$

and \mathbf{Q} satisfies

$$\mathbf{Q}^T \mathbf{Q} = \mathbf{I}_D. \quad (4.104)$$

Any constellation $\underline{\mathcal{X}}_D = \{\mathbf{x}_1, \mathbf{x}_2, \dots, \mathbf{x}_L\} \subset \mathbb{R}^{2NT \times 1}$ of cardinality L that is located in a D -dimensional subspace \mathcal{D} of $\mathbb{R}^{2NT \times 1}$ can be represented by a matrix $\mathbf{Q} \in \mathbb{R}^{2NT \times D}$ that satisfies (4.104) and a set $\mathcal{V}_D \triangleq \{\mathbf{v}_1, \mathbf{v}_2, \dots, \mathbf{v}_L\} \subset \mathbb{R}^{D \times 1}$ where $\mathbf{v}_\ell \triangleq \mathbf{Q}^T \mathbf{x}_\ell$. Clearly, for all $\mathbf{x}_\ell \in \underline{\mathcal{X}}_D$, $\mathbf{x}_\ell = \mathbf{Q}\mathbf{v}_\ell$. The matrix \mathbf{Q} represents the basis for the subspace in which $\underline{\mathcal{X}}_D$ is located and, given \mathbf{Q} , the elements of \mathcal{V}_D characterize the locations of $\mathbf{x}_1, \mathbf{x}_2, \dots, \mathbf{x}_L$ in this subspace.

As U is a function of the constellation, for constellations that are constrained to be located in a D -dimensional subspace, we can write

$$U = U(\underline{\mathcal{X}}_D) = U(\mathcal{V}_D, \mathbf{Q}).$$

Let

$$\text{for all } \mathcal{V}_D \subset \mathbb{R}^{D \times 1}, \quad \mathbf{Q}^{\text{opt}}(\mathcal{V}_D) \triangleq \underset{\substack{\mathbf{Q} \\ \mathbf{Q}^T \mathbf{Q} = \mathbf{I}_D}}{\arg \min} U(\mathcal{V}_D, \mathbf{Q}).$$

Furthermore, let us use the notation

$$\mathcal{V}_D^{\text{opt}} \triangleq \arg \min_{\mathcal{V}_D} U(\mathcal{V}_D, \mathbf{Q}^{\text{opt}}(\mathcal{V}_D)).$$

Clearly, $\underline{\mathcal{X}}_D^{\text{opt}} = \left\{ \mathbf{Q}^{\text{opt}}(\mathcal{V}_D^{\text{opt}}) \mathbf{v}_1^{\text{opt}}, \mathbf{Q}^{\text{opt}}(\mathcal{V}_D^{\text{opt}}) \mathbf{v}_2^{\text{opt}}, \dots, \mathbf{Q}^{\text{opt}}(\mathcal{V}_D^{\text{opt}}) \mathbf{v}_L^{\text{opt}} \right\}$ where $\mathbf{v}_\ell^{\text{opt}}$, $\ell = 1, 2, \dots, L$, denote the members of $\mathcal{V}_D^{\text{opt}}$. Now, we can write the problem of finding $\underline{\mathcal{X}}_D^{\text{opt}}$ as

$$\begin{aligned} \min_{\underline{\mathcal{X}}_D} U(\underline{\mathcal{X}}_D) &= \min_{\mathcal{V}_D} \min_{\substack{\mathbf{Q} \\ \mathbf{Q}^T \mathbf{Q} = \mathbf{I}_D}} U(\mathcal{V}_D, \mathbf{Q}) \\ &= \min_{\mathcal{V}_D} \min_{\substack{\mathbf{Q} \\ \mathbf{Q}^T \mathbf{Q} = \mathbf{I}_D}} \frac{1}{\pi L} \sum_i \sum_{\substack{\ell \\ \ell \neq i}} \int_0^{\frac{\pi}{2}} (\varphi(\theta, \sigma, \mathbf{Q}(\mathbf{v}_i - \mathbf{v}_\ell)))^{-RM} \\ &\quad \times \left(1 + \frac{1}{8\sigma^2 \sin^2 \theta} \frac{\|\mathbf{Q}(\mathbf{v}_i - \mathbf{v}_\ell)\|^2}{R} \right)^{-RM} d\theta \\ &= \min_{\mathcal{V}_D} \min_{\substack{\mathbf{Q} \\ \mathbf{Q}^T \mathbf{Q} = \mathbf{I}_D}} \frac{1}{\pi L} \sum_i \sum_{\substack{\ell \\ \ell \neq i}} \int_0^{\frac{\pi}{2}} (\varphi(\theta, \sigma, \mathbf{Q}(\mathbf{v}_i - \mathbf{v}_\ell)))^{-RM} \\ &\quad \times \left(1 + \frac{1}{8\sigma^2 \sin^2 \theta} \frac{\|\mathbf{v}_i - \mathbf{v}_\ell\|^2}{R} \right)^{-RM} d\theta \end{aligned} \quad (4.105)$$

subject to

$$\sum_{\ell=1}^L \|\mathbf{Q}\mathbf{v}_\ell\|^2 = \sum_{\ell=1}^L \|\mathbf{v}_\ell\|^2 = L E_X. \quad (4.106)$$

The inner minimization in (4.105) results in $\mathbf{Q}^{\text{opt}}(\mathcal{V}_D)$ for any \mathcal{V}_D , whereas the outer minimization results in $\mathcal{V}_D^{\text{opt}}$. In general, $\mathcal{V}_D^{\text{opt}}$ and $\mathbf{Q}^{\text{opt}}(\mathcal{V}_D)$ may not be unique. For any \mathcal{V}_D , we denote by $\mathcal{Q}^{\text{opt}}(\mathcal{V}_D)$ the set of matrices $\mathbf{Q}^{\text{opt}}(\mathcal{V}_D)$ that make the objective in (4.105) achieving the inner minimum.

Theorem 4.8.4 *If there exists a $2NT \times D$ real matrix $\tilde{\mathbf{Q}}$ such that $\tilde{\mathbf{Q}}^T \tilde{\mathbf{Q}} = \mathbf{I}_D$, and for any $\mathbf{v} \neq \mathbf{0}$ in $\mathbb{R}^{D \times 1}$ the matrix $\text{mat}_{T,N}(\tilde{\mathbf{Q}}\mathbf{v})$ is an MSUM, then*

1.

$$\text{for all } \mathcal{V}_D, \quad \tilde{\mathbf{Q}} \in \mathcal{Q}^{\text{opt}}(\mathcal{V}_D). \quad (4.107)$$

2. For any \mathcal{V}_D , and for all the members of $\mathcal{Q}^{\text{opt}}(\mathcal{V}_D)$, $\varphi = 1$.

3. As M goes to infinity, $\mathcal{V}_D^{\text{opt}}$ tends to the constellation in $\mathbb{R}^{D \times 1}$ with the largest minimum distance subject to the average energy constraint (4.106).

Proof.

1. In (4.105), only $\varphi(\theta, \sigma, \mathbf{Q}(\mathbf{v}_i - \mathbf{v}_\ell))$ depends on \mathbf{Q} and, because for any \mathbf{v} in $\mathbb{R}^{D \times 1}$ the matrix $\text{mat}_{T,N}(\tilde{\mathbf{Q}}\mathbf{v})$ is an MSUM, the choice of $\mathbf{Q} = \tilde{\mathbf{Q}}$ maximizes φ in (4.97) to its maximum possible value of 1, for any pair of elements in \mathcal{V}_D where \mathcal{V}_D can be any set of $D \times 1$ vectors. This, with noting that $\tilde{\mathbf{Q}}$ satisfies the constraint (4.104), proves (4.107).

2. Proof by contradiction: If any member $\mathbf{Q}^{\text{opt}}(\mathcal{V}_D)$ of $\mathcal{Q}^{\text{opt}}(\mathcal{V}_D)$ does not set φ to 1, then its corresponding U will be less than that of $\tilde{\mathbf{Q}}$, and this contradicts the optimality of $\mathbf{Q}^{\text{opt}}(\mathcal{V}_D)$.
3. Using item 2 above, we obtain that the minimization in (4.105) amounts to

$$\begin{aligned} & \min_{\mathcal{V}_D} \frac{1}{\pi L} \sum_i \sum_{\substack{\ell \\ \ell \neq i}} \int_0^{\frac{\pi}{2}} \left(1 + \frac{1}{8\sigma^2 \sin^2 \theta} \frac{\|\mathbf{v}_i - \mathbf{v}_\ell\|^2}{R} \right)^{-RM} d\theta \\ &= \min_{\mathcal{V}_D} \frac{1}{\pi L} \sum_i \sum_{\substack{\ell \\ \ell \neq i}} p \left(\frac{\|\mathbf{v}_i - \mathbf{v}_\ell\|^2}{8\sigma^2}, R, M \right) \end{aligned} \quad (4.108)$$

where for any positive x

$$p(x, R, M) \triangleq \int_0^{\frac{\pi}{2}} \left(1 + \frac{1}{\sin^2 \theta} \frac{x}{R} \right)^{-RM} d\theta$$

can easily be shown to be a decreasing function of all its arguments.

When M goes to infinity, the term in (4.108) with the smallest $\|\mathbf{v}_i - \mathbf{v}_\ell\|$ becomes dominant, and the problem becomes that of finding the \mathcal{V}_D with the largest minimum distance subject to (4.106). \square

The following remarks are in order.

- Theorem 4.8.4 establishes a sufficient condition for optimality of STBCs with dimension-constrained constellations. Essentially, it says that the optimal code can be obtained by selecting $\mathbf{Q} = \tilde{\mathbf{Q}}$ and choosing \mathcal{V}_D that minimizes (4.108).
- Not only the matrix $\tilde{\mathbf{Q}}$ minimizes the sum in (4.97), but it also minimizes each and every term in (4.97).
- Equation (4.108) provides a guideline for designing \mathcal{V}_D for any M and any SNR. In fact, the minimization problem of (4.108) is much simpler to solve as compared to (4.105), because the objective function in (4.108) depends only on the distances between the constellation points, with no dependence on the distribution of singular values or the rank of code differences. In this sense, the objective function in (4.108) becomes, to some extent, similar to the problem of constellation design for AWGN SISO channels.

4.8.2 Optimality of OSTBCs for dimension-constrained constellations

In this subsection, for a certain set of values of T , N , and D , we show the existence of matrices $\tilde{\mathbf{Q}}$ that satisfy the conditions of Theorem 4.8.4. We do this by showing that OSTBCs explicitly provide such matrices.

Theorem 4.8.5 *If for a given value of D , a $T \times N$ OSTBC with $2K \geq D$ exists, then*

$$\mathbf{Q}_{\text{OSTBC}} \triangleq \frac{1}{\sqrt{N}} \mathbb{G} \mathbf{M} \quad (4.109)$$

satisfies

$$\mathbf{Q}_{\text{OSTBC}}^T \mathbf{Q}_{\text{OSTBC}} = \mathbf{I}_D \quad (4.110)$$

where \mathbb{G} is defined as in (4.29) and \mathbf{M} is any row permutation of $\begin{bmatrix} \mathbf{I}_D \\ \mathbf{0}_{(2K-D) \times D} \end{bmatrix}$. Furthermore, for any $\mathbf{v} \in \mathbb{R}^{D \times 1}$, $\text{mat}_{T,N}(\mathbf{Q}_{\text{OSTBC}} \mathbf{v})$ is an MSUM when $\mathbf{v} \neq \mathbf{0}$. Thus, $\mathbf{Q}_{\text{OSTBC}}$ satisfies the conditions of $\tilde{\mathbf{Q}}$ in Theorem 4.8.4.

Proof. From (4.109) it is clear that the columns of $\mathbf{Q}_{\text{OSTBC}}$ are some D columns of $\frac{1}{\sqrt{N}} \mathbb{G}$ (taken in arbitrary order). Because of (4.36), the columns of $\frac{1}{\sqrt{N}} \mathbb{G}$ are orthonormal, therefore, the columns of $\mathbf{Q}_{\text{OSTBC}}$ are orthonormal as well. This proves (4.110).

From (4.10) it is clear that for all $\mathbf{s} \in \mathbb{C}^K$, the columns of $\mathbf{X}(\mathbf{s})$ are orthogonal with equal norms. Thus, because of (4.31), for all $\underline{\mathbf{s}} \in \mathbb{R}^{2K \times 1}$, the columns of $\text{mat}_{T,N}(\mathbb{G}\underline{\mathbf{s}})$ are also orthogonal with equal norms. Hence, for all $\mathbf{v} \in \mathbb{R}^{D \times 1}$, the columns of $\text{mat}_{T,N}(\mathbb{G}\mathbf{M}\mathbf{v})$ are orthogonal with equal norms, and therefore, $\text{mat}_{T,N}(\mathbf{Q}_{\text{OSTBC}} \mathbf{v})$ has equal singular values and is full rank when $\mathbf{v} \neq \mathbf{0}$. \square

Theorems 4.8.4 and 4.8.5 can be combined in the following theorem [40].

Theorem 4.8.6 *If there exists a $T \times N$ OSTBC with $2K \geq D$, then*

1. *For all \mathcal{V}_D , $\mathbf{Q}_{\text{OSTBC}} \in \mathcal{Q}^{\text{opt}}(\mathcal{V}_D)$.*
2. *For any \mathcal{V}_D and for all the members of $\mathcal{Q}_D^{\text{opt}}(\mathcal{V})$, $\varphi = 1$.*
3. *When M goes to infinity, $\mathcal{V}_D^{\text{opt}}$ tends to the constellation with the largest minimum distance subject to (4.106).*

4.8.3 Optimality of OSTBCs for small-size constellations

It is clear that any constellation of size L is located in a hyperplane of dimension $L - 1$. Thus, when $L - 1 \leq 2NT$, restricting the optimal constellation to be in a $D = L - 1$ dimensional hyperplane of $\mathbb{R}^{2NT \times 1}$ is no restriction at all. With this observation, Theorem 4.8.6 results in the following theorem [40].

Theorem 4.8.7 *If there exists a $T \times N$ OSTBC with $2K \geq L - 1$, then*

1. *For all \mathcal{V}_{L-1} , $\mathbf{Q}_{\text{OSTBC}} \in \mathcal{Q}^{\text{opt}}(\mathcal{V}_{L-1})$.*
2. *For any \mathcal{V}_{L-1} and for all the members of $\mathcal{Q}^{\text{opt}}(\mathcal{V}_{L-1})$, $\varphi = 1$.*
3. *When M goes to infinity, $\mathcal{V}_{L-1}^{\text{opt}}$ tends to a regular simplex constellation, and so does $\underline{\mathcal{X}}^{\text{opt}}$.*

Proof. Items 1 and 2 directly result from the corresponding items in Theorem 4.8.6. For item 3, we note that in Theorem 4.8.6 it was shown that when M is large, the problem of finding $\mathcal{V}_{L-1}^{\text{opt}}$ becomes that of finding the \mathcal{V}_{L-1} with the largest minimum distance subject to (4.106). When there is no dimensionality constraint, the solution to this problem is well known to be the regular simplex constellation [47]. \square

The following remarks can be made.

- Item 1 in Theorem 4.8.7 states that *any OSTBC is optimal for any constellation of its vector variable \mathbf{s} when*

$$L \leq 2K + 1. \quad (4.111)$$

In the special case, when the constellation of the vector variable \mathbf{s} is also selected optimally

$$\mathbf{s} \in \{\mathbf{Mv}_1^{\text{opt}}, \mathbf{Mv}_2^{\text{opt}}, \dots, \mathbf{Mv}_L^{\text{opt}}\}$$

the resulting matrix constellation $\tilde{\mathcal{X}}$ is also optimal. In light of item 3 in Theorem 4.8.7, this constellation is a regular simplex constellation when M is large.

- The key idea of Theorem 4.8.7 is that constraining $\tilde{\mathcal{X}}$ to be in an $(L - 1)$ -dimensional subspace does not affect the minimum U that it can achieve. Therefore, if there is an $(L - 1)$ -dimensional subspace that can guarantee that $\varphi(\theta, \sigma, \mathbf{X}_i - \mathbf{X}_\ell) = 1$ for every pair in $\tilde{\mathcal{X}}$, then by putting $\tilde{\mathcal{X}}$ in that subspace, we can maximize $\varphi(\theta, \sigma, \mathbf{X}_i - \mathbf{X}_\ell)$ without sacrificing our freedom in choosing the distances for minimization of U .
- It is worth noting that in Theorem 4.8.3 (which addresses the particular case $L = 2$), $\tilde{\mathcal{X}}^{\text{opt}}$ is also a regular simplex constellation, even though its optimality does not require M to be large.

We now provide explicit examples of the optimal constellations $\tilde{\mathcal{X}}^{\text{opt}}$ that follow from Theorem 4.8.7 for Alamouti's code with $N = T = 2$ [40]:

$$L = 2 : \quad \tilde{\mathcal{X}}^{\text{opt}} = \left\{ \frac{1}{\sqrt{2}} \begin{bmatrix} 0 & 1 \\ -1 & 0 \end{bmatrix}, \frac{1}{\sqrt{2}} \begin{bmatrix} 0 & -1 \\ 1 & 0 \end{bmatrix} \right\} \quad (4.112)$$

$$L = 3 : \quad \tilde{\mathcal{X}}^{\text{opt}} = \left\{ \frac{1}{\sqrt{2}} \begin{bmatrix} 0 & 1 \\ -1 & 0 \end{bmatrix}, \frac{1}{\sqrt{2}} \begin{bmatrix} -\frac{\sqrt{3}}{2} & -\frac{1}{2} \\ \frac{1}{2} & -\frac{\sqrt{3}}{2} \end{bmatrix}, \frac{1}{\sqrt{2}} \begin{bmatrix} \frac{\sqrt{3}}{2} & -\frac{1}{2} \\ \frac{1}{2} & \frac{\sqrt{3}}{2} \end{bmatrix} \right\} \quad (4.113)$$

$$L = 4 : \quad \tilde{\mathcal{X}}^{\text{opt}} = \left\{ \frac{1}{\sqrt{2}} \begin{bmatrix} 0 & 1 \\ -1 & 0 \end{bmatrix}, \frac{1}{\sqrt{2}} \begin{bmatrix} \frac{2\sqrt{2}}{3} & -\frac{1}{3} \\ \frac{1}{3} & \frac{2\sqrt{2}}{3} \end{bmatrix}, \frac{1}{\sqrt{2}} \begin{bmatrix} -\frac{\sqrt{2}}{3} & -\frac{1}{3} - j\frac{\sqrt{6}}{3} \\ \frac{1}{3} - j\frac{\sqrt{6}}{3} & -\frac{\sqrt{2}}{3} \end{bmatrix}, \frac{1}{\sqrt{2}} \begin{bmatrix} -\frac{\sqrt{2}}{3} & -\frac{1}{3} + j\frac{\sqrt{6}}{3} \\ \frac{1}{3} + j\frac{\sqrt{6}}{3} & -\frac{\sqrt{2}}{3} \end{bmatrix} \right\} \quad (4.114)$$

$$L = 5 : \quad \tilde{\mathcal{X}}^{\text{opt}} = \left\{ \frac{1}{\sqrt{2}} \begin{bmatrix} 0 & 1 \\ -1 & 0 \end{bmatrix}, \frac{1}{\sqrt{2}} \begin{bmatrix} \frac{\sqrt{15}}{4} & -\frac{1}{4} \\ \frac{1}{4} & \frac{\sqrt{15}}{4} \end{bmatrix}, \dots \right\}$$

$$\begin{aligned} & \frac{1}{\sqrt{2}} \begin{bmatrix} -\frac{\sqrt{15}}{12} & -\frac{1}{4} + j \frac{\sqrt{30}}{6} \\ \frac{1}{4} + j \frac{\sqrt{30}}{6} & -\frac{\sqrt{15}}{12} \end{bmatrix}, \\ & \frac{1}{\sqrt{2}} \begin{bmatrix} -\frac{\sqrt{15}}{12} - j \frac{\sqrt{10}}{4} & -\frac{1}{4} - j \frac{\sqrt{30}}{12} \\ \frac{1}{4} - j \frac{\sqrt{30}}{12} & -\frac{\sqrt{15}}{12} + j \frac{\sqrt{10}}{4} \end{bmatrix}, \\ & \frac{1}{\sqrt{2}} \begin{bmatrix} -\frac{\sqrt{15}}{12} + j \frac{\sqrt{10}}{4} & -\frac{1}{4} - j \frac{\sqrt{30}}{12} \\ \frac{1}{4} - j \frac{\sqrt{30}}{12} & -\frac{\sqrt{15}}{12} - j \frac{\sqrt{10}}{4} \end{bmatrix} \} \end{aligned} \quad (4.115)$$

As $K = 2$ in Alamouti's code, Theorem 4.8.6 proposes optimal constellations only for L in the range $2 \leq L \leq 2K + 1$ (i.e., $2 \leq L \leq 5$). Clearly, all these constellations are nonseparable. It is important to note that the constellations (4.112)–(4.115) are obtained analytically rather than via computer search.

Note that if we denote the transmission rate of a code in bits per channel use by ξ , then

$$\xi = \frac{\log_2(L)}{T}. \quad (4.116)$$

For the small-size constellations proposed in this subsection, we have

$$\xi \leq \frac{\log_2(2K + 1)}{T} \quad (4.117)$$

$$\leq \frac{\log_2(2T + 1)}{T} \quad (4.118)$$

$$\leq \frac{\log_2(5)}{2} \quad (4.119)$$

$$\approx 1.16 \quad (4.120)$$

where (4.117) is due to (4.111) and (4.116); (4.118) is due to (4.14); and (4.119) is obtained by noting that $\frac{\log_2(2T+1)}{T} \leq \frac{\log_2(5)}{2}$ for $T \geq 2$.

As a numerical example, let us consider a MIMO system with Rayleigh flat block-fading channel and $N = 2$ transmit antennas. The number of receive antennas is varied. We compare two versions of Alamouti's code. The first one uses the BPSK (binary phase shift keying) constellation to select each of the two random variables of the code, whereas the second one uses the optimal constellation of (4.114). Both constellations have the same size $L = 4$ and the same constellation energy. The BLERs of these two Alamouti's code-based systems are displayed in Figure 4.11 versus SNR and for different values of M .

Figure 4.11 demonstrates that Alamouti's code with the optimal constellation of (4.114) has better performance in terms of BLER for all the values of M tested, as compared to BPSK-based Alamouti's code. This result shows that, although theoretically the optimality of (4.114) has been proven only when M goes to infinity, it is also a good choice (as compared to the conventional BPSK constellation) in the case of finite and even quite small M .

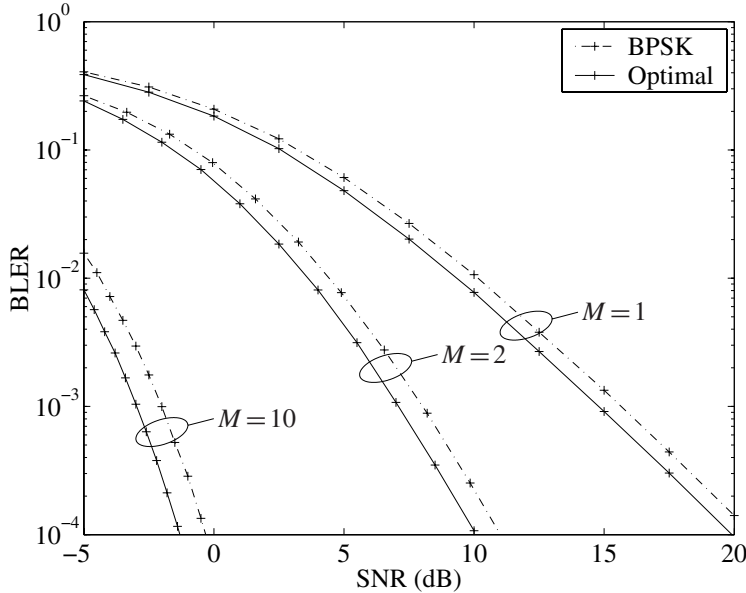


Figure 4.11 BLERs of Alamouti's code with the BPSK constellation and with the optimal constellation of (4.114) versus SNR.

4.8.4 Optimality of OSTBCs among LD codes with the same number of complex variables

Consider a $T \times N$ complex matrix \mathbf{X} where each element of \mathbf{X} is a function of K complex variables s_1, s_2, \dots, s_K . If we use the notation of (4.9), then the function $\mathbf{X}(\mathbf{s})$ is called an LD code [15] if its elements are linear functions of s_1, s_2, \dots, s_K and their complex conjugates. We will refer to s_1, s_2, \dots, s_K as the complex variables of the LD code.

Clearly, all OSTBCs are LD codes, but not all LD codes are OSTBCs. Any LD code may also be written in the form (4.31). However, in contrast to the case of OSTBCs, for LD codes the columns of \mathbb{G} are arbitrary and do not necessarily satisfy (4.36). In [15], certain optimized LD codes have been proposed for constructing space-time constellations.

For simplicity of notation and without loss of generality, let us assume that the rank of \mathbb{G} is $2K$. Then, we have the following theorem [40].

Theorem 4.8.8 *For any constellation size L , OSTBCs are optimal among LD codes with the same number of complex variables, where optimality is in the sense of minimizing (4.91) subject to (4.99).*

Proof. Using Theorem 4.8.6, we can make the observation that restricting a constellation to be generated from an LD code of K complex variables is equivalent to restricting $\tilde{\mathcal{X}}$ to be in a $2K$ -dimensional subspace of $\mathbb{R}^{2NT \times 1}$. This subspace can be represented by a matrix \mathbf{Q}_{LD} that satisfies $\mathbf{Q}_{\text{LD}}^T \mathbf{Q}_{\text{LD}} = \mathbf{I}_{2K}$, where the columns of \mathbf{Q}_{LD} make an orthonormal basis

for the range of the LD code. \mathbf{Q}_{LD} can be obtained by applying a QR decomposition to \mathbb{G} :

$$\mathbb{G} = \mathbf{Q}_{\text{LD}} \mathbf{R}_{\text{LD}} \quad (4.121)$$

where \mathbf{Q}_{LD} is a $2NT \times 2K$ real matrix with orthonormal columns and \mathbf{R}_{LD} is a $2K \times 2K$ upper triangular matrix. Then

$$\mathbb{G} \underline{\mathbf{s}} = \mathbf{Q}_{\text{LD}} \mathbf{R}_{\text{LD}} \underline{\mathbf{s}}.$$

Let us assume that $\underline{\mathbf{s}}$ belongs to the constellation $\tilde{\mathcal{S}} \triangleq \{\underline{\mathbf{s}}_1, \underline{\mathbf{s}}_2, \dots, \underline{\mathbf{s}}_L\} \subset \mathbb{R}^{2K \times 1}$. If we use the notation

$$\mathbf{v}_\ell \triangleq \mathbf{R}_{\text{LD}} \underline{\mathbf{s}}_\ell \quad (4.122)$$

then $\mathbb{G} \underline{\mathbf{s}}_\ell = \mathbf{Q}_{\text{LD}} \mathbf{v}_\ell$ and, therefore,

$$\mathbf{v}_\ell = \mathbf{Q}_{\text{LD}}^T \mathbb{G} \underline{\mathbf{s}}_\ell.$$

Note that \mathbf{Q}_{LD} and $\mathcal{V}_{2K} \triangleq \{\mathbf{v}_1, \mathbf{v}_2, \dots, \mathbf{v}_L\}$ fully represent an LD code and its constellation, respectively.

For any given LD code and its constellation, one can use (4.121) and (4.122) to obtain \mathbf{Q}_{LD} and \mathcal{V}_{2K} , respectively. For any given $\tilde{\mathcal{S}}$, the question of finding the optimal LD code is equivalent to the question of finding the optimal \mathbf{Q}_{LD} . According to Theorem 4.8.6, QOSTBC is the best choice of the matrix \mathbf{Q} and, therefore, QOSTBC is an optimal \mathbf{Q}_{LD} . \square

The following remarks are in order.

- Note that given N , T , and L , LD codes can be made for any value of K , whereas OSTBCs exist only for certain values of K . Theorem 4.8.8 states that for those values of K for which OSTBCs exist, no LD code can perform better than the OSTBC, no matter what is the input constellation. Clearly, there may be advantages in using optimized LD codes for values of K for which no OSTBC exists.
- Theorem 4.8.8 may sound contradictive to the results in [15] where it has been shown that certain optimized LD codes perform better than certain OSTBCs with the same N , T , and L . However, the optimized LD codes in [15] have the values of K larger than those of the corresponding OSTBC that are used to compare with. Indeed, the optimized LD codes used in comparisons of [15] are all for the values of K that are greater than or equal to T , for which no OSTBC with the same N , T and K exists.

4.9 Blind Decoding of OSTBCs

We have seen in Section 4.6 that if the exact CSI is available at the receiver and if (4.15) holds true, then the optimal ML decoder for OSTBCs is a simple linear MF processor followed by a symbol-by-symbol decoder. It is common to use training to obtain the CSI at the receiver. However, frequent use of training intervals reduces the bandwidth efficiency. Furthermore, in the presence of noise and/or when the duration and number of training intervals are limited, training-based approaches can result in inaccurate channel estimates. Using such imperfect CSI at the receiver, in turn, can substantially reduce the performance of the ML decoder.

To overcome these difficulties, several blind approaches such as differential space-time coding methods [48–52], unitary space-time modulation techniques [53, 54], and other approaches [55–62] have been presented in the literature. However, the approaches of [48–54] suffer from a substantial loss (typically 3 dB) as compared to the coherent ML receiver, whereas the techniques of [53, 54, 56–59] are based on computationally demanding decoding algorithms.

In this section, we consider the recent blind approach proposed in [60–62]. This technique uses OSTBCs as the underlying space-time coding scheme and exploits a specific structure of the array-processing-type model (4.34) of the vectorized received data $\underline{\mathbf{Y}}$ to provide a blind closed-form estimate of the channel matrix. This estimate can then be used in conjunction with the conventional OSTBC ML receiver to detect the information symbols.

4.9.1 Signal model and its properties

Let us assume that the channel coherence time is substantially larger than the data block length T and that the elements of \mathbf{s} in (4.9) are zero-mean mutually uncorrelated random variables. Note that $\mathbf{s} \in \tilde{\mathcal{S}}$ where $\tilde{\mathcal{S}} = \{\mathbf{s}^{(1)}, \mathbf{s}^{(2)}, \dots, \mathbf{s}^{(L)}\}$ is the set of all possible symbol vectors. We stress that hereafter we will use the superscript $(\cdot)^{(l)}$ rather than the subscript $(\cdot)_l$ to denote the l th point in the constellation $\tilde{\mathcal{S}}$.

Let us recall that, according to (4.34) and (4.37), we have the following array-processing-type model

$$\underline{\mathbf{Y}} = \mathbf{A}(\mathbf{H})\underline{\mathbf{s}} + \underline{\mathbf{V}} \quad (4.123)$$

where

$$\mathbf{A}^T(\mathbf{H})\mathbf{A}(\mathbf{H}) = \|\mathbf{H}\|_F^2 \mathbf{I}_{2K} \quad (4.124)$$

and

$$\mathbf{A}(\mathbf{H}) = [\underline{\mathbf{C}_1 \mathbf{H}} \cdots \underline{\mathbf{C}_K \mathbf{H}} \ \underline{\mathbf{D}_1 \mathbf{H}} \cdots \underline{\mathbf{D}_K \mathbf{H}}]. \quad (4.125)$$

The decoupling property of (4.124) plays a key role in the design of the blind channel estimation technique of [60–62].

As shown in Subsection 4.6, the optimal ML decoder for a given \mathbf{H} can be viewed as a linear MF receiver that computes the estimate

$$\hat{\underline{\mathbf{s}}} = \frac{1}{\|\mathbf{H}\|_F^2} \mathbf{A}^T(\mathbf{H}) \underline{\mathbf{Y}} \quad (4.126)$$

of $\underline{\mathbf{s}}$ and then estimates the vector \mathbf{s} as

$$\hat{\mathbf{s}} = [\mathbf{I}_K \ j\mathbf{I}_K] \hat{\underline{\mathbf{s}}}. \quad (4.127)$$

It should be noted that $\hat{\underline{\mathbf{s}}}$ in equation (4.126) is similar to $\underline{\mathbf{s}}_{\parallel}$ in equation (4.44). The k th entry of \mathbf{s} is then detected from $\hat{\underline{\mathbf{s}}}$ by means of the simple nearest neighbor decoder (quantizer). This procedure is repeated for all $k = 1, 2, \dots, K$.

Let us define the $2MN \times 1$ channel vector \mathbf{h} as

$$\mathbf{h} \triangleq \underline{\mathbf{H}} \quad (4.128)$$

and, for the sake of notational simplicity, use $\mathbf{A}(\mathbf{h})$ instead of $\mathbf{A}(\mathbf{H})$ below. Then, (4.124) can be rewritten as

$$\mathbf{A}^T(\mathbf{h})\mathbf{A}(\mathbf{h}) = \|\mathbf{h}\|^2 \mathbf{I}_{2K}. \quad (4.129)$$

As the matrix $\mathbf{A}(\mathbf{h})$ is linear in \mathbf{h} , there exists a unique matrix Φ with dimension $4KMT \times 2MN$ such that [60]

$$\text{vec}\{\mathbf{A}(\mathbf{h})\} = \Phi \mathbf{h} \quad (4.130)$$

where the k th column of the matrix Φ can be written as

$$[\Phi]_k = \text{vec}\{\mathbf{A}(\mathbf{e}_k)\} \quad (4.131)$$

and $[\cdot]_k$ denotes the k th column of a matrix. Note that, as before, \mathbf{e}_k is a vector having one in its k th entry and zeros elsewhere but now its dimension is $2MN \times 1$.

Let us discuss the properties of the covariance matrix of the real-valued vectorized data $\underline{\mathbf{Y}}$. Making use of (4.123) and exploiting the new notation $\mathbf{A}(\mathbf{h})$ instead of $\mathbf{A}(\mathbf{H})$, this covariance matrix can be written as [60–62]

$$\mathbf{R} \triangleq \mathbb{E}\{\underline{\mathbf{Y}}\underline{\mathbf{Y}}^T\} = \mathbf{A}(\mathbf{h})\Lambda_s\mathbf{A}^T(\mathbf{h}) + \sigma^2\mathbf{I}_{2MT} \quad (4.132)$$

where $\Lambda_s \triangleq \mathbb{E}\{\underline{\mathbf{s}}\underline{\mathbf{s}}^T\}$ is the covariance matrix of $\underline{\mathbf{s}}$. As we assumed that the elements of \mathbf{s} are uncorrelated, Λ_s is a diagonal matrix. Note that each diagonal element of Λ_s represents the average power of the real or imaginary part of the corresponding data symbol and depends only on the shape of the constellation of that particular symbol. Therefore, the matrix Λ_s is known at the receiver [60].

Multiplying (4.132) by $\mathbf{A}(\mathbf{h})$ and using (4.129), we have

$$\mathbf{R}\mathbf{A}(\mathbf{h}) = \mathbf{A}(\mathbf{h})\left(\|\mathbf{h}\|^2\Lambda_s + \sigma^2\mathbf{I}_{2K}\right). \quad (4.133)$$

As Λ_s is a diagonal matrix, (4.133) is nothing but the *characteristic equation* for \mathbf{R} . This implies that the diagonal elements of the matrix

$$\Lambda \triangleq \|\mathbf{h}\|^2\Lambda_s + \sigma^2\mathbf{I}_{2K} \quad (4.134)$$

are the $2K$ largest eigenvalues of \mathbf{R} while the columns of $\mathbf{A}(\mathbf{h})$ are the corresponding eigenvectors. Note that the other $2MT - 2K$ eigenvalues are all equal to σ^2 .

4.9.2 Blind channel estimation

A straightforward approach to estimate the channel vector \mathbf{h} would be to find the value of $\tilde{\mathbf{h}}$ for which the columns of $\mathbf{A}(\tilde{\mathbf{h}})$ span the same subspace as that of the $2K$ principal eigenvectors of \mathbf{R} . This approach implicitly involves the eigendecomposition of \mathbf{R} . In what follows, we show how the channel vector \mathbf{h} can be estimated without eigendecomposing the data covariance matrix.

Let \mathbf{P} be a $2MT \times 2K$ real matrix ($K \leq MT$). Then, the solution to the following optimization problem

$$\max_{\mathbf{P}} \text{tr}\{\mathbf{P}^T \mathbf{R} \mathbf{P}\} \quad \text{subject to} \quad \mathbf{P}^T \mathbf{P} = \mathbf{I}_{2K} \quad (4.135)$$

is given by any matrix \mathbf{P}_{opt} whose column space is the same as the subspace spanned by the $2K$ principal eigenvectors⁴ of \mathbf{R} , that is

$$\text{range}\{\mathbf{P}_{\text{opt}}\} = \text{range}\{\mathbf{A}(\mathbf{h})\} \quad (4.136)$$

⁴that is, the eigenvectors that correspond to the $2K$ largest eigenvalues.

and, for any such \mathbf{P}_{opt} , the value of the objective function in (4.135) is equal to the summation of the $2K$ principal eigenvalues of \mathbf{R} , that is,

$$\text{tr}\{\mathbf{P}_{\text{opt}}^T \mathbf{R} \mathbf{P}_{\text{opt}}\} = \text{tr}\{\Lambda\}. \quad (4.137)$$

For a proof of equations (4.136) and (4.137), we refer the reader to [63] and [64]. We now replace \mathbf{P} in (4.135) by $\mathbf{A}(\tilde{\mathbf{h}})/\|\tilde{\mathbf{h}}\|$ where $\tilde{\mathbf{h}}$ is a vector of optimization variables. In this case, the constraint in (4.135) becomes

$$\mathbf{A}^T(\tilde{\mathbf{h}})\mathbf{A}(\tilde{\mathbf{h}})/\|\tilde{\mathbf{h}}\|^2 = \mathbf{I}_{2K}. \quad (4.138)$$

According to (4.129), this constraint is satisfied for any $\tilde{\mathbf{h}}$ and, therefore, is redundant. Omitting it, we obtain the following unconstrained optimization problem [60]

$$\max_{\tilde{\mathbf{h}}} \frac{\text{tr}\{\mathbf{A}^T(\tilde{\mathbf{h}})\mathbf{R}\mathbf{A}(\tilde{\mathbf{h}})\}}{\|\tilde{\mathbf{h}}\|^2}. \quad (4.139)$$

As stressed in [60–62], the problems (4.135) and (4.139) are not equivalent to each other because the matrix $\mathbf{A}(\tilde{\mathbf{h}})$ in (4.139) has a particular structure, while the matrix \mathbf{P} in (4.135) is unstructured. This means that the sets of solutions to (4.135) and (4.139) for the matrices \mathbf{P} and $\mathbf{A}(\tilde{\mathbf{h}})$, respectively, may be different. This also means that the maximum value of the objective function in (4.139) cannot exceed the maximum value of the objective function in (4.135). However, it is easy to prove that the set of all possible solutions to (4.139) in terms of $\mathbf{A}(\tilde{\mathbf{h}})$ is a *subset* of the set of all possible solutions to (4.135) in terms of \mathbf{P} . Indeed, inserting (4.132) into the objective function (4.139) and using (4.129), it can be readily verified that [60]

$$\left. \frac{\text{tr}\{\mathbf{A}^T(\tilde{\mathbf{h}})\mathbf{R}\mathbf{A}(\tilde{\mathbf{h}})\}}{\|\tilde{\mathbf{h}}\|^2} \right|_{\tilde{\mathbf{h}}=\mathbf{h}} = \text{tr}\{\Lambda\}. \quad (4.140)$$

Comparing (4.137) and (4.140), we see that the maxima of the objective functions in (4.135) and (4.139) are the same and, hence, the set of all possible solutions to (4.139) in terms of $\mathbf{A}(\tilde{\mathbf{h}})$ is a subset of the set of all possible solutions to (4.135) in terms of \mathbf{P} . Using this property and (4.136), we see that for any $\tilde{\mathbf{h}}$ that achieves the maximum of (4.139),

$$\text{range}\{\mathbf{A}(\tilde{\mathbf{h}})\} = \text{range}\{\mathbf{A}(\mathbf{h})\}. \quad (4.141)$$

It is clear that \mathbf{h} belongs to the set of all values $\tilde{\mathbf{h}}$ that satisfy (4.141). To obtain the channel vector \mathbf{h} from this set, we now determine it by finding all solutions to (4.139).

The numerator of the cost function in (4.139) can be simplified as [60]

$$\text{tr}\{\mathbf{A}^T(\tilde{\mathbf{h}})\mathbf{R}\mathbf{A}(\tilde{\mathbf{h}})\} = \text{vec}\{\mathbf{A}(\tilde{\mathbf{h}})\}^T (\mathbf{I}_{2K} \otimes \mathbf{R}) \text{vec}\{\mathbf{A}(\tilde{\mathbf{h}})\}. \quad (4.142)$$

Using (4.130), we can write

$$\text{vec}\{\mathbf{A}(\tilde{\mathbf{h}})\} = \Phi \tilde{\mathbf{h}}. \quad (4.143)$$

Inserting (4.143) into (4.142), we can express (4.142) as

$$\text{tr}\{\mathbf{A}^T(\tilde{\mathbf{h}})\mathbf{R}\mathbf{A}(\tilde{\mathbf{h}})\} = \tilde{\mathbf{h}}^T \Phi^T (\mathbf{I}_{2K} \otimes \mathbf{R}) \Phi \tilde{\mathbf{h}} \quad (4.144)$$

and the optimization problem (4.139) can be rewritten as [60]

$$\max_{\tilde{\mathbf{h}}} \frac{\tilde{\mathbf{h}}^T \Phi^T (\mathbf{I}_{2K} \otimes \mathbf{R}) \Phi \tilde{\mathbf{h}}}{\|\tilde{\mathbf{h}}\|^2}. \quad (4.145)$$

We stress that all solutions to (4.145) belong to the subspace spanned by n linearly independent principal eigenvectors of the matrix $\Phi^T (\mathbf{I}_{2K} \otimes \mathbf{R}) \Phi$ where n is the *multiplicity order* of the largest eigenvalue of this matrix. Hence, the set of all values $\tilde{\mathbf{h}}$ that satisfy (4.141) forms the subspace spanned by these principal eigenvectors and the dimension of this subspace is equal to n [60].

If $n = 1$, finding any nonzero vector from this subspace enables us to obtain the true channel vector \mathbf{h} up to some scaling factor.

If $n > 1$, the true channel vector \mathbf{h} can be written as a linear combination of any n linearly independent principal eigenvectors of the matrix $\Phi^T (\mathbf{I}_{2K} \otimes \mathbf{R}) \Phi$. Thus, in the case $n > 1$ it is not possible to obtain \mathbf{h} (even up to a scalar) based only on the knowledge of the aforementioned subspace. To resolve this ambiguity, pilot symbols can be used. Such a pilot-assisted technique has been developed in [65] and [66] in the multiuser MIMO channel estimation context when OSTBCs are employed. However, the basic idea of [65] and [66] can be also used to estimate the channel vector of a single user in a semiblind way.

As shown in [60], for many OSTBCs $n = 1$. To illustrate this fact, note that the value of n depends on the symbol constellations as well as on the structure of the underlying OSTBC. If the symbol constellations are such that the average transmitted powers over the real and imaginary parts of all information symbols are different from each other, then the diagonal entries of Λ_s (and, consequently, those of Λ), are distinct. As a result, the corresponding $2K$ principal eigenvectors of \mathbf{R} are unique up to some real scaling factors. This implies that the solution to (4.139) in terms of $\mathbf{A}(\tilde{\mathbf{h}})$ is unique, and consequently, the corresponding $\tilde{\mathbf{h}}$ that achieves the maximum of (4.145) is also unique up to a real scaling factor. Therefore, in the case where the diagonal entries of the matrix Λ (or Λ_s) are distinct, the multiplicity order n of the principal eigenvalue of the matrix $\Phi^T (\mathbf{I}_{2K} \otimes \mathbf{R}) \Phi$ has to be equal to one. This fact can be used for designing the symbol constellations that guarantee the uniqueness property.

Now, let us consider the case when the given constellations do not result in a matrix Λ_s with distinct diagonal entries. In this case, the value of n depends on the matrix Φ that, in turn, depends on the structure of the underlying OSTBC [60]. It seems to be very difficult to find a relationship between the value of n and the structure of Φ . Because of this, the value of n has been obtained in [60] numerically for a variety of known OSTBCs based on the generalized orthogonal designs [5] as well as OSTBCs obtained using amicable designs [9]. Table 4.2 summarizes the results. In this table, it is assumed that all symbols are drawn from the same BPSK (QPSK) constellations in the real (complex) OSTBC case. It should be noted that although each particular value of n in Table 4.2 has been computed for multiple independently generated zero-mean Gaussian channel vectors, the value of n appears to be independent of \mathbf{h} , but depends only on the type of the OSTBC and the number of receive antennas.

As can be seen from this table, if $M > 1$, then the multiplicity order n is independent of the number of receive antennas M . We can also see that, if $M > 1$, then $n = 1$ almost in all cases. However, the Alamouti's OSTBC has $n > 1$ for any value of M . A related ambiguity

Table 4.2 The multiplicity order n of the principal eigenvalue of $\Phi^T(\mathbf{I}_{2K} \otimes \mathbf{R})\Phi$ for different OSTBCs

Rate (K/T)	Constell.	Number of transmit antennas N	Number of symbols per block K	Design method	Multiplicity order n ($M=1$)	Multiplicity order n ($1 < M \leq 10$)
1	real	2	2	Alamouti	2	2
1	real	3	4	gen. ort.	2	1
1	real	4	4	gen. ort.	4	4
1	real	5	8	gen. ort.	2	1
1	real	6	8	gen. ort.	2	1
1	real	7	8	gen. ort.	2	1
1	real	8	8	gen. ort.	2	1
1	real	9	16	gen. ort.	2	1
1	real	10	16	gen. ort.	2	1
1	complex	2	2	Alamouti	4	4
1/2	complex	3	4	gen. ort.	2	1
1/2	complex	4	4	gen. ort.	4	4
1/2	complex	5	8	gen. ort.	2	1
1/2	complex	6	8	gen. ort.	2	1
1/2	complex	7	8	gen. ort.	2	1
1/2	complex	8	8	gen. ort.	2	1
3/4	complex	3	3	amicable	2	1
3/4	complex	4	3	amicable	2	1
1/2	complex	5	4	amicable	1	1
1/2	complex	6	4	amicable	1	1
1/2	complex	7	4	amicable	1	1
1/2	complex	8	4	amicable	1	1
1/2	complex	8	4	[7]	2	1
2/3	complex	5	10	[8]	2	1
2/3	complex	5	10	[67]	2	1

of the Alamouti's scheme has been discovered in [68] where different linear precoders have been used for odd and even symbols to ensure channel identifiability.

Hereafter, only the case $n = 1$ is considered. For the case $n > 1$, the reader is referred to [69, 60].

If $n = 1$, then, ignoring the scaling ambiguity, the normalized solution to (4.145) can be expressed as [60]

$$\tilde{\mathbf{h}}_{\text{opt}} = \mathcal{P}\{\Phi^T(\mathbf{I}_{2K} \otimes \mathbf{R})\Phi\} \quad (4.146)$$

where $\mathcal{P}\{\cdot\}$ denotes the normalized principal eigenvector of a matrix ($\|\mathcal{P}\{\cdot\}\| = 1$). Then, the true channel vector \mathbf{h} can be written as

$$\mathbf{h} = \|\mathbf{h}\| \mathcal{P}\{\Phi^T(\mathbf{I}_{2K} \otimes \mathbf{R})\Phi\}. \quad (4.147)$$

Using (4.137) along with (4.134), it can be shown that [60]

$$\max_{\tilde{\mathbf{h}}} \frac{\text{tr}\{\mathbf{A}^T(\tilde{\mathbf{h}})\mathbf{R}\mathbf{A}(\tilde{\mathbf{h}})\}}{\|\tilde{\mathbf{h}}\|^2} = \|\mathbf{h}\|^2 \text{tr}\{\Lambda_s\} + 2K\sigma^2. \quad (4.148)$$

Making use of (4.146) and (4.148), the value of $\|\mathbf{h}\|$ can be found as

$$\|\mathbf{h}\| = \sqrt{\frac{\text{tr}\{\mathbf{A}^T(\tilde{\mathbf{h}}_{\text{opt}})\mathbf{R}\mathbf{A}(\tilde{\mathbf{h}}_{\text{opt}})\} - 2K\sigma^2}{\text{tr}\{\Lambda_s\}}}. \quad (4.149)$$

Inserting (4.147) into (4.149), we obtain the true channel vector \mathbf{h} in a closed form [60–62]

$$\mathbf{h} = \sqrt{\frac{\text{tr}\{\mathbf{A}^T(\tilde{\mathbf{h}}_{\text{opt}})\mathbf{R}\mathbf{A}(\tilde{\mathbf{h}}_{\text{opt}})\} - 2K\sigma^2}{\text{tr}\{\Lambda_s\}}} \tilde{\mathbf{h}}_{\text{opt}} \quad (4.150)$$

where $\tilde{\mathbf{h}}_{\text{opt}}$ is given by (4.146).

In practice, the true covariance matrix \mathbf{R} is unavailable. Instead, the sample covariance matrix

$$\hat{\mathbf{R}} = \frac{1}{n_B} \sum_{i=1}^{n_B} \underline{\mathbf{Y}(i)} \underline{\mathbf{Y}(i)}^T = \frac{1}{n_B} \mathbb{Y} \mathbb{Y}^T \quad (4.151)$$

can be used. Here,

$$\mathbb{Y} \triangleq [\underline{\mathbf{Y}(1)} \ \underline{\mathbf{Y}(2)} \ \cdots \ \underline{\mathbf{Y}(n_B)}] \quad (4.152)$$

is the matrix of the received data, $\mathbf{Y}(i)$ is the i th data block, and n_B is the number of data blocks used.

Replacing the true covariance matrix \mathbf{R} by the sample covariance matrix $\hat{\mathbf{R}}$ in (4.150) yields the following finite-sample closed-form blind channel estimate [60–62]:

$$\hat{\mathbf{h}} = \sqrt{\frac{\text{tr}\{\mathbf{A}^T(\hat{\mathbf{h}}_{\text{opt}})\hat{\mathbf{R}}\mathbf{A}(\hat{\mathbf{h}}_{\text{opt}})\} - 2K\sigma^2}{\text{tr}\{\Lambda_s\}}} \hat{\mathbf{h}}_{\text{opt}} \quad (4.153)$$

where

$$\hat{\mathbf{h}}_{\text{opt}} = \mathcal{P}\{\Phi^T(\mathbf{I}_{2K} \otimes \hat{\mathbf{R}})\Phi\} \quad (4.154)$$

is obtained by means of replacing \mathbf{R} by $\hat{\mathbf{R}}$ in (4.146).

It is worth noting that, if all the symbol constellations are *constant modulus*, then scaling the channel estimate by any real constant does not affect the performance of the ML receiver. Thus, for such constellations the factor $\sqrt{(\text{tr}\{\mathbf{A}^T(\hat{\mathbf{h}}_{\text{opt}})\hat{\mathbf{R}}\mathbf{A}(\hat{\mathbf{h}}_{\text{opt}})\} - 2K\sigma^2)/\text{tr}\{\Lambda_s\}}$ can be ignored in (4.153), and the value of $\hat{\mathbf{h}}_{\text{opt}}$ can be directly used as the channel estimate [60].

The blind OSTBC decoding algorithm of [60] can be summarized as follows.

1. Obtain the sample covariance matrix $\hat{\mathbf{R}}$ from n_B consecutive received data vectors using (4.151).
2. If the symbol constellations are not constant modulus, compute the estimate $\hat{\mathbf{h}}$ of the channel vector \mathbf{h} using (4.153). Otherwise, use $\hat{\mathbf{h}} = \hat{\mathbf{h}}_{\text{opt}}$ in (4.154) as the channel estimate.
3. Use the so-obtained $\hat{\mathbf{h}}$ in the ML receiver to find the estimates

$$\underline{\hat{s}} = \frac{1}{\|\hat{\mathbf{h}}\|^2} \mathbf{A}^T(\hat{\mathbf{h}}) \underline{\mathbf{Y}} \quad (4.155)$$

and

$$\hat{\mathbf{s}} = [\mathbf{I}_K \ j\mathbf{I}_K] \underline{\hat{s}} \quad (4.156)$$

where the “double-hat” symbol stresses that the signal detection is blind.

4. Decode the k th symbol ($k = 1, 2, \dots, K$) as the constellation point that is closest to the k th entry of $\hat{\mathbf{s}}$.

The following remarks are in order.

- The channel estimate (4.153) is consistent. At the same time, as will be shown through numerical examples, this blind algorithm also works properly in scenarios where the number of data blocks is small.
- The estimate (4.153) assumes that the noise power σ^2 is known. However, if symbol constellations are constant modulus (MPSK, M -ary phase shift keying), then the decoder performance is insensitive to rescaling the final channel estimate by any real constant and, therefore, knowledge of σ^2 is not required. In the nonconstant modulus case, the noise power can be estimated by averaging the $2MT - 2K$ smallest eigenvalues of the sample covariance matrix $\hat{\mathbf{R}}$. The so-obtained estimate $\hat{\sigma}^2$ of σ^2 can be used in (4.153) instead of the true σ^2 and, in this case, the value $\text{tr}\{\mathbf{A}^T(\hat{\mathbf{h}}_{\text{opt}})\hat{\mathbf{R}}\mathbf{A}(\hat{\mathbf{h}}_{\text{opt}})\} - 2K\hat{\sigma}^2$ under the square root in (4.153) is always nonnegative.
- The order of computational complexity of this approach is determined by the cost of evaluation of the matrix $\Phi^T(\mathbf{I}_{2K} \otimes \hat{\mathbf{R}})\Phi$ and the cost of finding the principal eigenvector of this matrix. In [60], a simple online implementation of this technique has been proposed, which can be used to adaptively update the channel vector estimate whenever a new data block is received.
- Because of the fact that real-valued data are processed, there is no phase ambiguity, but the channel estimate (4.153) suffers from a sign ambiguity. However, such a sign ambiguity is common to all blind detectors and can be easily resolved by appropriate decoding of each symbol sequence [70] or by assuming that the real part of one of the symbols are known.

- The above technique is applicable only to the single transmitter case. In the multiuser case, two different *semiblind* methods have been proposed in [65] and [66] that can be used to simultaneously estimate the channel matrices of several transmitters. The methods of [65] and [66] are based on generalizations of the well-known Capon and MUSIC parameter estimation techniques to the problem of multiuser MIMO channel estimation when OSTBCs are used as the underlying space-time coding scheme. As a result of such generalizations, one can blindly estimate the *subspace* spanned by user channel vectors. In fact, this subspace can be estimated on the basis of only the received data corresponding to the information bearing symbols. To estimate each channel vector from this subspace, one needs to use just a few training blocks. The semiblind techniques of [65] and [66] have been proven to enhance the quality of the channel estimates and to improve the bandwidth efficiency as compared to the standard least squares-type (LS-type) training-based techniques.

4.9.3 Relationship to the blind ML estimator

In this subsection, we show [71] that using the joint channel matrix estimation and symbol detection ML technique with relaxed finite-alphabet constraint leads exactly to the same channel matrix estimate as obtained in the previous subsection.

Let the i th ($i = 1, 2, \dots, n_B$) received data vector $\underline{\mathbf{Y}}(i)$ be given by

$$\underline{\mathbf{Y}}(i) = \mathbf{A}(\mathbf{h})\underline{\mathbf{s}}(i) + \underline{\mathbf{V}}(i) \quad (4.157)$$

where $\underline{\mathbf{s}}(i)$ is the i th vector of transmitted information symbols and $\underline{\mathbf{V}}(i)$ is the corresponding noise matrix.

In the ML approach to joint channel estimation and symbol detection, \mathbf{h} and $\{\underline{\mathbf{s}}(i)\}_{i=1}^{n_B}$ are assumed to be unknown deterministic parameters and their estimates are obtained as their values for which the log-likelihood function is maximized, that is,

$$\{\hat{\mathbf{h}}_{\text{ML}}, \hat{\mathbf{S}}_{\text{ML}}\} = \arg \max_{\mathbf{h}} \max_{\mathbf{S} \in \Omega} \log f(\underline{\mathbf{Y}}(1), \underline{\mathbf{Y}}(2), \dots, \underline{\mathbf{Y}}(n_B) | \mathbf{S}, \mathbf{h}) \quad (4.158)$$

where

$$\mathbf{S} \triangleq [\underline{\mathbf{s}}(1) \ \underline{\mathbf{s}}(2) \ \cdots \ \underline{\mathbf{s}}(n_B)]$$

and Ω is the set of all possible values of \mathbf{S} . It is, however, extremely difficult to solve (4.158) because its computational cost grows exponentially in n_B [59]. To simplify (4.158), let us relax the finite-alphabet constraint $\mathbf{S} \in \Omega$, that is, let us assume that $\mathbf{S} \in \mathbb{R}^{2K \times n_B}$. Then, we can rewrite (4.158) as

$$\{\hat{\mathbf{h}}_{\text{RML}}, \hat{\mathbf{S}}_{\text{RML}}\} = \arg \max_{\mathbf{h}} \max_{\mathbf{S}} \log f(\underline{\mathbf{Y}}(1), \underline{\mathbf{Y}}(2), \dots, \underline{\mathbf{Y}}(n_B) | \mathbf{S}, \mathbf{h}) \quad (4.159)$$

where the subscript “RML” stands for “relaxed ML”. Taking into account that $\underline{\mathbf{V}}(i)$ ($i = 1, 2, \dots, n_B$) are all zero-mean independent Gaussian vectors with the covariance matrix $E\{\underline{\mathbf{V}}(i) \underline{\mathbf{V}}(i)^T\} = \sigma^2 \mathbf{I}$, the conditional pdf of $\underline{\mathbf{Y}}(i)$ can be written as [65]

$$f(\underline{\mathbf{Y}}(i) | \underline{\mathbf{s}}(i), \mathbf{h}) = \frac{1}{(2\pi\sigma^2)^{MT}} \exp\left(-\frac{\|\underline{\mathbf{Y}}(i) - \mathbf{A}(\mathbf{h})\underline{\mathbf{s}}(i)\|^2}{2\sigma^2}\right). \quad (4.160)$$

Using the fact that all $\{\underline{\mathbf{Y}}(i)\}_{i=1}^{n_B}$ are independent, we obtain

$$f(\underline{\mathbf{Y}}(1), \underline{\mathbf{Y}}(2), \dots, \underline{\mathbf{Y}}(n_B) | \mathbf{S}, \mathbf{h}) = \prod_{i=1}^{n_B} f(\underline{\mathbf{Y}}(i) | \underline{\mathbf{s}}(i), \mathbf{h}). \quad (4.161)$$

Using equations (4.160) and (4.161), we can express equation (4.159) in the form

$$\{\hat{\mathbf{h}}_{\text{RML}}, \hat{\mathbf{S}}_{\text{RML}}\} = \arg \min_{\mathbf{h}} \min_{\mathbf{S}} \sum_{i=1}^{n_B} \|\underline{\mathbf{Y}}(i) - \mathbf{A}(\mathbf{h})\underline{\mathbf{s}}(i)\|^2. \quad (4.162)$$

In (4.162), the i th term of the sum is minimized with

$$\underline{\mathbf{s}}(i) = \frac{1}{\|\mathbf{h}\|^2} \mathbf{A}^T(\mathbf{h}) \underline{\mathbf{Y}}(i). \quad (4.163)$$

Using equation (4.163), the objective function in (4.162) can be concentrated with respect to \mathbf{S} and we obtain [65]

$$\begin{aligned} \hat{\mathbf{h}}_{\text{RML}} &= \arg \min_{\mathbf{h}} \sum_{i=1}^{n_B} \left\| \underline{\mathbf{Y}}(i) - \frac{\mathbf{A}(\mathbf{h})\mathbf{A}^T(\mathbf{h})\underline{\mathbf{Y}}(i)}{\|\mathbf{h}\|^2} \right\|^2 \\ &= \arg \min_{\mathbf{h}} \left\| \underline{\mathbb{Y}} - \frac{\mathbf{A}(\mathbf{h})\mathbf{A}^T(\mathbf{h})}{\|\mathbf{h}\|^2} \underline{\mathbb{Y}} \right\|_F^2 \\ &= \arg \min_{\mathbf{h}} \left\{ \|\underline{\mathbb{Y}}\|_F^2 - \frac{2}{\|\mathbf{h}\|^2} \text{tr} \left\{ \underline{\mathbb{Y}}^T \mathbf{A}(\mathbf{h}) \mathbf{A}^T(\mathbf{h}) \underline{\mathbb{Y}} \right\} \right. \\ &\quad \left. + \frac{1}{\|\mathbf{h}\|^4} \text{tr} \left\{ \underline{\mathbb{Y}}^T \mathbf{A}(\mathbf{h}) \mathbf{A}^T(\mathbf{h}) \mathbf{A}(\mathbf{h}) \mathbf{A}^T(\mathbf{h}) \underline{\mathbb{Y}} \right\} \right\} \\ &= \arg \max_{\mathbf{h}} \frac{1}{\|\mathbf{h}\|^2} \text{tr} \{ \mathbf{A}^T(\mathbf{h}) \underline{\mathbb{Y}} \underline{\mathbb{Y}}^T \mathbf{A}(\mathbf{h}) \} \\ &= \arg \max_{\mathbf{h}} \frac{1}{\|\mathbf{h}\|^2} \text{tr} \{ \mathbf{A}^T(\mathbf{h}) \hat{\mathbf{R}} \mathbf{A}(\mathbf{h}) \}. \end{aligned} \quad (4.164)$$

Comparing (4.164) and (4.139), it can be concluded that these two problems are identical. Therefore, in the Gaussian noise case the blind channel estimator (4.153) can be viewed as the ML channel estimator with relaxed finite alphabet constraint.

4.9.4 Numerical examples

We consider two numerical examples with different OSTBCs and/or different numbers of transmit and receive antennas. In both examples, the SNR is defined as σ_h^2/σ^2 where σ_h^2 is the variance of the real or imaginary part of the elements of \mathbf{H} . The performance of the blind algorithm of [60–62] is compared with that of the differential space-time coding technique and the coherent ML receiver. The latter receiver exploits exact CSI and is included in the figures only to illustrate performance losses of the blind techniques with respect to the ideal (informed receiver) case. In both examples, the multiplicity order n of the principal

eigenvalue of the matrix $\Phi^T(\mathbf{I}_{2K} \otimes \mathbf{R})\Phi$ is equal to one, and hence, the channel is blindly identifiable.

In the first example, we assume BPSK symbols and the full-rate OSTBC with $N = 3$, $M = 5$, and $K = T = 4$ (this code is given by eqn. (27) of [5]). The differential space-time coding scheme of [51] is used in this example. Figure 4.12 displays the SERs versus the SNR and Figure 4.13 shows the mean squared normalized channel estimation errors $\|\hat{\mathbf{H}} - \mathbf{H}\|_F^2 / \|\mathbf{H}\|_F^2$ versus SNR.

In the second example, QPSK symbols are assumed and the 3/4 rate OSTBC with $N = T = 4$ and $K = M = 3$ is chosen (this code is given by eqn. (7.4.10) of [9]). In this example, the differential space-time coding technique of [9] is used for comparisons. Figures 4.14 and 4.15 display, respectively, the SERs and the mean squared normalized channel estimation errors versus the SNR.

It can be seen from Figures 4.12–4.15 that, if there are enough received data blocks for each channel realization, then the blind approach of [60–62] has an excellent performance in terms of both blind channel estimation and symbol detection. As follows from Figures 4.12 and 4.14, this blind decoder performs substantially better than the differential approach even if $n_B \sim 10$. With $n_B \sim 30$, the performance of this decoder is within a fraction of dB from that of the coherent ML decoder.

It is interesting to observe that, as n_B is increased, the performance of the considered blind decoder closely approaches that of the coherent ML receiver (even though the blind technique corresponds to the *incoherent* ML decoder with *relaxed* finite alphabet constraint). This remarkable property is entirely due to the specific structure of OSTBCs.

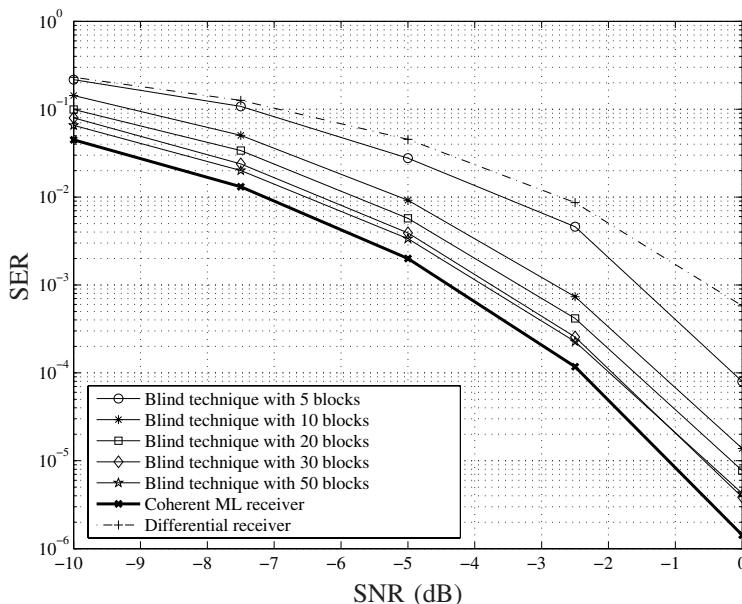


Figure 4.12 SERs versus SNR. First example of blind decoding.

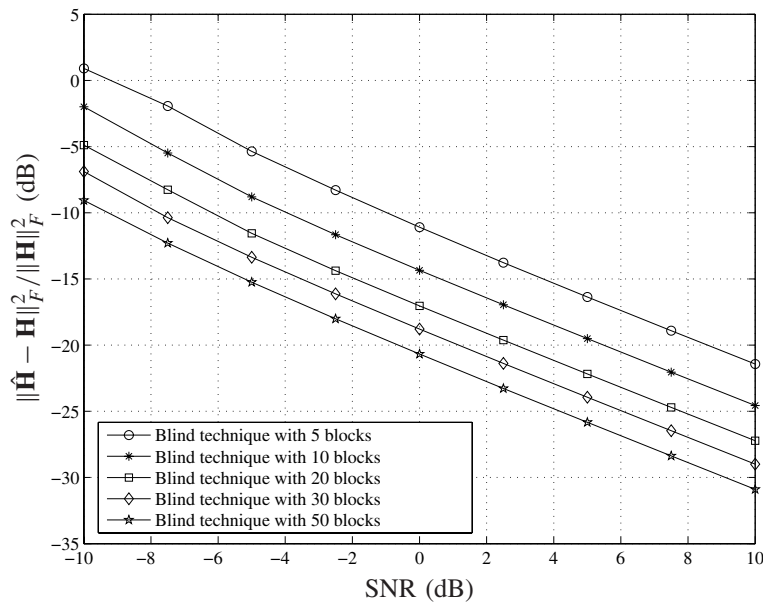


Figure 4.13 Mean squared normalized channel estimation error versus SNR. First example of blind decoding.

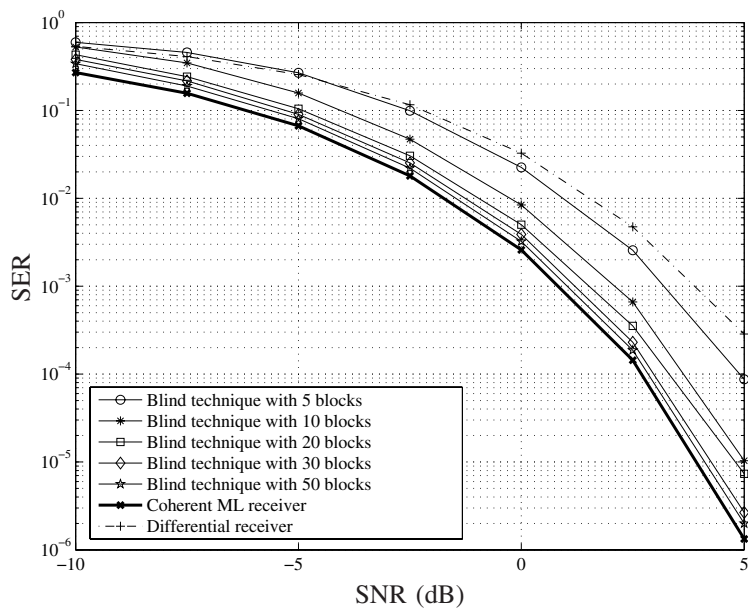


Figure 4.14 SERs versus SNR. Second example of blind decoding.

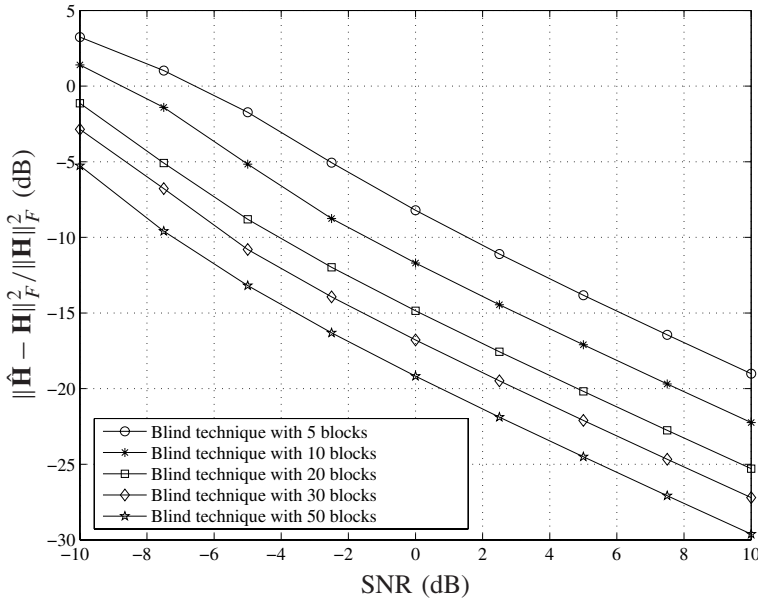


Figure 4.15 Mean squared channel estimation errors versus SNR. Second example of blind decoding.

4.10 Multiaccess MIMO Receivers for OSTBCs

So far we have considered the case of point-to-point OSTBC-based MIMO communications. In this section, we will consider the multiaccess MIMO case, when multiple multiantenna transmitters simultaneously communicate with a multiantenna receiver. In the latter case, the ML technique has a prohibitively high complexity as compared with the MF (single-user ML) receiver because its computational complexity grows exponentially with the number of users. Therefore, in multiaccess scenarios suboptimal but simple linear receivers are of particular interest [72–75, 18].

For example, a Capon-type linear receiver has been developed in [73] for direct sequence (DS) code-division multiple access (CDMA) systems that use multiple antennas and space-time block coding. Another promising approach has been proposed in [74] where a linear decorrelator receiver has been developed for a DS-CDMA based communication system. However, both of these techniques are restricted by the assumption that the transmitter consists of two antennas (Alamouti's code case) and that not more than two antennas are used at the receiver.

Another method has been presented in [75] where joint space-time decoding and interference suppression has been addressed. However, the approach of [75] is restricted to the case of only Alamouti's code and a single interferer.

In this section, we introduce the linear multiuser receiver methods developed in [16] and [18]. In contrast to the techniques of [73–75], the receivers of [18, 16] are not restricted to a specific type of OSTBC.

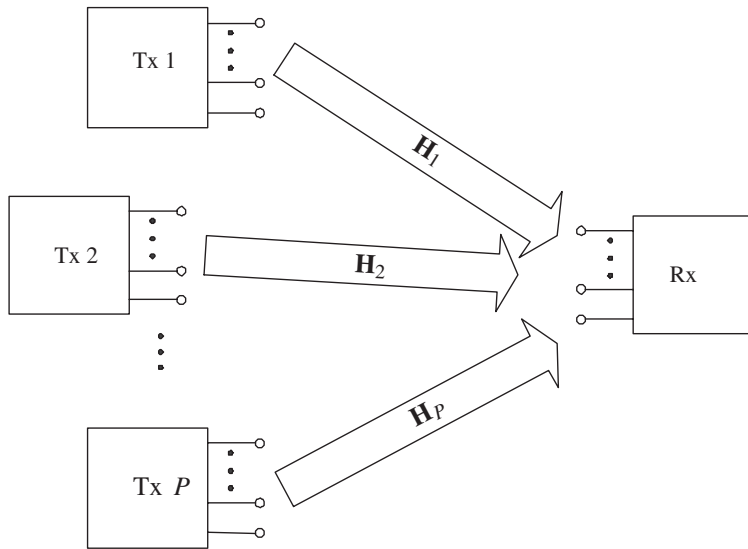


Figure 4.16 Multiaccess MIMO system.

4.10.1 Multiaccess MIMO model

Let us consider the case of a multiaccess MIMO communication system illustrated in Figure 4.16. Let P synchronous multiantenna transmitters communicate with a single multiantenna receiver. It is assumed that all the transmitters have the same number of transmit antennas and use the same OSTBC⁵ to encode the information symbols. Then, the received signal can be written as a superposition of signals received from different transmitters:

$$\mathbf{Y} = \sum_{p=1}^P \mathbf{X}(\mathbf{s}_p) \mathbf{H}_p + \mathbf{V} \quad (4.165)$$

where \mathbf{s}_p is a $K \times 1$ vector of information symbols of the p th transmitter, $\mathbf{X}(\mathbf{s}_p)$ is the matrix of its transmitted signals, and \mathbf{H}_p is the channel matrix between the p th transmitter and the receiver.

Applying the “underline” operator of (4.1) to (4.165), we have

$$\underline{\mathbf{Y}} = \sum_{p=1}^P \mathbf{A}(\mathbf{h}_p) \underline{\mathbf{s}}_p + \underline{\mathbf{V}} \quad (4.166)$$

where $\mathbf{h}_p \triangleq \underline{\mathbf{H}}_p$ and

$$\begin{aligned} \mathbf{A}(\mathbf{h}_p) &= \left[\underline{\mathbf{C}_1 \mathbf{H}_p} \cdots \underline{\mathbf{C}_K \mathbf{H}_p} \underline{\mathbf{D}_1 \mathbf{H}_p} \cdots \underline{\mathbf{D}_K \mathbf{H}_p} \right] \\ &\triangleq [\mathbf{a}_{p,1} \ \mathbf{a}_{p,2} \ \cdots \ \mathbf{a}_{p,2K}]. \end{aligned} \quad (4.167)$$

⁵These assumptions are only needed for simplicity of our notation and can be easily relaxed.

4.10.2 Minimum variance receivers

As mentioned earlier, the MF receiver provides a maximum output SNR for each transmitted data symbol. In the multiaccess MIMO case, however, the receiver performance is determined by the signal-to-interference-plus-noise ratio (SINR) rather than the SNR, and as a result, some kind of multiaccess interference (MAI) suppression is necessary. Motivated by this fact, in this subsection we consider linear receivers that maximize the SINR and achieve much better interference suppression performance than the MF receiver.

Let us assume, without any loss of generality, the first transmitter to be the user-of-interest. Then, we can express the output vector of a linear receiver as [18]

$$\hat{s}_1 = \mathbf{W}^T \underline{\mathbf{Y}} \quad (4.168)$$

where \hat{s}_1 can be viewed as the resulting estimate of the vector s_1 of symbols of the user-of-interest, and $\mathbf{W} = [\mathbf{w}_1 \mathbf{w}_2 \cdots \mathbf{w}_{2K}]$ is the $2MT \times 2K$ real matrix of the receiver coefficients. In fact, the vector \mathbf{w}_k can be interpreted as the receiver weight vector for the k th entry of s_1 . Note that for each user-of-interest, a separate matrix \mathbf{W} should be applied.

Given the matrix \mathbf{W} , the information symbols of the user-of-interest can be estimated as

$$\hat{s}_1 = [\mathbf{I}_K \ j\mathbf{I}_K] \hat{s}_1. \quad (4.169)$$

Using the linear estimate (4.169), the k th information symbol can be detected as the nearest neighbor constellation point to the k th entry of \hat{s}_1 .

The approach of [18] to the design of the matrix \mathbf{W} is to maximally suppress interference while preserving a distortionless response toward the signal of the transmitter-of-interest. The key idea behind this approach is inspired by the popular MV and minimum output energy (MOE) techniques used in adaptive beamforming [20] and multiuser detection [72], respectively. Specifically, for each entry of s_1 , the receiver output power can be minimized while preserving a unity gain (distortionless response) for that particular entry of s_1 . This is equivalent to solving the following optimization problem [18].

$$\min_{\mathbf{w}_k} \mathbf{w}_k^T \mathbf{R} \mathbf{w}_k \quad \text{subject to} \quad \mathbf{a}_{1,k}^T \mathbf{w}_k = 1 \quad \text{for all } k = 1, 2, \dots, 2K. \quad (4.170)$$

Note that the covariance matrix \mathbf{R} can be computed directly provided that all the channel matrices $\{\mathbf{H}_p\}_{p=1}^P$ and the noise variance are known at the receiver. However, in practice the knowledge of the channel matrices of some transmitters may be unavailable. In such cases, the true covariance matrix \mathbf{R} can be replaced in (4.170) by its sample estimate (4.151). Using such a replacement and taking into account that the problem (4.170) can be solved independently for each k , the finite-sample solution to (4.170) is given by [20, 18]

$$\mathbf{w}_k = \frac{1}{\mathbf{a}_{1,k}^T \hat{\mathbf{R}}^{-1} \mathbf{a}_{1,k}} \hat{\mathbf{R}}^{-1} \mathbf{a}_{1,k}, \quad k = 1, 2, \dots, 2K. \quad (4.171)$$

It is well-known that the receiver (4.171) is very sensitive to finite sample effects and self-nulling of the user-of-interest [76]. To provide robustness against such effects, the diagonal loading (DL) technique can be used [20, 76]. The DL-based receiver can be written as

$$\tilde{\mathbf{w}}_k = \frac{1}{\mathbf{a}_{1,k}^T (\hat{\mathbf{R}} + \nu \mathbf{I})^{-1} \mathbf{a}_{1,k}} (\hat{\mathbf{R}} + \nu \mathbf{I})^{-1} \mathbf{a}_{1,k}, \quad k = 1, 2, \dots, 2K \quad (4.172)$$

where ν is the diagonal loading factor.

Although the receivers (4.171) and (4.172) are able to maximally suppress MAI, they do not completely cancel *self-interference* [73]. Self-interference, for the k th entry of \mathbf{s}_1 , is the part of the interference caused by other entries of \mathbf{s}_1 than the k th one. In fact, self-interference is treated in (4.170) in the same way as MAI. Hence, when the MAI component is strong, self-interference may not be sufficiently rejected. Note, however, that complete cancellation of self-interference is a very desirable feature because, otherwise, the symbol-by-symbol detector becomes nonoptimal [18, 16]. Indeed, this detector is based on the assumption that the output of each linear receiver corresponding to any particular symbol does not depend on the other symbols. This assumption can be violated in the presence of even a small amount of noncancelled self-interference.

To guarantee complete cancellation of self-interference, it has been proposed in [18, 16] to add the following additional zero-forcing constraints to (4.170)

$$\mathbf{a}_{1,l}^T \mathbf{w}_k = 0 \quad \text{for all } l \neq k. \quad (4.173)$$

It can be readily verified that the optimization problems in (4.170) along with the additional constraints (4.173) can be equivalently written as

$$\min_{\mathbf{W}} \text{tr}\{\mathbf{W}^T \mathbf{R} \mathbf{W}\} \quad \text{subject to} \quad \mathbf{A}^T(\mathbf{h}_1) \mathbf{W} = \mathbf{I}_{2K}. \quad (4.174)$$

To solve the problem (4.174), the Lagrange multiplier method can be used. The Lagrangian function for this problem can be expressed as [18]

$$L(\mathbf{W}, \boldsymbol{\Lambda}) = \text{tr}\{\mathbf{W}^T \mathbf{R} \mathbf{W}\} - \text{tr}\{\boldsymbol{\Lambda}^T (\mathbf{A}^T(\mathbf{h}_1) \mathbf{W} - \mathbf{I}_{2K})\} \quad (4.175)$$

where $\boldsymbol{\Gamma}$ is a $2K \times 2K$ matrix of Lagrange multipliers. Differentiating (4.175) with respect to \mathbf{W} and equating it to zero yields

$$2\mathbf{R}\mathbf{W} = \mathbf{A}(\mathbf{h}_1)\boldsymbol{\Gamma} \quad (4.176)$$

or, equivalently,

$$\mathbf{W}_{\text{opt}} = \frac{1}{2} \mathbf{R}^{-1} \mathbf{A}(\mathbf{h}_1) \boldsymbol{\Gamma}. \quad (4.177)$$

Inserting (4.177) into the constraint $\mathbf{A}^T(\mathbf{h}_1) \mathbf{W} = \mathbf{I}_{2K}$, we obtain that

$$\boldsymbol{\Gamma} = 2(\mathbf{A}^T(\mathbf{h}_1) \mathbf{R}^{-1} \mathbf{A}(\mathbf{h}_1))^{-1}. \quad (4.178)$$

Substituting (4.178) to (4.177) yields the MV receiver of [18] in its final form:

$$\mathbf{W}_{\text{opt}} = \mathbf{R}^{-1} \mathbf{A}(\mathbf{h}_1) (\mathbf{A}^T(\mathbf{h}_1) \mathbf{R}^{-1} \mathbf{A}(\mathbf{h}_1))^{-1}. \quad (4.179)$$

Comparing (4.179) and (4.126) and using the property (4.124), we observe that the MV receiver (4.179) reduces to the MF receiver in the specific case of $\mathbf{R} = \beta \mathbf{I}$ for any positive real-valued β . This implies that the MF receiver ignores the effect of MAI treating it as a white noise. This also explains why the MF receiver is optimal only when MAI does not exist.

An interesting interpretation of the MV receiver (4.179) is based on the observation that it boils down to the combination of the prewhitener and decorrelator receiver.

To completely reject MAI caused by all the $P - 1$ interfering transmitters and, at the same time, to completely cancel self-interference, $4PK^2$ degrees of freedom are needed. Note that the available number of degrees of freedom is $4KMT$. Therefore, to warrant complete elimination of both MAI and self-interference, the condition

$$MT > PK \quad (4.180)$$

should be satisfied when using the receiver (4.179). As in orthogonal space-time coding, the parameter T is always greater than K , choosing $M > P$ is sufficient to satisfy (4.180).

Using the sample covariance matrix $\hat{\mathbf{R}}$ instead of the true covariance matrix \mathbf{R} , the finite-sample version of the MV receiver (4.179) can be written as [18]

$$\mathbf{W}_{\text{MV}} = \hat{\mathbf{R}}^{-1} \mathbf{A}(\mathbf{h}_1)(\mathbf{A}^T(\mathbf{h}_1)\hat{\mathbf{R}}^{-1}\mathbf{A}(\mathbf{h}_1))^{-1}. \quad (4.181)$$

Similar to (4.172), diagonal loading can be used in (4.181) to provide additional robustness against finite sample and signal self-nulling effects. This yields the following diagonally loaded MV receiver [18]:

$$\tilde{\mathbf{W}}_{\text{MV}} = (\hat{\mathbf{R}} + \nu \mathbf{I})^{-1} \mathbf{A}(\mathbf{h}_1)(\mathbf{A}^T(\mathbf{h}_1)(\hat{\mathbf{R}} + \nu \mathbf{I})^{-1}\mathbf{A}(\mathbf{h}_1))^{-1}. \quad (4.182)$$

An important observation is that the MV receivers in (4.172) and (4.182) do not exploit the assumptions that different transmitters use the same OSTBC and that they have the same number of antennas. Therefore, these receivers can also be used in the case when the numbers of antennas at the transmitters and their OSTBCs are different.

We end this subsection by mentioning that the MV linear receivers studied here are all based on the assumption that perfect CSI is available at the receiver. In practice, perfect CSI is not available and has to be estimated by means of training. As a result, the so-obtained training-based CSI is always erroneous, that is, is mismatched with respect to the exact CSI. Such a mismatch between the presumed and the exact CSI can result in a substantial performance degradation of the MV linear receivers considered. Therefore, the design of robust linear receivers is of great interest. Several robust MV techniques for the multiaccess MIMO case have been developed in [77, 78]. They use the worst-case optimization approach that has been successfully applied to develop robust adaptive beamformers and multiuser detectors, see [79–83]. More specifically, in [77] it is assumed that the mismatch between the true and the presumed CSI is norm-bounded, and two linear receivers are designed such that their performances are optimized for the worst-case mismatch within the uncertainty set. One of these receivers can be viewed as a robust version of the linear receiver (4.171), while the second robust receiver is a robust version of the receiver (4.181). Herein, we do not consider these robust techniques and refer our reader to [77] and [78] for more details.

4.10.3 Numerical examples

A multiaccess scenario with $P = 4$ transmitters is considered. Each transmitter is assumed to have $N = 2$ antennas and to use the Alamouti's code to encode its information symbols. The receiver has $M = 6$ antennas. The elements of all channel matrices are independently drawn from a zero-mean complex Gaussian distribution. The transmitted symbols are uniformly and independently drawn from the QPSK constellation. The SNR of the user-of-interest is defined as σ_1^2/σ^2 , where σ_1^2 is the variance of the real or imaginary part of the elements

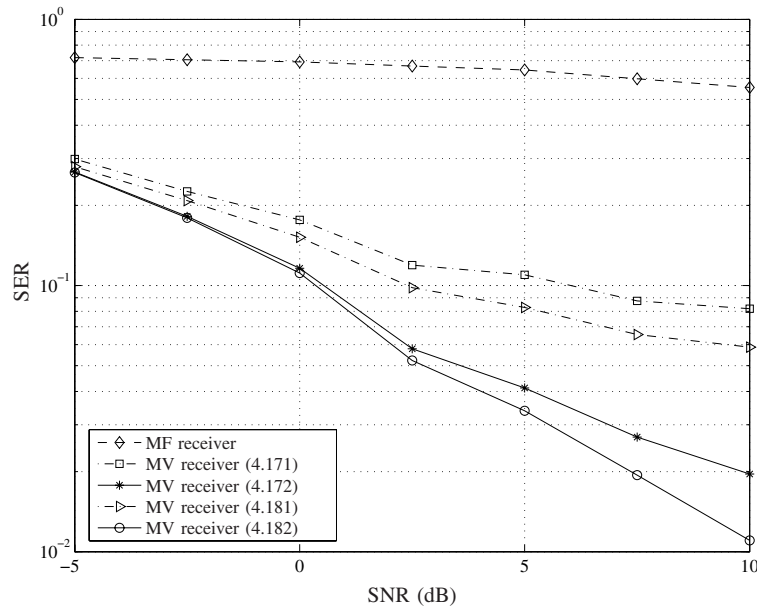


Figure 4.17 SERs versus SNR for the multiaccess example.

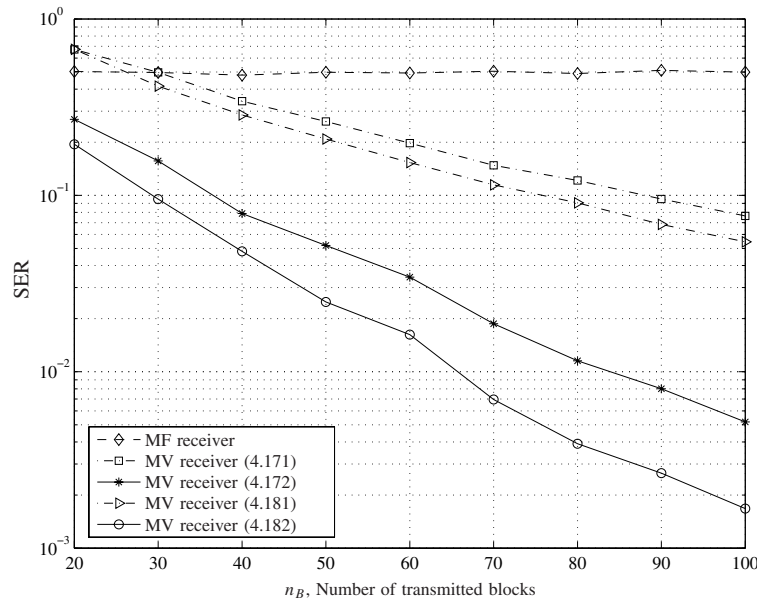


Figure 4.18 SERs versus n_B for the multiaccess example.

of \mathbf{H}_1 . The interference-to-noise ratio (INR) for the p th interfering transmitter is defined as σ_p^2/σ^2 where σ_p^2 is the variance of the real or imaginary part of the elements of \mathbf{H}_p .

Figure 4.17 shows SERs of the user-of-interest versus SNR. The linear receivers (4.171), (4.172), (4.181), and (4.182) are compared with the MF receiver. In this figure, $n_B = 100$ data blocks are used to obtain the sample covariance matrix and the INRs of all interfering transmitters are equal to 20 dB. It is clearly seen from this figure that all MV receivers greatly outperform the MF receiver. Interestingly, the MV receiver (4.181) with the self-interference ZF constraints outperforms the conventional MV receiver (4.171). Similarly, the DL-based MV receiver (4.182) with complete self-interference cancellation has better performance than the conventional DL-based MV receiver (4.172). As expected, performance improvements due to the ZF constraints are especially pronounced at high SNRs (i.e., in the region where self-interference affects the performance of the symbol-by-symbol detector at most).

Figure 4.18 shows SERs versus n_B for different receivers and for $\text{SNR} = 10$ dB and $\text{INR} = 20$ dB. As can be seen from this figure, all the MV receivers tested substantially outperform the MF receiver. Moreover, the receivers (4.181) and (4.182) have substantially better performance as compared to (4.171) and (4.172), respectively.

4.11 Conclusions

In this chapter, we have given an introduction to OSTBCs and reviewed some very recent results on different aspects of these codes. First of all, we have reviewed the conventional flat block fading MIMO model. Then, the constellation space invariance property of the OSTBCs have been proved and studied. Using this property, an intuitive equivalent array-processing-type MIMO model has been developed. The constellation space invariance property has been further used to obtain conceptually simple formulas for the ML decoder and to provide an exact and general symbol error probability analysis of OSTBCs. We have then considered optimality properties of OSTBCs and, in particular, have shown that OSTBCs are optimal among all LD codes with the same number of complex variables. A blind technique for incoherent decoding of OSTBCs has been then discussed, and its relationship to the incoherent ML decoder has been explored. At last, we have developed and studied several linear MV receivers for multiaccess MIMO communications and discussed their advantages with respect to the MF receiver.

References

- [1] E. Telatar, "Capacity of multi-antenna Gaussian channels," *Eur. Trans. Telecommun.*, vol. 10, no. 6, pp. 585–595, Nov./Dec. 1999.
- [2] T. L. Marzetta and B. M. Hochwald, "Capacity of a mobile multiple-antenna communication link in Rayleigh flat fading," *IEEE Trans. Inf. Theory*, vol. 45, no. 1, pp. 139–157, Jan. 1999.
- [3] V. Tarokh, N. Seshadri, and A. R. Calderbank, "Space-time codes for high data rate wireless communication: Performance criterion and code construction," *IEEE Trans. Inf. Theory*, vol. 44, no. 2, pp. 744–765, Mar. 1998.
- [4] S. M. Alamouti, "A simple transmit diversity technique for wireless communications," *IEEE J. Sel. Areas Commun.*, vol. 16, no. 8, pp. 1451–1458, Oct. 1998.
- [5] V. Tarokh, H. Jafarkhani, and A. R. Calderbank, "Space-time block codes from orthogonal designs," *IEEE Trans. Inf. Theory*, vol. 45, no. 5, pp. 1456–1467, July 1999.

- [6] G. Ganesan and P. Stoica, "Space-time block codes: A maximum SNR approach," *IEEE Trans. Inf. Theory*, vol. 47, no. 4, pp. 1650–1656, May 2001.
- [7] O. Tirkkonen and A. Hottinen, "Square-matrix embeddable space-time block codes for complex signal constellations," *IEEE Trans. Inf. Theory*, vol. 48, no. 2, pp. 384–395, Feb. 2002.
- [8] X.-B. Liang, "Orthogonal designs with maximal rates," *IEEE Trans. Inf. Theory*, vol. 49, no. 10, pp. 2468–2503, Oct. 2003.
- [9] E. G. Larsson and P. Stoica, *Space-time Block Coding for Wireless Communications*. Cambridge, U.K.: Cambridge University Press, May 2003.
- [10] I. Stakgold, *Green's Functions and Boundary Value Problems*, 2nd ed. New York: Wiley, 1998.
- [11] M. Gharavi-Alkhansari and A. B. Gershman, "Constellation space invariance of space-time block codes with application to optimal antenna subset selection," in *Proc. Fourth IEEE Workshop Signal Process. Adv. Wireless Commun.*, Rome, Italy, June 15–18, 2003, pp. 269–273.
- [12] M. Gharavi-Alkhansari and A. B. Gershman, "Constellation space invariance of space-time block codes with application to optimal ML decoding," in *Proc. IEEE Veh. Technol. Conf.*, vol. 1, Orlando, FL, Oct. 6–9, 2003, pp. 637–641.
- [13] M. Gharavi-Alkhansari and A. B. Gershman, "Constellation space invariance of orthogonal space-time block codes with application to evaluation of the probability of error," in *Proc. IEEE GLOBECOM*, vol. 4, San Francisco, CA, Dec. 1–5, 2003, pp. 1920–1924.
- [14] M. Gharavi-Alkhansari and A. B. Gershman, "Constellation space invariance of orthogonal space-time block codes," *IEEE Trans. Inf. Theory*, vol. 51, no. 1, Jan. 2005, pp. 331–334.
- [15] B. Hassibi and B. M. Hochwald, "High-rate codes that are linear in space and time," *IEEE Trans. Inf. Theory*, vol. 48, no. 7, pp. 1804–1824, July 2002.
- [16] S. Shahbazpanahi, M. Beheshti, A. B. Gershman, M. Gharavi-Alkhansari, and K. M. Wong, "Minimum variance linear receiver for multi-access interference rejection in a space-time block code based communication system," in *Conf. Rec. Thirty-Seventh Asilomar Conf. Signals, Syst., Comput.*, vol. 1, Pacific Grove, CA, Nov. 9–12, 2003, pp. 1017–1021.
- [17] S. Shahbazpanahi, M. Beheshti, A. B. Gershman, M. Gharavi-Alkhansari, and K. M. Wong, "Linear receivers for multiple-access MIMO systems with space-time block coding," in *Proc. IEEE Int. Conf. Commun.*, vol. 1, Paris, France, June 20–24, 2004, pp. 608–612.
- [18] S. Shahbazpanahi, M. Beheshti, A. B. Gershman, M. Gharavi-Alkhansari, and K. M. Wong, "Minimum variance linear receiver for multiaccess MIMO wireless systems with space-time block coding," *IEEE Trans. Signal Process.*, vol. 52, no. 12, pp. 3306–3313, Dec. 2004.
- [19] M. Gharavi-Alkhansari and A. B. Gershman, "Exact symbol error probability analysis for orthogonal space-time block codes: Two- and higher-dimensional constellations cases," *IEEE Trans. Commun.*, vol. 52, no. 7, pp. 1068–1073, July 2004.
- [20] H. L. Van Trees, *Optimum Array Processing*. New York: Wiley, 2002.
- [21] V. Tarokh, H. Jafarkhani, and A. R. Calderbank, "Space-time block coding for wireless communications: Performance results," *IEEE J. Sel. Areas Commun.*, vol. 17, no. 3, pp. 451–460, Mar. 1999.
- [22] S. Sandhu and A. Paulraj, "Space-time block codes: A capacity perspective," *IEEE Commun. Lett.*, vol. 4, no. 12, pp. 384–386, Dec. 2000.
- [23] G. Bauch, J. Hagenauer, and N. Seshadri, "Turbo processing in transmit antenna diversity systems," *Ann. Telecomm.*, vol. 56, no. 7–8, pp. 455–471, Aug. 2001.
- [24] S. Sandhu and A. Paulraj, "Union bound on error probability of linear space-time block codes," in *Proc. IEEE ICASSP*, Salt Lake City, UT, May 7–11, 2001, pp. 2473–2476.
- [25] G. Bauch and J. Hagenauer, "Analytical evaluation of space-time transmit diversity with FEC-coding," in *Proc. IEEE GLOBECOM*, vol. 1, San Antonio, TX, Nov. 25–29, 2001, pp. 435–439.

- [26] C. Gao, A. M. Haimovich, and D. Lao, "Bit error probability for space-time block code with coherent and differential detection," in *Proc. IEEE Veh. Technol. Conf.*, vol. 1, Vancouver, BC, Canada, Sept. 24–28, 2002, pp. 410–414.
- [27] H. Shin and J. H. Lee, "Exact symbol error probability of orthogonal space-time block codes," in *Proc. IEEE GLOBECOM*, vol. 2, Taipei, Taiwan, Nov. 17–21, 2002, pp. 1197–1201.
- [28] E. A. Jorswieck and A. Sezgin, "Impact of spatial correlation on the performance of orthogonal space-time block codes," *IEEE Commun. Lett.*, vol. 8, no. 1, pp. 21–23, Jan. 2004.
- [29] J. P. Kermoal, L. Schumacher, K. I. Pedersen, P. E. Mogensen, and F. Frederiksen, "A stochastic MIMO radio channel model with experimental validation," *IEEE J. Sel. Areas Commun.*, vol. 20, no. 6, pp. 1211–1226, Aug. 2002.
- [30] M. Gharavi-Alkhansari and A. B. Gershman, "Exact symbol error probability of orthogonal space-time block codes," in *Conf. Rec. Thirty-Seventh Asilomar Conf. Signals, Syst., Comput.*, vol. 2, Pacific Grove, CA, Nov. 9–12, 2003, pp. 1835–1839.
- [31] M. Gharavi-Alkhansari, A. B. Gershman, and M. Haardt, "Exact symbol error probability analysis of orthogonal space-time block codes over correlated fading channels," in *Proc. Fifth IEEE Int. Workshop Signal Process. Adv. Wireless Commun.*, Lisbon, Portugal, July 11–14, 2004.
- [32] M. Gharavi-Alkhansari, A. B. Gershman, and M. Haardt, "Exact error probability analysis of orthogonal space-time block codes with spatially correlated Rician fading," submitted to *IEEE Trans. Commun.*
- [33] J. M. Wozencraft and I. M. Jacobs, *Principles of Communication Engineering*. New York: Wiley, 1965.
- [34] J. G. Proakis, *Digital Communications*, 4th ed. New York: McGraw-Hill, 2001.
- [35] N. L. Johnson and S. Kotz, *Distributions in Statistics: Continuous Univariate Distributions*—2. New York: Wiley, 1970.
- [36] M. K. Simon and M.-S. Alouini, *Digital Communication Over Fading Channels: A Unified Approach to Performance Analysis*. New York: Wiley, 2000.
- [37] A. J. Paulraj, R. U. Nabar, and D. A. Gore, *Introduction to Space-Time Wireless Communications*. Cambridge, U.K.: Cambridge University Press, May 2003.
- [38] G. D. Forney Jr. and L.-F. Wei, "Multidimensional constellations—Part I: Introduction, figures of merit, and generalized cross constellations," *IEEE J. Sel. Areas Commun.*, vol. 7, no. 6, pp. 877–892, Aug. 1989.
- [39] A. Stuart, J. K. Ord, S. Arnold, and M. G. Kendall, *Kendall's Advanced Theory of Statistics: Classical Inference and the Linear Model*, 6th ed. New York: Oxford University Press, 1999, vol. 2A.
- [40] M. Gharavi-Alkhansari and A. B. Gershman, "On diversity and coding gains and optimal matrix constellations for space-time block codes," to appear in *IEEE Trans. Signal Process.*
- [41] S. Sandhu and A. Paulraj, "Unified design of linear space-time block codes," in *Proc. IEEE GLOBECOM*, San Antonio, TX, Nov. 25–29, 2001, pp. 1073–1077.
- [42] J.-C. Guey, M. P. Fitz, M. R. Bell, and W.-Y. Kuo, "Signal design for transmitter diversity wireless communication systems over Rayleigh fading channels," *IEEE Trans. Commun.*, vol. 47, no. 4, pp. 527–537, Apr. 1999.
- [43] D. M. Ionescu, "On space-time code design," *IEEE Trans. Wireless Commun.*, vol. 2, no. 1, pp. 20–28, Jan. 2003.
- [44] H.-F. Lu, Y. Wang, P. V. Kumar, and K. M. Chugg, "Remarks on space-time codes including a new lower bound and an improved code," *IEEE Trans. Inf. Theory*, vol. 49, no. 10, pp. 2752–2757, Oct. 2003.

- [45] J. W. Craig, "A new, simple and exact result for calculating the probability of error for two-dimensional signal constellations," in *Conf. Rec. IEEE MILCOM*, vol. 2, McLean, VA, Nov. 4–7, 1991, pp. 571–575.
- [46] M.-K. Byun and B. G. Lee, "New bounds of pairwise error probability for space-time codes in Rayleigh fading channels," in *Proc. IEEE WCNC*, vol. 1, Orlando, FL, Mar. 17–21, 2002, pp. 89–93.
- [47] C. L. Weber, *Elements of Detection and Signal Design*. Springer-Verlag, 1987.
- [48] V. Tarokh and H. Jafarkhani, "A differential detection scheme for transmit diversity," *IEEE J. Sel. Areas Commun.*, vol. 18, no. 7, pp. 1169–1174, July 2000.
- [49] B. L. Hughes, "Differential space-time modulation," *IEEE Trans. Inf. Theory*, vol. 46, no. 7, pp. 2567–2578, Nov. 2000.
- [50] B. M. Hochwald and W. Sweldens, "Differential unitary space-time modulation," *IEEE Trans. Commun.*, vol. 48, no. 12, pp. 2041–2052, Dec. 2000.
- [51] H. Jafarkhani and V. Tarokh, "Multiple transmit antenna differential detection from generalized orthogonal designs," *IEEE Trans. Inf. Theory*, vol. 47, no. 6, pp. 2626–2631, Sept. 2001.
- [52] G. Ganesan and P. Stoica, "Differential modulation using space-time block codes," *IEEE Signal Process. Lett.*, vol. 9, no. 2, pp. 57–60, Feb. 2002.
- [53] B. M. Hochwald and T. L. Marzetta, "Unitary space-time modulation for multiple-antenna communications in Rayleigh flat fading," *IEEE Trans. Inf. Theory*, vol. 46, no. 3, pp. 543–564, Mar. 2000.
- [54] B. M. Hochwald, T. L. Marzetta, T. J. Richardson, W. Sweldens, and R. Urbanke, "Systematic design of unitary space-time constellations," *IEEE Trans. Inf. Theory*, vol. 46, no. 6, pp. 1962–1973, Sept. 2000.
- [55] A. L. Swindlehurst and G. Leus, "Blind and semi-blind equalization for generalized space-time block codes," *IEEE Trans. Signal Process.*, vol. 50, no. 10, pp. 2489–2498, Oct. 2002.
- [56] P. Stoica and G. Ganesan, "Space-time block codes: Trained, blind, and semi-blind detection," *Digital Signal Process.*, vol. 13, no. 1, pp. 93–105, Jan. 2003.
- [57] E. G. Larsson, P. Stoica, and J. Li, "Orthogonal space-time block codes: Maximum-likelihood detection for unknown channels and unstructured interferences," *IEEE Trans. Signal Process.*, vol. 51, no. 2, pp. 362–372, Feb. 2003.
- [58] N. D. Sidiropoulos and R. S. Budampati, "Khatri-Rao space-time codes," *IEEE Trans. Signal Process.*, vol. 50, no. 10, pp. 2396–2407, Oct. 2002.
- [59] W.-K. Ma, P. C. Ching, T. N. Davidson, and X.-G. Xia, "Blind maximum likelihood decoding for orthogonal space-time block codes: A semidefinite relaxation approach," in *Proc. IEEE GLOBECOM*, San Francisco, CA, Dec. 1–5, 2003, pp. 2094–2098.
- [60] S. Shahbazpanahi, A. B. Gershman, and J. H. Manton, "Blind decoding of orthogonal space-time block codes using closed-form channel estimation," to appear in *IEEE Trans. Signal Process.*
- [61] S. Shahbazpanahi, A. B. Gershman, and J. H. Manton, "Closed-form channel estimation for blind decoding of orthogonal space-time block codes," in *Proc. IEEE Int. Conf. Commun.*, vol. 1, Paris, France, June 20–24, 2004, pp. 603–607.
- [62] S. Shahbazpanahi, A. B. Gershman, and J. H. Manton, "Closed-form blind decoding of orthogonal space-time block codes," in *Proc. IEEE ICASSP*, vol. 4, Montreal, Quebec, Canada, May 17–21, 2004, pp. 473–476.
- [63] U. Helmke and J. B. Moore, *Optimization and Dynamical Systems*. New York: Springer-Verlag, 1994.
- [64] J. H. Manton, "Optimization algorithms exploiting unitary constraints," *IEEE Trans. Signal Process.*, vol. 50, no. 3, pp. 635–650, Mar. 2002.

- [65] S. Shahbazpanahi, A. B. Gershman, and G. B. Giannakis, "Semi-blind MIMO channel estimation for space-time coded multi-user systems," in *Proc. IEEE Sensor Array Multichannel Signal Process. Workshop*, Sitges, Spain, July 18–21, 2004.
- [66] S. Shahbazpanahi, A. B. Gershman, and G. B. Giannakis, "Semi-blind multi-user MIMO channel estimation based on Capon and MUSIC techniques," submitted to *IEEE Trans. Signal Process.*
- [67] X.-B. Liang, "A high-rate orthogonal space-time block code," *IEEE Commun. Lett.*, vol. 7, no. 5, pp. 222–223, May 2003.
- [68] S. Zhou, B. Muquet, and G. B. Giannakis, "Semi-blind channel estimation for block precoded space-time OFDM transmissions," in *Proc. IEEE Workshop Stat Signal Process.*, Singapore, 2001, pp. 381–384.
- [69] S. Shahbazpanahi, A. B. Gershman, and J. H. Manton, "A linear precoding approach to resolve ambiguity of blind decoding of orthogonal space-time block codes in slowly fading channels," in *Proc. Fifth IEEE Int. Workshop Signal Process. Adv. Wireless Commun.*, Lisbon, Portugal, July 11–14, 2004.
- [70] S. Talwar, M. Viberg, and A. Paulraj, "Blind separation of synchronous cochannel digital signals using an antenna array – Part I: Algorithms," *IEEE Trans. Signal Process.*, vol. 44, no. 5, pp. 1184–1197, May 1996.
- [71] S. Shahbazpanahi, A. B. Gershman, and J. H. Manton, "A relaxed maximum likelihood approach to blind channel estimation and symbol detection in MIMO systems with orthogonal space-time block codes," in *Proc. IEEE Veh. Technol. Conf.*, Milan, Italy, May 17–19, 2004.
- [72] M. Honig and M. K. Tsatsanis, "Adaptive techniques for multiuser CDMA receivers," *IEEE Signal Process. Mag.*, vol. 17, no. 3, pp. 49–61, May 2000.
- [73] H. Li, X. Lu, and G. B. Giannakis, "Capon multiuser receiver for CDMA systems with space-time coding," *IEEE Trans. Signal Process.*, vol. 50, no. 5, pp. 1193–1204, May 2002.
- [74] D. Reynolds, X. Wang, and H. V. Poor, "Blind adaptive space-time multiuser detection with multiple transmitter and receiver antennas," *IEEE Trans. Signal Process.*, vol. 50, no. 6, pp. 1261–1276, June 2002.
- [75] A. F. Naguib, N. Seshadri, and A. R. Calderbank, "Applications of space-time block codes and interference suppression for high capacity and high data rate wireless systems," in *Conf. Rec. 32nd Asilomar Conf. Signals, Syst., Comput.*, vol. 2, Pacific Grove, CA, Nov. 1998, pp. 1803–1810.
- [76] A. B. Gershman, "Robustness issues in adaptive beamforming and high-resolution direction finding," in *High-Resolution and Robust Signal Processing*, Y. Hua, A. B. Gershman, and Q. Cheng, Eds. New York: Marcel Dekker, 2003, ch. 2.
- [77] Y. Rong, S. Shahbazpanahi, and A. B. Gershman, "Robust linear receivers for space-time block-coded multi-access MIMO systems with imperfect channel state information," to appear in *IEEE Trans. Signal Process.*
- [78] Y. Rong, S. Shahbazpanahi, and A. B. Gershman, "Robust linear receivers for space-time block-coded multiple-access MIMO wireless systems," in *Proc. IEEE ICASSP*, vol. 2, Montreal, Quebec, Canada, May 17–22, 2004, pp. 9–12.
- [79] S. A. Vorobyov, A. B. Gershman, and Z.-Q. Luo, "Robust adaptive beamforming using worst-case performance optimization: A solution to the signal mismatch problem," *IEEE Trans. Signal Process.*, vol. 51, no. 2, pp. 313–324, Feb. 2003.
- [80] S. Shahbazpanahi, A. B. Gershman, Z.-Q. Luo, and K. M. Wong, "Robust adaptive beamforming for general-rank signal models," *IEEE Trans. Signal Process.*, vol. 51, no. 9, pp. 2257–2269, Sept. 2003.
- [81] R. Lorenz and S. P. Boyd, "Robust minimum variance beamforming," submitted to *IEEE Trans. Signal Process.*

- [82] S. Shahbazpanahi and A. B. Gershman, "Robust blind multiuser detection for synchronous CDMA systems using worst-case performance optimization," *IEEE Trans. Wireless Commun.*, vol. 3, no. 6, pp. 2232–2245, Nov. 2004.
- [83] K. Zarifi, S. Shahbazpanahi, A. B. Gershman, and Z.-Q. Luo, "Robust blind multiuser detection based on the worst-case performance optimization of the MMSE receiver," *IEEE Trans. Signal Process.*, vol. 53, no. 1, pp. 295–305, Jan. 2005.

5

Trace-Orthogonal Full Diversity Cyclotomic Space-Time Codes

Jian-Kang Zhang, Jing Liu, and Kon Max Wong

5.1 Introduction

The explosive expansion in wireless communications in recent years encounters severe technical challenges such as the demand of transmitting speech, data and video at high rates in an environment rich of scattering. Multi-input multi-output (MIMO) wireless links are an important recent development in wireless communication systems because of their significant potential in terms of meeting these challenges caused by fading channels together with power and bandwidth limitations. The importance of MIMO communication channels lies in the fact that they are able to provide a significant increase in capacity over single-input single-output (SISO) channels. Existing MIMO designs rely on the use of M transmitter antennas and N receiver antennas, enabling the communication system to exploit either the high performance provided by the space diversity available or the high data rate provided by the capacity available in MIMO channels [1, 2], or both. Full diversity is achieved when the total degrees of freedom ($M \times N$) offered in the multiantenna system are utilized. This will ensure a low pairwise probability of error for detecting the transmitted symbols at high signal-to-noise ratio (SNR) when a maximum likelihood (ML) detector is employed. Full symbol rate, on the other hand, is achieved when one symbol is transmitted by each of the multiple transmitter antennas per time slot (often called a “channel”), and, in the case of M transmitter antennas, we will have M symbols per channel use (pcu) at full rate.

One approach, which attempts to achieve high data rate, is the Vertical Bell Labs Layered Space-times (V-BLAST) scheme [3], the architecture of which breaks the original data stream into substreams to be transmitted on the individual antennas. The V-BLAST receiver

decodes the substreams using a sequence of nulling and cancelling steps. Although V-BLAST offers full symbol rate in data transmission and its multiplexing design allows ergodic capacity to be achieved, this is done at the expense of performance in fading channels. Furthermore, V-BLAST suffers from its inability to work with fewer receiver antennas than transmitter antennas.

Since then, there has been considerable work on a variety of space-time transmission schemes such as the space-time trellis codes [4] and space-time block codes for known channels [5, 6] and for unknown channels [7–15]. Orthogonal space-time block codes [5, 16, 6, 17–19] can provide full diversity with a linear processing maximum likelihood detector, however, they suffer from having a limited transmission rate [19–22], and thus do not achieve full capacity in MIMO channels [23].

Therefore, Hassibi and Hochwald [24] proposed linear dispersion (LD) codes, in which the transmitted codeword is a linear combination of certain weighted matrices. The key to LD code design is that the basis matrices are optimized such that the resulting codes maximize the *ergodic* capacity of the LD coded MIMO system. Unfortunately, for the LD codes proposed in [24], good error probability performance is not strictly guaranteed. To bridge the gap between multiplexing and diversity gains, Heath and Paulraj [25] proposed a LD code design using frame theory that typically performs well in terms of both ergodic capacity as well as error performance. However, their design still cannot guarantee full diversity.

More recent research [26–28] in the design of linear space-time block codes based on number theory has shown that it is possible to provide full rate and full diversity without information loss, that is, the ergodic capacity of the space-time coded MIMO channel is equal to that of the original MIMO channel. The key steps to successfully design such linear space-time block codes are as follows.

- Design a rotation matrix [57, 29–33] for the diagonal space-time (DAST) code [34] of each layer such that each point from the transmitted signal constellation is mapped into a new constellation such that each information symbol affects all transmitted space-time coded symbols. This enables the recovery of any point of the transmitted constellation lost in a deep fade. Here, a powerful tool used for constructing full diversity linear space-time block codes is algebraic number theory [26, 27, 33, 50, 34, 37, 28].
- While the substream data in the same layer can be identified by a corresponding rotation matrix, circularly organize the substream data from different layers for transmission such that both full ergodic channel capacity and full diversity are achieved simultaneously [35]. On the basis of this idea, the interlayer can be identified by simply using a *Diophantine number* [26, 27]. Here, the two vital points to successfully provide full diversity are (i) that the nonzero coefficient of highest order in the determinant expansion of a signal matrix in terms of the Diophantine number is just the product of the same layer (DAST) data and, (ii) that the Diophantine number is linearly independent over this coefficient domain.

For the above design of a full-rate, full-diversity and information lossless code, there are two important issues as follows.

1. Systematic design of rotation matrices in different layers and constellation – The rotation matrix in [26, 27] arose from [57, 29–31, 33, 36], where the number of

transmitter antennas is restricted to $2^m 3^n$ and the corresponding constellations are limited to PAM or QAM. Therefore, the systematic and efficient joint design of the rotation matrix, the constellation, and the Diophantine number for an arbitrary number of transmitter antennas and receiver antennas is an important issue. Recently, Wang [37] *et al.* have obtained a profound result on a *cyclotomic* linear diagonal space-time block code design. They proposed a systematic method to jointly design a generating matrix and corresponding constellation set. However, the resulting optimal generating matrix is not unitary, and the number of transmitter antennas is limited only to a specific rational integer).

2. Relaxing the present restrictions of the space-time block code design – the signal matrix in [26, 27] is square; i.e., the number of channel uses T must be equal to the number of transmitter antennas. This is particularly restrictive in the case when the channel is not known to either the transmitter or the receiver, since, under this condition, a noncoherent receiver that needs a nonsquare space-time code design [7–11] has to be employed. Recently, Kammoun and Belfiore [38] listed several examples of nonsquare coding matrices for noncoherent MIMO systems without showing how they were designed. It would be very useful to have the currently available code design generalized to a rectangular signal matrix and to full diversity LD code designs as well.

In this chapter, we address the above two issues of designing a full rate, full diversity and information lossless code. We focus on understanding the architecture of an LD code and, from the view points of information theory and detection theory, on exploring the structures of a good code. Since there are a large number of parameters to be considered in a space-time code design, it is very difficult to exhaustively search for a good solution, particularly if the number of transmitter antennas, the number of channel uses, or the constellation size is large. Therefore, confining to the consideration of the possible necessary conditions that a good space-time code should satisfy can dramatically reduce the parameter space and hence could provide us with a systematic and efficient way of finding a good space-time code.

Notation: Throughout this chapter, we use the following notation: Matrices are denoted by uppercase boldface characters (e.g., \mathbf{A}), while column vectors are denoted by lowercase boldface characters (e.g., \mathbf{b}). The i -th entry of \mathbf{b} is denoted by b_i . The columns of an $M \times N$ matrix \mathbf{A} are denoted by $\mathbf{a}_1, \mathbf{a}_2, \dots, \mathbf{a}_N$. The k -th diagonal entry of a matrix \mathbf{A} is denoted by $[\mathbf{A}]_{kk}$. The conjugate of matrix \mathbf{A} is denoted by \mathbf{A}^* . The transpose of \mathbf{A} is denoted by \mathbf{A}^T . The Hermitian transpose of \mathbf{A} (i.e., the conjugate transpose of \mathbf{A}) is denoted by \mathbf{A}^H . K denotes the total number of symbols to be transmitted, and M and N denote the number of transmitter antennas and receiver antennas, respectively. \mathbb{Z} denotes the ring of integers; \mathbb{Q} denotes the field of rational numbers; \mathbb{R} denotes the field of real numbers; \mathbb{C} denotes the field of complex numbers; $\gcd(m, n)$ denotes the greatest common divisor of positive integers m and n ; $\varphi(n)$ denotes the Euler function over \mathbb{Z} ; ζ_m denotes the m th root of unity, that is, $\zeta_m = \exp\left(\frac{j2\pi}{m}\right)$ with $j = \sqrt{-1}$; $\mathbb{Z}[\zeta_m]$ denotes the cyclotomic ring generated by \mathbb{Z} and the cyclotomic number ζ_m . $\mathbb{Q}(\zeta_m)$ denotes the field generated by \mathbb{Q} and ζ_m . \mathbf{W}_P denotes the $P \times P$ discrete Fourier transform matrix and \mathbf{C}_P denotes the $P \times P$ circular generator matrix,

$$\mathbf{C}_P = \begin{pmatrix} \mathbf{0}_{1 \times (P-1)} & 1 \\ \mathbf{I}_{P-1} & \mathbf{0}_{(P-1) \times 1} \end{pmatrix}$$

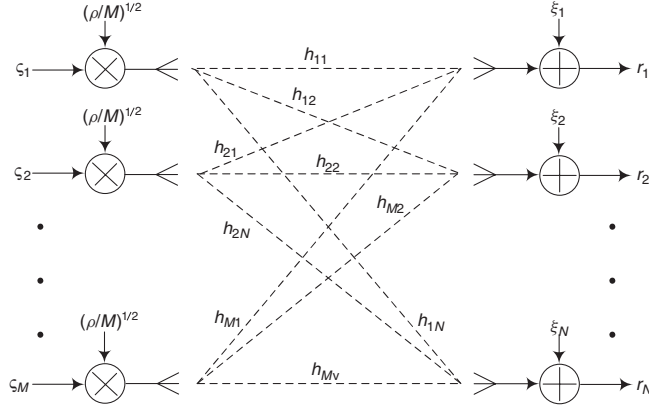


Figure 5.1 A MIMO system with M transmitter antennas and N receiver antennas.

where \mathbf{I}_{P-1} denotes the $(P - 1) \times (P - 1)$ identity matrix. Notation \otimes and $\text{vec}(\cdot)$ denotes the Kronecker product and vectorization operation [39], respectively. For two positive semidefinite matrices \mathbf{X} and \mathbf{Y} , the notation $\mathbf{X} \succeq \mathbf{Y}$ denotes that $(\mathbf{X} - \mathbf{Y})$ is a positive definite matrix. A diagram representing this MIMO system is shown in Fig. 5.1.

5.2 Channel Model with Linear Dispersion Codes

At any time slot of transmission, the discrete-time equivalent model of a baseband MIMO communication system equipped with M antennas at the transmitter and N antennas at the receiver can be represented in a compact matrix form as

$$\mathbf{r} = \sqrt{\frac{\rho}{M}} \mathbf{H} \boldsymbol{\varsigma} + \boldsymbol{\xi} \quad (5.1)$$

where \mathbf{r} is a $N \times 1$ received signal vector, \mathbf{H} is a $N \times M$ channel matrix, $\boldsymbol{\varsigma}$ is an $M \times 1$ transmitted signal vector each element of which represents a code of the information symbols to be transmitted, and $\boldsymbol{\xi}$ is a $N \times 1$ complex noise vector. Throughout this chapter, we assume that \mathbf{H} , $\boldsymbol{\varsigma}$ and $\boldsymbol{\xi}$ are independent, the entries of \mathbf{H} and $\boldsymbol{\varsigma}$ are samples of circularly symmetric zero-mean complex white Gaussian random variables with unit variances and the signal vector \mathbf{s} has an identical covariance matrix, so that the normalization factor $\sqrt{\frac{\rho}{M}}$ in Eq. (5.1) ensures that ρ is the SNR per receiver antenna, independent of M .

Let us consider T transmission time slots (i.e., the number of channel uses = T) of the MIMO channel model of Eq. (5.1). Then there will be T coded signal vectors to be transmitted, forming an $M \times T$ coded signal matrix. If we employ an LD code, this coded signal matrix $\boldsymbol{\Sigma}(\mathbf{s})$ is defined as [24]

$$\boldsymbol{\Sigma}(\mathbf{s}) = \sum_{k=1}^K \mathbf{A}_k s_k + \sum_{k=1}^K \mathbf{B}_k s_k^* \quad (5.2)$$

Here, K denotes the total number of information symbols, \mathbf{s} denotes a $K \times 1$ transmission symbol vector $\mathbf{s} = [s_1, s_2, \dots, s_K]^T$, and each of \mathbf{A}_k and \mathbf{B}_k denotes an $M \times T$ matrix.

Note that if all $\mathbf{B}_k = \mathbf{0}$ in Eq. (5.2), then the linear dispersion code is reduced to a linear space-time block code [27, 26]. Therefore, a linear dispersion code is a generalization of a linear space-time block code. In addition, we note that the linear dispersion code in Eq. (5.2) is linear with respect to the real parts and the imaginary parts of all symbols \mathbf{s}_k , but not linear with respect to the complex symbols themselves, since $\Sigma(j\mathbf{s}) \neq j\Sigma(\mathbf{s})$ in general.

The purpose of the transmitter is to transmit all the coded symbols in the coded matrix $\Sigma(\mathbf{s})$. However, at each time slot t , instead of transmitting a particular column vector of M symbols, we may select M symbols, each from a different signal vectors of $\Sigma(\mathbf{s})$ to be fed to the M transmitter antennas for transmission. This can be facilitated by multiplying the code matrix $\Sigma(\mathbf{s})$ by a circulant matrix \mathbf{C}_M^ℓ before transmission. At each time slot t , the selected symbols from the M different rows of $\Sigma(\mathbf{s})$ for transmission are usually called a *layer*. This concept of creating different layers will be addressed later on in the design of the coding matrix. For simplicity of the model, we assume for the time being that the circulant matrix used for the formation of layers is \mathbf{I} so that at the receiver all the T received signal vectors can be organized in a more compact matrix form into

$$\mathbf{R} = \sqrt{\frac{\rho}{M}} \mathbf{H} \Sigma(\mathbf{s}) + \boldsymbol{\Xi} \quad (5.3)$$

where $\mathbf{R} = [\mathbf{r}_1, \mathbf{r}_2, \dots, \mathbf{r}_T]$ denotes an $N \times T$ received signal matrix and $\boldsymbol{\Xi} = [\boldsymbol{\xi}_1, \boldsymbol{\xi}_2, \dots, \boldsymbol{\xi}_T]$ denotes a $N \times T$ noise matrix. An equivalent model can be established by vectoring both sides of Eq. (5.3) such that

$$\text{vec}(\mathbf{R}) = \sqrt{\frac{\rho}{M}} \mathcal{H} (\mathcal{A}\mathbf{s} + \mathcal{B}\mathbf{s}^*) + \text{vec}(\boldsymbol{\Xi}) \quad (5.4)$$

with $\mathcal{H} = \mathbf{I}_T \otimes \mathbf{H}$. In order to obtain an equivalent expression of model (5.4) for a real input and real output as well as preserve the matrix structure, it is very useful to take the conjugate of the vector $\text{vec}(\mathbf{R})$. By doing so, the model of Eq. (5.4) can be equivalently rewritten as

$$\begin{pmatrix} \text{vec}(\mathbf{R}) \\ \text{vec}(\mathbf{R}^*) \end{pmatrix} = \sqrt{\frac{\rho}{M}} \begin{pmatrix} \mathcal{H} & \mathbf{0} \\ \mathbf{0} & \mathcal{H}^* \end{pmatrix} \begin{pmatrix} \mathcal{A} & \mathcal{B} \\ \mathcal{B}^* & \mathcal{A}^* \end{pmatrix} \begin{pmatrix} \mathbf{s} \\ \mathbf{s}^* \end{pmatrix} + \begin{pmatrix} \text{vec}(\boldsymbol{\Xi}) \\ \text{vec}(\boldsymbol{\Xi})^* \end{pmatrix} \quad (5.5)$$

Equation. (5.5) now becomes a precoded MIMO channel model with the precoder \mathcal{F} given by

$$\mathcal{F} = \begin{pmatrix} \mathcal{A} & \mathcal{B} \\ \mathcal{B}^* & \mathcal{A}^* \end{pmatrix} \quad (5.6)$$

where

$$\mathcal{A} = [\text{vec}(\mathbf{A}_1), \text{vec}(\mathbf{A}_2), \dots, \text{vec}(\mathbf{A}_K)] \quad (5.7a)$$

$$\mathcal{B} = [\text{vec}(\mathbf{B}_1), \text{vec}(\mathbf{B}_2), \dots, \text{vec}(\mathbf{B}_K)] \quad (5.7b)$$

On the other hand, the complex MIMO model in Eq. (5.5) can also be expressed as one involving real multiinputs and real multioutputs by employing a transformation matrix \mathbf{T} such that,

$$\begin{pmatrix} \boldsymbol{\varsigma} \\ \boldsymbol{\varsigma}^* \end{pmatrix} = \sqrt{2} \mathbf{T} \begin{pmatrix} \boldsymbol{\varsigma}_{\text{re}} \\ \boldsymbol{\varsigma}_{\text{im}} \end{pmatrix} \quad (5.8)$$

where ς_{re} and ς_{im} denote the real and imaginary parts of ς , respectively, and \mathbf{T} is defined as

$$\mathbf{T} = \frac{1}{\sqrt{2}} \begin{pmatrix} \mathbf{I} & j\mathbf{I} \\ \mathbf{I} & -j\mathbf{I} \end{pmatrix} \quad (5.9)$$

Note that \mathbf{T} is unitary. Applying this transformation \mathbf{T} , the model in Eq. (5.5) can be equivalently written as

$$\begin{pmatrix} \text{vec}(\mathbf{R}_{\text{re}}) \\ \text{vec}(\mathbf{R}_{\text{im}}) \end{pmatrix} = \sqrt{\frac{\rho}{M}} \mathbf{T}^H \tilde{\mathcal{H}} \mathcal{F} \mathbf{T} \begin{pmatrix} \mathbf{s}_{\text{re}} \\ \mathbf{s}_{\text{im}} \end{pmatrix} + \begin{pmatrix} \text{vec}(\boldsymbol{\Xi}_{\text{re}}) \\ \text{vec}(\boldsymbol{\Xi}_{\text{im}}) \end{pmatrix} \quad (5.10)$$

where matrix $\tilde{\mathcal{H}}$ is defined as

$$\tilde{\mathcal{H}} = \begin{pmatrix} \mathcal{H} & \mathbf{0} \\ \mathbf{0} & \mathcal{H}^* \end{pmatrix} \quad (5.11)$$

Equation (5.10) is useful to analyze the detection of a linear dispersion code and also to compare the ergodic capacity of the original channel in Eq. (5.1) with that of the linear dispersion coded channel of Eq. (5.5).

5.3 Good Structures for LD Codes: Trace Orthogonality

In this section, we examine the structure of an LD code used in MIMO communications and try to establish, from two different points of view, a good structure of the code to be designed. From an information-theoretic viewpoint, we establish that a good LD code should have a *inter*-unitary structure, while from a detection error viewpoint a good LD code should have a *intra*-unitary structure. We called a code having the combined interunitary and intraunitary structure a *trace orthogonal* LD code [40].

5.3.1 An information-theoretic viewpoint

In the design of space-time LD codes, it is important that the ergodic capacity of the equivalent channel of Eq. (5.5) employing the LD code be made as close as possible to that of the original channel in Eq. (5.1). Here, in the analysis of the ergodic capacity, we assume that the entries of the channel matrix \mathbf{H} are independently Gaussian distributed with the unit variances and are known to the receiver but not to the transmitter. We also assume that ξ is circularly symmetric complex Gaussian noise with the identity covariance matrix. Under these assumptions, the ergodic capacity of the channel modeled in Eq. (5.1) is given by [1, 2],

$$C = \mathbb{E} \left[\log \det \left(\mathbf{I}_N + \frac{\rho}{M} \mathbf{H} \mathbf{H}^H \right) \right] \quad (5.12)$$

where the expectation $\mathbb{E}[\cdot]$ is taken over the random channel coefficients. For the channel of Eq. (5.5), the corresponding ergodic channel capacity is determined by [24, 25]

$$C_{\text{LDC}} = \max_{\mathcal{F}} \frac{1}{2T} \mathbb{E} \left[\log \det \left(\mathbf{I}_{2K} + \frac{\rho}{M} \tilde{\mathcal{H}} \mathcal{F} \mathcal{F}^H \tilde{\mathcal{H}}^H \right) \right] \quad (5.13)$$

where the coding matrix \mathcal{F} is subject to some suitable power constraint. Typically, the total transmission power of the coding matrices is fixed; that is,

$$\sum_{k=1}^K \text{tr}(\mathbf{A}_k \mathbf{A}_k^H + \mathbf{B}_k \mathbf{B}_k^H) = MT \quad (5.14)$$

Now, an important question arises: Under this power constraint, what structure of the coding matrix \mathcal{F} will render the ergodic capacity of the LD coded channel given in Eq. (5.13) equal to that of the original channel given by Eq. (5.12)? The answer is given in the following theorem [52].

Theorem 5.3.1 *Let $K = MT$ (i.e., consider full symbol rate transmission). Then, subject to the power constraint given by Eq. (5.14), \mathcal{F} is capacity-optimal if and only if \mathcal{F} is unitary, or equivalently, $C = C_{\text{LDC}}$ if and only if the following conditions hold*

$$\text{tr}(\mathbf{A}_k \mathbf{A}_{k'}^H + \mathbf{B}_k \mathbf{B}_{k'}^H) = \delta(k - k') \quad (5.15a)$$

$$\text{tr}(\mathbf{B}_k \mathbf{A}_{k'}^H + \mathbf{B}_{k'} \mathbf{A}_k^H) = 0 \quad (5.15b)$$

for $k, k' = 1, 2, \dots, K$, where $\delta(k - k')$ is the Kronecker delta.

Proof. First, we note that the mutual information I between the input vector signal and the output vector signal of the LD coded channel of Eq. (5.5) can be written as

$$\begin{aligned} I &= \frac{1}{2T} \mathbb{E}_{\mathbf{H}} \left[\log \det \left(\mathbf{I} + \frac{\rho}{M} \mathcal{F}^H \tilde{\mathcal{H}}^H \tilde{\mathcal{H}} \mathcal{F} \right) \right] \\ &= \frac{1}{2T} \mathbb{E}_{\mathbf{H}} \left[\log \det \left(\mathbf{I} + \frac{\rho}{M} \tilde{\mathcal{H}} \Phi \tilde{\mathcal{H}}^H \right) \right] \end{aligned} \quad (5.16)$$

where

$$\Phi = \mathcal{F} \mathcal{F}^H \quad (5.17)$$

is a $2MT \times 2MT$ matrix, $\mathbb{E}_{\mathbf{H}}$ denotes that the expected value is taken over all possible channels, \mathbf{H} is the original channel in Eq. (5.1), and we have used the fact that for any matrix \mathbf{W} , $\det(\mathbf{I} + \mathbf{W}^H \mathbf{W}) = \det(\mathbf{I} + \mathbf{W} \mathbf{W}^H)$. Now, applying Fischer inequality [42] that states that for a positive semidefinite matrix its determinant is less than or equal to the product of the determinants of its diagonal block matrices, to the determinant in Eq. (5.16), we have

$$\begin{aligned} &\det \left(\mathbf{I} + \frac{\rho}{M} \tilde{\mathcal{H}} \Phi \tilde{\mathcal{H}}^H \right) \\ &\leq \prod_{t=1}^T \det \left(\mathbf{I} + \frac{\rho}{M} \mathbf{H} \Phi_{tt} \mathbf{H}^H \right) \prod_{t=T+1}^{2T} \det \left(\mathbf{I} + \frac{\rho}{M} \mathbf{H}^* \Phi_{tt} \mathbf{H}^T \right) \end{aligned} \quad (5.18)$$

$$= \prod_{t=1}^T \left(\det \left(\mathbf{I} + \frac{\rho}{M} \mathbf{H} \Phi_{tt} \mathbf{H}^H \right) \right)^2 \quad (5.19)$$

where Φ_{tt} , $t = 1, \dots, 2T$ denote the $M \times M$ diagonal block sub-matrices of Φ and we have used the structure of \mathcal{F} given by Eq. (5.6) in the definition of Φ in Eq. (5.17) so

that $\Phi_{tt} = \Phi_{(T+t)(T+t)}^*$ for $t = 1, 2, \dots, T$. Equality in Eq. (5.18) holds if and only if Φ is itself block-diagonal. Thus, using Eq. (5.19), an achievable upper bound of the mutual information in Eq. (5.16) can be established such that

$$I \leq \frac{1}{T} \sum_{t=1}^T \mathbb{E}_{\mathbf{H}} \left[\log \det \left(\mathbf{I} + \frac{\rho}{M} \mathbf{H} \Phi_{tt} \mathbf{H}^H \right) \right] \quad (5.20)$$

with equality holding if and only if Φ is block-diagonal, i.e.,

$$\Phi_{ij} = \mathbf{0} \quad \text{for } i, j = 1, 2, \dots, T, \quad i \neq j \quad (5.21)$$

We now apply eigen decomposition to each of the positive definite matrices Φ_{tt} such that $\Phi_{tt} = \mathbf{U}_{tt} \Lambda_{tt} \mathbf{U}_{tt}^H$, where \mathbf{U}_{tt} is unitary and Λ_{tt} is nonnegative diagonal. Since \mathbf{H} is independent and identically Gaussian distributed, its stochastic properties will not change if it is right-multiplied by any unitary matrix [43], that is,

$$\begin{aligned} & \frac{1}{T} \sum_{t=1}^T \mathbb{E}_{\mathbf{H}} \left[\log \det \left(\mathbf{I} + \frac{\rho}{M} \mathbf{H} \Phi_{tt} \mathbf{H}^H \right) \right] \\ &= \frac{1}{T} \sum_{t=1}^T \mathbb{E}_{\mathbf{H}} \left[\log \det \left(\mathbf{I} + \frac{\rho}{M} \mathbf{H} \Lambda_{tt} \mathbf{H}^H \right) \right] \end{aligned} \quad (5.22)$$

Furthermore, we note that the function $\log \det(\cdot)$ is concave over the set of positive definite matrices [42]. Therefore, applying Jensen's inequality [44], which states that for any convex function $f(x)$, and for $x_1, \dots, x_N \in \mathcal{D}_x$ where \mathcal{D}_x is the domain of x , we have $\frac{1}{N} \sum_{n=1}^N f(x_n) \geq f(\frac{1}{N} \sum_{n=1}^N x_n)$, with equality holding if and only if all x_n are equal, yields

$$\begin{aligned} & \frac{1}{T} \sum_{t=1}^T \mathbb{E}_{\mathbf{H}} \left[\log \det \left(\mathbf{I} + \frac{\rho}{M} \mathbf{H} \Lambda_{tt} \mathbf{H}^H \right) \right] \\ & \leq \mathbb{E}_{\mathbf{H}} \left[\log \det \left(\mathbf{I} + \frac{\rho}{M} \mathbf{H} \Lambda \mathbf{H}^H \right) \right] \end{aligned} \quad (5.23)$$

where we have denoted $\Lambda = \frac{1}{T} \sum_{t=1}^T \Lambda_{tt}$. Equality in Eq. (5.23) holds if and only if all Λ_{tt} are equal, that is,

$$\Lambda_{tt} = \Lambda \quad \text{for } t = 1, 2, \dots, T \quad (5.24)$$

Here, we note that there are M eigenvalues in each Λ_{tt} and that there are $M!$ ways of permuting them. Utilizing a similar technique to that in [1] such that multiplying Λ_{tt} by any of the $M!$ permutation matrices \mathbf{P}_i and averaging over the $M!$ possible ways of permuting, the expectation in Eq. (5.22) remains unchanged, i.e.,

$$\begin{aligned} & \mathbb{E}_{\mathbf{H}} \left[\log \det \left(\mathbf{I} + \frac{\rho}{M} \mathbf{H} \Lambda \mathbf{H}^H \right) \right] \\ &= \frac{1}{M!} \sum_{i=1}^{M!} \mathbb{E}_{\mathbf{H}} \left[\log \det \left(\mathbf{I} + \frac{\rho}{M} \mathbf{H} \mathbf{P}_i \Lambda \mathbf{P}_i^H \mathbf{H}^H \right) \right]. \end{aligned} \quad (5.25)$$

Again, employing the concavity of function $\log \det(\cdot)$ and Jensen's inequality to Eq. (5.25) yields

$$\begin{aligned} & \frac{1}{M!} \sum_{i=1}^{M!} \mathbb{E}_{\mathbf{H}} \left[\log \det \left(\mathbf{I} + \frac{\rho}{M} \mathbf{H} \mathbf{P}_i \Lambda \mathbf{P}_i^H \mathbf{H}^H \right) \right] \\ & \leq \mathbb{E}_{\mathbf{H}} \left[\log \det \left(\mathbf{I} + \frac{\rho}{M} \mathbf{H} \mathbf{H}^H \right) \right] \end{aligned} \quad (5.26)$$

where we have used the fact that $\frac{1}{M!} \sum_{i=1}^{M!} \mathbf{P}_i \Lambda \mathbf{P}_i^H = \mathbf{I}$. We note that the right side of Eq. (5.26) is independent of the design parameter and is equal to the capacity of the original channel model of Eq. (5.12). The upper bound in Eq. (5.26) is reached if and only if all $\mathbf{P}_i \Lambda \mathbf{P}_i$ are equal to each other since $\mathbf{H}^H \mathbf{H}$ or $\mathbf{H} \mathbf{H}^H$ is non-singular with probability one [43], i.e., for $i = 1, \dots, M!$,

$$\mathbf{P}_i \Lambda \mathbf{P}_i^H = \mathbf{I} \quad (5.27)$$

Finally, combining Eqs. (5.20), (5.23) with (5.26) leads to

$$I \leq \mathbb{E}_{\mathbf{H}} \left[\log \det \left(\mathbf{I} + \frac{\rho}{M} \mathbf{H}^H \mathbf{H} \right) \right] \quad (5.28)$$

where the equality in Eq. (5.28) holds (i.e., $C_{\text{LDC}} = C$) if and only if the three conditions of Eqs. (5.21), (5.24) and (5.27) are met simultaneously. This is equivalent to the fact that \mathcal{F} is unitary. \square

Remarks on Theorem 5.3.1:

1. Theorem 5.3.1 provides us with the necessary and sufficient condition for the capacity of the LD coded channel to remain the same as that of the original channel when $K = MT$. That condition is fulfilled when \mathcal{F} is unitary. Since \mathcal{F} contains all the coding matrices \mathbf{A}_k and \mathbf{B}_k , we describe this unitary structure of \mathcal{F} as *inter-unitary* and therefore, to maintain information lossless transmission employing LD codes in MIMO communications, the code design should strive for such a structure. In fact, that the condition of \mathcal{F} being unitary is sufficient for information lossless transmission has been shown by Hassibi and Hochwald [24] as well as Heath and Paulraj [25]. However, in the proof presented here, we have shown that the condition is both necessary and sufficient because the inequalities used are satisfied *if and only if* the conditions are fulfilled.
2. When $K \neq MT$, e.g., in the case when there are more transmitter antennas than receiver antennas, we often choose to transmit at a lower rate to accommodate a simpler structure of the receiver, then $K < MT$ and \mathcal{F} becomes a $2MT \times 2K$ “tall” matrix. When this is the case, Eq. (5.13) can no longer be guaranteed to be equal to Eq. (5.12) even though the condition of $\mathcal{F}^H \mathcal{F} = \mathbf{I}$ holds.

5.3.2 A detection error viewpoint

In this section, we examine the use of an LD code in a MIMO environment from the point of view of detection. We establish a structure of the code necessary to minimize the detection error. For the development of the analysis, we first put forward the following assumptions:

1. The signal vector \mathbf{s} is normalized so that $E[\mathbf{s}\mathbf{s}^H] = \mathbf{I}_K$ and its elements are uncoded and are equally likely signaling points from a fixed constellation;
2. The channel coefficients $h_{m,n}$ are samples of circularly symmetric zero-mean complex white Gaussian random variables with unit variances and are fixed during one time frame (T time slots) but may change independently from one time frame to the next;
3. ξ is circularly symmetric complex Gaussian noise with covariance matrix \mathbf{I} ;
4. Complete channel state information is available at the receiver and maximum likelihood (ML) detection is employed.

On the basis of these assumptions, given a channel realization \mathbf{H} , we can evaluate the probability of transmitting \mathbf{s} and deciding in favor of $\mathbf{s}' \neq \mathbf{s}$ at the ML detector such that

$$P(\mathbf{s} \rightarrow \mathbf{s}' | \mathbf{H}) = Q\left(\frac{d(\mathbf{s}, \mathbf{s}')}{2}\right), \quad \mathbf{s} \neq \mathbf{s}' \quad (5.29)$$

where $Q(z) = (1/\sqrt{2\pi}) \int_z^\infty e^{-\zeta^2/2} d\zeta$ and $d(\mathbf{s}, \mathbf{s}')$ is the Euclidean distance between the received code words $\mathcal{HF}\mathbf{s}$ and $\mathcal{HF}\mathbf{s}'$; i.e.,

$$d^2(\mathbf{s}, \mathbf{s}') = \frac{\rho}{M} \operatorname{tr} \left[\Sigma^H(\mathbf{s} - \mathbf{s}') \mathbf{H}^H \mathbf{H} \Sigma(\mathbf{s} - \mathbf{s}') \right] \quad (5.30)$$

where $\Sigma(\cdot)$ is defined in Eq. (5.2). To evaluate this probability, it is convenient to use the following alternative expression for the Q -function [45], [46]

$$Q(z) = \frac{1}{\pi} \int_0^{\pi/2} \exp\left(-\frac{z^2}{2 \sin^2 \theta}\right) d\theta \quad (5.31)$$

Also, utilizing the property of trace [39], we can rewrite Eq. (5.30) as

$$d^2(\mathbf{s}, \mathbf{s}') = \frac{\rho}{M} [\operatorname{vec}(\mathbf{H})]^H \left[\Sigma^*(\mathbf{e}) \Sigma^T(\mathbf{e}) \otimes \mathbf{I}_N \right] \operatorname{vec}(\mathbf{H}) \quad (5.32)$$

where $\mathbf{e} = \mathbf{s} - \mathbf{s}'$. By substituting Eqs. (5.31) and (5.32) into Eq. (5.29) and then taking the average over the random vector $\operatorname{vec}(\mathbf{H})$ whose statistics are given in Assumption 2) above, the average pairwise error probability at the ML detector can be written as

$$P(\mathbf{s} \rightarrow \mathbf{s}') = \frac{1}{\pi} \int_0^{\pi/2} \frac{d\theta}{\det \left(\mathbf{I}_M + \frac{\rho}{8M \sin^2 \theta} \Sigma(\mathbf{e}) \Sigma^H(\mathbf{e}) \right)^N} \quad (5.33)$$

Eq. (5.33) expresses the exact probability of the pairwise error. From this expression, since $|\sin \theta| \leq 1$, we can obtain the Chernoff bound such that

$$P(\mathbf{s} \rightarrow \mathbf{s}') \leq \frac{1}{2} \det \left(\mathbf{I}_M + \frac{\rho}{8M} \Sigma(\mathbf{e}) \Sigma^H(\mathbf{e}) \right)^{-N} \quad (5.34)$$

The pairwise error probability can be employed as a design criterion to obtain good space-time codes. Indeed, several authors have made use of the Chernoff bound to arrive at

general guidelines for designing good codes [47, 4]. We note that

$$\begin{aligned} \det \left(\mathbf{I}_N + \frac{\rho}{8M} \boldsymbol{\Sigma}(\mathbf{e}) \boldsymbol{\Sigma}^H(\mathbf{e}) \right)^{-N} &\leq \prod_{m=1}^M \left(1 + \frac{\rho}{8M} \cdot \lambda_m \right)^{-N} \\ &\leq \prod_{m=1}^r \left(\frac{\rho}{8M} \cdot \lambda_m \right)^{-N} = \left(\frac{\rho}{8M} \right)^{-rN} \left(\prod_{m=1}^r \lambda_m \right)^{-N} \end{aligned} \quad (5.35)$$

where r ($\leq M$) is the rank, and $\{\lambda_m\}, m = 1, \dots, r$ are the nonzero eigenvalues of the matrix $\boldsymbol{\Sigma}(\mathbf{e}) \boldsymbol{\Sigma}^H(\mathbf{e})$. To arrive at a code that may keep the Chernoff bound in Eq. (5.34) low, we must examine the two terms in Eq. (5.35):

- The Rank Criterion: At high SNR, the first term in Eq. (5.35) dominates and therefore, to keep the Chernoff bound in Eq. (5.34) as low as possible, we should make the exponent part rN as large as possible. The minimum rank of $\boldsymbol{\Sigma}(\mathbf{e}) = \boldsymbol{\Sigma}(\mathbf{s}) - \boldsymbol{\Sigma}(\mathbf{s}')$ taken over all distinct pairs $\{\mathbf{s}, \mathbf{s}'\}$ is the diversity gain and should be maximized, that is, the matrix $\boldsymbol{\Sigma}(\mathbf{e}) \boldsymbol{\Sigma}^H(\mathbf{e})$ should be of full rank. Thus, maximum diversity or *full diversity* is, therefore, equal to MN if number of channel used $T \geq M$.
- The Determinant Criterion: The second term consists of the product of the nonzero eigenvalues of $\boldsymbol{\Sigma}(\mathbf{e}) \boldsymbol{\Sigma}^H(\mathbf{e})$. The value of $(\prod_{m=1}^r \lambda_m)^{1/r}$, taken over all distinct symbol vector pairs $\{\mathbf{s}, \mathbf{s}'\}$, is called the *coding gain* and must be maximized.

Thus, to achieve good pairwise error probability, we should design a code such that the matrix $\boldsymbol{\Sigma}(\mathbf{e}) \boldsymbol{\Sigma}^H(\mathbf{e})$ is of full rank and the minimum product of its eigenvalues [47, 4] is maximized.

In the following, we further carry out the exploration of a good code by first establishing the lower bound of the worst-case exact pairwise error probability and then by considering the necessary code structure for the lower bound to be reached. To do that, we first introduce the following definition.

Definition 5.3.2 Let s be an element of \mathbf{s} . Then, the minimum distance of the constellation \mathcal{S} is defined as

$$d_{\min}(\mathcal{S}) = \min_{s, s' \in \mathcal{S}, s \neq s'} |s - s'| \quad (5.36)$$

Now we formally state the following theorem on the universal lower bound of the worst-case pairwise error probability for any linear dispersion code [41]:

Theorem 5.3.3 Let \mathcal{S}_{re} and \mathcal{S}_{im} denote two constellations consisting of, respectively, the real and the imaginary parts of the elements in constellation \mathcal{S} . If \mathcal{S} satisfies the following geometrical property,

$$d_{\min}(\mathcal{S}) = d_{\min}(\mathcal{S}_{\text{re}}) = d_{\min}(\mathcal{S}_{\text{im}}) \quad (5.37)$$

then, for any LD code \mathcal{F} with a power budget $\text{tr}(\mathcal{F}\mathcal{F}^H) \leq MT$, the worst-case pairwise error probability of the ML detector is lower bounded by

$$\max_{s, s' \in \mathcal{S}^K, s \neq s'} P_{\mathcal{F}}(s \rightarrow s') \geq J \left(\frac{\rho T d_{\min}^2(\mathcal{S})}{8MK} \right) \quad (5.38)$$

where $J(a)$ is given by

$$J(a) = \frac{1}{\pi} \int_0^{\pi/2} \left(1 + \frac{a}{\sin^2 \theta}\right)^{-MN} d\theta \quad \text{for } a > 0 \quad (5.39)$$

Furthermore, a necessary condition for the lower bound to be achieved is that the pair of matrices, \mathbf{A}_k and \mathbf{B}_k , associated with each individual symbol must satisfy the following conditions

$$\mathbf{A}_k \mathbf{A}_k^H + \mathbf{B}_k \mathbf{B}_k^H = \frac{T}{K} \mathbf{I}_M \quad (5.40a)$$

$$\mathbf{A}_k \mathbf{B}_k^H + \mathbf{B}_k \mathbf{A}_k^H = \mathbf{0} \quad (5.40b)$$

Proof. Let the $M \times M$ coding matrices be defined such that $\mathbf{F}_k = \mathbf{A}_k + \mathbf{B}_k$ and $\mathbf{F}_{K+k} = j(\mathbf{A}_k - \mathbf{B}_k)$ for $k = 1, 2, \dots, K$. Then,

$$\begin{pmatrix} \mathbf{A}_k \\ \mathbf{B}_k \end{pmatrix} = \frac{1}{\sqrt{2}} \mathbf{T}^* \begin{pmatrix} \mathbf{F}_k \\ \mathbf{F}_{K+k} \end{pmatrix} \quad (5.41)$$

where \mathbf{T} is the transformation matrix given by Eq. (5.9). With this relationship, it is easy to verify that the conditions in Eq. (5.40) are equivalent to:

$$\mathbf{F}_k \mathbf{F}_k^H = \frac{T}{K} \mathbf{I}_M \quad (5.42a)$$

$$\text{and} \quad \mathbf{F}_{K+k} \mathbf{F}_{K+k}^H = \frac{T}{K} \mathbf{I}_M \quad (5.42b)$$

Let us consider the case when the error is such that $|e_{k'}| = d_{\min}(\mathcal{S})$ and $e_k = 0$, $k = 1, 2, \dots, K$, $k \neq k'$, the denominator in the integral of Eq. (5.33) can be written as

$$\det \left(\mathbf{I} + \frac{\rho \Sigma_{\mathcal{F}}(\mathbf{e}) \Sigma_{\mathcal{F}}^H(\mathbf{e})}{8M \sin^2 \theta} \right) = \det \left(\mathbf{I} + \frac{\rho d_{\min}^2(\mathcal{S}) \mathbf{F}_{k'} \mathbf{F}_{k'}^H}{8M \sin^2 \theta} \right) \quad (5.43)$$

Using Hardamard's inequality [42] and then employing the relationship between the arithmetic mean and the geometrical mean, we have

$$\begin{aligned} \det \left(\mathbf{I} + \frac{\rho d_{\min}^2(\mathcal{S}) \mathbf{F}_{k'} \mathbf{F}_{k'}^H}{8M \sin^2 \theta} \right) &\leq \prod_{\ell=1}^M \left(1 + \frac{\rho d_{\min}^2(\mathcal{S}) [\mathbf{F}_{k'} \mathbf{F}_{k'}^H]_{\ell\ell}}{8M \sin^2 \theta} \right) \\ &\leq \left(1 + \frac{\rho d_{\min}^2(\mathcal{S}) \text{tr}(\mathbf{F}_{k'} \mathbf{F}_{k'}^H)}{8M^2 \sin^2 \theta} \right)^M \end{aligned} \quad (5.44)$$

where, respectively, equalities in the first and second parts of Eq. (5.44) hold if and only if:

- (i) $\mathbf{F}_{k'} \mathbf{F}_{k'}^H$ is a diagonal matrix, and
- (ii) $[\mathbf{F}_{k'} \mathbf{F}_{k'}^H]_{\ell\ell} = [\mathbf{F}_{k'} \mathbf{F}_{k'}^H]_{mm}$, for $\ell, m = 1, 2, \dots, M$.

The upper bound on the right side of Eq. (5.44) is still a function of the design parameters $\mathbf{F}_{k'}$. Now, if in particular, this coding matrix is the one that has been allocated the minimum power among all the coding matrices $\{\mathbf{F}_k\}$, that is, let \mathbf{F}_{m0} be the coding matrix such that $\text{tr}(\mathbf{F}_{m0}\mathbf{F}_{m0}^H) = \min [\text{tr}(\mathbf{F}_k\mathbf{F}_k^H)], 1 \leq k \leq 2K$, we then have

$$\text{tr}(\mathbf{F}_{m0}\mathbf{F}_{m0}^H) \leq \frac{1}{2K} \sum_{k=1}^{2K} \text{tr}(\mathbf{F}_k\mathbf{F}_k^H) = \frac{MT}{K} \quad (5.45)$$

where the last part of Eq. (5.45) is due to the power constraint. Equality in (5.45) holds if and only if the following condition is satisfied

$$\text{tr}(\mathbf{F}_k\mathbf{F}_k^H) = \frac{MT}{K} \quad \text{for } k = 1, 2, \dots, 2K \quad (5.46)$$

Combining Eq. (5.45) with the upper bound on the right side of (5.44) yields

$$\left(1 + \frac{\rho d_{\min}^2(\mathcal{S}) \text{tr}(\mathbf{F}_{m0}\mathbf{F}_{m0}^H)}{8M^2 \sin^2 \theta}\right)^M \leq \left(1 + \frac{\rho T d_{\min}^2(\mathcal{S})}{8MK \sin^2 \theta}\right)^M \quad (5.47)$$

for which equality holds if and only if the condition in Eq. (5.46) holds.

The upper bound in Eq. (5.47) is now independent of the design parameter and is therefore the maximum value attainable by $\det(\mathbf{I} + \frac{\rho d_{\min}^2(\mathcal{S}) \mathbf{F}_{m0}\mathbf{F}_{m0}^H}{8M^2 \sin^2 \theta})$ for the coding matrix allocated the lowest power. On the other hand, we note that Conditions (i) and (ii) above as well as Eq. (5.46) are simultaneously satisfied if

$$\mathbf{F}_{k'}\mathbf{F}_{k'}^H = \frac{T}{K}\mathbf{I}_M \quad \text{for } k' = 1, 2, \dots, 2K \quad (5.48)$$

which, because of the fact that Conditions (i) and (ii) are met, will render the upper bound on the right side of Eq. (5.44) attainable for all the coding matrices $\mathbf{F}_k, k = 1, \dots, 2K$. As stated before (see Eqs. (5.42)), these conditions of Eq. (5.48) are equivalent to the condition that $\mathbf{A}_m\mathbf{A}_m^H + \mathbf{B}_m\mathbf{B}_m^H = \frac{T}{K}\mathbf{I}_M$ and $\mathbf{A}_m\mathbf{B}_m^H + \mathbf{B}_m\mathbf{A}_m^H = \mathbf{0}$. Hence, by substituting this upper bound value in Eq. (5.47) into Eq. (5.33), the probability of the particular case of error when $|e_m| = d_{\min}(\mathcal{S})$ and $e_k = 0, k = 1, 2, \dots, K, k \neq m$ is lower bounded by $J\left(\frac{\rho T d_{\min}^2(\mathcal{S})}{8MK}\right)$.

Therefore, we can conclude that the *worst-case* pairwise error probability is bounded by¹

$$\max_{\mathbf{s}, \mathbf{s}' \in \mathcal{S}^K, \mathbf{s} \neq \mathbf{s}'} P_{\mathcal{F}}(\mathbf{s} \rightarrow \mathbf{s}') \geq J\left(\frac{\rho T d_{\min}^2(\mathcal{S})}{8MK}\right)$$

□

Theorem 5.3.3 establishes from a detection viewpoint that *each individual code matrix of a good LD code should also have an intra-unitary structure*. We would like to make the following comments on Theorem 5.3.3:

¹We note that a similar lower bound for a *linear space-time block code* based on the Chernoff bound was given in [48].

1. The square q -ary QAM satisfies Condition (5.37), whereas the standard q -ary PSK $\{\exp(\frac{2k\pi j}{q})\}_{k=0}^{q-1}$ does not.
2. Although the constellation for LD codes is limited to satisfy Condition (5.37), from the proof of Theorem 5.3.3, we see that in linear STBC case, Theorem 5.3.3 is true for any constellation.
3. Conditions (5.40) is necessary but not sufficient. For example, when $M = N = 2$, $\mathbf{B}_k = \mathbf{0}$ for $k = 1, 2, 3, 4$ and $\mathbf{A}_1 = \begin{pmatrix} 1 & 0 \\ 0 & 1 \end{pmatrix}$, $\mathbf{A}_2 = \begin{pmatrix} 1 & 0 \\ 0 & -1 \end{pmatrix}$, $\mathbf{A}_3 = \begin{pmatrix} 0 & 1 \\ 1 & 0 \end{pmatrix}$, $\mathbf{A}_4 = \begin{pmatrix} 0 & -1 \\ 1 & 0 \end{pmatrix}$, the resulting coding signal matrix $\Sigma(\mathbf{s}) = \begin{pmatrix} s_1 + s_2 & s_3 - s_4 \\ s_3 + s_4 & s_1 - s_2 \end{pmatrix}$ cannot provide full diversity and thus cannot achieve the lower bound (5.38) either.
4. It can be verified that under the condition of an allowable symbol rate, the orthogonal STBCs achieve the lower bound (5.38). In Section 5.7, we will design a family of high symbol rate linear STBCs achieving this lower bound.

5.4 Trace-orthogonal LD Codes

Theorem 5.3.1 and Theorem 5.3.3 in the previous section together suggest that from both the information-theoretic and the detection error viewpoints, we should strive for both inter-unitary and intra-unitary structures in the design of an LD code. We call such structures of an LD code *trace orthogonality* [40, 49, 41].

5.4.1 Trace orthogonality

Let us now give a formal definition of a trace-orthogonal code:

Definition 5.4.1 Let $T \geq M$. A sequence of $M \times T$ matrices \mathbf{A}_k and \mathbf{B}_k , $k = 1, 2, \dots, K$ and $K \leq MT$, is said to constitute a trace-orthogonal LD code if the following conditions are satisfied,

$$\mathbf{A}_k \mathbf{A}_k^H + \mathbf{B}_k \mathbf{B}_k^H = \frac{T}{K} \mathbf{I}_M \quad (5.49a)$$

$$\mathbf{A}_k \mathbf{B}_k^H + \mathbf{B}_k \mathbf{A}_k^H = \mathbf{0} \quad (5.49b)$$

$$\text{tr} \left(\mathbf{A}_k \mathbf{A}_{k'}^H + \mathbf{B}_{k'} \mathbf{B}_k^H \right) = \frac{MT}{K} \delta(k - k') \quad (5.49c)$$

$$\text{tr} \left(\mathbf{B}_k \mathbf{A}_{k'}^H + \mathbf{B}_{k'} \mathbf{A}_k^H \right) = 0 \quad (5.49d)$$

for $k, k' = 1, 2, \dots, K$. Particularly when $K = MT$, it is said to constitute a trace-orthogonal LD code of full transmission symbol rate.

We would like to make the following remarks on the trace-orthogonal LD codes.

1. The conditions for designing *complex orthogonal space-time block codes* are [5, 18, 16, 6, 17]:

$$\begin{aligned}\mathbf{A}_k \mathbf{A}_{k'}^H + \mathbf{B}_{k'} \mathbf{B}_k^H &= \frac{T}{K} \delta(k - k') \mathbf{I}_M \\ \mathbf{B}_k \mathbf{A}_{k'}^H + \mathbf{B}_{k'} \mathbf{A}_k^H &= \mathbf{0}\end{aligned}$$

These conditions imply but are not implied by, Eqs. (5.49a), (5.49c) and (5.49d). Therefore, we can say that trace-orthogonal LD codes are a generalization of orthogonal complex space-time block codes.

2. The space-time codes in [26, 27] are trace-orthogonal linear STBCs.
3. Eqs. (5.49c) and (5.49d) are equivalent to \mathcal{F} being column-wise orthonormal unitary and thus, as shown in Theorem 5.3.1 in the previous section, a trace-orthogonal full dimension LD code is information lossless [25, 24, 50].
4. Eqs. (5.49a) and (5.49b) ensure that the LD code satisfies the necessary conditions of being intraunitary as required in Theorem 5.3.3 in the previous section.
5. The conditions of Eqs. (5.49a)–(5.49d) ensure that the output signal power of each symbol after super-channel matrix $\tilde{\mathcal{H}}\mathcal{F}$ is evenly distributed and, at the same time, also ensure that the output noise power or the interference and noise power of each subchannel after the linear equalizer (zero-forcing or minimum mean square error) are evenly distributed if $N \geq M$ and $K = MT$ [51, 41, 53].

5.4.2 Optimality of trace-orthogonal LD codes from a linear MMSE receiver viewpoint

We now proceed to examine trace-orthogonal codes from a point of view of using a linear minimum mean square error (MMSE) receiver. We consider the transmission of a full rate LD code in a MIMO system with $N \geq M$. For such a communication channel model as in Eq. (5.10), an MMSE equalizer is given by [54]

$$\mathcal{G} = \sqrt{\frac{\rho}{M}} \left(\mathbf{I}_{2MT} + \frac{\rho}{M} \mathbf{T}^H \mathcal{F}^H \tilde{\mathcal{H}}^H \tilde{\mathcal{H}} \mathcal{F} \mathbf{T} \right)^{-1} \mathbf{T}^H \mathcal{F}^H \tilde{\mathcal{H}}^H \quad (5.50)$$

In this case, the signal to the interference and noise ratio (SINR) at the receiver of the k th subchannel can be shown to be [54]

$$\rho_k = \frac{1}{[\mathbf{P}]_{kk}} - 1 \quad (5.51)$$

where

$$\mathbf{P} = \left(\mathbf{I}_{2TM} + \frac{\rho}{M} \mathbf{T}^H \mathcal{F}^H \tilde{\mathcal{H}}^H \tilde{\mathcal{H}} \mathcal{F} \mathbf{T} \right)^{-1} \quad (5.52)$$

In order to determine the bit error rate (BER) for such a receiver, we must specify a particular signal constellation. For convenience of analysis, we specify that our transmitted

symbols are selected randomly from a QPSK set and that all symbols are equally likely. Then, the BER of the k th subchannel is given by

$$P_{ek}(\mathbf{H}, \mathcal{F}) = Q(\sqrt{\rho_k}) \quad (5.53)$$

where $Q(z) = \frac{1}{\sqrt{2\pi}} \int_z^\infty \exp(-\zeta^2/2) d\zeta$ and ρ_k is the SINR of the k th subchannel. The average BER for all subchannels of the MMSE detector is thus

$$P_e(\mathbf{H}, \mathcal{F}) = \frac{1}{2MT} \sum_{k=1}^{2MT} Q(\sqrt{\rho_k}) \quad (5.54)$$

Therefore, taking the average over all random channel coefficients yields

$$P_e(\mathcal{F}) = \frac{1}{2MT} \sum_{k=1}^{2MT} E[Q(\sqrt{\rho_k})] \quad (5.55)$$

We now seek to design an LD code such that the average bit error probability in Eq. (5.55) is minimized, which can be formally formulated as the following optimization problem:

$$\mathcal{F}_{\text{opt}} = \arg \min_{\text{tr}(\mathcal{F}^H \mathcal{F}) \leq MT} P_e(\mathcal{F})$$

To solve this problem, we introduce the following lemma [55]:

Lemma 5.4.2 *The function $G(x)$ defined by*

$$G(x) = Q(\sqrt{x^{-1} - 1}) \quad (5.56)$$

is convex in an interval $0 < x \leq 1$.

Lemma 5.4.2 can easily be proved by showing $d^2G(x)/dx^2$ to be positive in the range of values of x . From Eq. (5.52), $\mathbf{P}^{-1} = (\mathbf{I}_{2TM} + \frac{\rho}{2M} \mathbf{T}^H \mathcal{F}^H \tilde{\mathcal{H}}^H \tilde{\mathcal{H}} \mathcal{F} \mathbf{T}) \succeq \mathbf{I}_{2MT}$, $\mathbf{P} \preceq \mathbf{I}_{2MT}$ and as a result, $0 < [\mathbf{P}]_{kk} \leq 1$. Using this fact in Lemma 5.4.2, we can apply Jensen's inequality [44] to the function $G(x)$ in Eq. (5.55) and obtain that

$$\frac{1}{2MT} \sum_{k=1}^{2MT} G([\mathbf{P}]_{kk}) \geq G\left(\frac{\text{tr}(\mathbf{P})}{2MT}\right) \quad (5.57)$$

where equality in Eq. (5.57) holds if and only if

$$[\mathbf{P}]_{11} = [\mathbf{P}]_{22} = \dots = [\mathbf{P}]_{(2MT)(2MT)} \quad (5.58)$$

To arrive at an expression of $\text{tr}(\mathbf{P})$ in Eq. (5.57) in terms of the original channel matrix \mathbf{H} for the design parameter \mathcal{F} , we introduce the following two lemmas to facilitate the manipulation of the trace of a matrix:

Lemma 5.4.3 *For an $M \times M$ matrix \mathbf{Q} , and a non-singular $M \times M$ matrix \mathbf{Y} , we have*

$$\text{tr}[(\mathbf{I} + \mathbf{Y}^H \mathbf{Q} \mathbf{Y})^{-1}] = \text{tr}[(\mathbf{I} + \mathbf{Q} \mathbf{Y} \mathbf{Y}^H)^{-1}] \quad (5.59)$$

Proof. Since $\mathbf{I} = \mathbf{Y}^H \mathbf{Y}^{-H}$, the left side of Eq. (5.59) can be written as

$$\text{tr}[(\mathbf{Y}^{-H} + \mathbf{Q}\mathbf{Y})^{-1}\mathbf{Y}^{-H}] = \text{tr}[\mathbf{Y}^{-H}(\mathbf{Y}^{-H} + \mathbf{Q}\mathbf{Y})^{-1}] = \text{tr}[(\mathbf{I} + \mathbf{Q}\mathbf{Y}\mathbf{Y}^H)^{-1}]$$

where we have used the property [42] that moving the matrices circularly does not change the value of the trace. \square

Lemma 5.4.4 *For any positive definite matrix [42]*

$$\mathbf{Z} = \begin{bmatrix} \mathbf{Z}_{11} & \mathbf{Z}_{12} \\ \mathbf{Z}_{12}^H & \mathbf{Z}_{22} \end{bmatrix}$$

we have

$$\text{tr}[\mathbf{Z}^{-1}] \geq \text{tr}[\mathbf{Z}_{11}^{-1}] + \text{tr}[\mathbf{Z}_{22}^{-1}]$$

where equality holds if and only if $\mathbf{Z}_{12} = \mathbf{0}$, that is, \mathbf{Z} is block diagonal.

Applying Lemma 5.4.3 to the error covariance matrix \mathbf{P} in Eq. (5.52) yields

$$\text{tr}(\mathbf{P}) = \text{tr}\left(\left(\mathbf{I}_{2MT} + \frac{\rho}{M}(\mathbf{I} \otimes \tilde{\mathcal{H}}^H \tilde{\mathcal{H}})\mathcal{F}\mathcal{F}^H\right)^{-1}\right) \quad (5.60)$$

Furthermore, letting $\Phi = \mathcal{F}\mathcal{F}^H$ and applying Lemma 5.4.4 to it on Eq. (5.60), we have

$$\begin{aligned} \text{tr}(\mathbf{P}) &\geq \sum_{t=1}^T \text{tr}\left(\left(\mathbf{I}_M + \frac{\rho}{M}\mathbf{H}^H \mathbf{H}\Phi_{tt}\right)^{-1}\right) \\ &\quad + \sum_{t=1}^T \text{tr}\left(\left(\mathbf{I}_M + \frac{\rho}{M}\mathbf{H}^T \mathbf{H}^*\Phi_{(T+t)(T+t)}\right)^{-1}\right) \end{aligned} \quad (5.61)$$

$$= 2 \sum_{t=1}^T \text{tr}\left(\left(\mathbf{I}_M + \frac{\rho}{M}\mathbf{H}^H \mathbf{H}\Phi_{tt}\right)^{-1}\right) \quad (5.62)$$

where Φ_{tt} for $t = 1, \dots, 2T$ are $M \times M$ matrices on the diagonal of Φ and in Eq. (5.62), again we have used the fact that $\Phi_{tt} = \Phi_{(T+t)(T+t)}^*$ for $t = 1, 2, \dots, T$ according to the definition of \mathcal{F} given by Eq. (5.6). Equality in Eq. (5.61) holds if and only if Φ is block diagonal; i.e.,

$$\Phi_{ij} = \mathbf{0} \quad \text{for } i, j = 1, 2, \dots, T, \quad i \neq j \quad (5.63)$$

Now, since $\text{tr}(\mathbf{P}^{-1})$ is convex with respect to positive definite matrix \mathbf{P} [42], applying Jensen's inequality to this convex function and employing Lemma 5.4.3 lead to

$$\frac{1}{T} \sum_{t=1}^T \text{tr}\left(\left(\mathbf{I}_M + \frac{\rho}{M}\mathbf{H}^H \mathbf{H}\Phi_{tt}\right)^{-1}\right) \geq \text{tr}\left(\left(\mathbf{I}_M + \frac{\rho}{M^2}\mathbf{H}^H \mathbf{H}\Psi\right)^{-1}\right) \quad (5.64)$$

where matrix Ψ is defined by

$$\Psi = \frac{1}{T} \sum_{k=1}^T \Phi_{tt} \quad (5.65)$$

Equality in Eq. (5.64) holds if and only if all Φ_{tt} are equal to each other, i.e.,

$$\Phi_{tt} = \Psi \quad \text{for } t = 1, 2, \dots, T \quad (5.66)$$

Using the results in Eqs. (5.61) through (5.66), we can establish a new lower bound for the right-hand side of Eq. (5.57) (and hence for Eq. (5.55)) such that

$$P_e(\mathcal{F}) \geq \mathbb{E}_{\mathbf{H}} \left[G \left(\frac{\text{tr}((\mathbf{I}_M + \frac{\rho}{M} \mathbf{H}^H \mathbf{H} \Psi)^{-1})}{M} \right) \right] \quad (5.67)$$

where, under our assumptions, Ψ is a positive definite matrix and can be decomposed such that $\Psi = \mathbf{U}_\Psi \Lambda_\Psi \mathbf{U}_\Psi^H$ where \mathbf{U}_Ψ is the unitary eigenvector matrix and Λ_Ψ is the diagonal eigenvalue (positive) matrix. Since the channel matrix \mathbf{H} is independently identically Gaussian distributed, for which the stochastic properties will not change when postmultiplied by a unitary eigenvector matrix [43], thus, the unitary eigenvector matrices have no bearing on the average value over the random channels and can be ignored. Furthermore, following a similar argument to the one in the proof of Theorem 5.3.1 in the previous section (adopted from a strategy in [1]), we note that there are $M!$ ways of permuting the columns of the channel matrix \mathbf{H} by postmultiplying each time with a permutation (unitary) matrix $\Pi_k, k = 1, \dots, M!$ without changing the average value of the matrix and, we can average these $M!$ convex functions of permuted matrices yielding

$$\begin{aligned} & \mathbb{E}_{\mathbf{H}} \left[G \left(\frac{\text{tr}((\mathbf{I}_M + \frac{\rho}{M} \mathbf{H}^H \mathbf{H} \Lambda_\Psi)^{-1})}{M} \right) \right] \\ &= \frac{1}{M!} \sum_{k=1}^{M!} \mathbb{E}_{\mathbf{H}} \left[G \left(\frac{\text{tr}((\mathbf{I}_M + \frac{\rho}{M} \mathbf{H}^H \mathbf{H} \Pi_k \Lambda_\Psi \Pi_k^H)^{-1})}{M} \right) \right] \end{aligned} \quad (5.68)$$

Using Jensen's inequalities, on the convex function $G(\cdot)$ on the right side of Eq. (5.68) and then, again on the convex function $\text{tr}(\mathbf{P}^{-1})$ inside the summation sign yield

$$\begin{aligned} & \frac{1}{M!} \sum_{k=1}^{M!} \mathbb{E}_{\mathbf{H}} \left[G \left(\frac{\text{tr}((\mathbf{I}_M + \frac{\rho}{M} \mathbf{H}^H \mathbf{H} \Pi_k \Lambda_\Psi \Pi_k^H)^{-1})}{M} \right) \right] \\ & \geq \mathbb{E}_{\mathbf{H}} \left[G \left(\frac{1}{MM!} \sum_{k=1}^{M!} \text{tr} \left((\mathbf{I}_M + \frac{\rho}{M} \mathbf{H}^H \mathbf{H} \Pi_k \Lambda_\Psi \Pi_k^H)^{-1} \right) \right) \right] \end{aligned} \quad (5.69)$$

$$\geq \mathbb{E}_{\mathbf{H}} \left[G \left(\frac{\text{tr}(\mathbf{I}_M + \frac{\rho}{M} \mathbf{H}^H \mathbf{H})^{-1}}{M} \right) \right] \quad (5.70)$$

where for the second inequality, we have also used the fact that averaging the sum of all permuted eigenvalue matrices together with the power constraints results in an identity matrix. We also note that both equalities in Eq. (5.70) hold if and only if Λ_Ψ , and hence Ψ , is an identity matrix; i.e.,

$$\Psi = \mathbf{I}. \quad (5.71)$$

Finally, combining Eqs. (5.67) and (5.68) with Eq. (5.70), we obtain

$$P_e(\mathcal{F}) \geq \mathbb{E}_{\mathbf{H}} \left[G \left(\frac{\text{tr}(\mathbf{I}_M + \frac{\rho}{M} \mathbf{H}^H \mathbf{H})^{-1}}{M} \right) \right] \quad (5.72)$$

The lower bound in Eq. (5.72) is independent of the design matrix \mathcal{F} and is achieved if and only if the four conditions in Eqs. (5.58), (5.63), (5.66) and (5.71) are met simultaneously. These four conditions together amount to the equivalent necessary and sufficient condition that the sequence of coding matrices $\{\mathbf{A}_k, \mathbf{B}_k\}_{k=1}^{MT}$ is trace-orthogonal. Therefore, we can arrive at the following conclusion [53]:

The minimum of the average BER for an LD-coded MIMO system transmitting QPSK signals and equipped with an MMSE receiver is given by

$$P_e(\mathcal{F}) = \mathbb{E}_{\mathbf{H}} \left[G \left(\frac{\text{tr}(\mathbf{I}_M + \frac{\rho}{M} \mathbf{H}^H \mathbf{H})^{-1}}{M} \right) \right] \quad (5.73)$$

This minimum is reached if and only if the LD code matrix sequence $\{\mathbf{A}_k, \mathbf{B}_k\}_{k=1}^{MT}$ is trace-orthogonal.

From the above analysis, we see the following two points:

1. The minimization of the average BER is achieved by evenly distributing the output signal power in each real dimension after channel matrix $\tilde{\mathcal{H}}\mathcal{FT}$ and at the same time evenly distributing the output noise power after the MMSE equalizer in each real dimension even without the channel state information at the transmitter. Therefore, we have actually proved that for an arbitrarily given channel realization, the trace-orthogonal LD code family is one among all unitary matrices \mathcal{F} that minimizes the BER of the MMSE detector without any channel information at the transmitter.
2. While our conclusion has been made only by considering the QPSK modulation, we notice that at high SNRs, the key performance index of determining the MMSE detector is the maximum diagonal entry of the error covariance matrix \mathbf{P} , just as the free distance is the key performance index for the ML detector [56]. Therefore, loosely speaking, to minimize the maximum diagonal entry of \mathbf{P} is to minimize the average symbol error probability of the MMSE detector. Since $\max_{1 \leq k \leq MT} [\mathbf{P}]_{k,k} \geq \frac{\text{tr}((\mathbf{I}_M + \frac{\rho}{M} \mathbf{H}^H \mathbf{H})^{-1})}{M}$ if \mathcal{F} is unitary, where the equality holds when the resulting LD code is trace-orthogonal, at high SNRs, the trace-orthogonal LD code family is still one among all unitary matrices \mathcal{F} that minimizes the symbol error probability of the MMSE detector without any channel information at the transmitter.

5.5 Construction of Trace Orthogonal LD Codes

Our purpose in space-time coding is to transform the original information symbols to be transmitted each time by multiplying the M symbols by a *rotation matrix* to generate a code matrix. This code matrix may be scaled by a *Diophantine number* ψ_n [26] and then multiplied by a circulant matrix \mathbf{C}_M^ℓ forming the various *layers* for transmission. For easy illustration, we show a simple example of a three transmitter antenna and three

receiver antenna MIMO system coded by a linear STBC. Here, information symbols $s_{m,n}$ for $m, n = 1, 2, 3$ to be transmitted during three time slots are first rotated by a 3×3 unitary matrix \mathcal{R} ; that is,

$$\mathbf{x}_n = \begin{pmatrix} x_{1,n} \\ x_{2,n} \\ x_{3,n} \end{pmatrix} = \frac{1}{\sqrt{3}} \begin{pmatrix} 1 & 1 & 1 \\ 1 & \zeta_3 & \zeta_3^2 \\ 1 & \zeta_3^2 & \zeta_3^4 \end{pmatrix} \text{diag}(1, \zeta_9, \zeta_9^2) \begin{pmatrix} s_{1,n} \\ s_{2,n} \\ s_{3,n} \end{pmatrix}$$

Then, these coded signal vectors \mathbf{x}_n are scaled by the diophantine numbers $\psi_1 = 1$, ψ_2 and ψ_3 , respectively, and are put into three layers corresponding to \mathbf{I} , \mathbf{C}_3 and \mathbf{C}_3^2 . Finally, the resulting coding signal matrix is

$$\Sigma(\mathbf{s}) = \begin{pmatrix} x_{1,1} & \psi_3 x_{2,3} & \psi_2 x_{3,2} \\ \psi_2 x_{1,2} & x_{2,1} & \psi_3 x_{3,3} \\ \psi_3 x_{1,3} & \psi_2 x_{2,2} & x_{3,1} \end{pmatrix}$$

Now, we have seen in the previous sections that trace orthogonality is a very desirable structure for the design of LD codes. Therefore, in transforming the information symbols, we aim at a code that has the trace-orthogonal structure. Here in this section, we develop such a scheme for the construction of trace-orthogonal LD codes.

For the systematic construction of LD codes possessing the properties of trace-orthogonality, we first need to have the following definition:

Definition 5.5.1 Let $T = LM$, where L is a positive integer. A $2T \times 2T$ unitary matrix \mathbf{V} satisfying

$$\mathbf{V} = \begin{pmatrix} \mathbf{X} & \mathbf{Y} \\ \mathbf{Y}^* & \mathbf{X}^* \end{pmatrix} \quad (5.74)$$

is said to be of V-structure if:

a) The entries of the $T \times T$ matrices \mathbf{X} and \mathbf{Y} satisfy

$$\sum_{n=0}^{L-1} |x_{t,(Mn+m)}|^2 + \sum_{n=0}^{L-1} |y_{k,(Mn+m)}|^2 = \frac{1}{M} \quad (5.75)$$

for $t = 1, 2, \dots, T$ and $m = 1, 2, \dots, M$.

b) The cross terms between \mathbf{X} and \mathbf{Y} satisfy

$$\sum_{n=0}^{L-1} (x_{t,(Mn+m)} y_{t,(Mn+m)}^* + x_{t,(Mn+m)}^* y_{t,(Mn+m)}) = 0 \quad (5.76)$$

for $t = 1, 2, \dots, T$ and $m = 1, 2, \dots, M$.

The following is an example for such a V-structured matrix.

Example 1 For $M = 2, L = 1$ and $T = 2$, we construct a 4×4 V-structured matrix as

$$\mathbf{V} = \frac{1}{\sqrt{2}} \begin{pmatrix} \cos \theta & \cos \theta & -j \sin \theta & j \sin \theta \\ \sin \theta & \sin \theta & j \cos \theta & -j \cos \theta \\ j \sin \theta & -j \sin \theta & \cos \theta & \cos \theta \\ -j \cos \theta & j \cos \theta & \sin \theta & \sin \theta \end{pmatrix} \quad (5.77)$$

The following proposition indicates that V-structured matrices are closed under the Kronecker product operation and that a new V-structured matrix with a larger dimension can be generated from a given V-structured matrix with a smaller dimension.

Proposition 5.5.2 *Let $T_1 = L_1 M$ and $T_2 = L_2 T_1$. If \mathbf{V}_1 is a $2T_1 \times 2T_1$ V-structured matrix formed with \mathbf{X}_1 and \mathbf{Y}_1 according to Eq. (5.74), which satisfies Eqs. (5.75) and (5.76), then, for any $L_2 \times L_2$ unitary matrix \mathbf{U} , the following matrix \mathbf{V}_2 is a $2T_2 \times 2T_2$ V-structured matrix,*

$$\mathbf{V}_2 = \begin{pmatrix} \mathbf{U} \otimes \mathbf{X}_1 & \mathbf{U} \otimes \mathbf{Y}_1 \\ \mathbf{U}^* \otimes \mathbf{Y}_1^* & \mathbf{U}^* \otimes \mathbf{X}_1^* \end{pmatrix} \quad (5.78)$$

We now present two methods for the systematic construction of such a V-structured matrix, which can be easily verified by Definition 5.5.1 of a V-structured matrix.

Construction 1 *Let \mathbf{U} denote an $M \times M$ unitary matrix with all its elements having equal magnitude. Let $\mathbf{V}(m : n, :)$ a matrix formed by taking row m to row n of \mathbf{V} , while retaining all its columns. We now form the $T \times T$ matrices \mathbf{X} and \mathbf{Y} such that*

$$\mathbf{X} = \begin{pmatrix} \mathbf{V}(1 : M_1, :) \\ \mathbf{0}_{M_2 \times M} \end{pmatrix}, \quad \mathbf{Y} = \begin{pmatrix} \mathbf{0}_{M_1 \times M} \\ \mathbf{V}^*(M_1 + 1 : M, :) \end{pmatrix} \quad (5.79)$$

where the nonnegative integers M_1 and M_2 satisfy $M_1 + M_2 = M$. Then, the matrix \mathbf{V} defined by Eq. (5.74) with such \mathbf{X} and \mathbf{Y} is of V-structure.

Construction 2 *Let \mathbf{X} and \mathbf{Y} denote a pair of $M \times M$ real matrices satisfying the conditions (i) $x_{k,m}^2 + y_{k,m}^2 = 1/M$, for $k, m = 1, 2, \dots, M$, (ii) $\mathbf{XX}^T + \mathbf{YY}^T = \mathbf{I}_M$, and (iii) $\mathbf{XY}^T + \mathbf{Y}^T \mathbf{X} = \mathbf{0}$. Then, the matrix \mathbf{V} given by*

$$\mathbf{V} = \begin{pmatrix} \mathbf{X} & j\mathbf{Y} \\ -j\mathbf{Y} & \mathbf{X} \end{pmatrix} \quad (5.80)$$

is a $2M \times 2M$ V-structured matrix.

As mentioned in Sections 5.1 and 5.2, often, we create different “layers” for transmission by multiplying code matrix by a circulant matrix \mathbf{C}_M^ℓ so that we select the appropriate symbols of the coded signal vectors to be transmitted at any time instant t . We first introduce the following lemma concerning an important property of a circulant generator matrix that will facilitate the proofs of some of the theorems in the ensuing sections:

Lemma 5.5.3 *For any $P \times P$ circulant generator matrix \mathbf{C}_P , the diagonal entries of its m th power \mathbf{C}_P^m , $m = 1, 2, \dots, P - 1$, are all zero, that is,*

$$[\mathbf{C}_P^m]_{pp} = \delta(m)$$

for $m = 0, 1, \dots, P - 1$ and $p = 1, 2, \dots, P$.

Proof. First we notice that \mathbf{C}_P can be decomposed as

$$\mathbf{C}_P = \mathbf{W}_P^H \mathbf{\Lambda}_C \mathbf{W}_P \quad (5.81)$$

where $\mathbf{\Lambda}_C = \text{diag}(1, e^{-\frac{j2\pi}{P}}, \dots, e^{-\frac{j2(P-1)\pi}{P}})$ and \mathbf{W}_P denotes the $P \times P$ discrete Fourier transform matrix. Then, the p th diagonal element of its m th power is given by

$$[\mathbf{C}_P^m]_{pp} = [\mathbf{W}_P^H \mathbf{\Lambda}_C^m \mathbf{W}_P]_{pp} = \frac{1}{P} \sum_{\ell=0}^{P-1} e^{-\frac{j2\pi\ell m}{P}} = \delta(m)$$

□

With a V-structured matrix constructed as above, together with different circulant matrices to create the different layers of transmission, we are now in a position to examine the systematic generation of trace-orthogonal LD codes. Our method of producing trace-orthogonal LD codes applies when the number of time slots T is a multiple of the number of transmitter antennas and the total number of information symbols is a multiple of the number of transmission time slots. We now formally state our methods of designing trace-orthogonal LD codes in the following theorem.

Theorem 5.5.4 *Let $T = LM$, $K = RT$ and $0 \leq i_1 < i_2 < \dots < i_R \leq M - 1$ be arbitrarily given R numbers out of $\{0, 1, \dots, M - 1\}$. Let each $2T \times 2T$ matrix \mathbf{V}_r be of V-structure and $\mathbf{D}_{i_r T+t}$ and $\Delta_{i_r T+t}$ denote the following matrices,*

$$\begin{aligned} \mathbf{D}_{i_r T+t} &= [\text{diag}(\mathbf{x}_t^{(r)}(1 : M)), \dots, \text{diag}(\mathbf{x}_t^{(r)}(L - 1)M + 1 : LM))] \\ \Delta_{i_r T+t} &= [\text{diag}(\mathbf{y}_t^{(r)}(1 : M)), \dots, \text{diag}(\mathbf{y}_t^{(r)}(L - 1)M + 1 : LM))] \end{aligned}$$

for $r = 1, 2, \dots, R$ and $t = 1, 2, \dots, T$, where $\mathbf{x}_t^{(r)}(LM + 1 : (L + 1)M)$ and $\mathbf{y}_t^{(r)}(LM + 1 : (L + 1)M)$ denote the $M \times 1$ column vectors consisting of the entries subtracted from the $LM + 1$ to $(L + 1)M$ elements of the t th column of matrices \mathbf{X}_r and \mathbf{Y}_r in the V-structured matrix \mathbf{V}_r , respectively. Two sequences of matrices $\mathbf{A}_{i_r T+t}$ and $\mathbf{B}_{i_r T+t}$, each of which is $T \times T$, are defined as follows:

$$\mathbf{A}_{i_r T+t} = \sqrt{\frac{MT}{K}} \mathbf{C}_M^{i_r} \mathbf{D}_{i_r M+n} \quad (5.82)$$

$$\mathbf{B}_{i_r T+t} = \sqrt{\frac{MT}{K}} \mathbf{C}_M^{i_r} \Delta_{i_r M+n} \quad (5.83)$$

where \mathbf{C}_M denotes an $M \times M$ circulant matrix. Then, the matrix family $\{\mathbf{A}_{i_r T+t}, \mathbf{B}_{i_r T+t}\}$ constitute a trace-orthogonal LD code with a symbol rate R per channel use.

Proof. First we notice that

$$\begin{aligned} \text{tr}(\mathbf{A}_{T i_m + n} \mathbf{A}_{T i_{m'} + n'}^H) &= \frac{MT}{K} \text{tr} \left(\mathbf{C}_M^{i_m} \mathbf{D}_{T i_m + n} \mathbf{D}_{T i_{m'} + n'}^H \mathbf{C}_M^{-i_{m'}} \right) \\ &= \frac{MT}{K} \text{tr} \left(\mathbf{C}_M^{i_m - i_{m'}} \mathbf{D}_{T i_m + n} \mathbf{D}_{T i_{m'} + n'}^H \right) \end{aligned}$$

$$\begin{aligned}
&= \frac{MT}{K} \sum_{k=1}^M \left[\mathbf{C}_M^{i_m - i_{m'}} \mathbf{D}_{Ti_m + n} \mathbf{D}_{Ti_{m'} + n'}^H \right]_{kk} \\
&= \frac{MT}{K} \sum_{k=1}^M [\mathbf{C}_M^{i_m - i_{m'}}]_{kk} [\mathbf{D}_{Ti_m + n} \mathbf{D}_{Ti_{m'} + n'}^H]_{kk}
\end{aligned} \tag{5.84}$$

where in the last step (5.84) we have used the fact that $\mathbf{D}_{Ti_m + n} \mathbf{D}_{Ti_{m'} + n'}^H$ is a diagonal matrix. Similarly, we have that

$$\text{tr}(\mathbf{B}_{Ti_{m'} + n'} \mathbf{B}_{Ti_m + n}^H) = \frac{MT}{K} \sum_{k=1}^M [\mathbf{C}_M^{i_m - i_{m'}}]_{kk} [\Delta_{Ti_m + n} \Delta_{Ti_{m'} + n'}^H]_{kk} \tag{5.85}$$

Combining Lemma 5.5.3, Eq. (5.85) with Eq. (5.84) yields

$$\text{tr} \left(\mathbf{A}_{Ti_m + n} \mathbf{A}_{Ti_{m'} + n'}^H + \mathbf{B}_{Ti_{m'} + n'} \mathbf{B}_{Ti_m + n}^H \right) = \frac{MT}{K} \delta(m - m') \delta(n - n')$$

where we have used the fact that each matrix \mathbf{V}_m has the V-structure. Similarly, we can obtain

$$\text{tr} \left(\mathbf{A}_{Ti_m + n} \mathbf{B}_{Ti_{m'} + n'}^H + \mathbf{B}_{Ti_{m'} + n'} \mathbf{A}_{Ti_m + n}^H \right) = 0$$

□

We note that Theorem 5.5.4 can be applied to any type of modulated symbol, that is, for all types of communication symbols, the resulting code is trace-orthogonal. We now present an example of generating a trace-orthogonal LD code family using the above theorem:

Example 2 Using the V-structured matrix in Example 1 and Theorem 5.5.4, we have

$$\begin{aligned}
\mathbf{A}_1 = \mathbf{A}_4 &= \frac{1}{\sqrt{2}} \begin{pmatrix} \cos \theta & 0 \\ 0 & \sin \theta \end{pmatrix}, \quad \mathbf{A}_2 = \mathbf{A}_3 = \frac{1}{\sqrt{2}} \begin{pmatrix} 0 & \sin \theta \\ \cos \theta & 0 \end{pmatrix} \\
\mathbf{B}_1 = -\mathbf{B}_4 &= \frac{j}{\sqrt{2}} \begin{pmatrix} -\sin \theta & 0 \\ 0 & \cos \theta \end{pmatrix}, \quad \mathbf{B}_2 = -\mathbf{B}_3 = \frac{j}{\sqrt{2}} \begin{pmatrix} 0 & \cos \theta \\ -\sin \theta & 0 \end{pmatrix}
\end{aligned}$$

Correspondingly, the unitary matrix \mathcal{F} is

$$\mathcal{F} = \frac{1}{\sqrt{2}} \begin{pmatrix} \cos \theta & 0 & 0 & \cos \theta & -j \sin \theta & 0 & 0 & j \sin \theta \\ 0 & \cos \theta & \cos \theta & 0 & 0 & -j \sin \theta & j \sin \theta & 0 \\ 0 & \sin \theta & \sin \theta & 0 & 0 & j \cos \theta & -j \cos \theta & 0 \\ \sin \theta & 0 & 0 & \sin \theta & j \cos \theta & 0 & 0 & -j \cos \theta \\ j \sin \theta & 0 & 0 & -j \sin \theta & \cos \theta & 0 & 0 & \cos \theta \\ 0 & j \sin \theta & -j \sin \theta & 0 & 0 & \cos \theta & \cos \theta & 0 \\ 0 & -j \cos \theta & j \cos \theta & 0 & 0 & \sin \theta & \sin \theta & 0 \\ -j \cos \theta & 0 & 0 & j \cos \theta & \sin \theta & 0 & 0 & \sin \theta \end{pmatrix}$$

5.6 Design of Full Diversity LD Codes

In the previous section, we have developed the way to design trace-orthogonal LD codes. In this section, we will consider the design of *full diversity* LD codes. We will show how to properly select the V-structured matrices from the trace-orthogonal LD code family such that the resulting codes will provide full diversity. To achieve this purpose, we make use of some fundamentals of algebraic number theory.

5.6.1 Some basic definitions and results in algebraic number theory

For completeness of the exposition, we begin by briefly introducing some necessary definitions and results extracted from [57, 31, 36, 58, 30, 59–61, 29], which hold the key in the systematical and efficient designing of a full diversity rotation matrix and the Diophantine number, and hence, full diversity LD codes.

Definition 5.6.1 (*The Euler Function*). *For a rational positive integer n , i.e., $n \in \{1, 2, \dots\}$, the Euler function $\varphi(n)$ is defined as the number of all positive rational integers that do not exceed n and are prime to n .*

The Euler function has the following properties:

1. $\varphi(1) = 1$;
2. $\varphi(p^\alpha) = p^{\alpha-1}(p - 1)$, where p is prime and α is a positive rational integer;
3. (Multiplicative Property) If $\gcd(m, n) = 1$, that is, if m and n are relatively prime rational integers, then $\varphi(mn) = \varphi(m)\varphi(n)$;
4. Let $m = \prod_{k=1}^r p_k^{\alpha_k}$ where p_k are prime and α_k are positive rational integers. Then, $\varphi(m) = m \prod_{k=1}^r (1 - \frac{1}{p_k})$.

We denote the rational integer ring $\{\dots, 0, \pm 1, \pm 2, \dots\}$ by \mathbb{Z} , the Gaussian integer ring, i.e., $\{a + jb; a, b \in \mathbb{Z}\}$ by $\mathbb{Z}[j]$, and the Eisenstein ring, i.e., $\{a + \zeta_3b; a, b \in \mathbb{Z}\}$ by $\mathbb{Z}[\zeta_3]$ with ζ_n being the n th root of unity, i.e., $\zeta_n = \exp(j \frac{2\pi}{n})$. We also denote the corresponding quotient fields by \mathbb{Q} , by $\mathbb{Q}(j)$, i.e., $\mathbb{Q}(j) = x + jy$; $x, y \in \mathbb{Q}$, and by $\mathbb{Q}(\zeta_3)$, i.e., $\mathbb{Q}(\zeta_3) = x + \zeta_3y$; $x, y \in \mathbb{Q}$, respectively. (Our notation here uses square brackets for rings and parentheses for fields).

Definition 5.6.2 *An n th “order” cyclotomic polynomial is defined as*

$$\Phi_n(x) = \prod_{k=1, \gcd(n,k)=1}^{n-1} (x - \zeta_n^k) \quad (5.86)$$

The degree of $\Phi_n(x)$ is the Euler function $\varphi(n)$. Furthermore, $\mathbb{Q}(\zeta_n)$ is called a cyclotomic field and its integer ring $\mathbb{Z}[\zeta_n]$ is called a cyclotomic ring.

In the following, we use \mathbb{I}_n to denote the rational integer ring \mathbb{Z} or the Gaussian integer ring $\mathbb{Z}[j]$ or the Eisenstein ring $\mathbb{Z}[\zeta_3]$, whereas \mathbb{K} is used to denote their respective quotient fields, that is, $\mathbb{K} = \mathbb{Q}$, or $\mathbb{K} = \mathbb{Q}(j)$, or $\mathbb{K} = \mathbb{Q}(\zeta_3)$.

Definition 5.6.3 (*Algebraic Number and Algebraic Integer*) A field \mathbb{L} is said to be an extension of field \mathbb{K} provided that \mathbb{K} is a subfield of \mathbb{L} . An element $\theta \in \mathbb{C}$ is said to be algebraic over \mathbb{K} provided that θ is a root of some nonzero polynomial $f(x) = \sum_{\ell=0}^d a_\ell x^\ell \in \mathbb{K}[x]$, the ring of polynomials with coefficients in \mathbb{K} , and θ is not a root of such a polynomial of degree less than d . Such a polynomial is called a minimal polynomial. If $f(x)$ can be chosen monic (having coefficient of the highest power term being unity), with coefficients in \mathbb{I}_n , the number θ is said to be integral over \mathbb{I}_n .

Definition 5.6.4 (*Trace and Norm*). Let θ be algebraic over \mathbb{K} with a degree d . Let σ_ℓ for $\ell = 1, 2, \dots, d$ be d automorphisms of \mathbb{K} in \mathbb{C} that fix \mathbb{K} pointwise (i.e., $\sigma_\alpha = \alpha$). Then, the trace $\text{Tr}(\theta)$ and the norm $\text{Nr}(\theta)$ of θ from \mathbb{K} are defined, respectively, as

$$\text{Tr}(\theta) = \sum_{\ell=1}^d \sigma_\ell(\theta) \quad (5.87)$$

$$\text{Nr}(\theta) = \prod_{\ell=1}^d \sigma_\ell(\theta) \quad (5.88)$$

The following lemma plays an important role in the diagonal space-time block code (DAST) design [34] based on algebraic number theory:

Lemma 5.6.5 Let \mathcal{O} be the set of elements of \mathbb{K} that are integral over \mathbb{I}_n . Then, \mathcal{O} is the number ring (subset of integer ring) of \mathbb{K} over \mathbb{I}_n and both the trace and norm of $\theta \in \mathcal{O} \setminus \{0\}$ belong to $\mathbb{I}_n \setminus \{0\}$. As a result, $|\text{Tr}(\theta)|, |\text{Nr}(\theta)| \geq 1$.

A profound result for designing cyclotomic diagonal linear space-time codes was recently obtained by Wang *et al* [37] and is important to the development of the ensuing material. We state this result without proof in the following.

Lemma 5.6.6 Let $P = L J$ and $L_t = \frac{\varphi(P)}{\varphi(L)}$. Then, all the L_t automorphisms σ_i , $1 \leq i \leq L_t$, of field $\mathbb{Q}(\zeta_P)$ that fix subfield $\mathbb{Q}(\zeta_L)$ can be represented by

$$\sigma_i(\zeta_P) = \zeta_P^{1+P_i L} \text{ for } 1 \leq i \leq L_t \quad (5.89)$$

where P_i , $1 \leq i \leq L_t$, are the integers that satisfy $0 = P_1 < P_2 < \dots < P_{L_t} \leq J - 1$ and $1 + P_i L$ and P are coprime for $1 \leq i \leq L_t$. Furthermore, if we let \mathbf{G}_{LJ} denote a generating matrix such that $[\mathbf{G}_{LJ}]_{mn} = \{\sigma_m(\zeta_P^n)\}_{1 \leq m, n \leq L_t}$ and $\mathbf{x} = [x_1, x_2, \dots, x_{L_t}]^T = \mathbf{G}_{LJ} \mathbf{s}$, where $\mathbf{s} \in \mathbb{Z}^{L_t}[\zeta_L]$, then the generating matrix \mathbf{G}_{LJ} is of full diversity over $\mathbb{Z}^{L_t}[\zeta_L]$, i.e., $\prod_{k=1}^{L_t} x_k \neq 0$ for any nonzero symbol vector \mathbf{s} belonging to $\mathbb{Z}^{L_t}[\zeta_L]$.

For a properly fixed positive rational integer L_t , Wang *et al* [37] optimized L and J such that the resulting cyclotomic lattice is as dense as possible. Unfortunately, the optimal generating matrix is not unitary and the number of transmitter antennas, L_t , is limited to a specific rational integer. Nonetheless, Lemma 5.6.6 is central to our joint design of a cyclotomic rotation matrix, the corresponding constellation and the Diophantine number such that the resulting LD code can guarantee full diversity.

5.6.2 Design of full diversity LD codes

In order to employ Lemma 5.6.6 to design a trace-orthogonal full diversity LD code, we first propose the following lemma.

Lemma 5.6.7 *Let $M = \prod_{k=1}^r p_k^{\alpha_k}$, where each p_k is prime and $\alpha_k \geq 1$. Then, for a positive rational integer $P = LM$, its Euler number $\varphi(P) = M\varphi(L)$ if and only if $L = L_1 \prod_{k=1}^r p_k^{\beta_k}$, where each $\beta_k \geq 1$ and L_1 is prime to M .*

Proof. First we prove the sufficient condition. Suppose that $L = L_1 \prod_{k=1}^r p_k^{\beta_k}$, where $\gcd(p_k, L_1) = 1$ for $k = 1, 2, \dots, r$. Then, in this case, employing the multiplicative property of the Euler function yields $\varphi(P) = \varphi(L_1) \prod_{k=1}^r \varphi(p_k^{\alpha_k + \beta_k}) = (\varphi(L_1) \prod_{k=1}^r p_k^{\beta_k - 1})(p_k - 1)(\prod_{k=1}^r p_k^{\alpha_k}) = \varphi(L)M$, which gives the proof of the sufficient condition.

Now we prove the necessary condition. Suppose that $\varphi(P) = \varphi(L)M$. Then, we claim that L and M are not coprime. Otherwise, if L and M were coprime, then, using Result 1 would result in $\varphi(P) = \varphi(L)\varphi(M)$. By the definition of the Euler function, we know that $\varphi(M) < M$ if $M > 1$. This would lead to $\varphi(P) = \varphi(L)\varphi(M) < \varphi(L)M$ for $M > 1$, which would contradict with the assumption. Therefore, L and M are not coprime. Let p_1, p_2, \dots, p_t ($t \geq 1$) be the common prime divisors of L and M ; that is, L and M can be decomposed as $L = \prod_{k=1}^t p_k^{\gamma_k} L_1$ and $M = \prod_{k=1}^t p_k^{\alpha_k} M_1$, where $t \geq 1$, $\alpha_k, \gamma_k \geq 1$, each p_k is coprime to both L_1 and M_1 , and $\gcd(L_1, M_1) = 1$. Hence, $\varphi(P) = \varphi(L_1)\varphi(M_1) \prod_{k=1}^t \varphi(p_k^{\alpha_k + \gamma_k})$. Since $\varphi(p_k^{\alpha_k + \gamma_k}) = p_k^{\alpha_k + \gamma_k - 1}(p_k - 1)$,

$$\begin{aligned} \varphi(P) &= \left(\varphi(L_1) \prod_{k=1}^t p_k^{\gamma_k - 1}(p_k - 1) \right) \left(\prod_{k=1}^t p_k^{\alpha_k} \varphi(M_1) \right) \\ &= \varphi(L) \left(\prod_{k=1}^t p_k^{\alpha_k} \varphi(M_1) \right) \\ &\leq \varphi(L) \left(\prod_{k=1}^t p_k^{\alpha_k} M_1 \right) \\ &= \varphi(L)M \end{aligned} \tag{5.90}$$

Where the equality in (5.90) holds if and only if $M_1 = 1$. Therefore, in this case, $L = L_1 \prod_{k=1}^r p_k^{\beta_k}$. This completes the proof of Lemma 5.6.7. \square

Directly applying Lemma 5.6.7 and Lemma 5.6.6, the following full diversity cyclotomic rotation matrix and a corresponding cyclotomic ring are immediate results.

Corollary 5.6.8 *Let $M = \prod_{k=1}^r p_k^{\alpha_k}$, where each p_k is prime and $\alpha_k \geq 1$, and let $P = LM$, where $L = L_1 \prod_{k=1}^r p_k^{\beta_k}$, $\beta_k \geq 1$ with L_1 being prime to M . The matrix $\mathcal{R}_0 = \mathbf{W}_M \text{diag}(1, \zeta_P, \dots, \zeta_P^{M-1})$ is unitary and is of full diversity over the cyclotomic ring $\mathbb{Z}[\zeta_L]$.*

Proof. Using Lemma 5.6.6 and Lemma 5.6.7, where $R = M$, $P = LM$ and thus $L_t = M$ because of Property 3 of the Euler function, we obtain that $P_i = i - 1$ for $i = 1, 2, \dots, M$, since, in this case, $1 + (i - 1)L$ is prime to P . As a result, $\sigma_m(\zeta_P) = \zeta_P^{1+(m-1)L}$ and hence, $\mathcal{R}_0(P, M) = \mathbf{W}_M^H \text{diag}(1, \zeta_P, \dots, \zeta_P^{M-1})$. \square

Using Corollary 5.6.8, for a fixed M , we can choose L as small as possible such that

1. $L = \prod_{k=1}^r p_k$ if $M \neq 2^n$ for any rational positive integer n ;
2. $L = 4$ or $L = 6$ if $M = 2^n$ for some rational positive integer n .

For the particular case of $M = 3^m 2^n$, it has been shown [57, 31, 36, 30, 29] that a unitary rotation matrix can be obtained. Here, we can choose the Gaussian integer ring $\mathbb{Z}[\zeta_4]$ or the Eisenstein integer ring $\mathbb{Z}[\zeta_3]$ in Corollary 5.6.8 and arrive at the same result of a unitary rotation matrix. Hence, we can conclude that Corollary 5.6.8 is a generalization of the available result for the case of $M = 3^m 2^n$ and also extends the result in [62].

Before we state our main results, we need a result from matrix theory [42]:

Lemma 5.6.9 *For $M \times M$ nonnegative definite matrices Ω_1 and Ω_2*

$$\det(\Omega_1 + \Omega_2) \geq \det(\Omega_1) + \det(\Omega_2) \quad (5.91)$$

If Ω_1 is positive definite, equality in (5.91) holds if and only if $\Omega_2 = \mathbf{0}$

Now we are in the position to formally state our main result in the design of trace-orthogonal full diversity LD codes [49]:

Theorem 5.6.10 *Let $\gcd(M, R)$ denote the greatest common divisor of M and R such that $\gcd(M, R) = D$, and $K = RT$ with $T = ML$ and $0 < R \leq M$. Let $0 \leq i_1 < i_2 < \dots < i_R \leq M - 1$ be arbitrarily given R numbers out of $\{0, 1, \dots, M - 1\}$. Also, let $M = \prod_{m=1}^d q_m^{\lambda_m} \prod_{k=1}^{d_M} p_k^{\alpha_k}$, $R = \prod_{m=1}^d q_m^{\mu_i} \prod_{\ell=1}^{d_R} \tilde{p}_\ell^{\beta_\ell}$ and $L_0 = L \prod_{i=1}^d q_m^{\tau_m} \prod_{k=1}^{d_M} p_k^{\gamma_k} \prod_{\ell=1}^{d_R} \tilde{p}_\ell^{\rho_\ell}$, where q_m , p_k and \tilde{p}_ℓ are primes and coprime to each other, and $\alpha_k, \beta_\ell, \gamma_i, \rho_\ell \geq 1$ and L is prime to both M and R . If we choose the V-structured matrices in Theorem 5.5.4 as follows,*

$$\mathbf{X}_r = \zeta_{LRM^2}^{r-1} \mathbf{U} \otimes \begin{pmatrix} \mathcal{R}_0[1 : M_1, :] \\ \mathbf{0}_{M_2 \times M} \end{pmatrix} \quad (5.92a)$$

$$\mathbf{Y}_r = \zeta_{LRM^2}^{r-1} \mathbf{U} \otimes \begin{pmatrix} \mathbf{0}_{M_1 \times M} \\ \mathcal{R}_0^*[M_1 + 1 : M, :] \end{pmatrix} \quad (5.92b)$$

for $r = 1, 2, \dots, R$, where $M_1 + M_2 = M$, $M_1, M_2 \geq 0$ and \mathcal{R}_0 is the unitary rotation matrix defined in Corollary 5.6.8, then the resulting signal matrix $\Sigma(\mathbf{s})$ provides full diversity over any constellation carved from $\mathbb{Z}^K[\zeta_L]$ with a symbol transmission rate R per channel use.

PROOF: By Theorem 5.5.4, the LD code constructed in Theorem 5.6.10 is trace-orthogonal. In the following, we prove that such resulting signal coding matrix $\Sigma(\mathbf{s})$ provides full diversity. To this end, first generate the k -th DAST. Let

$$\mathbf{s}_{m,k} = \begin{pmatrix} \mathcal{R}_0[1 : M_1, :] \\ \mathbf{0}_{M_2 \times M} \end{pmatrix} \mathbf{s}_{m,k} + \begin{pmatrix} \mathbf{0}_{M_1 \times M} \\ \mathcal{R}_0^*[M_1 + 1 : M, :] \end{pmatrix} \mathbf{s}_{m,k}^*$$

where $\mathbf{s}_{m,k} = [s_{mT+kM+1}, s_{mT+kM+2}, \dots, s_{mT+kM+M}]^T$. Then, the k -th DAST is generated by $\mathbf{D}(\mathbf{s}_t) = \text{diag}(\mathbf{S}_t)$. By circularly placing stream data of each DAST, we form the following matrix

$$\mathcal{X}_k(\mathbf{s}) = \sum_{m=1}^R \mathbf{C}^{i_m} \mathbf{D}(\mathbf{s}_m) \quad \text{for } k = 1, 2, \dots, K \quad (5.93)$$

where $\mathbf{s}_k = [\mathbf{s}_{0,k}^T, \mathbf{s}_{1,k}^T, \dots, \mathbf{s}_{M-1,k}^T]^T$. Therefore, a signal matrix $\Sigma(\mathbf{s})$ is built by Theorem 5.5.4

$$\Sigma(\mathbf{s}) = [\Sigma_1(\mathbf{s}), \Sigma_2(\mathbf{s}), \dots, \Sigma_K(\mathbf{s})] \quad (5.94)$$

where $\mathbf{s} = [\mathbf{s}_0^T, \mathbf{s}_1^T, \dots, \mathbf{s}_{K-1}^T]^T = [s_1, s_2, \dots, s_{TM}]^T$ and the k th subsignal matrix $\Sigma_k(\mathbf{s})$ is determined by

$$\Sigma_\ell(\mathbf{s}) = \sum_{k=0}^{K-1} u_{k,\ell} \mathcal{X}(\mathbf{s}_k) \quad \text{for } \ell = 1, 2, \dots, K \quad (5.95)$$

We have from Eq. (5.94) and Eq. (5.95) that

$$\Sigma(\mathbf{e}) \Sigma^H(\mathbf{e}) = \sum_{\ell=0}^{K-1} \Sigma_\ell(\mathbf{e}) \Sigma_\ell^H(\mathbf{e}) = \sum_{k=0}^{K-1} \mathcal{X}(\mathbf{e}_k) \mathcal{X}^H(\mathbf{e}_k) \quad (5.96)$$

This shows that the autocorrelation matrix $\Sigma(\mathbf{e}) \Sigma^H(\mathbf{e})$ of the signal matrix $\Sigma(\mathbf{s})$ constructed by Theorem 5.5.4 does not rely on the way in choosing the unitary matrix \mathbf{U} . Now it suffices to prove that for any point \mathbf{e} there exists at least one k such that $\mathcal{X}(\mathbf{e}_k)$ has a full rank. Since $\mathbf{e} \neq \mathbf{0}$, there exists at least one k such that $\mathbf{e}_k \neq \mathbf{0}$ and as a result there exists the maximum \bar{R} such that $\mathbf{e}_{\bar{R},k} \neq \mathbf{0}$. In other words, $\mathbf{e}_{m,k} = \mathbf{0}$ for $\bar{R} \leq m \leq R-1$, but $\mathbf{e}_{\bar{R},k} \neq \mathbf{0}$. Therefore, $\det(\mathbf{D}(\mathbf{e}_{\bar{R},k})) \neq 0$. Now following the proof in [26, 27], where the Diophantine numbers are chosen as $\psi_1 = 1$, $\psi_2 = \zeta_{LRM^2}, \dots, \psi_{R-1} = \zeta_{LRM^2}^{R-1}$, and expanding the determinant of $\mathcal{X}(\mathbf{e}_k)$ according to the power of ζ_{LRM} , we have that

$$\det(\mathcal{X}(\mathbf{e}_k)) = \sum_{\ell=0}^{\bar{R}} c_\ell \zeta_{LRM}^\ell \quad (5.97)$$

where $c_\ell \in \mathbb{Z}[\zeta_{LM}]$ for $\ell = 0, 1, \dots, \bar{R}$. By Corollary 5.6.8, $c_{\bar{R}} = \det(\mathbf{D}(\mathbf{e}_{\bar{R},k})) \neq 0$. In addition, by Lemma 5.6.6 and the properties of Euler functions, we know that $1, \zeta_{LRM}, \zeta_{LRM}^2, \dots, \zeta_{LRM}^{R-1}$ is linearly independent over $\mathbb{Z}[\zeta_{LM}]$ and as a result, we claim that the determinant of $\mathcal{X}(\mathbf{e}_k)$ is not zero. Therefore, using Lemma 5.6.9, we conclude from (5.96) that

$$\begin{aligned} \det(\Sigma(\mathbf{e}) \Sigma^H(\mathbf{e})) &= \det\left(\sum_{k=1}^K \mathcal{X}(\mathbf{e}_k) \mathcal{X}^H(\mathbf{e}_k)\right) \\ &\geq \sum_{k=1}^K \det(\mathcal{X}(\mathbf{e}_k) \mathcal{X}^H(\mathbf{e}_k)) > 0 \end{aligned} \quad (5.98)$$

for any $\mathbf{e} \in \mathbb{Z}^K[\zeta_L] \setminus \{0\}$. This completes the proof of Theorem 5.6.10. \square

Here, the following remarks help put the result in perspective.

1. When $M_2 = 0$, the resulting code reduces to a full diversity linear space-time block code [26, 27].

2. $\zeta_{LRM^2}^{r-1}$ in Eqs. (5.92) scales the rotation matrix and is thus a Diophantine number. Therefore, Theorem 5.6.10 not only provides a unified framework to systematically design a full diversity cyclotomic LD code at any symbol transmission rate less than or equal to the number of transmitter antennas but also provides a method to properly select the rotation matrices and the corresponding Diophantine number.
3. If $R = M$, our resulting LD code is information lossless and provides full rate and full diversity. If $N < M$, for full-rate transmission, there will be more symbols than receiver antennas and the detection has to be carried out by an ML detector. To avoid the need of a complex detector, the rule of having $R \leq \min\{M, N\}$ [24, 26] is a good choice for the constraint on the rate R , however, our resulting code in this case will lose its mutual information rate.
4. The structure of a coding signal matrix $\Sigma(\mathbf{s})$ depends on the V-structured rotation matrices. Different V-structured matrices result in different coding matrices and hence, different coding gains. How to choose a V-structured matrix such that the resulting coding signal matrix has a good coding gain is still an open problem.

5.7 Design of Full Diversity Linear Space-time Block Codes for $N < M$

The design of LD codes provided in the previous section necessitates that the number of receiver antennas is larger than or equal to the number of transmitter antennas to maintain full rate and full diversity. However, when the number of transmitter antennas is greater than the number of receiver antennas, i.e., $N < M$, then we should set the symbol rate to be $R = N$ to avoid using a complex ML detector. In this case, since $N < M$, the code will no longer be of full rate. Furthermore, as mentioned in Subsection 5.3.1, the capacity of the coded channel can no longer be guaranteed to reach the capacity of the original channel. In this section, we focus our attention on the design of linear space-time block codes for $N < M$. While some currently available linear space-time block codes can provide *full rate* and *full diversity* [26, 27] using ML detector, there is no guarantee that optimal coding gain is achieved. In the following, by taking advantage of the delay, we propose [41] the trace-orthogonal linear cyclotomic space-time block codes having a symbol rate equal to the number of receiver antennas N (not full-rate) per channel use, which, in turn, is a generalization of the linear diagonal space-time block code (LD-STBC) [33, 63]. In particular, when the number of the transmitter antennas is equal to 2^m , we show that our proposed code minimizes the worst-case pairwise error probability of the ML detector for an q -ary QAM signal, that is, optimal coding gain is achieved. Hence, by setting a reduced symbol rate to $R = N$, we achieve optimal coding gain. The following theorem formally states the conditions and results in the design of the trace-orthogonal full diversity cyclotomic space-time block code [41].

Theorem 5.7.1 *Let $M = \prod_{k=1}^r p_k^{\alpha_k}$, $L = L_1 \prod_{k=1}^r p_k^{\beta_k}$, where each p_k is prime, $\alpha_k, \beta_k \geq 1$ and L_1 is prime to M . Also, let $\gcd(M, N) = D$, $K = NT$, $T = \frac{MT_1}{D}$ and $T_2 = \frac{NT_1}{D}$ with $T_1 = \lceil \frac{(M-1)D}{M-N} \rceil$. If we let \mathbf{D}_{Mm+n} denote the following matrices,*

$$\mathbf{D}_{Mm+n} = [\text{diag}(\mathcal{R}_0[:, n]), \mathbf{0}_{M \times (T-M)}]$$

for $m = 0, 1, \dots, T_2 - 1$, $n = 1, 2, \dots, M$, where $\mathcal{R}_0[:, n]$ denotes the n -th column vector of matrix $\mathcal{R}_0 = \mathbf{W}_M \text{diag}(1, \zeta_P, \dots, \zeta_P^{M-1})$ defined in Corollary 5.6.8 of the previous section, and

$$\mathbf{A}_{Mm+n} = \sqrt{\frac{MT}{K}} \mathbf{D}_{Mm+n} \mathbf{C}_T^m$$

then, we have the following three statements:

1. matrix family $\{\mathbf{A}_k\}_{k=1}^{NT}$ constitutes a trace-orthogonal linear triangular space-time block code with a symbol rate N per channel use.
2. The resulting coding signal matrix $\Sigma_{\mathcal{A}}(\mathbf{s})$ provides full diversity over any constellation carved from a cyclotomic ring $\mathbb{Z}[\zeta_L]$.
3. In particular, when the number of transmitter antennas is equal to 2^m , the so designed code minimizes the worst-case pairwise error probability for q -ary QAM; i.e.,

$$\begin{aligned} \mathcal{A} &= \arg \min_{\text{tr}(\mathcal{F}\mathcal{F}^H) \leq K} \max_{\mathbf{s}, \mathbf{s}' \in \mathcal{S}^K, \mathbf{s} \neq \mathbf{s}'} P_{\mathcal{F}}(\mathbf{s} \rightarrow \mathbf{s}') \\ &\min_{\text{tr}(\mathcal{F}\mathcal{F}^H) \leq K} \max_{\mathbf{s}, \mathbf{s}' \in \mathcal{S}^K, \mathbf{s} \neq \mathbf{s}'} P_{\mathcal{F}}(\mathbf{s} \rightarrow \mathbf{s}') = J \left(\frac{\rho d_{\min}^2}{8MN} \right) \end{aligned}$$

Proof.

- 1) The proof of Statement 1 follows that of Theorem 5.5.4.
- 2) To show Statement 2, it suffices to prove that $\Sigma_{\mathcal{A}}(\mathbf{e})\Sigma_{\mathcal{A}}^H(\mathbf{e})$ is always invertible for any nonzero vector $\mathbf{e} \in \mathbb{Z}^K[\zeta_L]$. Since $\mathbf{e} \neq \mathbf{0}$, there exists some layer i_m such that

$$\mathbf{e}_{i_m} = [e_{Mi_m+1}, e_{Mi_m+2}, \dots, e_{Mi_m+M}]^T \neq \mathbf{0}$$

By code construction, we can always assume that $\sigma_{i_m} = \mathbf{V}\mathbf{e}_{i_m}$ is located in the diagonal line of the triangular submatrix, say, $\Sigma_1(\mathbf{e})$, consisting of the first M columns of the signal coding matrix $\Sigma(\mathbf{e})$. If this is not the case, then we permute the column or row of $\Sigma_{\mathcal{A}}(\mathbf{e})$ to obtain this placement. This permutation does not change the determinant of $\Sigma_{\mathcal{A}}(\mathbf{e})\Sigma_{\mathcal{A}}^H(\mathbf{e})$. In other words, without loss of generality, we can always assume that $\Sigma_{\mathcal{A}}(\mathbf{e})$ can be written as

$$\Sigma_{\mathcal{A}}(\mathbf{e}) = [\Sigma_1(\mathbf{e}) \vdots \Sigma_2(\mathbf{e})] \quad (5.99)$$

where $\Sigma_1(\mathbf{e})$ is a triangular matrix with nonzero diagonal entries $[\Sigma_1(\mathbf{e})]_k = \sigma_{i_m}(k) \neq 0$ for $k = 1, 2, \dots, M$. Together with this structure as well as Lemma 5.6.9 in the previous section, we obtain

$$\begin{aligned} \det(\Sigma_{\mathcal{A}}(\mathbf{e})\Sigma_{\mathcal{A}}^H(\mathbf{e})) &= \det(\Sigma_1(\mathbf{e})\Sigma_1^H(\mathbf{e}) + \Sigma_2(\mathbf{e})\Sigma_2^H(\mathbf{e})) \\ &\geq \det(\Sigma_1(\mathbf{e})\Sigma_1^H(\mathbf{e})) + \det(\Sigma_2(\mathbf{e})\Sigma_2^H(\mathbf{e})) \\ &\geq \det(\Sigma_1(\mathbf{e})\Sigma_1^H(\mathbf{e})) \\ &= \prod_{k=1}^M |\sigma_{i_m}(k)|^2 > 0 \end{aligned} \quad (5.100)$$

where both of the equalities hold if and only if $\Sigma_2(\mathbf{e}) = \mathbf{0}$. This completes the proof of Statement 2.

- 3) We now prove Statement 3. Let us first establish an upper bound of the worst-case pairwise error probability for this code. To that end, we apply Minkowski's inequality [42]), which states that if Ω_1 and Ω_2 are both $M \times M$ positive definite matrices, then

$$\det(\Omega_1 + \Omega_2)^{1/M} \geq \det(\Omega_1)^{1/M} + \det(\Omega_2)^{1/M} \quad (5.101)$$

where the equality holds if and only if $\Omega_2 = c\Omega_1$ for some constant c . Here, we substitute $\Omega_1 = \mathbf{I}_M$ and $\Omega_2 = \Sigma_{\mathcal{A}}(\mathbf{e})\Sigma_{\mathcal{A}}^H(\mathbf{e})$ in Eq. (5.101) and applying Eq. (5.100) and Lemma 5.6.5, we obtain, for any nonzero vector \mathbf{e} and nonzero θ in the interval $[0, \pi/2]$,

$$\begin{aligned} & \det\left(\mathbf{I}_M + \frac{\rho}{8M \sin^2 \theta} \Sigma_{\mathcal{A}}(\mathbf{e})\Sigma_{\mathcal{A}}^H(\mathbf{e})\right)^{1/M} \\ & \geq 1 + \frac{\rho}{8M \sin^2 \theta} \det\left(\Sigma_{\mathcal{A}}(\mathbf{e})\Sigma_{\mathcal{A}}^H(\mathbf{e})\right)^{1/M} \end{aligned} \quad (5.102)$$

$$\begin{aligned} & \geq 1 + \frac{\rho}{8MN \sin^2 \theta} |\text{Nr}(\mathbf{e}_{i_m})|^{2/M} \\ & \geq 1 + \frac{\rho d_{\min}^2}{8MN \sin^2 \theta} \end{aligned} \quad (5.103)$$

Here, the first equality holds if and only if $\Sigma_{\mathcal{A}}(\mathbf{e})\Sigma_{\mathcal{A}}^H(\mathbf{e})$ is a scaled identity matrix and the second equality holds if and only if $\Sigma_2(\mathbf{e}) = \mathbf{0}$. Therefore, both equalities hold if and only if \mathbf{s} and \mathbf{s}' are neighbor points, i.e., $\|\mathbf{s} - \mathbf{s}'\| = d_{\min}$. We conclude from this that

$$\det\left(\mathbf{I}_M + \frac{\rho}{8M \sin^2 \theta} \Sigma_{\mathcal{A}}(\mathbf{e})\Sigma_{\mathcal{A}}^H(\mathbf{e})\right) \geq \left(1 + \frac{\rho d_{\min}^2}{8MN \sin^2 \theta}\right)^M$$

This results in

$$\max_{\mathbf{s}, \mathbf{s}' \in \mathcal{S}^Q, \mathbf{s} \neq \mathbf{s}'} P_{\mathcal{A}}(\mathbf{s} \rightarrow \mathbf{s}') \leq J\left(\frac{\rho d_{\min}^2}{8MN}\right) \quad (5.104)$$

where the equality in Eq. (5.104) holds if and only if $\|\mathbf{s} - \mathbf{s}'\| = d_{\min}$. Combining (5.104) with Theorem 5.3.3 in Section 5.3B yields

$$\min_{\text{tr}(\mathcal{F}^H \mathcal{F}) \leq K} \max_{\substack{\mathbf{s}, \mathbf{s}' \in \mathcal{S}^K \\ \mathbf{s} \neq \mathbf{s}'} } P_{\mathcal{F}}(\mathbf{s} \rightarrow \mathbf{s}') = J\left(\frac{\rho d_{\min}^2}{8MN}\right)$$

This completes the proof of Statements 3 and hence Theorem 5.7.1. \square

Remarks on Theorem 5.7.1:

- When $N = 1$, we have that $D = T_1 = T_2 = 1$ and our code is reduced to an LD-STBC [63], which has been shown to achieve optimum coding gain when $M = 2^n$ and $N < M$ [33]. Thus, Theorem 5.7.1 shows stronger and more general results than those for LD-STBC.

- There are three key points in Theorem 5.7.1:
 - a) The cyclotomic rotation matrix \mathbf{V} here guarantees that each layer provides full diversity;
 - b) Similar to the role of the Diophantine number, the decoding delay T guarantees that different layers provide full diversity;
 - c) The structure of the non-singular triangular submatrix of the code matrix assures the existence of $\Sigma_{\mathcal{A}}(\mathbf{e})$, $\mathbf{e} = \mathbf{s} - \mathbf{s}' \neq \mathbf{0}$, which guarantees that the worst-case pairwise error probability is minimized for q -ary QAM when $M = 2^m$. As a result, optimal coding gain is achieved.

5.8 Design Examples and Simulations

In this section, we present some examples of trace-orthogonal space-time code designs and examine their performance in comparison to other codes available in literature.

Example 3 In this example, we consider a MIMO system with two transmitter antennas and two receiver antennas. We design an information lossless full rate full diversity linear dispersion code over Gaussian integer ring $\mathbb{Z}[i]$. A coded signal matrix is given by

$$\Sigma(\mathbf{s}) = \frac{1}{\sqrt{2}} \begin{pmatrix} \Sigma_{11}, & \Sigma_{12} \\ \Sigma_{21}, & \Sigma_{22} \end{pmatrix}$$

where

$$\begin{aligned} \Sigma_{11} &= (s_1 + s_2) \cos \theta + (s_2^* - s_1^*) \sin \theta \\ \Sigma_{12} &= e^{\frac{j\pi}{4}} ((s_3 + s_4) \sin \theta + (s_4^* - s_3^*) \cos \theta) \\ \Sigma_{21} &= e^{\frac{j\pi}{4}} ((s_3 + s_4) \cos \theta + (s_3^* - s_4^*) \sin \theta) \\ \Sigma_{22} &= (s_1 + s_2) \sin \theta + (s_1^* - s_2^*) \cos \theta \end{aligned}$$

Therefore, we have that

$$\begin{aligned} 2 \det(\Sigma(\mathbf{e})) &= \frac{(s_1 + s_2)^2 - (s_1^* - s_2^*)^2}{2} \sin 2\theta + (s_1 + s_2)(s_1^* - s_2^*) \cos 2\theta \\ &\quad - j \left(\frac{(s_3 + s_4)^2 - (s_3^* - s_4^*)^2}{2} \sin 2\theta + (s_3 + s_4)(s_3^* - s_4^*) \cos 2\theta \right) \end{aligned}$$

Now choosing $\sin 2\theta = \frac{1}{\sqrt{5}}$ and $\cos 2\theta = \frac{2}{\sqrt{5}}$, we have in this case

$$\begin{aligned} 4\sqrt{5} \det(\Sigma(\mathbf{e})) &= (s_1 + s_2 + 2(s_1^* - s_2^*))^2 - 5(s_1^* - s_2^*)^2 \\ &\quad - j \left((s_3 + s_4 + 2(s_3^* - s_4^*))^2 - 5(s_3^* - s_4^*)^2 \right) \end{aligned}$$

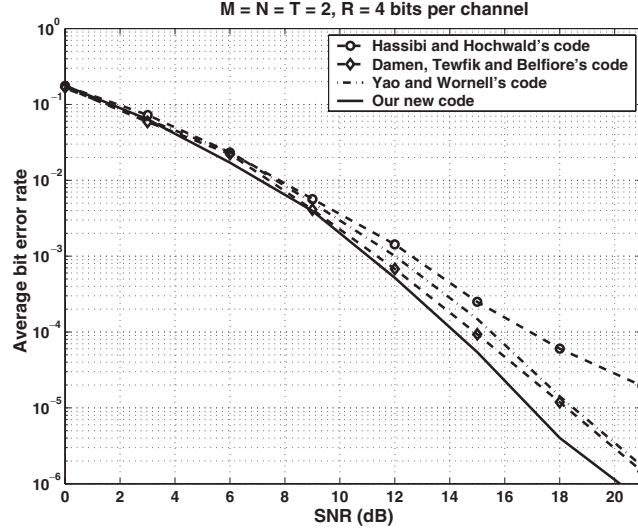


Figure 5.2 The error-performance comparison of our new code with the current available codes in [24, 50, 64].

If we let

$$\begin{aligned} S_1 &= (s_1 + s_2 + 2(s_1^* - s_2^*))^2 \\ S_2 &= (s_1^* - s_2^*)^2 \\ S_3 &= (s_3 + s_4 + 2(s_3^* - s_4^*))^2 \\ S_4 &= (s_3^* - s_4^*)^2 \end{aligned}$$

then, $4\sqrt{5}\det(\Sigma(\mathbf{e})) = S_1^2 - 5S_2^2 - j(S_3^2 - 5S_4^2) = (S_1^2 - jS_3^2) - 5(S_2^2 - jS_4^2)$. Similar to [64], it can be verified [64] by checking the remainders of S_k^2 divided by 5 that $\det(\Sigma(\mathbf{e})) = 0$ if and only if $\mathbf{e} = \mathbf{0}$. On the other hand, since $((S_1^2 - jS_3^2) - 5(S_2^2 - jS_4^2)) - ((S_1^2 - S_2^2) - j(S_3^2 - S_4^2))$ is divided by 4, while both $S_1^2 - S_2^2$ and $S_3^2 - S_4^2$ is divided by 4, we conclude that $4\sqrt{5}\det(\Sigma(\mathbf{e}))$ is divided by 4. As a result, $|4\sqrt{5}\det(\Sigma(\mathbf{e}))| \geq 4$, which² implies $|\det(\Sigma(\mathbf{e}))| \geq \frac{1}{\sqrt{5}}$. Fig. 2 shows that the error performance comparison of our code with those in [50, 64, 66].

Example 4 For three transmitter antennas and three receiver antennas, we can directly apply Theorem 5.6.10 to design an information lossless full rate full diversity linear space-time block code. In this case, the determinant of a signal matrix is easy to be evaluated.

²More recently, Dayal and Varanasi [65], Belfiore, Rekaya and Viterbo [66] constructed a linear space-time block code that has the same coding gain with a nonvanishing determinant.

Hence, we can first take special care of its coefficients in the expansion of its determinant and then use Theorem 5.5.4, where the V-structured matrices are carefully chosen as $\mathbf{V}_1 = \mathbf{W}_3^H \text{diag}(1, \zeta_9, \zeta_9^2)$, $\mathbf{V}_2 = \zeta_{27} \mathbf{C}_3 \mathbf{W}_3^H \text{diag}(1, \zeta_9, \zeta_9^2)$, $\mathbf{V}_3 = \zeta_{27} \mathbf{C}_3^2 \mathbf{W}_3^H \text{diag}(1, \zeta_9, \zeta_9^2)$. The resulting coding signal matrix is

$$\Sigma(\mathbf{s}) = \begin{pmatrix} S_{11} & \zeta_{27}^2 S_{33} & \zeta_{27} S_{22} \\ \zeta_{27} S_{23} & S_{12} & \zeta_{27}^2 S_{31} \\ \zeta_{27}^2 S_{32} & \zeta_{27} S_{21} & S_{13} \end{pmatrix}$$

where $\mathbf{S}_k = [S_{k1}, S_{k2}, S_{k3}]^T = \mathbf{W}^H \text{diag}(1, \zeta_9, \zeta_9^2) \mathbf{s}_k$ with $\mathbf{s}_k = [s_{3k-2}, s_{3k-1}, s_{3k}]^T$ for $k = 1, 2, 3$. Hence, the determinant of $\Sigma(\mathbf{s})$ is

$$\begin{aligned} \det(\Sigma(\mathbf{s})) &= S_{11} S_{12} S_{13} + \zeta_9 S_{21} S_{22} S_{23} + \zeta_9^2 S_{31} S_{32} S_{33} - S_{11} S_{21} S_{31} \\ &\quad - S_{12} S_{22} S_{32} - S_{13} S_{23} S_{33} \\ &= \text{Nr}(\theta_1) + \zeta_9 \text{Nr}(\theta_2) + \zeta_9^2 \text{Nr}(\theta_3) - \text{Tr}(\theta_1 \theta_2 \theta_3) \end{aligned}$$

where $\theta_k = s_{3k-2} + s_{3k-1}\zeta_9 + s_{3k}\zeta_9^2$ for $k = 1, 2, 3$. Since $\mathbf{s}_k \in \mathbb{Z}^3[\zeta_3]$, by Lemma 5.6.5, both the norm $\text{Nr}(\mathbf{s}_k)$ and the trace $\text{Tr}(\mathbf{s}_k)$ belong to the Eisenstein ring $\mathbb{Z}[\zeta_3]$ for $k = 1, 2, 3$. By Lemma 5.6.6, $\{1, \zeta_9, \zeta_9^2\}$ is independent over the Eisenstein cyclotomic ring $\mathbb{Z}[\zeta_3]$. Therefore, $\det(\Sigma(\mathbf{s}))$ is nonzero over any constellation carved from $\mathbb{Z}^9[\zeta_3] \setminus 0$, and hence, $\Sigma(\mathbf{s})$ provides full rate full diversity without information loss over any constellation carved from $\mathbb{Z}[\zeta_3]$. Such designed code has the Diophantine number with a smaller degree than that constructed by directly using Theorem 5.6.10. An error-performance comparison of our code with those in [25–27] is shown in Fig 5.3.

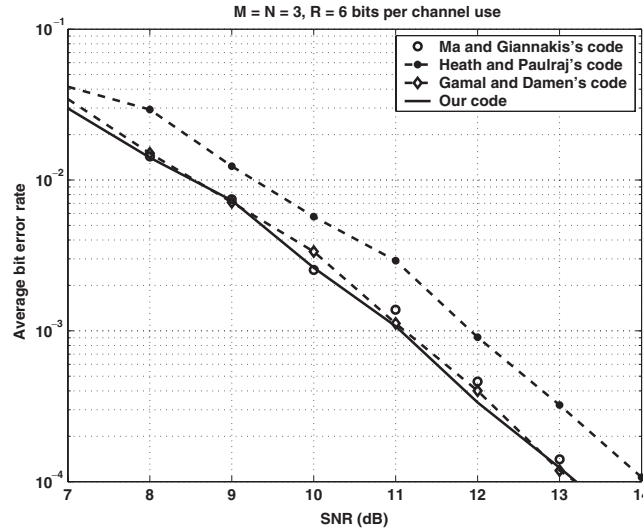


Figure 5.3 The error-performance comparison of our new code with the current available codes in [25–27].

Example 5 For a MIMO system with three transmitter antennas and two receiver antennas, we design a full diversity linear space-time block code with a symbol rate two per channel use as follows.

$$\Sigma_{\mathcal{A}}(\mathbf{s}) = \frac{\sqrt{2}}{2} \begin{pmatrix} X_{11} & 0 & 0 & X_{41} & X_{31} & X_{21} \\ X_{22} & X_{12} & 0 & 0 & X_{42} & X_{32} \\ X_{33} & X_{23} & X_{13} & 0 & 0 & X_{43} \end{pmatrix}$$

where

$$\begin{pmatrix} X_{i1} \\ X_{i2} \\ X_{i3} \end{pmatrix} = \begin{pmatrix} 1 & 1 & 1 \\ 1 & \zeta_3 & \zeta_3^2 \\ 1 & \zeta_3^2 & \zeta_3^4 \end{pmatrix} \begin{pmatrix} s_{i1} \\ s_{i2}\zeta_9 \\ s_{i3}\zeta_9^2 \end{pmatrix}$$

for $i = 1, 2, 3, 4$. It can be shown that $\det(\Sigma_{\mathcal{A}}(\mathbf{e})\Sigma_{\mathcal{A}}^H(\mathbf{e})) \neq 0$ for any constellation carved from $\mathbb{Z}[\zeta_3] \setminus 0$. An error-performance comparison of our code with that in [26] is provided in Fig 5.4.

Example 6 In this example, we examine the performance of trace-orthogonal space-time codes when a linear receiver is employed. As shown in Subsection 5.4.2, trace-orthogonality is the necessary and sufficient condition for an LDC to achieve minimum bit error probability for QPSK signals when an MMSE detector is employed. We compare our code with the code presented in [67], which is the best-known ML code so far. Let us first examine Rekaya, Belfiore and Viterbo's code from the point of the view of trace-orthogonality. Their code

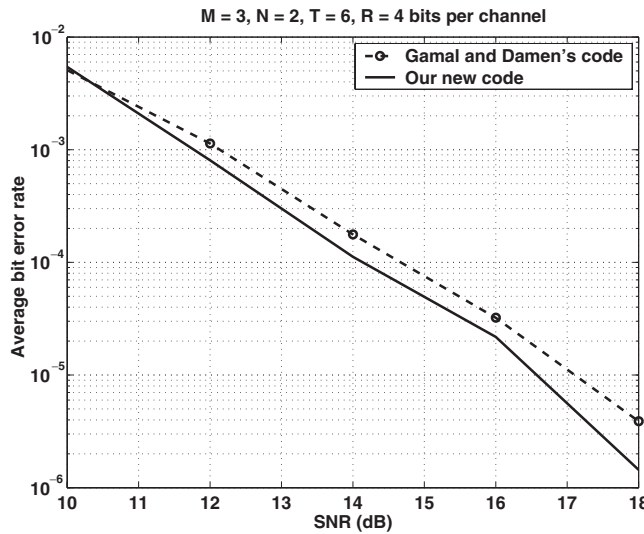


Figure 5.4 The error-performance comparison of our new code with Gamal and Damen's code [26].

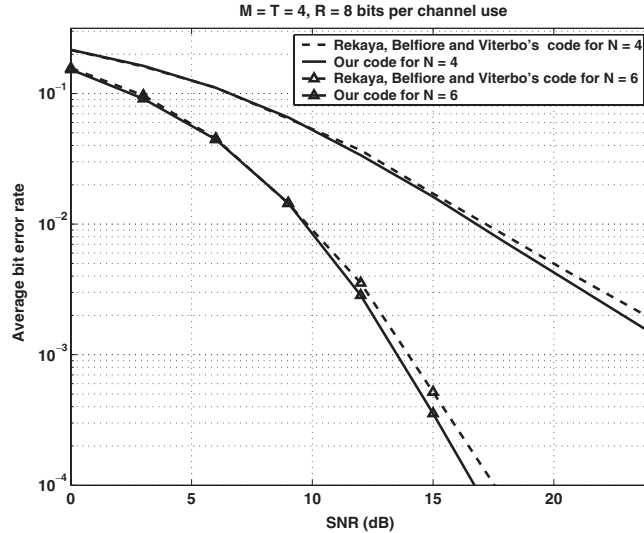


Figure 5.5 The error-performance comparison of our new code with Rekaya, Belfiore and Viterbo's code [67].

satisfies the intraunitary requirement. However, it is interorthogonal but not orthonormal. Therefore, it is expected that their code has slightly worse performance than our code under the condition that both are detected by a linear receiver. Simulation results are shown in Fig. 5.5, which supports our arguments.

5.9 Conclusion

In this chapter, we examine the design of LD space-time codes applied to a MIMO communication system from both the information-theoretic and detection error viewpoints. We arrive at the conclusion that a good LD code should have a trace-orthogonal structure. In particular, when the signal is QPSK modulated and an MMSE detector is employed at the receiver, we have shown that the necessary and sufficient condition for an LD space-time code to minimize the average bit error probability is that the code is trace-orthogonal. This desirable structure has prompted us to come up with a method to construct such a code family by the way of the V-structured matrix. Furthermore, by applying cyclotomic field theory, we have developed a systematic method to jointly design the rotation matrix, the Diophantine number and constellation. This has led us to arrive at a very efficient design of full diversity rectangular LD code at a symbol transmission rate less than or equal to the number of the transmitter antennas. We emphasize that the method is applicable to a MIMO system with any number of transmitter antennas and receiver antennas, i.e., it generalizes the currently available full diversity square linear space-time block design to a rectangular design. In particular, when the number of the transmitter antennas is $M = 2^m$, and the number of the receiver antennas is less than M , we proposed a linear space-time block code

design that possesses a submatrix of an isosceles-triangular structure at a symbol rate N per channel use. This code has been shown to minimize the worst-case average pairwise error probability of the ML detector for a QAM signal and, as a result, achieves the optimal coding gain.

References

- [1] I. Teletar, "Capacity of multi-antenna Gaussian channels," *European Trans. Telecommun.*, vol. 10, pp. 585–595, Nov. 1999.
- [2] G. Foschini and M. Gans, "On limits of wireless communications in a fading environment when using multiple antenna," *Wireless Pers. Commun.*, vol. 6, pp. 311–335, Mar. 1998.
- [3] G. D. Golden, G. J. Foschini, R. A. Valenzuela, and P.-W. Wolniansky, "Detection algorithm and initial laboratory results using V-BLAST space-time communication architecture," *Electr. Lett.*, vol. 35, pp. 14–15, Jan. 1999.
- [4] V. Tarokh, H. Jafarkhani, and A. R. Calderbank, "Space-time codes for high date rate wireless communication: Performance criterion and code construction," *IEEE Trans. Inf. Theory*, vol. 44, pp. 744–765, Mar. 1998.
- [5] S. M. Alamouti, "A simple transmitter diversity scheme for wireless communications," *IEEE J. Sel. Areas Commun.*, vol. 16, pp. 1451–1458, Oct. 1998.
- [6] V. Tarokh, H. Jafarkhani, and A. R. Calderbank, "Space-time block codes from orthogonal designs," *IEEE Trans. Inf. Theory*, vol. 45, pp. 1456–1467, Jul. 1999.
- [7] B. M. Hochwald and T. L. Marzetta, "Unitary space-time modulation for multiple-antenna communication in Rayleigh flat-fading," *IEEE Trans. Inf. Theory*, vol. 46, pp. 543–564, Mar. 2000.
- [8] B. M. Hochwald and W. Sweldens, "Differential unitary space-time modulation," *IEEE Trans. Commun.*, vol. 48, pp. 2041–2052, Dec. 2000.
- [9] B. Hughes, "Differential space-time modulation," *IEEE Trans. Inf. Theory*, pp. 2567–2578, Nov. 2000.
- [10] A. Shokrollahi, B. Hassibi, B. Hochwald, and W. Sweldens, "Representation theory for high-rate multiple-antenna code design," *IEEE Trans. Inf. Theory*, 2001.
- [11] M. Brehler and M. K. Varanasi, "Asymptotic error probability analysis of quadratic receiver in Rayleigh-fading channels with applications to a unified analysis of coherent and noncoherent space-time receivers," *IEEE Trans. Inf. Theory*, vol. 47, pp. 2383–2399, Sept. 2001.
- [12] A. L. Swindlehurst and G. Leus, "Blind and semi-blind equalization for generalized space-time block codes," *IEEE Trans. Signal Process.*, vol. 50, pp. 2489–2498, Oct. 2002.
- [13] N. D. Sidiropoulos and R. S. Budampati, "Khatri-Rao space-time codes," *IEEE Trans. Signal Process.*, vol. 50, pp. 2396–2407, Oct. 2002.
- [14] S. Shahbazpanahi, A. B. Gershman, and J. H. Manton, "Closed-form channel estimation for blind decoding of orthogonal space-time block codes," in *IEEE Int. Conf. Commun.*, vol. 1, (Paris), pp. 20–24, Jun. 2004.
- [15] W.-K. Ma, P. C. Ching, and T. N. Davidson, "Blind symbol identifiability of orthogonal space-time block codes," in *Int. Conf. Acoust., Speech, Signal Process.*, (Montreal, Canada), pp. 821–824, May 2004.
- [16] A. V. Geramita and J. Seberry, "Orthogonal design, quadratic forms and hadamard matrices," in *Lecture Notes in Pure and Applied Mathematics*, New York: Marcel Dekker, 1979.
- [17] G. Ganesan and P. Stoica, "Space-time block codes: a maximum SNR approach," *IEEE Trans. Inf. Theory*, vol. 47, pp. 1650–1656, May. 2001.

- [18] O. Tirkkonen and A. Hottinen, "Square-matrix embeddable space-time codes for complex signal constellations," *IEEE Trans. Inf. Theory*, vol. 48, pp. 1122–1126, Feb. 2002.
- [19] X.-B. Liang, "Orthogonal designs with maximal rates," *IEEE Trans. Inf. Theory*, vol. 49, pp. 2468–2503, Oct. 2003.
- [20] X.-B. Liang and X.-G. Xia, "Nonexistence of rate one space-time blocks from generalized complex linear processing orthogonal designs for more than two transmit antennas," in *Int. Symp. Inf. Theory*, (Washington, DC), Jun. 2001.
- [21] W. Su and X.-G. Xia, "Two generalized complex orthogonal space-time block codes of rates 7/11 and 3/5 for 5 and 6 transmit antennas," in *Int. Symp. Inf. Theory*, (Washington DC), Jun. 2001.
- [22] H. Wang and X.-G. Xia, "Upper bounds of rates of complex orthogonal space-time block codes," in *Int. Symp. Inf. Theory*, (Lausanne, Switzerland), Jun. 2002.
- [23] S. Sandhu and A. J. Paulraj, "Space-time block coding: A capacity perspective," *IEEE Commun. Lett.*, vol. 4, pp. 384–386, Dec. 2000.
- [24] B. Hassibi and B. M. Hochwald, "High-rate codes that are linear in space and time," *IEEE Trans. Inf. Theory*, vol. 50, pp. 1804–1824, Jul. 2002.
- [25] R. W. Heath and A. J. Paulraj, "Linear dispersion codes for MIMO systems based on frame theory," *IEEE Trans. Signal Process.*, vol. 50, pp. 2429–2441, Oct. 2002.
- [26] H. E. Gamal and M. O. Damen, "Universal space-time coding," *IEEE Trans. Inf. Theory*, vol. 49, pp. 1097–1119, May. 2003.
- [27] X.-Ma and G. B. Giannakis, "Full-diversity full rate complex-field space-time coding," *IEEE Trans. Signal Process.*, vol. 51, pp. 2917–2930, Nov. 2003.
- [28] B. A. Sethuraman, B. S. Rajan, and V. Shashidhar, "Full-diversity, high rate space-time block codes from division algebras," *IEEE Trans. Inf. Theory*, vol. 49, pp. 2596–2616, Oct. 2003.
- [29] J. Boutros and E. Viterbo, "Signal space diversity: A power-and bandwidth-efficient diversity technique for the Rayleigh fading channel," *IEEE Trans. Inf. Theory*, vol. 44, pp. 1453–1467, Jul. 1998.
- [30] X. Giraud and J. C. Belfiore, "Constellations matched to the Rayleith fading channel," *IEEE Trans. Inf. Theory*, vol. 42, pp. 106–115, Jan. 1996.
- [31] X. Giraud and J. C. Belfiore, "Algebraic tools build modulation schemes for fading channels," *IEEE Trans. Inf. Theory*, vol. 43, pp. 938–952, May 1997.
- [32] M. O. Damen and N. C. Beaulieu, "On two high-rate algebraic space-time codes," *IEEE Trans. Inf. Theory*, vol. 49, pp. 1059–1063, Apr. 2003.
- [33] Y. Xin, Z. Wang, and G. B. Giannakis, "Space-time constellation-rotating codes maximizing diversity and coding gains," in *Proc. Global Telecommun. Conf.*, vol. 1, pp. 455–459, 2001.
- [34] M. O. Damen, K. A. Meraim, and J. C. Belfiore, "Diagonal algebraic space-time block codes," *IEEE Trans. Inf. Theory*, vol. 48, pp. 628–636, Mar. 2002.
- [35] H. E. Gamal and A. R. Hammons, "A new approach to layered space-time coding and signal processing," *IEEE Trans. Inf. Theory*, vol. 47, pp. 2321–2334, Sept. 2001.
- [36] K. Boulle and J.-C. Belfiore, "Modulation schemes designed for the Rayleigh fading channel," in *Proc. CISS*, (Princeton, NJ), Mar. 1992.
- [37] G.-Y. Wang, H.-Y. Liao, H.-Q. Wang, and X.-G. Xia, "Systematic and optimal cyclotomic lattices and diagonal space-time block code designs," *IEEE Trans. Inform. Theory*, vol. 50, pp. 3348–3360, Dec. 2004.
- [38] I. Kammoun and J. C. Belfiore, "A new family of Grassmann space-time codes for non-coherent MIMO systems," *IEEE Commun. Letters*, vol. 7, pp. 528–530, Nov. 2003.

- [39] R. A. Horn and C. R. Johnson, *Topics in Matrix Analysis*. The Pitt Building, Trumpington Street, Cambridge CB2 1RP England: Cambridge University Press, 1991.
- [40] J.-K. Zhang, K. M. Wong, and T. N. Davidson, "Information lossless full rate full diversity cyclotomic linear dispersion codes," in *Int. Conf. Acoust., Speech, Signal Process.*, (Montreal, Canada), May 2004.
- [41] J.-K. Zhang, J. Liu, and K. M. Wong, "Trace-orthonormal full diversity triangular cyclotomic space-time minimizing worst-case pairwise error probability," in *Int. Conf. Sensor Array and Multichannel Signal Processing*, (Sitges, Barcelona, Spain), July 2004.
- [42] R. A. Horn and C. R. Johnson, *Matrix Analysis*. Cambridge, MA: Cambridge University Press, 1985.
- [43] R. J. Muirhead, *Aspects of Multivariate Statistical Theory*. New York: John Wiley & Sons, 1982.
- [44] T. M. Cover and J. A. Thomas, *Elements of Information Theory*. New York: John Wiley and Sons, 1991.
- [45] J. W. Craig, "A new, simple, and exact result for calculating the probability of error for two-dimensional signal constellations," in *Proc. IEEE Milit. Commun. Conf.*, (McLean, VA), pp. 571–575, Oct. 1991.
- [46] M. K. Simon and M.-S. Alouini, "A unified approach to the performance analysis of digital communication over generalized fading channels," *Proc. IEEE*, vol. 86, pp. 1860–1877, Sept. 1998.
- [47] J.-C. Guey, M. P. Fitz, M. R. Bell, and W.-Y. Kuo, "Signal design for high data rate wireless communication systems over Rayleigh fading channels," in *Proc. IEEE Veh. Technol. Conf.*, pp. 136–140, 1996.
- [48] M. O. Damen, H. E. Gamal, and N. C. Beaulieu, "Linear threaded algebraic space-time constellation," *IEEE Trans. Inf. Theory*, vol. 49, pp. 2372–2388, Oct. 2003.
- [49] J.-K. Zhang, J. Liu, and K. M. Wong, "Trace-orthonormal full diversity cyclotomic linear dispersion codes," in *Proc. IEEE Int. Symp. Inf. Theory*, (Chicago, ill), Jun. 2004.
- [50] M. O. Damen, A. Tewfik, and J. C. Belfiore, "A construction of a space-time code based on number theory," *IEEE Trans. Inf. Theory*, vol. 48, pp. 658–661, Mar. 2002.
- [51] J. Liu, J.-K. Zhang, and K. M. Wong, "Design of optimal orthogonal linear codes in MIMO systems for MMSE receiver," in *Int. Conf. Acoust., Speech, Signal Process.*, (Montreal, Canada), May 2004.
- [52] J. Liu, "Optimal linear STBC design for MIMO systems with MMSE receivers" M.A.Sc. Thesis, Department of Electrical and Computer Engineering, McMaster University, (Hamilton, Canada), Jun. 2004.
- [53] J. Liu, J.-K. Zhang, and K. M. Wong, "On the design of minimum BER linear space-time block codes for MIMO systems with MMSE receivers," submitted to *IEEE Trans. Signal Process.*, Oct. 2004.
- [54] U. Madhow and M. L. Honig, "MMSE interference suppression for direct-sequence spread-spectrum CDMA," *IEEE Trans. Commun.*, vol. 42, pp. 3178–3187, Dec. 1994.
- [55] Y.-P. Lin and S.-M. Phoong, "BER minimized OFDM systems with channel independent precoders," *IEEE Trans. Signal Process.*, vol. 51, pp. 2369–2380, Sept. 2003.
- [56] G. D. Forney and G. U. Ungerboeck, "Modulation and coding for linear Gaussian channel," *IEEE Trans. Inf. Theory*, vol. 44, pp. 2384–2415, May 1998.
- [57] J. Boutros, E. Viterbo, C. Rastello, and J. C. Belfiore, "Good lattice constellations for both Rayleigh fading and Gaussian channels," *IEEE Trans. Inf. Theory*, vol. 42, pp. 502–518, Mar. 1996.
- [58] D. A. Marcus, *Number Fields*. New York: Springer-Verlag, 1977.

- [59] P. Ribenboim, *13 Lectures on Fermat's Last Theorem*. New York: Springer-Verlag, 1979.
- [60] S. Lang, *Algebraic Number Theory*. New York: Spring-Verlag, 1986.
- [61] P. Morandi, *Field and Galois Theory*. New York: Springer, 1996.
- [62] M. O. Damen, H. E. Gamal, and N. C. Beaulieu, "Systematic construction of full diversity algebraic constellations," *IEEE Trans. Inf. Theory*, vol. 49, pp. 3344–3340, Dec 2003.
- [63] M. O. Damen and N. C. Beaulieu, "On diagonal algebraic space-time block codes," *IEEE Trans. Commun.*, vol. 51, pp. 911–919, Jun. 2003.
- [64] H. Yao and G. W. Wornell, "Achieving the full MIMO diversity-vs-multiplexing frontier with rotation-based space-time codes," in *41th Annu. Allerton Conf. Commun. Control, Comput.*, (Monticello, IL), Oct. 2003.
- [65] P. Dayal and M. K. Varanasi, "An optimal two transmit antenna space-time code and its stacked extensions," in *Asilomar Conf. Signals, Syst. Comput.*, (Monterey, CA), Nov. 2003.
- [66] J. C. Belfiore, G. R. Rekaya, and E. Viterbo, "The Golden code: A 2×2 full rate space-time code with non-vanishing determinants," in *Proc. IEEE Int. Symp. Inf. Theory*, (Chicago, ill), Jun. 2004.
- [67] G. Rekaya, J.-C. Belfiore, and E. Viterbo, "Algebraic 3×3 , 4×4 and 6×6 space-time codes with non-vanishing determinants," in *ISITA*, (Parma, Italy), Oct. 2004.

6

Linear and Dirty-Paper Techniques for the Multiuser MIMO Downlink

Christian B. Peel, Quentin H. Spencer, A. Lee Swindlehurst, Martin Haardt, and Bertrand M. Hochwald

6.1 Introduction

Multi-input, multi-output (MIMO) communications systems have attracted considerable attention over the past decade, mostly for single-user, point-to-point scenarios. The multiuser MIMO case has attracted less attention; most of the research on this problem has focused on uplink communications. Only recently has the multiuser MIMO downlink been addressed, beginning with information-theoretic capacity results [1–4, 17], and followed by practical implementations, including those based on linear techniques [5, 6] and non-linear precoding [7–9, 83]. In this chapter we review these techniques and discuss some important open problems.

6.1.1 Problem overview

The term *multiuser MIMO downlink* typically refers to situations in which a multiantenna transmitter (e.g., a base station) simultaneously communicates with several cochannel users. In the communications and information theory literature, this scenario is referred to as the *MIMO broadcast channel*. We will also use the term *spatial multiplexing* to describe this problem, although we note that this term is also used in connection with point-to-point MIMO links when multiple independent data streams are transmitted to a single user (e.g., as in vertical Bell Labs space-time (V-BLAST) techniques [10, 11]). The users in

a multiuser MIMO network may have a single antenna, and hence no ability for spatial discrimination, or they may have multiple antennas and the ability to perform some type of interference suppression. This is to be contrasted with the MIMO uplink problem, where a multiple antenna receiver must separate the signals arriving from several different users. This scenario is often referred to as the *MIMO multiple access* channel (MAC) or space-division multiple access (SDMA). In this paper, we focus on the multiuser MIMO downlink or broadcast channel. Although less frequently addressed in the literature, there is still a considerable body of work on this topic, which is too extensive to adequately cover in this chapter. As discussed below, we will focus on two classes of approaches to this problem: linear beamforming techniques and nonlinear precoding.

Single-user MIMO systems have generated considerable excitement in the wireless communications literature because of their potential for significant gains in capacity over single-antenna links. Of particular note is that these gains are often independent of whether or not channel state information (CSI) is available at the transmitter. The situation is considerably different in the multiuser case, where interference must be taken into account and balanced against the need for high throughput. A transmission scheme that maximizes the capacity for one user in the network might result in unacceptably high interference for the other users, rendering their links useless. If high throughput is the goal, a better approach might be to maximize the *sum* capacity of the network or the maximum sum transmission rate, where the interuser interference is taken into consideration. Transmit CSI is the key to achieving such a goal. While in principle the receivers themselves could perform some interference cancellation via multiuser detection, for example, the desire to keep costs low and preserve battery life for the end user in cellular networks usually leads to simpler receiver architectures.

Maximizing the sum capacity of a multiuser downlink channel does not always lead to a desirable solution. For example, if one of the users has a channel with considerably higher SNR than the others, the sum capacity solution might come at the expense of the weaker users who will receive little or no throughput. An alternative in such cases is to attempt to achieve a certain Quality of Service level (QoS), *for example*, measured in terms of signal-to-interference-plus-noise ratio (SINR) or bit-error rate (BER). The problem of meeting QoS constraints with minimum transmit power is often referred to as the downlink *power control* or *interference-balancing* problem. As with sum capacity maximization, channel knowledge at the transmitter is crucial to finding a solution.

Channel state information is most often obtained by means of uplink training data, as in a time-division duplex system, or via feedback from the users, as in the frequency-division duplex case. Each approach has its advantages and disadvantages in terms of throughput penalty and latency. CSI can be in the form of deterministic channel estimates, or it can be described in probabilistic terms (e.g., channel mean and covariance). While we will focus on the deterministic case in this chapter, statistical CSI may be directly applied in most cases. For an excellent and comprehensive treatment of the issues involved with different types of CSI, see [12].

6.1.2 Literature survey

Algorithms for multiuser MIMO downlink processing can be classified according to a number of criteria: whether they attempt to approach the sum capacity bound, eliminate interuser interference or achieve minimum QoS constraints, whether the users have single or multiple antennas, whether or not multiple data streams are transmitted to each user, and so on. We

begin with the case that has received the most attention: users with single-antenna receivers. The most direct approach in this case is referred to as *channel inversion* [13, 14], which amounts to using a set of transmit beamformers that “preinverts” the channel and ideally removes all interuser interference at the receivers. One can think of this approach as zero-forcing transmit beamforming. As with zero-forcing receive beamformers, problems arise when the channel is nearly rank deficient, although we will see it is not noise amplification that occurs but rather signal attenuation. Minimum mean-squared error (MMSE) or regularized transmit beamforming can be used as an alternative to reduce sensitivity to low-rank channels, in which case dramatically improved performance is obtained [5, 15]. Although the gain of regularized channel inversion is significant, there is still a considerable gap between its performance and the capacity bound. Algorithms from the class of so-called “dirty paper” coding techniques have recently been shown to more closely approach the sum capacity for the multiuser channel, and in some cases achieve it [2, 3, 16–18]. We will describe one such technique, referred to as *vector modulo precoding* [7, 15, 19, 20], that can be framed as an extension of the channel inversion algorithms described earlier.

The algorithms mentioned above attempt to maximize the overall throughput of the network for a fixed transmit power, under the constraint of zero (or nearly zero) interference. On the other hand, power control or interference-balancing algorithms relax the zero interference constraint and minimize the total transmitted power subject to meeting given QoS constraints. Iterative methods have been found that are guaranteed to find the optimal solution to this problem, assuming a solution exists [21, 22]. The problem can also be posed as a semidefinite optimization with convex constraints and solved using more efficient numerical procedures [23].

To this point, the research cited has assumed that each user possesses only one receive antenna. These algorithms can be trivially extended to multiple antenna receivers by viewing each as a separate “user,” provided that the total number of receive antennas for all users is no greater than the number of transmit antennas. While this allows for extremely simple receiver architectures, it ignores the ability of the receivers to perform spatial discrimination of their own and is only practical for networks with a small number of cochannel users. The result can be either (i) a significant gap between the achievable throughput of these techniques and the capacity of the system in cases where the receivers can obtain CSI or (ii) a dramatic increase in required transmit power to achieve a desired QoS, especially in situations in which the channels to adjacent receive antennas are not uncorrelated.

Instead of completely diagonalizing the channel as some of the techniques above attempt to do, one could find an optimal *block* diagonalization when the users have multiple antennas. Such an approach removes interuser interference but leaves the receiver responsible for separating the multiple data streams sent to it [6, 24–29]. This approach still has the drawback of requiring more transmit antennas than the total number of receive antennas among all the users. As a means of relaxing this constraint, suppose that each user employs a beamformer or beamformers of its own to receive the data stream(s) destined for it. If the transmitter knew what those beamformers were in advance, then it could consider the *effective* channel to each user to be the combination of the propagation channel for that user and the beamformers that user employs. As long as the total number of data streams to all users does not exceed the number of transmit antennas, then any of the algorithms discussed above could be used. The problem of course is that the optimal receive beamformers depend on the choice of the transmit beamformers, and vice versa. Iterative techniques have been proposed in which the

transmitter postulates a set of receive beamformers, designs a corresponding set of transmit weights, updates the receive beamformers accordingly, and so on [6, 29–35].

6.1.3 Chapter organization

In the next section, we describe the mathematical model we will assume for our discussion of the multiuser MIMO downlink and establish a common notation. Section 6.3 describes algorithms for the case where each user has only a single receive antenna and presents some simulation results illustrating their performance. Section 6.4 does the same for cases involving multiple antennas per user. We finally summarize and review open problems in the area in Section 6.5, including references to related work that we did not address in this chapter.

6.2 Background and Notation

We will consider a standard scenario involving a base station that simultaneously transmits data to K users, whose channels have been determined earlier either through the use of uplink training data (as in a time-division duplex system) or via a feedback channel (as in a frequency-division duplex system). The base station is assumed to have n_T antennas, user j has n_{R_j} antennas, and the total number of receive antennas is $n_R = \sum_{j=1}^K n_{R_j}$. In a flat-fading propagation environment, the channel between the base and user j is described by the $n_{R_j} \times n_T$ matrix \mathbf{H}_j , whose rows we denote by \mathbf{h}_{ij}^* as follows.

$$\mathbf{H}_j^* = [\mathbf{h}_{1j} \dots \mathbf{h}_{n_{R_j} j}] .$$

The symbol $(\cdot)^*$ is used to denote the complex conjugate (Hermitian) transpose. In Section 6.3, we will focus on cases where $n_{R_j} = 1$, in which case we will simply denote the channel as $\mathbf{H}_j = \mathbf{h}_j^*$. We will follow the convention of denoting matrices by capital boldface letters, vectors in lowercase boldface, and scalars as either upper or lowercase letters without boldface.

The base station may desire to send data at different rates to each of the K active users. This can be accomplished by an appropriate choice of the symbol constellation for each user or by changing the number of independent data streams that are simultaneously sent to each user. We will let m_j denote the number of data streams transmitted to user j . Suitable values for m_1, \dots, m_K will not only depend on the desired data rate for user j but also on the available transmit power, the achievable SINR, and the number of transmit and receive antennas. We will see that, typically, $m_j \leq n_{R_j}$ without some type of additional coding or multiplexing, and that $\sum m_k \leq n_T$. We will assume that m_j has been determined beforehand, recognizing the fact that this resource allocation step is critical if optimal system performance is required. Thus, at symbol time t , the transmitter desires to send the $m_j \times 1$ vector of symbols $\mathbf{d}_j(t)$ to user j . The signal destined for user j that is actually broadcast from the transmit antennas at time t is denoted by the $n_T \times 1$ vector $\mathbf{s}_j(t)$. In many cases, the transmitted signal is a linear function of the symbols, that is, $\mathbf{s}_j(t) = \mathbf{B}_j \mathbf{d}_j(t)$, where the columns of \mathbf{B}_j , denoted $\mathbf{B}_j = [\mathbf{b}_{1j} \dots \mathbf{b}_{m_j j}]$, correspond to the transmit beamformers for each symbol. In cases where $m_j = 1$, we will simply write $\mathbf{B}_j = \mathbf{b}_j$, $\mathbf{d}_j(t) = d_j(t)$, and $\mathbf{s}_j(t) = \mathbf{b}_j d_j(t)$. We will also consider algorithms that employ a nonlinear mapping of the symbols to the transmitted data: $\mathbf{s}_j(t) = \mathbf{f}_j(\mathbf{d}_j(t))$.

User j not only receives its desired signal through the channel \mathbf{H}_j but also contributions from the signals destined for other users:

$$\mathbf{x}_j(t) = \sum_{k=1}^K \mathbf{H}_j \mathbf{s}_k(t) + \mathbf{e}_j(t), \quad (6.1)$$

where $\mathbf{e}_j(t)$ is assumed to represent spatially white noise and interference with covariance $\mathcal{E}\{\mathbf{e}_j(t)\mathbf{e}_j^*(t)\} = \mathbf{I}$. If linear beamforming is used on the transmit side, then stacking the data together from all of the receivers leads to the following compact expression.

$$\mathbf{x}(t) = \begin{bmatrix} \mathbf{x}_1(t) \\ \vdots \\ \mathbf{x}_K(t) \end{bmatrix} = \begin{bmatrix} \mathbf{H}_1 \\ \vdots \\ \mathbf{H}_K \end{bmatrix} [\mathbf{B}_1 \dots \mathbf{B}_K] \begin{bmatrix} \mathbf{d}_1(t) \\ \vdots \\ \mathbf{d}_K(t) \end{bmatrix} + \begin{bmatrix} \mathbf{e}_1(t) \\ \vdots \\ \mathbf{e}_K(t) \end{bmatrix} \quad (6.2)$$

$$= \mathbf{H}\mathbf{B}\mathbf{d}(t) + \mathbf{e}(t), \quad (6.3)$$

where the definitions of $\mathbf{x}(t)$, \mathbf{H} , \mathbf{B} , $\mathbf{d}(t)$ and $\mathbf{e}(t)$ should be obvious from context. For the sake of simplicity, in what follows we will drop the explicit dependence of the above equations on time. In some figures we will use the notation $\{n_{R_1}, \dots, n_{R_K}\} \times n_T$ to describe the configuration of the antennas. Thus, a $\{1, 1, 1, 1\} \times 4$ system has $K = 4$ users, each with one antenna, and a base station with 4 antennas, while $\{1, 1, 2, 2\} \times 4$ describes the same case, with the exception that two of the users have two antennas.

6.2.1 Capacity

A fundamental tool for characterizing any communication channel is capacity. In a single-user channel, capacity is the maximum amount of information that can be transmitted as a function of available bandwidth, given a constraint on transmitted power. In single-user MIMO channels, it is common to assume that there is a constraint on the total power broadcast by all transmit antennas. For the multiuser MIMO channel, the problem is somewhat more complex. Given a constraint on the total transmitted power, it is possible to allocate varying fractions of that power to different users in the network, so a single power constraint can yield many different information rates. The result is a “capacity region” like that illustrated in Figure 6.1 for a two-user channel. The maximum capacity for user 1 is achieved when 100% of the power is allocated to user 1; for user 2 the maximum capacity is also obtained when it has all the power. For every possible power distribution in between, there is an achievable information rate, which results in the capacity regions depicted in the illustration. Two regions are shown in Figure 6.1, the bigger one for the case where both users have roughly the same maximum capacity, and the other for a case where they are different (due, for example, to user 2’s channel being attenuated relative to user 1). For K users, the capacity region is characterized by a K -dimensional volume.

The maximum achievable throughput of the entire system is given by the point on the curve that maximizes the sum of all of the users’ information rates and is referred to as the *sum capacity* of the channel. This point is illustrated in Figure 6.1 by dots. Achieving

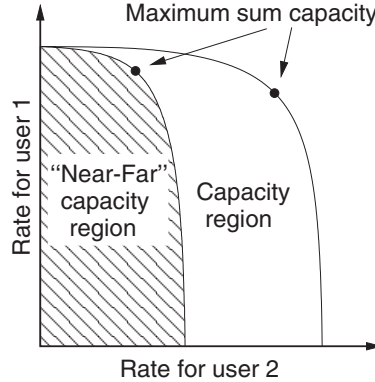


Figure 6.1 An illustration of a multiuser capacity region. The sum capacity may penalize certain users, depending on the shape of the capacity region.

the sum capacity point may not necessarily be the goal of a system designer. One example where this may be the case is when the “near-far” problem occurs, where one user has a strongly attenuated channel compared to other users. As depicted in Figure 6.1, obtaining the sum capacity in such a situation would come at the expense of the user with the attenuated channel.

The sum capacity for a system described by (6.1) has been formulated using the dirty paper coding (DPC) framework (see, for example, [2, 3, 16–18] and [36–39]) for the case of Gaussian noise. The capacity is defined in terms of the achievable rate for each user given the set of covariance matrices for each transmitted data vector $\mathbf{S}_k = \mathcal{E}\{\mathbf{s}_k\mathbf{s}_k^*\}$:

$$R_k = \frac{\log \left| \mathbf{I} + \mathbf{H}_k \left(\sum_{j=1}^k \mathbf{S}_j \right) \mathbf{H}_k^* \right|}{\log \left| \mathbf{I} + \mathbf{H}_k \left(\sum_{j=1}^{k-1} \mathbf{S}_j \right) \mathbf{H}_k^* \right|}, \quad (6.4)$$

assuming that the data for each user is uncorrelated with the others. The sum capacity is then

$$C_S = \max_{\mathbf{S}_k \geq 0; \sum \text{tr}(\mathbf{S}_k) \leq \rho} \sum_{k=1}^K R_k, \quad (6.5)$$

where ρ is the upper bound on the total transmit power. The input distributions are arbitrary, though the sum capacity can be achieved with Gaussian signals [16, 17]. The capacity region C_R of a given multiuser MIMO system is defined to be the set of all achievable rates $\{R_1, \dots, R_K\}$ given the power constraint. In general, determining C_R is an unsolved problem, but a solution for the Gaussian case has been reported in [4] building on work in [40].

In the case of users with single receive antennas ($n_{R_j} = 1$ for all j) the sum capacity expression is much simpler:

$$C_S = \max_{\mathbf{D} \in \mathbf{A}} \log |\mathbf{I} + \mathbf{H}\mathbf{D}\mathbf{H}^*|, \quad (6.6)$$

where \mathbf{A} is the set of all $K \times K$ nonnegative diagonal matrices \mathbf{D} with $\text{tr}(\mathbf{D}) \leq \rho$. This equation looks much like the capacity of a point-to-point MIMO system with M transmit antennas and K receive antennas, where only the receiver has knowledge of the channel: $\log |\mathbf{I} + (\rho/n_T)\mathbf{H}\mathbf{H}^*|$. This comparison makes it easy to see that multiuser sum capacity grows linearly with $\min(M, K)$ under the same conditions as for the single-user case.

6.2.2 Dirty-paper coding

As mentioned above, capacity results for the multiuser problem have been achieved using the notion of *dirty-paper coding*, which originates in a 1983 paper [41] by M. H. M. Costa. He studies a channel with Gaussian noise and interference that is known to the transmitter and makes an analogy to the problem of writing on dirty paper. To describe this idea, let

$$y = s + i + w , \quad (6.7)$$

where s is the signal used to transmit a codeword d , i is interference with power Q known deterministically at the transmitter, but unknown to the receiver, $w \sim \mathcal{CN}(0, N)$ is Gaussian noise, and the received data is y . Costa presented the encouraging result that the capacity of this system is the same as if there were no interference present. If the signal has power constraint $|s|^2 \leq \rho$, then the capacity of this system is

$$C = \log \left(1 + \frac{\rho}{N} \right) \quad (6.8)$$

regardless of what Q is. To extend the dirty-paper analogy, the “capacity” of dirty paper is the same as for a sheet without this known “dirt.”

This result has been applied to a variety of systems: using what is nominally “analog” spectrum for both analog and digital signals [42], information-embedding applications [43], and in finding the capacity of the MIMO broadcast channel [1–4, 17]. These theoretical results have motivated progress in the development of practical algorithms [44–46] that approach the capacity bound (6.8).

To illustrate dirty-paper principles, we describe a simple technique based on the use of a simple modulo operator. Although this method is very simple, it performs within a few dB of capacity. We define the modulo function f as

$$f_\tau(y) = y - \left\lfloor \frac{y + \tau/2}{\tau} \right\rfloor \tau . \quad (6.9)$$

The signal s is created using information about the interference i and the codeword d , as follows.

$$s = f_\tau(d - i) = d - i - \tau k , \quad (6.10)$$

where k is an integer. The modulo function reduces the power of the transmitted signal from what it would be if the simple method of $s = d - i$ were used. Applying the modulo function to the received data (6.7) gives

$$\begin{aligned} f_\tau(y) &= f_\tau(s + i + w) = f_\tau(d - i - \tau k + i + w) \\ &= f_\tau(d + w) . \end{aligned}$$

The interference has been cancelled; there remains only a penalty from applying the modulo function to $d + w$, which may lie outside the interval $(-\tau/2, \tau/2)$, and cause $f_\tau(d + w) \neq d + w$. In a practical system τ would be a function of the codeword constellation, chosen, for example, as described in Section 6.3.3.

To completely overcome this shaping loss, coding must occur over n consecutive samples and the modulo operation is applied with respect to a “good” n -dimensional lattice rather than with respect to an interval. Finally, as $n \rightarrow \infty$, the shaping error disappears and capacity is achieved (See [37] for more information, including how to handle low SNR situations and to find a discussion on what a “good” lattice is). The shaping loss is 1.56 dB when using the simple cubical lattice defined by (6.9) as compared with an infinite-dimensional lattice on a scalar Gaussian interference channel. In Section 6.3.3, we use these DPC ideas to describe and analyze a coding technique for the MIMO downlink channel.

6.2.3 Discussion

We have assumed a data model with a flat fading or narrow-band channel. However, in many current and next-generation wireless communications applications, this assumption does not hold. Wideband or frequency-selective fading channels suffer from intersymbol interference and a fading characteristic that varies significantly across the frequency band. There are several ways to apply the matrix channel model to this case. In channels where the use of orthogonal frequency division multiplexing (OFDM) is considered, it is possible to implement MIMO processing algorithms separately for each frequency bin, where the channel fading characteristic can be considered to be narrowband. In what follows, we assume a narrow-band channel model but note that our discussion can be applied to the wideband case using either OFDM or other common techniques for frequency-selective channels.

One additional property of radio propagation channels that must also be considered in the multiuser MIMO context is how they vary with time, particularly for applications that assume mobility of one or both ends of the wireless link. Two likely applications for multiuser MIMO transmission are wireless local area networks (LANs) and cellular telephony. Wireless LANs are a natural fit for MIMO technology because the rich multipath environment in the places where they are usually deployed (indoors, office or college campuses, etc.) is an important criterion for achieving high capacity. In this type of channel, user mobility is likely to be very slow, and the channel can be viewed as being quasi-static. Cellular telephone applications are more challenging because of higher user mobility, and the small size and cost constraints of manufacturing mobile devices make the use of multiple antennas problematic. While time-varying channel models have been considered in analyzing simple MIMO systems [47–49], most applications assume quasi-static fading. Further research on techniques for obtaining and tracking channel state information is needed for highly mobile scenarios. Recent research suggests that the prediction horizon for MIMO systems may be much longer than in the SISO case (which has usually proven to be too short to be useful), since multiple antennas reveal more information about the physical structure of the channel [50].

Perhaps the most critical assumption common to all of the recent multiuser MIMO research is the availability of CSI at the transmitter. While single-user MIMO systems

benefit from having CSI at the transmitter only when $n_T > n_R$ or at low SNR, a base station transmitting to multiple cochannel users will almost always benefit from CSI. This is because the CSI is not only useful in achieving high SNR at the desired receiver but also in reducing the interference produced at other points in the network by the desired user's signal. The most common method for obtaining CSI at the transmitter is through the use of training or pilot data in the uplink (*e.g.*, for time-division duplex systems) or via feedback of the receiver's channel estimate found using downlink training data (*e.g.*, for frequency-division duplex transmission). In either case, obtaining CSI at the transmitter is a very challenging and costly problem, but appears justifiable for multiuser channels.

6.3 Single Antenna Receivers

We begin our discussion of multiuser MIMO downlink algorithms with the case most commonly treated in the research literature, namely situations involving users with only one receive antenna: $n_{R_j} = 1$. With only one antenna, the receiver is unable to perform any spatial interference suppression of its own, and the transmitter is responsible for precoding the data in such a way that the interference seen by each user is tolerable. In the discussion that follows, we consider four techniques for solving this problem: channel inversion, regularized channel inversion, sphere encoding and iterative interference balancing, or power control.

6.3.1 Channel inversion

Channel inversion [13, 14] simply amounts to undoing the effects of the channel via pre-coding; in other words, we precode the data with the (pseudo-)inverse of the channel prior to transmission, as illustrated in Figure 6.2 for the case where \mathbf{H} is square. More generally, we define

$$\mathbf{s} = \frac{1}{\sqrt{\gamma}} \mathbf{H}^* (\mathbf{H}\mathbf{H}^*)^{-1} \mathbf{d}, \quad (6.11)$$

where it is assumed that $n_T \geq K = n_R$. The scaling factor γ is present to limit the total transmitted power to some predetermined value ρ :

$$\|\mathbf{s}\|^2 = \rho \Rightarrow \gamma = \frac{1}{\rho} \mathbf{d}^* (\mathbf{H}\mathbf{H}^*)^{-1} \mathbf{d}. \quad (6.12)$$

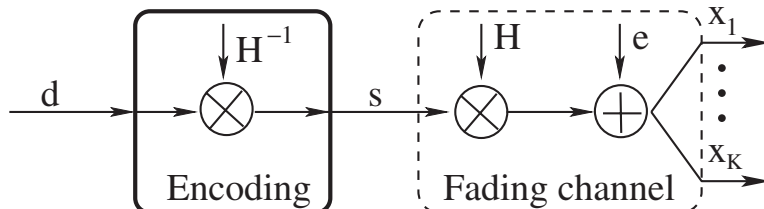


Figure 6.2 Channel Inversion cancels all interference but requires high power to cancel the small elements of \mathbf{H} .

Ideally, all interuser interference is canceled by this approach, reducing the problem to K separate scalar channels, and each user sees only the desired symbol in additive noise:

$$x_j = \frac{1}{\sqrt{\gamma}} d_j + e_j . \quad (6.13)$$

One issue that may be a problem in practice is the fact that the scaling γ is data-dependent and will in general change from symbol to symbol. To avoid this problem, γ can be chosen so that the *average* transmit power is ρ , which leads to

$$\gamma = \frac{1}{\rho} \text{trace} \left[(\mathbf{H}\mathbf{H}^*)^{-1} \right] \quad (6.14)$$

if the users' symbols are independent and have average unit power.

Obviously, a more serious problem arises if the channel is ill-conditioned. In such cases, at least one of the singular values of $(\mathbf{H}\mathbf{H}^*)^{-1}$ is very large, γ will be large, and the SNR at the receivers will be low. It is interesting to contrast channel inversion with least-squares or “zero-forcing” (ZF) receive beamforming, which applies a dual of the transformation in (6.11) to the receive data. Such beamformers are well known to cause noise amplification when the channel is nearly rank deficient. Here, on the transmit side, ZF produces signal attenuation instead. In fact, as shown in [5], the problem is very serious, even for what one might consider the “ideal” case, *i.e.*, where the elements of \mathbf{H} are independent, identically distributed Rayleigh random variables. If the elements of \mathbf{d} are modeled as independent zero-mean unit-variance Gaussian random variables, it can be shown [5] that the probability density function of γ is given by

$$p(\gamma) = K \frac{\gamma^{K-1}}{(1+\gamma)^{K+1}} , \quad (6.15)$$

when $n_T = K = n_R$, and γ has an infinite mean! As a consequence, the capacity of channel inversion does not increase linearly with K , unlike the capacity bound.

6.3.2 Regularized channel inversion

When rank-deficient channels are encountered in ZF receive beamforming, a common approach to reducing the effects of noise amplification is to regularize the inverse in the ZF filter. If the noise is spatially white and an appropriate regularization value is chosen, this approach is equivalent to using a minimum mean-squared error (MMSE) criterion to design the beamformer weights. Applying this principle to the transmit side suggests the following solution:

$$\mathbf{s} = \frac{1}{\sqrt{\gamma}} \mathbf{H}^* (\mathbf{H}\mathbf{H}^* + \zeta \mathbf{I})^{-1} \mathbf{d} , \quad (6.16)$$

where ζ is the regularization parameter. The presence of a nonzero value for ζ will mean that the transmit beamformer does not exactly cancel the “mixing” effect of the channel, resulting in some level of interuser interference. The key is to define a value for ζ that optimally trades off the numerical condition of the matrix inverse (which impacts the normalization required for the power constraint) against the amount of interference that is produced. In [5], it is shown that choosing $\zeta = K/\rho$ approximately maximizes the SINR at each receiver, and unlike standard channel inversion, leads to linear capacity growth with K .

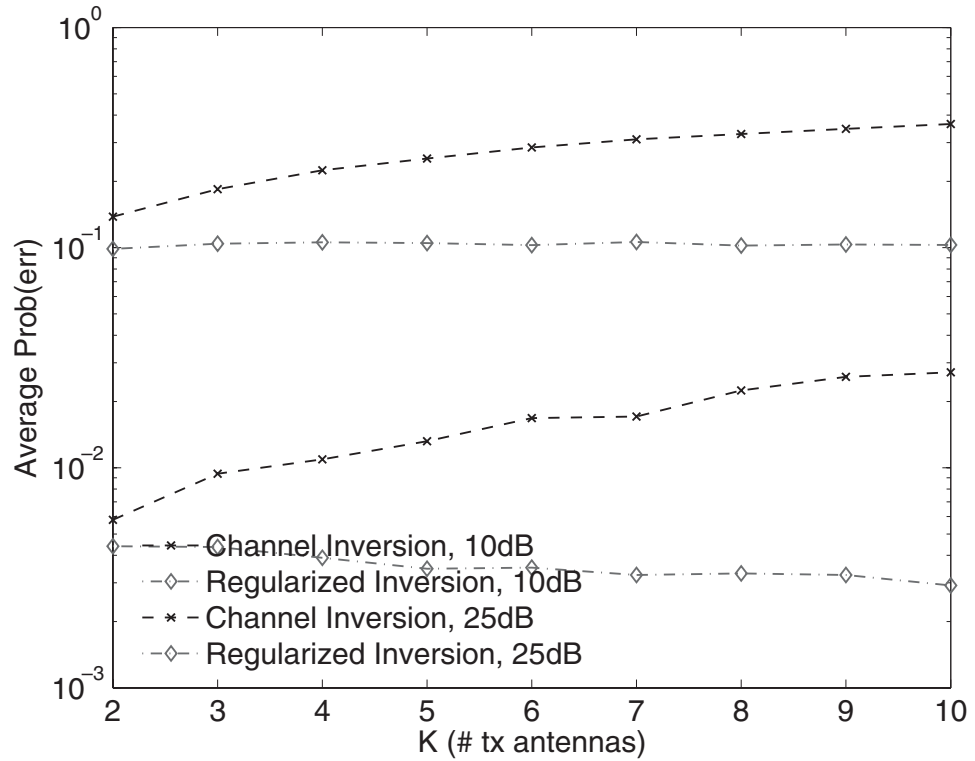


Figure 6.3 Comparing uncoded symbol error rates for standard and regularized channel inversion for as a function of K . The performance of channel inversion decreases with K , while regularized inversion improves slightly at high transmit power.

Figures 6.3 and 6.4 compare respectively the symbol error rates and capacity of standard and regularized channel inversion. Figure 6.3 shows average error rates as a function of K for QPSK signaling (the SNR is defined as ρ since the elements of \mathbf{e} are assumed to have unit power). The elements of the channel matrices were simulated as independent, unit-variance Rayleigh random variables. Note that the performance of standard channel inversion degrades as K increases, while the performance of regularized inversion is approximately constant. Figure 6.4 plots capacity as a function of K assuming $n_T = K = n_R$ and $\rho = 10$ dB. The plot also shows that there is still a considerable gap between the performance of regularized inversion and the sum capacity of the system.

6.3.3 Sphere encoding

The simulation results of the previous section indicate that channel inversion techniques are not capacity optimal. As mentioned above, dirty-paper coding (DPC) techniques more closely approach (and in some cases achieve) multiuser capacity, and thus may be of interest when capacity is the primary design criterion. DPC is different from other downlink

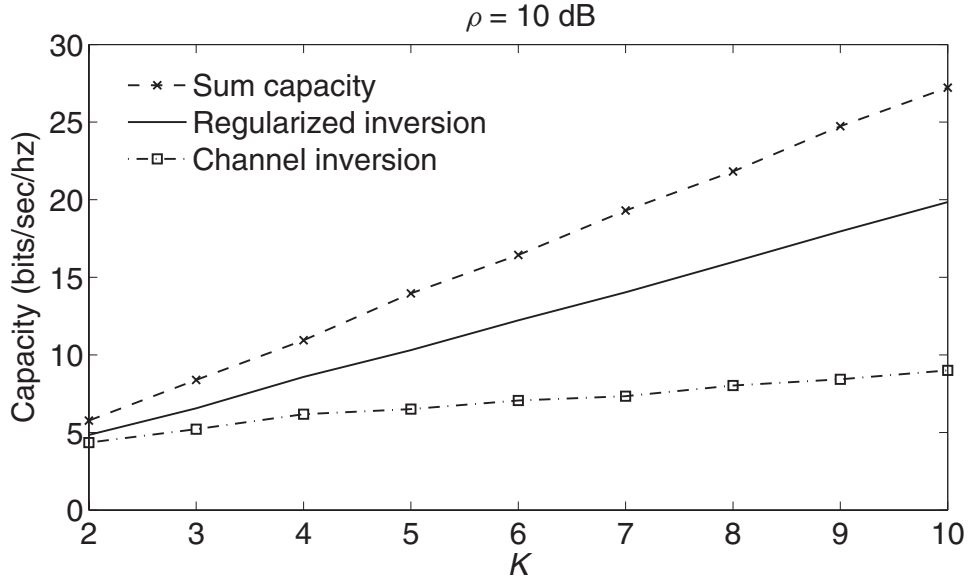


Figure 6.4 Comparison of the sum capacity (dashed line) as a function of K (where $n_T = K$) for $\rho = 10 \text{ dB}$ with the regularized channel inversion sum-rate (solid line) and the standard channel inversion sum-rate (dash-dotted line).

approaches in that the transmitted data is a nonlinear function of the information symbols, as well as the interference environment. For this reason, DPC is sometimes referred to as *interference-dependent coding*. Because of their nonlinear nature and their need for high-dimensional lattices, DPC techniques are often difficult to implement in practice.

In this section, we present a simple DPC technique that fits in well with the channel inversion algorithms already discussed. Figure 6.5 illustrates the approach we will consider, which is referred to as *vector precoding*. As discussed above, channel inversion performs poorly because the scaling factor γ in (6.12) can be large when the channel is ill-conditioned, and the vector \mathbf{d} happens to (nearly) align itself with a right singular vector of $(\mathbf{H}\mathbf{H}^*)^{-1}$ with large singular value. The idea behind the technique proposed in [7, 15] is to “perturb” the symbol vector \mathbf{d} by some value $\bar{\mathbf{d}}$ such that $\mathbf{d} + \bar{\mathbf{d}}$ is directed toward singular vectors of $(\mathbf{H}\mathbf{H}^*)^{-1}$ with smaller singular values, and in such a way that the receivers can still decode \mathbf{d} without knowledge of $\bar{\mathbf{d}}$. In particular, [7, 15] constrains $\bar{\mathbf{d}}$ to lie on a (complex) integer lattice:

$$\bar{\mathbf{d}} = \tau(\mathbf{a} + j\mathbf{b}), \quad (6.17)$$

where \mathbf{a}, \mathbf{b} are vectors of integers and τ is a real-valued constant, and calculates $\bar{\mathbf{d}}$ on the basis of the following optimization problem.

$$\begin{aligned} \bar{\mathbf{d}} &= \arg \min_{\bar{\mathbf{d}}} (\mathbf{d} + \bar{\mathbf{d}})^* (\mathbf{H}\mathbf{H}^*)^{-1} (\mathbf{d} + \bar{\mathbf{d}}) \\ \text{s.t. } \bar{\mathbf{d}} &= \tau(\mathbf{a} + j\mathbf{b}). \end{aligned} \quad (6.18)$$

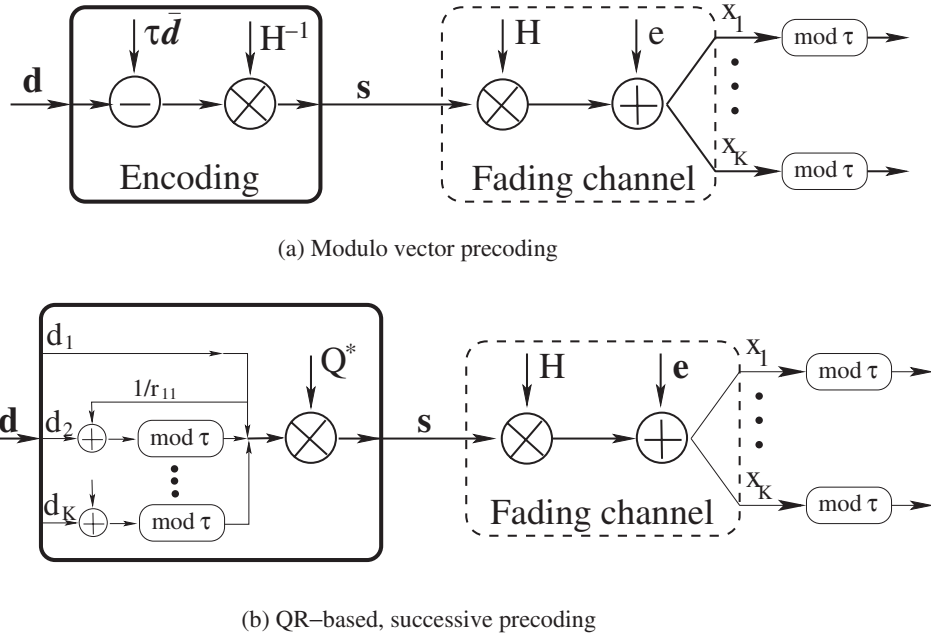


Figure 6.5 Part (a) shows the vector precoding technique; a vector chosen to minimize the signal power is added to the data to be transmitted. Part (b) shows that QR-based techniques successively cancel interference from previous users.

This is an integer-lattice least-squares problem and can be solved using standard sphere algorithm methods [51–53] and other related techniques [54, 55]. Since it is used on the transmit side for this application, in [7, 9, 15] it is referred to as *sphere encoding* or *sphere precoding*. Using this method, the vector of data at the receivers is given by

$$\mathbf{x} = \frac{1}{\sqrt{\gamma}} \mathbf{d} + \frac{1}{\sqrt{\gamma}} \tau (\mathbf{a} + j\mathbf{b}) + \mathbf{e}, \quad (6.19)$$

where, as before, γ is chosen to maintain a constant (average) transmit power ρ .

To eliminate the contribution of the vector perturbation, the receivers employ the modulo function (6.9). If τ and γ (or $\mathcal{E}\{\gamma\}$) are known at the receivers, then in the absence of noise,

$$f_\tau(\sqrt{\gamma}x_j) = f_\tau(d_j + \tau a_j + \tau b_j) = d_j. \quad (6.20)$$

Small values of τ are advantageous because they allow for a denser perturbation lattice and hence more flexibility in maximizing received SINR. However, τ must be chosen large enough to allow for unambiguous decoding. In [7, 15], it is suggested that τ be chosen as

$$\tau = 2(d_{max} + \Delta/2), \quad (6.21)$$

where d_{max} is the distance from the origin to the farthest constellation point, and Δ is the maximum distance between any two constellation points.

A simple numerical example is now presented to illustrate the algorithm. For simplicity, we consider the special case of binary pulse-amplitude modulated (PAM) signaling over real-valued channels with $K = 2$ and $\rho = 1$. A near-singular channel matrix is chosen to illustrate the benefit of nonlinear precoding:

$$\mathbf{H} = \begin{bmatrix} -0.0521 & 0.17 \\ -0.661 & 1.80 \end{bmatrix}. \quad (6.22)$$

Suppose the data to be transmitted is $\mathbf{d} = [-1, 1]^T$, with noise $\mathbf{e} = [0.011, 0.001]^T$. Simple channel inversion gives the signal $\mathbf{H}^{-1}\mathbf{d} = [-106, -38.4]^T$, which results in $\gamma = 12,700$. Transmitting the normalized signal through the channel results in $\mathbf{x} = [0.00213, 0.00987]^T$, which gives decoded PAM symbols [1, 1] when using the sign of the elements of \mathbf{x} to decode. In contrast, sphere encoding results in $\bar{\mathbf{d}} = \tau[0, 2]^T$, which results in a signal with a more attractive $\gamma = 36.5$. For our 2-PAM constellation, we choose $\tau = 4$, resulting in the received signal $\mathbf{x} = [-0.154, -1.82]^T$ and $f_\tau(\mathbf{x}) = [-0.154, 0.166]^T$. In this case, decoding based on $f_\tau(\mathbf{x})$ returns the correct symbols $[-1, 1]^T$.

Figure 6.6 shows a plot of the uncoded symbol error probability of the algorithms discussed thus far for a case with $n_T = 10$, $n_R = 10$, a Rayleigh fading channel and QPSK signaling. “Sphere Encoder” denotes the modulo precoding algorithm described above, and “Reg. Sphere Encoder” refers to the use of vector modulo precoding together with regularized channel inversion. Regularization improves performance, but by a smaller margin than in the case of standard channel inversion. It is clear from the plot that, for SNRs high enough to achieve reliable decoding, modulo precoding offers a significant improvement

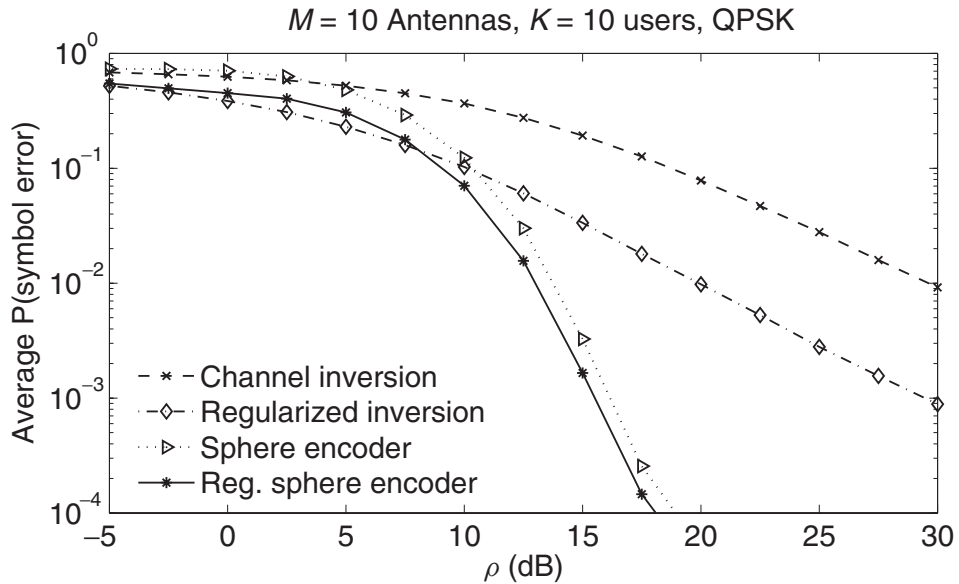


Figure 6.6 Uncoded probability of symbol error for various downlink algorithms as a function of transmit power ρ .

in performance over channel inversion and regularized inversion. The modulo precoding technique presented here represents perhaps the simplest form of DPC for the multiuser MIMO problem, that is, one involving a simple cubical lattice. As reported in [7], improved performance can be expected if more complicated, higher-dimensional lattices [37, 56] are employed. In particular, these techniques may improve the low-SNR performance of the modulo precoding techniques, which perform slightly worse than their linear counterparts in Figure 6.6. Finally, we note that a suboptimal but more computationally efficient version of the modulo precoding algorithm has recently been presented in [8].

A full analysis of the algorithm appears difficult, due in part to the difficulty in obtaining a distribution for γ . We focus instead on understanding the performance gains seen in our simulations. The precoding process aligns $\mathbf{d} - \bar{\mathbf{d}}$ with the singular values of the inverse channel. Let $\mathbf{UDV}^* = \mathbf{H}^{-1}$ be the singular value decomposition (SVD) of the channel inverse, so that $\delta_{CI} = |\mathbf{V}^* \mathbf{d}|$ is the channel-inversion data vector rotated by the right singular vectors of \mathbf{H}^{-1} , and $\delta_{SE} = |\mathbf{V}^* (\mathbf{d} - \bar{\mathbf{d}})|$, is the equivalent for the sphere encoded data. The sphere encoder minimizes the cost function

$$\gamma = \|\delta_{SE}^* \boldsymbol{\sigma}\|^2 \quad (6.23)$$

over $\bar{\mathbf{d}}$, where $\boldsymbol{\sigma}$ is a vector containing the singular values of \mathbf{H}^{-1} . For channel inversion, we have $\gamma = \|\delta_{CI}^* \boldsymbol{\sigma}\|^2$. In [5] it is shown that $\mathcal{E}\{\gamma\} = \infty$ for plain channel inversion. In contrast, for the sphere encoder, $\mathcal{E}\{\gamma\}$ is shown in [7, 15] to be approximately constant with K . Specifically, $\mathbf{d} - \bar{\mathbf{d}}$ is chosen to orient itself toward each singular vector in inverse proportion to the singular value of the inverse channel matrix:

$$\mathcal{E}\{\sigma_1 \delta_1\} = \dots = \mathcal{E}\{\sigma_K \delta_K\}. \quad (6.24)$$

We illustrate this in Figure 6.7, where $\delta_k \sigma_k$ are shown averaged over 10,000 samples for a case where $K = n_T = 10$ users and a 16-QAM constellation is employed. While basic channel inversion does not modify or perturb the transmitted symbols, the sphere encoding technique attempts to orient the symbol vector toward each singular vector in inverse proportion to the singular values $\boldsymbol{\sigma}$. For comparison, we also show results for regularized inversion and regularized vector precoding, both with $\zeta = K/\rho$; for these curves the $\boldsymbol{\sigma}$ is obtained from the regularized inverse.

6.3.4 Computationally efficient precoding

Though the vector precoding technique in the previous section is very powerful, it is somewhat expensive computationally. There are several ways to increase the speed of the integer least-squares search, including successive algorithms based on the QR and V-BLAST decompositions, and on the use of lattice-reduction algorithms. We will present a simplified technique that generates the integer offset $\bar{\mathbf{d}}$ by repeated application of a modulo operation inspired by scalar Tomlinson-Harashima Precoding (THP) [57, 58]. The method uses a QR decomposition of the channel matrix \mathbf{H} , where the resulting triangular structure leads to the k th user seeing interference only from users $1, \dots, k-1$. The transmitter compensates for this interference by using its knowledge of s_1, \dots, s_{k-1} to generate s_k from u_k , for $k = 2, \dots, K$. Methods based on the QR decomposition have been explored for use with DPC codes in [1]. Similar algorithms have been used for crosstalk cancellation in digital subscriber lines [59] and for CDMA transmission to distributed receivers [60]. The

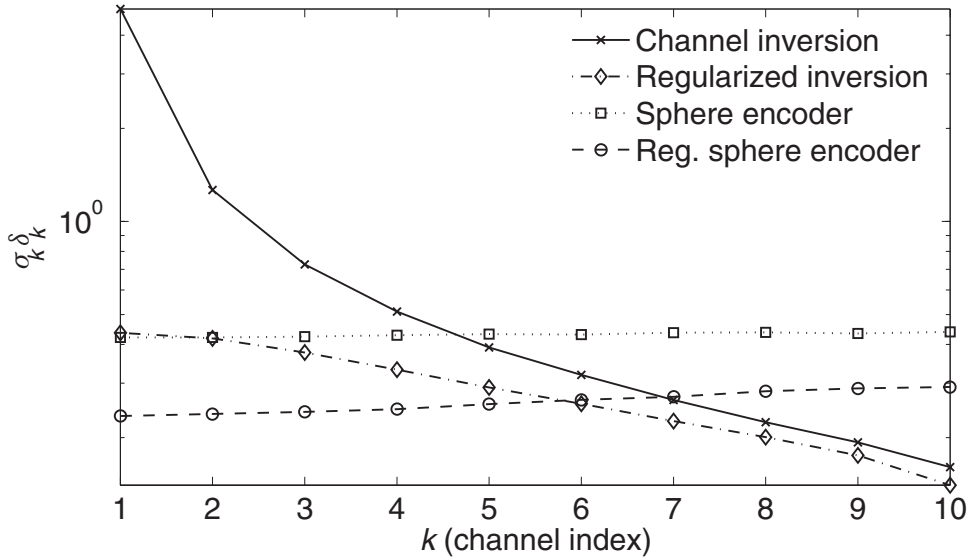


Figure 6.7 The integer offset vector $\bar{\mathbf{d}}$ is chosen such that it orients itself toward each singular vector in inverse proportion to the singular values σ . Values of $\delta_k \sigma_k$ are shown, averaged over 1000 samples.

achievable capacity of a greedy form of this scheme is analyzed in [83], where it is shown to be close to the sum capacity.

Let $\mathbf{H} = \mathbf{R}\mathbf{Q}$, where \mathbf{R} is a lower triangular matrix, and \mathbf{Q} is a unitary matrix; let \mathbf{D} be a diagonal matrix composed of the diagonal entries of \mathbf{R} , and $\alpha = \rho/(1 + \rho)$. We first generate the signal $\tilde{\mathbf{s}}$, and then form the transmitted signal $\mathbf{s} = \mathbf{Q}^*\tilde{\mathbf{s}}$. Because the matrix $\mathbf{R} - \mathbf{D}$ is zero on and above the diagonal, a successive technique can be used to generate $\tilde{\mathbf{s}}$:

$$\begin{aligned} \tilde{s}_1 &= d_1 \\ \tilde{s}_2 &= f_\tau \left(d_2 - \alpha \frac{r_{21}}{r_{22}} \tilde{s}_1 \right) \\ &\vdots \\ \tilde{s}_K &= f_\tau \left(d_K - \alpha \sum_{i=1}^{K-1} \frac{r_{Ki}}{r_{KK}} \tilde{s}_i \right), \end{aligned} \quad (6.25)$$

where d_k is the k th diagonal entry of D , and r_{ij} is the entry on the i th row and in the j th column of \mathbf{R} . We may write this equation in terms of the vector of integers $\bar{\mathbf{d}}$ that the modulo function effectively adds to the signal:

$$\tilde{\mathbf{s}} = \left((1 - \alpha)I + \alpha \mathbf{D}^{-1} \mathbf{R} \right)^{-1} (\mathbf{d} + \tau \bar{\mathbf{d}}). \quad (6.26)$$

The signal $\mathbf{s} = \mathbf{Q}^* \tilde{\mathbf{s}}$ is formed, normalized, and then sent through the channel. The K users receive

$$\mathbf{x} = \frac{1}{\sqrt{\gamma}} \mathbf{H} \mathbf{s} + \mathbf{e} = \frac{1}{\sqrt{\gamma}} \mathbf{R} \left((1 - \alpha) I + \alpha \mathbf{D}^{-1} \mathbf{R} \right)^{-1} (\mathbf{d} + \tau \bar{\mathbf{d}}) + \mathbf{e}.$$

The parameter α increases the SINR for each user, similar to what the parameter ζ does with regularized inversion in Section 6.3.2. Let y_k be the data received at the k th user; decoding occurs at user k based on [1, 37]

$$y'_k = f_{\tilde{\tau}_k}(\alpha y_k),$$

where $\tilde{\tau}_k = \tau \frac{r_{kk}}{\sqrt{\gamma}}$. Each receiver models the received data as

$$y'_k = \alpha \frac{r_{kk}}{\sqrt{\gamma}} d_k + w'_k,$$

where w'_k combines the additive receiver noise w_k and the interference. We do not analyze the algorithm but simply mention that at high ρ (where $\alpha \rightarrow 1$),

$$\mathbf{s} = \mathbf{Q}^* \mathbf{R}^{-1} \mathbf{D} (\mathbf{d} + \tau \bar{\mathbf{d}}), \quad (6.27)$$

which yields

$$y'_k = f_{\tilde{\tau}_k} \left(\frac{r_{kk}}{\sqrt{\gamma}} d_k + \tau l_k + w_k \right). \quad (6.28)$$

When $\alpha = 1$, there is no interference at user k from the other users' signals. The algorithm described here differs slightly from those of [59, 60] in our introduction of the parameter α . However, our use of α is well known in the DPC literature [1, 37], including in the original paper by Costa [41]. An important characteristic of these QR-based algorithms is that they do not achieve full diversity, although they do provide a significant computational advantage. For $K = N_R$, the complexity is of order K^2 . This is much less than for typical integer least-squares algorithms, which have expected complexity of order K^3 as described in [61]. A high peak-to-average power ratio can cause clipping in power amplifiers and accuracy problems in processors with limited wordlength. We note that the technique described here explicitly limits the peak signal strength; further research is needed on the use of a modulo function to minimize the peak-to-average power ratio.

A V-BLAST-type ordering of the users can also be applied to the QR decomposition [8, 62], with similar complexity in the resulting precoding algorithm. In this case, a permutation of the users is obtained as part of the V-BLAST decomposition; the rest of the algorithm is similar to that above for the QR-based techniques. An MMSE V-BLAST decomposition returns \mathbf{Q} and \mathbf{R} matrices that are no longer orthogonal and triangular, respectively. Some interference is allowed at each user in order to increase the overall SINR. For a full description and analysis of the basic V-BLAST technique, see [62]. The MMSE version of this technique performs especially well [63]; however, it also does not achieve the full spatial/multiuser diversity available. This can be easily seen by noting that at least one channel is processed linearly; at high SNR this channel will give an upper bound on performance and result in the same diversity as the linear techniques described in Section 6.3.1.

In contrast to the above techniques, an algorithm for finding the integer offset vector using the Lenstra-Lenstra-Lovász (LLL) algorithm [64] does give full diversity; at high SNR the slope of the error curves for this technique is the same as for vector precoding. The LLL matrix decomposition of the channel results in an integer matrix with unit determinant, and a reduced matrix \mathbf{B} :

$$\mathbf{H} = \mathbf{BT}, \quad \text{such that } |\mathbf{T}| = \pm 1 . \quad (6.29)$$

Thus, \mathbf{B} has the same determinant as \mathbf{H} . This decomposition can be used to obtain the Babai estimate of the integer offset:

$$\bar{\mathbf{d}} = \tau \mathbf{T} \left\lfloor \frac{\mathbf{T}^{-1} \mathbf{d}}{\tau} \right\rfloor . \quad (6.30)$$

MMSE versions of this algorithm exist for the uplink [65], though they have not been explored as much in the downlink setting.

6.3.5 Power control

As mentioned above, sum rate maximization in “near-far” scenarios may result in one or two strong users taking a dominant share of the available power, potentially leaving weak users with little or no throughput. Consequently, in practice, the dual *power control* problem is often of more interest, that is, minimizing power output at the transmitter subject to achieving a desired QoS for each user. We illustrate this approach below for the case where QoS is measured in terms of SINR. Assuming linear transmit beamformers and unit-power data symbols and noise, the SINR for user j can be expressed as:

$$\text{SINR}_j = \frac{\mathbf{b}_j^* \mathbf{R}_j \mathbf{b}_j}{\sum_{k \neq j} \mathbf{b}_k^* \mathbf{R}_j \mathbf{b}_k + 1} , \quad (6.31)$$

where either $\mathbf{R}_j = \mathbf{h}_j \mathbf{h}_j^*$ or $\mathbf{R}_j = \mathcal{E}\{\mathbf{h}_j \mathbf{h}_j^*\}$ depending on the type of CSI available at the transmitter.

Given a desired minimum SINR for each user, which we denote by η_j , the power control problem can be formulated as follows.

$$\begin{aligned} & \min_{b_1, \dots, b_K} \sum_{k=1}^K \mathbf{b}_k^* \mathbf{b}_k \\ \text{s.t. } & \frac{\mathbf{b}_j^* \mathbf{R}_j \mathbf{b}_j}{\sum_{k \neq j} \mathbf{b}_k^* \mathbf{R}_j \mathbf{b}_k + 1} \geq \eta_j , \quad j = 1, \dots, K . \end{aligned} \quad (6.32)$$

In [21, 22], iterative algorithms are presented that solve this problem when a feasible solution exists (i.e., if the SINR constraints can be met). An alternative formulation of the problem is presented in [23], where (6.32) is recast as a minimization over the matrices $\mathbf{W}_j = \mathbf{b}_j \mathbf{b}_j^*$ rather than the beamformers \mathbf{b}_j directly. It is shown that the constraint that \mathbf{W}_j be rank one can be relaxed, and the resulting optimization problem will still have an optimal rank-one solution. The advantage of this approach is that the problem becomes a semidefinite optimization, for which efficient numerical algorithms exist. While the above discussion has focused on linear beamforming, an approach based on vector precoding would be a natural extension of this work.

6.4 Multiple Antenna Receivers

With only a single antenna, the users in the network can perform no spatial interference suppression of their own, and can only receive data over a single spatial channel. With multiple antennas, these restrictions are removed, provided that the transmitter and receiver can coordinate their spatial processing, and appropriately allocate the available spatial resources. In this chapter, we present several methods that take advantage of the presence of multiple antennas at the receivers for increased throughput, enhanced interference suppression, or both.

6.4.1 Channel block diagonalization

The single-antenna techniques of the previous section could be directly applied in the multiple-antenna receiver case, provided that $n_R \leq n_T$, that is, the number of transmit antennas is greater than the number of receive antennas summed over all the users. In such cases, each receive antenna is considered to be a separate “user,” and each transmitted data stream is decoded independently on each receive antenna as if it were a SISO channel. As mentioned above, while this approach results in a very simple receiver, it overly constrains the problem and will lead to suboptimal performance.

Rather than forcing \mathbf{HB} in (6.2) to be diagonal (or nearly so), an alternative is to make it block-diagonal [6, 24–28]. This removes interuser interference but requires that the receiver perform some type of spatial demultiplexing to separate and decode the individual data streams sent to it. To be precise, the goal is to find \mathbf{B} such that

$$\mathbf{HB} = \begin{bmatrix} \mathbf{M}_1 & & \\ & \ddots & \\ & & \mathbf{M}_K \end{bmatrix}, \quad (6.33)$$

where \mathbf{M}_j is $n_{R_j} \times n_{R_j}$ assuming that up to n_{R_j} data streams are transmitted to user j (some of the columns of \mathbf{M}_j could be zero so that $m_j \leq n_{R_j}$). There are several criteria that could be used to determine \mathbf{M}_j . Below, we present an algorithm that is sum-capacity-achieving under the block-diagonal constraint [6].

Define $\tilde{\mathbf{H}}_j$ as the following $(n_R - n_{R_j}) \times n_T$ matrix:

$$\tilde{\mathbf{H}}_j = \left[\mathbf{H}_1^T \dots \mathbf{H}_{j-1}^T \mathbf{H}_{j+1}^T \dots \mathbf{H}_K^T \right]^T. \quad (6.34)$$

If we denote the rank of $\tilde{\mathbf{H}}_j$ as \tilde{L}_j , then the nullspace of $\tilde{\mathbf{H}}_j$ has dimension $n_T - \tilde{L}_j \geq n_{R_j}$. The SVD of $\tilde{\mathbf{H}}_j$ is partitioned as follows:

$$\tilde{\mathbf{H}}_j = \tilde{\mathbf{U}}_j \tilde{\Sigma}_j \left[\tilde{\mathbf{V}}_j^{(1)} \ \tilde{\mathbf{V}}_j^{(0)} \right]^*, \quad (6.35)$$

where $\tilde{\mathbf{V}}_j^{(0)}$ holds the $n_T - \tilde{L}_j$ singular vectors in the nullspace of $\tilde{\mathbf{H}}_j$. The columns of $\tilde{\mathbf{V}}_j^{(0)}$ are candidates for user j 's beamforming matrix \mathbf{B}_j , since they will produce zero interference at the other users. Since $\tilde{\mathbf{V}}_j^{(0)}$ potentially holds more beamformers than the number of data streams that user j can support, an optimal linear combination of these vectors must be

found to form \mathbf{B}_j , which can have at most n_{R_j} columns. To do this, the following SVD is formed:

$$\mathbf{H}_j \tilde{\mathbf{V}}_j^{(0)} = \left[\mathbf{U}_j^{(1)} \mathbf{U}_j^{(0)} \right] \left[\begin{array}{cc} \boldsymbol{\Sigma}_j & 0 \\ 0 & 0 \end{array} \right] \left[\mathbf{V}_j^{(1)} \mathbf{V}_j^{(0)} \right]^*, \quad (6.36)$$

where $\boldsymbol{\Sigma}_j$ is $L_j \times L_j$ and $\mathbf{V}_j^{(1)}$ represents the L_j singular vectors with nonzero singular values. The $L_j \leq n_{R_j}$ columns of the product $\tilde{\mathbf{V}}_j^{(0)} \mathbf{V}_j^{(1)}$ represent (to within a power loading factor) the beamformers that maximize the information rate for user j subject to producing zero interuser interference.

The transmit beamformer matrix will thus have the following form:

$$\mathbf{B} = \left[\tilde{\mathbf{V}}_1^{(0)} \mathbf{V}_1^{(1)} \dots \tilde{\mathbf{V}}_K^{(0)} \mathbf{V}_K^{(1)} \right] \boldsymbol{\Lambda}^{1/2}, \quad (6.37)$$

where $\boldsymbol{\Lambda}$ is a diagonal matrix whose elements scale the power allocated to each “subchannel.” With \mathbf{B} chosen as in (6.37), the capacity of the block diagonalization (BD) method becomes

$$C_{BD} = \max_{\boldsymbol{\Lambda}} \log_2 \left| \mathbf{I} + \boldsymbol{\Sigma}^2 \boldsymbol{\Lambda} \right| \quad \text{s.t. } \text{Tr}(\boldsymbol{\Lambda}) = \rho, \quad (6.38)$$

where

$$\boldsymbol{\Sigma} = \begin{bmatrix} \boldsymbol{\Sigma}_1 & & \\ & \ddots & \\ & & \boldsymbol{\Sigma}_K \end{bmatrix}. \quad (6.39)$$

The optimal power loading coefficients in $\boldsymbol{\Lambda}$ are then found using water-filling on the diagonal elements of $\boldsymbol{\Sigma}$. Forcing the interuser interference to zero also allows for a power control formulation of the above approach. This is done by performing water-filling on each $\boldsymbol{\Sigma}_j$ individually in order to achieve the desired rate for user j , then forming $\boldsymbol{\Lambda}$ from the diagonal matrices that result for each user.

Figure 6.8 illustrates the performance of the BD algorithm and several alternatives for a case involving $n_T = 4$ and $n_R = 4$ with $\rho = 10$ dB. The elements of \mathbf{H} were independent Rayleigh random variables with unit variance, and the cumulative distribution function of the capacity achieved by each method is plotted. The BD algorithm is implemented for three different scenarios: four users with one antenna each ($\{1, 1, 1, 1\} \times 4$), two users with two antennas each ($\{2, 2\} \times 4$), and a single user with four antennas (referred to as “1 User” in the figure). “Inversion” refers to channel inversion with equal power distributed to each data stream, and “TDM” refers to the case where no channel information is available and the users are simply time-multiplexed. Note that the difference between channel inversion and BD in the $\{1, 1, 1, 1\} \times 4$ case is due to the fact that BD employs an optimal power allocation via water-filling. The single-user performance is obviously the best, since it does not require the block-diagonal constraint. The improved performance of BD in the $\{2, 2\} \times 4$ case compared with the $\{1, 1, 1, 1\} \times 4$ scenario demonstrates the advantage of relaxing the requirement that the channel be identically diagonalized.

6.4.2 Combined block diagonalization and MMSE THP precoding

Block diagonalization (BD) always outperforms channel inversion, but it is still worse than MMSE THP transmit filtering when the users are equipped with one antenna each. In a

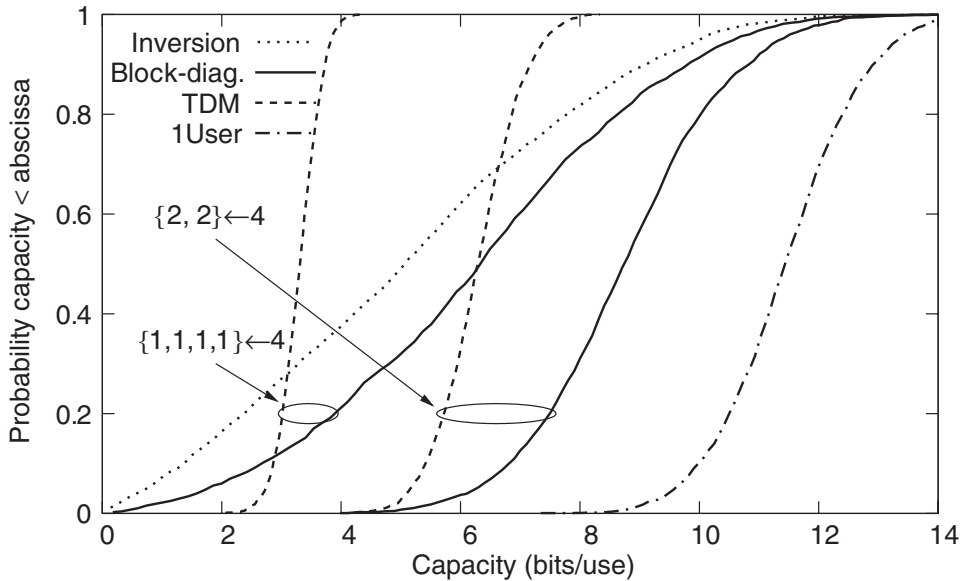


Figure 6.8 Cumulative distributions of the sum capacity for $n_T = n_R = 4$ achieved by several transmit beamforming strategies.

scenario where we have multiple users equipped with one or more antennas, the performance of the single-antenna users degrades the overall system performance. In [66], a combination of MMSE THP and block diagonalization is proposed, where MMSE THP is used for the single-antenna users and BD for the multiple-antenna users. This approach significantly improves the performance of the single-antenna users, and hence also that of the overall system.

In the combined BD and MMSE THP approach, the modulation matrices for multiple-antenna users are chosen to lie in the null space of the channel matrices of the other users including those with single antennas. In this way, the equivalent channel for the single-antenna users looks as if there are no multiple-antenna users present. This improves diversity for these users, which in turn improves their BER performance. MMSE THP is applied on the network channel corresponding to these single-antenna users. The data transmitted to the multiple-antenna users is also precoded using THP in order to eliminate the multiuser interference, which in this case only originates from the single-antenna users.

Figures 6.9 and 6.10 illustrate the performance of this combined technique. In the simulations, the data rate for each user is assumed to be proportional to the number of receive antennas. In Figure 6.9, we compare the performance of the multiple- and single-antenna users in a system with the configuration $\{1, 1, 2, 2\} \times 6$. The BER performance of the single-antenna users is represented using dashed lines. Here we compare the following algorithms: BD with dominant eigenmode transmission (DET), MMSE THP, and BD MMSE THP. In the case of MMSE THP, both single- and multiple-antenna users have similar performance. For BD DET and BD MMSE THP, there is a difference between the performance of the single- and multiple-antenna users. From the results for BD DET and BD MMSE THP,

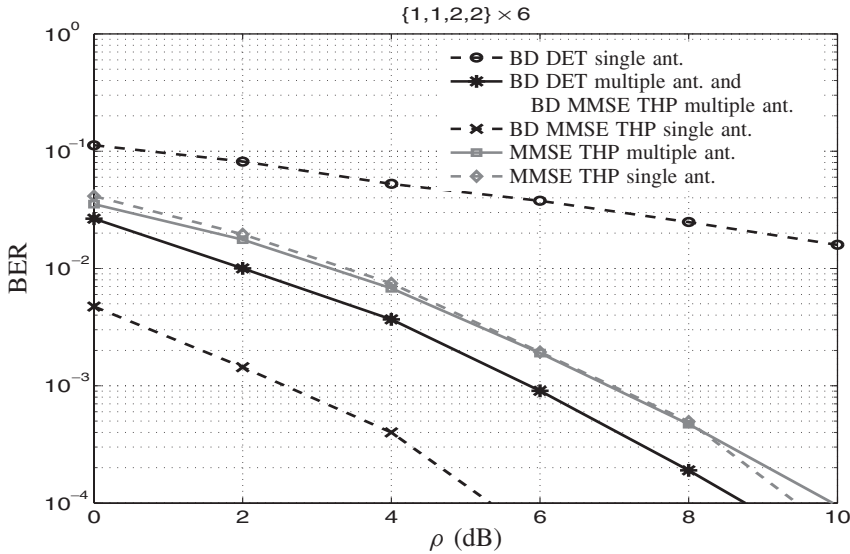


Figure 6.9 Average BER of the single- as well as the multiple-antenna users as a function of the SNR. For the single-antenna users, we use either BD or MMSE THP.

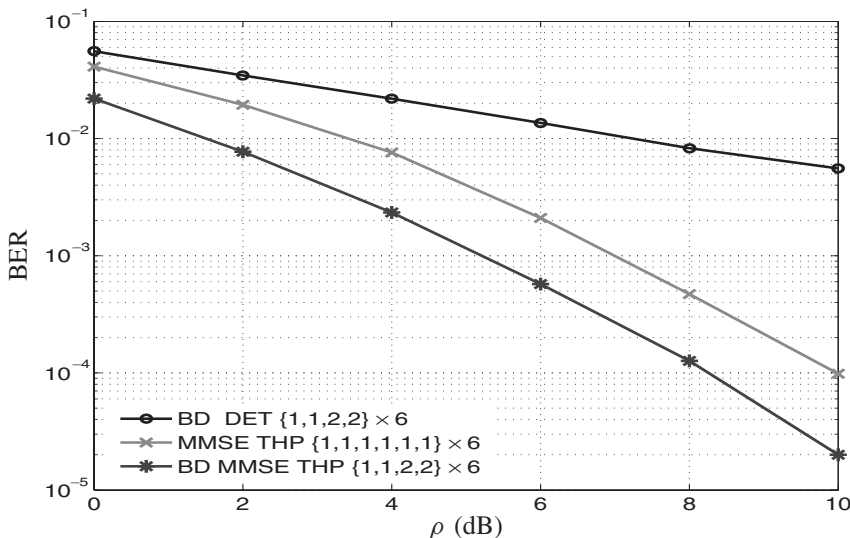


Figure 6.10 Overall BER of all users as a function of the SNR.

where the only difference is that in the first case we use BD for single-antenna users and in the second case we use MMSE THP, we can see that MMSE THP clearly outperforms BD for single-antenna users. In Fig. 6.10, the overall system performance is depicted comparing MMSE THP, BD, and the combination of BD and MMSE THP. The combination of BD and MMSE THP achieves an SNR gain of about 2 dB with respect to MMSE THP.

6.4.3 Coordinated Tx/Rx beamforming

Strictly speaking, the BD algorithm does not require $n_T \geq n_R$. However, when there are more than just a couple of users, n_R is usually close to the lower bound on the number of transmit antennas.¹ In this section, we examine methods that have a less stringent constraint on n_T , namely that n_T be no smaller than the total number of data streams to be transmitted. For example, if $m_j = 1$ for all j , then $n_T \geq K$ would be required. Obviously, in a real system where the total number of users serviced by a base station is very large, spatial multiplexing must be augmented by other multiple access techniques such as time and frequency multiplexing. A key question is how best to group the K users to be spatially multiplexed together into a given time/frequency slot.

To begin, consider the case where $m_j = 1$, and each receiver uses a beamformer \mathbf{w}_j in decoding the symbol d_j that is sent to it:

$$\bar{x}_j = \mathbf{w}_j^* \mathbf{x}_j = \sum_{k=1}^K \mathbf{w}_j^* \mathbf{H}_j \mathbf{b}_k d_k + \mathbf{w}_j^* \mathbf{e}_j \quad (6.40)$$

$$= \sum_{k=1}^K \bar{\mathbf{h}}_j^* \mathbf{b}_k d_k + \bar{e}_j , \quad (6.41)$$

where $\bar{\mathbf{h}}_j^* = \mathbf{w}_j^* \mathbf{H}_j$ represents the effective channel from the transmit array to the output of the receive beamformer, and $\bar{e}_j = \mathbf{w}_j^* \mathbf{e}_j$ represents the noise at the output of the receive beamformer. If we define $\bar{\mathbf{H}}^* = [\bar{\mathbf{h}}_1 \dots \bar{\mathbf{h}}_K]$, then we obtain an equation identical in form to (6.2):

$$\bar{\mathbf{x}} = \bar{\mathbf{H}} \mathbf{B} \mathbf{d} + \bar{\mathbf{e}} . \quad (6.42)$$

Each receiver has a single element of $\bar{\mathbf{x}}$ associated with it, so (6.42) has the same dimensions as (6.2) when $n_{R_j} = 1$. The implication is that, if the transmitter somehow has knowledge of $\mathbf{w}_1, \dots, \mathbf{w}_K$, then it knows $\bar{\mathbf{H}}$, and hence any of the downlink algorithms in Section 6.3 for the single-antenna-per-user case could be used. The coordinated transmit–receive beamforming technique is illustrated in Figure 6.11.

The composite channel $\bar{\mathbf{H}}$ could be estimated directly by the transmitter using uplink training data in a reciprocal time-division duplex (TDD) system, assuming that the receiver

¹Technically, the BD approach requires

$$n_T > \max \{ \text{rank}(\tilde{\mathbf{H}}_1), \dots, \text{rank}(\tilde{\mathbf{H}}_K) \} .$$

Since $\text{rank}(\tilde{\mathbf{H}}_j) \leq n_R - n_{R_j}$, it is clear that n_R can be larger than n_T . For example, two users with three antennas each could be accommodated by a transmit array with no more than four antennas, and possibly fewer depending on the rank of $\tilde{\mathbf{H}}_1$ and $\tilde{\mathbf{H}}_2$.

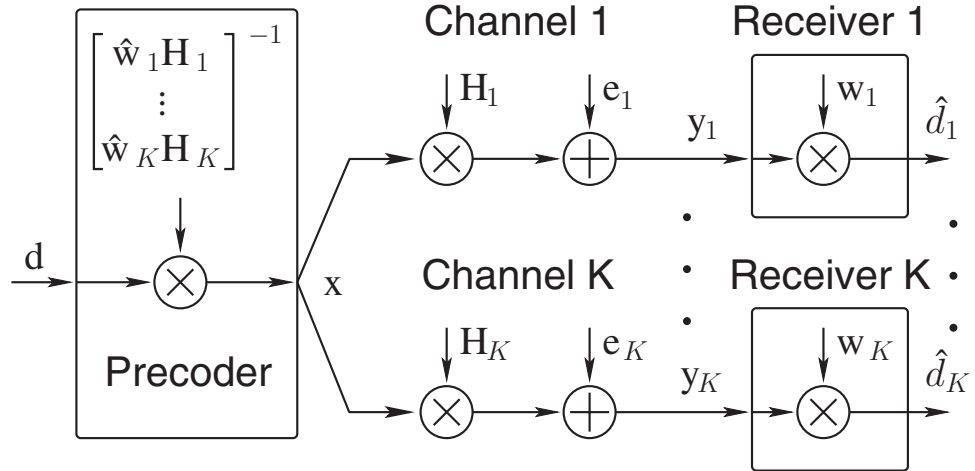


Figure 6.11 An illustration of coordinated transmitter-receiver beamforming, where the transmitter estimates what beamformers the receivers are using, creates a “virtual channel” matrix with one row per user, and uses channel inversion to create the transmit-side beamformers.

will use the conjugate of its transmit weights for downlink reception. However, this approach begs the question of how the receiver chose its beamformer, and whether or not any type of optimal solution is possible. An alternative is to assume the base station knows what algorithm each receiver uses in computing its own “optimal” receive beamformer. Since the base generates the interference that each user sees, given CSI it can predict what each user’s beamformer will be. For example, suppose it is known that user j employs MMSE receive beamforming. Then

$$\mathbf{w}_j = \left[\mathcal{E} \left\{ \mathbf{x}_j \mathbf{x}_j^* \right\} \right]^{-1} \mathcal{E} \left\{ \mathbf{x}_j d_j^* \right\} \quad (6.43)$$

$$= \left[\sum_{k \neq j} \mathbf{H}_j \mathbf{b}_k \mathbf{b}_k^* \mathbf{H}_j^* + \mathbf{I} \right]^{-1} \mathbf{H}_j \mathbf{b}_j, \quad (6.44)$$

which can be computed at the transmitter. Alternatively, if the receiver uses maximal ratio combining (MRC), then $\mathbf{w}_j = \mathbf{H}_j \mathbf{b}_j$, which is also a function of information known at the transmitter. Whatever the criterion chosen by the receiver, it is likely that the optimal value for \mathbf{w}_j will depend on one or more of the transmit beamformers in \mathbf{B} . On the other hand, the choice of \mathbf{B} in (6.42) depends on $\bar{\mathbf{H}}$, which in turn depends on the receive beamformers \mathbf{w}_j .

The interdependency of \mathbf{w}_j and \mathbf{B} suggests the following iterative approach:

1. Find an initial value for $\mathbf{w}_1, \dots, \mathbf{w}_K$. For example, they could be chosen as the principle left singular vectors of the respective channel matrices \mathbf{H}_j .
2. Repeat steps 3–4 until convergence.

3. Given $\mathbf{w}_1, \dots, \mathbf{w}_K$, calculate $\tilde{\mathbf{H}}$ and find \mathbf{B} using any of the algorithms discussed above (MMSE, MRC, or other).
4. Given \mathbf{B} , recalculate the receive beamformers $\mathbf{w}_1, \dots, \mathbf{w}_K$ according to their respective algorithms.

Convergence can be said to have occurred, for example, when no appreciable change in the achieved SINR or sum rate is observed from one iteration to the next. Algorithms of this general form have been presented in [6, 30–35]. While analytical results for these approaches are scarce, empirical evidence suggests they have reliable convergence behavior.

In situations where $m_j \geq 1$, solutions similar to those in Section 6.4.1 are possible, where in this case it is the effective channel $\tilde{\mathbf{H}}$ that is block-diagonalized. For this case, step 3 in the above iterative algorithm is replaced by either the capacity or the power control formulation of the BD algorithm, and rather than computing the $\mathbf{w}_1, \dots, \mathbf{w}_K$ vectors in step 4 independently, they are taken from the left singular vectors $\mathbf{U}_j^{(1)}$ in equation (6.36) with \mathbf{H}_j replaced by $\tilde{\mathbf{H}}_j$ (when $m_j = 1$, this is equivalent to using MRC beamformers). Figure 6.12 plots the cumulative distribution functions of capacity for the coordinated Tx/Rx beamforming algorithm described above. The SNR for this example is 10 dB, and the channels were all composed of independent, Rayleigh-distributed entries. Several base/user geometries were considered: 4×4 (single-user case), $\{2, 2\} \times 4$ with $m_1 = m_2 = 2$, $\{4, 4\} \times 4$ also with $m_1 = m_2 = 2$, $\{2, 2, 2, 2\} \times 4$ and $\{4, 4, 4, 4\} \times 4$. In the latter two scenarios, one subchannel is allocated to each user, and channel inversion is used to determine \mathbf{B} . When $m_j = 2$, the BD algorithm is assumed. As expected, the more total receive antennas

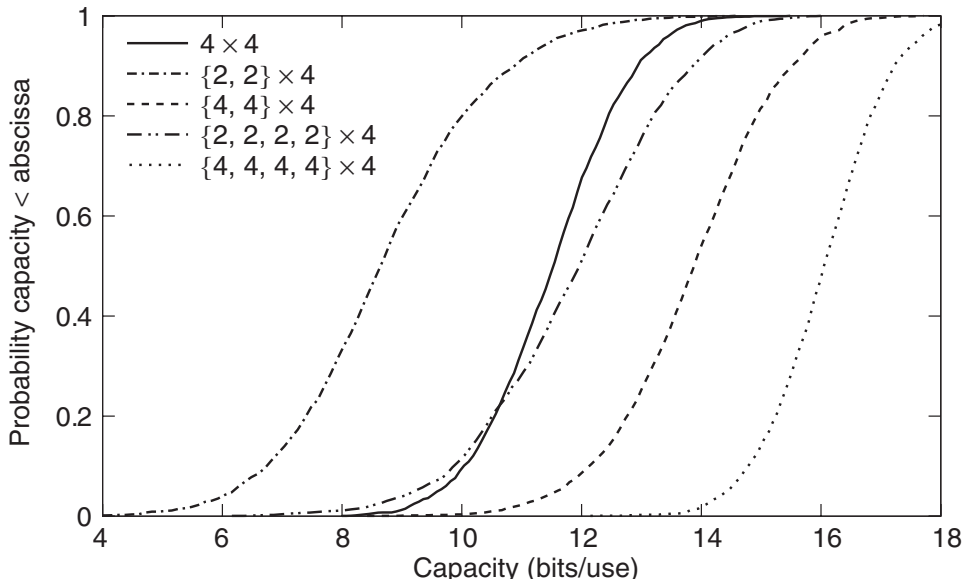


Figure 6.12 Cumulative distributions of the sum capacity for coordinated Tx/Rx beamforming in several scenarios.

that are available, the more flexibility there is in finding a good solution, and the higher the capacity. The 4×4 single-user system outperforms the $\{2, 2\} \times 4$ case since it does not require the block-diagonal constraint. Similarly, the $\{4, 4\} \times 4$ channel achieves higher capacity than the $\{2, 2, 2, 2\} \times 4$ system since the block-diagonal constraint is less restrictive than full channel diagonalization.

An obvious extension of this work is to combine the joint transmit–receive beamforming technique with the vector precoding approach of Section 6.3.3. At the transmitter, the nonlinear integer offset would be applied on the basis of the effective channel, which would include the transmit beamformers, with the modulo operation at the receivers occurring after the receive beamformers are applied. Similar to the significant diversity gain seen in Section 6.3.3 over linear techniques, the combined technique is anticipated to provide a significant diversity gain over linear joint transmit–receive beamforming.

6.5 Open Problems

6.5.1 Coding and capacity

A method for determining the multiuser capacity region in arbitrary scenarios is the most visible open problem in the area of multiantenna multiuser coding. The case of Gaussian noise was recently solved [4], but the general problem has not been solved. This and other theoretical results for the broadcast channel have built on dirty-paper coding techniques, which are rather complex. An important area of research is finding simple techniques for approaching the dirty-paper limit. In Section 6.3.3, we used a simple modulo operation to approach capacity; this idea may be extended to higher-dimensional lattices. Though these lattices are difficult to use for encoding and decoding, low-complexity techniques [8, 65] based on the LLL [64] algorithm exist.

A classic coding approach would be to use a QR-type approach as in Section 6.3.4, but with a more complex dirty-paper coding scheme replacing the simple modulo function. Candidate coding schemes include those based on nested lattices [56], repeat-accumulate codes [38], low-density-parity-check codes [44, 45], and trellis precoding [46]. It remains to be seen if the complexity of these schemes are prohibitive in practical MIMO systems. Though we have focused on the frequency-flat case with CSI assumed known, future wireless cellular systems will include appropriate coding to obtain temporal and frequency diversity as well as the spatial and multiuser diversity mentioned above.

6.5.2 Partial or imperfect CSI

Almost all of the work on both theoretical and practical coding approaches for the MIMO broadcast channel has assumed that the transmitter and receivers all know the channel exactly [1, 3, 7–9, 17, 67]. Accurate CSI may be easy to obtain when the channel is changing slowly, for example, as for indoor scenarios, but it is much more difficult in situations where the base station or users are highly mobile. An analysis of the penalty for using imperfect or outdated feedback of channel information would be of significant benefit to system designers; preliminary simulations indicate that the techniques of Section 6.3.3 are robust to channel estimation error or “stale” CSI. The sum capacity when only the transmitter or when no one knows the channel would also provide insight for practical coding schemes.

A related area of open research is analysis of a system where the transmitter and/or receiver know only the statistics of the channel coefficients. References to several papers that have addressed this problem can be found in [12].

It has been proposed [50] that MIMO channel prediction has the ability to lengthen the time between training intervals over that obtained by SISO prediction techniques. This is especially intriguing for multiuser scenarios where the CSI burden at the transmitter is considerably higher than in the single-user case. Other CSI-related issues that require additional research include algorithms that take the statistics of the channel estimation error into account, channel feedback methods that consume minimal bandwidth, and analysis of the trade-off between the amount of CSI fed back to the transmitter and the gain available from using the CSI. A comparison of the resources needed for channel estimation in a time-division duplex versus a frequency-division duplex system is given in [68].

6.5.3 Scheduling

In systems with a single base-station antenna, it is well known [69] that transmitting to the user with the strongest channel at any given time achieves the sum-rate capacity. The resulting “multi-user diversity” is expected to be present as well in the multiantenna case. The idea is that when a large number of users are sharing a network with rapidly time-varying channels, a base station may use intelligent scheduling algorithms to improve capacity by transmitting to a subset of users. In situations where $K \gg n_T$, one obvious possibility is to transmit to a set of n_T users at each symbol time. The n_T users with strongest average channel strength could be selected, or some orthogonality criterion could be used [70].

In situations where minimal channel variation is to be found, *opportunistic beamforming* has been used to create artificial channel variation in situations where it might not otherwise exist [71]. *Proportional fair scheduling* is also investigated in [71] as a way to ensure that users are treated fairly over some time interval. Some work has been done in extending the opportunistic beamforming idea to the case where base station and mobile stations all have multiple antennas [73], but this has not been studied extensively. Multiple random beams are used in [72] with limited feedback to communicate with many users. Other recent studies in the area of scheduling include [73–87].

6.5.4 Resource allocation

Related to the scheduling problem are numerous issues that arise when considering practical network implementations. For example, a typical scenario involves more users than transmit antennas; if spatial multiplexing (SDMA) is used to supplement existing TDMA and FDMA implementations, it is important to consider how the users in the network will be grouped together. In particular, since the different spatial channels are nonorthogonal, it is critical that only “spatially compatible” users be chosen to be time- or frequency-coincident [88]. Efficient methods are needed to determine how to optimally determine which users in a network should be spatially multiplexed.

Downlink processing is only one aspect of the multiuser MIMO problem. The uplink MIMO MAC has received significant attention in recent years (see [2, 3, 12] for a discussion of the MIMO MAC and some of the duality relationships it shares with the MIMO broadcast channel). We have focused solely on the cellular network architecture with a base terminal and users that communicate with the base. Ad hoc networks composed of multiple antenna

nodes are of increasing interest, especially in military applications. An important question is how MIMO nodes could be exploited in message relaying, where signal “hops” are required to connect widely separated network nodes. When considering all of these ideas together in the context of a network where all users have arrays, complexity grows very quickly; it is unlikely that globally optimal solutions can be easily found. The ability of heuristic algorithms for scheduling and relaying to achieve the available capacity remains an important area for future research. Some preliminary studies on the application of MIMO techniques to ad hoc networks have been conducted (e.g., see [89–92]).

Though the general area of multiuser communications has been well studied, the addition of multiple antennas in a wireless network opens up many new areas of research that have not yet been addressed. Space does not permit a complete treatment of this topic; in addition to the references cited above, there have been a number of other important results that have not been mentioned, including methods based on estimating physical channel parameters (e.g., directions of arrival, etc.) [93–97], “multicell” or multi-basestation MIMO [98, 99], and others [100–104].

6.6 Summary

A brief overview of coding techniques for the multiuser MIMO downlink has been given in this chapter. We began with a description of techniques for the special case where each user in the network has a single antenna. The capacity of channel inversion was shown to approach a constant as the number of antennas grows, a fact that indicates its inefficiency. A combination of regularized channel inversion and integer perturbation of the data to be transmitted is shown to operate near capacity when combined with an appropriate channel code. Linear techniques for multiple-antenna receivers were also presented, including block diagonalization of the channel and joint transmit–receive beamforming.

Despite the progress in this area, many open problems remain. Efficient techniques for multiuser scheduling, acquisition of CSI at the base station, and coding must be developed. Future wireless cellular systems may include channel tracking techniques at the base station, and use of this CSI with appropriate coding to obtain temporal, frequency, spatial, and multiuser diversity. The complexity of this system is a serious challenge for researchers, since it grows rapidly with the number of antennas, users, bandwidth, and code length.

Acknowledgments

Work for this paper was supported in part by the U.S. National Science Foundation under Information Technology Research Grants CCR-0081476 and CCR-0313056. In addition to other prior work by the authors cited above, portions of this chapter are based on results presented in [105–107].

References

- [1] G. Caire and S. Shamai, “On the achievable throughput of a multi-antenna Gaussian broadcast channel,” *IEEE Transactions on Information Theory*, vol. 43, pp. 1691–1706, July 2003.

- [2] P. Viswanath and D. Tse, "Sum capacity of the vector Gaussian broadcast channel and uplink-downlink duality," *IEEE Transactions on Information Theory*, vol. 49, no. 8, pp. 1912–1921, August 2003.
- [3] S. Vishwanath, N. Jindal, and A. Goldsmith, "Duality, achievable rates and sum capacity of Gaussian MIMO broadcast channels," *IEEE Transactions on Information Theory*, vol. 49, no. 10, pp. 2658–2668, August 2003.
- [4] H. Weingarten, Y. Steinberg, and S. Shamai, "The capacity region of the Gaussian MIMO broadcast channel," in *Proceedings Conference on Information Sciences and Systems (CISS)*, Princeton, NJ, March 2004.
- [5] C. B. Peel, B. M. Hochwald, and A. L. Swindlehurst, "A vector-perturbation technique for near-capacity multiantenna multiuser communication – Part I: Channel inversion and regularization," *IEEE Transactions on Communications*, vol. 53, no. 1, pp. 195–202, January 2005.
- [6] Q. H. Spencer, A. L. Swindlehurst, and M. Haardt, "Zero-forcing methods for downlink spatial multiplexing in multi-user MIMO channels," *IEEE Transactions on Signal Processing*, vol. 52, no. 2, pp. 461–471, February 2004.
- [7] C. B. Peel, B. M. Hochwald, and A. L. Swindlehurst, "A vector-perturbation technique for near-capacity multi-antenna multi-user communication – Part II: perturbation," *Accepted for publication in IEEE Transactions on Communications*, available from <http://mars.bell-labs.com/>.
- [8] C. Windpassinger, R. F. H. Fischer, and J. B. Huber, "Lattice-reduction-aided broadcast precoding," *IEEE Transactions on Communications*, vol. 52, no. 12, pp. 2057–2060, December 2004.
- [9] S. Shi and M. Schubert, "Precoding and power loading for multi-antenna broadcast channels," in *Proceedings Conference on Information Sciences and Systems*, Princeton, NJ, March 2004.
- [10] P. Wolniansky, G. Foschini, G. Golden, and R. Valenzuela, "V-BLAST: An architecture for realizing very high data rates over the rich scattering wireless channel," in *Proceedings IEEE International Symposium on Signals, Systems, and Electronics Conference*, Pisa, Italy, September 1998.
- [11] G. Golden, G. Foschini, R. Valenzuela, and P. Wolniansky, "Detection algorithm and initial laboratory results using the V-BLAST space-time communications architecture," *Electronics Letters*, vol. 35, no. 1, pp. 14–15, January 1999.
- [12] A. Goldsmith, S. Jafar, N. Jindal, and S. Vishwanath, "Capacity limits of MIMO channels," *IEEE Journal on Selected Areas in Communications*, vol. 21, no. 5, pp. 684–702, June 2003.
- [13] D. Gerlach and A. Paulraj, "Adaptive transmitting antenna arrays with feedback," *IEEE Signal Processing Letters*, vol. 1, no. 10, pp. 150–152, October 1994.
- [14] T. Haustein, C. von Helmolt, E. Jorwieck, V. Jungnickel, and V. Pohl, "Performance of MIMO systems with channel inversion," in *Proceedings IEEE Vehicular Technology Conference*, Birmingham, AL, May 2002.
- [15] B. M. Hochwald and C. B. Peel, "Vector precoding for the multi-antenna, multi-user channel," in *Proceedings Allerton Conference on Communication, Control, and Computing*, Monticello, IL, October 2003.
- [16] W. Yu and J. Cioffi, "Trellis precoding for the broadcast channel," in *Proceedings of 2001 IEEE GlobeCom*, San Antonio, TX, November 2001, pp. 1344–1348.
- [17] W. Yu and J. Cioffi, "Sum capacity of a Gaussian vector broadcast channel," *IEEE Transactions on Information Theory*, vol. 50, no. 9, pp. 1875–1892, September 2004.
- [18] G. Caire and S. Shamai, "On the achievable throughput of a multi-antenna Gaussian broadcast channel," *IEEE Transactions on Information Theory*, vol. 49, no. 7, pp. 1691–1706, July 2003.
- [19] C. B. Peel, "Studies in multiple-antenna wireless communications," Ph.D. dissertation, Brigham Young University, Provo UT (USA), January 2004, <http://contentdm.lib.byu.edu/ETD/image/etd331.pdf>.

- [20] S. Shi and M. Schubert, "Precoding and power loading for multi-antenna broadcast channels," in *Proceedings Conference on Information Sciences and Systems*, Princeton, NJ, March 2004.
- [21] F. Rashid-Farrokhi, K. R. Liu, and L. Tassiulas, "Transmit beamforming and power control for cellular wireless systems," *IEEE Journal on Selected Areas in Communications*, vol. 16, no. 8, pp. 1437–1450, October 1998.
- [22] E. Visotsky and U. Madhow, "Optimum beamforming using transmit antenna arrays," in *Proceedings of the IEEE Vehicular Technology Conference*, vol. 1. Houston, TX: IEEE, May 16–20 1999, pp. 851–856.
- [23] M. Bengtsson and B. Ottersten, "Optimal and suboptimal beamforming," in *Handbook of Antennas in Wireless Communications*, L. Godara, Ed. CRC Press, August 2001.
- [24] R. L.-U. Choi and R. D. Murch, "A downlink decomposition transmit pre-processing technique for multi-user MIMO systems," in *Proceedings of IST Mobile & Wireless Telecommunications Summit*, Thessaloniki, Greece, June 2002.
- [25] A. Bourdoux and N. Khaled, "Joint Tx-Rx optimization for MIMO-SDMA based on a null-space constraint," in *Proceedings of the IEEE Vehicular Technology Conference*, Vancouver, BC, September 2002, pp. 171–174.
- [26] Q. H. Spencer and M. Haardt, "Capacity and downlink transmission algorithms for a multi-user MIMO channel," in *Conference Record of the 36th Asilomar Conference on Signals, Systems and Computers*. IEEE, Monterrey, CA, November 2002.
- [27] M. Rim, "Multi-user downlink beamforming with multiple transmit and receive antennas," *Electronics Letters*, vol. 38, no. 25, pp. 1725–1726, 5th December 2002.
- [28] R. Choi and R. Murch, "A transmit preprocessing technique for multiuser MIMO systems using a decomposition approach," *IEEE Transactions on Wireless Communications*, vol. 3, no. 1, pp. 20–24, January 2004.
- [29] Q. H. Spencer, "Transmission strategies for wireless multi-user, multiple-input, multiple-output communication channels," Ph.D. dissertation, Brigham Young University, March 2004, <http://contentdm.lib.byu.edu/ETD/image/etd378.pdf>.
- [30] J.-H. Chang, L. Tassiulas, and F. Rashid-Farrokhi, "Joint transmitter receiver diversity for efficient space division multiaccess," *IEEE Transactions on Wireless Communications*, vol. 1, no. 1, pp. 16–27, January 2002.
- [31] Z. Pan, K.-K. Wong, and T. Ng, "MIMO antenna system for multi-user multi-stream orthogonal space division multiplexing," in *Proceedings of the IEEE International Conference on Communications*, vol. 5. Anchorage, Alaska: IEEE, May 2003, pp. 3220–3224.
- [32] K.-K. Wong, R. Murch, and K. B. Letaief, "A joint-channel diagonalization for multiuser MIMO antenna systems," *IEEE Transactions on Wireless Communications*, vol. 2, no. 4, pp. 773–786, July 2003.
- [33] Q. H. Spencer, A. L. Swindlehurst, and M. Haardt, "Fast power minimization with QoS constraints in multi-user MIMO downlinks," in *Proceedings of the IEEE International Conference on Acoustics, Speech, and Signal Processing*. IEEE, April 2003.
- [34] R. L.-U. Choi, M. T. Ivrlač, R. D. Murch, and J. A. Nossek, "Joint transmit and receive multi-user MIMO decomposition approach for the downlink of multi-user MIMO systems," in *Proceedings of the IEEE 58th Vehicular Technology Conference*. Orlando, FL: IEEE, October 6–9 2003.
- [35] Q. H. Spencer and A. L. Swindlehurst, "A hybrid approach to spatial multiplexing in multi-user MIMO downlinks," *EURASIP Journal on Wireless Communications and Networking*, vol. 2004, no. 2, pp. 236–247, December 2004.
- [36] S. Vishwanath, N. Jindal, and A. Goldsmith, "On the capacity of multiple input multiple output broadcast channels," in *Proceedings of the IEEE International Conference on Communications*,

New York, NY, April 2002, see also http://wsl.stanford.edu/Andrea_publications.html for journal version.

- [37] U. Erez, S. Shamai, and R. Zamir, "Capacity and lattice strategies for cancelling known interference," in *Proceedings International Symposium on Information Theory and its Applications*, Honolulu, Hawaii, November 2000, pp. 681–684.
- [38] U. Erez and S. ten Brink, "Approaching the dirty paper limit for canceling known interference," in *Proceedings Allerton Conference on Communication, Control, and Computing*, Monticello, IL, October 2003.
- [39] H. Viswanathan, S. Venkatesan, and H. Huang, "Downlink capacity evaluation of cellular networks with known interference cancellation," *IEEE Journal on Selected Areas in Communications*, vol. 21, no. 5, pp. 802–811, June 2003.
- [40] S. Vishwanath, G. Kramer, S. S. Shitz, S. Jafar, and A. Goldsmith, "Capacity bounds for Gaussian vector broadcast channels," in *Proceedings DIMACS Workshop on Signal Processing for Wireless Transmission*, Piscataway, NJ, October 2002.
- [41] M. H. M. Costa, "Writing on dirty paper," *IEEE Transactions on Information Theory*, vol. 29, pp. 439–441, May 1983.
- [42] S. S. Pradhan and K. Ramchandran, "Enhancing analog image transmission systems using digital side information: A new wavelet-based image coding paradigm," in *Proceedings of the Data Compression Conference*, Snowbird, Utah, March 2001, pp. 63–72.
- [43] J. J. Eggers, J. K. Su, and B. Girod, "A blind watermarking scheme based on structured codebooks," in *Proceedings of IEE Secure Images and Image Authentication*, vol. 4, London, UK, April 2000, pp. 1–6.
- [44] G. Caire and S. Shamai, "LDPC coding for interference mitigation at the transmitter," in *Proceedings 40th annual Allerton Conference on Communication, Control, and Computing*, Monticello, IL, October 2002.
- [45] G. Caire and S. Shamai, "Writing on dirty tape with LDPC codes," in *Multiantenna Channels: Capacity, Coding and Signal Processing*, ser. DIMACS Series in Discrete Mathematics and Theoretical Computer Science, vol. 62, 2002, pp. 123–140.
- [46] T. Philosof, U. Erez, and R. Zamir, "Precoding for interference cancellation at low SNR," *22nd Convention of IEEE Israel Section*, Tel-Aviv University, December 2002.
- [47] C. B. Peel and A. L. Swindlehurst, "Effective SNR for space-time modulation over a time-varying Rician channel," *IEEE Transactions on Communications*, vol. 52, no. 1, pp. 17–23, Jan 2004.
- [48] C. B. Peel and A. L. Swindlehurst, "Performance of space-time modulation for a generalized time-varying Rician channel model," *IEEE Transactions on Wireless Communications*, vol. 3, no. 3, pp. 1003–1012, May 2004.
- [49] C. B. Peel and A. L. Swindlehurst, "Capacity-optimal training for space-time modulation in time varying fading," in *The 2003 International Conference on Communications*, vol. 4, May 2003, pp. 2698–2702.
- [50] T. Svantesson and A. L. Swindlehurst, "A performance bound for prediction of a multipath MIMO channel," in *Proceedings of the 37th Asilomar Conference on Signals, Systems, and Computers, Session: Array Processing for Wireless Communications*, Pacific Grove, CA, November 2003.
- [51] U. Fincke and M. Pohst, "Improved methods for calculating vectors of short lengths in a lattice, including a complexity analysis," *Mathematics of Computation*, vol. 44, pp. 463–471, April 1985.
- [52] M. O. Damen, A. Chkeif, and J.-C. Belfiore, "Lattice code decoder for space-time codes," *IEEE Communications Letters*, vol. 4, no. 5, pp. 161–163, May 2000.

- [53] A. M. Chan and I. Lee, "A new reduced-complexity sphere decoder for multiple antenna systems," in *Proceedings International Conference on Communications*, vol. 1, New York, April 2002, pp. 460–464.
- [54] R. Kannan, "Improved algorithms for integer programming and related lattice problems," in *Proceedings of the ACM Symposium on the Theory of Computing*, Boston, MA, April 1983, pp. 193–206.
- [55] E. Agrell, T. Eriksson, A. Vardy, and K. Zeger, "Closest point searches in lattices," *IEEE Transactions on Information Theory*, vol. 48, no. 8, pp. 2201–2214, August 2002.
- [56] R. Zamir, S. Shamai, and U. Erez, "Nested linear/lattice codes for structured multiterminal binning," *IEEE Transactions on Information Theory*, vol. 48, no. 6, pp. 1250–1276, June 2002.
- [57] M. Tomlinson, "New automatic equalizer employing modulo arithmetic," *Electronics Letters*, vol. 7, pp. 138–139, March 1971.
- [58] H. Harashima and H. Miyakawa, "Matched-transmission technique for channels with intersymbol interference," *IEEE Transactions on Communications*, vol. 20, no. 4, pp. 774–780, August 1972.
- [59] G. Ginis and J. Cioffi, "A multi-user precoding scheme achieving crosstalk cancellation with application to DSL systems," in *Conference Record of the Thirty-Fourth Asilomar Conference on Signals, Systems and Computers*, vol. 2, Monterrey, CA, 2000, pp. 1627–1631.
- [60] R. Fischer, C. Windpassinger, A. Lampe, and J. Huber, "MIMO precoding for decentralized receivers," in *Proceedings IEEE International Symposium on Information Theory*, Lausanne, Switzerland, June/July 2002, p. 496.
- [61] B. Hassibi and H. Vikalo, "On the expected complexity of integer least-squares problems," in *Proceedings ICASSP*, Orlando, FL, 2002.
- [62] C. Windpassinger, T. Vencel, and R. F. H. Fischer, "Precoding and loading for blast-like systems," in *Proceedings of the IEEE International Conference on Communications*, vol. 5, Anchorage, Alaska, May 2003, pp. 3061–3065.
- [63] M. Joham, J. Brehmer, and W. Utschick, "MMSE approaches to multiuser spatio-temporal tomlinson-harashima precoding," in *Proceedings of the 5th International ITG Conference on Source and Channel Coding (ITG SCC'04)*, Erlangen, Germany, January 2004, pp. 387–394.
- [64] A. K. Lenstra, H. W. Lenstra, and L. Lovász, "Factoring polynomials with rational coefficients," *Mathematische Annalen*, vol. 261, pp. 515–534, 1982.
- [65] D. Wübben, R. Böhnke, V. Kühn, and K.-D. Kammeyer, "MMSE-based lattice-reduction for near-ML detection of MIMO systems," in *ITG Workshop on Smart Antennas*, Munich, Germany, March 2004.
- [66] V. Stankovic, M. Haardt, and M. Fuchs, "Combination of block diagonalization and THP transmit filtering for downlink beamforming in multi-user MIMO systems," in *Proceedings of the European Conference on Wireless Technology (ECWT 2004)*, Amsterdam, The Netherlands, October 2004, to be published.
- [67] P. Viswanath and D. Tse, "Sum capacity of the multi-antenna broadcast channel," in *Proceedings IEEE International Symposium on Information Theory*, July 2002, p. 497.
- [68] T. L. Marzetta and B. M. Hochwald, "Fast transfer of channel state information in wireless systems," *Submitted to IEEE Transactions on Signal Processing*, 2004, <http://mars.bell-labs.com>.
- [69] R. Knopp and P. A. Humblet, "Information capacity and power control in single-cell multiuser communications," in *Proceedings of the IEEE International Conference on Communications*, Seattle, WA, June 1995.
- [70] M. J. Lopez, "Multiplexing, scheduling, and multicasting strategies for antenna arrays in wireless networks," Ph.D. dissertation, Massachusetts Institute of Technology, 2002.

- [71] P. Viswanath, D. N. C. Tse, and R. Laroia, "Opportunistic beamforming using dumb antennas," *IEEE Transactions on Information Theory*, vol. 48, no. 6, pp. 1277–1294, June 2002.
- [72] M. Sharif and B. Hassibi, "On the capacity of MIMO broadcast channel with partial side information," *IEEE Transactions on Information Theory*, vol. 51, no. 2, pp. 506–522, February 2005.
- [73] R. W. Heath Jr., M. Airy, and A. Paulraj, "Multiuser Diversity for MIMO Wireless Systems with Linear Receivers," in *35th Asilomar Conference on Signals, Systems and Computers*, Asilomar, CA, November 2001, pp. 1194–1199.
- [74] H. Viswanathan and K. Kumaran, "Rate scheduling in multiple antenna downlink wireless systems," in *Proceedings of the 39th Annual Allerton Conference on Communication, Control, and Computing*, Monticello, IL, October 3–5 2001.
- [75] I. Koutsopoulos and L. Tassiulas, "Adaptive resource allocation in SDMA-based wireless broadband networks with OFDM signaling," in *Proceedings of IEEE INFOCOM 2002*, vol. 3, New York, NY, 2002, pp. 1376–1385.
- [76] V. Lau, Y. Liu, and T.-A. Chen, "Optimal multi-user space time scheduling for wireless communications," in *Proceedings IEEE Vehicular Technology Conference*, Vancouver, BC, September 2002, pp. 1939–1942.
- [77] R. Gozali, R. Buehrer, and B. Woerner, "On the performance of scheduling over space-time architectures," in *Proceedings Vehicular Technology Conference*, Vancouver, BC, September 2002, pp. 415–419.
- [78] M. Demirkol and M. Ingram, "Stream control in networks with interfering MIMO links," in *Proceedings of IEEE Wireless Communications and Networking Conference*, New Orleans, LA, March 2003, pp. 343–348.
- [79] B. Farhang-Boroujeny and Q. Spencer, "Layering techniques for space-time communication in multi-user networks," in *Proceedings of the IEEE 58th Vehicular Technology Conference*. Orlando, FL: IEEE, October 6–9 2003.
- [80] D. Mazzarese and W. Krzymien, "High throughput downlink cellular packet data access with multiple antennas and multiuser diversity," in *Proceedings IEEE Vehicular Technology Conference*, vol. 2, Seoul, Korea, 2003, pp. 1079–1083.
- [81] J. Chung, C.-S. Hwang, K. Kim, and Y. Kim, "A random beamforming technique in MIMO systems exploiting multiuser diversity," *IEEE Journal on Selected Areas in Communications*, vol. 21, no. 5, pp. 848–855, June 2003.
- [82] H. Boche and M. Wiczanowski, "Stability region of arrival rates and optimal scheduling for MIMO-MAC-A cross-layer approach," in *Proceedings of 2004 International Zurich Seminar on Communications*, Zurich, Switzerland, February 2004, pp. 18–21.
- [83] Z. Tu and R. Blum, "Multiuser diversity for a dirty paper approach," *IEEE Communications Letters*, vol. 7, no. 8, pp. 370–372, August 2003.
- [84] L. Dong, T. Li, and Y.-F. Huang, "Opportunistic transmission scheduling for multiuser MIMO systems," in *Proceedings ICASSP*, vol. 5, April 2003, pp. V65–V68.
- [85] O.-S. Shin and K. Bok, "Antenna-assisted round robin scheduling for MIMO cellular systems," *IEEE Communications Letters*, vol. 7, no. 3, pp. 109–111, March 2003.
- [86] D. Aktas and H. Gamal, "Multiuser scheduling for MIMO wireless systems," in *Proceedings IEEE Vehicular Technology Conference*, Orlando, FL, October 2003, pp. 1743–1747.
- [87] K.-K. Wong, "Adaptive space-division-multiplexing and bit-and-power allocation in multiuser MIMO flat fading broadcast channels," in *Proceedings of the IEEE 58th Vehicular Technology Conference*. Orlando, FL: IEEE, October 6–9 2003.
- [88] Q. H. Spencer and A. L. Swindlehurst, "Channel allocation in multi-user MIMO wireless communications systems," in *Proceedings of the IEEE International Conference on Communications*. Paris: IEEE, June 2004.

- [89] M. Dohler, A. Gkelias, and H. Aghvami, "A resource allocation strategy for distributed MIMO multi-hop communication systems," *IEEE Communications Letters*, vol. 8, no. 2, pp. 99–101, February 2004.
- [90] M. Dohler, J. Dominguez, and H. Aghvami, "Link capacity analysis for virtual antenna arrays," in *Proceedings IEEE Vehicular Technology Conference*, Vancouver, BC, September 2002, pp. 440–443.
- [91] S. Bellofiore, J. Foutz, R. Govindarajula, I. Bahceci, C. Balanis, A. Spanias, J. Capone, and T. Duman, "Smart antenna system analysis, integration and performance for mobile ad-hoc networks (MANETs)," *IEEE Transactions on Antennas and Propagation*, vol. 50, pp. 571–581, May 2002.
- [92] Y. Chang and Y. Hua, "Application of space-time linear block codes to parallel wireless relays in mobile ad hoc networks," in *Proceedings of the 37th Asilomar Conference on Signals, Systems, and Computers*, Monterrey, CA, 2003, pp. 1002–1006.
- [93] P. Zetterberg and B. Ottersten, "The spectrum efficiency of a base station antenna array system for spatially selective transmission," *IEEE Transactions on Vehicular Technology*, vol. VT-44, no. 3, pp. 651–660, August 1995.
- [94] J. Fonollosa, J. Goldberg, and G. Vazquez, "Downlink beamforming in cellular mobile communications," in *Proceedings of SPAWC Workshop*, Paris, France, 1997, pp. 197–200.
- [95] C. Farsakh and J. A. Nossek, "Spatial covariance based downlink beamforming in an SDMA mobile radio system," *IEEE Transactions on Communications*, vol. 46, no. 11, pp. 1497–1506, November 1998.
- [96] T. Asté, P. Forster, L. Féty, and S. Mayrargue, "Downlink beamforming avoiding DOA estimation for cellular mobile communications," in *Proceedings ICASSP*, vol. 6, Seattle, WA, 1998, pp. 3313–3316.
- [97] K. Hugl, J. Laurila, and E. Bonek, "Downlink beamforming for frequency division duplex systems," in *Proceedings IEEE Vehicular Technology Conference*, vol. 3, Houston, TX, 1999, pp. 1449–1453.
- [98] S. Shamai and B. Zaidel, "Enhancing the cellular downlink capacity via co-processing at the transmitting end," in *Proceedings Vehicular Technology Conference*, Rhodes, Greece, May 2001, pp. 1745–1749.
- [99] G. J. Foschini, S. A. Jafar and A. Goldsmith, "PhantomNet : Exploring optimal multicellular multiple-antenna systems," in *Proceedings IEEE Vehicular Technology Conference*, Vancouver, Canada, September 2002, pp. 24–28.
- [100] K.-K. Wong, R. Murch, and K. Letaief, "Performance enhancement of multiuser MIMO wireless communication systems," *IEEE Transactions on Communications*, vol. 50, no. 12, pp. 1960–1970, December 2002.
- [101] M. Schubert and H. Boche, "Joint 'dirty paper' pre-coding and downlink beamforming," in *Proceedings of the IEEE 7th International Symposium on Spread Spectrum Techniques and Applications*, vol. 2. Prague, Czech Republic: IEEE, September 2–5 2002, pp. 536–540.
- [102] H. Boche, M. Scubert, and E. A. Jorswieck, "Trace balancing for multiuser MIMO downlink transmission," in *Conference Record of the 36th Asilomar Conference on Signals, Systems and Computers*. Pacific Grove, CA: IEEE, November 2002, pp. 1379–1383.
- [103] M. T. Ivrlač, R. L.-U. Choi, R. D. Murch, and J. A. Nossek, "Effective use of long-term transmit channel state information in multi-user MIMO communication systems," in *Proceedings of the IEEE 58th Vehicular Technology Conference*. Orlando, FL: IEEE, October 6–9 2003.
- [104] M. Schubert and H. Boche, "Solution of the multiuser downlink beamforming problem with individual SINR constraints," *IEEE Transactions on Vehicular Technology*, vol. 53, no. 1, pp. 18–28, January 2004.

- [105] C. Peel, "On dirty-paper coding," *IEEE Signal Processing Magazine*, vol. 20, no. 3, pp. 112–113, May 2003.
- [106] C. Peel, Q. Spencer, A. Swindlehurst, and M. Haardt, "Downlink transmit beamforming in multi-user MIMO systems," in *Proceedings of the IEEE Workshop on Sensor Array and Multi-channel Signal Processing*, Stiges, Spain, 2004.
- [107] Q. Spencer, C. Peel, A. Swindlehurst, and M. Haardt, "An introduction to the multi-user MIMO downlink," *IEEE Communications Magazine*, vol. 42, no. 10, pp. 60–67, Oct. 2004.

Antenna Subset Selection in MIMO Communication Systems

Alexei Gorokhov, Dhananjay A. Gore, and Arogyaswami J. Paulraj

7.1 Introduction

Although multiple-input multiple-output (MIMO) technology improves reliability and transmission rates achievable in wireless systems [1–6], the improvement comes at the expense of higher hardware cost. Indeed, every extra transmit/receive antenna requires its own hardware chain (power amplifier, low noise amplifier (LNA), analog to digital (A/D) convertors, etc.). Therefore, cost-effective implementation of MIMO technology remains a major challenge. Antenna subset selection, where transmission/reception is performed through a subset of the available antenna elements, helps in reducing the implementation cost while retaining most of the benefits of MIMO technology.

This chapter summarizes the state of the art in MIMO antenna selection research. We begin by reviewing some well-known results on maximum ratio combining and receive antenna selection for single-input-multiple-output (SIMO) antenna systems. Our overview is followed by a summary of recent efforts on antenna selection in MIMO systems. The core of this chapter is dedicated to information theoretic analysis of antenna selection performance in MIMO systems. Therein, we cite recent results that shed light on the diversity gains of MIMO systems with antenna selection. Beyond simple intuition on the diversity achievable in MIMO systems with antenna selection, we establish a fundamental relationship between multiplexing gains and diversity gains for these systems.

We highlight some simple practical selection rules that achieve a hefty fraction of the optimal selection gain. Finally, we provide an example of a practical MIMO OFDM system and comment on the practical gains of MIMO antenna selection.

7.1.1 Signal and channel model

In this section, we specify the notation, signal model and channel model.

Notation

We use bold lowercase (uppercase) letters to denote vectors (matrices). A matrix variable indexed with a single integer denotes the corresponding row. The notation $(a : b)$ stands for indices a through b , whereas $(:)$ stands for the whole scope of indices. Matrix transpose and matrix conjugate transpose are denoted by superscripts $(^T)$ and $(^*)$, respectively, and $\|\cdot\|$ is the Euclidean vector norm.

Signal model

The matrix channel between the M_T transmit and M_R receive antennas is assumed to be non-selective, that is, flat fading and linear time invariant. The signal model is

$$\mathbf{x}[k] = \sqrt{\rho} \mathbf{H} \mathbf{s}[k] + \mathbf{n}[k], \quad (7.1)$$

where $\mathbf{x}[k] = [\mathbf{x}_1[k], \dots, \mathbf{x}_{M_R}[k]]^T$ is the $M_R \times 1$ vector corresponding to the signal received at the M_R receivers and sampled at the symbol rate, $\mathbf{s}[k] = [s_1[k], \dots, s_{M_T}[k]]^T$ corresponds to the $M_T \times 1$ symbol vector transmitted by the M_T transmit antennas, ρ is the average signal energy per receive antenna and per channel use, $\mathbf{n}[k] = [n_1[k], \dots, n_{M_R}[k]]^T$ is the additive white Gaussian noise (AWGN) with variance 1/2 per real dimension and $\mathbf{H} = [\mathbf{H}_{:,1}, \dots, \mathbf{H}_{:,M_T}]$ is the $M_R \times M_T$ channel matrix, $\mathbf{H}_{:,q} = [\mathbf{H}_{1,q}, \dots, \mathbf{H}_{M_T,q}]^T$, $1 \leq q \leq M_T$, where $\mathbf{H}_{p,q}$ is a scalar channel between the p -th receive and the q -th transmit antenna.

Antenna selection

Assume the presence of M_T transmit antenna elements and M_R receive antenna elements, see Fig. 7.1. For a given channel instantiation, N_T out of M_T transmit antenna elements and N_R out of M_R receive antenna elements are selected and used for transmission and reception, respectively.

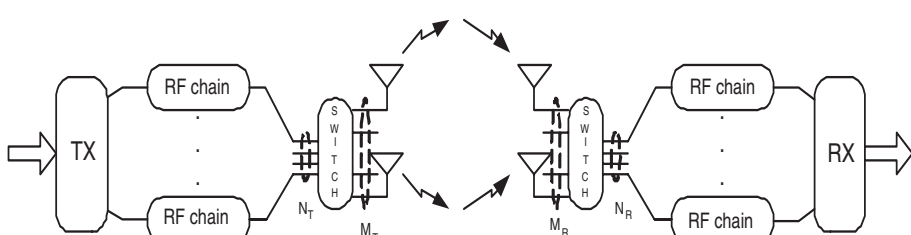


Figure 7.1 Selection in MIMO systems, N_T out of M_T transmit and N_R out of M_R receive antennas.

Channel model

In this chapter, we mainly focus on flat, Rayleigh faded, i.i.d. channel, that is, the entries of \mathbf{H} are i.i.d. zero mean circular Gaussian random variables with variance one¹. We always assume that the receiver has perfect channel knowledge.

Channel capacity

The capacity $C(\mathbf{H}, \rho)$ of a fixed MIMO channel specified by \mathbf{H} is given by, see [8, 3, 5]:

$$C(\mathbf{H}, \rho) = \log_2 \det(\mathbf{I}_{M_T} + \rho \mathbf{H}^* \mathbf{H}), \quad (7.2)$$

where $\det(\cdot)$ denotes determinant and \mathbf{I}_{M_T} is the $M_T \times M_T$ identity matrix.

7.2 SIMO/MISO Selection

In this section, we discuss receive antenna selection in SIMO systems. Although there are multiple antennas at either the receiver (for SIMO) or the transmitter (for MISO), the transmit/receive processing of signals is such that these systems may be treated similar to a SISO system with appropriately modified signal-to-noise ratio (SNR). Mathematical analysis of such systems is therefore especially tractable and reveals useful insight. There has been extensive work in this area, see, for example, [9, 10], and is briefly summarized below.

For a SIMO system, (7.1) may be rewritten as

$$\mathbf{x}[k] = \sqrt{\rho} \mathbf{h} s[k] + \mathbf{n}[k], \quad (7.3)$$

where $s[k]$ is a scalar transmitted signal while $\mathbf{x}[k]$, \mathbf{h} and $\mathbf{n}[k]$ are all vectors of dimension M_R corresponding to the observed signal, channel and AWGN, respectively. We reiterate that the receiver is assumed to have perfect channel knowledge.

7.2.1 Maximum ratio combining

The optimal receiver strategy for a SIMO system is to use a matched filter, that is,

$$\mathbf{h}^* \mathbf{x}[k] = \sqrt{\rho} \|\mathbf{h}\|^2 s[k] + \mathbf{h}^* \mathbf{n}[k]. \quad (7.4)$$

This filtering, commonly known as *maximum ratio combining*, results in a SISO equivalent channel between the transmitter and receiver. The postprocessing SNR (γ_{mrc}) is

$$\gamma_{mrc} = \rho \|\mathbf{h}\|^2, \quad (7.5)$$

and, given the channel model assumption, is readily recognized as a gamma distributed variable with M_R degrees of freedom. The cumulative distribution function (c.d.f.) for the received SNR of the equivalent SISO system is:

$$\mathbb{P} \left\{ \|\mathbf{h}\|^2 < x \right\} = \Gamma_i(x; M_R), \quad (7.6)$$

¹Many results presented in this chapter also apply in some scenarios of correlated transmit and/or receive antennas, see, for example, [7].

where $\mathbb{P}\{\cdot\}$ stands for the probability of the event (\cdot) and $\Gamma_i(x; M_R) = (\Gamma(M_R))^{-1} \int_0^x u^{M_R-1} e^{-u} du$ is the *incomplete gamma function* with parameter M_R . The channel capacity (C_{mrc}) and average received SNR may be written directly as

$$C_{mrc} = \log_2(1 + \rho \|\mathbf{h}\|^2), \quad (7.7)$$

$$\mathbb{E}\{\gamma_{mrc}\} = \rho M_R. \quad (7.8)$$

7.2.2 Antenna selection

In antenna selection, a subset of the total number of receive antennas is selected and used for reception. Assuming that only one antenna is to be selected, the post-processing SNR is maximized by choosing the best receive antenna, that is, the received SNR (γ_{sel}) is

$$\gamma_{sel} = \rho \max_p |\mathbf{h}_p|^2, \quad (7.9)$$

where \mathbf{h}_p is the p^{th} element of \mathbf{h} and corresponds to the channel between the single transmit and p^{th} receive antenna. The cumulative distribution function of the equivalent SISO channel is

$$\mathbb{P}\left\{\max_p |\mathbf{h}_p|^2 < x\right\} = (1 - e^{-x})^{M_R}. \quad (7.10)$$

The capacity C_{sel} and average received SNR with optimal selection may be written as [10]

$$C_{sel} = \log_2(1 + \rho \max_p |\mathbf{h}_p|^2), \quad (7.11)$$

$$\mathbb{E}\{\gamma_{sel}\} = \rho \sum_{k=1}^{M_R} \frac{1}{k}. \quad (7.12)$$

7.2.3 MRC versus antenna selection: performance comparison

It is clear that the analytical characterization of MRC and antenna selection depends on the receive SNR.

Average received signal-to-noise ratio

Fig. 7.2 compares the average received SNR of MRC and antenna selection, with one optimally selected antenna, as a function of the number of receive antennas. Note that with increasing number of receive antenna elements, the performance “gap” between MRC and antenna selection becomes quite substantial. This is hardly surprising since using fewer antennas ought to lead to a loss in average received energy.

A performance comparison based on this metric alone is overly pessimistic. The real gain of antenna selection in a fading environment is the improved diversity benefit. In fact, we shall see that *the diversity benefit through antenna selection is the same as that with MRC* [11, 7].

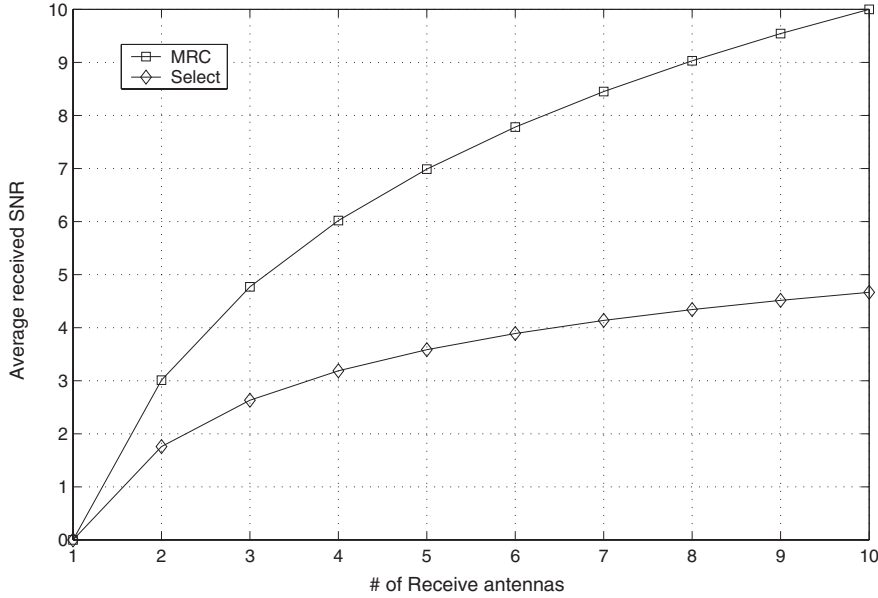


Figure 7.2 Average received SNR in MRC and antenna selection (with one optimally selected antenna), $\rho = 0$ dB.

Diversity performance

Adequate diversity is important in random fading environments since it is a key factor influencing the relationship between the link quality, for example, outage rate or average error rate, and system performance, for example, throughput. The relationship is especially important at small outage rates since high reliability is mandatory in many situations. The slope of the outage capacity versus outage rate, in the region of small outage rates, is often used to characterize the diversity order.

From (7.7) and (7.11), it can be easily verified that the analytical characterization of outage capacity depends directly on the received SNR. The c.d.f. in (7.6) represents the outage rate $\mathbb{P}\{\cdot\}$ with outage SNR x and outage capacity $\log_2(1+x)$. From (7.6) and (7.10), observe that in the region of small outage rates [12, 7],

$$\begin{aligned}
 \mathbb{P} \left\{ \max_p |\mathbf{h}_p|^2 < x \right\} &= (1 - e^{-x})^{M_R} \\
 &= (1 - (1 - x + o(x)))^{M_R} \\
 &= x^{M_R} (1 + o(x)), \\
 \mathbb{P} \left\{ \|\mathbf{h}\|^2 < x \right\} &= (\Gamma(M_R))^{-1} \int_0^x u^{M_R-1} e^{-u} du \\
 &= (M_R!)^{-1} x^{M_R} (1 + o(x)).
 \end{aligned}$$

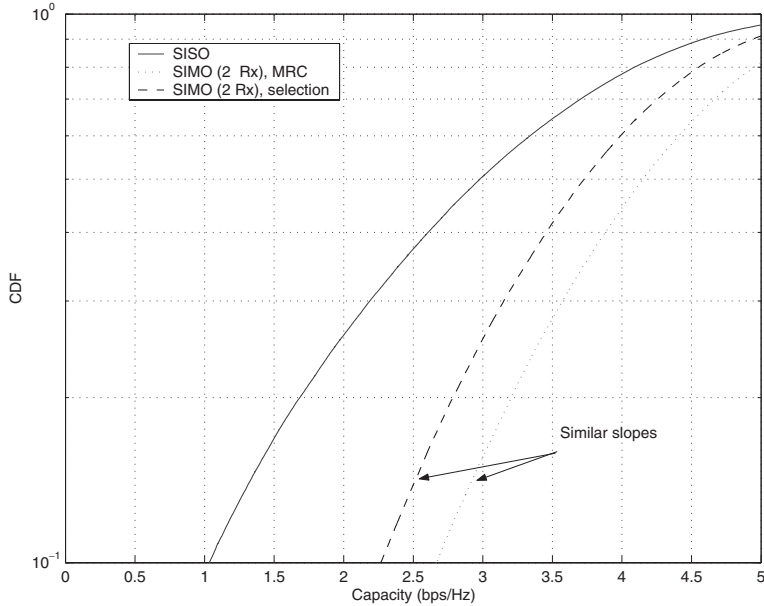


Figure 7.3 MRC and selection in SIMO systems deliver same diversity.

Notice that in the region of small outage rates, both c.d.f.s behave as M_R -th power of SNR x . Given that the diversity order is characterized by the relationship (slope) between outage capacity and outage rate this observation allows us to conclude that both schemes have the same diversity order. This equivalence in diversity is in fact the primary motivation for antenna selection in a fading environment. Fig. 7.3 plots the c.d.f. of the capacity for a SIMO system with MRC, antenna selection and when the receiver has only one receive antenna (SISO). The similarity in slope (in the outage region) of the curves corresponding to MRC and selection is apparent.

The difference in average SNR, however, is fundamental and grows rapidly with the number of receive elements, see Fig. 7.2. Selecting more than one receive antenna reduces this gap. The authors of [13, 10] discuss a hybrid MRC/selection scheme where a subset N_R of the available antennas is used for reception. The antennas with the N_R highest channel gains are used for reception. The average SNR is [13, 10]:

$$\gamma_{sel} = \rho N_R \left(1 + \sum_{k=N_R+1}^{M_R} \frac{1}{k} \right). \quad (7.13)$$

Since the performance with more than one receive antenna is superior to that with a single antenna, it is clear that the diversity order is the same as that of MRC. This equivalence is also visible through the following inequality [12]

$$(1/M_R) \sum_p \|\mathbf{h}\|^2 \leq \max_p |\mathbf{h}_p|^2 \leq \sum_p \|\mathbf{h}\|^2. \quad (7.14)$$

The inequality states that the SNR through selection is bounded above by the squared channel Frobenius norm (upper bound through MRC) and below by the average power over all antennas. Since both quantities are gamma distributed with parameter M_R the post-selection SNR is bounded above and below by two quantities with the same diversity. This implies that receive selection delivers the same diversity as MRC.

7.3 MIMO Selection

In this section, we review recent results on MIMO selection analysis and present some conclusions.

7.3.1 Antenna selection for practical space-time processing

Earlier, we noted that SIMO/MISO selection algorithm development and analysis is simplified because of the possibility of recasting a SIMO/MISO system into an equivalent SISO system. This is no longer the case in MIMO. In fact, MIMO framework allows for a wide range of transmit/receive processing schemes ranging from those that provide full diversity [14–16] to full spatial-multiplexing [17, 18] and trade-offs that “go in between” [19–21]. This gives rise to a vast variety of MIMO antenna selection algorithms requiring sophisticated analysis. Existing literature includes antenna selection for maximizing channel diversity [22–29], most of which focuses on selecting the transmit and/or receive antennas that maximize the channel Frobenius norm. The work on antenna selection for spatial-multiplexing includes [30–34] where the emphasis is on selecting antennas that minimize the error rate. An in-depth discussion of this work is not included in this chapter. Instead, the interested reader is pointed to the excellent references listed above.

This chapter focuses on antenna selection for maximizing Shannon capacity, the goal being to evolve an understanding of the information theoretic aspects of antenna selection in MIMO systems.

7.3.2 Antenna selection to maximize Shannon capacity

We denote $\underline{\mathbf{H}}$, a $N_R \times N_T$ submatrix of the $M_R \times M_T$ channel matrix \mathbf{H} corresponding to the channel between the selected N_T transmit and N_R receive antennas. According to (7.2), the capacity of channel $\underline{\mathbf{H}}$ is:

$$C(\underline{\mathbf{H}}, \rho) = \log_2 \det(\mathbf{I}_{M_T} + \rho \underline{\mathbf{H}}^* \underline{\mathbf{H}}). \quad (7.15)$$

The optimal set of receive antennas should be chosen so as to maximize the capacity of the resultant channel. There is a wide body of work [35–41, 7, 12, 42–44] in this area. In [35], the authors show that transmit selection in low rank environments can increase capacity. However, the first attempt to characterize the capacity gains of antenna selection in MIMO systems was made in [38]. In that work, the authors show that the capacity of receive antenna selection, that is, $N_T = M_T$, in Rayleigh faded i.i.d. channels can be upper bounded by:

$$\sum_{k=M_R-N_R+1}^{M_R} \log_2 (1 + \rho \Gamma_k),$$

where Γ_i is the i^{th} order statistic of a set of M_R i.i.d. gamma distributed random variables with parameter N_T . This bound can be tightened further [38] for the case of $N_R \geq M_T$.

In [12, 7], we show that for the case of $N_R = M_T = N_T$, that is, when the number of selected receive antenna elements is equal to the number of transmit antenna elements, the channel capacity may be lower bounded:

$$C(\underline{\mathbf{H}}, \rho) \geq \log_2 \det(\mathbf{I}_{M_R} + \rho \mathbf{H} \mathbf{H}^*) + \log_2 \det(\tilde{\mathbf{U}}^* \tilde{\mathbf{U}}), \quad (7.16)$$

where $\tilde{\mathbf{U}}$ is the $N_R \times M_T$ block of \mathbf{U} corresponding to the selected receive antennas and \mathbf{U} is the orthonormal basis of the column space of \mathbf{H} . Note that

$$\log_2 \det(\tilde{\mathbf{U}}^* \tilde{\mathbf{U}}) \leq 1, \quad (7.17)$$

so that the optimal set of receive antennas is the one that maximizes $\det(\tilde{\mathbf{U}}^* \tilde{\mathbf{U}})$. After some analysis [7, 12], it is possible to show that at high ρ and/or high M_R , we have:

$$C(\underline{\mathbf{H}}, \rho) > \sum_{k=1}^{M_T} \log_2 \left(1 + \rho \eta_k^2 \right), \quad (7.18)$$

where η_k^2 is statistically equivalent to the maximum squared absolute value of a vector of $(M_R - k + 1)$ i.i.d. zero mean unit variance complex circular Gaussian variables. In other words, η_k^2 is equal to the gain of SIMO selection with $(M_R - k + 1)$ antennas.

The above result implies that we can statistically lower bound (at high ρ and/or high M_R) the capacity of a MIMO channel with receive selection by the capacity of M_T independent SIMO channels with each SIMO link undergoing selection combining at the receiver. This “lower bound” equivalent channel is depicted by a block diagram in Fig. 7.4.

The result also allows us to relate selection and MRC in SIMO systems to selection and optimal processing in MIMO systems. The relationship follows from Foschini’s lower bound statistical representation for MIMO capacity without selection:

$$C(\mathbf{H}, \rho) > \sum_{k=1}^{M_T} \log_2 \left(1 + \rho \gamma_{M_R-k+1}^2 \right), \quad (7.19)$$

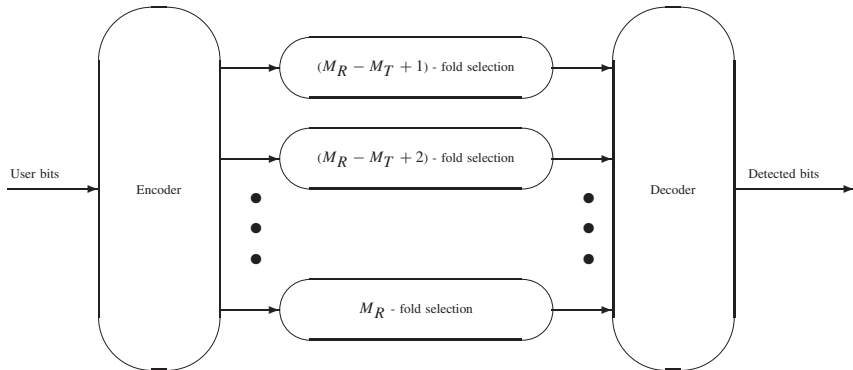


Figure 7.4 MIMO capacity with receive selection.

where γ_n^2 has gamma distribution with n degrees of freedom with c.d.f. $\mathbb{P}\{\gamma_n^2 < x\} \leq \Gamma_i(x; n)$, see [8, 4]. Comparing each term in the sum (7.19) with the MRC capacity given by (7.7) and the corresponding distribution described in the left-hand side of (7.6), we see that the MIMO capacity $C(\mathbf{H}, \rho)$ may be lower bounded by the capacity of M_T parallel SIMO channels with the respective diversity orders ranging from $(M_R - M_T + 1)$ up to M_R . The block diagram of this equivalent channel is shown in Fig. 7.5.

We may now develop a link, illustrated in Fig. 7.6, between selection and optimal processing in SIMO systems and selection and optimal processing in MIMO systems.

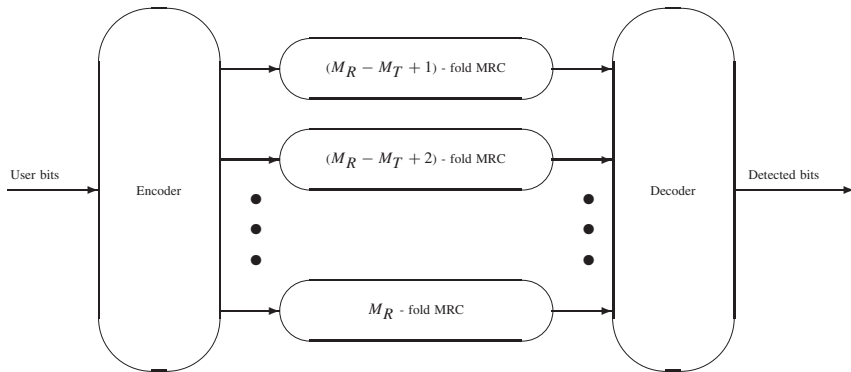


Figure 7.5 MIMO capacity.

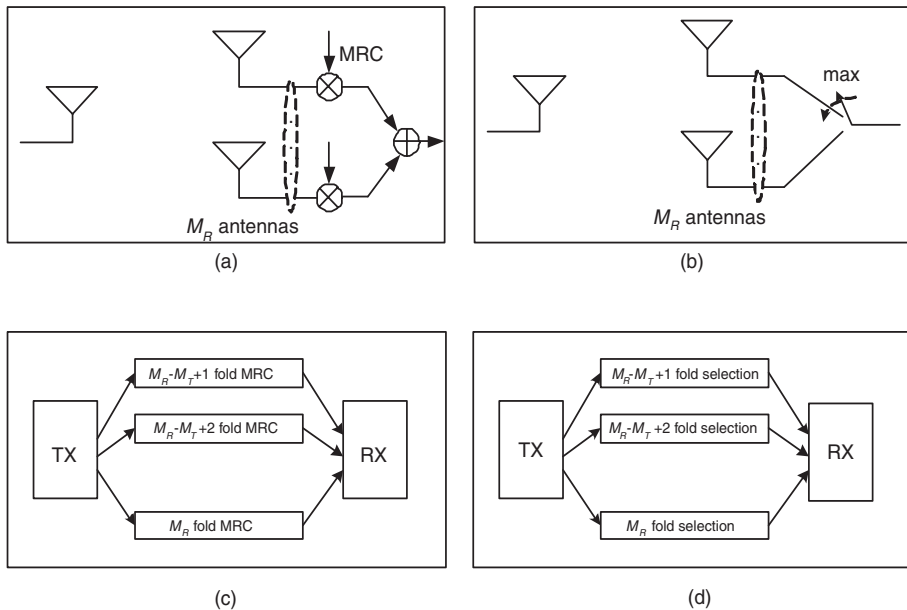


Figure 7.6 (a) SIMO MRC, (b) SIMO selection, (c) Full MIMO, (d) MIMO selection.

7.4 Diversity and Multiplexing with MIMO Antenna Selection

Diversity and spatial multiplexing gain are recognized to be the main benefits of MIMO communication systems. While diversity reduces the outage on random fading channels, thereby increasing reliably achievable rates, spatial multiplexing achieves a similar goal by expanding channel dimensions. The importance of diversity versus multiplexing gain depends on the desired link reliability, channel conditions and rate requirements. As both diversity and multiplexing gain come from the spatial dimensions of the MIMO channel, there exists an inherent trade-off between these two benefits. The “diversity versus multiplexing” issue remained a Gordian knot of the optimal MIMO design problem over many years. A tractable solution to this fundamental issue has been recently proposed by Zheng and Tse. Indeed, the achievable upper bound on the amount of diversity versus multiplexing gain presented in [21] offers a unified framework for the comparison of MIMO schemes.

In this contribution, our interest is focused on the effect of antenna subset selection, at either side of a MIMO link, for the so-called diversity/multiplexing trade-off. While it is easy to see that subset selection cannot increase MIMO dimensions and therefore enhance multiplexing gain in a MIMO system, the intuition based on SISO/SIMO/MISO results suggests possibility of non-negligible diversity improvement. Recall that several (sub)optimal subset selection algorithms allowed us to achieve full diversity, corresponding to the entire set of antennas, in SIMO/MISO systems. Moreover, many recent MIMO designs are shown to be capable of achieving full diversity subject to certain (minimum) multiplexing gain. The challenge of this section is to derive the entire relationship between diversity and multiplexing gain in MIMO systems with transmit/receive antenna selection. The main results presented in this section have been summarized in [43]. Interestingly, it turns out that even simple antenna selection algorithms are able to achieve the diversity/multiplexing curve of the full MIMO system, thereby offering the diversity gains of a MIMO system that makes use of all antennas.

7.4.1 Diversity versus multiplexing

Let us first set the mathematical framework of trade-off between diversity and multiplexing gains in MIMO systems [21]. We consider a family of MIMO transmission (coding) schemes that can sustain rate $R(\rho)$ with probability $(1 - P_{out}(\rho))$, subject to signal-to-noise ratio ρ . Here $P_{out}(\rho)$ is the *outage* probability. The multiplexing gain r and diversity gain d are defined as follows.

$$r = \lim_{\rho \rightarrow \infty} \frac{R(\rho)}{\log_2 \rho}, \quad d = - \lim_{\rho \rightarrow \infty} \frac{\log P_{out}(\rho)}{\log \rho}. \quad (7.20)$$

In other words, r defines scaling of the achievable data rate $R(\rho)$ w.r.t. $\log_2 \rho$, whereas d defines the exponent of the corresponding outage rate:

$$R(\rho) \doteq r \log_2 \rho, \quad P_{out}(\rho) \doteq \rho^{-d}, \quad (7.21)$$

where (\doteq) means asymptotic equality as $\rho \rightarrow \infty$. Intuitively, a well-designed MIMO transmission scheme will be capable of trading-off the achievable rate and reliability. Hence, we are interested in the achievable region of the pairs (r, d) or equivalently the maximum diversity gain $d(r)$ for a given multiplexing gain r . Since the maximum achievable data rate is given by the capacity in (7.1), the maximum achievable diversity gain $d_{\bullet}(r)$ subject to a fixed multiplexing gain satisfies

$$d_{\bullet}(r) = - \lim_{\rho \rightarrow \infty} \frac{\log \mathbb{P}\{C(\mathbf{H}, \rho) < r \log_2 \rho\}}{\log \rho}, \quad (7.22)$$

The authors of [21] showed that for uncorrelated MIMO flat Rayleigh fading channel, the maximum achievable diversity gain $d_{\bullet}(r)$ is the piecewise linear function of r connecting the points $(m, d_{\bullet}(m))$, with integer $0 \leq m \leq M_0$, where $M_0 = \min\{M_T, M_R\}$ and

$$d_{\bullet}(m) = (M_R - m)(M_T - m). \quad (7.23)$$

7.4.2 Transmit/receive antenna selection

As earlier, we assume a MIMO system equipped with M_T transmit and M_R receive antennas, whereas the numbers of actual transmit/receive chains are N_T and N_R , respectively. By successively sounding all the transmit and receive antennas with the available transmit and receive chains, the receiver can estimate the channel matrix \mathbf{H} of the full system. However, only N_T transmit and N_R receive antennas may be used at once. Since the goal is to maximize channel capacity, we search for the $N_R \times N_T$ block of \mathbf{H} that maximizes the capacity:

$$C(\underline{\mathbf{H}}, \rho) = \log_2 \det(\mathbf{I}_{N_T} + \rho \underline{\mathbf{H}}^* \underline{\mathbf{H}}), \quad (7.24)$$

where maximization is over $\underline{\mathbf{H}}$ in the set $\mathbb{H}_{N_R, N_T}(\mathbf{H})$ of all $N_R \times N_T$ blocks of \mathbf{H} . This maximum capacity may be written as

$$C_{\star}(\mathbf{H}, \rho) = \sup\{C(\underline{\mathbf{H}}, \rho) : \underline{\mathbf{H}} \in \mathbb{H}_{N_R, N_T}(\mathbf{H})\}. \quad (7.25)$$

Note that $C_{\star}(\mathbf{H}, \rho)$ is the maximum of $C(\underline{\mathbf{H}}, \rho)$ over all $\binom{M_R}{N_R} \binom{M_T}{N_T}$ blocks $\underline{\mathbf{H}}$ of \mathbf{H} . We will extend (7.23) to the described model of antenna selection. According to (7.25), we have

$$d_{\star}(r) = - \lim_{\rho \rightarrow \infty} \frac{\log \mathbb{P}\{C_{\star}(\mathbf{H}, \rho) < r \log_2 \rho\}}{\log \rho}. \quad (7.26)$$

First, we specify a simplified suboptimal selection rule that is based on two steps. At the first step, N_T transmit antennas are selected while keeping all M_R receive antennas. At the second step, N_R receive antennas are selected, with the fixed subset of N_T transmit antennas. The selection at both steps is based on the maximum capacity criterion. The proposed selection algorithm is stated below.

ALGORITHM I
DECOPLED TX/RX SELECTION

Find a set \mathcal{I}_T of N_T transmit antennas through the maximization over all possible subsets $\mathcal{I} \subset \{1, \dots, M_T\}$ of size N_T :

$$\mathcal{I}_T = \arg \max_{\mathcal{I}} \det(\mathbf{I}_{N_T} + \rho \mathbf{H}_{:, \mathcal{I}}^* \mathbf{H}_{:, \mathcal{I}}).$$

Find a set \mathcal{I}_R of N_R receive antennas through the maximization over all possible subsets $\mathcal{I} \subset \{1, \dots, M_R\}$ of size N_R :

$$\mathcal{I}_R = \arg \max_{\mathcal{I}} \det(\mathbf{I}_{N_T} + \rho \mathbf{H}_{\mathcal{I}, \mathcal{I}_T}^* \mathbf{H}_{\mathcal{I}, \mathcal{I}_T}).$$

Note that, owing to the symmetry of the capacity criterion w.r.t. rows and columns of \mathbf{H} , the order of transmit/receive antenna selection may be exchanged.

Some remarks pertaining to practical implementation and complexity are in order. First of all, notice a substantial reduction in the complexity of the proposed algorithm compared to the exhaustive search. In fact, Algorithm I requires computing $\binom{M_R}{N_R} + \binom{M_T}{N_T}$ determinants of size $N_T \times N_T$ matrices, instead of $\binom{M_R}{N_R} \binom{M_T}{N_T}$ determinants of the same size for the exhaustive search. Further simplifications may be achieved by replacing the exhaustive search of transmit and receive selection by a recursive maximization approach as explained later in Section 7.5. Also, some extensions to the frequency selective fading scenario may be developed along the lines of [37].

In the remainder of this section, we focus on extension of the result (7.23) by Zheng and Tse to the case of transmit and receive selection. We will use Algorithm I as a baseline selection rule and will show that maximum diversity gain may be achieved with this algorithm, for any feasible multiplexing gain. Note that the maximum achievable multiplexing gain is limited by the minimum number of the available chains at the transmitter or receiver: $0 \leq r \leq N_0$, where $N_0 = \min\{N_T, N_R\}$.

In the following paragraphs, we sketch the proof of our main result formulated in Theorem 7.4.1. As a first step, we establish the following upper bound on the capacity in (7.25).

Lemma 7.4.1 *The capacity $C_*(\mathbf{H}, \rho)$ achieved with optimal antenna selection satisfies*

$$\begin{aligned} C_*(\mathbf{H}, \rho) &\geq C_o(\mathbf{H}, \rho) - \log_2 \binom{M_T}{N_0} - \log_2 \binom{M_R}{N_0}, \\ C_o(\mathbf{H}, \rho) &= \sum_{k=1}^{N_0} \log_2 \left(1 + \rho \Lambda_k^2 \right), \end{aligned} \tag{7.27}$$

where $\Lambda_1 \geq \dots \geq \Lambda_{N_0}$ are the N_0 principal singular values of \mathbf{H} .

The proof of Lemma 7.4.1 is rather technical and is not presented here. The importance of this result lies in the fact that channel capacity after transmit/receive selection can be lower bounded by the term $C_o(\mathbf{H}, \rho)$ from (7.27) less a constant $A = (\log_2 \binom{M_R}{N_0} + \log_2 \binom{M_T}{N_0})$.

The latter constant is independent of ρ and therefore has no effect on the limit in (7.26). Indeed, from (7.26) and the above lemma,

$$\begin{aligned} d_{\star}(r) &\geq - \lim_{\rho \rightarrow \infty} \frac{\log \mathbb{P}\{C_o(\mathbf{H}, \rho) - A < r \log_2 \rho\}}{\log \rho} \\ &= - \lim_{\rho \rightarrow \infty} \frac{\log \mathbb{P}\{C_o(\mathbf{H}, \rho) < r \log_2 \rho (1 + A/(r \log_2 \rho))\}}{\log \rho} \\ &= - \lim_{\rho \rightarrow \infty} \frac{\log \mathbb{P}\{C_o(\mathbf{H}, \rho) < r \log_2 \rho\}}{\log \rho} \end{aligned} \quad (7.28)$$

It is easy to see that the term $C_o(\mathbf{H}, \rho)$ from the last equation is a MIMO capacity expression where only N_0 principal components (singular values Λ_k) of the total set of $\min\{M_T, M_R\}$ components have been retained. On the basis of the intuition developed in [21], diversity gain $d_{\bullet}(r)$ of channel (system) capacity corresponds to the order of the $(r+1)$ -th largest singular value involved in the capacity term. From (7.27), we readily conclude that $d_{\bullet}(r)$ is associated with the $(r+1)$ -th singular value of the $M_R \times M_T$ channel matrix \mathbf{H} “before” antenna selection. Hence, it is natural to expect that $d_{\circ}(r)$ defined as

$$d_{\circ}(r) = - \lim_{\rho \rightarrow \infty} \frac{\log \mathbb{P}\{C_o(\mathbf{H}, \rho) < r \log_2 \rho\}}{\log \rho} \quad (7.29)$$

which according to (7.28) is a lower bound on $d_{\star}(r)$, achieves diversity advantage of the $M_R \times M_T$ channel and hence coincides with $d_{\bullet}(r)$, which is clearly an upper bound on $d_{\star}(r)$.

The above discussion leads to the following statement that is based on Laplace principle (see, for example, [21]) applied to the joint distribution of the M_0 principal singular values $\Lambda_1, \dots, \Lambda_{M_0}$ of \mathbf{H} .

Theorem 7.4.1 *Assume that the entries of \mathbf{H} are i.i.d. complex circular Gaussian with zero mean and unit variance. The maximum achievable diversity gain $d_{\star}(r)$ is a piecewise linear function of $r \in [0, N_0]$ connecting the points $(m, d_{\star}(m))$ defined by*

$$d_{\star}(m) = (M_R - m)(M_T - m), \quad 0 \leq m \leq N_0. \quad (7.30)$$

Proof: According to (7.28) and (7.29), we have $d_{\star}(r) \geq d_{\circ}(r)$ for $r \in [0, N_0]$. Note also that $d_{\star}(r) \leq d_{\bullet}(r)$ since this latter term stands for the maximum diversity of the “full” $M_R \times M_T$ system. Given this observation and the existing results for $d_{\bullet}(m)$ revisited earlier in this section, it is sufficient to show that $d_{\circ}(r)$ is a piecewise linear function of $r \in [0, N_0]$ connecting the points $(m, d_{\star}(m))$ defined by

$$d_{\circ}(m) = (M_R - m)(M_T - m), \quad 0 \leq m \leq N_0. \quad (7.31)$$

Let us show the aforementioned sufficient condition. Define

$$\hat{\alpha}_k = \begin{cases} 1, & 1 \leq k \leq M_0 - N_0; \\ -(\log \Lambda_k^2)/(\log \rho), & M_0 - N_0 + 1 \leq k \leq M_0. \end{cases} \quad (7.32)$$

According to (7.27), we can write

$$\begin{aligned}\mathbb{P}\{C_o(\mathbf{H}, \rho) < r \log_2 \rho\} &= \mathbb{P}\left\{\sum_{k=1}^{M_0} \frac{\log_2(1 + \rho \Lambda_k^2)}{\log_2 \rho} < r\right\} \\ &= \mathbb{P}\left\{\sum_{k=1}^{M_0} \frac{\log_2(1 + \rho^{1-\hat{\alpha}_k})}{\log_2 \rho} < r\right\}.\end{aligned}$$

By the definition of $d_o(r)$, we have

$$\begin{aligned}d_o(r) &= -\lim_{\rho \rightarrow \infty} \frac{\mathbb{P}\left\{\sum_{k=1}^{M_0} \frac{\log_2(1 + \rho^{1-\hat{\alpha}_k})}{\log_2 \rho} < r\right\}}{\log \rho} \\ &= -\lim_{\rho \rightarrow \infty} \frac{\mathbb{P}\left\{\sum_{k=1}^{M_0} (1 - \hat{\alpha}_k)^+ < r\right\}}{\log \rho},\end{aligned}$$

where $(\cdot)^+ = \max\{\cdot, 0\}$. Given the definition of $\{\alpha_k\}$ and the statistical properties of the eigenvalues $\Lambda_1^2, \dots, \Lambda_{M_0}^2$ for the channel model under consideration, we can make use of the results from [21] (Theorem 4). With $\{\hat{\alpha}_k\}$ defined in (7.32), we find

$$d_o(r) = \min_{\alpha \in \mathcal{A}} \sum_{k=1}^{M_0} (2k - 1 + |M_R - M_T|) \alpha_k, \quad r \in [0, N_0], \quad (7.33)$$

where $\alpha = [\alpha_1, \dots, \alpha_{M_0}]$ and

$$\begin{aligned}\mathcal{A} = \{ \alpha \in \mathbb{R}^{M_0} : \alpha_1 = \dots = \alpha_{M_0-N_0} = 1, \\ 1 \geq \alpha_{M_0-N_0+1} \geq \dots \geq \alpha_{M_0} \geq 0, \quad \sum_k (1 - \alpha_k)^+ \leq r \}.\end{aligned}$$

A slight difference w.r.t. [21] is in the definition of the set \mathcal{A} , which contains an additional constraint $\alpha_1 = \dots = \alpha_{M_0-N_0} = 1$ (unlike \mathcal{A}' in [21]). One can check that this difference does not affect the proof and the final result.

To obtain the closed form of $d_o(r)$, we will represent $r \in [0, N_0]$ as follows.

$$r = m + \delta, \quad \text{where} \quad 0 \leq m \leq N_0 \quad \text{and} \quad \delta \in (0, 1).$$

Check that for such r , the minimum in (7.33) will be reached with

$$\alpha_1 = \dots = \alpha_{M_0-m-1} = 1, \quad \alpha_{M_0-m} = 1 - \delta, \quad \alpha_{M_0-m+1} = \dots = \alpha_{M_0} = 0.$$

Consequently,

$$\begin{aligned}d_o(m + \delta) &= \sum_{k=1}^{M_0-m-1} (2k - 1 + |M_R - M_T|) \\ &\quad + (2(M_0 - m) - 1 + |M_R - M_T|)(1 - \delta), \\ &\quad 0 \leq m \leq M_0, \quad \delta \in (0, 1).\end{aligned}$$

Note that $d_{\circ}(m + \delta)$ is a piecewise linear function of $(m + \delta)$ connecting the points $(m, d_{\circ}(m))$, $0 \leq m \leq M_0$, and

$$\begin{aligned} d_{\circ}(m) &= \sum_{k=1}^{M_0-m} (2k - 1 + |M_R - M_T|) \\ &= (M_0 - m)^2 + (M_0 - m) |M_R - M_T| \\ &= (M_0 - m) (M_0 + |M_R - M_T| - m) = (M_R - m) (M_T - m). \end{aligned}$$

□

In other words, a MIMO system that selects $N_T \leq M_T$ out of M_T transmit antennas and $N_R \leq M_R$ out of M_R receive antennas achieves the same diversity gain as a system that makes use of all M_T transmit and M_R receive antennas.

It is worthwhile reiterating that the lower bound from Lemma 7.4.1 is based on the sub-optimal antenna selection rule of Algorithm I. Hence, the conclusion of the Theorem 7.4.1 also carries over to the results of Algorithm I:

Corollary 7.4.1 *The suboptimal antenna subset selection rule of Algorithm I achieves the same diversity gain $d_{\star}(r)$ as the optimal subset selection.*

7.4.3 Diversity and multiplexing: numerical example

Let us illustrate the results of the previous section via simulations. We consider three scenarios. In the first scenario, there is no antenna selection and $M_T = M_R = N_T = N_R = 2$. In the second scenario, we set $M_T = M_R = 3$ and $N_T = N_R = 2$. In the third scenario, $M_T = M_R = 4$ and $N_T = N_R = 3$. For each scenario, we choose the SNR of 20 dB ($\rho = 10^2$) and simulate 100000 independent runs of the channel matrix \mathbf{H} . The optimal set of transmit/receive antennas is selected and the associated Shannon capacity is determined. On the basis of this data, we compute the ratio $\log \mathbb{P}\{C_{\star}(\mathbf{H}, \rho) < r \log_2 \rho\} / (\log \rho)$ and plot it versus the multiplexing gain r in Fig. 7.7. The results for the three scenarios are shown by the solid (—), dashed (---) and dash-dotted (—·—) lines correspondingly. This simple numerical example validates our theoretical results, namely for $r = \{1, 2\}$ (first scenario), $r = 2$ (second scenario) and $r = 3$ (third scenario). Let us emphasize that it is difficult to obtain data points for higher diversity gains ($d_{\star} \geq 3$) as these latter correspond to very small outage rates.

7.5 Receive Antenna Selection Algorithms

Thus far we have omitted discussing specific algorithms for MIMO antenna selection. This section focuses on this topic, in particular, on receive antenna selection algorithms. In most cases, optimal antenna selection requires a combinatorial search, that is, if we select N_R out of M_R , we have to potentially search over $\binom{M_R}{N_R}$ possibilities. When the goal is to perform transmit *and* receive selection, then the number of choices increases to $\binom{M_R}{N_R} \binom{M_T}{N_T}$. For large M_R and/or M_T , the search complexity can be prohibitive. It is therefore important to

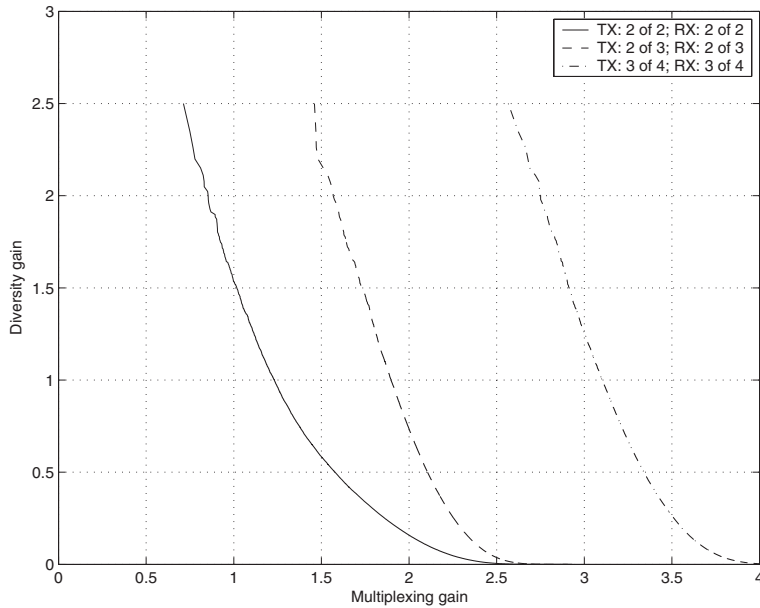


Figure 7.7 Diversity gain (d_*) versus multiplexing gain (r), 20 dB SNR.

develop low-complexity selection algorithms with good performance that allow tractable analysis. These algorithms have to be designed to maximize/minimize a certain metric, such as received SNR, throughput, minimum error rate, that depends on the transmit/receive processing scheme. Given the vast multiplicity of such schemes in MIMO systems, there is no single metric ² that can be used in the antenna selection algorithm. In other words, there is no single antenna subset that is optimal for all transmit/receive algorithms, and the selection algorithms have to be tailored to meet the requirements of a particular space-time processing scheme.

In the following, rather than enumerating antenna selection algorithms for each and every space-time processing technique we choose instead to present two selection methodologies that may be readily adapted for use with practical space-time processing schemes [40, 12].

7.5.1 Incremental and decremental selection

As mentioned earlier, receive antenna selection to maximize channel capacity requires a search over all $\binom{M_R}{N_R}$ subsets. The resulting complexity may be excessive, especially for large M_T and/or M_R . In the rest of this section, we briefly describe two approaches. The interested reader is pointed to [40, 7, 12] for a more detailed treatment.

²This is as opposed to the SIMO case where selecting the subset with maximum SNR is usually optimal for almost all criteria.

Incremental selection

The idea of incremental selection is to successively add N_R antennas so that, at every stage, the antenna that yields the maximum increase of the capacity is added to the set r of receive antennas. Suppose that after n steps, the antennas indexed with $\{r_1, \dots, r_n\}$ have been selected and $\mathbf{H}_{r_1, \dots, r_n}$ is the corresponding $n \times M_T$ submatrix of \mathbf{H} . Appending the l -th antenna yields

$$\begin{aligned} C(\mathbf{H}_{r_1, \dots, r_n, l}, \rho) &= \log_2 \det(\mathbf{I}_{M_T} + \rho (\mathbf{H}_{r_1, \dots, r_n}^* \mathbf{H}_{r_1, \dots, r_n} + \mathbf{H}_l^* \mathbf{H}_l)), \\ &= \log_2 \det(\mathbf{I}_{M_T} + \rho \mathbf{H}_{r_1, \dots, r_n}^* \mathbf{H}_{r_1, \dots, r_n}) \\ &\quad + \log_2 \left(1 + \rho \mathbf{H}_l (\mathbf{I}_{M_T} + \rho \mathbf{H}_{r_1, \dots, r_n}^* \mathbf{H}_{r_1, \dots, r_n})^{-1} \mathbf{H}_l^* \right). \end{aligned} \quad (7.34)$$

Maximization of $C(\mathbf{H}_{r_1, \dots, r_n, l}, \rho)$ w.r.t. l yields:

$$r_{n+1} = \arg \max_{l \notin \{r_1, \dots, r_n\}} \mathbf{H}_l (\rho^{-1} \mathbf{I}_{M_T} + \mathbf{H}_{r_1, \dots, r_n}^* \mathbf{H}_{r_1, \dots, r_n})^{-1} \mathbf{H}_l^*. \quad (7.35)$$

The matrix inverses in the selection rule defined above may be efficiently computed using the matrix inversion lemma [45]. Let \mathbf{A} and \mathbf{a} denote a $n \times n$ positive definite matrix and a $n \times 1$ vector, respectively. Then,

$$(\mathbf{A} + \mathbf{a} \mathbf{a}^*)^{-1} = \mathbf{A}^{-1} - \mathbf{A}^{-1} \mathbf{a} (1 + \mathbf{a}^* \mathbf{A}^{-1} \mathbf{a})^{-1} \mathbf{a}^* \mathbf{A}^{-1}. \quad (7.36)$$

The incremental selection algorithm can now be defined, making use of (7.35) and (7.36).

ALGORITHM II INCREMENTAL SELECTION

```

Set  $\mathbf{A} := \rho \mathbf{I}_{M_T}$  and  $r_1 := \arg \max_{1 \leq l \leq N_R} \|\mathbf{H}_l\|^2$ .
for  $n = 1$  to  $(N_R - 1)$ 
    update  $\mathbf{A} := \mathbf{A} - \mathbf{A} \mathbf{H}_{r_n}^* (1 + \mathbf{H}_{r_n} \mathbf{A} \mathbf{H}_{r_n}^*)^{-1} \mathbf{H}_{r_n} \mathbf{A}$ ;
    compute  $r_{n+1} = \arg \max_{l \notin \{r_1, \dots, r_n\}} \mathbf{H}_l \mathbf{A} \mathbf{H}_l^*$ ;
end

```

Decremental selection

The idea of decremental selection, introduced in [37], is to start with the whole set of M_R antennas and to remove one antenna in each of $(M_R - N_R)$ stages. At each stage, the algorithm identifies and removes the antenna that yields the minimum reduction in capacity. Observe that the effect of removing the l -th antenna from a given set $\{r_1, \dots, r_n\}$ amounts to replacing the term $(\mathbf{H}_l^* \mathbf{H}_l)$ in (7.34) by $(-\mathbf{H}_l^* \mathbf{H}_l)$. This observation allows the procedure outlined in the development of the incremental selection algorithm to be easily extended to develop decremental selection.

ALGORITHM III
DECREMENTAL SELECTION

```

Set  $\mathbf{A} := (\rho^{-1} \mathbf{I}_{M_T} + \mathbf{H}^* \mathbf{H})^{-1}$ ,
 $p = \arg \min_{1 \leq l \leq N_R} \mathbf{H}_l \mathbf{A} \mathbf{H}_l^*$ , and
 $r := \{1, \dots, p - 1, p + 1, \dots, N_R\}$ .
for  $n = 1$  to  $(N_R - M_R - 1)$ 
    update  $\mathbf{A} := \mathbf{A} + \mathbf{A} \mathbf{H}_p^* (1 - \mathbf{H}_p \mathbf{A} \mathbf{H}_p^*)^{-1} \mathbf{H}_p \mathbf{A}$ ;
    compute  $p = \arg \min_{l \in r} \mathbf{H}_l \mathbf{A} \mathbf{H}_l^*$ ,  $r := p \setminus r$ ;
end

```

For the same number of selection steps, decremental selection is more complex but expected to perform better than incremental selection. This is because of the fact that the decremental selection algorithm factors in the contributions of all remaining antennas while the incremental selection algorithm is based on individual contributions of the appended antennas. Finally, note that Algorithm III is strictly optimal when $M_R = N_R + 1$.

7.5.2 Numerical study

In this section, we compare the performance of the algorithms outlined above. Fig. 7.8 depicts the outage capacity with outage rate 10% versus the total received SNR per receive antenna ($M_T \rho$) for $M_R = 8$. The figure contains two sets of curves corresponding to $M_T = N_T = \{2, 4\}$ and $N_R = N_T$ (i.e., post selection, the channel matrix is square). Each set consists of six cases corresponding to different selection algorithms. The performance without antenna selection and with all receive antennas provide boundaries for the performance of antenna selection. Note that the curves corresponding to incremental and decremental selection algorithms overlap with the optimal selection curve, indicating that Algorithms I and II are near optimal. The performance of the ‘maximum norm’ based selection algorithm that selects the receive antennas with the maximum norm [27, 24] (or, equivalently, selects the antennas that maximizes the total received energy) is provided for the sake of comparison. At high SNR, there is a fixed gap between the outage capacity with antenna selection and the outage capacity when all antennas are used. This gap indicates the array loss incurred because of the use of fewer (N_R) than the available (M_R) receive antennas. Fig. 7.9 depicts the outage capacity versus the total number M_R of receive antennas for $M_T \rho = 10$ dB. The two sets of curves correspond to $M_T = N_T = \{2, 4\}$ and $N_R = N_T$. Notice that even a relatively simple selection algorithm based on maximizing the total received energy provides significant selection gain.

7.6 Antenna Selection in MIMO Wireless LAN Systems

In this section, we discuss a possible use of MIMO antenna selection in a practical MIMO-OFDM system. We will consider Wireless Local Area Network (WLAN) as a driving application. Our interest in WLAN is motivated by a rapid proliferation of MIMO technology in WLAN market space, in the form of the new (IEEE 802.11n) standard that is being

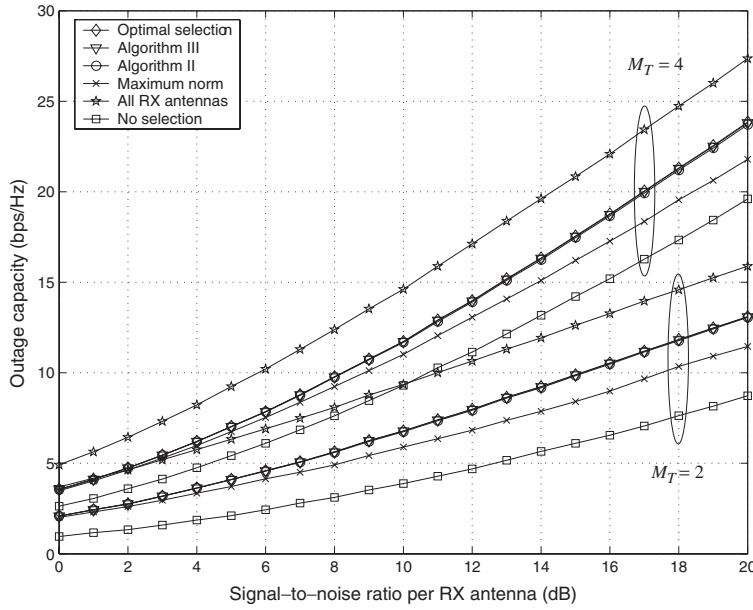


Figure 7.8 10% outage capacity of antenna selection versus SNR (ρM_T), $M_R = 8$. Incremental and decremental selection algorithms are near optimal.

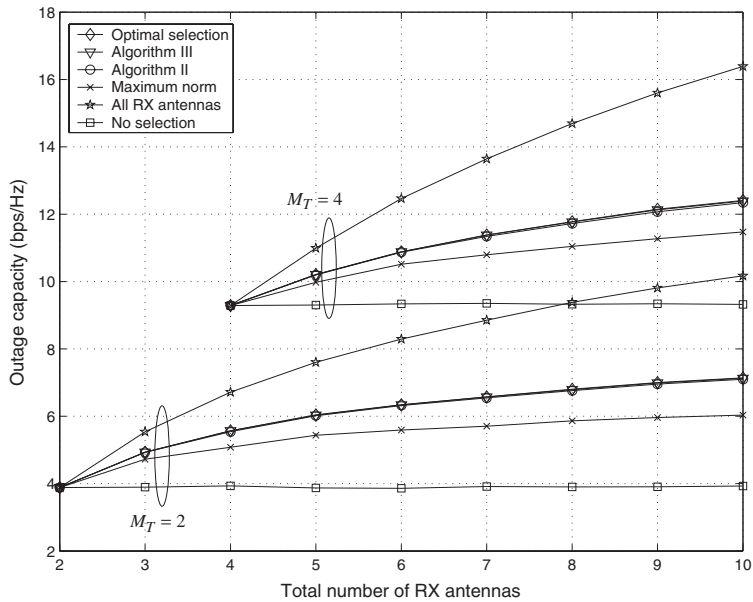


Figure 7.9 10% outage capacity of antenna selection versus M_R , $M_T \rho = 10$ dB.

defined. It is worth mentioning that implementation cost has been a major obstacle to widespread use of MIMO technology for WLANs, thereby making MIMO antenna selection particularly attractive.

The block diagram of a typical MIMO-OFDM system considered for WLAN is depicted in Fig. 7.10. Such a transceiver performs spatial multiplexing over N_T transmit antennas in order to increase the data rate by a factor of N_T compared to the standard 802.11 a/g systems. At the receiver, the original data stream is reconstructed from N_R received signals. When antenna subset selection is used, these N_T transmit (N_R receive) antennas are selected from the total M_T transmit (M_R receive) available antennas. Antenna selection algorithms will be applied to the main tap of the (frequency selective) $M_R \times M_T$ MIMO channel. This approach is justified in typical WLAN environments since the RMS delay spread is often less than 10ns, for the total signal bandwidth of 20 MHz. At the transmitter, user bits are encoded by the standard (133₈,171₈) convolutional FEC code with coding rate 3/4 achieved through puncturing. The coded bits are distributed in a round robin fashion between the N_T transmit streams. Next, the standard frequency interleaving scheme is applied to every stream. In Fig. 7.10, these operations are carried out by the space-frequency interleaver. The sequences of interleaved bits are mapped into N_T sequences of 64 QAM symbols and further transmitted via N_T antennas after the OFDM modulation as per 802.11 a/g.

At the receiver, the captured signals are sampled and, after frequency and timing recovery, mapped to the frequency domain. In a MIMO-OFDM system, the N_R received signals at each subcarrier are instantaneous mixtures of the N_T symbols transmitted at this subcarrier. In this paper, we assume that the N_T symbols are retrieved from their N_R noisy mixtures by the optimal linear filter (MMSE) at every subcarrier. The set of N_T signal-to-interference-and-noise ratio (SINR) values at the respective outputs of the filter are also computed and subsequently used in the soft demapper along with the output signals of the filter.

In the remainder of this paper, we set the number of transmit/receive data streams to $N_T = N_R = 2$. We simulate the system in Fig. 7.10 with the optimal combined transmit receive antenna selection specified in (7.25) as well as the suboptimal selection defined by Algorithm I.

In Fig. 7.11, we plot packet error rate (PER) versus the average SNR per receive antenna for optimal and suboptimal antenna selection, for different values of M_T and M_R . Note that

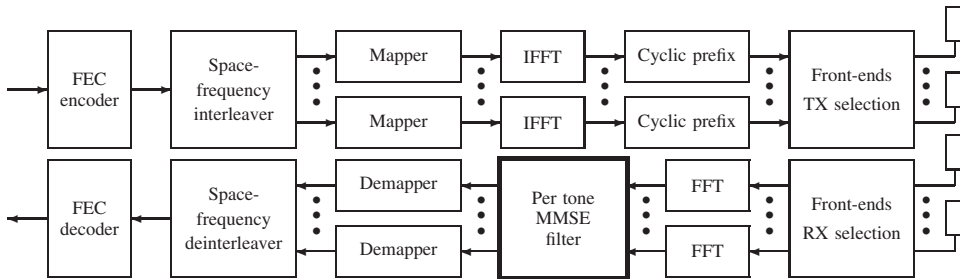


Figure 7.10 MIMO-OFDM transceiver: block diagram.

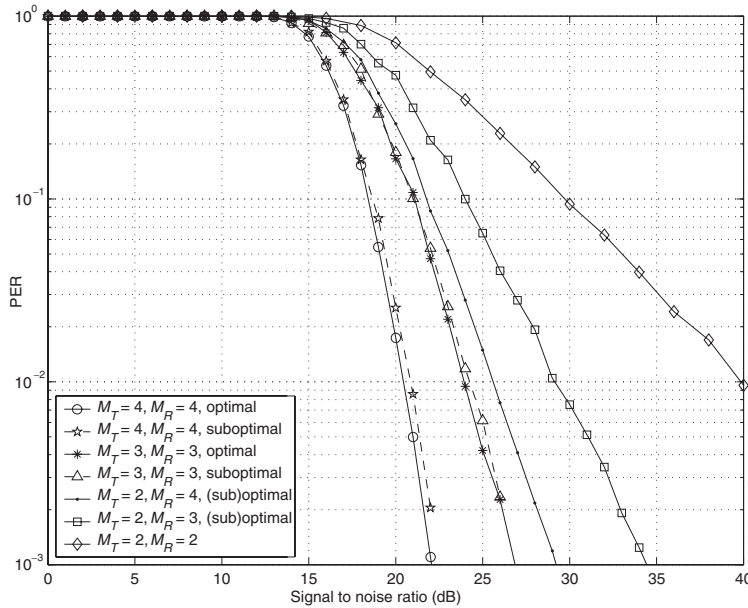


Figure 7.11 Packet error rates versus SNR per RX antenna: 108 Mbps, 1000 bytes/packet, $N_T = N_R = 2$.

PER will approximate the outage rate in a high SNR mode and/or with a powerful FEC. According to the definition (7.20), the slope of the PER curve in the log-scale will approach the diversity gain d in high SNR region. It is possible to show that for a MIMO transceiver with MMSE multiplexing and $N_T = 2$, the multiplexing gain satisfies $1 \leq r \leq 2$, with the lower limit ($r = 1$) attained at high SNR. This observation is due to the fact that the output SINR of the MMSE filter is dominated by the “worst” eigenvalue of the channel matrix, which is the N_T -th ordered eigenvalue (nonincreasing order) corresponding to the multiplexing gain $r = (N_T - 1)$ (note that $N_T = 1$ corresponds to $r = 0$ for a fixed rate and high SNR limit). Hence, we can apply (7.30) with $m = 1$ to predict the diversity gains. These gains should resemble the slope of the respective PER curves at high SNR. We find $d(1) = 1$ for $M_T = M_R = 2$, $d(1) = 2$ for $M_T = 2$ and $M_R = 3$, $d(1) = 3$ for $M_T = 2$ and $M_R = 4$, $d(1) = 4$ for $M_T = M_R = 3$ and finally $d(1) = 9$ for $M_T = M_R = 4$. Check that these numbers correspond to the slopes in Fig. 7.11. Also note that the suboptimal selection produces the same slopes as the optimal selection, with a slight loss in SNR.

7.7 Summary

In this chapter, we covered recent advances in the art of MIMO antenna selection. One of the main theoretical conclusions is that selecting a subset of antennas at the transmitter and/or receiver delivers the diversity gain of a “full” system that makes use of all available transmit/receive antennas. This fundamental result extends the well-known observation that selecting a single receive antenna delivers the full diversity gain in a system with a single

transmit antenna. Additionally, we extended the framework of diversity versus multiplexing trade-off of MIMO systems to systems with antenna selection. The second part of the chapter describes reduced complexity approaches to antenna selection. Interestingly, these simple techniques provide a hefty fraction of the total gains achievable through antenna selection. Finally, we presented an example of a MIMO-WLAN communication system indicating possibility of substantial gains using antenna selection.

References

- [1] J. Winters, "On the capacity of radio communication systems with diversity in a rayleigh fading environment," *IEEE J. Sel. Areas Commun.*, vol. 5, no. 5, pp. 871–878, Jun. 1987.
- [2] A. Paulraj and T. Kailath, "Increasing capacity in wireless broadcast systems using distributed transmission/directional reception," *U. S. Patent*, no. 5,345,599, 1994.
- [3] I. Telatar, "Capacity of multi-antenna Gaussian channels," AT & T Bell Laboratories, Tech. Rep. #BL0112170-950615-07TM, 1995.
- [4] G. Foschini, "Layered space-time architecture for wireless communication in a fading environment when using multi-element antennas," *Bell Labs Tech. J.*, vol. 1, no. 2, pp. 41–59, 1996.
- [5] I. Telatar, "Capacity of multi-antenna Gaussian channels," *Eur. Trans. Telecommun.*, vol. 10, no. 6, pp. 585–595, Nov./Dec. 1999.
- [6] A. Paulraj, R. Nabar, and D. Gore, *Introduction to Space-time Wireless Communications*. Cambridge University Press, May 2003.
- [7] A. Gorokhov, D. Gore, and A. Paulraj, "Receive antenna selection for MIMO flat-fading channels," *IEEE Trans. Inf. Theory*, vol. 49, pp. 2687–2696, Oct. 2003.
- [8] G. Foschini and M. Gans, "On limits of wireless communications in a fading environment when using multiple antennas," *Wireless Pers. Commun.*, vol. 6, no. 3, pp. 311–335, Mar. 1998.
- [9] T. Eng, N. Kong, and L. Milstein, "Comparison of diversity combining techniques for Rayleigh fading channels," *IEEE Trans. Commun.*, vol. 44, no. 9, pp. 1117–1129, Sept. 1996.
- [10] M. Win and J. Winters, "Virtual branch analysis of symbol error probability for hybrid selection/maximal-ratio combining in Rayleigh fading," *IEEE Trans. Commun.*, vol. 49, no. 11, pp. 1926–1934, Nov. 2001.
- [11] M. Win, N. Beaulieu, L. Shepp, B. Logan, and J. Winters, "On the SNR penalty of MPSK with hybrid selection/maximal ratio combining over i.i.d. Rayleigh fading channels," *IEEE Trans. Commun.*, vol. 51, pp. 1012–1023, Jun. 2003.
- [12] A. Gorokhov, D. Gore, and A. Paulraj, "Receive antenna selection for spatial multiplexing: theory and algorithms," *IEEE Trans. Signal Proc.*, vol. 51, pp. 2796–2807, Nov. 2003.
- [13] M. Win and J. Winters, "Analysis of hybrid selection/maximal-ratio combining in Rayleigh fading," *IEEE Trans. Commun.*, vol. 47, no. 12, pp. 1773–1776, Dec. 1999.
- [14] S. Alamouti, "A simple transmit diversity technique for wireless communications," *IEEE J. Sel. Areas Commun.*, vol. 16, no. 8, pp. 1451–1458, Oct. 1998.
- [15] V. Tarokh, A. Naguib, N. Seshadri, and A. Calderbank, "Space-time codes for high data rate wireless communication: Performance criteria in the presence of channel estimation errors, mobility, and multiple paths," *IEEE Trans. Commun.*, vol. 47, no. 2, pp. 199–207, Feb. 1999.
- [16] V. Tarokh, H. Jafarkhani, and A. Calderbank, "Space-time block coding for wireless communications: Performance results," *IEEE J. Sel. Areas Commun.*, vol. 17, no. 3, pp. 451–460, Mar. 1999.

- [17] P. Wolniansky, G. Foschini, G. Golden, and R. Valenzuela, "V-BLAST: An architecture for realizing very high data rates over the rich-scattering wireless channel," in *Proc. URSI ISSSE*, Sept. 1998, pp. 295–300, Pisa, Italy.
- [18] G. Golden, G. Foschini, R. Valenzuela, and P. Wolniansky, "Detection algorithm and initial laboratory results using V-BLAST space-time communication architecture," *Electron. Lett.*, vol. 35, no. 1, pp. 14–16, Jan. 1999.
- [19] L. Zheng and D. Tse, "Optimal diversity-multiplexing trade-off in multi-antenna channels," in *Proc. Allerton Conf. Commun., Control Comput.*, Monticello, IL, Oct. 2001.
- [20] R. Heath and A. Paulraj, "Linear dispersion codes for MIMO systems based on frame theory," *IEEE Trans. Signal Proc.*, vol. 50, no. 10, pp. 2429–2441, Oct. 2002.
- [21] L. Zheng and D. Tse, "Diversity and multiplexing: A fundamental tradeoff in multiple-antenna channels," *IEEE Trans. Inf. Theory*, vol. 49, no. 5, pp. 1073–1096, May 2003.
- [22] D. Gore and A. Paulraj, "MIMO antenna sub-set selection for space-time coding," *IEEE Trans. Signal Proc.*, vol. 50, no. 10, pp. 2580–2588, Oct. 2002.
- [23] I. Bahceci, T. Duman, and Y. Altunbasak, "Antenna selection for multiple-antenna transmission systems: Performance analysis and code construction," *IEEE Trans. Inf. Theory*, vol. 49, no. 10, pp. 2669–2681, Oct. 2003.
- [24] A. Ghayeb and T. Duman, "Performance analysis of MIMO systems with antenna selection over quasi-static fading channels," *IEEE Trans. Veh. Technol.*, vol. 52, no. 3, pp. 281–288, Mar. 2003.
- [25] W. Wong and E. Larsson, "Orthogonal space-time block coding with antenna selection and power allocation," *Electron. Lett.*, vol. 39, no. 4, pp. 379–381, Feb. 2003.
- [26] Z. Chen, B. Vucetic, and Y. Jinhong, "Space-time trellis codes with transmit antenna selection," *Electron. Lett.*, vol. 39, no. 11, pp. 854–855, May 2003.
- [27] A. Molisch, M. Win, and J. Winters, "Reduced-complexity transmit/receive-diversity systems," *IEEE Trans. Signal Proc.*, vol. 51, no. 11, pp. 2729–2738, Nov. 2003.
- [28] Z. Chen, Y. Jinhong, B. Vucetic, and Z. Zhou, "Performance of Alamouti scheme with transmit antenna selection," *Electron. Lett.*, vol. 39, no. 23, pp. 1666–1668, Nov. 2003.
- [29] X. Zheng and A. Ghayeb, "Performance bounds for space-time block codes with receive antenna selection," *IEEE Trans. Inf. Theory*, vol. 50, pp. 2130–2137, Sept. 2004.
- [30] R. Heath and A. Paulraj, "Antenna selection for spatial multiplexing systems based on minimum error rate," in *Proc. IEEE ICC*, vol. 7, Helsinki, Finland, June 2001, pp. 2276–2280.
- [31] R. Narasimhan, "Spatial multiplexing with transmit antenna and constellation selection for correlated MIMO fading channels," *IEEE Trans. Signal Proc.*, vol. 51, no. 11, pp. 2829–2838, Nov. 2003.
- [32] Z. Hairuo, D. Lin, Z. Shidong, and Y. Yan, "Low complexity per-antenna rate and power control approach for closed-loop V-BLAST," *IEEE Trans. Commun.*, vol. 51, no. 11, pp. 1783–1787, Nov. 2003.
- [33] P. Voltz, "Characterization of the optimum transmitter correlation matrix for MIMO with antenna subset selection," *IEEE Trans. Commun.*, vol. 51, pp. 1779–1782, Nov. 2003.
- [34] I. Berenguer, X. Wang, and I. Wassell, "Transmit antenna selection in linear receivers: geometrical approach," *Electron. Lett.*, vol. 40, no. 5, pp. 292–293, Mar. 2004.
- [35] D. Gore, R. U. Nabar, and A. Paulraj, "Selecting an optimal set of transmit antennas for a low rank matrix channel," in *Proc. IEEE ICASSP*, vol. 5, Istanbul, Turkey, May 2000, pp. 2785–2788.
- [36] S. Sandhu, R. Nabar, D. Gore, and A. Paulraj, "Near-optimal selection of transmit antennas for a MIMO channel based on Shannon capacity," in *Proc. Asilomar Conf. Signals, Syst. Comput.*, vol. 1, Pacific Grove, CA, Nov. 2000, pp. 567–571.

- [37] A. Gorokhov, "Antenna selection algorithms for MEA transmission systems," in *Proc. IEEE ICASSP*, vol. 3, Orlando, FL, May 2002, pp. 2857–2860.
- [38] A. Molisch, M. Win, and J. Winters, "Capacity of MIMO systems with antenna selection," in *Proc. IEEE ICC*, vol. 2, Helsinki, Finland, June 2001, pp. 570–574.
- [39] R. Blum and J. Winters, "On optimum MIMO with antenna selection," *IEEE Commun. Lett.*, vol. 6, no. 8, pp. 322–324, Aug. 2002.
- [40] D. Gore, A. Gorokhov, and A. Paulraj, "Joint MMSE vs V-BLAST and receive selection," in *Proc. Asilomar Conf. Signals, Syst. Comput.*, vol. 1, Nov. 2002, pp. 505–509.
- [41] R. Blum, "MIMO capacity with antenna selection and interference," in *Proc. IEEE ICASSP*, vol. 4, Hong Kong, April 2003, pp. 824–827.
- [42] A. Molisch and M. Win, "MIMO systems with antenna selection," *IEEE Microw. Mag.*, vol. 5, no. 1, pp. 46–56, Mar. 2004.
- [43] A. Gorokhov, M. Collados, D. Gore, and A. Paulraj, "Transmit/receive MIMO antenna subset selection," in *Proc. IEEE ICASSP*, vol. II, Montreal, Canada, May 2004, pp. 13–16.
- [44] M. Gharavi-Alkhansari and A. Gershman, "Fast antenna sub-set selection in MIMO systems," *IEEE Trans. Signal Proc.*, vol. 52, pp. 339–347, Feb. 2004.
- [45] T. Kailath, *Linear Systems*. Englewood Cliffs (NJ): Prentice Hall, 1980.

Convex Optimization Theory Applied to Joint Transmitter-Receiver Design in MIMO Channels

Daniel Pérez Palomar, Antonio Pascual-Iserte, John M. Cioffi, and Miguel Angel Lagunas

8.1 Introduction

Multiantenna MIMO channels have recently become a popular means to increase the spectral efficiency and quality of wireless communications by the use of spatial diversity at both sides of the link [1–4]. In fact, the MIMO concept is much more general and embraces many other scenarios such as wireline digital subscriber line (DSL) systems [5] and single-antenna frequency-selective channels [6]. This general modeling of a channel as an abstract MIMO channel allows for a unified treatment using a compact and convenient vector-matrix notation.

MIMO systems are not just mathematically more involved than SISO systems but also conceptually different and more complicated, since several substreams are typically established in MIMO channels (multiplexing property) [7]. The existence of several substreams,

This work was supported in part by the Fulbright Program and Spanish Ministry of Education and Science; the Spanish Government under projects TIC2002-04594-C02-01 (GIRAFÁ, jointly financed by FEDER) and FIT-070000-2003-257 (MEDEA+ A111 MARQUIS); and the European Commission under project IST-2002-2.3.1.4 (NEWCOM).

each with its own quality, makes the definition of a global measure of the system quality very difficult; as a consequence, a variety of design criteria have been adopted in the literature. In fact, the design of such systems is a multiobjective optimization problem characterized by not having just optimal solutions (as happens in single-objective optimization problems) but a set of Pareto-optimal solutions [8].

The fundamental limits of MIMO communications have been known since 1948, when Shannon, in his ground-breaking paper [9], defined the concept of channel capacity—the maximum reliably achievable rate—and obtained the capacity-achieving signaling strategy. For a given realization of a MIMO channel, such a theoretical limit can be achieved by a Gaussian signaling with a waterfilling power profile over the channel eigenmodes [10, 3, 2]. In real systems, however, rather than with Gaussian codes, the transmission is done with practical signal constellations and coding schemes. To simplify the analysis and design of such systems, it is convenient to divide them into an uncoded part, which transmits symbols drawn from some constellations, and a coded part that builds upon the uncoded system. It is important to bear in mind that the ultimate system performance depends on the combination of both parts (in fact, for some systems, such a division does not apply).

The signaling scheme in a MIMO channel depends on the quantity and the quality of the channel state information (CSI) available at both sides of the communication link. For the case of no CSI at the transmitter, a wide family of techniques—termed *space-time* coding—have been proposed in the literature [1, 11, 12]. The focus of this chapter is on communication systems with CSI, either perfect (i.e., sufficiently good) or imperfect, and, more specifically, on the design of the uncoded part of the system in the form of linear MIMO transceivers (or transmit-receive beamforming strategies) under the framework of convex optimization theory.

In the last two decades, a number of fundamental and practical results have been obtained in convex optimization theory [13, 14]. It is a well-developed area both in the theoretical and practical aspects. Many convex problems, for example, can be analytically studied and solved using the optimality conditions derived from Lagrange duality theory. In any case, a convex problem can always be solved in practice with very efficient algorithms such as interior-point methods [14]. The engineering community has greatly benefited from these recent advances by finding applications. This chapter describes another application in the design of beamforming for MIMO channels.

This chapter starts with a brief overview of convex optimization theory in Section 8.2, with special emphasis on the art of unveiling the hidden convexity of problems (illustrated with some recent examples). Then, after introducing the system model in Section 8.3, the design of linear MIMO transceivers is considered in Section 8.4 under the framework of convex optimization theory. The derivation of optimal designs focuses on how the originally nonconvex problem is reformulated in convex form, culminating with closed-form expressions obtained from the optimality conditions. This work presents in a unified fashion the results obtained in [15] and [16] (see also [17]) and generalizes some of the results as well. The practical problem of imperfect CSI is addressed in Section 8.5, deriving a robust design less sensitive to errors in the CSI.

Notation: Boldface upper-case letters denote matrices, boldface lower-case letters denote column vectors, and italics denote scalars. The superscripts $(\cdot)^T$, $(\cdot)^*$, and $(\cdot)^H$ denote transpose, complex conjugate, and Hermitian operations, respectively. $\mathbb{R}^{m \times n}$ and $\mathbb{C}^{m \times n}$ represent the set of $m \times n$ matrices with real- and complex-valued entries, respectively (the

subscript $_+$ is sometimes used to restrict the elements to nonnegative values). $\text{Re}\{\cdot\}$ and $\text{Im}\{\cdot\}$ denote the real and imaginary part, respectively. $\text{Tr}(\cdot)$ and $\det(\cdot)$ denote the trace and determinant of a matrix, respectively. $\|\mathbf{x}\|$ is the Euclidean norm of a vector \mathbf{x} and $\|\mathbf{X}\|_F$ is the Frobenius norm of a matrix \mathbf{X} (defined as $\|\mathbf{X}\|_F \triangleq \sqrt{\text{Tr}(\mathbf{X}^H \mathbf{X})}$). $[\mathbf{X}]_{i,j}$ (also $[\mathbf{X}]_{ij}$) denotes the (i th, j th) element of matrix \mathbf{X} . $\mathbf{d}(\mathbf{X})$ and $\boldsymbol{\lambda}(\mathbf{X})$ denote the diagonal elements and eigenvalues, respectively, of matrix \mathbf{X} . A block-diagonal matrix with diagonal blocks given by the set $\{\mathbf{X}_k\}$ is denoted by $\text{diag}(\{\mathbf{X}_k\})$. The operator $(x)^+ \triangleq \max(0, x)$ is the projection on the nonnegative orthant.

8.2 Convex Optimization Theory

In the last two decades, several fundamental and practical results have been obtained in convex optimization theory [13, 14]. The engineering community not only has benefited from these recent advances by finding applications but has also fueled the mathematical development of both the theory and efficient algorithms. The two classical mathematical references on the subject are [18] and [19]. Two more recent engineering-oriented excellent references are [13] and [14].

Traditionally, it was a common believe that linear problems were easy to solve as opposed to nonlinear problems. However, as stated by Rockafellar in a 1993 survey [20], “the great watershed in optimization isn’t between linearity and nonlinearity, but convexity and nonconvexity” [14]. In a nutshell, convex problems can always be solved optimally either in closed form (by means of the optimality conditions derived from Lagrange duality) or numerically (with very efficient algorithms that exhibit a polynomial convergence). As a consequence, roughly speaking, one can say that once a problem has been expressed in convex form, it has been solved.

Unfortunately, most engineering problems are not convex when directly formulated. However, many of them have a potential hidden convexity that engineers have to unveil in order to be able to use all the machinery of convex optimization theory.

This section introduces the basic ideas of convex optimization (both the theory and practice) and then focuses on the art of reformulating engineering problems in convex form by means of recent real examples.

8.2.1 Definitions and classes of convex problems

Basic definitions

An optimization problem with arbitrary equality and inequality constraints can always be written in the following standard form [14]:

$$\begin{aligned} & \underset{\mathbf{x}}{\text{minimize}} && f_0(\mathbf{x}) \\ & \text{subject to} && f_i(\mathbf{x}) \leq 0 \quad 1 \leq i \leq m, \\ & && h_i(\mathbf{x}) = 0 \quad 1 \leq i \leq p, \end{aligned} \tag{8.1}$$

where $\mathbf{x} \in \mathbb{R}^n$ is the optimization variable, f_0 is the *cost* or *objective function*, f_1, \dots, f_m are the m inequality constraint functions, and h_1, \dots, h_p are the p equality constraint functions.

If the objective and inequality constraint functions are convex¹ and the equality constraint functions are linear (or, more generally, affine), the problem is then a *convex optimization problem* (or *convex program*). A point \mathbf{x} in the domain of the problem (set of points for which the objective and all constraint functions are defined) is *feasible* if it satisfies all the constraints $f_i(\mathbf{x}) \leq 0$ and $h_i(\mathbf{x}) = 0$. The problem (8.1) is said to be feasible if there exists at least one feasible point and *infeasible* otherwise. The *optimal value* (minimal value) is denoted by f^* and is achieved at an optimal solution \mathbf{x}^* , that is, $f^* = f_0(\mathbf{x}^*)$.

Classes of convex problems

When the functions f_i and h_i in (8.1) are linear (affine), the problem is called a *linear program* (LP) and is much simpler to solve. If the objective function is quadratic and the constraint functions are linear (affine), then it is called a *quadratic program* (QP); if, in addition, the inequality constraints are also quadratic, it is called *quadratically constrained quadratic program* (QCQP). QPs include LPs as a special case.

A problem that is closely related to quadratic programming is the *second-order cone program* (SOCP) [21, 14] that includes constraints of the form

$$\|\mathbf{Ax} + \mathbf{b}\| \leq \mathbf{c}^T \mathbf{x} + d \quad (8.2)$$

where $\mathbf{A} \in \mathbb{R}^{k \times n}$, $\mathbf{b} \in \mathbb{R}^k$, $\mathbf{c} \in \mathbb{R}^n$, and $d \in \mathbb{R}$ are given and fixed. Note that (8.2) defines a convex set because it is an affine transformation of the second-order cone $\mathcal{C}^n = \{(\mathbf{x}, t) \in \mathbb{R}^n \mid \|\mathbf{x}\| \leq t\}$, which is convex since both $\|\mathbf{x}\|$ and $-t$ are convex. If $\mathbf{c} = \mathbf{0}$, then (8.2) reduces to a quadratic constraint (by squaring both sides).

A more general problem than an SOCP is a *semidefinite program* (SDP) [22, 14] that has matrix inequality constraints of the form

$$x_1 \mathbf{F}_1 + \cdots + x_n \mathbf{F}_n + \mathbf{G} \leq \mathbf{0} \quad (8.3)$$

where $\mathbf{F}_1, \dots, \mathbf{F}_n, \mathbf{G} \in \mathcal{S}^k$ (\mathcal{S}^k is the set of Hermitian $k \times k$ matrices) and $\mathbf{A} \geq \mathbf{B}$ means that $\mathbf{A} - \mathbf{B}$ is positive semidefinite.

A very useful generalization of the standard convex optimization problem (8.1) is obtained by allowing the inequality constraints to be vector valued and using generalized inequalities [14]:

$$\begin{aligned} & \underset{\mathbf{x}}{\text{minimize}} && f_0(\mathbf{x}) \\ & \text{subject to} && \mathbf{f}_i(\mathbf{x}) \preceq_{\mathcal{K}_i} \mathbf{0} \quad 1 \leq i \leq m, \\ & && \mathbf{h}_i(\mathbf{x}) = \mathbf{0} \quad 1 \leq i \leq p, \end{aligned} \quad (8.4)$$

where the generalized inequalities² $\preceq_{\mathcal{K}_i}$ are defined by the proper cones \mathcal{K}_i ($\mathbf{a} \preceq_{\mathcal{K}} \mathbf{b} \Leftrightarrow \mathbf{b} - \mathbf{a} \in \mathcal{K}$) [14] and f_i are \mathcal{K}_i -convex.³

¹A function $f : \mathbb{R}^n \rightarrow \mathbb{R}$ is convex if, for all $\mathbf{x}, \mathbf{y} \in \text{dom } f$ and $\theta \in [0, 1]$, $\theta\mathbf{x} + (1 - \theta)\mathbf{y} \in \text{dom } f$ (i.e., the domain is a convex set) and $f(\theta\mathbf{x} + (1 - \theta)\mathbf{y}) \leq \theta f(\mathbf{x}) + (1 - \theta)f(\mathbf{y})$.

²A generalized inequality is a partial ordering on \mathbb{R}^n that has many of the properties of the standard ordering on \mathbb{R} . A common example is the matrix inequality defined by the cone of positive semidefinite $n \times n$ matrices \mathcal{S}_+^n .

³A function $\mathbf{f} : \mathbb{R}^n \rightarrow \mathbb{R}^{k_i}$ is \mathcal{K}_i -convex if the domain is a convex set and, for all $\mathbf{x}, \mathbf{y} \in \text{dom } f$ and $\theta \in [0, 1]$, $\mathbf{f}(\theta\mathbf{x} + (1 - \theta)\mathbf{y}) \preceq_{\mathcal{K}_i} \theta\mathbf{f}(\mathbf{x}) + (1 - \theta)\mathbf{f}(\mathbf{y})$.

Among the simplest convex optimization problems with generalized inequalities are the *cone programs* (CP) (or *conic form problems*), which have a linear objective and one inequality constraint function [23, 14]:

$$\begin{aligned} & \underset{\mathbf{x}}{\text{minimize}} && \mathbf{c}^T \mathbf{x} \\ & \text{subject to} && \mathbf{F}\mathbf{x} + \mathbf{g} \preceq_{\mathcal{K}} \mathbf{0} \\ & && \mathbf{A}\mathbf{x} = \mathbf{b}. \end{aligned} \tag{8.5}$$

CPs particularize nicely to LPs, SOCPs, and SDPs as follows: (i) if $\mathcal{K} = \mathbb{R}_+^n$ (nonnegative orthant), the partial ordering $\preceq_{\mathcal{K}}$ is the usual componentwise inequality between vectors and (8.5) reduces to LP; (ii) if $\mathcal{K} = \mathcal{C}^n$ (second-order cone), $\preceq_{\mathcal{K}}$ corresponds to a constraint of the form (8.2) and the problem (8.5) becomes an SOCP; (iii) if $\mathcal{K} = \mathcal{S}_+^n$ (positive semidefinite cone), the generalized inequality $\preceq_{\mathcal{K}}$ reduces to the usual matrix inequality as in (8.3) and the problem (8.5) simplifies to an SDP.

There is yet another very interesting and useful class of problems, the family of *geometric programs* (GP), that are not convex in their natural form but can be transformed into convex problems [14].

8.2.2 Reformulating a problem in convex form

As has been previously said, convex problems can always be solved in practice, either in closed form or numerically. However, the natural formulation of most engineering problems is not convex. In many cases, fortunately, there is a hidden convexity that can be unveiled by properly reformulating the problem. The main task of an engineer is then to cast the problem in convex form and, if possible, in any of the well-known classes of convex problems (so that specific and optimized algorithms can be used).

Unfortunately, there is not a systematic way to reformulate a problem in convex form. In fact, it is rather an art that can only be learned by examples (see §8.2.5). There are two main ways to reformulate a problem in convex form. The main one is to devise a convex problem equivalent to the original nonconvex one by using a series of clever changes of variables. As an example, consider the minimization of $1/(1+x^2)$ subject to $x^2 \geq 1$, which is a nonconvex problem (both the cost function and the constraint are nonconvex). The problem can be rewritten in convex form, after the change of variable $y = x^2$, as the minimization of $1/(1+y)$ subject to $y \geq 1$ (and the optimal x can be recovered from the optimal y as $x = \sqrt{y}$). A more realistic example is briefly described in §8.2.5 for robust beamforming. The class of geometric problems is a very important example of nonconvex problems that can be reformulated in convex form by a change of variable [14]. Another example is the beamforming design for MIMO channels treated in detail in §8.4.

Nevertheless, it is not really necessary to devise a convex problem that is exactly equivalent to the original one. In fact, it suffices if they both have the same set of optimal solutions (related by some mapping). In other words, both problems have to be equivalent only within the set of optimal solutions but not otherwise. Of course, the difficulty is how to obtain such a magic convex problem without knowing beforehand the set of optimal solutions. One very popular way to do this is by relaxing the problem (removing some of the constraints) such that it becomes convex, in a way that the “relaxed” optimal solutions can be shown to satisfy the removed constraints as well. A remarkable example of this approach

is described in §8.2.5 for multiuser beamforming. Several relaxations are also employed in the beamforming design for MIMO channels in §8.4.

8.2.3 Lagrange duality theory and KKT optimality conditions

Lagrange duality theory is a very rich and mature theory that links the original minimization problem (8.1), termed *primal problem*, with a dual maximization problem. In some occasions, it is simpler to solve the dual problem than the primal one. A fundamental result in duality theory is given by the optimality Karush-Kuhn-Tucker (KKT) conditions that any primal-dual solution must satisfy. By exploring the KKT conditions, it is possible in many cases to obtain a closed-form solution to the original problem (see, for example, the iterative waterfilling described in §8.2.5 and the closed-form results obtained in §8.4 for MIMO beamforming). In the following, the basic results on duality theory including the KKT conditions are stated (for details, the reader is referred to [13, 14]).

The basic idea in Lagrange duality is to take the constraints of (8.1) into account by augmenting the objective function with a weighted sum of the constraint functions. The *Lagrangian* of (8.1) is defined as

$$L(\mathbf{x}, \boldsymbol{\lambda}, \mathbf{v}) = f_0(\mathbf{x}) + \sum_{i=1}^m \lambda_i f_i(\mathbf{x}) + \sum_{i=1}^p v_i h_i(\mathbf{x}) \quad (8.6)$$

where λ_i and v_i are the *Lagrange multipliers* associated with the i th inequality constraint $f_i(\mathbf{x}) \leq 0$ and with the i th equality constraint $h_i(\mathbf{x}) = 0$, respectively.

The optimization variable \mathbf{x} is called the *primal variable* and the Lagrange multipliers $\boldsymbol{\lambda}$ and \mathbf{v} are also termed the *dual variables*. The original objective function $f_0(\mathbf{x})$ is referred to as the *primal objective*, whereas the *dual objective* $g(\boldsymbol{\lambda}, \mathbf{v})$ is defined as the minimum value of the Lagrangian over \mathbf{x} :

$$g(\boldsymbol{\lambda}, \mathbf{v}) = \inf_{\mathbf{x}} L(\mathbf{x}, \boldsymbol{\lambda}, \mathbf{v}), \quad (8.7)$$

which is concave even if the original problem is not convex because it is the pointwise infimum of a family of affine functions of $(\boldsymbol{\lambda}, \mathbf{v})$. Note that the infimum in (8.7) is with respect all \mathbf{x} (not necessarily feasible points). The dual variables $(\boldsymbol{\lambda}, \mathbf{v})$ are *dual feasible* if $\boldsymbol{\lambda} \geq \mathbf{0}$.

It turns out that the primal and dual objectives satisfy $f_0(\mathbf{x}) \geq g(\boldsymbol{\lambda}, \mathbf{v})$ for any feasible \mathbf{x} and $(\boldsymbol{\lambda}, \mathbf{v})$. Therefore, it makes sense to maximize the dual function to obtain a lower bound on the optimal value f^* of the original problem (8.1):

$$\begin{aligned} & \underset{\boldsymbol{\lambda}, \mathbf{v}}{\text{maximize}} \quad g(\boldsymbol{\lambda}, \mathbf{v}) \\ & \text{subject to} \quad \boldsymbol{\lambda} \geq \mathbf{0}, \end{aligned} \quad (8.8)$$

which is always a convex optimization problem even if the original problem is not convex. It is interesting to point out that a primal-dual feasible pair $(\mathbf{x}, (\boldsymbol{\lambda}, \mathbf{v}))$ localizes the optimal value of the primal (and dual) problem in an interval:

$$f^* \in [g(\boldsymbol{\lambda}, \mathbf{v}), f_0(\mathbf{x})]. \quad (8.9)$$

This property can be used in optimization algorithms to provide nonheuristic stopping criteria.

The difference between the optimal primal objective f^* and the optimal dual objective g^* is called the *duality gap*, which is always nonnegative $f^* - g^* \geq 0$ (weak duality). A central result in convex analysis [19, 18, 13, 14] is that when the problem is convex, under some mild technical conditions (called *constraint qualifications*⁴), the duality gap reduces to zero at the optimal (i.e., strong duality holds). Hence, the primal problem (8.1) can be equivalently solved by solving the dual problem (8.8) (see, for example, the simultaneous routing and resource allocation described in §8.2.5).

The optimal solutions of the primal and dual problems, \mathbf{x}^* and (λ^*, ν^*) , respectively, are linked together through the KKT conditions:

$$h_i(\mathbf{x}^*) = 0, \quad f_i(\mathbf{x}^*) \leq 0, \quad (8.10)$$

$$\lambda_i^* \geq 0, \quad (8.11)$$

$$\nabla_{\mathbf{x}} f_0(\mathbf{x}^*) + \sum_{i=1}^m \lambda_i^* \nabla_{\mathbf{x}} f_i(\mathbf{x}^*) + \sum_{i=1}^p \nu_i^* \nabla_{\mathbf{x}} h_i(\mathbf{x}^*) = \mathbf{0}, \quad (8.12)$$

$$(\text{complementary slackness}) \quad \lambda_i^* f_i(\mathbf{x}^*) = 0. \quad (8.13)$$

The KKT conditions are necessary and sufficient for optimality (when strong duality holds) [13, 14]. Hence, if they can be solved, both the primal and dual problems are implicitly solved.

8.2.4 Efficient numerical algorithms to solve convex problems

During the last decade, there has been a tremendous advance in developing efficient algorithms for solving wide classes of convex optimization problems. The most recent breakthrough in convex optimization theory is probably the development of interior-point methods for nonlinear convex problems. This was well established by Nesterov and Nemirovski in 1994 [24], where they extended the theory of linear programming interior-point methods (Karmarkar, 1984) to nonlinear convex optimization problems (based on the convergence theory of Newton's method for self-concordant functions).

The traditional optimization methods are based on gradient descent algorithms, which suffer from slow convergence and sensitivity to the algorithm initialization and stepsize selection. The recently developed methods for convex problems enjoy excellent convergence properties (polynomial convergence) and do not suffer from the usual problems of the traditional methods. In addition, it is simple to employ nonheuristic stopping criteria based on a desired resolution, since the difference between the cost value at each iteration and the optimum value can be upper-bounded using duality theory as in (8.9) [13, 14].

Many different software implementations have been recently developed and many of them are publicly available for free. It is worth pointing out that the existing packages not only provide the optimal primal variables of the problem but also the optimal dual variables. Currently, one of the most popular software optimization packages is **SeDuMi** [25], which is a Matlab toolbox for solving optimization problems over symmetric cones.

⁴One simple version of the constraint qualifications is Slater's condition, which is satisfied when the problem is strictly feasible (i.e., when there exists \mathbf{x} such that $f_i(\mathbf{x}) < 0$ for $1 \leq i \leq m$ and $h_i(\mathbf{x}) = 0$ for $1 \leq i \leq p$) [13, 14].

In the following, the most common optimization methods are briefly described with emphasis in interior-point methods.

Interior-point methods

Interior-point methods solve constrained problems by solving a sequence of smooth (continuous second derivatives are assumed) unconstrained problems, usually using Newton's method [13, 14]. The solutions at each iteration are all strictly feasible (they are in the interior of the domain), hence the name interior-point method. They are also called *barrier methods* since at each iteration a barrier function is used to guarantee that the obtained solution is strictly feasible.

Suppose that the following problem is to be solved:

$$\begin{aligned} & \underset{\mathbf{x}}{\text{minimize}} && f_0(\mathbf{x}) \\ & \text{subject to} && f_i(\mathbf{x}) \leq 0 \quad 1 \leq i \leq m. \end{aligned} \tag{8.14}$$

(Note that equality constraints can always be eliminated by a reparameterization of the affine feasible set.⁵) An interior-point method is easily implemented, for example, by forming the logarithmic barrier $\phi(\mathbf{x}) = -\sum_i \log(-f_i(\mathbf{x}))$, which is defined only on the feasible set and tends to $+\infty$ as any of the constraint functions goes to 0. At this point, the function $f_0(\mathbf{x}) + \frac{1}{t}\phi(\mathbf{x})$ can be easily minimized for a given t since it is an unconstrained minimization, obtaining the solution $x^*(t)$, which of course is only an approximation of the solution to the original problem x^* . Interestingly, $x^*(t)$ as a function of t describes a curve called the central path, with the property that $x^*(t) \rightarrow x^*$ as $t \rightarrow \infty$. In practice, instead of choosing a large value of t and solving the approximated unconstrained problem (which would be very difficult to minimize since its Hessian would vary rapidly near the boundary of the feasible set), it is much more convenient to start with a small value of t and successively increase it (this way, the unconstrained minimization for some t can use as a starting point the optimal solution obtained in the previous unconstrained minimization). Note that it is not necessary to compute $x^*(t)$ exactly since the central path has no significance beyond the fact that it leads to a solution of the original problem as $t \rightarrow \infty$.

It can be shown from a worst-case complexity analysis that the total number of Newton steps grows as \sqrt{m} (polynomial complexity), although in practice this number is between 10 and 50 iterations [14].

Cutting-plane and ellipsoid methods

Cutting-plane methods are based on a completely different philosophy and do not require differentiability of the objective and constraint functions [26, 13]. They start with the feasible space and iteratively divide it into two halfspaces to reject the one that is known not to contain any optimal solution. Ellipsoid methods are related to cutting-plane methods in that they sequentially reduce an ellipsoid known to contain an optimal solution [26]. In general, cutting-plane methods are less efficient for problems to which interior-point methods apply.

⁵The set $\{\mathbf{x} \mid \mathbf{Ax} = \mathbf{b}\}$ is equal to $\{\mathbf{Fz} + \mathbf{x}_0\}$, where \mathbf{x}_0 is any solution that satisfies the constraints $\mathbf{Ax}_0 = \mathbf{b}$ and \mathbf{F} is any matrix whose range is the nullspace of \mathbf{A} . Hence, instead of minimizing $f(\mathbf{x})$ subject to the equality constraints, one can equivalently minimize the function $\tilde{f}(\mathbf{z}) = f(\mathbf{Fz} + \mathbf{x}_0)$ with no equality constraints [14].

Primal-dual interior-point methods

Primal-dual interior-point methods are similar to (primal) interior-point methods in the sense that they follow the central path, but they are more sophisticated since they solve the primal and dual linear programs simultaneously by generating iterates of the primal-dual variables [13, 14]. For several basic problem classes, such as linear, quadratic, second-order cone, geometric, and semidefinite programming, customized primal-dual methods outperform the barrier method. For general nonlinear convex optimization problems, primal-dual interior-point methods are still a topic of active research, but show great promise.

8.2.5 Applications in signal processing and communications

The number of applications of convex optimization theory has exploded in the last eight years. An excellent source of examples and applications is [14] (see also [27] for an overview of recent applications).

The following is a nonexhaustive list of several illustrative recent results that make a strong use of convex optimization theory, with special emphasis on examples that have successfully managed to reformulate nonconvex problems in convex form.

Filter/beamforming design

The design of finite impulse response (FIR) filters and, similarly, of antenna array weighting (beamforming), has greatly benefited from convex optimization theory. Some examples are: [28], where the design of the antenna array weighting to satisfy some specifications in different directions is formulated as an SOCP; [29], where the design of FIR filters subject to upper and lower bounds on the discrete-frequency response magnitude is formulated in convex form using a change of variables and spectral factorization; and [30], where FIR filters are designed enforcing piecewise constant and piecewise trigonometric polynomial masks in a finite and convex manner via linear matrix inequalities.

Worst-case robust beamforming

A classical approach to design receive beamforming is Capon's method, also termed *minimum variance distortionless response* (MVDR) beamformer [31]. Capon's method obtains the beamvector \mathbf{w} as the minimization of the weighted array output power $\mathbf{w}^H \mathbf{R} \mathbf{w}$ subject to a unity-gain constraint in the desired look direction $\mathbf{w}^H \mathbf{s} = 1$, where \mathbf{R} is the covariance matrix of the received signal and \mathbf{s} is the steering vector of the desired signal. Under ideal conditions, this design maximizes the signal to interference-plus-noise ratio (SINR). However, a slight mismatch between the presumed and actual steering vectors, $\hat{\mathbf{s}}$ and \mathbf{s} , respectively, can cause a severe performance degradation. Therefore, robust approaches to adaptive beamforming are needed.

A worst-case robust approach essentially models the estimated parameters with an uncertainty region [32–35]. As formulated in [33], an effective worst-case robust design is obtained by considering that the actual steering vector is close to the estimated one $\mathbf{s} = \hat{\mathbf{s}} + \mathbf{e}$, where \mathbf{e} is an error vector with bounded norm $\|\mathbf{e}\| \leq \varepsilon$ that describes the uncertainty region (more general uncertainty regions and different formulations were considered in [32, 34]). The robust formulation can be formulated by imposing a good response along

all directions in the uncertainty region:

$$\begin{aligned} & \underset{\mathbf{w}}{\text{minimize}} \quad \mathbf{w}^H \mathbf{R} \mathbf{w} \\ & \text{subject to} \quad |\mathbf{w}^H \mathbf{c}| \geq 1 \quad \forall \mathbf{c} = \hat{\mathbf{s}} + \mathbf{e}, \quad \|\mathbf{e}\| \leq \varepsilon. \end{aligned} \quad (8.15)$$

Such a problem is a semi-infinite nonconvex quadratic problem that needs to be simplified. The single constraint $\min_{\|\mathbf{e}\| \leq \varepsilon} |\mathbf{w}^H (\hat{\mathbf{s}} + \mathbf{e})| \geq 1$ is equivalent to the original semi-infinite set of constraints and then, by applying the triangle and Cauchy-Schwarz inequalities along with $\|\mathbf{e}\| \leq \varepsilon$, the following is obtained.

$$|\mathbf{w}^H \hat{\mathbf{s}} + \mathbf{w}^H \mathbf{e}| \geq |\mathbf{w}^H \hat{\mathbf{s}}| - |\mathbf{w}^H \mathbf{e}| \geq |\mathbf{w}^H \hat{\mathbf{s}}| - \varepsilon \|\mathbf{w}\| \quad (8.16)$$

where the lower bound is indeed achieved if \mathbf{e} is proportional to \mathbf{w} with a phase such that $\mathbf{w}^H \mathbf{e}$ has opposite direction as $\mathbf{w}^H \hat{\mathbf{s}}$ [33]. Now, since \mathbf{w} admits any arbitrary rotation without affecting the problem, $\mathbf{w}^H \hat{\mathbf{s}}$ can be forced to be real and nonnegative. The problem can be finally formulated in convex form

$$\begin{aligned} & \underset{\mathbf{w}}{\text{minimize}} \quad \mathbf{w}^H \mathbf{R} \mathbf{w} \\ & \text{subject to} \quad \mathbf{w}^H \hat{\mathbf{s}} \geq 1 + \varepsilon \|\mathbf{w}\| \\ & \quad \text{Im} \{ \mathbf{w}^H \hat{\mathbf{s}} \} = 0. \end{aligned} \quad (8.17)$$

In addition, the problem can be further manipulated to be expressed as an SOCP [33].

This type of worst-case robust formulation generally leads to a diagonal loading on \mathbf{R} [32–35], where the loading factor is optimally calculated as opposed to the more traditional ad hoc techniques (the computation of the diagonal loading was explicitly characterized in [34] in a simple form). A similar problem was considered in [35] for a general-rank signal model, that is, by considering the constraint $\mathbf{w}^H \mathbf{R}_s \mathbf{w} = 1$, where \mathbf{R}_s is the covariance matrix of the desired signal with arbitrary rank (in the previous case, $\mathbf{R}_s = \mathbf{s} \mathbf{s}^H$, which is rank one).

Multiuser beamforming

Beamforming for transmission in a wireless network was addressed in [36] within a convex optimization framework for a scenario with multiantenna base stations transmitting simultaneously to several single-antenna users. The design problem can be formulated as the minimization of the total transmitted power subject to independent SINR constraints on each user:

$$\begin{aligned} & \underset{\{\mathbf{w}_k\}}{\text{minimize}} \quad \sum_{k=1}^K \mathbf{w}_k^H \mathbf{w}_k \\ & \text{subject to} \quad \frac{\mathbf{w}_k^H \mathbf{R}_{k,\beta(k)} \mathbf{w}_k}{\sum_{l \neq k} \mathbf{w}_l^H \mathbf{R}_{k,\beta(l)} \mathbf{w}_l + \sigma_k^2} \geq \gamma_k \quad 1 \leq k \leq K \end{aligned} \quad (8.18)$$

where K is the total number of users and, for the k th user, $\beta(k)$ is the corresponding base station, \mathbf{w}_k is the beamvector, γ_k is the minimum required SINR, $\mathbf{R}_{k,\beta(l)} = \mathbb{E} [\mathbf{h}_{k,\beta(l)} \mathbf{h}_{k,\beta(l)}^H]$ is the channel correlation matrix of the downlink channel $\mathbf{h}_{k,\beta(l)}$ between the base station $\beta(l)$ and the user k , and σ_k^2 is the noise power. This problem can be easily written as a quadratic optimization problem but with quadratic nonconvex constraints.

The problem can be reformulated in convex form as an SDP by defining the change of variable $\mathbf{W}_k = \mathbf{w}_k \mathbf{w}_k^H$:

$$\begin{aligned} & \underset{\{\mathbf{W}_k\}}{\text{minimize}} \quad \sum_{k=1}^K \text{Tr}(\mathbf{W}_k) \\ & \text{subject to} \quad \text{Tr}(\mathbf{R}_{k,\beta(k)} \mathbf{W}_k) - \gamma_k \sum_{l \neq k} \text{Tr}(\mathbf{R}_{k,\beta(l)} \mathbf{W}_l) \geq \gamma_k \sigma_k^2 \quad 1 \leq k \leq K \\ & \quad \mathbf{W}_k = \mathbf{W}_k^H \geq 0. \end{aligned} \quad (8.19)$$

This problem, however, is a relaxation of the original one since it lacks the rank-one constraint $\text{rank}(\mathbf{W}_k) = 1$, which would make the problem nonconvex again. Surprisingly, as was shown in [36], it turns out that the relaxed problem (8.19) always has one solution where all \mathbf{W}_k 's have rank one and, as a consequence, it is not just a relaxation but actually an equivalent reformulation of (8.18).

In addition, if each user knows its instantaneous channel, it follows that $\mathbf{R}_{k,\beta(k)} = \mathbf{h}_{k,\beta(k)} \mathbf{h}_{k,\beta(k)}^H$, then $\mathbf{w}_k^H \mathbf{R}_{k,\beta(k)} \mathbf{w}_k = |\mathbf{w}_k^H \mathbf{h}_{k,\beta(k)}|^2$, and the original problem (8.18) can be expressed as an SOCP. This is achieved, as was done in the previous application of robust beamforming, by imposing without loss of generality $\text{Im}\{\mathbf{w}_k^H \mathbf{h}_{k,\beta(k)}\} = 0$ and $\mathbf{w}_k^H \mathbf{h}_{k,\beta(k)} \geq 0$ (such that $|\mathbf{w}_k^H \mathbf{h}_{k,\beta(k)}|^2 = (\mathbf{w}_k^H \mathbf{h}_{k,\beta(k)})^2$), and by taking the square root on both sides of the inequality constraints to finally obtain a linear transformation of the second-order convex cone:

$$\mathbf{w}_k^H \mathbf{h}_{k,\beta(k)} \geq \sqrt{\gamma_k \sum_{l \neq k} \mathbf{w}_l^H \mathbf{R}_{k,\beta(l)} \mathbf{w}_l + \gamma_k \sigma_k^2}. \quad (8.20)$$

Duality between channel capacity and rate distortion

As Shannon himself pointed out in 1959 [37], the two fundamental limits of data transmission and data compression are “somewhat dual”. However, such a relation between the two problems is not a “duality by mapping” (in the sense that both problems cannot be related by simple mappings of variables, constant parameters, and mathematical operations). As was unveiled in [38], using convex optimization tools, it turns out that the Lagrange dual formulation of the two problems exhibit a precise “duality by mapping” in the form of two geometric problems, resolving the apparent asymmetry between the two original problems. This is an example of how convex optimization can be used to perform an analytical study of a problem.

Network optimization problems

In wireless networks, the optimal routing of data depends on the link capacities that, in turn, are determined by the allocation of communications resources (such as powers and bandwidths) to the links. Traditionally, the link capacities are assumed fixed and the routing problem is often formulated as a convex multicommodity network flow problem. However, the optimal performance of the network can only be achieved by simultaneous optimization of routing and resource allocation. In [39], such a problem was formulated as a convex optimization problem over the network flow variables and the communications variables. In addition, the structure of the problem was exploited to obtain efficient algorithms based on a decomposition approach of the dual problem.

Many existing multihop networks are based on the TCP protocol with some mechanism of congestion control such as Reno or Vegas (which essentially control the transmission rate of each source). Indeed, not only TCP is the predominant protocol in the Internet but it is also being extended to wireless networks. It was recently shown in [40] that this type of congestion control can be interpreted as a distributed primal-dual algorithm carried out by sources and links over the network to solve a global network utility maximization problem (different protocols correspond to different objective functions in the global problem). For example, it turns out that the congestion avoidance mechanism of Vegas can be interpreted as an approximate gradient projection algorithm to solve the dual problem. In [41], such an interpretation was extended to ad hoc wireless networks with flexible link capacities as a function of the allocated powers and interference, obtaining joint congestion control and power control iterative algorithms.

Iterative waterfilling

The iterative waterfilling algorithm for the multiple-access channel [42] is an example of a simple resolution of a convex problem based on the KKT conditions. Just to give a flavor of the solution, it turns out that the following convex problem that obtains the transmit covariance matrices $\{\mathbf{Q}_k\}$ that achieve the sum-capacity for the K -user multiple-access channel with channels $\{\mathbf{H}_k\}$ and noise covariance matrix \mathbf{R}_n :

$$\begin{aligned} & \underset{\{\mathbf{Q}_k\}}{\text{maximize}} \quad \log \det \left(\sum_{k=1}^K \mathbf{H}_k \mathbf{Q}_k \mathbf{H}_k^H + \mathbf{R}_n \right) \\ & \text{subject to} \quad \text{Tr}(\mathbf{Q}_k) \leq P_k \quad 1 \leq k \leq K \\ & \quad \mathbf{Q}_k \geq \mathbf{0} \end{aligned} \tag{8.21}$$

can be solved very efficiently in practice by solving a sequence of simpler problems. In particular, each user k should solve in a sequential order the convex problem

$$\begin{aligned} & \underset{\mathbf{Q}_k}{\text{maximize}} \quad \log \det (\mathbf{H}_k \mathbf{Q}_k \mathbf{H}_k^H + \mathbf{R}_k) \\ & \text{subject to} \quad \text{Tr}(\mathbf{Q}_k) \leq P_k \\ & \quad \mathbf{Q}_k \geq \mathbf{0} \end{aligned} \tag{8.22}$$

where $\mathbf{R}_k = \sum_{l \neq k} \mathbf{H}_l \mathbf{Q}_l \mathbf{H}_l^H + \mathbf{R}_n$. This problem has a well-known solution [10, 3] given by a \mathbf{Q}_k with eigenvectors equal to the those of $\mathbf{R}_{H,k} = \mathbf{H}_k^H \mathbf{R}_k^{-1} \mathbf{H}_k$ and eigenvalues given by a waterfilling solution (easily derived from the KKT conditions) of the form $\lambda_i(\mathbf{Q}_k) = (\mu_k - \lambda_i^{-1}(\mathbf{R}_{H,k}))^+$.

This sequential updating of the \mathbf{Q}_k 's is in fact a particular instance of the nonlinear Gauss-Seidel algorithm [43].

Linear MIMO transceiver design

The design of linear transceivers for point-to-point MIMO systems was formulated in convex form in [15] and [16] (see also [17]) for a wide family of measures of the system quality, after a change of variable based on majorization theory [44]. This problem is treated in detail in §8.4.

The design of linear transceivers in the multiuser case is even more difficult and a general result is still missing. However, an interesting convex formulation as an SDP was

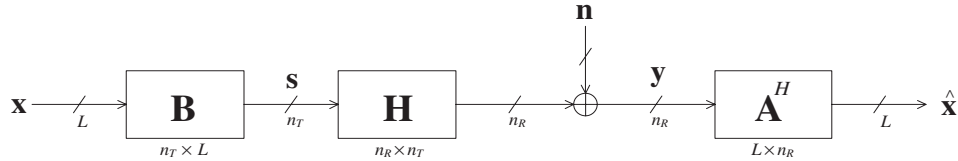


Figure 8.1 Scheme of a general MIMO communication system with a linear transceiver.

obtained in [45] (see also [27]) for the particular case of minimizing the average of the mean square errors (MSEs) of all substreams and users.

8.3 System Model and Preliminaries

8.3.1 Signal model

The baseband signal model corresponding to a transmission through a general MIMO communication channel with n_T transmit and n_R receive dimensions is

$$\mathbf{y} = \mathbf{H}\mathbf{s} + \mathbf{n} \quad (8.23)$$

where $\mathbf{s} \in \mathbb{C}^{n_T \times 1}$ is the transmitted vector, $\mathbf{H} \in \mathbb{C}^{n_R \times n_T}$ is the channel matrix, $\mathbf{y} \in \mathbb{C}^{n_R \times 1}$ is the received vector, and $\mathbf{n} \in \mathbb{C}^{n_R \times 1}$ is a zero-mean circularly symmetric complex Gaussian interference-plus-noise vector with arbitrary covariance matrix \mathbf{R}_n .

The focus is on systems employing linear transceivers (composed of a linear precoder at the transmitter and a linear equalizer at the receiver), as opposed to nonlinear ones, such as those including a maximum likelihood (ML) receiver, for reasons of practical complexity (decision-feedback receivers are an interesting alternative in terms of performance/complexity).

The transmitted vector can be written as (see Figure 8.1)

$$\mathbf{s} = \mathbf{B}\mathbf{x} \quad (8.24)$$

where $\mathbf{B} \in \mathbb{C}^{n_T \times L}$ is the transmit matrix (linear precoder) and $\mathbf{x} \in \mathbb{C}^{L \times 1}$ is the data vector that contains the L symbols to be transmitted (zero-mean,⁶ normalized and uncorrelated, that is, $\mathbb{E}[\mathbf{x}\mathbf{x}^H] = \mathbf{I}$) drawn from a set of constellations. For the sake of notation, it is assumed that $L \leq \min(n_R, n_T)$. The total average transmitted power (in units of energy per transmission) is

$$P_T = \mathbb{E}[\|\mathbf{s}\|^2] = \text{Tr}(\mathbf{B}\mathbf{B}^H). \quad (8.25)$$

Similarly, the estimated data vector at the receiver is (see Figure 8.1)

$$\hat{\mathbf{x}} = \mathbf{A}^H\mathbf{y} \quad (8.26)$$

where $\mathbf{A}^H \in \mathbb{C}^{L \times n_R}$ is the receive matrix (linear equalizer).

⁶If a constellation does not have zero-mean, the receiver can always remove the mean and then proceed as if the mean was zero, resulting in a loss of transmitted power. Indeed, the mean of the signal does not carry any information and can always be set to zero, saving power at the transmitter.

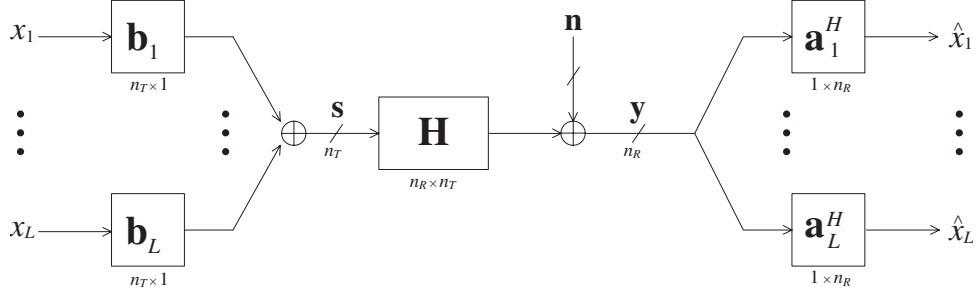


Figure 8.2 Interpretation of a linear MIMO transceiver as a multiple beamforming scheme.

It is interesting to observe that the i th column of \mathbf{B} and \mathbf{A} , \mathbf{b}_i and \mathbf{a}_i , respectively, can be interpreted as the transmit and receive beamvectors associated to the i th transmitted symbol x_i :

$$\hat{x}_i = \mathbf{a}_i^H (\mathbf{H}\mathbf{b}_i x_i + \mathbf{n}_i) \quad (8.27)$$

where $\mathbf{n}_i = \sum_{j \neq i} \mathbf{H}\mathbf{b}_j x_j + \mathbf{n}$ is the equivalent noise seen by the i th substream, with covariance matrix $\mathbf{R}_{n_i} = \sum_{j \neq i} \mathbf{H}\mathbf{b}_j \mathbf{b}_j^H \mathbf{H}^H + \mathbf{R}_n$. Therefore, the linear MIMO transceiver scheme (see Figure 8.1) can be equivalently interpreted as a multiple beamforming transmission (see Figure 8.2).

The previously introduced complex-valued signal model could have been similarly written with an augmented real-valued notation, simply by augmenting the n -dimensional complex vectors to $2n$ -dimensional real vectors (stacking the real and imaginary parts). However, the use of a complex-valued notation is always preferred since it models the system in a simpler and more compact way. Interestingly, it turns out that complex linear filtering is equivalent to (augmented) real linear filtering if the random vectors involved are proper [46] or circular [47]; otherwise, complex linear filtering is suboptimal and it is necessary to consider either real linear filtering or widely complex linear filtering [47, 48]. Fortunately, many of the commonly employed constellations, such as the family of QAM constellations, are proper [49], and this allows the use of a nice complex notation (although some other constellations, such as BPSK and GMSK, are improper and a complex notation is not adequate anymore).

As a final comment, it is worth noting that multicarrier systems, although they can always be modeled as in (8.23) by properly defining the channel matrix \mathbf{H} as a block-diagonal matrix containing in each diagonal block the channel at each carrier, may be more conveniently modeled as a set of parallel and noninterfering MIMO channels (c.f. §8.4.4).

8.3.2 Measures of quality

The quality of the i th established substream or link in (8.27) can be conveniently measured, among others, in terms of MSE, SINR, or bit error rate (BER), defined, respectively, as

$$\text{MSE}_i \triangleq \mathbb{E}[|\hat{x}_i - x_i|^2] = |\mathbf{a}_i^H \mathbf{H}\mathbf{b}_i - 1|^2 + \mathbf{a}_i^H \mathbf{R}_{n_i} \mathbf{a}_i \quad (8.28)$$

$$\text{SINR}_i \triangleq \frac{\text{desired component}}{\text{undesired component}} = \frac{|\mathbf{a}_i^H \mathbf{H} \mathbf{b}_i|^2}{\mathbf{a}_i^H \mathbf{R}_{n_i} \mathbf{a}_i} \quad (8.29)$$

$$\text{BER}_i \triangleq \frac{\# \text{ bits in error}}{\# \text{ transmitted bits}} \approx \tilde{g}_i(\text{SINR}_i) \quad (8.30)$$

where \tilde{g}_i is a function that relates the BER to the SINR at the i th substream. For most types of modulations, the BER can indeed be analytically expressed as a function of the SINR when the interference-plus-noise term follows a Gaussian distribution [50–52]. Otherwise, it is an approximation, although when the number of interfering signals is sufficiently large, the central limit theory can be invoked to show that the distribution converges almost surely to a Gaussian distribution (c.f. [53]) (see [54] for a more detailed discussion). For example, for square M -ary QAM constellations, the BER is [50, 52]

$$\text{BER}(\text{SINR}) \approx \frac{4}{\log_2 M} \left(1 - \frac{1}{\sqrt{M}} \right) \mathcal{Q} \left(\sqrt{\frac{3}{M-1}} \text{SINR} \right) \quad (8.31)$$

where \mathcal{Q} is defined as $\mathcal{Q}(x) \triangleq \frac{1}{\sqrt{2\pi}} \int_x^\infty e^{-\lambda^2/2} d\lambda$ [51].⁷ It is sometimes convenient to use the Chernoff upper bound of the tail of the Gaussian distribution function $\mathcal{Q}(x) \leq \frac{1}{2}e^{-x^2/2}$ [51] to approximate the symbol error probability (which becomes a reasonable approximation for high values of the SINR).

It is worth pointing out that expressing the BER as in (8.30) implicitly assumes that the different links are independently detected after the joint linear processing with the receive matrix \mathbf{A} . This reduces the complexity drastically compared to a joint ML detection and is indeed the main advantage of using the receive matrix \mathbf{A} .

Any properly designed system should attempt to somehow minimize the MSEs, maximize the SINRs, or minimize the BERs, as is mathematically formulated in §8.4.1.

8.3.3 Optimum linear receiver

The optimum linear receiver can be easily designed independently of the particular criterion chosen to design the system (c.f. §8.4.1), provided that the system quality improves with smaller MSEs, higher SINRs, and smaller BERs (for more details, the reader is referred to [15, 17]).

It is notationally convenient to define the MSE matrix as

$$\begin{aligned} \mathbf{E} &\triangleq \mathbb{E}[(\hat{\mathbf{x}} - \mathbf{x})(\hat{\mathbf{x}} - \mathbf{x})^H] \\ &= (\mathbf{A}^H \mathbf{H} \mathbf{B} - \mathbf{I}) (\mathbf{B}^H \mathbf{H}^H \mathbf{A} - \mathbf{I}) + \mathbf{A}^H \mathbf{R}_n \mathbf{A} \end{aligned} \quad (8.32)$$

from which the MSE of the i th link is obtained as the i th diagonal element of \mathbf{E} , that is, $\text{MSE}_i = [\mathbf{E}]_{ii}$.

The receive matrix \mathbf{A} can be easily optimized for a given fixed transmit matrix \mathbf{B} , since the minimization of the MSE of a substream with respect to \mathbf{A} does not incur any penalty

⁷The \mathcal{Q} -function and the commonly used complementary error function “erfc” are related as $\text{erfc}(x) = 2\mathcal{Q}(\sqrt{2}x)$ [51].

on the other substreams (see, for example, (8.27) where \mathbf{a}_i only affects \hat{x}_i). In other words, there is no trade-off among the MSEs and the problem decouples. Therefore, it is possible to minimize simultaneously all MSEs and this is precisely how the well-known linear MMSE receiver, also termed *Wiener filter*, is obtained [55] (see also [15, 16]). If the additional ZF constraint $\mathbf{A}^H \mathbf{H} \mathbf{B} = \mathbf{I}$ is imposed to avoid crosstalk among the substreams (which happens with the MMSE receiver), then the well-known linear ZF receiver is obtained. Interestingly, the MMSE and ZF linear receivers are also optimum (within the class of linear receivers) in the sense that they maximize simultaneously all SINRs and, consequently, minimize simultaneously all BERs under the Gaussian approximation (c.f. [15, 17]).

The MMSE and ZF linear receivers can be compactly written as

$$\mathbf{A} = \mathbf{R}_n^{-1} \mathbf{H} \mathbf{B} \left(\nu \mathbf{I} + \mathbf{B}^H \mathbf{H}^H \mathbf{R}_n^{-1} \mathbf{H} \mathbf{B} \right)^{-1} \quad (8.33)$$

where ν is a parameter defined as $\nu \triangleq \begin{cases} 1 & \text{for the MMSE receiver} \\ 0 & \text{for the ZF receiver} \end{cases}$. The MSE matrix (8.32) reduces then to the following concentrated MSE matrix

$$\mathbf{E} = \left(\nu \mathbf{I} + \mathbf{B}^H \mathbf{R}_H \mathbf{B} \right)^{-1} \quad (8.34)$$

where $\mathbf{R}_H \triangleq \mathbf{H}^H \mathbf{R}_n^{-1} \mathbf{H}$ is the squared whitened channel matrix.

Relation among different measures of quality

It is convenient now to relate the different measures of quality, namely, MSE, SINR, and BER, to the concentrated MSE matrix in (8.34). From the definition of MSE matrix, the individual MSEs are given by the diagonal elements:

$$\text{MSE}_i = \left[\left(\nu \mathbf{I} + \mathbf{B}^H \mathbf{R}_H \mathbf{B} \right)^{-1} \right]_{ii}. \quad (8.35)$$

It turns out that the SINRs and the MSEs are trivially related when using the MMSE or ZF linear receivers as [15–17]

$$\text{SINR}_i = \frac{1}{\text{MSE}_i} - \nu. \quad (8.36)$$

Finally, the BERs can also be written as a function of the MSEs:

$$\text{BER}_i = g_i(\text{MSE}_i) \triangleq \tilde{g}_i \left(\text{SINR}_i = \text{MSE}_i^{-1} - \nu \right) \quad (8.37)$$

where \tilde{g}_i was defined in (8.30).

8.4 Beamforming Design for MIMO Channels: A Convex Optimization Approach

The design of transmit-receive beamforming or linear MIMO transceivers has been studied since the 1970s where cable systems were the main application [56, 57]. The traditional

results existing in the literature have dealt with the problem from a narrow perspective (due to the complexity of the problem); the basic approach has been to choose a measure of quality of the system sufficiently simple such that the problem can be analytically solved. Some examples include the minimization of the (weighted) sum of the MSEs of the substreams or, equivalently, the trace of the MSE matrix [56–58, 6, 59]; the minimization of the determinant of the MSE matrix [60]; and the maximization of the SINR with a ZF constraint [6]. For these criteria, the original complicated design problem is greatly simplified because the channel turns out to be diagonalized by the optimal transmit-receive processing and the transmission is effectively performed on a diagonal or parallel fashion. The diagonal transmission allows a *scalarization* of the problem (meaning that all matrix equations are substituted with scalar ones) with the consequent simplification.

Recent results have considered more elaborated and meaningful measures of quality. In [61], the minimization of the BER (and also of the Chernoff upper bound) averaged over the channel substreams was treated in detail when a diagonal structure is imposed. The minimum BER design without the diagonal structure constraint has been independently obtained in [62] and [15], resulting in an optimal nondiagonal structure. This result, however, only holds when the constellations used in all channel substreams are equal. The general case of different constellations was treated and optimally solved in [54] (different constellations are typically obtained when some kind of bit allocation strategy is used such as the gap-approximation method [63, Part II], which chooses the constellations as a function of the channel realization). In [15], a general unifying framework was developed that embraces a wide range of different design criteria; in particular, the optimal design was obtained for the family of Schur-concave and Schur-convex cost functions [44].

Clearly, the problem faced when designing a MIMO system not only lies on the design itself but also on the choice of the appropriate measure of the system quality (which may depend on the application at hand and/or on the type of coding used on top of the uncoded system). In fact, to fully characterize such a problem, a multiobjective optimization approach should be taken to characterize the Pareto-optimal set.⁸ Following the results in [16, 17], this section deals first with the optimal design subject to a set of independent QoS constraints for each of the channel substreams. This allows the characterization of the Pareto-optimal set and the feasible region (see the numerical example in Figure 8.7). However, since it is generally more convenient to use a single measure of the system quality to simplify the characterization, the optimal design subject to a global QoS constraint that measures the system quality is also considered on the basis of [15, 17].

8.4.1 Problem formulation

The problems addressed in this section are the minimization of the transmitted power $\text{Tr}(\mathbf{B}\mathbf{B}^H)$ subject to either independent QoS constraints or a global QoS constraint. The problems are originally formulated in terms of the variables \mathbf{A} and \mathbf{B} . However, as was obtained in §8.3.3, the optimal receive matrix \mathbf{A} is always given by (8.33), and the problems can then be rewritten as optimization problems with respect to only the transmit matrix \mathbf{B} .

⁸A Pareto-optimal solution is an optimal solution to a multiobjective optimization problem; it is defined as any solution that cannot be improved with respect to any component without worsening the others [8].

Independent QoS constraints

Independent QoS constraints can always be expressed in terms of MSE constraints $\text{MSE}_i \leq \rho_i$, where ρ_i denotes the maximum MSE value for the i th substream (recall that SINR and BER constraints can always be rewritten as MSE constraints, c.f. §8.3.3). The problem can then be formulated as

$$\begin{aligned} & \underset{\mathbf{A}, \mathbf{B}}{\text{minimize}} \quad \text{Tr}(\mathbf{B}\mathbf{B}^H) \\ & \text{subject to} \quad \text{MSE}_i \leq \rho_i \quad 1 \leq i \leq L. \end{aligned} \tag{8.38}$$

This problem is optimally solved in §8.4.2 and is then used in a numerical example in §8.4.5 to obtain the achievable region for a given power budget P_0 (a given set of constraints $\{\rho_i\}$ is achievable if and only if the minimum required power is no greater than P_0).

Global QoS constraint

In this case, it is assumed that the performance of the system is measured by a global cost function f of the MSEs (as before, cost functions of the SINRs and BERs can always be rewritten in terms of MSEs, c.f. §8.3.3). The problem can be formulated as

$$\begin{aligned} & \underset{\mathbf{A}, \mathbf{B}}{\text{minimize}} \quad \text{Tr}(\mathbf{B}\mathbf{B}^H) \\ & \text{subject to} \quad f(\{\text{MSE}_i\}) \leq \alpha_0 \end{aligned} \tag{8.39}$$

where α_0 is the required level of the global performance as measured by the cost function f . In principle, any function can be used to measure the system quality as long as it is increasing in each argument (this is a mild and completely reasonable assumption: if the quality of one of the substream improves while the rest remain unchanged, any reasonable function should properly reflect this difference).

It is important to point out that this problem can be similarly formulated as the minimization of the cost function subject to a given power budget P_0 . Both formulations are essentially equivalent since they describe the same trade-off curve of performance versus power. In fact, numerically speaking, each problem can be solved by iteratively solving the other combined with the bisection method [14, Alg. 4.1].

Illustrative example

As a motivation to the need of solving problems (8.38) and (8.39) optimally, the following example shows that a simple design imposing a diagonal transmission is not necessarily good.

Consider a system with the following characteristics: a diagonal 2×2 MIMO channel $\mathbf{H} = \text{diag}(\{1, \epsilon\})$, a white normalized noise $\mathbf{R}_n = \mathbf{I}$, two established substreams $L = 2$ with an MMSE receiver (see (8.33) with $v = 1$), with a power budget P_0 , and a design based on maximizing the minimum of the SINRs of the substreams $\text{SINR}_0 = \min\{\text{SINR}_1, \text{SINR}_2\}$.

A naive design imposing a diagonal transmission is suboptimal in this case (c.f. Theorem 8.4.3) and is given by

$$\mathbf{B} = \begin{bmatrix} \sqrt{p_1} & 0 \\ 0 & \sqrt{p_2} \end{bmatrix}, \quad \mathbf{A} = \begin{bmatrix} \sqrt{p_1}/(1+p_1) & 0 \\ 0 & \epsilon\sqrt{p_2}/(1+\epsilon^2 p_2) \end{bmatrix} \tag{8.40}$$

with SINRs given by $\text{SINR}_1 = p_1$ and $\text{SINR}_2 = \epsilon^2 p_2$. The optimal power allocation is given by $p_1 = P_0 \epsilon^2 / (1 + \epsilon^2)$ and $p_2 = P_0 / (1 + \epsilon^2)$, and then both substreams have the same SINR given by $\text{SINR}_0 = P_0 \epsilon^2 / (1 + \epsilon^2)$.

An optimal design yields a nondiagonal transmission (c.f. Theorem 8.4.3) given by

$$\mathbf{B} = \begin{bmatrix} \sqrt{p_1} & 0 \\ 0 & \sqrt{p_2} \end{bmatrix} \bar{\mathbf{H}}_2, \quad \mathbf{A} = \begin{bmatrix} \sqrt{p_1} / (1 + p_1) & 0 \\ 0 & \epsilon \sqrt{p_2} / (1 + \epsilon^2 p_2) \end{bmatrix} \bar{\mathbf{H}}_2 \quad (8.41)$$

with equal SINRs given by $\text{SINR}_0 = \text{MSE}_0^{-1} - 1$ (from (8.36)), where $\bar{\mathbf{H}}_2$ is a 2×2 unitary Hadamard matrix (c.f. Theorem 8.4.3) and $\text{MSE}_0 = \frac{1}{2} (1/(1+p_1) + 1/(1+\epsilon^2 p_2))$ (from (8.61)). The optimal power allocation in this case is $p_1 = (\mu - 1)^+$ and $p_2 = (\mu \epsilon^{-1} - \epsilon^{-2})^+$ (from (8.63)), which simplifies to $p_1 = P_0$ and $p_2 = 0$ for sufficiently small ϵ ($\epsilon < 1/(1+P_0)$) with a final SINR given by $\text{SINR}_0 = P_0 / (2 + P_0)$.

Both solutions can be easily compared for small ϵ : the performance of the suboptimal diagonal transmission goes to zero with ϵ , whereas the optimal transmission is robust and less sensitive.

8.4.2 Optimal design with independent QoS constraints

Using the optimal receive matrix (8.33), problem (8.38) can be rewritten as

$$\begin{aligned} & \underset{\mathbf{B}}{\text{minimize}} \quad \text{Tr}(\mathbf{B}\mathbf{B}^H) \\ & \text{subject to} \quad \mathbf{d}((\nu\mathbf{I} + \mathbf{B}^H \mathbf{R}_H \mathbf{B})^{-1}) \leq \boldsymbol{\rho} \end{aligned} \quad (8.42)$$

where the elements of $\boldsymbol{\rho}$ are assumed in decreasing order without loss of generality (by properly relabeling the elements).

It is now possible to write a simpler and equivalent problem by using a fundamental result of majorization theory [44] that says that a matrix with given eigenvalues λ and diagonal elements less than \mathbf{d} can be constructed if and only if λ weakly majorizes \mathbf{d} , that is, $\lambda \succ^w \mathbf{d}$ [44, 9.B.1, 9.B.2, & 5.A.9.a].⁹ Defining $\tilde{\mathbf{B}} = \mathbf{B}\mathbf{Q}^H$, where \mathbf{Q}^H is a unitary matrix that diagonalizes $\mathbf{B}^H \mathbf{R}_H \mathbf{B}$ (with the resulting diagonal elements in increasing order), the equivalent problem is

$$\begin{aligned} & \underset{\tilde{\mathbf{B}}}{\text{minimize}} \quad \text{Tr}(\tilde{\mathbf{B}}\tilde{\mathbf{B}}^H) \\ & \text{subject to} \quad \tilde{\mathbf{B}}^H \mathbf{R}_H \tilde{\mathbf{B}} \quad \text{diagonal (increasing diag. elements)} \\ & \quad \lambda((\nu\mathbf{I} + \tilde{\mathbf{B}}^H \mathbf{R}_H \tilde{\mathbf{B}})^{-1}) \succ^w \boldsymbol{\rho}. \end{aligned} \quad (8.43)$$

Conversely, given $\tilde{\mathbf{B}}$, it is not difficult to compute a unitary matrix \mathbf{Q} and form $\mathbf{B} = \tilde{\mathbf{B}}\mathbf{Q}$ such that $\mathbf{d}((\nu\mathbf{I} + \mathbf{B}^H \mathbf{R}_H \mathbf{B})^{-1}) \leq \boldsymbol{\rho}$ (with equality at an optimal solution) with the practical algorithm given in [64, IV-A].

Since $\tilde{\mathbf{B}}^H \mathbf{R}_H \tilde{\mathbf{B}}$ is diagonal with diagonal elements in increasing order, it can be shown [15, Lem. 12] [17, Lem. 5.11] that $\tilde{\mathbf{B}}$ can be assumed without loss of optimality of the

⁹The weakly majorization relation $\mathbf{y} \succ^w \mathbf{x}$ is defined as $\sum_{j=i}^n y_j \leq \sum_{j=i}^n x_j$ for $1 \leq i \leq n$, where the elements of \mathbf{y} and \mathbf{x} are assumed in decreasing order [44].

form $\tilde{\mathbf{B}} = \mathbf{U}_{H,1} \Sigma_B$, where $\mathbf{U}_{H,1} \in \mathbb{C}^{nT \times L}$ is a (semi-)unitary matrix that has as columns the eigenvectors of \mathbf{R}_H corresponding to the L largest eigenvalues $\{\lambda_{H,i}\}$ in increasing order and $\Sigma_B = \text{diag}(\{\sqrt{p_i}\}) \in \mathbb{R}^{L \times L}$ is a diagonal matrix with a power allocation $\{p_i\}$ over the channel eigenmodes (note the need for the additional constraints $p_i \geq 0$).

Using the form of the optimal $\tilde{\mathbf{B}}$ and writing the weakly majorization relation explicitly, the problem finally becomes

$$\begin{aligned} & \underset{\mathbf{p}}{\text{minimize}} && \sum_{i=1}^L p_i \\ & \text{subject to} && \sum_{j=i}^L \frac{1}{v + p_j \lambda_{H,j}} \leq \sum_{j=i}^L \rho_j \quad 1 \leq i \leq L \\ & && p_i \geq 0 \end{aligned} \quad (8.44)$$

which is a very simple convex problem. In principle, problem (8.44) is a relaxation since it lacks the constraints $p_i \lambda_{H,i} \leq p_{i+1} \lambda_{H,i+1}$ (to guarantee that the diagonal elements of $\tilde{\mathbf{B}}^H \mathbf{R}_H \tilde{\mathbf{B}}$ are in increasing order). However, it is not difficult to see that any optimal point must necessarily satisfy them and, hence, problem (8.44) is indeed equivalent to the original one (suppose $p_i \lambda_{H,i} > p_{i+1} \lambda_{H,i+1}$ for some i , then the terms $p_i \lambda_{H,i}$ and $p_{i+1} \lambda_{H,i+1}$ could be swapped to satisfy the ordering constraint without affecting the problem (8.44), but this cannot be at an optimal point because the objective value could be further reduced by using the optimal increasing ordering of the $\lambda_{H,i}$'s). The following theorem summarizes the whole simplification.

Theorem 8.4.1 *The original complicated nonconvex problem (8.42), with the elements of ρ in decreasing order w.l.o.g., is equivalent to the simple convex problem (8.44), where the $\lambda_{H,i}$'s are the L largest eigenvalues of \mathbf{R}_H in increasing order. The mapping from (8.44) to (8.42) is given by*

$$\mathbf{B} = \mathbf{U}_{H,1} \text{diag}(\{\sqrt{p_i}\}) \mathbf{Q}, \quad (8.45)$$

where $\mathbf{U}_{H,1}$ diagonalizes the channel matrix, $\{p_i\}$ is the power allocation over the channel eigenmodes, and \mathbf{Q} is a “rotation”, chosen such that $\mathbf{d}((v\mathbf{I} + \mathbf{B}^H \mathbf{R}_H \mathbf{B})^{-1}) = \rho$ (e.g., with the algorithm in [64, IV-A]), that spreads the transmitted symbols over the channel eigenmodes (see Figure 8.3).

Furthermore, the convex problem (8.44) can be easily solved in practice with a simple multilevel waterfilling algorithm as given in [16, 17].

The global transmit-receive process $\hat{\mathbf{x}} = \mathbf{A}^H (\mathbf{H} \mathbf{B} \mathbf{x} + \mathbf{n})$ using the optimal transmission structure of Theorem 8.4.1 can be written as

$$\hat{\mathbf{x}} = \mathbf{Q}^H \left(v\mathbf{I} + \Sigma_B^H \mathbf{D}_{H,1} \Sigma_B \right)^{-1} \Sigma_B^H \mathbf{D}_{H,1}^{1/2} \left(\mathbf{D}_{H,1}^{1/2} \Sigma_B \mathbf{Q} \mathbf{x} + \mathbf{w} \right) \quad (8.46)$$

or, equivalently, as

$$\hat{x}_i^Q = \alpha_i \left(\sqrt{p_i \lambda_{H,i}} x_i^Q + w_i \right) \quad 1 \leq i \leq L \quad (8.47)$$

where \mathbf{w} is an equivalent normalized white noise ($\mathbb{E}[\mathbf{w} \mathbf{w}^H] = \mathbf{I}$), $\mathbf{D}_{H,1} = \mathbf{U}_{H,1}^H \mathbf{R}_H \mathbf{U}_{H,1}$, $\mathbf{x}^Q = \mathbf{Q} \mathbf{x}$, and $\alpha_i = \sqrt{p_i \lambda_{H,i}} / (v + p_i \lambda_{H,i})$ (see Figure 8.3 with $\lambda_i \triangleq \lambda_{H,i}$).

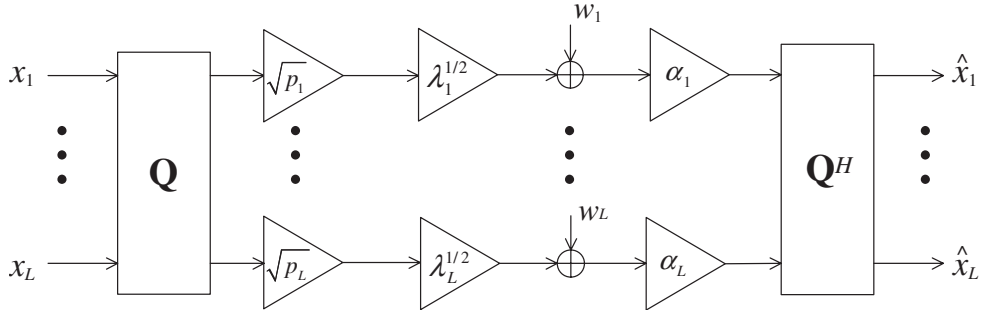


Figure 8.3 Decomposition of the optimal transmission through a MIMO channel.

8.4.3 Optimal design with a global QoS constraint

Using the optimal receive matrix (8.33), problem (8.39) reduces to

$$\begin{aligned} & \underset{\mathbf{B}}{\text{minimize}} \quad \text{Tr}(\mathbf{B}\mathbf{B}^H) \\ & \text{subject to} \quad f\left(\mathbf{d}\left(v\mathbf{I} + \mathbf{B}^H \mathbf{R}_H \mathbf{B}\right)^{-1}\right) \leq \alpha_0. \end{aligned} \quad (8.48)$$

This problem can be easily simplified by using the previous result in Theorem 8.4.1. First, rewrite (8.48) as

$$\begin{aligned} & \underset{\mathbf{B}, \rho}{\text{minimize}} \quad \text{Tr}(\mathbf{B}\mathbf{B}^H) \\ & \text{subject to} \quad \mathbf{d}\left(v\mathbf{I} + \mathbf{B}^H \mathbf{R}_H \mathbf{B}\right)^{-1} \leq \rho \\ & \quad f(\rho) \leq \alpha_0 \end{aligned} \quad (8.49)$$

which can always be done since f is increasing in each argument. Then, use Theorem 8.4.1 to reformulate the problem as

$$\begin{aligned} & \underset{\mathbf{p}, \rho}{\text{minimize}} \quad \sum_{i=1}^L p_i \\ & \text{subject to} \quad \sum_{j=i}^L \frac{1}{v+p_j \lambda_{H,j}} \leq \sum_{j=i}^L \rho_{[j]} \quad 1 \leq i \leq L \\ & \quad p_i \geq 0 \\ & \quad f(\rho_1, \dots, \rho_L) \leq \alpha_0 \end{aligned} \quad (8.50)$$

where the ordering constraints $p_i \lambda_{H,i} \leq p_{i+1} \lambda_{H,i+1}$ are not necessary for the same reasons as in (8.44) and $\rho_{[i]}$ denotes the ρ_i 's in decreasing order, which can be explicitly written as [14]:

$$\sum_{j=i}^L \rho_{[j]} = \min \left\{ \rho_{j_1} + \dots + \rho_{j_{L-i+1}} \mid 1 \leq j_1 < \dots < j_{L-i+1} \leq L \right\}. \quad (8.51)$$

This is clearly a concave function since it is the pointwise minimum of concave (affine) functions.

To avoid the constraint (8.51), it is convenient to assume that the cost function f is minimum when the arguments are sorted in decreasing order.¹⁰ The problem can then be rewritten as

$$\begin{aligned} & \underset{\mathbf{p}, \boldsymbol{\rho}}{\text{minimize}} \quad \sum_{i=1}^L p_i \\ & \text{subject to} \quad \sum_{j=i}^L \frac{1}{v + p_j \lambda_{H,j}} \leq \sum_{j=i}^L \rho_j \quad 1 \leq i \leq L \\ & \quad p_i \geq 0 \\ & \quad \rho_i \geq \rho_{i+1} \\ & \quad f(\rho_1, \dots, \rho_L) \leq \alpha_0. \end{aligned} \quad (8.52)$$

If, in addition, the cost function f is convex, then the constraints $\rho_i \geq \rho_{i+1}$ are not necessary (since any optimal solution cannot have $\rho_i < \rho_{i+1}$ because the problem would have a lower objective value by using instead $\tilde{\rho}_i = \tilde{\rho}_{i+1} = (\rho_i + \rho_{i+1})/2$ [54]) and the problem can be finally written in convex form as

$$\begin{aligned} & \underset{\mathbf{p}, \boldsymbol{\rho}}{\text{minimize}} \quad \sum_{i=1}^L p_i \\ & \text{subject to} \quad \sum_{j=i}^L \frac{1}{v + p_j \lambda_{H,j}} \leq \sum_{j=i}^L \rho_j \quad 1 \leq i \leq L \\ & \quad p_i \geq 0 \\ & \quad f(\rho_1, \dots, \rho_L) \leq \alpha_0. \end{aligned} \quad (8.53)$$

The following theorem summarizes the simplification.

Theorem 8.4.2 *The original complicated nonconvex problem (8.48), with a cost function f increasing in each variable, is equivalent to the simple problem (8.50), where the $\lambda_{H,i}$'s are the L largest eigenvalues of \mathbf{R}_H in increasing order. In addition, if f is convex and is minimum when its arguments are sorted in decreasing order, the problem further simplifies to the convex problem (8.53). The mapping from (8.53) to (8.48) is given by*

$$\mathbf{B} = \mathbf{U}_{H,1} \text{diag}(\{\sqrt{p_i}\}) \mathbf{Q},$$

where $\mathbf{U}_{H,1}$ diagonalizes the channel matrix, $\{p_i\}$ is the power allocation over the channel eigenmodes, and \mathbf{Q} is a “rotation”, chosen such that $\mathbf{d}((v\mathbf{I} + \mathbf{B}^H \mathbf{R}_H \mathbf{B})^{-1}) = \boldsymbol{\rho}$ (e.g., with the algorithm in [64, IV-A]), that spreads the transmitted symbols over the channel eigenmodes (see Figure 8.3).

Interestingly, Theorem 8.4.2 can be further simplified for the family of Schur-concave and Schur-convex functions as shown next. First, rewrite the MSE constraints of (8.49) (knowing that they are satisfied with equality at an optimal point) as

$$\boldsymbol{\rho} = \mathbf{d}(\mathbf{Q}^H (v\mathbf{I} + \tilde{\mathbf{B}}^H \mathbf{R}_H \tilde{\mathbf{B}})^{-1} \mathbf{Q}). \quad (8.54)$$

Now it suffices to use the definition of Schur-concavity/convexity to obtain the desired result. In particular, if f is Schur-concave, it follows from the definition of Schur-concavity [44] (the diagonal elements and eigenvalues are assumed in decreasing order) that

$$f(\mathbf{d}(\mathbf{X})) \geq f(\boldsymbol{\lambda}(\mathbf{X})) \quad (8.55)$$

¹⁰In practice, most cost functions are minimized when the arguments are in a specific ordering (if not, one can always use instead the function $\tilde{f}_0(\mathbf{x}) = \min_{\mathbf{P} \in \mathcal{P}} f_0(\mathbf{Px})$, where \mathcal{P} is the set of all permutation matrices) and, hence, the decreasing ordering can be taken without loss of generality.

which means that $f(\rho)$ is minimum when $\mathbf{Q} = \mathbf{I}$ in (8.54) (since $(v\mathbf{I} + \tilde{\mathbf{B}}^H \mathbf{R}_H \tilde{\mathbf{B}})^{-1}$ is already diagonal with diagonal elements in decreasing order by definition). If f is Schur-convex, the opposite happens:

$$f(\mathbf{d}(\mathbf{X})) \geq f(\mathbf{1} \times \text{Tr}(\mathbf{X}) / L) \quad (8.56)$$

where $\mathbf{1}$ denotes the all-one vector. This means that $f_0(\rho)$ is minimum when \mathbf{Q} is such that ρ has equal elements in (8.54), that is, when $\mathbf{Q}^H(v\mathbf{I} + \tilde{\mathbf{B}}^H \mathbf{R}_H \tilde{\mathbf{B}})^{-1}\mathbf{Q}$ has equal diagonal elements. The following theorem summarizes this results.

Theorem 8.4.3 *The solution to the original problem (8.48) can be further characterized for two particular families of cost functions:*

- *If f is Schur-concave, then an optimal solution is*

$$\mathbf{B} = \mathbf{U}_{H,1} \text{diag}(\{\sqrt{p_i}\}) . \quad (8.57)$$

- *If f is Schur-convex, then an optimal solution is*

$$\mathbf{B} = \mathbf{U}_{H,1} \text{diag}(\{\sqrt{p_i}\}) \mathbf{Q}, \quad (8.58)$$

where \mathbf{Q} is a unitary matrix such that $(\mathbf{I} + \mathbf{B}^H \mathbf{R}_H \mathbf{B})^{-1}$ has identical diagonal elements. This “rotation” matrix \mathbf{Q} can be computed with the algorithm in [64, IV-A], as well as with any unitary matrix that satisfies $|\mathbf{Q}|_{ik} = |\mathbf{Q}|_{il}|, \forall i, k, l$ such as the unitary Discrete Fourier Transform (DFT) Transform matrix or the unitary Hadamard matrix (when the dimensions are appropriate such as a power of two [51, p. 66]).

Interestingly, Theorem 8.4.3 implies that Schur-concave cost functions lead to parallel transmissions (from the fully channel diagonalization), whereas Schur-convex cost functions result in transmission schemes that spread all the symbols equally through all channel eigenmodes in a CDMA fashion (see Figure 8.4). Hence, the designs obtained with Schur-convex cost functions are inherently more robust to ill-conditioned substreams (due, for example, to fading) and exhibit a better performance (as can be observed from the numerical results in §8.4.5).

It is important to remark that all the results obtained in this section are directly applicable to the opposite problem formulation consisting in the minimization of a cost function subject to a power constraint.

Schur-concave cost functions

For Schur-concave cost functions, the optimal rotation is $\mathbf{Q} = \mathbf{I}$ (from Theorem 8.4.3) and the MSEs are given by

$$\text{MSE}_i = \frac{1}{v + p_i \lambda_{H,i}} \quad 1 \leq i \leq L. \quad (8.59)$$

Note that the SINRs in this case are easily given by $\text{SINR}_i = p_i \lambda_{H,i}$ (from (8.36) and (8.59)), which do not depend on v .

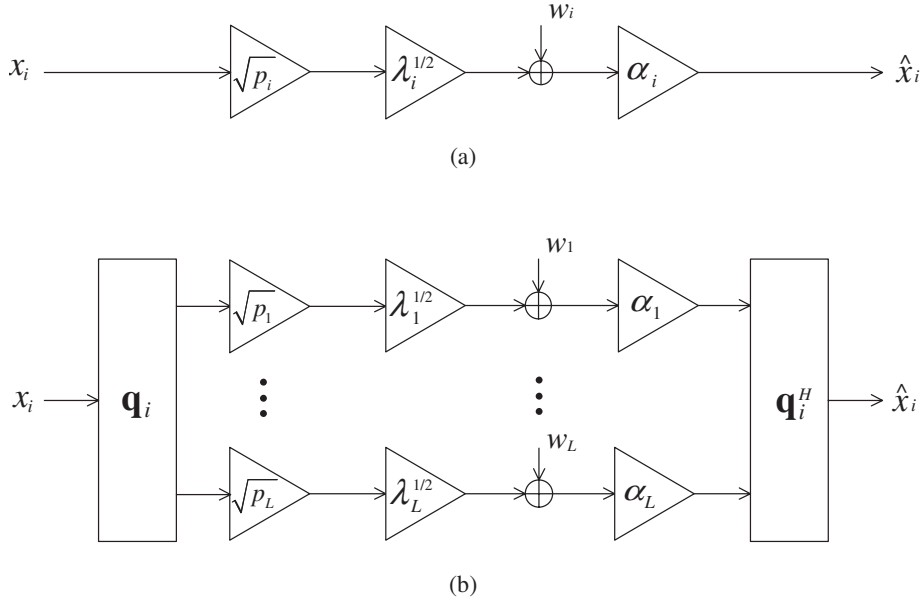


Figure 8.4 Transmission structure for the i -th symbol: (a) Diagonal (parallel) transmission for Schur-concave functions; and (b) Nondiagonal (distributed or spread) transmission for Schur-convex functions.

The original optimization problem (8.48) can be finally written as

$$\begin{aligned} & \underset{\mathbf{p}}{\text{minimize}} \quad \sum_{j=1}^L p_j \\ & \text{subject to} \quad f\left(\left\{\frac{1}{v+p_i \lambda_{H,i}}\right\}\right) \leq \alpha_0 \\ & \quad p_i \geq 0 \quad 1 \leq i \leq L, \end{aligned} \quad (8.60)$$

whose solution clearly depends on the particular choice of f .

Schur-convex cost functions

For Schur-concave cost functions, the diagonal elements of the MSE matrix \mathbf{E} are equal at the optimal solution (Theorem 8.4.3) and the MSEs are then given by

$$\text{MSE}_i = \frac{1}{L} \text{Tr}(\mathbf{E}) = \frac{1}{L} \sum_{j=1}^L \frac{1}{v + p_j \lambda_{H,j}} \quad 1 \leq i \leq L. \quad (8.61)$$

The original optimization problem (8.48) can be finally written as

$$\begin{aligned} & \underset{\mathbf{p}}{\text{minimize}} \quad \sum_{j=1}^L p_j \\ & \text{subject to} \quad \frac{1}{L} \sum_{j=1}^L \frac{1}{v + p_j \lambda_{H,j}} \leq \rho_0 \\ & \quad p_i \geq 0 \quad 1 \leq i \leq L \end{aligned} \quad (8.62)$$

where $\rho_0 \triangleq \{\rho \mid f(\mathbf{1} \times \rho) = \alpha_0\}$ is the MSE level required on all substreams to achieve the required global quality.

Surprisingly, this simplified problem for Schur-convex functions does not explicitly depend on the cost function f ; in other words, once the required MSE level ρ_0 has been calculated, problem (8.62) is independent of f . The reason is that since all the MSEs are equal, the cost function simply defines a one-to-one mapping between α_0 and ρ_0 . In addition, problem (8.62) is solved by the following waterfilling solution obtained from the KKT optimality conditions:

$$p_i = \left(\mu \lambda_{H,i}^{-1/2} - \nu \lambda_{H,i}^{-1} \right)^+ \quad 1 \leq i \leq L \quad (8.63)$$

where μ is the waterlevel chosen such that $\frac{1}{L} \sum_{j=1}^L \frac{1}{\nu + p_j \lambda_{H,j}} = \rho_0$ (see [16, 17] for a practical numerical evaluation of the waterfilling expression). Note that for the ZF receiver ($\nu = 0$), the waterfilling solution (8.63) simplifies to $p_i = \lambda_{H,i}^{-1/2} / \sum_{j=1}^L \lambda_{H,j}^{-1/2} / (L\rho_0)$.

List of Schur-concave and Schur-convex cost functions

The following list of Schur-concave and Schur-convex functions, along with the corresponding closed-form solutions obtained from the KKT conditions, illustrates how powerful is the unifying framework developed in Theorem 8.4.3 (see [15, 17] for a detailed treatment of each case).

Examples of Schur-concave functions (when expressed as functions of the MSEs) for which the diagonal transmission is optimal:

- Minimization of the sum of the MSEs or, equivalently, of $\text{Tr}(\mathbf{E})$ [58, 6] with solution $p_i = \left(\mu \lambda_{H,i}^{-1/2} - \nu \lambda_{H,i}^{-1} \right)^+$.
- Minimization of the weighted sum of the MSEs or, equivalently, of $\text{Tr}(\mathbf{WE})$, where $\mathbf{W} = \text{diag}(\{w_i\})$ is a diagonal weighting matrix, [59] with solution

$$p_i = \left(\mu w_i^{1/2} \lambda_{H,i}^{-1/2} - \nu \lambda_{H,i}^{-1} \right)^+.$$

- Minimization of the (exponentially weighted) product of the MSEs with solution $p_i = \left(\mu w_i - \nu \lambda_{H,i}^{-1} \right)^+$.
- Minimization of $\det(\mathbf{E})$ [60] with solution $p_i = \left(\mu - \nu \lambda_{H,i}^{-1} \right)^+$.
- Maximization of the mutual information, for example, [10], with solution $p_i = \left(\mu - \lambda_{H,i}^{-1} \right)^+$.
- Maximization of the (weighted) sum of the SINRs with solution given by allocating the power on the eigenmode with maximum weighted gain $w_i \lambda_{H,i}$.
- Maximization of the (exponentially weighted) product of the SINRs with solution $p_i \propto w_i / \sum_j w_j$ (for the unweighted case, it results in a uniform power allocation).

Examples of Schur-convex functions for which the optimal transmission is nondiagonal with solution given by $p_i = (\mu \lambda_{H,i}^{-1/2} - \nu \lambda_{H,i}^{-1})^+$ plus the rotation \mathbf{Q} :

- Minimization of the maximum of the MSEs.
- Maximization of the minimum of the SINRs.
- Maximization of the harmonic mean of the SINRs.¹¹
- Minimization of the average BER (with equal constellations).
- Minimization of the maximum of the BERs.

A practical example: Minimum BER design

The average (uncoded) BER is a good measure of the uncoded part of a system. Hence, guaranteeing a minimum average BER may be regarded as an excellent criterion:

$$\frac{1}{L} \sum_{i=1}^L g_i(\text{MSE}_i) \leq \text{BER}_0 \quad (8.64)$$

where the functions g_i were defined in (8.37) and happen to be convex increasing in the MSE for sufficiently small values of the argument (see Figure 8.5) [15, 17]. As a rule of thumb, the BER is convex in the MSE for a BER less than 2×10^{-2} (this is a mild assumption, since practical systems have in general a smaller uncoded BER¹²); interestingly, for BPSK and QPSK constellations the BER function is always convex [15, 17].

The optimal receive matrix is given by (8.33) and the problem is

$$\begin{aligned} & \underset{\mathbf{B}}{\text{minimize}} \quad \text{Tr}(\mathbf{B}\mathbf{B}^H) \\ & \text{subject to} \quad \frac{1}{L} \sum_i g_i\left(\left[(\nu\mathbf{I} + \mathbf{B}^H \mathbf{R}_H \mathbf{B})^{-1}\right]_{ii}\right) \leq \text{BER}_0 \end{aligned} \quad (8.65)$$

where it has been implicitly assumed that the constellations used have been previously chosen with some bit allocation strategy such as the gap-approximation method [63, Part II] or simply equal fixed constellations. Theorem 8.4.2 can now be invoked (provided that the constellations are chosen with increasing cardinality) to simplify the problem and reformulate it in convex form as in (8.53). This problem was extensively treated in [54] for the multicarrier case via a primal decomposition approach, which allowed the resolution of the problem with extremely simple algorithms (rather than using general purpose iterative algorithms such as interior-point methods).

In the particular case when the constellations used in the L substreams are equal, the average BER cost function turns out to be Schur-convex, since it is the sum of identical convex functions [44, 3.H.2]. Hence, the final problem to be solved is (8.62) with $\rho_0 = g^{-1}(\text{BER}_0)$ and the solution is given by (8.63) (recall that the rotation matrix \mathbf{Q} is needed as indicated in Theorem 8.4.3).

¹¹For the ZF receiver, the maximization of the harmonic mean of the SINRs is equivalent to the minimization of the unweighted sum of the MSEs, which can be classified as both Schur-concave and Schur-convex (since it is invariant to rotations).

¹²Given an uncoded bit error probability of at most 10^{-2} and using a proper coding scheme, coded bit error probabilities with acceptable low values such as 10^{-6} can be obtained.

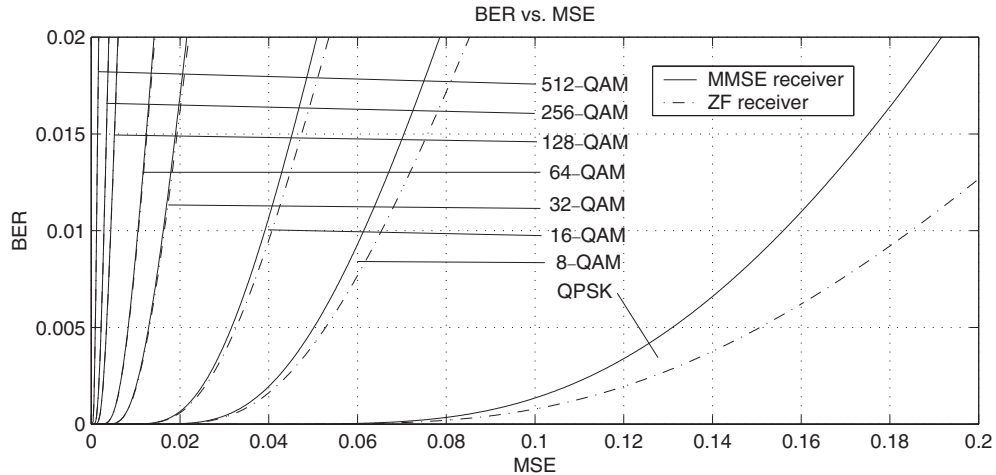


Figure 8.5 BER as a function of the MSE for different QAM constellations.

8.4.4 Extension to multicarrier systems

As mentioned in §8.3, multicarrier systems may be more conveniently modeled as a communication through a set of parallel MIMO channels

$$\mathbf{y}_k = \mathbf{H}_k \mathbf{s}_k + \mathbf{n}_k \quad 1 \leq k \leq N, \quad (8.66)$$

where N is the number of carriers and k is the carrier index, rather than as a single MIMO channel as in (8.23) with $\mathbf{H} = \text{diag}(\{\mathbf{H}_k\})$. The parallel modeling in (8.66) is useful when the signal processing operates independently at each MIMO channel (implying block diagonal matrices $\mathbf{B} = \text{diag}(\{\mathbf{B}_k\})$ and $\mathbf{A} = \text{diag}(\{\mathbf{A}_k\})$), whereas the modeling with a single MIMO channel is more convenient when the signal processing operates jointly over all carriers (meaning full matrices \mathbf{B} and \mathbf{A}).

The optimal linear receiver and MSE matrix for multiple MIMO channels as in (8.66) still have the same form as (8.33) and (8.34), respectively, for each MIMO channel (L_k denotes the number of established substreams at the k th MIMO channel).

The extension of the design with independent QoS constraint of §8.4.2 to the case of a set of N parallel MIMO channels is straightforward. In fact, the minimization of the total power is equivalent to the independent minimization of the power used at each carrier; hence, the original problem decouples into N subproblems like (8.42).

The design with a global QoS constraint of §8.4.3 can also be extended to N parallel MIMO channels, under the mild assumption that the quality of each carrier k is measured by an increasing function f_k and the global quality of the system, as measured by f , depends only on the f_k 's:

$$\begin{aligned} & \underset{\{\mathbf{A}_k, \mathbf{B}_k, \alpha_k\}}{\text{minimize}} && \sum_{k=1}^N \text{Tr}(\mathbf{B}_k \mathbf{B}_k^H) \\ & \text{subject to} && f_k \left(\{\text{MSE}_{k,i}\}_{i=1}^{L_k} \right) \leq \alpha_k \quad 1 \leq k \leq N \\ & && f(\alpha_1, \dots, \alpha_N) \leq \alpha_0 \end{aligned} \quad (8.67)$$

where the optimization is also over the α_k 's that measure the quality of each carrier. If the α_k 's are held fixed, problem (8.67) decouples into a set of N parallel optimization subproblems like (8.48), for which all the results of §8.4.3 apply. However, problem (8.67) has the additional difficulty that the α_k 's have to be optimized as well. Such a problem can sometimes be directly solved as was done in [17] for some particular cases, obtaining more complicated solutions than the simple waterfillings expressions previously listed for Schur-concave/convex functions. Alternatively, the problem can also be easily tackled with a decomposition approach [13], by which (8.67) is conveniently decomposed into a set of parallel subproblems controlled by a master problem, c.f. [54].

Single beamforming

A significant simplification occurs when a single substream is established per MIMO channel, that is, when $L_k = 1 \forall k$. In such a case, the structure of each transmit matrix \mathbf{B}_k is trivially given by a vector (or beamvector, hence the name single beamforming) \mathbf{b}_k parallel to the eigenvector corresponding to the maximum eigenvalue at the k th MIMO channel and with squared norm p_k (from Theorems 8.4.1–8.4.3). Problem (8.67) then reduces to (see [65] for a comparison of several criteria)

$$\begin{aligned} & \underset{\{p_k, \alpha_k\}}{\text{minimize}} && \sum_{k=1}^N p_k \\ & \text{subject to} && f_k(\{\text{MSE}_k\}) \leq \alpha_k \quad 1 \leq k \leq N \\ & && f(\alpha_1, \dots, \alpha_N) \leq \alpha_0. \end{aligned} \tag{8.68}$$

8.4.5 Numerical results

This section illustrates with numerical results the power of the tools developed for the design of linear MIMO transceivers in §8.4.2 and §8.4.3. Once the design criterion has been chosen, the transceiver is optimally designed using the general framework of Theorems 8.4.1–8.4.3.

A simple model has been used to randomly generate different realizations of the MIMO channel. In particular, the channel matrix \mathbf{H} has been generated from a Gaussian distribution with i.i.d. zero-mean unit-variance elements, and the noise has been modeled as white $\mathbf{R}_n = \sigma_n^2 \mathbf{I}$, where σ_n^2 is the noise power. (For simulations with more realistic wireless multiantenna channel models including spatial and frequency correlation, the reader is referred to [15–17].) The SNR is defined as $\text{SNR} = P_T / \sigma_n^2$, which is essentially a measure of the transmitted power normalized with respect to the noise.

In the first example, four different methods have been simulated by minimizing a cost function subject to a power constraint (recall that this is equivalent to minimizing the power subject to a global constraint as in §8.4.3): the classical minimization of the sum of the MSEs (SUM-MSE), the minimization of the product of the MSEs (PROD-MSE), the minimization of the maximum of the MSEs (MAX-MSE), and the minimization of the average/sum of the BERs (SUM-BER). The methods are evaluated in terms of BER averaged over the substreams; to be more precise, the outage BER¹³ (over different realizations of \mathbf{H}) is considered since it is a more realistic measure than the average BER (which only makes

¹³The outage BER is the BER that is attained with some given probability (when it is not satisfied, an outage event is declared).

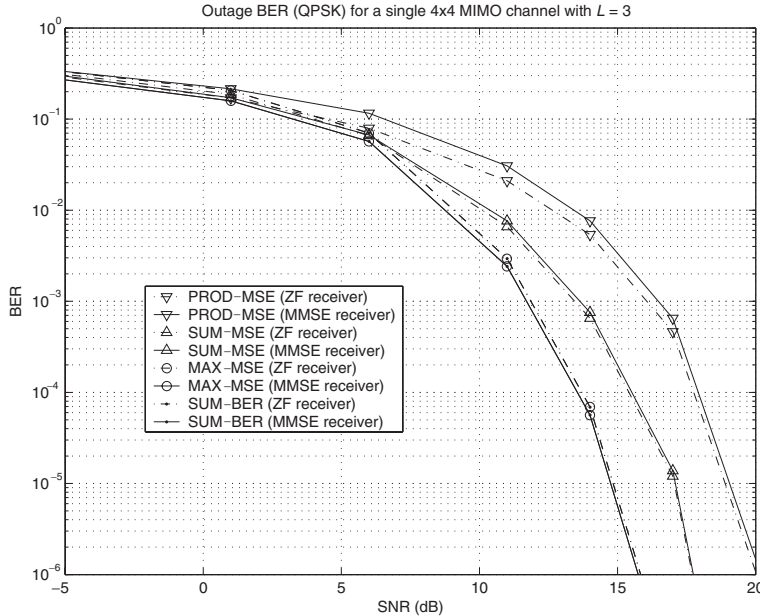


Figure 8.6 BER (at an outage probability of 5%) versus SNR when using QPSK in a 4×4 MIMO channel with $L = 3$ (with MMSE and ZF receivers) for the methods: PROD-MSE, SUM-MSE, MAX-MSE, and SUM-BER.

sense when the system does not have delay constraints and the duration of the transmission is sufficiently long such that the fading statistics of the channel can be averaged out).

In Figure 8.6, the BER (for a QPSK constellation) is plotted as a function of the SNR for a single 4×4 MIMO channel with $L = 3$ for the cases of ZF and MMSE receivers. It can be observed that the ZF receiver performs almost the same as the MMSE receiver thanks to the joint optimization of the transmitter and receiver (as opposed to the typically worse performance of the ZF receiver in the classical equalization setup where only the receiver is optimized). The methods MAX-MSE and SUM-BER correspond to Schur-convex functions and, as expected, are exactly the same (c.f. §8.4.3). The superiority of Schur-convex designs (MAX-MSE and SUM-BER) with respect to Schur-concave designs (SUM-MSE and PROD-MSE) is very clear from Figure 8.6, as was argued in §8.4.3, because of the increase in robustness against fading of the channel eigenmodes.

In Figure 8.7, the achievable region in terms of MSEs is plotted for a given realization of a single 4×4 MIMO channel with $L = 2$ (MMSE receiver) and with an SNR of 15 dB. The achievable region has been computed with the method developed in §8.4.2 that allows to specify independent QoS constraints on each substream. The boundary between the achievable and non-achievable regions corresponds to the Pareto-optimal designs, characterized by not being outperformed by any other solution simultaneously in all substreams. The solutions corresponding to the previous methods, SUM-MSE, PROD-MSE, Schur-convex method (which includes MAX-MSE and SUM-BER), are also indicated. They clearly lie on the Pareto-optimal frontier, although in different points of it. In fact, since Schur-convex

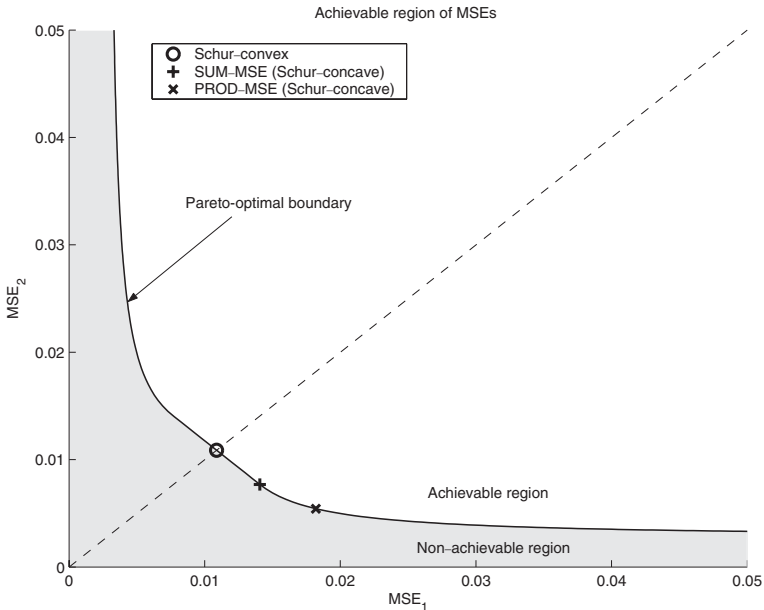


Figure 8.7 Achievable region of the MSEs for a given channel realization of a 4×4 MIMO channel with $L = 2$, along with the location of the design with the methods: PROD-MSE, SUM-MSE, and a Schur-convex (MAX-MSE and SUM-BER).

methods have equal MSEs on all substreams, they all correspond to the intersection of the Pareto-optimal boundary with the line $\rho_1 = \rho_2 = \dots = \rho_L$, which corresponds to a complete fairness among substreams.

8.5 An Application to Robust Transmitter Design in MIMO Channels

8.5.1 Introduction and state-of-the-art

In §8.4, a general framework has been presented to jointly design optimum linear transmitters and receivers according to a set of optimization criteria based on convex optimization theory. In those cases, it has been assumed that a perfect channel estimate or CSI is available during the design stage. In a realistic scenario, however, the channel knowledge is generally imperfect. In such a situation, the design should explicitly take into account the errors in the channel estimate, leading to the so-called *robust designs*, which are less sensitive to these errors. It is interesting to note that the first applications of robust designs were not for wireless communications but for control theory (see [66, 67] and references therein). Indeed, the concepts of signal state space and MIMO were originally used in that area. Afterwards, all these techniques and concepts were extended to other fields because of their potential benefits.

In some works such as [65, 68–70], the performance degradation of several nonrobust designs for multiantenna systems was analyzed, in which the errors in the CSI were considered negligible. The main conclusion is that this degradation increases rapidly with the error level.

In a communication system, the receiver usually acquires the channel estimate using a training sequence (pilot symbols). At the transmitter, the CSI can be obtained through a feedback channel or from previous received signals, exploiting the channel reciprocity principle in a time division duplexing (TDD) system (see [36] for an overview of different channel estimation strategies).

Different sources of errors in the CSI can be identified. In case of exploiting the channel reciprocity, the Gaussian noise from the estimation process and the outdated estimate due to the channel variability have to be considered. If a feedback channel is used, additional effects arise, such as the quantization of the channel estimate and the errors in the communication through the feedback channel.

According to the way the error in the channel estimate is modeled, the robust techniques can be classified into two families: the Bayesian (or stochastic) and the maximin (or worst-case) approaches [14, 17]. In the Bayesian philosophy, the statistics of the error are assumed to be known and a stochastic measure of the system performance is optimized, such as the mean value. On the other hand, the maximin approach considers that the error belongs to a predefined uncertainty region, and the final objective is the optimization of the worst system performance for any error in this region.

The Bayesian philosophy has been considered in works such as [71], where a multiantenna transmitter was designed to maximize the mean SNR and the mutual information assuming two sources of errors: the Gaussian noise and the quantization errors. The minimization of the BER was considered in [72]. Transmit FIR filters in a multiantenna frequency-selective channel were designed in [73] to maximize the mean SNR and minimize the MSE assuming Gaussian errors. The more general case of MIMO flat fading channels was considered in [74], where the transmitter was composed of an orthogonal space-time block code (OSTBC) and a matrix performing a linear transformation. This matrix was designed to minimize an upper bound of the BER assuming Gaussian errors. A similar scheme consisting of the combination of an OSTBC a set of beamformers was considered in [75] to minimize the error probability. The same objective was taken in [76] and [77] for a MIMO frequency-selective channel using a multicarrier modulation: in [76], the transmitter and the receiver were based on matrices performing a linear transformation, whereas in [77], the transmitter was composed of an Alamouti's code [11] combined with two beamformers.

Regarding the maximin approach, [78] and [79] provide a general insight using a game theoretic formulation and describing several applications in signal processing. See also [18] for a reference on the theory of saddle-functions and maximin. This approach has been recently used in the classical problem of designing a receive beamformer under mismatches in the presumed model, as in [33], where the errors were assumed to be in the estimated steering vector and to belong to a spherical uncertainty region. This was afterwards generalized in [35] to embrace uncertainties both in the array response and the covariance matrix. The classical Capon's beamformer [31] was extended to its robust version in [32, 34], and [80], taking generic uncertainty regions and different formulations. In some of these examples, the robustness was obtained by minimizing the output power of the beamformer

while guaranteeing a minimum gain for any direction modeled by the uncertainty region (see §8.2.5 for a more detailed description). Finally, several applications of this robust approach to multiuser systems with multiantenna base stations can also be found in [36, 81], and [82].

This subsection starts with the presentation of the generic formulation of the Bayesian and the maximin approaches in §8.5.2. Afterwards, a MIMO system is considered, where the robust transmitter is designed under the maximin philosophy and the receiver is based on an optimum ML detector assuming a perfect channel knowledge. This follows and extends the results obtained in [83].

8.5.2 A generic formulation of robust approaches

A generic formulation can be stated for both the Bayesian and the maximin approaches (see [17] for more details). In all the cases, the imperfect CSI can be represented as

$$\mathbf{H} = \widehat{\mathbf{H}} + \Delta \quad (8.69)$$

where \mathbf{H} is the actual MIMO channel matrix (as defined in §8.3), $\widehat{\mathbf{H}}$ is the channel estimate, and Δ is the error. The system performance is usually measured by a cost function f , whose minimization is the objective of the design (usual cost functions are based on the BER, the MSE, or the SINR, among others, c.f. §8.3.2).

In the Bayesian approach, the error and the actual channel are modeled statistically with the probability density functions (pdf's) $p_\Delta(\Delta)$ and $p_{\mathbf{H}}(\mathbf{H})$, respectively, which are assumed to be known. Note that knowing these pdf's is equivalent to knowing the pdf of the actual channel conditioned to the channel estimate $p_{\mathbf{H}|\widehat{\mathbf{H}}}(\mathbf{H}|\widehat{\mathbf{H}})$, which is equal to $p_\Delta(\mathbf{H} - \widehat{\mathbf{H}})p_{\mathbf{H}}(\mathbf{H})/p_{\widehat{\mathbf{H}}}(\widehat{\mathbf{H}})$ by the Bayes rule. A possible design strategy consists in the minimization of the mean value of the cost function f (note, however, that other stochastic measures of the performance could have been used, such as the outage performance). If this criterion is adopted and the average transmitted power is upper bounded by P_0 , the following optimization problem has to be solved:

$$\begin{aligned} & \underset{\mathbf{A}, \mathbf{B}}{\text{minimize}} \quad \mathbb{E}_{\mathbf{H}|\widehat{\mathbf{H}}} [f(\mathbf{H}, \mathbf{A}, \mathbf{B})] \\ & \text{subject to} \quad \text{Tr}(\mathbf{B}\mathbf{B}^H) \leq P_0 \end{aligned} \quad (8.70)$$

where the optimization variables are the transmit \mathbf{B} and the receive \mathbf{A} matrices. Note that, in this case, although the average performance is optimized, no guarantee can be given in terms of the instantaneous performance.

In the maximin approach, instead of modeling the error statistically, it is assumed that it belongs to a predefined uncertainty region \mathcal{R} , that is, $\Delta \in \mathcal{R}$. Then, the worst performance for any error in \mathcal{R} is expressed as $\sup_{\Delta \in \mathcal{R}} f(\mathbf{H}, \mathbf{A}, \mathbf{B})$. The robust design problem consists in the optimization of the worst performance, which can be formulated as

$$\begin{aligned} & \underset{\mathbf{A}, \mathbf{B}}{\text{minimize}} \quad \sup_{\Delta \in \mathcal{R}} f(\mathbf{H}, \mathbf{A}, \mathbf{B}) \\ & \text{subject to} \quad \text{Tr}(\mathbf{B}\mathbf{B}^H) \leq P_0. \end{aligned} \quad (8.71)$$

In this case, a full statistical characterization is not necessary. Besides, this approach guarantees a minimum instantaneous performance for any error modeled by the uncertainty region, that is, when the actual error behaves as expected (in a real situation, this will be satisfied with a high probability, declaring an outage otherwise). Note that this guarantee cannot be provided by the Bayesian approach optimizing the average performance.

8.5.3 Problem formulation

As in §8.3 and §8.4, in the following, the transmission through a MIMO channel \mathbf{H} is considered corresponding to the signal model $\mathbf{y} = \mathbf{H}\mathbf{s} + \mathbf{n}$ (see (8.23)). In particular, a multiantenna flat fading wireless channel is assumed, where the number of transmit and receive antennas is n_T and n_R , respectively. The interference-plus-noise covariance matrix is $\mathbf{R}_n = \sigma_n^2 \mathbf{I}$, corresponding to a scenario with only additive white Gaussian noise (AWGN). Note, however, that the derived design strategy can be applied to other kinds of MIMO channels as well.

The objective is to obtain a maximin robust design of the system, as in (8.71), according to an imperfect channel estimate $\widehat{\mathbf{H}}$ at the transmitter as modeled in (8.69). The CSI at the receiver will be assumed to be perfect.

The transmitter architecture

Consider that one symbol is to be transmitted at one time instant. From §8.4 it is concluded that, in the case of having a perfect CSI, the optimum solution is based on single beamforming ($L = 1$), consisting in the transmission through the eigenvector of $\mathbf{H}^H \mathbf{H}$ associated to the maximum eigenvalue (note that the squared whitened channel matrix is $\mathbf{R}_H = \frac{1}{\sigma_n^2} \mathbf{H}^H \mathbf{H}$). In case that the channel knowledge is imperfect, transmitting through the maximum eigenmode of $\widehat{\mathbf{H}}^H \widehat{\mathbf{H}}$ constitutes the naive or nonrobust solution, which may be quite sensitive to the errors in the CSI. Therefore, a robust design is expected to use more eigenmodes than the maximum one.

The design of the robust transmitter will be based on a linear processing, as in §8.3 ($\mathbf{s} = \mathbf{Bx}$), whereas at the receiver, a ML detector will be used assuming a perfect CSI. The direct design of a robust transmit matrix \mathbf{B} seems very complicated and, therefore, a structure will be imposed on it to simplify the problem. The proposed robust solution consists in the transmission of the symbols through all the eigenmodes of $\widehat{\mathbf{H}}^H \widehat{\mathbf{H}}$ using an adequate power distribution among them, as will be shown later and as opposed to the nonrobust design, where only the maximum eigenmode is used.

Consider the simultaneous transmission of R independent complex symbols over N_t periods (leading to a transmission rate equal to R/N_t), corresponding to the following linear signal model, similarly to linear dispersion codes [84] and OSTBC [85–87]:

$$\mathbf{S} = \sum_{l=1}^R \left(\mathbf{B}_l^{(r)} x_l^{(r)} + j \mathbf{B}_l^{(i)} x_l^{(i)} \right) \in \mathbb{C}^{n_T \times N_t} \quad (8.72)$$

where x_l is the l th transmitted complex symbol with a normalized energy ($\mathbb{E}[|x_l|^2] = 1$), $x_l^{(r)}$ and $x_l^{(i)}$ are its real and imaginary parts, respectively, $\mathbf{B}_l^{(r)}, \mathbf{B}_l^{(i)} \in \mathbb{C}^{n_T \times N_t}$ are the associated complex transmit matrices for $x_l^{(r)}$ and $x_l^{(i)}$, and the rows of \mathbf{S} are the N_t signal samples transmitted through each antenna. The structure imposed on the transmit matrices is

$$\mathbf{B}_l^{(r)} = \widehat{\mathbf{U}} \operatorname{diag}(\{\sqrt{p_i}\}) \mathbf{T}_l^{(r)}, \quad \mathbf{B}_l^{(i)} = \widehat{\mathbf{U}} \operatorname{diag}(\{\sqrt{p_i}\}) \mathbf{T}_l^{(i)} \quad (8.73)$$

where $\widehat{\mathbf{U}} = [\widehat{\mathbf{u}}_1 \cdots \widehat{\mathbf{u}}_{n_T}] \in \mathbb{C}^{n_T \times n_T}$ is the unitary matrix containing the n_T eigenvectors of $\widehat{\mathbf{H}}^H \widehat{\mathbf{H}}$ with eigenvalues $\{\widehat{\lambda}_i\}$ sorted in decreasing order, p_i is the power allocated to the i th

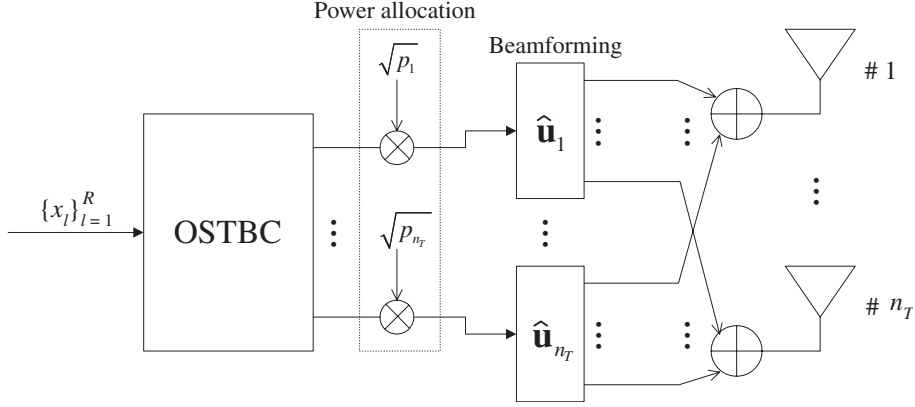


Figure 8.8 General architecture for the transmitter based on the combination of an OSTBC block, a power allocation, and a beamforming stage.

estimated eigenmode, and $\mathbf{T}_l^{(r)}, \mathbf{T}_l^{(i)} \in \mathbb{C}^{n_T \times N_t}$ are matrices modeling a temporal spreading of the symbols and fulfilling $\mathbf{T}_l^{(r)} \mathbf{T}_l^{(r)H} = \mathbf{I}$ and $\mathbf{T}_l^{(i)} \mathbf{T}_l^{(i)H} = \mathbf{I}$. These matrices $\mathbf{T}_l^{(r)}$ and $\mathbf{T}_l^{(i)}$ are based on the Hurwitz-Radon family of matrices (see [86] and [85]), so that the ML detector reduces to a bank of linear filters, and the detection scheme is the same as that used for OSTBC.

This apparently complicated signaling scheme (8.72) can be represented as shown in Figure 8.8, where it is seen that the symbols are encoded by an OSTBC, and each output of the OSTBC is transmitted through a different estimated eigenmode. Finally, the parameters $\{p_i\}$ distribute the available power among the eigenmodes. This transmission scheme is similar to those presented in [74, 75, 88], among others, in which the transmitter architecture also consisted in the combination of an OSTBC and a beamforming stage, although the design of the power allocation was different to the one proposed in the following.

Note that, in the signal model (8.72), not only the spatial but also the temporal dimensions are exploited. This signal model can be rewritten using the generic matrix-vector notation presented in §8.3 as follows. Let \mathbf{s}_n be the n th column of \mathbf{S} representing the transmitted vector during the n th period of time. This vector can be expressed as

$$\mathbf{s}_n = \bar{\mathbf{B}}_n^{(r)} \mathbf{x}_r + j \bar{\mathbf{B}}_n^{(i)} \mathbf{x}_i \quad (8.74)$$

where $\bar{\mathbf{B}}_n^{(r)} = \widehat{\mathbf{U}} \text{diag}(\{\sqrt{p_i}\}) \bar{\mathbf{T}}_n^{(r)}$ and $\bar{\mathbf{B}}_n^{(i)} = \widehat{\mathbf{U}} \text{diag}(\{\sqrt{p_i}\}) \bar{\mathbf{T}}_n^{(i)}$, the matrices $\bar{\mathbf{T}}_n^{(r)}$ and $\bar{\mathbf{T}}_n^{(i)}$ contain the n th columns of $\mathbf{T}_l^{(r)}$ and $\mathbf{T}_l^{(i)}$ for $l = 1, \dots, R$, and $\mathbf{x}_r = [x_1^{(r)} \dots x_R^{(r)}]^T$, $\mathbf{x}_i = [x_1^{(i)} \dots x_R^{(i)}]^T$.

The design objective is to calculate the optimum power allocation strategy $\{p_i\}$ subject to a transmit power constraint and adopting an adequate performance criterion. If the transmit power budget is P_0 , the power constraint can be expressed in terms of the factors $\{p_i\}$ as

$$\frac{1}{2} (\|\mathbf{B}_l^{(r)}\|_F^2 + \|\mathbf{B}_l^{(i)}\|_F^2) = \sum_{i=1}^{n_T} p_i \leq P_0, \quad p_i \geq 0. \quad (8.75)$$

Note that the set of feasible power distributions is convex, since all the constraints given above are linear.

For the considered system ((8.72) and (8.73)), using an OSTBC with ML detection, the performance can be measured by the SNR expressed as (see [86] and [85])

$$\text{SNR} = \frac{1}{\sigma_n^2} \text{Tr} \left(\widehat{\mathbf{U}}^H \mathbf{H}^H \mathbf{H} \widehat{\mathbf{U}} \text{diag}(\mathbf{p}) \right) \quad (8.76)$$

where $\mathbf{p} = [p_1 \cdots p_{n_T}]^T$. Based on this, the performance function f is defined as

$$f(\mathbf{p}, \Delta) = \text{Tr} \left(\widehat{\mathbf{U}}^H \mathbf{H}^H \mathbf{H} \widehat{\mathbf{U}} \text{diag}(\mathbf{p}) \right) \quad (8.77)$$

$$= \text{Tr} \left(\widehat{\mathbf{U}}^H (\widehat{\mathbf{H}} + \Delta)^H (\widehat{\mathbf{H}} + \Delta) \widehat{\mathbf{U}} \text{diag}(\mathbf{p}) \right), \quad (8.78)$$

whose maximization is the objective of the design and where the error model (8.69) has been used. This function is linear in \mathbf{p} and, therefore, concave; and convex-quadratic in the error Δ . Note that, in this case, an opposite strategy is taken from that presented in §8.4, in which the transmitted power was minimized subject to QoS constraints, although both kinds of problems are essentially equivalent, as explained in §8.4.1.

The maximin problem formulation

As stated in §8.5.2, the maximin approach can be used to include robustness in the design. Accordingly, an uncertainty region \mathcal{R} for Δ has to be defined, which, in the following, will be assumed to be convex.¹⁴ The robust power distribution \mathbf{p}^* , which optimizes the worst performance for any error in the uncertainty region, can be found as the solution to the following optimization problem:

$$\begin{aligned} & \underset{\mathbf{p}}{\text{maximize}} && \inf_{\Delta \in \mathcal{R}} f(\mathbf{p}, \Delta) \\ & \text{subject to} && \mathbf{1}^T \mathbf{p} \leq P_0 \\ & && p_i \geq 0 \end{aligned} \quad (8.79)$$

where $\mathbf{1} = [1 \cdots 1]^T \in \mathbb{R}^{n_T \times 1}$ is the all-one vector.

The direct way to solve the maximin problem is to obtain the minimization of f with respect to Δ in an analytical way and then solve the outer maximization. Such an approach, however, is difficult because it is not clear what is the minimizing Δ for a given \mathbf{p} in closed form.

Of course, one can also consider solving the problem numerically, that is, solving the inner minimization

$$\tilde{f}(\mathbf{p}) = \inf_{\Delta \in \mathcal{R}} f(\mathbf{p}, \Delta) \quad (8.80)$$

numerically for a given \mathbf{p} , and then solving the outer maximization $\max_{\mathbf{p}} \tilde{f}(\mathbf{p})$ also numerically. Note that the inner minimization is a convex problem, since f is convex in Δ and the

¹⁴The set \mathcal{R} is convex if $\Delta = \theta \Delta_1 + (1 - \theta) \Delta_2 \in \mathcal{R}$ for any $\Delta_1, \Delta_2 \in \mathcal{R}$ and $\theta \in [0, 1]$.

constraint set \mathcal{R} is also convex. The outer maximization is also a convex problem since the constraint set for \mathbf{p} is convex and the function \tilde{f} is concave. Consequently, the numerical algorithms referenced in §8.2.4 could be used. The proof that \tilde{f} is concave is given below, where \mathbf{p}_1 and \mathbf{p}_2 are any feasible power distributions, and $\theta \in [0, 1]$:

$$\begin{aligned}\tilde{f}(\theta\mathbf{p}_1 + (1 - \theta)\mathbf{p}_2) &= \inf_{\Delta \in \mathcal{R}} f(\theta\mathbf{p}_1 + (1 - \theta)\mathbf{p}_2, \Delta) \\ &= \inf_{\Delta \in \mathcal{R}} [\theta f(\mathbf{p}_1, \Delta) + (1 - \theta)f(\mathbf{p}_2, \Delta)] \\ &\geq \theta \inf_{\Delta \in \mathcal{R}} f(\mathbf{p}_1, \Delta) + (1 - \theta) \inf_{\Delta \in \mathcal{R}} f(\mathbf{p}_2, \Delta) \\ &= \theta \tilde{f}(\mathbf{p}_1) + (1 - \theta) \tilde{f}(\mathbf{p}_2)\end{aligned}\tag{8.81}$$

where the linearity of f in \mathbf{p} has been used in the second equality. This numerical procedure guarantees that the desired solution \mathbf{p}^* is found, however, it is computationally costly because each iteration of the method for the outer maximization requires an evaluation of $\tilde{f}(\mathbf{p})$ (and possibly its gradient as well), which in turn requires solving the inner minimization numerically with as many iterations as needed to converge.

Other kinds of numerical iterative methods could be used, such as the algorithm proposed in [89] to find saddle-points of maximin problems based on the method of steepest descent. In [90], an alternative algorithm for the same problem is derived on the basis of the interior-point approach.

8.5.4 Reformulating the problem in a simplified convex form

The objective is to rewrite the maximin problem (8.79), which is already convex but not amenable for efficient resolution, into an equivalent simplified convex problem so that it can be solved requiring less computational effort (see §8.2).

The function $f(\mathbf{p}, \Delta)$, which is concave-convex, and the optimization sets for the power distribution and the error satisfy the conditions given in Corollary 37.6.2 in [18]. From it, it can be concluded that there exists a saddle-point of the maximin problem, that is, there exist \mathbf{p}^* and Δ^* fulfilling the constraints and satisfying

$$f(\mathbf{p}, \Delta^*) \leq f(\mathbf{p}^*, \Delta^*) \leq f(\mathbf{p}^*, \Delta)\tag{8.82}$$

for any feasible \mathbf{p} and Δ . The solution to the original maximin problem (8.79) can be shown to be \mathbf{p}^* , and the saddle-value $f^* \triangleq f(\mathbf{p}^*, \Delta^*)$ is the minimum value of f , given \mathbf{p}^* , that is, $\tilde{f}(\mathbf{p}^*)$ (see Lemma 36.2 in [18]). The existence of the saddle-point allows to rewrite the original maximin problem (8.79) using a minimax formulation, that is, the inner and the outer optimizations can be interchanged:

$$\begin{array}{ll}\text{minimize}_{\Delta} & \sup_{\mathbf{1}^T \mathbf{p} \leq P_0, p_i \geq 0} f(\mathbf{p}, \Delta) \\ \text{subject to} & \Delta \in \mathcal{R},\end{array}\tag{8.83}$$

with the advantage that the inner maximization is now very simple. In particular, $\sup_{\mathbf{p}} f(\mathbf{p}, \Delta)$ gives as a result the maximum element of the diagonal of the matrix $\widehat{\mathbf{U}}^H (\widehat{\mathbf{H}} + \Delta)^H (\widehat{\mathbf{H}} + \Delta) \widehat{\mathbf{U}}$ multiplied by the power budget P_0 , that is:

$$\sup_{\mathbf{1}^T \mathbf{p} \leq P_0, p_i \geq 0} f(\mathbf{p}, \Delta) = P_0 \max_i \left[\widehat{\mathbf{U}}^H (\widehat{\mathbf{H}} + \Delta)^H (\widehat{\mathbf{H}} + \Delta) \widehat{\mathbf{U}} \right]_{ii} \quad (8.84)$$

$$= P_0 \max_i \left\{ \widehat{\mathbf{u}}_i^H (\widehat{\mathbf{H}} + \Delta)^H (\widehat{\mathbf{H}} + \Delta) \widehat{\mathbf{u}}_i \right\}. \quad (8.85)$$

Note that the power allocation \mathbf{p} achieving this optimum value is not unique if the maximum value is attained by more than one element of the diagonal of the matrix $\widehat{\mathbf{U}}^H (\widehat{\mathbf{H}} + \Delta)^H (\widehat{\mathbf{H}} + \Delta) \widehat{\mathbf{U}}$.

As a consequence from the previous result, the original problem can now be written as the following simple convex minimization problem:

$$\begin{aligned} & \underset{t, \Delta}{\text{minimize}} && t \\ & \text{subject to} && t \geq P_0 \widehat{\mathbf{u}}_i^H (\widehat{\mathbf{H}} + \Delta)^H (\widehat{\mathbf{H}} + \Delta) \widehat{\mathbf{u}}_i \quad \forall i \\ & && \Delta \in \mathcal{R}. \end{aligned} \quad (8.86)$$

Solving the previous problem gives the saddle-value $f^* = f(\mathbf{p}^*, \Delta^*) = t^*$ and the worst-case error Δ^* of the saddle-point of the problem (see [18]); however, the optimal robust power distribution is still unknown. It turns out that the optimum Lagrange multipliers γ_i^* associated with the constraints $t \geq P_0 \widehat{\mathbf{u}}_i^H (\widehat{\mathbf{H}} + \Delta)^H (\widehat{\mathbf{H}} + \Delta) \widehat{\mathbf{u}}_i$ in problem (8.86) provide the optimum normalized power distribution p_i^* , that is, $p_i^* = P_0 \gamma_i^*$, as proved below.

The problem (8.86) can be solved by formulating the KKT conditions, which are satisfied by the worst-case error Δ^* along with the optimum dual variables (see §8.2.3). On the other hand, it is clear that the worst-case error Δ^* is also the solution to the problem $\inf_{\Delta} f(\mathbf{p}^*, \Delta)$ (from (8.82)), where $\mathbf{p}^* = \arg \max_{\mathbf{p}} f(\mathbf{p}, \Delta^*)$ is the robust power distribution, and, therefore, the worst-case error Δ^* must satisfy the KKT conditions for the problem $\inf_{\Delta} f(\mathbf{p}^*, \Delta)$. By a simple comparison of the KKT conditions for both problems, it is straightforward to see that for $p_i^* = P_0 \gamma_i^*$, the worst-case error Δ^* satisfies both sets of KKT conditions and, hence, that is an optimal robust power allocation.

The Lagrangian of the optimization problem (8.86) (characterizing for convenience and w.l.o.g. the uncertainty convex region \mathcal{R} as the intersection of a set of convex constraints of the form $f_i(\Delta) \leq 0$) is

$$\begin{aligned} L_1 &= t + \sum_{i=1}^{n_T} \gamma_i \left(P_0 \widehat{\mathbf{u}}_i^H (\widehat{\mathbf{H}} + \Delta)^H (\widehat{\mathbf{H}} + \Delta) \widehat{\mathbf{u}}_i - t \right) + \sum_i \mu_i f_i(\Delta) \\ &= t \left(1 - \sum_{i=1}^{n_T} \gamma_i \right) + P_0 \operatorname{Tr} \left((\widehat{\mathbf{H}} + \Delta)^H (\widehat{\mathbf{H}} + \Delta) \widehat{\mathbf{U}} \operatorname{diag}(\{\gamma_i\}) \widehat{\mathbf{U}}^H \right) + \sum_i \mu_i f_i(\Delta), \end{aligned} \quad (8.87)$$

where the relation $\sum_{i=1}^{n_T} \gamma_i \hat{\mathbf{u}}_i \hat{\mathbf{u}}_i^H = \hat{\mathbf{U}} \text{diag}(\{\gamma_i\}) \hat{\mathbf{U}}^H$ has been used. The KKT conditions for this problem are

$$f_i(\Delta^*) \leq 0, \quad t^* \geq P_0 \hat{\mathbf{u}}_i^H (\hat{\mathbf{H}} + \Delta^*)^H (\hat{\mathbf{H}} + \Delta^*) \hat{\mathbf{u}}_i, \quad (8.88)$$

$$\mu_i^* \geq 0, \quad \gamma_i^* \geq 0, \quad (8.89)$$

$$\sum_{i=1}^{n_T} \gamma_i^* = 1, \quad P_0 (\hat{\mathbf{H}} + \Delta^*) \hat{\mathbf{U}} \text{diag}(\{\gamma_i^*\}) \hat{\mathbf{U}}^H + \sum_i \mu_i^* \nabla f_i(\Delta^*) = \mathbf{0}, \quad (8.90)$$

$$\mu_i^* f_i(\Delta^*) = 0, \quad \gamma_i^* \left(P_0 \hat{\mathbf{u}}_i^H (\hat{\mathbf{H}} + \Delta^*)^H (\hat{\mathbf{H}} + \Delta^*) \hat{\mathbf{u}}_i - t^* \right) = 0. \quad (8.91)$$

On the other hand, the Lagrangian for the problem $\inf_{\Delta} f(\mathbf{p}^*, \Delta)$ is

$$L_2 = \text{Tr} \left(\hat{\mathbf{U}}^H (\hat{\mathbf{H}} + \Delta)^H (\hat{\mathbf{H}} + \Delta) \hat{\mathbf{U}} \text{diag}(\mathbf{p}^*) \right) + \sum_i \alpha_i f_i(\Delta) \quad (8.92)$$

and the KKT conditions for the optimal error and multipliers are:

$$f_i(\Delta^*) \leq 0, \quad (8.93)$$

$$\alpha_i^* \geq 0, \quad (8.94)$$

$$(\hat{\mathbf{H}} + \Delta^*) \hat{\mathbf{U}} \text{diag}(\mathbf{p}^*) \hat{\mathbf{U}}^H + \sum_i \alpha_i^* \nabla f_i(\Delta^*) = \mathbf{0}, \quad (8.95)$$

$$\alpha_i^* f_i(\Delta^*) = 0. \quad (8.96)$$

From the comparison of both sets of KKT conditions (8.88)-(8.91) and (8.93)-(8.96), it is clear that they are satisfied by the same worst-case error Δ^* if $\alpha_i^* = \mu_i^*$ and $p_i^* = P_0 \gamma_i^*$. Note that the transmit power constraints are automatically fulfilled, since the optimum dual variables $\{\gamma_i^*\}$ are required to satisfy $\gamma_i^* \geq 0$ (see (8.89)) and $\sum_{i=1}^{n_T} \gamma_i^* = 1$ (see (8.90)).

It is important to remark that the saddle-value t^* can be attained by more than one element of the diagonal of the matrix $P_0 \hat{\mathbf{U}}^H (\hat{\mathbf{H}} + \Delta^*)^H (\hat{\mathbf{H}} + \Delta^*) \hat{\mathbf{U}}$. Taking this into account, and using the condition $\gamma_i^* (P_0 \hat{\mathbf{u}}_i^H (\hat{\mathbf{H}} + \Delta^*)^H (\hat{\mathbf{H}} + \Delta^*) \hat{\mathbf{u}}_i - t^*) = 0$ in (8.91), it is concluded that there can exist more than one Lagrange multiplier γ_i^* that can be different from zero; in other words, the robust power distribution can use more than one estimated eigenmode for transmission, as expected. This will be proved with some examples in the simulations section.

Summarizing, the original maximin robust power allocation problem (8.79) can be solved by means of the simplified convex problem (8.86). The values of the optimum Lagrange multipliers of this simplified problem provide the normalized power distribution to be applied among the estimated eigenmodes. Currently, most of the existing software packages simultaneously provide the optimum values of both the primal and the dual variables and, therefore, they could be applied to find the optimum solution to this robustness problem (see §8.2.4 and references therein).

8.5.5 Convex uncertainty regions

The definition of the uncertainty region \mathcal{R} may impact importantly on the system performance. The size and the shape of this region should take into account the quality of the channel estimate and the imperfections that generate the error (see §8.5.1 for some examples of sources of errors).

In the following, two sources of errors are identified and three different uncertainty regions, jointly with their sizes, are described. In all the cases, the proposed uncertainty regions are convex, as required to solve the optimization problem.

Estimation Gaussian noise

A common situation when estimating the channel corresponds to the presence of AWGN, especially in TDD systems, where the transmitter can estimate the channel while receiving in the reverse link, and use it as an estimate in the forward link, because of the channel reciprocity principle.

The following assumptions are considered: all the components of the actual channel \mathbf{H} are i.i.d. and follow a zero-mean circularly symmetric Gaussian distribution with a variance equal to σ_h^2 , whereas the estimation AWGN is also zero-mean and circularly symmetric with variance σ_e^2 . Based on this, the estimation SNR, that is, the received SNR during the transmission of the training sequence, is defined as $\text{SNR}_{\text{est}} = \sigma_h^2/\sigma_e^2$.

Under these assumptions, the actual channel \mathbf{H} conditioned to the channel estimate follows a circularly symmetric complex Gaussian distribution with a mean value equal to the MMSE Bayesian channel estimate and a white covariance matrix with diagonal elements equal to $\frac{\sigma_h^2 \sigma_e^2}{\sigma_h^2 + \sigma_e^2} = \frac{\sigma_h^2}{1 + \text{SNR}_{\text{est}}}$ (see [55]), that is, the actual channel can be assumed to be in a region near the MMSE Bayesian channel estimate, where the distance to it is measured indirectly by $\frac{\sigma_h^2}{1 + \text{SNR}_{\text{est}}}$. Therefore, in this case, it is natural to identify $\widehat{\mathbf{H}}$ as the MMSE Bayesian estimate of the MIMO channel and to define the uncertainty region \mathcal{R} as a sphere centered at $\widehat{\mathbf{H}}$ with a radius equal to $\sqrt{\epsilon}$ as follows:

$$\mathcal{R} = \left\{ \Delta : \|\Delta\|_F^2 \leq \epsilon \right\}. \quad (8.97)$$

Since the error Δ is Gaussian distributed, it will be inside the region \mathcal{R} with a certain probability P_{in} lower than 1. This probability will be equal to the probability of providing the required QoS to the user. The mathematical relationship between the size of the uncertainty region, measured by ϵ , and P_{in} is given by $\epsilon = \varphi^{-1}(P_{\text{in}})$, where the function φ is the cumulative density function of the chi-square distribution corresponding to $\|\Delta\|_F^2$ with $2n_{RNT}$ degrees of freedom and normalized variance $\frac{\sigma_h^2}{2 + 2\text{SNR}_{\text{est}}}$.

Quantization errors

In frequency division duplexing (FDD) systems, the estimate of the channel at the transmitter is typically obtained through a feedback channel from the receiver to the transmitter. Since this feedback is expected to be discrete, the channel estimate has to be quantized, introducing

an error in the CSI available at the transmitter. Assuming that the receiver has a perfect knowledge of the channel response \mathbf{H} , let us consider, for illustrative purposes, that a suboptimum uniform quantization is applied to the real and imaginary parts of all the components of \mathbf{H} using a quantization step equal to Δ_q , obtaining $\widehat{\mathbf{H}}$. In this situation, the quantization SNR is given by $\text{SNR}_q = 6\sigma_h^2/\Delta_q^2$. Consequently, the uncertainty region can be defined as a cube centered at $\widehat{\mathbf{H}}$ as

$$\mathcal{R} = \left\{ \Delta : |\text{Re}\{[\Delta]_{ij}\}| \leq \frac{\Delta_q}{2}, |\text{Im}\{[\Delta]_{ij}\}| \leq \frac{\Delta_q}{2} \right\}. \quad (8.98)$$

As the capacity of the feedback channel increases, more bits can be used in the quantization and, therefore, the size of the uncertainty region can be reduced.

Combined estimation and quantization errors

In a realistic scenario with feedback, the two effects considered previously, that is, the presence of AWGN and the quantization errors, are expected to be combined. This can be modeled mathematically by defining an appropriate uncertainty region as

$$\mathcal{R} = \left\{ \Delta = \Delta_1 + \Delta_2 : \|\Delta_1\|_F^2 \leq \epsilon, \quad \begin{aligned} &|\text{Re}\{[\Delta_2]_{ij}\}| \leq \frac{\Delta_q}{2}, \quad |\text{Im}\{[\Delta_2]_{ij}\}| \leq \frac{\Delta_q}{2} \end{aligned} \right\}, \quad (8.99)$$

which is convex because it is described by linear and norm constraints [14]. With this region, the optimization problem (8.86) can be rewritten as the following quadratic convex minimization problem.

$$\begin{aligned} &\underset{t, \Delta_1, \Delta_2}{\text{minimize}} \quad t \\ &\text{subject to} \quad t \geq P_0 \widehat{\mathbf{u}}_i^H (\widehat{\mathbf{H}} + \Delta_1 + \Delta_2)^H (\widehat{\mathbf{H}} + \Delta_1 + \Delta_2) \widehat{\mathbf{u}}_i \quad \forall i \\ &\quad \text{Tr}(\Delta_1^H \Delta_1) \leq \epsilon \\ &\quad |\text{Re}\{[\Delta_2]_{ij}\}| \leq \frac{\Delta_q}{2}, \quad |\text{Im}\{[\Delta_2]_{ij}\}| \leq \frac{\Delta_q}{2}, \end{aligned} \quad (8.100)$$

which comprises the previous uncertainty regions and the corresponding optimization problems as particular cases.

Figure 8.9 illustrates the shape of the three considered uncertainty regions for the concrete case of a scalar error Δ , where $\Delta_r = \text{Re}\{\Delta\}$ and $\Delta_i = \text{Im}\{\Delta\}$.

8.5.6 Numerical results

This section provides some numerical results to illustrate the performance of the proposed robust design when compared to other known transmission techniques.

The robust design takes into account the uncertainty in the channel knowledge to find an optimum power distribution among the estimated eigenmodes. When the channel estimate is perfect, the robust solution must lead to the same power distribution as for the nonrobust

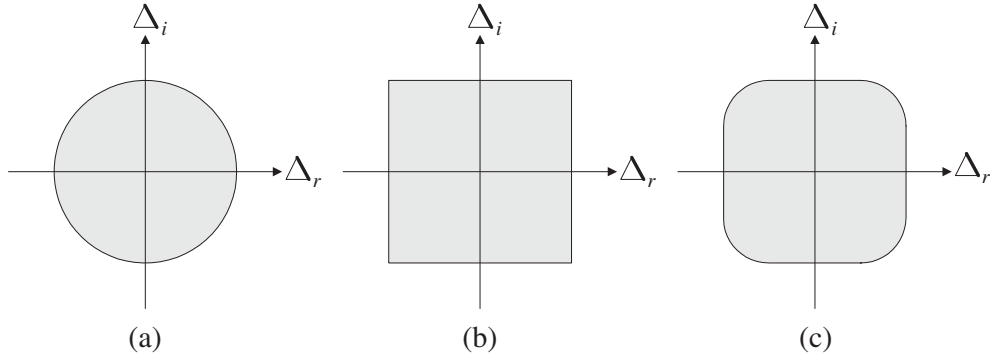


Figure 8.9 Different uncertainty regions for the case of a scalar error Δ , where $\Delta_r = \text{Re}\{\Delta\}$ and $\Delta_i = \text{Im}\{\Delta\}$. (a) estimation Gaussian noise, (b) quantization errors, and (c) combined estimation and quantization errors.

beamforming. As stated in §8.5.3, the nonrobust design consists in transmitting all the symbols only through the maximum estimated eigenmode, which can be formulated in terms of the power distribution as $p_1 = P_0$, $p_i = 0$, $i = 2, \dots, n_T$, that is, all the power is allocated to the maximum eigenmode. When the channel uncertainty increases, the robust design tends to distribute the power in a more uniform way, increasing the power for the weaker eigenmodes.

In the first example, a system with four transmit and six receive antennas is studied. Spherical uncertainty regions with a radius equal to $\sqrt{\epsilon} = g\|\widehat{\mathbf{H}}\|_F$, $0 < g \leq 1$ are considered. Note that for these uncertainty regions, $\mathbf{H} = \widehat{\mathbf{H}} + \Delta \neq \mathbf{0}$, $\forall \Delta \in \mathcal{R}$. This condition is imposed since, otherwise, the saddle-value would be equal to 0. In Figure 8.10, the spherical uncertainty regions for different sizes are represented. Since $n_T = 4$, the total transmitted power has to be distributed among the four estimated eigenmodes. Figure 8.11 shows the mean value of the normalized robust power distribution given by $\{\gamma_i^*\}$, that is, assuming $P_0 = 1$. As seen, for $g = 0$ the power distribution corresponds to the nonrobust approach, as expected. As g increases, the errors in the channel estimate are higher and the power allocation profile changes so that the power is distributed in a more uniform way.

Figures 8.12 and 8.13 show some simulations results in order to compare three different techniques: the proposed maximin robust approach, the nonrobust technique, and a pure OSTBC in which no CSI is available at the transmitter. The techniques are compared in terms of the minimum required transmitted power so that the resulting SNR is higher than a target $\text{SNR}_0 = 10$ dB for any error in the uncertainty region. These results are given as a function of the estimation and the quantization SNR.

In Figure 8.12, a TDD system has been considered with Gaussian estimation noise and assuming spherical uncertainty regions. The number of antennas is $n_T = 2$, $n_R = 2$ and, therefore, the transmission rate is 1. Two different probabilities of providing the required QoS have been considered: $P_{\text{in}} = 0.6$ and $P_{\text{in}} = 0.85$. As P_{in} increases, more power is

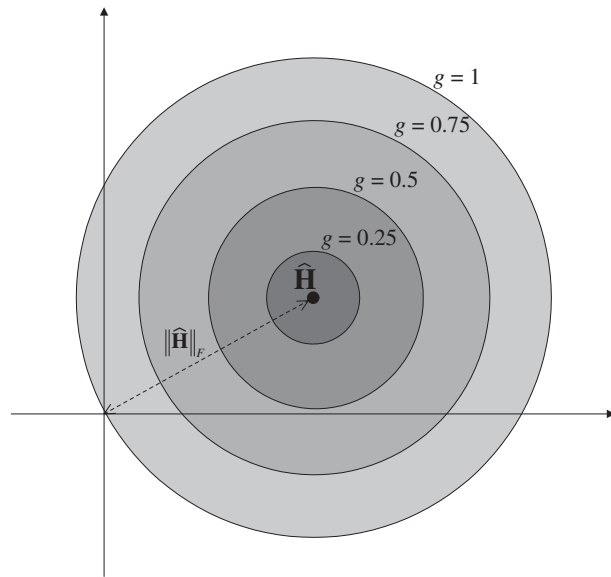


Figure 8.10 Spherical uncertainty regions for different values of the parameter g .

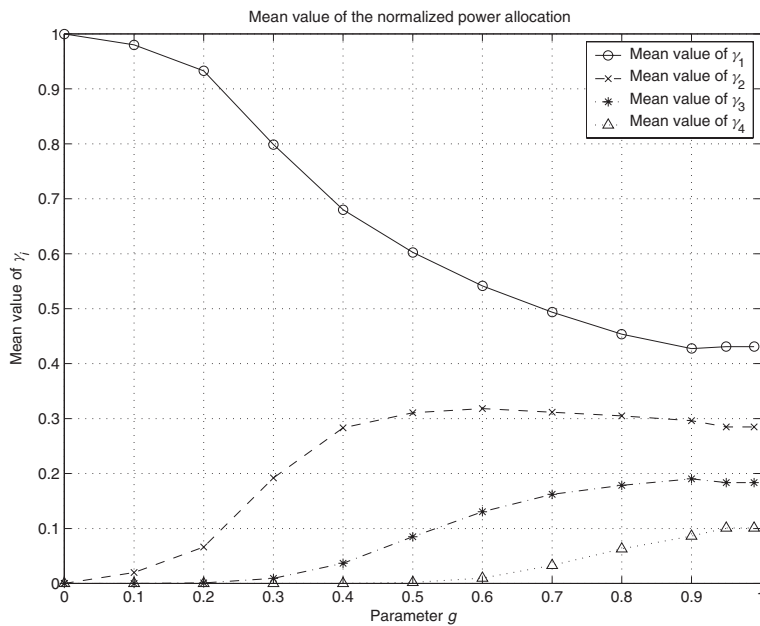


Figure 8.11 Mean value of the normalized robust power distribution for different sizes of the uncertainty regions.

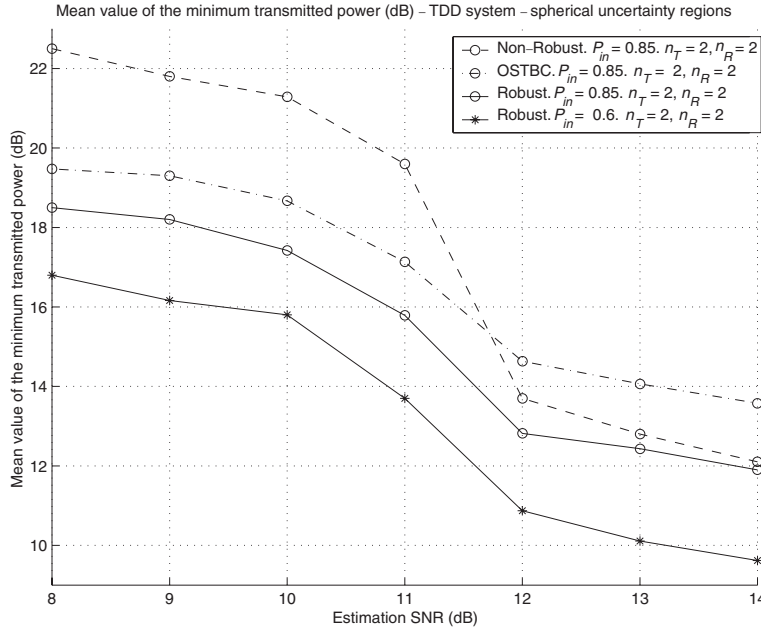


Figure 8.12 Minimum transmitted power in a TDD system assuming spherical uncertainty regions.

necessary since the uncertainty region grows in order to guarantee the required performance with a higher probability. Besides, as the estimation SNR increases, less power is necessary, since the quality of the CSI improves. An interesting conclusion obtained from the figure is that, if the estimation SNR is high enough, the OSTBC technique needs more power than the nonrobust and the robust solutions, since it does not exploit the channel knowledge. On the contrary, if the estimation SNR is low enough, the nonrobust solution may need more power than OSTBC, concluding that in case that the CSI has a very low quality, it is not convenient to exploit that knowledge, unless using the robust solution. Note that, for all the estimation SNR range, the robust technique is the one requiring less power.

Very similar conclusions can be obtained from Figure 8.13 in terms of the quantization SNR. Once again, the robust technique needs less transmitted power than the other ones to fulfill the performance requirements represented by $\text{SNR}_0 = 10$ dB. In the same figure, the performance is also compared for two different antennas configurations: $n_T = 4, n_R = 4$ (rate 3/4) and $n_T = 6, n_R = 6$ (rate 1/2). From the simulations it is concluded that, as expected, increasing the number of antennas implies a reduction in the required transmitted power.

8.6 Summary

This chapter has given an overview of convex optimization theory with emphasis on the art of unveiling the hidden convexity of engineering problems and then has considered

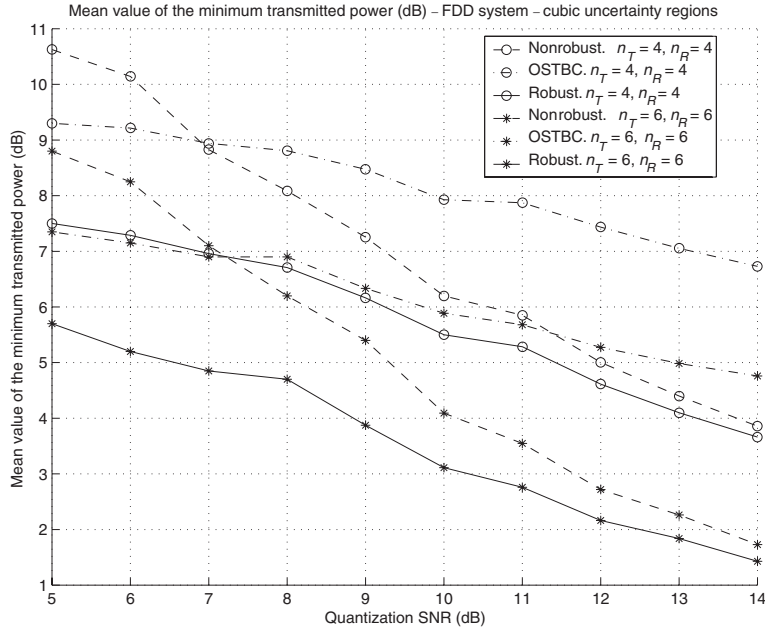


Figure 8.13 Minimum transmitted power in an FDD system assuming cubic uncertainty regions.

the design of linear MIMO transceivers or beamforming under the powerful framework of convex optimization theory.

The design of linear MIMO transceivers is a complicate nonconvex problem with matrix-valued variables. After several manipulations, the problem has been reformulated as a simple convex problem with scalar-valued variables. Then, the theory of convex optimization has been used to derive simple and efficient algorithms to compute the achievable region and, in particular, closed-form solutions have been obtained for the family of Schur-concave/convex functions such as the minimization of the average BER of the system.

Finally, a robust transmission scheme for MIMO channels has been proposed based on this combination of an OSTBC, a power allocation, and a beamforming stage. The design of the power allocation is performed according to an imperfect channel estimate under the maximin philosophy, by which the worst performance is optimized for any error in the channel estimate described by an uncertainty region. The original maximin optimization problem corresponding to the design of the robust power allocation, which consists of two stages (inner and outer optimizations), is first formulated and then is transformed into a simple single-stage convex optimization problem, whose optimal Lagrange multipliers provide the optimum power allocation. For several examples of uncertainty regions, this optimization problem is shown to reduce to a convex quadratic problem.

References

- [1] G. J. Foschini, "Layered space-time architecture for wireless communication in a fading environment when using multi-element antennas," *Bell Labs Tech. J.*, vol. 1, no. 2, pp. 41–59, Autumn 1996.
- [2] G. G. Raleigh and J. M. Cioffi, "Spatio-temporal coding for wireless communication," *IEEE Trans. Commun.*, vol. 46, no. 3, pp. 357–366, Mar. 1998.
- [3] I. E. Telatar, "Capacity of multi-antenna Gaussian channels," *Eur. Trans. Telecommun.*, vol. 10, no. 6, pp. 585–595, Nov.-Dec. 1999.
- [4] G. Foschini and M. Gans, "On limits of wireless communications in a fading environment when using multiple antennas," *Wireless Pers. Commun.*, vol. 6, pp. 311–335, 1998.
- [5] M. L. Honig, K. Steiglitz, and B. Gopinath, "Multichannel signal processing for data communications in the presence of crosstalk," *IEEE Trans. Commun.*, vol. 38, no. 4, pp. 551–558, Apr. 1990.
- [6] A. Scaglione, G. B. Giannakis, and S. Barbarossa, "Redundant filterbank precoders and equalizers Part I: Unification and optimal designs," *IEEE Trans. Signal Process.*, vol. 47, no. 7, pp. 1988–2006, Jul. 1999.
- [7] H. Bölcseki and A. J. Paulraj, "Multiple-input multiple-output (MIMO) wireless systems," in *The Communications Handbook*, 2nd ed., J. Gibson, Ed. CRC Press, 2002, pp. 90.1–90.14.
- [8] K. Miettinen, *Multi-Objective Optimization*. Kluwer Academic Publishers, 1999.
- [9] C. E. Shannon, "A mathematical theory of communication," *Bell Syst. Tech. J.*, vol. 27, pp. 379–423, 623–656, July-Oct. 1948.
- [10] T. M. Cover and J. A. Thomas, *Elements of Information Theory*. New York: Wiley, 1991.
- [11] S. M. Alamouti, "A simple transmit diversity technique for wireless communications," *IEEE J. Sel. Areas Commun.*, vol. 16, no. 8, pp. 1451–1458, Oct. 1998.
- [12] V. Tarokh, N. Seshadri, and A. R. Calderbank, "Space-time codes for high data rate wireless communications: Performance criterion and code construction," *IEEE Trans. Inf. Theory*, vol. 44, no. 2, pp. 744–765, Mar. 1998.
- [13] D. P. Bertsekas, *Nonlinear Programming*, 2nd ed. Belmont, MA: Athena Scientific, 1999.
- [14] S. Boyd and L. Vandenberghe, *Convex Optimization*. Cambridge University Press, 2004.
- [15] D. P. Palomar, J. M. Cioffi, and M. A. Lagunas, "Joint Tx-Rx beamforming design for multicarrier MIMO channels: A unified framework for convex optimization," *IEEE Trans. Signal Process.*, vol. 51, no. 9, pp. 2381–2401, Sept. 2003.
- [16] D. P. Palomar, M. A. Lagunas, and J. M. Cioffi, "Optimum linear joint transmit-receive processing for MIMO channels with QoS constraints," *IEEE Trans. Signal Process.*, vol. 52, no. 5, pp. 1179–1197, May 2004.
- [17] D. P. Palomar, "A unified framework for communications through MIMO channels," Ph.D. dissertation, Technical University of Catalonia (UPC), Barcelona, Spain, May 2003.
- [18] R. T. Rockafellar, *Convex Analysis*, 2nd ed. Princeton, NJ: Princeton Univ. Press, 1970.
- [19] D. G. Luenberger, *Optimization by Vector Space Methods*. New York: Wiley, 1969.
- [20] R. T. Rockafellar, "Lagrange multipliers and optimality," *SIAM Rev.*, vol. 35, no. 2, pp. 183–238, 1993.
- [21] M. S. Lobo, L. Vandenberghe, S. Boyd, and H. Lebret, "Applications of second-order cone programming," *Linear Algebra Appl.*, vol. 284, no. 1–3, pp. 193–228, Jul. 1998.

- [22] L. Vandenberghe and S. Boyd, "Semidefinite programming," *SIAM Rev.*, vol. 38, no. 1, pp. 49–95, Mar. 1996.
- [23] A. Ben-Tal and A. Nemirovski, *Lectures on Modern Convex Optimization: Analysis, Algorithms, and Engineering Applications*. Society for Industrial and Applied Mathematics, 2001.
- [24] Y. Nesterov and A. Nemirovski, "Interior-point polynomial algorithms in convex programming," *SIAM Stud. Appl. Math.*, vol. 13, 1994.
- [25] J. F. Sturm, "Using sedumi 1.02, a MATLAB toolbox for optimization over symmetric cones," *Optimiz. Methods Softw.*, vol. 11–12, pp. 625–653, 1999.
- [26] J.-L. Goffin and J.-P. Vial, "Convex nondifferentiable optimization: A survey focussed on the analytic center cutting plane method," Department of Management Studies, University of Geneva, Switzerland, Tech. Rep., Feb. 1999.
- [27] Z.-Q. Luo, "Applications of convex optimization in signal processing and digital communication," *Math. Program., Ser. B*, vol. 97, no. 1–2, pp. 177–207, Jul. 2003.
- [28] H. Lebret and S. Boyd, "Antenna array pattern synthesis via convex optimization," *IEEE Trans. Signal Process.*, vol. 45, no. 3, pp. 526–532, Mar. 1997.
- [29] S.-P. Wu, S. Boyd, and L. Vandenberghe, "FIR filter design via spectral factorization and convex optimization," in *Applied and Computational Control, Signals and Circuits*, vol. 1, ch. 5, B. Datta, Ed. Boston, MA: Birkhauser, 1999, pp. 215–245.
- [30] T. N. Davidson, Z.-Q. Luo, and J. F. Sturm, "Linear matrix inequality formulation of spectral mask constraints with applications to FIR filter design," *IEEE Trans. Signal Process.*, vol. 50, no. 11, pp. 2702–2715, Nov. 2002.
- [31] R. A. Monzingo and T. W. Miller, *Introduction to Adaptive Arrays*. New York: Wiley, 1980.
- [32] R. Lorenz and S. P. Boyd, "Robust minimum variance beamforming," *IEEE Trans. Signal Process.*, vol. 53, no. 5, May 2005.
- [33] S. A. Vorobyov, A. B. Gershman, and Z.-Q. Luo, "Robust adaptive beamforming using worst-case performance optimization: A solution to the signal mismatch problem," *IEEE Trans. Signal Process.*, vol. 51, no. 2, pp. 313–324, Feb. 2003.
- [34] J. Li, P. Stoica, and Z. Wang, "On robust Capon beamforming and diagonal loading," *IEEE Trans. Signal Process.*, vol. 51, no. 7, pp. 1702–1715, Jul. 2003.
- [35] S. Shahbazpanahi, A. B. Gershman, Z.-Q. Luo, and K. M. Wong, "Robust adaptive beamforming for general-rank signal models," *IEEE Trans. Signal Process.*, vol. 51, no. 9, pp. 2257–2269, Sept. 2003.
- [36] M. Bengtsson and B. Ottersten, "Optimal and suboptimal transmit beamforming," in *Handbook of Antennas in Wireless Communications*, L. C. Godara, Ed. Boca Raton, FL: CRC Press, 2001.
- [37] C. E. Shannon, "Coding theorems for a discrete source with a fidelity criterion," *IRE Nat. Conv. Rec.*, vol. 7 (Part 4), pp. 142–163, Mar. 1959.
- [38] M. Chiang and S. Boyd, "Geometric programming duals of channel capacity and rate distortion," *IEEE Trans. Inf. Theory*, vol. 50, no. 2, pp. 245–258, Feb. 2004.
- [39] L. Xiao, M. Johansson, and S. Boyd, "Simultaneous routing and resource allocation via dual decomposition," *IEEE Trans. Commun.*, vol. 52, no. 7, pp. 1136–1144, Jul. 2004.
- [40] S. H. Low, L. L. Peterson, and L. Wang, "Understanding vegas: A duality model," *J. ACM*, vol. 49, no. 2, pp. 207–235, Mar. 2002.
- [41] M. Chiang, "To layer or not to layer: balancing transport and physical layers in wireless multihop networks," in *Proceedings of IEEE INFOCOM*, Hong Kong, China, Mar. 2004.
- [42] W. Yu, W. Rhee, S. Boyd, and J. M. Cioffi, "Iterative water-filling for Gaussian vector multiple-access channels," *IEEE Trans. Inf. Theory*, vol. 50, no. 1, pp. 145–152, Jan. 2004.

- [43] D. P. Bertsekas and J. N. Tsitsiklis, *Parallel and Distributed Computation: Numerical Methods*. Prentice Hall, 1989.
- [44] A. W. Marshall and I. Olkin, *Inequalities: Theory of Majorization and Its Applications*. New York: Academic Press, 1979.
- [45] Z.-Q. Luo, T. N. Davidson, G. B. Giannakis, and K. M. Wong, "Transceiver optimization for block-based multiple access through ISI channels," *IEEE Trans. Signal Process.*, vol. 52, no. 4, pp. 1037–1052, Apr. 2004.
- [46] F. D. Neeser and J. L. Massey, "Proper complex random processes with applications to information theory," *IEEE Trans. Inf. Theory*, vol. 39, no. 4, pp. 1293–1302, Jul. 1993.
- [47] B. Picinbono, "On circularity," *IEEE Trans. Signal Process.*, vol. 42, no. 12, pp. 3473–3482, Dec. 1994.
- [48] B. Picinbono and P. Chevalier, "Widely linear estimation with complex data," *IEEE Trans. Signal Process.*, vol. 43, no. 8, pp. 2030–2033, Aug. 1995.
- [49] P. J. Schreier and L. L. Scharf, "Second-order analysis of improper complex random vectors and processes," *IEEE Trans. Signal Process.*, vol. 51, no. 3, pp. 714–725, Mar. 2003.
- [50] S. Benedetto and E. Biglieri, *Principles of Digital Transmission: with Wireless Applications*. New York: Kluwer Academic, 1999.
- [51] S. Verdú, *Multiuser Detection*. New York: Cambridge University Press, 1998.
- [52] K. Cho and D. Yoon, "On the general BER expression of one- and two-dimensional amplitude modulations," *IEEE Trans. Commun.*, vol. 50, no. 7, pp. 1074–1080, Jul. 2002.
- [53] H. V. Poor and S. Verdú, "Probability of error in MMSE multiuser detection," *IEEE Trans. Inf. Theory*, vol. 43, no. 3, pp. 858–871, May 1997.
- [54] D. P. Palomar, M. Bengtsson, and B. Ottersten, "Minimum BER linear transceivers for MIMO channels via primal decomposition," *accepted in IEEE Trans. Signal Process.*, to appear 2005.
- [55] S. M. Kay, *Fundamentals of Statistical Signal Processing: Estimation Theory*. Englewood Cliffs, NJ: Prentice Hall, 1993.
- [56] K. H. Lee and D. P. Petersen, "Optimal linear coding for vector channels," *IEEE Trans. Commun.*, vol. COM-24, no. 12, pp. 1283–1290, Dec. 1976.
- [57] J. Salz, "Digital transmission over cross-coupled linear channels," *At&T Tech. J.*, vol. 64, no. 6, pp. 1147–1159, Jul.–Aug. 1985.
- [58] J. Yang and S. Roy, "On joint transmitter and receiver optimization for multiple-input-multiple-output (MIMO) transmission systems," *IEEE Trans. Commun.*, vol. 42, no. 12, pp. 3221–3231, Dec. 1994.
- [59] H. Sampath, P. Stoica, and A. Paulraj, "Generalized linear precoder and decoder design for MIMO channels using the weighted MMSE criterion," *IEEE Trans. Commun.*, vol. 49, no. 12, pp. 2198–2206, Dec. 2001.
- [60] J. Yang and S. Roy, "Joint transmitter-receiver optimization for multi-input multi-output systems with decision feedback," *IEEE Trans. Inf. Theory*, vol. 40, no. 5, pp. 1334–1347, Sept. 1994.
- [61] E. N. Onggosanusi, A. M. Sayeed, and B. D. V. Veen, "Efficient signaling schemes for wide-band space-time wireless channels using channel state information," *IEEE Trans. Veh. Technol.*, vol. 52, no. 1, pp. 1–13, Jan. 2003.
- [62] Y. Ding, T. N. Davidson, Z.-Q. Luo, and K. M. Wong, "Minimum BER block precoders for zero-forcing equalization," *IEEE Trans. Signal Process.*, vol. 51, no. 9, pp. 2410–2423, Sept. 2003.
- [63] J. M. Cioffi, G. P. Dudevoir, M. V. Eyuboglu, and G. D. Forney, "MMSE decision-feedback equalizers and coding - Parts I-II: Equalization results and coding results," *IEEE Trans. Commun.*, vol. 43, no. 10, pp. 2582–2604, Oct. 1995.

- [64] P. Viswanath and V. Anantharam, "Optimal sequences and sum capacity of synchronous CDMA systems," *IEEE Trans. Inf. Theory*, vol. 45, no. 6, pp. 1984–1991, Sept. 1999.
- [65] A. Pascual-Iserte, A. I. Pérez-Neira, and M. A. Lagunas, "On power allocation strategies for maximum signal to noise and interference ratio in an OFDM-MIMO system," *IEEE Trans. Wireless Commun.*, vol. 3, no. 3, pp. 808–820, May 2004.
- [66] K. Zhou, J. C. Doyle, and K. Glover, *Robust and Optimal Control*. Upper Saddle River, NJ: Prentice-Hall, 1996.
- [67] B. Hassibi, A. H. Sayed, and T. Kailath, *Indefinite Quadratic Estimation and Control: A Unified Approach to \mathcal{H}_2 and \mathcal{H}_∞ Theories*. Philadelphia, PA: SIAM, 1999.
- [68] S. Zhou and G. B. Giannakis, "How accurate channel prediction needs to be for transmit-beamforming with adaptive modulation over Rayleigh MIMO channels?" *IEEE Trans. Wireless Commun.*, vol. 3, no. 4, pp. 1285–1294, July 2004.
- [69] J. Choi, "Performance analysis for transmit antenna diversity with/without channel information," *IEEE Trans. Veh. Technol.*, vol. 51, no. 1, pp. 101–113, Jan. 2002.
- [70] J. Choi, "Performance limitation of closed-loop transmit antenna diversity over fast rayleigh fading channels," *IEEE Trans. Veh. Technol.*, vol. 51, no. 4, pp. 771–775, Jul. 2002.
- [71] A. Narula, M. J. Lopez, M. D. Trot, and G. W. Wornell, "Efficient use of side information in multiple-antenna data transmission over fading channels," *IEEE J. Sel. Areas Commun.*, vol. 16, no. 8, pp. 1423–1436, Oct. 1998.
- [72] A. Wittneben, "Optimal predictive TX combining diversity in correlated fading for microcellular mobile radio applications," in *Proceedings of the IEEE Global Telecommunications Conference (GLOBECOM 1995)*, pp. 13–17, Nov. 1995.
- [73] A. Pascual-Iserte, A. I. Pérez-Neira, and M. A. Lagunas, "Exploiting transmission spatial diversity in frequency selective systems with feedback channel," in *Proceedings of the IEEE International Conference on Acoustics, Speech, and Signal Processing (ICASSP 2003)*, vol. 4, pp. 85–88, April 2003.
- [74] G. Jöngren, M. Skoglund, and B. Ottersen, "Combining beamforming and orthogonal space-time block coding," *IEEE Trans. Inf. Theory*, vol. 48, no. 3, pp. 611–627, Mar. 2002.
- [75] S. Zhou and G. B. Giannakis, "Optimal transmitter eigen-beamforming and space-time block coding based on channel mean feedback," *IEEE Trans. Signal Process.*, vol. 50, no. 10, pp. 2599–2613, Oct. 2002.
- [76] F. Rey, M. Lamarca, and G. Vázquez, "Transmit filter optimization based on partial CSI knowledge for wireless applications," in *Proceedings IEEE 2003 International Conference on Communications (ICC 2003)*, vol. 4, pp. 2567–2571, Anchorage, AK, May 11–15, 2003.
- [77] P. Xia, S. Zhou, and G. B. Giannakis, "Adaptive MIMO-OFDM based on partial channel state information," *IEEE Trans. Signal Process.*, vol. 52, no. 1, pp. 202–213, Jan. 2004.
- [78] S. A. Kassam and H. V. Poor, "Robust techniques for signal processing: A survey," *Proc. IEEE*, vol. 73, no. 3, pp. 433–481, Mar. 1985.
- [79] S. Verdú and V. Poor, "On minimax robustness: A general approach and applications," *IEEE Trans. Inf. Theory*, vol. 30, no. 2, pp. 328–340, Mar. 1984.
- [80] P. Stoica, Z. Wang, and J. Li, "Robust Capon beamforming," *IEEE Signal Process. Lett.*, vol. 10, no. 6, pp. 172–175, Jun. 2003.
- [81] M. Bengtsson and B. Ottersten, "Optimal downlink beamforming using semidefinite optimization," in *Proceedings of the 37th Annual Allerton Conference on Communications, Control, and Computing*, pp. 987–996, Sept. 1999.
- [82] M. Biguesh, S. Shahbazpanahi, and A. B. Gershman, "Robust power adjustment for transmit beamforming in cellular communications systems," in *Proceedings of the IEEE International*

- Conference on Acoustics, Speech, and Signal Processing (ICASSP 2003)*, vol. 5, pp. 105–108, April 2003.
- [83] A. Pascual-Iserte, A. I. Pérez-Neira, and M. A. Lagunas, “A maximin approach for robust MIMO design: Combining OSTBC and beamforming with minimum transmission power requirements,” in *Proceedings of the IEEE International Conference on Acoustics, Speech, and Signal Processing (ICASSP 2004)*, vol. 2, pp. 1–4, May 2004.
 - [84] B. Hassibi and B. M. Hochwald, “High-rate codes that are linear in space and time,” *IEEE Trans. Inf. Theory*, vol. 48, no. 7, pp. 1804–1824, Jul. 2002.
 - [85] G. Ganesan and P. Stoica, “Space-time block codes: A maximum SNR approach,” *IEEE Trans. Inf. Theory*, vol. 47, no. 4, pp. 1650–1656, May 2001.
 - [86] V. Tarokh, H. Jafarkhani, and A. R. Calderbank, “Space-time block codes from orthogonal designs,” *IEEE Trans. Inf. Theory*, vol. 45, no. 5, pp. 1456–1467, Jul. 1999.
 - [87] E. G. Larsson and P. Stoica, *Space-Time Block Coding for Wireless Communications*. Cambridge University Press, 2003.
 - [88] S. Zhou and G. B. Giannakis, “Optimal transmitter eigen-beamforming and space-time block coding based on channel correlations,” *IEEE Trans. Inf. Theory*, vol. 49, no. 7, pp. 1673–1690, Jul. 2003.
 - [89] R. T. Rockafellar, “Saddle-points and convex analysis,” in *Differential Games and Related Topics*, H. W. Kuhn and G. P. Szego, Eds. North-Holland, 1971, pp. 109–127.
 - [90] S. Žaković and C. Pantelides, “An interior point method algorithm for computing saddle points of constrained continuous minimax,” *Ann. Oper. Res.*, vol. 99, pp. 59–77, Dec. 2000.

9

MIMO Communications with Partial Channel State Information

Shengli Zhou and Georgios B. Giannakis

9.1 Introduction

Optimal transmitter designs obeying the water-filling principle are well-documented and widely applied when the propagation channel is deterministically known and regularly updated at the transmitter. Albeit reasonable for wireline links, adaptive transmissions based on perfect channel state information (CSI) in wireless systems can be justified only when the channel fading is sufficiently slow. On the other hand, the proliferation of space-time (ST) coding research we have witnessed lately testifies to the efforts put toward the other extreme: nonadaptive (and thus conservative) designs requiring no CSI to be available at the transmitter. As no-CSI leads to robust but rather pessimistic designs, and perfect-CSI is probably a utopia for most wireless links, recent efforts geared toward quantification and exploitation of partial CSI promise to have great practical value not only because they are capable of offering a “jack of both trades” but also because they encompass the perfect-CSI and no-CSI paradigms.

This chapter highlights recent advances on multiinput multioutput (MIMO) communications based on partial CSI from both information- and communication-theoretic perspectives. After summarizing commonly used partial CSI models, we first investigate the impact partial CSI has on MIMO capacity. We then focus on practical constructions of adaptive transmitters based on partial CSI, which either improve the system error performance for a given transmission rate or enhance the system throughput for a target error performance.

9.2 Partial CSI Models

As depicted in Fig. 9.1, we consider a system with N_t transmit- and N_r receive- antennas, operating over frequency-flat fading channels. Let $h_{\nu\mu}$ denote the channel coefficient from

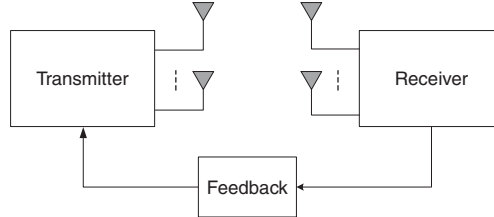


Figure 9.1 The MIMO system with channel feedback

the μ th transmit antenna to the ν th receive antenna. Corresponding to each receive antenna ν , we define the $N_t \times 1$ vector¹ $\mathbf{h}_\nu := [h_{\nu 1}, \dots, h_{\nu N_t}]^T$. We then concatenate \mathbf{h}_ν 's into a composite channel vector of length $N_t N_r$ as

$$\mathbf{h} = \begin{bmatrix} \mathbf{h}_1 \\ \vdots \\ \mathbf{h}_{N_r} \end{bmatrix}. \quad (9.1)$$

The receiver estimates the channel \mathbf{h} and then feeds relevant information back to the transmitter through a feedback channel. In the ideal case with perfect CSI, the transmitter knows each realization of \mathbf{h} deterministically.

For most wireless links, however, communication with perfect CSI is probably a utopia, owing to imperfections originating from various sources such as estimation errors, quantization effects, feedback delay and feedback errors. Modeling and exploiting imperfect, or partial, channel knowledge is thus important for practical systems.

Partial CSI can be modeled in different ways. We next describe two commonly used approaches.

9.2.1 Statistical models

Since deterministic knowledge of \mathbf{h} is not available with partial CSI, the transmitter views the channel as being random with statistics dictated by the feedback information. Let us denote the conceived random channel vector at the transmitter as $\check{\mathbf{h}}$ to differentiate it from the true channel \mathbf{h} (obviously, $\check{\mathbf{h}}$ and \mathbf{h} have quite different statistics, since the statistics of $\check{\mathbf{h}}$ change every time new feedback information becomes available). The *statistical distribution* of $\check{\mathbf{h}}$ constitutes the partial CSI the transmitter can utilize.

One widely used distribution is the Gaussian, which is described only through first- and second-order statistics. Specifically, the transmitter models $\check{\mathbf{h}}$ as Gaussian distributed

$$\check{\mathbf{h}} \sim \mathcal{CN}(\bar{\mathbf{h}}, \Sigma_h), \quad (9.2)$$

¹We use the following notational conventions in this chapter. Bold upper- and lowercase letters denote matrices and column vectors, respectively; $\|\cdot\|$ denotes the vector 2-norm; $\|\cdot\|_F$ denotes the Frobenius norm of a matrix; $|\cdot|$ denotes the absolute value of a scalar and the determinant of a matrix; $\text{tr}\{\cdot\}$ denotes the trace; $(\cdot)^*$, $(\cdot)^T$, and $(\cdot)^\mathcal{H}$ stand for conjugate, transpose, and Hermitian transpose, respectively; $E\{\cdot\}$ denotes expectation; $E_A\{\cdot\}$ denotes expectation with respect to variable A ; \mathbf{I}_N stands for an identity matrix of size N , and $\mathbf{0}_{M \times N}$ for an $M \times N$ all zero matrix; $[\mathbf{A}]_{i,j}$ stands for the (i, j) th entry of \mathbf{A} ; \mathcal{C}^N stands for the N -dimensional complex vector space; and $\mathcal{CN}(\mathbf{b}, \Sigma)$ denotes the circularly symmetric complex Gaussian distribution with mean \mathbf{b} and covariance Σ .

where $\bar{\mathbf{h}}$ is the mean and Σ_h is the covariance when conditioned on the received feedback. When $\Sigma_h = \mathbf{0}$, the channel uncertainty disappears, and perfect CSI $\check{\mathbf{h}} = \bar{\mathbf{h}}$ is obtained. The Gaussian assumption may not be always satisfied in practice but greatly simplifies the system design, which also provides valuable insight on transmitter optimization based on partial CSI.

The Gaussian model in Eq. (9.2) assumes arbitrary mean and covariance. We next specify two simplified models, termed as *mean feedback* and *covariance feedback* [25, 32], respectively.

Mean feedback

In mean feedback, the channel covariance matrix is assumed to be proportional to an identity matrix as:

$$\check{\mathbf{h}} \sim \mathcal{CN}(\bar{\mathbf{h}}, \sigma_\epsilon^2 \mathbf{I}_{N_t N_r}), \quad (9.3)$$

where σ_ϵ^2 is the variance for each entry of $\check{\mathbf{h}}$. Let us now look at an example where the mean-feedback model fits nicely.

Example 1 (delayed feedback): We consider an application scenario where

- i) the antennas are well separated, so that the channel coefficients are independent and identically distributed (i.i.d.), as $\mathbf{h} \sim \mathcal{CN}(\mathbf{0}_{N_t N_r \times 1}, \sigma_h^2 \mathbf{I}_{N_t N_r})$;
- ii) the channel coefficients are slowly time varying according to Jakes' model with Doppler frequency f_d ; and,
- iii) the channel is acquired perfectly at the receiver and is fed back to the transmitter via a noiseless channel, which introduces a delay τ .

Assume that the receiver feeds back the estimated channel $\hat{\mathbf{h}}_f$. Notice that both \mathbf{h} and $\hat{\mathbf{h}}_f$ are complex Gaussian vectors, drawn from the same random process. Thus, \mathbf{h} and $\hat{\mathbf{h}}_f$ are jointly Gaussian with $E\{\mathbf{h}\hat{\mathbf{h}}_f^\mathcal{H}\} = \rho \sigma_h^2 \mathbf{I}_{N_t N_r}$, where

$$\rho := J_0(2\pi f_d \tau) \quad (9.4)$$

is the correlation coefficient and $J_0(\cdot)$ is the zero-order Bessel function of the first kind. The minimum mean square error (MMSE) estimator of \mathbf{h} based on $\hat{\mathbf{h}}_f$ is given by $E\{\mathbf{h}|\hat{\mathbf{h}}_f\} = \rho \hat{\mathbf{h}}_f$, with estimation error having covariance matrix $\sigma_h^2(1 - |\rho|^2) \mathbf{I}_{N_t N_r}$. For each realization of $\hat{\mathbf{h}}_f = \hat{\mathbf{h}}_{f,0}$, the transmitter obtains the following parameters in the mean feedback model.

$$\bar{\mathbf{h}} = \rho \hat{\mathbf{h}}_{f,0}, \quad \sigma_\epsilon^2 = \sigma_h^2(1 - |\rho|^2). \quad (9.5)$$

The values of $\bar{\mathbf{h}}$ are updated when the next feedback becomes available. ■

In the delayed feedback model, a single parameter ρ compactly represents the feedback quality. When $\rho = 0$, there is no useful instantaneous CSI, while when $\rho = 1$ the transmitter has perfect CSI with no ambiguity. Varying ρ between the two extreme cases $\rho = 0$ and $\rho = 1$, various degrees of partial CSI can be conveniently modeled. We will use this delayed feedback model for numerical results on mean feedback.

Aiming to track the instantaneous channel value, mean feedback is suitable for slowly time-varying channels, in contrast to the case of covariance feedback that follows.

Covariance feedback

In covariance feedback, we assume that the channel \mathbf{h} varies too rapidly for the transmitter to track its instantaneous value. In this case, the channel mean is set to zero, and the relative geometry of the propagation paths manifests itself in a nonwhite covariance matrix Σ_h . In this case, (9.2) simplifies to

$$\check{\mathbf{h}} \sim \mathcal{CN}(\mathbf{0}_{N_t N_r \times 1}, \Sigma_h). \quad (9.6)$$

Matrix Σ_h is invariant as long as the channel remains wide-sense stationary, which implies that this form of partial CSI only needs to be updated infrequently.

Through field measurements, ray-tracing simulations, or using physical channel models, the transmitter can acquire such statistical CSI a priori. For certain applications such as fixed wireless, the spatial fading correlations can be determined from physical parameters such as antenna spacing, antenna arrangement, angle of arrival, and angle spread. Alternatively, the receiver can estimate the channel correlations by long-term time averaging of the channel realizations and feed them back reliably to the transmitter through a low data rate feedback channel. In applications involving Time Division Duplex (TDD) protocols, the transmitter can also obtain channel statistics directly since the forward and backward channels share the same physical (and statistically invariant) channel characteristics, even when the time separation between the forward and the backward link is long enough to render the deterministic instantaneous channel estimates outdated. In Frequency Division Duplex (FDD) systems with small angle spread, the downlink channel covariance estimates can be also obtained accurately from the uplink channel covariance through proper frequency calibration processing [18].

Equation (9.6) specifies a general correlation matrix Σ_h for covariance feedback. The correlation matrix Σ_h , however, is highly structured in a number of applications.

Example 2 Consider a scenario where

- i) the transmit-correlation matrix corresponding to each receive antenna is the same; that is, $\Sigma_t = E\{\mathbf{h}_v \mathbf{h}_v^H\}$, $\forall v$; and,
- ii) the receive-correlation matrix corresponding to each transmit antenna is the same; that is, $\Sigma_r = E\{\tilde{\mathbf{h}}_\mu \tilde{\mathbf{h}}_\mu^H\}$, $\forall \mu$, where $\tilde{\mathbf{h}}_\mu := [h_{1\mu}, \dots, h_{N_r\mu}]^T$.

In this case, the correlation matrix Σ_h has the nice structure as

$$\Sigma_h = \Sigma_r \otimes \Sigma_t, \quad (9.7)$$

where \otimes stands for Kronecker's product. This model has been widely used in the literature and been verified through field measurements for some practical MIMO setups, see, for example, [16, 10]. The limitations of this model were pointed out recently in [26]. ■

9.2.2 Finite-rate feedback model

Another very practical way of modeling partial CSI is to directly impose a bandwidth constraint on the feedback channel. For example, the feedback channel is only able to communicate a finite number of (say, B) feedback bits, as depicted in Fig. 9.2.

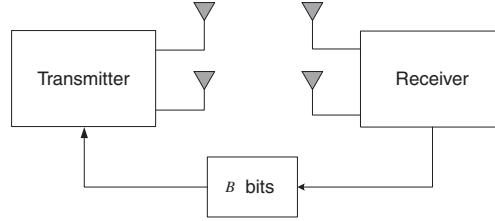


Figure 9.2 The MIMO system with finite rate feedback

Naturally, finite-rate feedback is linked to vector quantization, since with B feedback bits, the receiver can feed back only $N = 2^B$ different channel representations (codewords). This implies that the channel space at the receiver is partitioned in N nonoverlapping regions, with each region represented by a distinct codeword. Partial CSI through finite-rate feedback corresponds to informing the transmitter which region the current channel belongs to.

Responding to the finite-rate feedback, the transmitter switches to a desirable transmission mode, where each transmission mode consists of a collection of different transmission parameters corresponding to transmission power, constellation size, and space-time coding formats. With B feedback bits, the transmitter only needs to construct a total of N transmission modes.

Transceiver design based only on finite-rate feedback has been considered from a broad range of perspectives, as we will see later on. The design process is in general complex. With a given performance metric, one has to perform two design tasks jointly:

- i) partitioning the channel space into N nonoverlapping regions, with each region associated with one index represented by B bits; and,
- ii) selecting a proper transmission mode for each partitioned channel region.

9.3 Capacity-Optimal Designs

In this section, we investigate MIMO communications with partial CSI from an information-theoretic perspective. We will develop capacity-optimal transmissions under different partial CSI forms.

Let x_μ denote the transmitted symbol from the μ th transmit antenna, and y_v the received symbol at the v th receive antenna. Define $\mathbf{x} := [x_1, \dots, x_{N_t}]^T$ and $\mathbf{y} := [y_1, \dots, y_{N_r}]^T$. For the MIMO system depicted in Fig. 9.1, the channel input–output relationship is:

$$\mathbf{y} = \mathbf{H}\mathbf{x} + \mathbf{v}, \quad (9.8)$$

where the channel matrix \mathbf{H} is of size $N_r \times N_t$ with entries $[\mathbf{H}]_{v,\mu} = h_{v\mu}$, and \mathbf{v} denoting additive white Gaussian noise with zero mean and covariance $N_0\mathbf{I}_{N_r}$. The channel matrix \mathbf{H} and the channel vector \mathbf{h} in (9.1) are linked as follows.

$$\mathbf{h} = \text{vec}(\mathbf{H}^T), \quad \mathbf{H} = [\mathbf{T}_1\mathbf{h}, \dots, \mathbf{T}_{N_t}\mathbf{h}], \quad (9.9)$$

where vec denotes the column-stacking operator, and \mathbf{T}_i is a $N_r \times N_t N_r$ selection matrix with entries $[\mathbf{T}_i]_{j,i+(j-1)N_t} = 1$, $\forall j \in [1, N_r]$, and zero otherwise.

With perfect CSI at the receiver side, the mutual information between the input \mathbf{x} and the output \mathbf{y} is maximized when \mathbf{x} is zero-mean Gaussian distributed [31]. For a Gaussian input with covariance matrix $\mathbf{R}_x := \text{E}\{\mathbf{x}\mathbf{x}^H\}$, the mutual information conditioned on each realization of \mathbf{H} is [31]:

$$I(\mathbf{x}; \mathbf{y}|\mathbf{H}, \mathbf{R}_x) = \log_2 \left| \mathbf{I}_{N_r} + \frac{1}{N_0} \mathbf{H} \mathbf{R}_x \mathbf{H}^H \right|. \quad (9.10)$$

On the basis of this expression, we next derive capacity-optimal transmissions based on partial CSI.

9.3.1 Capacity optimization with statistical CSI

With statistical CSI as in (9.2), the transmitter deals with a random channel $\check{\mathbf{h}}$, from which we define the matrix channel

$$\check{\mathbf{H}} = [\mathbf{T}_1 \check{\mathbf{h}}, \dots, \mathbf{T}_{N_t} \check{\mathbf{h}}]. \quad (9.11)$$

Hence, the mutual information $I(\mathbf{x}; \mathbf{y}|\check{\mathbf{H}}, \mathbf{R}_x)$ is a random variable. A good performance measure will be the expected mutual information averaged over all possible realizations of $\check{\mathbf{h}}$. The maximum average mutual information optimized over the input-covariance matrix yields the average capacity conditioned on statistical CSI:

$$C(\bar{\mathbf{h}}, \Sigma_h) = \max_{\mathbf{R}_x; \text{tr}(\mathbf{R}_x)=P_0} \text{E}_{\check{\mathbf{h}}} \{ I(\mathbf{x}; \mathbf{y}|\check{\mathbf{H}}, \mathbf{R}_x) \}, \quad (9.12)$$

where P_0 is the total transmit-power. Notice that we use $C(\bar{\mathbf{h}}, \Sigma_h)$ to signify the dependence of the average capacity C on partial CSI. In a transmission with infinite block length, $C(\bar{\mathbf{h}}, \Sigma_h)$ would indicate the maximum achievable rate for the portion of transmission whose available CSI at the transmitter is $(\bar{\mathbf{h}}, \Sigma_h)$.

The optimal input covariance can then be found as the solution of the following optimization problem:

$$\mathbf{R}_{x,\text{opt}} = \arg \max_{\mathbf{R}_x; \text{tr}(\mathbf{R}_x)=P_0} \text{E}_{\check{\mathbf{h}}} \{ I(\mathbf{x}; \mathbf{y}|\check{\mathbf{H}}, \mathbf{R}_x) \}, \quad (9.13)$$

where $\check{\mathbf{h}}$ is distributed as in (9.2). Unfortunately, the solution of (9.13) for the general MIMO case is difficult to obtain analytically. For illustration purposes, we derive next the solution for a multiinput single-output (MISO) system that is analytically tractable.

MISO case

With $N_r = 1$, the channel matrix $\check{\mathbf{H}}$ reduces to a row vector $\check{\mathbf{h}}^T$. Let us denote $I(\mathbf{x}; \mathbf{y}|\check{\mathbf{h}}^T, \mathbf{R}_x)$ as I for brevity. From (9.10), the mutual information can be simplified as

$$\begin{aligned} I &= \log_2 \left(1 + \frac{1}{N_0} \check{\mathbf{h}}^T \mathbf{R}_x \check{\mathbf{h}}^* \right) \\ &= \frac{1}{\ln 2} \ln(1 + \bar{\gamma} \check{\mathbf{h}}^T \bar{\mathbf{R}}_x \check{\mathbf{h}}^*) \end{aligned} \quad (9.14)$$

where for notational simplicity we defined the average transmit signal-to-noise ratio (SNR) as

$$\bar{\gamma} = \frac{P_0}{N_0}, \quad (9.15)$$

and the normalized channel input-covariance matrix as

$$\bar{\mathbf{R}}_x = \frac{1}{P_0} \mathbf{R}_x. \quad (9.16)$$

The trace constraint of $\text{tr}(\mathbf{R}_x) = P_0$ translates to $\text{tr}(\bar{\mathbf{R}}_x) = 1$.

Since \mathbf{R}_x is Hermitian symmetric, we can rewrite (9.14) as

$$I = \frac{1}{\ln 2} \ln(1 + \bar{\gamma} \check{\mathbf{h}}^H \bar{\mathbf{R}}_x^* \check{\mathbf{h}}). \quad (9.17)$$

Following the approach in [23] that is based on the identity $\ln(x) = \int_0^\infty \frac{1}{y} (e^{-y} - e^{-xy}) dy$, we obtain:

$$\begin{aligned} \mathbb{E}\{I\} &= \frac{1}{\ln 2} \mathbb{E} \left\{ \int_0^\infty \frac{1}{y} (e^{-y} - e^{-(1+\bar{\gamma} \check{\mathbf{h}}^H \bar{\mathbf{R}}_x^* \check{\mathbf{h}})y}) dy \right\} \\ &= \frac{1}{\ln 2} \int_0^\infty \frac{1}{y} e^{-y} \left[1 - \mathbb{E}\{e^{-y \bar{\gamma} \check{\mathbf{h}}^H \bar{\mathbf{R}}_x^* \check{\mathbf{h}}}\} \right] dy. \end{aligned} \quad (9.18)$$

Applying the identity (9.123) in the Appendix to (9.18), we arrive at

$$\mathbb{E}\{I\} = \frac{1}{\ln 2} \int_0^\infty \frac{1}{y} e^{-y} \left[1 - \frac{\exp(-\check{\mathbf{h}}^H [\Sigma_h^{-1} - (\Sigma_h + y \bar{\gamma} \Sigma_h \bar{\mathbf{R}}_x^* \Sigma_h)^{-1}] \check{\mathbf{h}})}{|\mathbf{I}_{N_t} + y \bar{\gamma} \Sigma_h \bar{\mathbf{R}}_x^*|} \right] dy. \quad (9.19)$$

We now represent $\bar{\mathbf{R}}_x$ by its eigen decomposition as

$$\bar{\mathbf{R}}_x = \mathbf{U}_x^* \Delta_x \mathbf{U}_x^T, \quad (9.20)$$

where \mathbf{U}_x contains its eigenvectors, and

$$\Delta_x := \text{diag}(\delta_{x,1}, \dots, \delta_{x,N_t}) \quad (9.21)$$

contains its nonnegative eigenvalues. With the closed-form expression (9.19) of the average mutual information, and the eigen decomposition on $\bar{\mathbf{R}}_x$ in (9.20), one can derive the following results for mean feedback and covariance feedback.

Result 1 In a MISO system with mean feedback $\check{\mathbf{h}} \sim \mathcal{CN}(\bar{\mathbf{h}}, \sigma_\epsilon^2 \mathbf{I}_{N_t})$, let the eigen decomposition of $\check{\mathbf{h}} \check{\mathbf{h}}^H$ be

$$\check{\mathbf{h}} \check{\mathbf{h}}^H = \mathbf{U}_h \Lambda_h \mathbf{U}_h^H, \quad (9.22)$$

where $\Lambda_h = \text{diag}(\lambda, 0, \dots, 0)$ with $\lambda = \|\bar{\mathbf{h}}\|^2$. Subject to the total transmit power P_0 and the average transmit SNR $\bar{\gamma} = P_0/N_0$, the capacity-achieving input covariance matrix is

$$\mathbf{R}_{x,\text{opt}} = P_0 \mathbf{U}_{x,\text{opt}}^* \Delta_{x,\text{opt}} \mathbf{U}_{x,\text{opt}}^T \quad (9.23)$$

where

$$\mathbf{U}_{x,\text{opt}} = \mathbf{U}_h, \quad (9.24)$$

and the diagonal entries of $\Delta_{x,\text{opt}}$ are:

$$\delta_{x,1} = 1 - (N_t - 1)\delta_o, \quad \delta_{x,2} = \dots = \delta_{x,N_t} = \delta_o. \quad (9.25)$$

with the optimal value $\delta_o \in [0, 1/N_t]$ found by numerically maximizing

$$E\{I\} = \frac{1}{\ln 2} \int_0^\infty \frac{1}{y} e^{-y} \left[1 - \frac{\exp(-\lambda/\sigma_\epsilon^2) \exp\left(\frac{\lambda}{\sigma_\epsilon^2(1+y\bar{\gamma}\sigma_\epsilon^2\delta_{x,1})}\right)}{(1+y\bar{\gamma}\sigma_\epsilon^2\delta_{x,1})(1+y\bar{\gamma}\sigma_\epsilon^2\delta_{x,2})^{N_t-1}} \right] dy. \quad (9.26)$$

Proof: With $\Sigma_h = \sigma_\epsilon^2 \mathbf{I}_{N_t}$ and $\lambda = \bar{\mathbf{h}}^H \bar{\mathbf{h}}$, we simplify (9.19) to

$$E\{I\} = \frac{1}{\ln 2} \int_0^\infty \frac{1}{y} e^{-y} \left[1 - \frac{\exp(-\lambda/\sigma_\epsilon^2) \exp\left(\bar{\mathbf{h}}^H (\mathbf{I}_{N_t} + y\bar{\gamma}\sigma_\epsilon^2 \bar{\mathbf{R}}_x^*)^{-1} \bar{\mathbf{h}}/\sigma_\epsilon^2\right)}{|\mathbf{I}_{N_t} + y\bar{\gamma}\sigma_\epsilon^2 \Delta_x|} \right] dy. \quad (9.27)$$

For any given Δ_x , we select \mathbf{U}_x to minimize

$$\bar{\mathbf{h}}^H (\mathbf{I}_{N_t} + y\bar{\gamma}\sigma_\epsilon^2 \bar{\mathbf{R}}_x^*)^{-1} \bar{\mathbf{h}} = \text{tr} \left\{ \mathbf{U}_x^H \mathbf{U}_h \Delta_h \mathbf{U}_h^H \mathbf{U}_x (\mathbf{I}_{N_t} + y\bar{\gamma}\sigma_\epsilon^2 \Delta_x)^{-1} \right\}. \quad (9.28)$$

Recall that for each Δ_x , we can arrange the diagonal entries of Δ_x in a nonincreasing order by reordering the eigenvectors in \mathbf{U}_x . Applying the inequality (9.124) in the Appendix to (9.28), we find the optimal \mathbf{U}_x in (9.24). Subsequently, the average mutual information can be expressed as in (9.26) as a function of $\delta_{x,\mu}$'s. The fact that $\delta_{x,2} = \dots = \delta_{x,N_t} = \delta_o$ in the optimal solution is due to their equal contribution to the overall mutual information, while $\delta_{x,1} = 1 - (N_t - 1)\delta_o$ is due to the power constraint. Since strong subchannels get more power, we shall have $\delta_{x,1} \geq \delta_{x,2}$, which leads to $0 \leq \delta_o \leq 1/N_t$. ■

We now present numerical results for MISO mean feedback. We use the delayed feedback setup in Example 1, with $N_t = 4$, $N_r = 1$ and $\sigma_h^2 = 1$. We average the capacity $C(\bar{\mathbf{h}}, \sigma_\epsilon^2 \mathbf{I}_{N_t})$ over different feedback realizations, and plot

$$\bar{C} = E_{\hat{\mathbf{h}}_f} \{ C(\bar{\mathbf{h}}, \sigma_\epsilon^2 \mathbf{I}_{N_t}) \}$$

in Fig. 9.3, where $\hat{\mathbf{h}}_f \sim \mathcal{CN}(\mathbf{0}_{N_t \times 1}, \mathbf{I}_{N_t})$, $\bar{\mathbf{h}} = \rho \hat{\mathbf{h}}_f$, and $\sigma_\epsilon^2 = 1 - |\rho|^2$. The feedback quality is thus controlled by the single parameter ρ . The no-CSI case corresponds to $\rho = 0$, while perfect CSI corresponds to $\rho = 1$. The capacity with perfect CSI is larger than the capacity with no CSI by about $\log_2(N_t) = 2$ bits at high SNR, as predicted in [31]. The average capacity with partial CSI increases when the feedback quality improves, as expected.

For covariance feedback, we have the following result.

Result 2 In a MISO system with covariance feedback $\check{\mathbf{h}} \sim \mathcal{CN}(\mathbf{0}_{N_t \times 1}, \Sigma_h)$, let the eigen decomposition of Σ_h be:

$$\Sigma_h = \mathbf{U}_h \text{diag}(\lambda_1, \dots, \lambda_{N_t}) \mathbf{U}_h^H, \quad (9.29)$$

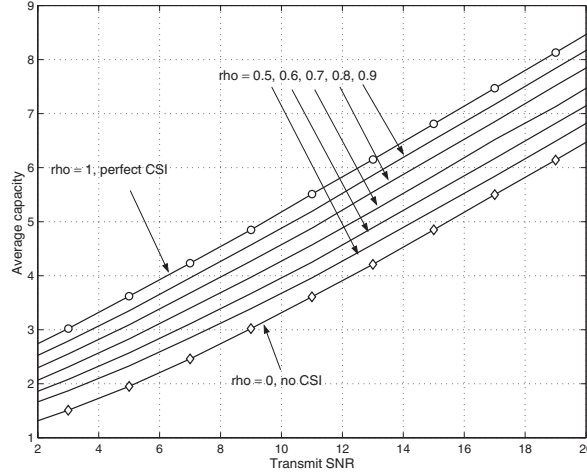


Figure 9.3 Capacity results with MISO mean feedback

with the eigenvalues arranged in a nonincreasing order: $\lambda_1 \geq \dots \geq \lambda_{N_t}$. Subject to the total transmit power P_0 and the average transmit SNR $\bar{\gamma} = P_0/N_0$, the capacity-achieving input covariance matrix is

$$\mathbf{R}_{x,\text{opt}} = P_0 \mathbf{U}_{x,\text{opt}}^* \boldsymbol{\Delta}_{x,\text{opt}} \mathbf{U}_{x,\text{opt}}^T, \quad (9.30)$$

where

$$\mathbf{U}_{x,\text{opt}} = \mathbf{U}_h, \quad (9.31)$$

and the diagonal entries of $\boldsymbol{\Delta}_{x,\text{opt}}$ are found by numerically maximizing

$$E\{I\} = \frac{1}{\ln 2} \int_0^\infty \frac{1}{y} e^{-y} \left[1 - \prod_{\mu=1}^{N_t} (1 + y\bar{\gamma}\lambda_\mu \delta_{x,\mu})^{-1} \right] dy \quad (9.32)$$

subject to the constraints

$$\sum_{\mu=1}^{N_t} \delta_{x,\mu} = 1, \quad \delta_{x,1} \geq \dots \geq \delta_{x,N_t} \geq 0. \quad (9.33)$$

Proof: With covariance feedback, we simplify (9.19) as

$$E\{I\} = \frac{1}{\ln 2} \int_0^\infty \frac{1}{y} e^{-y} \left[1 - \frac{1}{|\mathbf{I}_{N_t} + y\bar{\gamma}\mathbf{\Sigma}_h \mathbf{R}_x^*|} \right] dy. \quad (9.34)$$

The determinant $|\mathbf{I}_{N_t} + y\bar{\gamma}\mathbf{\Sigma}_h \mathbf{R}_x^*| = |\mathbf{I}_{N_t} + y\bar{\gamma}\mathbf{U}_x^H \mathbf{\Sigma}_h \mathbf{U}_x \boldsymbol{\Delta}_x|$ is maximized when $\mathbf{U}_x = \mathbf{U}_h$, in accordance with the Hadamard's inequality; hence, (9.31) holds true. Subsequently, we can simplify (9.34) to (9.32), from which the optimal $\delta_{x,\mu}$'s can be found numerically. Because λ_μ 's are arranged in a nonincreasing order, the same ordering on $\delta_{x,\mu}$'s in (9.33) is necessary to maximize the expression inside the bracket in (9.32) for any value of y , resembling a water-filling principle, as can be easily verified. ■

We now present numerical results for MISO covariance feedback, with $N_t = 4$ and $N_r = 1$. We consider the “broadside” configuration in [27] where the angle of arrival is perpendicular to the transmitter antenna array. With the antenna spacing to be half of the wavelength, and the angle spread $\Delta_1 = 5^\circ$ and $\Delta_2 = 25^\circ$, we generate two channel covariance matrices as:

$$\Sigma_1 = \begin{bmatrix} 1.00 & 0.98 & 0.93 & 0.84 \\ 0.98 & 1.00 & 0.98 & 0.93 \\ 0.93 & 0.98 & 1.00 & 0.98 \\ 0.84 & 0.93 & 0.98 & 1.00 \end{bmatrix}, \quad \Sigma_2 = \begin{bmatrix} 1.00 & 0.58 & -0.16 & -0.39 \\ 0.58 & 1.00 & 0.58 & -0.16 \\ -0.16 & 0.58 & 1.00 & 0.58 \\ -0.39 & -0.16 & 0.58 & 1.00 \end{bmatrix}. \quad (9.35)$$

With a larger angle spread, channel 2 is less correlated than channel 1. The eigenvalues for the first channel are $\Lambda_1 = \text{diag}(3.81, 0.18, 0.007, 0.00)$, while for the second channel are $\Lambda_2 = \text{diag}(1.79, 1.74, 0.45, 0.02)$. For comparison, we also present results for an i.i.d. channel.

First, we assume that the transmitter does not have CSI and uses the input covariance matrix $\mathbf{R}_x = (P_0/N_t)\mathbf{I}_{N_t}$. Fig. 9.4 shows that the i.i.d. channel has larger capacity than channel 2, and both of them have larger capacity than channel 1. This demonstrates that with no CSI, antenna correlation reduces channel capacity.

With covariance feedback, however, the capacity of channel 1 is larger than that of channel 2, and both are larger than that of the i.i.d. channel. This reveals the interesting fact that with partial CSI based on the covariance, antenna correlation can actually increase capacity. In this scenario, it is beneficial to deploy antenna arrays with closely spaced elements. Our observations here agree with the theoretical results in [3], that the ergodic capacity with no CSI at the transmitter is Schur-concave and the ergodic capacity with covariance knowledge at the transmitter is Schur-convex with respect to correlation properties.

In the MISO setup with mean and covariance feedback, the optimal matrix $\mathbf{U}_{x,\text{opt}}$ [c.f. (9.24) and (9.31)] was first derived in [32], while the numerical search for $\Delta_{x,\text{opt}}$ based on

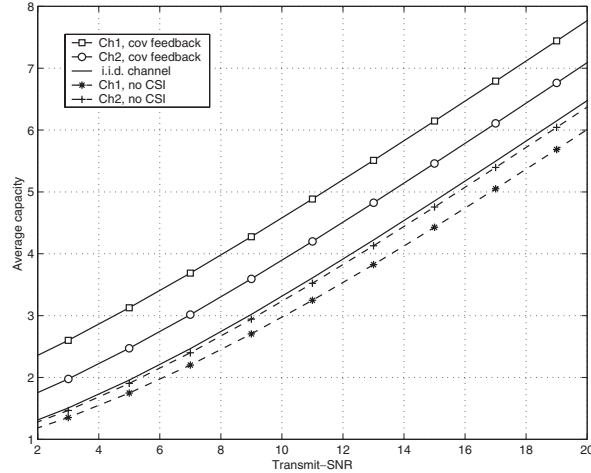


Figure 9.4 MISO Covariance Feedback

analytical expressions [c.f. (9.26) and (9.32)] is due to [23]. With the optimal covariance matrix $\mathbf{R}_{x,\text{opt}}$ in (9.23), or, (9.30), the optimal input \mathbf{x} can be constructed as

$$\mathbf{x}_{\text{opt}} = P_0^{\frac{1}{2}} \mathbf{U}_{x,\text{opt}}^* \boldsymbol{\Delta}_{x,\text{opt}}^{\frac{1}{2}} \mathbf{s}_g, \quad (9.36)$$

where \mathbf{s}_g contains i.i.d. Gaussian entries with unit variance. From this point of view, one could interpret \mathbf{U}_x as a beamforming matrix, and $\boldsymbol{\Delta}_x$ as a power loading matrix, operating on the N_t parallel data streams of \mathbf{s}_g .

Alternative configurations

Using the average capacity as figure of merit, we have presented in Results 1 and 2 the optimal solutions for MISO mean and covariance feedback. We now briefly summarize other scenarios that have been investigated in the literature. With the average capacity criterion, the following cases have been reported.

- MIMO mean feedback with a *rank one* mean channel matrix $\bar{\mathbf{H}} = [\mathbf{T}_1 \bar{\mathbf{h}}, \dots, \mathbf{T}_{N_t} \bar{\mathbf{h}}]$, in [12].
- MIMO covariance feedback with *one-sided* covariance $\boldsymbol{\Sigma}_h = \mathbf{I}_{N_r} \otimes \boldsymbol{\Sigma}_t$, in [13, 4, 29].

In addition to average capacity, transmitter designs optimizing the outage capacity have also been pursued [29, 23]. As mentioned before, the mutual information I is a random variable when conditioned on channel feedback. Hence, one can define an outage probability

$$P_{\text{out}} = \Pr(I < I_{\text{out}}), \quad (9.37)$$

that I is less than a threshold I_{out} . For a *fixed* P_{out} , outage capacity is defined as

$$C(P_{\text{out}}) = \max_{\mathbf{R}_x; \text{tr}\{\mathbf{R}_x\}=P_0} I_{\text{out}}, \quad (9.38)$$

where the maximization is over the input-covariance matrix \mathbf{R}_x conditioned on channel feedback. The following cases have been investigated.

- MISO mean feedback and covariance feedback [23].
- MIMO covariance feedback with $N_t = 2$ and arbitrary N_r [29].

Notice that if the optimal input-covariance matrix in (9.36) has rank one, then $\mathbf{x}_{\text{opt}} = \sqrt{P_0} \mathbf{u}_1^* s_{g,1}$, where \mathbf{u}_1 is the first column of $\mathbf{U}_{x,\text{opt}}$, and $s_{g,1}$ is the first entry of \mathbf{s}_g . This corresponds to one-dimensional (1D) beamforming, where only one data stream is transmitted. Having low decoding complexity, the resulting transceiver is appealing in practice. The conditions under which 1D beamforming actually achieves optimality have been extensively studied for all the aforementioned cases in [11, 12, 4, 29, 23].

9.3.2 Capacity optimization with finite-rate feedback

In this subsection, we formulate the capacity optimization problem based on finite-rate feedback. For simplicity, we assume that the feedback channel can convey B bits back to the transmitter without error and delay. With B bits, the receiver partitions the channel space into $N = 2^B$ nonoverlapping regions denoted as $\{\mathcal{H}_n\}_{n=1}^N$. If the channel realization

at the receiver falls into the n th region, then the index of this region is conveyed back to the transmitter through B bits. Correspondingly, the transmitter needs to prepare a codebook comprising N transmission modes, and switch to the desirable mode depending on the feedback. Using *capacity* as criterion, the transmission modes are characterized by the input covariance matrices $\{\mathbf{R}_{x,n}\}_{n=1}^N$.

The channel space partition at the receiver and the transmission design at the transmitter are interdependent and shall be accomplished jointly. With $A_n = \Pr(\mathbf{h} \in \mathcal{H}_n)$ denoting the probability that \mathbf{h} falls into the n th region, the mutual information averaged over all possible channel realizations is

$$\mathbb{E} \left\{ I(\mathbf{x}; \mathbf{y} | \{\mathcal{H}_n, \mathbf{R}_{x,n}\}_{n=1}^N) \right\} = \sum_{n=1}^N \mathbb{E}_{\mathbf{h} \in \mathcal{H}_n} \left\{ \log_2 \left| \mathbf{I}_{N_r} + \frac{1}{N_0} \mathbf{H} \mathbf{R}_{x,n} \mathbf{H}^\mathcal{H} \right| \right\} A_n, \quad (9.39)$$

where \mathbf{H} is related to \mathbf{h} as in (9.9). The ergodic capacity of the system is thus:

$$C = \max_{\{\mathcal{H}_n, \mathbf{R}_{x,n}\}} \mathbb{E} \left\{ I(\mathbf{x}; \mathbf{y} | \{\mathcal{H}_n, \mathbf{R}_{x,n}\}_{n=1}^N) \right\}, \quad (9.40)$$

subject to either an instantaneous power constraint

$$\text{tr}\{\mathbf{R}_{x,n}\} = P_0, \quad \forall n, \quad (9.41)$$

or an average power constraint

$$\sum_{n=1}^N A_n \text{tr}\{\mathbf{R}_{x,n}\} = P_0. \quad (9.42)$$

Capacity optimization with the instantaneous power constraint (9.41) is formulated in [2], while that with the average power constraint (9.42) is provided in [17].

The capacity optimization with constant power over all transmission modes (9.41) is linked to a vector quantization problem, for which the generalized Lloyd's algorithm [9] can be applied. Specifically, the generalized Lloyd's algorithm consists of the following two steps, which are applied iteratively until convergence.

- S1) Given transmission modes $\{\mathbf{R}_{x,n}\}_{n=1}^N$, partition the channels according to a *nearest neighbor* rule:

$$\mathbf{h} \in \mathcal{H}_i \quad \text{if} \quad d(\mathbf{h}, \mathbf{R}_{x,i}) \leq d(\mathbf{h}, \mathbf{R}_{x,j}), \quad \forall j \neq i, \quad (9.43)$$

where $d(\mathbf{h}, \mathbf{R}_x) = -\log_2 |\mathbf{I}_{N_r} + (1/N_0) \mathbf{H} \mathbf{R}_x \mathbf{H}^\mathcal{H}|$ corresponds to a distance metric [17] replacing the Euclidean distance typically used in vector quantization problems.

- S2) Given channel space partitions $\{\mathcal{H}_n\}_{n=1}^N$, determine transmission modes $\{\mathbf{R}_{x,n}\}_{n=1}^N$ via a *centroid condition*:

$$\mathbf{R}_{x,n} = \arg \min_{\mathbf{R}_x; \text{tr}\{\mathbf{R}_x\}=P_0} \mathbb{E}_{\mathbf{h} \in \mathcal{H}_n} d(\mathbf{h}, \mathbf{R}_x). \quad (9.44)$$

Although clearly formulated, the solution of (9.44) is in general difficult to find. Approximate solutions are usually pursued in such cases [2, 17].

On the other hand, capacity optimization with the average power constraint corresponds to a vector quantization problem with an additional entropy constraint on the codeword probabilities [5]. The generalized Lloyd algorithm can still be applied to maximize an alternative objective function $E\{I(\mathbf{x}; \mathbf{y}|\{\mathcal{H}_n, \mathbf{R}_{x,n}\}_{n=1}^N)\} + \lambda \sum_{n=1}^N A_n \text{tr}\{\mathbf{R}_{x,n}\}$, where λ is the Lagrange multiplier, as detailed in [17].

9.4 Error Performance Oriented Designs

Capacity specifies the theoretical limit on the achievable data rate over the underlying communication channel without complexity and delay constraints. We now focus on practical transceiver designs, aiming to improve error performance of existing space-time coding schemes by exploiting partial CSI at the transmitter.

Notice that from the plethora of available space-time coding and modulation schemes that assuming no CSI at the transmitter, one can just pick up a specific scheme and improve its performance by making partial CSI available at the transmitter. In this section, we will focus on two particular setups: (i) orthogonal space-time block coding (STBC) with statistical CSI; and ii) transmit-beamforming with finite-rate feedback.

9.4.1 Combining orthogonal STBC with linear precoding

Orthogonal STBC is an attractive modulation scheme, achieving the full diversity provided by multiple antennas with low-complexity optimal linear decoding. For detailed discussion, we refer the readers to the chapter by Gharavi-Alkhansari *et al* in this book.

Let \mathcal{O}_{N_t} denote the orthogonal STBC matrix for N_t transmit antennas. As examples, the space-time code words for \mathcal{O}_2 [1] and \mathcal{O}_4 [30, 8] are:

$$\mathcal{O}_2 = \begin{bmatrix} s_1 & -s_2^* \\ s_2 & s_1^* \end{bmatrix}, \quad \mathcal{O}_4 = \begin{bmatrix} s_1 & 0 & -s_2^* & s_3^* \\ 0 & s_1 & -s_3 & -s_2 \\ s_2 & s_3^* & s_1^* & 0 \\ -s_3 & s_2^* & 0 & s_1^* \end{bmatrix}, \quad (9.45)$$

where s_i 's are information-bearing symbols. Taking any three rows of \mathcal{O}_4 , one can easily construct \mathcal{O}_3 .

Orthogonal STBC is designed with no CSI at the transmitter. With $(1/\sqrt{N_t})\mathcal{O}_{N_t}$ transmitted, where the constant $1/\sqrt{N_t}$ is introduced for power scaling, the received space time matrix codeword is:

$$\mathbf{Y} = \frac{1}{\sqrt{N_t}} \mathbf{H} \mathcal{O}_{N_t} + \mathbf{V}, \quad (9.46)$$

where \mathbf{V} denotes additive white Gaussian noise with zero mean and variance N_0 per entry. Capitalizing on statistical CSI at the transmitter, it becomes possible to improve the error performance of orthogonal (CSI-unaware) STBC. In [14] and [37, 38], the idea of combining orthogonal STBC with linear precoding was proposed independently. Let \mathbf{C} denote the precoding matrix, and for the moment let it be square of size $N_t \times N_t$. Instead of transmitting $(1/\sqrt{N_t})\mathcal{O}_{N_t}$, the idea is to transmit $\mathbf{C}\mathcal{O}_{N_t}$ and adaptively change \mathbf{C} according to partial CSI. With $\mathbf{C}\mathcal{O}_{N_t}$ transmitted, the received code word is now

$$\mathbf{Y} = \mathbf{H} \mathbf{C} \mathcal{O}_{N_t} + \mathbf{V}. \quad (9.47)$$

Compared with (9.46), Eq. (9.47) reveals that the original orthogonal STBC matrix \mathcal{O}_{N_t} now sees an equivalent channel $\mathbf{H}_{\text{equ}} := \mathbf{H}\mathbf{C}$. This observation leads to the following conclusions. (i) The receiver complexity is not increased, when the optimal linear decoding is applied with a modified channel \mathbf{H}_{equ} ; (ii) The orthogonal property of STBC is preserved, and each symbol can be detected independently without the interference from other symbols. Equivalently, each symbol passes through a scalar channel of the form

$$y_k = \|\mathbf{H}\mathbf{C}\|_F s_k + v_k, \quad (9.48)$$

where the noise v_k has variance N_0 and the subscript F denotes the Frobenius norm.

If the average symbol energy for s_k as E_s , the instantaneous SNR in (9.48) is given by

$$\gamma_k = \|\mathbf{H}\mathbf{C}\|_F^2 \frac{E_s}{N_0}. \quad (9.49)$$

Since $\mathbf{h} = \text{vec}(\mathbf{H}^T)$ and thus $\text{vec}(\mathbf{C}^T \mathbf{H}^T) = (\mathbf{I}_{N_r} \otimes \mathbf{C}^T) \mathbf{h}$, we have

$$\begin{aligned} \gamma_k &= \|(\mathbf{I}_{N_r} \otimes \mathbf{C}^T) \mathbf{h}\|_F^2 \frac{E_s}{N_0} \\ &= \mathbf{h}^H (\mathbf{I}_{N_r} \otimes \mathbf{C}^* \mathbf{C}^T) \mathbf{h} \frac{E_s}{N_0}. \end{aligned} \quad (9.50)$$

Notice that the SNR, and thus error performance, depend on \mathbf{C} only through the Hermitian matrix $\mathbf{C}^* \mathbf{C}^T$. Let its eigen decomposition be

$$\mathbf{C}^* \mathbf{C}^T = \mathbf{U}_c \Delta_c \mathbf{U}_c^H, \quad (9.51)$$

where \mathbf{U}_c contains the eigenvectors, and the diagonal matrix

$$\Delta_c = \text{diag}(\delta_{c,1}, \dots, \delta_{c,N_t}) \quad (9.52)$$

contains on its diagonal the eigenvalues of $\mathbf{C}^* \mathbf{C}^T$. We can then express \mathbf{C} as $\mathbf{C} = \mathbf{U}_c^* \Delta_c^{\frac{1}{2}} \Phi$, where Φ is an arbitrary unitary matrix. Since unitary matrices do not affect error performance, without loss of generality we take $\Phi = \mathbf{I}_{N_t}$, and thus

$$\mathbf{C} = \mathbf{U}_c^* \Delta_c^{\frac{1}{2}}. \quad (9.53)$$

The final transmitted space-time code word is then:

$$\mathbf{X} = \mathbf{U}_c^* \Delta_c^{\frac{1}{2}} \mathcal{O}_{N_t}. \quad (9.54)$$

One can interpret Δ_c as power loading on the parallel data streams created from the orthogonal STBC, and the unitary precoding \mathbf{U}_c^* as a beamformer. The system diagram is shown in Fig. 9.5.

Our goal is to find Δ_c and \mathbf{U}_c , on the basis of whatever partial is CSI available, to minimize error performance. To this end, we first need to know how the performance depends on Δ_c and \mathbf{U}_c .

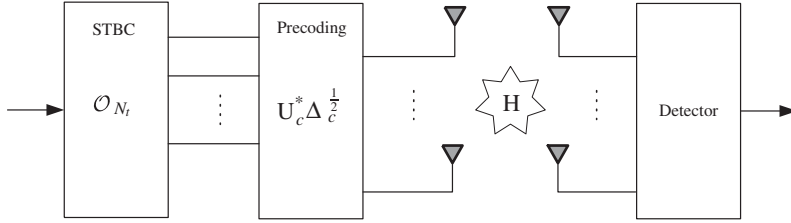


Figure 9.5 The combined orthogonal STBC with power loaded beamforming

Closed-form SER performance

Let us evaluate the system performance in terms of symbol error rate (SER) for commonly used signal constellations. We present here results for phase-shift keying (PSK), rectangular and square quadrature amplitude modulations (QAM). Other constellations can be similarly treated.

Relying on the convenient integral representation of the Gaussian $Q(\cdot)$ function [28], we list the instantaneous symbol error rate (SER) for all signal constellations as

$$\text{SER}_{\text{PSK}}(\gamma) = \frac{1}{\pi} \int_0^{\frac{(M-1)\pi}{M}} \exp\left(-\frac{g_{\text{PSK}}\gamma}{\sin^2 \theta}\right) d\theta, \quad (9.55)$$

$$\begin{aligned} \text{SER}_{\text{QAM}}^{\text{rectangular}}(\gamma) &= \frac{4}{\pi} \left(\frac{3}{\sqrt{8M}} - \frac{1}{M} \right) \int_0^{\frac{\pi}{4}} \exp\left(-\frac{g_{\text{QAM}}^{\text{rect}}\gamma}{\sin^2 \theta}\right) d\theta \\ &\quad + \frac{4}{\pi} \left(1 - \frac{3}{\sqrt{8M}} \right) \int_{\frac{\pi}{4}}^{\frac{\pi}{2}} \exp\left(-\frac{g_{\text{QAM}}^{\text{rect}}\gamma}{\sin^2 \theta}\right) d\theta, \end{aligned} \quad (9.56)$$

$$\begin{aligned} \text{SER}_{\text{QAM}}^{\text{square}}(\gamma) &= \frac{4}{\pi} \left(\frac{1}{\sqrt{M}} - \frac{1}{M} \right) \int_0^{\frac{\pi}{4}} \exp\left(-\frac{g_{\text{QAM}}^{\text{square}}\gamma}{\sin^2 \theta}\right) d\theta \\ &\quad + \frac{4}{\pi} \left(1 - \frac{1}{\sqrt{M}} \right) \int_{\frac{\pi}{4}}^{\frac{\pi}{2}} \exp\left(-\frac{g_{\text{QAM}}^{\text{square}}\gamma}{\sin^2 \theta}\right) d\theta, \end{aligned} \quad (9.57)$$

where the constellation-specific constant g is defined as

$$g_{\text{PSK}} = \sin^2\left(\frac{\pi}{M}\right) \quad \text{for } M\text{-ary PSK}, \quad (9.58)$$

$$g_{\text{QAM}}^{\text{rect}} = \frac{6}{5M-4} \quad \text{for } M\text{-ary rectangular QAM}, \quad (9.59)$$

$$g_{\text{QAM}}^{\text{square}} = \frac{3}{2(M-1)} \quad \text{for } M\text{-ary square QAM}. \quad (9.60)$$

For notational convenience, we define

$$\mathbf{Z} = \mathbf{I}_{N_r} \otimes (\mathbf{C}^* \mathbf{C}^T) \frac{E_s}{N_0}. \quad (9.61)$$

With the mean-feedback CSI in (9.2), the transmitter views γ_k in (9.50) as a random variable $\gamma_k = \check{\mathbf{h}}^H \mathbf{Z} \check{\mathbf{h}}$. With the identity in (9.123), we obtain the average error performance over all possible realizations of γ_k as

$$\overline{\text{SER}}_{\text{PSK}} = \frac{1}{\pi} \int_0^{\frac{(M-1)\pi}{M}} \frac{\exp\left(-\bar{\mathbf{h}}^H g \mathbf{Z} [\mathbf{I} \sin^2 \theta + g \Sigma_h \mathbf{Z}]^{-1} \bar{\mathbf{h}}\right)}{|\mathbf{I} + g \Sigma_h \mathbf{Z} / \sin^2 \theta|} d\theta \quad (9.62)$$

$$\begin{aligned} \overline{\text{SER}}_{\text{QAM}}^{\text{square}} &= \frac{4}{\pi} \left(\frac{1}{\sqrt{M}} - \frac{1}{M} \right) \int_0^{\frac{\pi}{4}} \frac{\exp\left(-\bar{\mathbf{h}}^H g \mathbf{Z} [\mathbf{I} \sin^2 \theta + g \Sigma_h \mathbf{Z}]^{-1} \bar{\mathbf{h}}\right)}{|\mathbf{I} + g \Sigma_h \mathbf{Z} / \sin^2 \theta|} d\theta \\ &\quad + \frac{4}{\pi} \left(1 - \frac{1}{\sqrt{M}} \right) \int_{\frac{\pi}{4}}^{\frac{\pi}{2}} \frac{\exp\left(-\bar{\mathbf{h}}^H g \mathbf{Z} [\mathbf{I} \sin^2 \theta + g \Sigma_h \mathbf{Z}]^{-1} \bar{\mathbf{h}}\right)}{|\mathbf{I} + g \Sigma_h \mathbf{Z} / \sin^2 \theta|} d\theta, \end{aligned} \quad (9.63)$$

where g takes values as in (9.58) and (9.60), respectively, and the identity matrix \mathbf{I} has size $N_t N_r$.

For any given precoder \mathbf{C} , the transmitter can now evaluate the average SER based on the partial CSI in (9.2). However, for transmitter design these integral forms of the exact SER expressions are not convenient to optimize. They also require constellation-dependent optimization. To bypass this problem, we propose to optimize \mathbf{C} based on a unifying upper bound on the SER, which allows us to treat all signal constellations at once.

Optimal designs based on SER bounds

By observing that the integrands in (9.55)–(9.57) and (9.62)–(9.63) peak at $\theta = \pi/2$, we obtain a unifying SER upper bound as [39]:

$$\overline{\text{SER}}_{\text{bound}} = \alpha \exp\left(-\bar{\mathbf{h}}^H g \mathbf{Z} [\mathbf{I} + g \Sigma_h \mathbf{Z}]^{-1} \bar{\mathbf{h}}\right) |\mathbf{I} + g \Sigma_h \mathbf{Z}|^{-1}, \quad (9.64)$$

where $\alpha := (M - 1)/M$. This bound has been confirmed to be tight [39].

To set up the power constraint, we let $\text{tr}\{\mathbf{C}^H \mathbf{C}\} = \text{tr}\{\Delta_c\} = 1$. This way, the total transmitted power for each information symbol is E_s in one space-time code word, consistent with the transmission in (9.46) with no CSI. The optimization problem is then formulated as

$$(\mathbf{U}_{c,\text{opt}}, \Delta_{c,\text{opt}}) = \arg \min_{\mathbf{U}_c, \Delta_c; \text{tr}\{\Delta_c\}=1} \overline{\text{SER}}_{\text{bound}}. \quad (9.65)$$

The general solution for the optimization in (9.65) is difficult to find. We next present results for the mean feedback case [37], and for the covariance feedback case [38].

Result 3 Consider a MIMO system with mean feedback $\check{\mathbf{h}} \sim \mathcal{CN}(\bar{\mathbf{h}}, \sigma_\epsilon^2 \mathbf{I}_{N_t N_r})$. Define the mean channel matrix $\bar{\mathbf{H}} = [\mathbf{T}_1 \bar{\mathbf{h}}, \dots, \mathbf{T}_{N_t} \bar{\mathbf{h}}]$, and let the eigen decomposition of $\bar{\mathbf{H}}^T \bar{\mathbf{H}}^*$ be

$$\bar{\mathbf{H}}^T \bar{\mathbf{H}}^* = \mathbf{U}_H \Lambda_H \mathbf{U}_H^H, \quad (9.66)$$

where $\Lambda_H = \text{diag}(\lambda_1, \lambda_2, \dots, \lambda_{N_t})$ contains the eigenvalues in a nonincreasing order: $\lambda_1 \geq \dots \geq \lambda_{N_t}$. The optimally precoded orthogonal STBC transmission minimizing a tight SER upperbound, is

$$\mathbf{X}_{\text{opt}} = \mathbf{U}_{c,\text{opt}}^* \Delta_{c,\text{opt}}^{\frac{1}{2}} \mathcal{O}_{N_t} \quad (9.67)$$

where

$$\mathbf{U}_{c,\text{opt}} = \mathbf{U}_H, \quad (9.68)$$

and the diagonal entries of $\Delta_{c,\text{opt}}$ are found by numerically minimizing

$$\overline{\text{SER}}_{\text{bound}} = \alpha \left[\prod_{\mu=1}^{N_t} \frac{1}{1 + \delta_{c,\mu}\beta} \exp \left(\frac{-\mathcal{K}_\mu \delta_{c,\mu}\beta}{1 + \delta_{c,\mu}\beta} \right) \right]^{N_r} \quad (9.69)$$

subject to $\sum_{\mu=1}^{N_t} \delta_{c,\mu} = 1$. The constants in (9.69) are defined as

$$\alpha = \frac{M-1}{M}, \quad \beta = g\sigma_\epsilon^2 \frac{E_s}{N_0}, \quad \mathcal{K}_\mu = \frac{\lambda_\mu}{N_r \sigma_\epsilon^2}, \quad (9.70)$$

where M is the constellation size, E_s is the total transmit energy per information symbol in one STBC codeword, N_0 is the noise variance, and g is the constellation-specific constant in (9.58)–(9.60) for different constellations.

Proof: Substituting $\Sigma_h = \sigma_\epsilon^2 \mathbf{I}_{N_t N_r}$, (9.51) and (9.61) into (9.64), and after straightforward manipulation, we obtain

$$\overline{\text{SER}}_{\text{bound}} = \frac{\alpha}{|\mathbf{I}_{N_t} + \beta \Delta_c|^{N_r}} \exp \left(-\frac{1}{\sigma_\epsilon^2} \text{tr} \left\{ \bar{\mathbf{H}}^* \mathbf{U}_c \beta \Delta_c (\mathbf{I}_{N_t} + \beta \Delta_c)^{-1} \mathbf{U}_c^H \bar{\mathbf{H}}^T \right\} \right). \quad (9.71)$$

For each fixed Δ_c , the optimal \mathbf{U}_c maximizes

$$\begin{aligned} & \text{tr} \left\{ \mathbf{U}_c^H \bar{\mathbf{H}}^T \bar{\mathbf{H}}^* \mathbf{U}_c \beta \Delta_c (\mathbf{I}_{N_t} + \beta \Delta_c)^{-1} \right\} \\ &= \text{tr} \{ \Lambda_H \} - \text{tr} \left\{ \mathbf{U}_c^H \mathbf{U}_H \Lambda_H \mathbf{U}_H^H \mathbf{U}_c (\mathbf{I}_{N_t} + \beta \Delta_c)^{-1} \right\}. \end{aligned} \quad (9.72)$$

Recall that for each Δ_c we can arrange the diagonal entries of Δ_c in a nonincreasing order by reordering the eigenvectors in \mathbf{U}_c . Applying the inequality (9.124) in the Appendix to (9.72), we have $\mathbf{U}_{c,\text{opt}} = \mathbf{U}_H$. Subsequently, eq. (9.71) simplifies to (9.69), from which the optimal power splitting is found. ■

Example 3 Exact power loading for MISO with mean feedback

It turns out that $\Delta_{c,\text{opt}}$ can be found in closed form only when $N_r = 1$ in Result 3, where only one eigen-value λ_1 is nonzero. In this case, our equivalent constrained optimization problem is

$$\begin{aligned} \Delta_{c,\text{opt}} &= \arg \min_{\Delta_c \geq 0; \text{tr}(\Delta_c)=1} \ln(\overline{\text{SER}}_{\text{bound}}) \\ &= \arg \min_{\Delta_c \geq 0; \text{tr}(\Delta_c)=1} \ln \alpha - \sum_{\mu=1}^{N_t} \ln(1 + \delta_{c,\mu}\beta) - \frac{\lambda_1 \delta_{c,1}\beta}{\sigma_\epsilon^2(1 + \delta_{c,1}\beta)}. \end{aligned} \quad (9.73)$$

Using Lagrange's multiplier method on (9.73), we find the solution as follows; see also [37] for details. With constants defined as

$$\begin{aligned} a &:= \left(1 + \frac{N_t}{\beta}\right)^2, \quad c := N_t(N_t - 1), \\ b &:= \left[\frac{\lambda}{\beta\sigma_\epsilon^2} + \left(1 + \frac{N_t}{\beta}\right)(2N_t - 1)\right], \end{aligned} \quad (9.74)$$

the optimal power splitting solution is

$$\begin{aligned} \delta_{c,2} = \dots = \delta_{c,N_t} &= \left[\frac{2a}{b + \sqrt{b^2 - 4ac}} - \frac{1}{\beta} \right]_+, \\ \delta_{c,1} &= 1 - (N_t - 1)\delta_{c,2}, \end{aligned} \quad (9.75)$$

where the notation $[x]_+ = \max(x, 0)$. ■

For $N_r > 1$, there exist multiple nonzero λ_μ 's, which prevents a closed-form optimal power loading solution. One can resort to numerical search in this case. Alternatively, an approximate solution has been found in [37], through approximating the objective function in (9.69) by replacing the Ricean distribution with its equivalent Nakagami distribution.

For covariance feedback, we have the following result for MIMO systems with transmit-side correlation only.

Result 4 For a MIMO system with covariance feedback $\check{\mathbf{h}} \sim \mathcal{CN}(\mathbf{0}_{N_t N_r \times 1}, \mathbf{I}_{N_r} \otimes \boldsymbol{\Sigma}_t)$, let the eigen decomposition of $\boldsymbol{\Sigma}_t$ be:

$$\boldsymbol{\Sigma}_t = \mathbf{U}_H \boldsymbol{\Lambda}_H \mathbf{U}_H^\mathcal{H}, \quad (9.76)$$

where $\boldsymbol{\Lambda}_H = \text{diag}(\lambda_1, \dots, \lambda_{N_t})$ contains the eigenvalues in a nonincreasing order $\lambda_1 \geq \dots \geq \lambda_{N_t}$. The optimally precoded orthogonal STBC transmission minimizing a tight upper-bound on the average SER is:

$$\mathbf{X}_{\text{opt}} = \mathbf{U}_{c,\text{opt}}^* \boldsymbol{\Delta}_{c,\text{opt}}^{\frac{1}{2}} \mathcal{O}_{N_t}, \quad (9.77)$$

where

$$\mathbf{U}_{c,\text{opt}} = \mathbf{U}_H, \quad (9.78)$$

and the diagonal entries of $\boldsymbol{\Delta}_{c,\text{opt}}$ satisfy

$$\delta_{c,\mu} = \left[-\frac{1}{\zeta} - \frac{N_0}{\lambda_\mu g E_s} \right]_+, \quad \sum_{\mu=1}^{N_t} \delta_{c,\mu} = 1. \quad (9.79)$$

In (9.79), ζ is the Lagrange multiplier, E_s is the total transmit energy per information symbol in one STBC codeword, N_0 is the noise variance, and g is the constellation-specific constant in (9.58)-(9.60) for different constellations.

Proof: Substituting $\bar{\mathbf{h}} = \mathbf{0}$, $\Sigma_h = \mathbf{I}_{N_r} \otimes \Sigma_t$, (9.51), (9.61), and (9.76) into (9.64), we obtain:

$$\overline{\text{SER}}_{\text{bound}} = \alpha \left| \mathbf{I}_{N_t} + \Lambda_H^{\frac{1}{2}} \mathbf{U}_H^H \mathbf{U}_c \Delta_c \mathbf{U}_c^H \mathbf{U}_H \Lambda_H^{\frac{1}{2}} g \frac{E_s}{N_0} \right|^{-N_r}. \quad (9.80)$$

On the basis of Hadamard's inequality, the $\overline{\text{SER}}_{\text{bound}}$ is minimized when $\mathbf{U}_{c,\text{opt}} = \mathbf{U}_H$. Subsequently, the optimal Δ_c is found as

$$\begin{aligned} \Delta_{c,\text{opt}} &= \arg \min_{\Delta_c \geq 0; \text{tr}(\Delta_c)=1} \ln(\overline{\text{SER}}_{\text{bound}}) \\ &= \arg \min_{\Delta_c \geq 0; \text{tr}(\Delta_c)=1} \ln \alpha - N_r \ln \left| \mathbf{I}_{N_t} + \Lambda_H \Delta_c \frac{g E_s}{N_0} \right|. \end{aligned} \quad (9.81)$$

Using Lagrange's method, we obtain the standard water-filling solution in (9.79). ■

The optimal beamforming directions in (9.78) coincide with the eigenvectors of the channel correlation matrix; hence one can term it as *eigen-beamforming*. The transmission in (9.77) first decorrelates the channel and then balances the strengths of the decorrelated channels to some degree, followed by orthogonal STBC transmission.

Two-dimensional coding-beamforming

We now recall rate properties of orthogonal STBC. For complex symbols, a rate 1 orthogonal design only exists for $N_t = 2$. For $N_t = 3, 4$, rate 3/4 orthogonal STBC designs exist, while for $N_t > 4$, only rate 1/2 codes have been constructed. Therefore, for complex symbols the transmitter of (9.54) achieves optimal performance with no rate loss only when $N_t = 2$, and pays a rate penalty up to 50%, when $N_t > 2$ and complex constellations are used. To make up for this loss, the transmitter has to enlarge the constellation size, which for the same performance necessitates more transmit-power.

To maintain constant rate of 1 symbol per channel use, it is possible to send Alamouti's matrix code along the two strongest directions. Specifically, the following $N_t \times 2$ space-time coded matrix for the two-dimensional (2D) coder-beamformer has been introduced by [37, 38]:

$$\mathbf{X} = \underbrace{\begin{bmatrix} \mathbf{u}_{c,1}^* & \mathbf{u}_{c,2}^* \end{bmatrix}}_{\mathbf{U}_c^*} \underbrace{\begin{bmatrix} \sqrt{\delta_{c,1}} & 0 \\ 0 & \sqrt{\delta_{c,2}} \end{bmatrix}}_{\Delta_c^{1/2}} \underbrace{\begin{bmatrix} s_1 & -s_2^* \\ s_2 & s_1^* \end{bmatrix}}_{\mathcal{O}_2}. \quad (9.82)$$

The implementation of (9.82) is depicted in Fig. 9.6.

The transmission of (9.82) amounts to choosing a tall precoding matrix \mathbf{C} of size $N_t \times 2$, and applying it on \mathcal{O}_2 . Following the same steps we used to establish Results 3 and 4, one can easily prove that

Result 5 *In the special case of mean feedback and covariance feedback, the optimal beam directions for the 2D coder-beamformer are:*

$$\mathbf{u}_{c,1} = \mathbf{u}_{H,1}, \quad \mathbf{u}_{c,2} = \mathbf{u}_{H,2}, \quad (9.83)$$

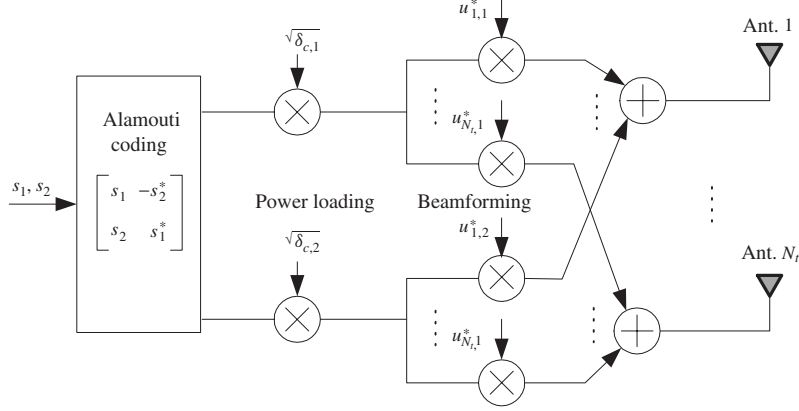


Figure 9.6 The two-directional (2D) coder-beamformer, $u_{p,q} := [\mathbf{U}_c]_{p,q}$

where $(\mathbf{u}_{H,1}, \mathbf{u}_{H,2})$ are the first two eigenvectors of \mathbf{U}_H in (9.66) for mean feedback, or, of \mathbf{U}_H in (9.76) for covariance feedback.

With only two beams, the 2D coder-beamformer transforms a MIMO system into a virtual system with only two transmit- and N_r receive- antennas. By virtually setting $N_t = 2$, we only need to solve for $\delta_{c,1}$ and $\delta_{c,2}$ following the steps of Result 3 and 4. Since only two beam directions are used in the 2D coder-beamformer, only the first two eigenvalues λ_1 and λ_2 will be loaded nonzero power.

Notice that if we set $\delta_{c,2} = 0$ in the 2D beamformer, (9.82) reduces to:

$$\mathbf{X} = [\mathbf{u}_{c,1}^* s_1 \quad -\mathbf{u}_{c,1}^* s_2^*], \quad (9.84)$$

which corresponds to transmitting information symbols s_1 and $-s_2^*$ in two consecutive time slots, using only one beamforming vector. The scheme in (9.84) is the conventional one-dimensional (1D) beamforming. We thus have the following observation.

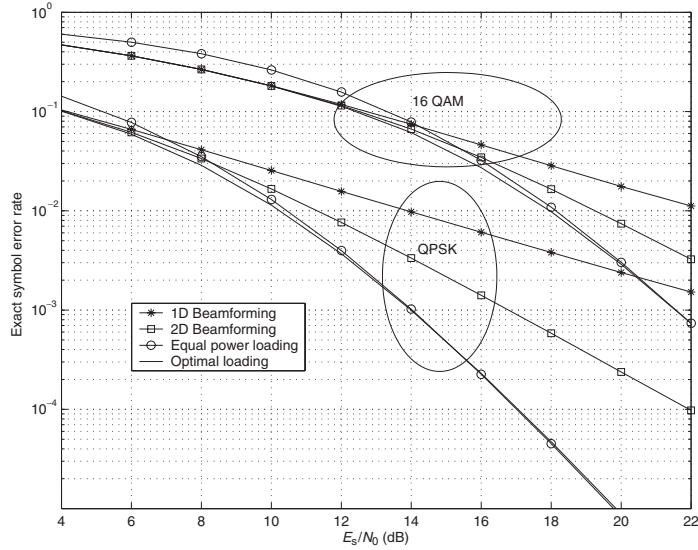
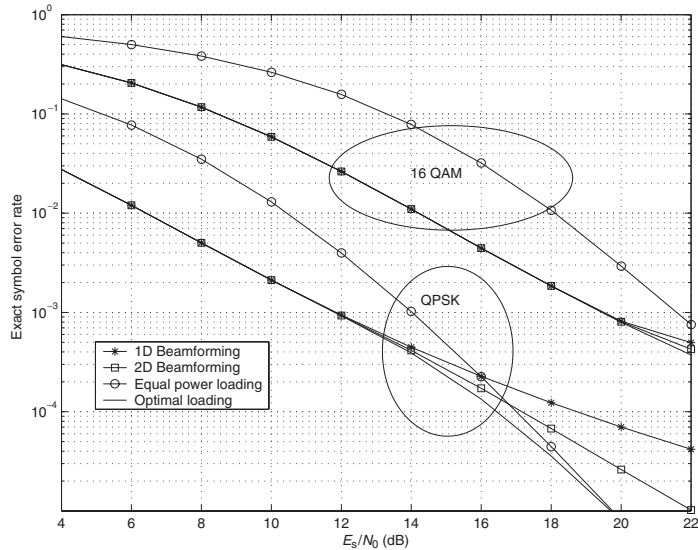
The 2D coder-beamformer includes the 1D-beamformer as a special case and outperforms it uniformly, without rate reduction, and without essential increase in complexity.

Therefore, the 2D coder-beamformer is more attractive than the conventional 1D beamformer. Thanks to its full-rate capability and superior performance (that will be demonstrated soon), the 2D coder-beamformer is appealing in practice. For this reason, we will also construct an adaptive system that combines adaptive modulation with the 2D coder-beamformer in Section 9.5.

Numerical results

We now present numerical results for the mean and covariance feedback case.

We first consider mean feedback. We use the delayed feedback setup in Example 1, with $N_t = 4$, $N_r = 1$ and, $\sigma_h^2 = 1$. We average the SER performance over all possible feedback realizations, where $\hat{\mathbf{h}}_f \sim \mathcal{CN}(\mathbf{0}_{N_t \times 1}, \mathbf{I}_{N_t})$.

Figure 9.7 SER versus E_s/N_0 ($\rho = 0.6$, $N_t = 4$, $N_r = 1$)Figure 9.8 SER versus E_s/N_0 ($\rho = 0.9$, $N_t = 4$, $N_r = 1$)

Figs. 9.7 and 9.8 compare the optimal power loading, the equal power loading with $\Delta_c = (1/N_t)\mathbf{I}_{N_t}$ (that has the same performance as plain STBC without linear precoding), the 1D and 2D beamforming, for both QPSK and 16QAM constellations. When the feedback quality is low ($\rho = 0.6$), Fig. 9.7 shows that optimal power loading performs close to equal

power loading, while it considerably outperforms conventional 1D beamforming. On the other hand, when the feedback quality improves to $\rho = 0.9$, equal power loading is highly suboptimum. The conventional beamforming performs close to the optimal power loading at low SNR, while it becomes inferior at sufficiently high SNR. Notice that the 2D beamformer outperforms the 1D beamformer uniformly.

We now turn to covariance feedback. We set $N_t = 4$, $N_r = 1$ and adopt the two channel covariance matrices in (9.35), where channel 2 is less correlated than channel 1.

With channel 1, the curves in Fig. 9.9 depict the exact SER, and the SER upper bound for optimal power loading, equal power loading (that has the same performance as plain STBC without linear precoding), and 1D beamforming. Since channel 1 is highly correlated, it turns out that only 2 beams are used in the considered SNR range for optimal loading. Therefore, the 2D coder-beamformer is overall optimal for channel 1 in the considered SNR range, and its performance curves coincide with those of the optimal loading. Fig. 9.9 confirms that the optimal allocation outperforms both the equal power allocation and the 1D beamforming. The difference between optimal loading and equal power loading is about 3 dB as SNR increases, since 2 out of 4 beams are so weak that the power allocated to them is wasted. The differences between the upper bound and the exact SER in Fig. 9.9 justifies the approach that pushes down the upper bound to minimize the exact SER.

For the less correlated channel 2, all four beams are used at high SNR. Equal power loading approaches the optimal loading when SNR is sufficiently high but is inferior to both the 2D eigen-beamforming and the optimal loading at low to medium SNR, as confirmed by Fig. 9.10. It is also shown that 2D beamforming outperforms 1D beamforming uniformly, and the difference is quite significant at moderate to high SNR. This observation corroborates the advantage of 2D beamforming relative to 1D beamforming.

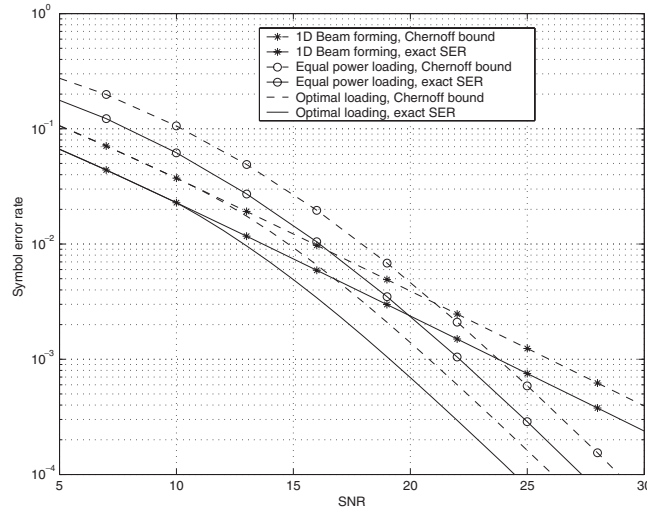


Figure 9.9 SER versus E_s/N_0 : Channel 1, QPSK

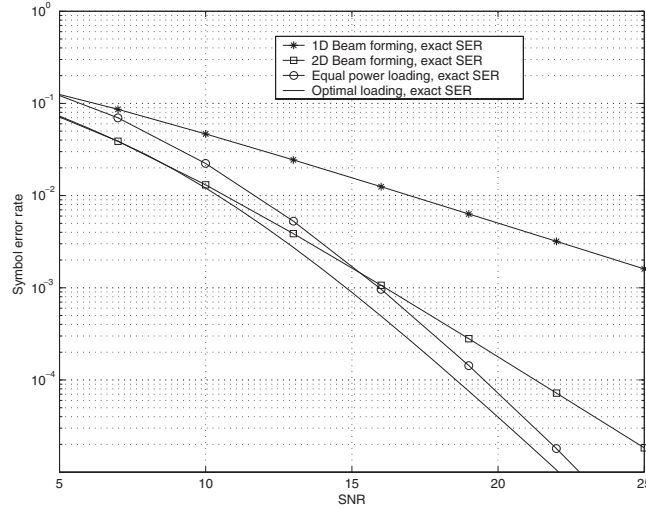
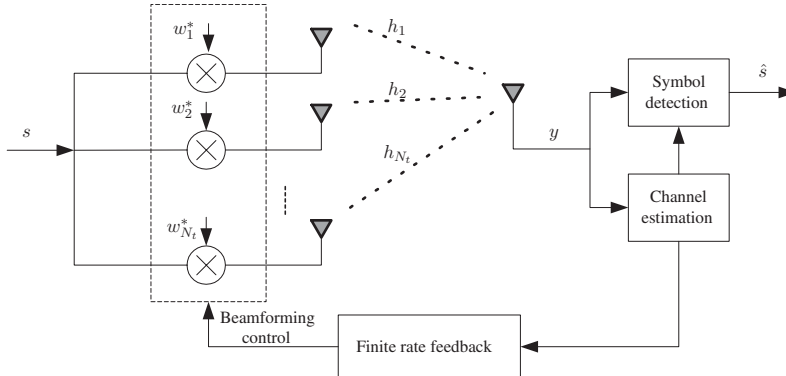
Figure 9.10 SER versus E_s/N_0 : Channel 2, QPSK

Figure 9.11 The transmit beamforming system based on finite rate feedback

9.4.2 Finite-rate one-dimensional beamforming

In this subsection, we focus on one-dimensional transmit beamforming in a MISO setting with finite-rate feedback [24, 22, 40]. As depicted in Fig. 9.11, each information symbol s is multiplied by a beamforming vector \mathbf{w}^* , where $\mathbf{w} := [w_1, w_2, \dots, w_{N_t}]^T$ has unit norm $\|\mathbf{w}\| = 1$. The N_t entries of the vector $s\mathbf{w}^*$ are transmitted simultaneously from N_t antennas, which leads to a received sample:

$$y = \mathbf{w}^H \mathbf{h} s + v, \quad (9.85)$$

where v is the additive complex Gaussian noise with zero mean and variance N_0 .

We assume that the transmission power and the signal constellation are fixed. Our objective is to improve error performance by adapting the beamforming directions based on finite-rate feedback. With B bits, the transmitter needs to construct a total of $N = 2^B$ transmission modes, where each mode is now characterized by one beamforming vector. Let us denote these vectors as $\mathbf{w}_1, \mathbf{w}_2, \dots, \mathbf{w}_N$ and collect them into a matrix (the codebook of beamforming vectors):

$$\mathbf{W} := [\mathbf{w}_1, \mathbf{w}_2, \dots, \mathbf{w}_N]. \quad (9.86)$$

Given \mathbf{W} , channel partitioning at the receiver is straightforward. With E_s denoting the average symbol energy, the instantaneous SNR in (9.85) is

$$\gamma = |\mathbf{w}^H \mathbf{h}|^2 E_s / N_0. \quad (9.87)$$

To optimize system performance, the receiver selects the beamforming vector to maximize the instantaneous SNR; that is, channel partitioning amounts to having

$$\mathbf{h} \in \mathcal{H}_i \quad \text{if} \quad |\mathbf{w}_i^H \mathbf{h}| > |\mathbf{w}_j^H \mathbf{h}|, \quad \forall j \neq i. \quad (9.88)$$

When $\mathbf{h} \in \mathcal{H}_i$, the index i is coded into B feedback bits. After receiving the B feedback bits, the transmitter switches to the optimal beamforming vector \mathbf{w}_i .

Assuming that the feedback link is error-free and delay-free, the instantaneous SNR in (9.87) is:

$$\gamma = \max_{1 \leq i \leq N} \{|\mathbf{w}_i^H \mathbf{h}|^2\} E_s / N_0, \quad (9.89)$$

which shows that error performance depends critically on the design of the beamforming vectors $\{\mathbf{w}_i\}_{i=1}^N$. The design of transmit-beamformers based on finite-rate feedback boils down to specifying the codebook \mathbf{W} .

Good beamformer designs

Optimizing the columns $\{\mathbf{w}_i\}_{i=1}^N$ of the codebook has been thoroughly investigated in [24] and [22], where [24] uses the outage probability as figure of merit, and [22] the average receive-SNR. Albeit starting from different perspectives, these two criteria lead to identical beamformer designs. Specifically, with i.i.d. channels

$$\mathbf{h} \sim \mathcal{CN}(\mathbf{0}, \mathbf{I}_{N_t}), \quad (9.90)$$

a good beamformer should minimize the maximum correlation between any pair of beamforming vectors; that is,

$$\mathbf{W}_{\text{opt}} = \min_{\mathbf{W} \in \mathcal{C}^{N_t \times N}} \max_{1 \leq i < j \leq N} |\mathbf{w}_i^H \mathbf{w}_j|. \quad (9.91)$$

In [22], the beamformer design problem is explicitly linked to the Grassmannian line packing problem in [7]. Specifically, \mathbf{w}_i is viewed as the coordinates of a point on the surface of a hypersphere with unit radius centered around origin. This point dictates a straight line

in a complex space \mathcal{C}^{N_t} that passes through the origin. The two lines generated by \mathbf{w}_i and \mathbf{w}_j have a distance defined as:

$$\begin{aligned} d(\mathbf{w}_i, \mathbf{w}_j) &:= \sin(\theta_{i,j}) \\ &= \sqrt{1 - |\mathbf{w}_i^H \mathbf{w}_j|^2}, \end{aligned} \quad (9.92)$$

where $\theta_{i,j}$ denotes the angle between these two lines. The distance $d(\mathbf{w}_i, \mathbf{w}_j)$ is known as “chordal distance” [7]. So the beamformer design in (9.91) is equivalent to

$$\mathbf{W}_{\text{opt}} = \max_{\mathbf{W} \in \mathcal{C}^{N_t \times N}} \min_{1 \leq i < j \leq N} d(\mathbf{w}_i, \mathbf{w}_j). \quad (9.93)$$

The beamformer design in (9.93) is challenging only when the codebook size $N > N_t$. When $N \leq N_t$, \mathbf{W} can be formed using any N columns of an arbitrary $N_t \times N_t$ unitary matrix, which leads to the minimal chordal distance $1 = \sin(90^\circ)$. The resulting beamforming system has identical performance as a selection combining (SC) system with N diversity branches [24, 22].

Example 4 For illustration purposes, we list here some code design examples [19, 22, 33].

1) For $N_t = 2$ and $N = 4$ ($B = 2$ feedback bits), \mathbf{W} is constructed in [22] as:

$$\mathbf{W}^T = \begin{bmatrix} -0.1612 - 0.7348j & -0.5135 - 0.4128j \\ -0.0787 - 0.3192j & -0.2506 + 0.9106j \\ -0.2399 + 0.5985j & -0.7641 - 0.0212j \\ -0.9541 & 0.2996 \end{bmatrix}. \quad (9.94)$$

The achieved maximum correlation is $\max_{1 \leq i < j \leq N} |\mathbf{w}_i^H \mathbf{w}_j| = 0.57735$ and the achieved minimum chordal distance is $\min_{1 \leq i < j \leq N} d(\mathbf{w}_i, \mathbf{w}_j) = \sqrt{0.6713} = \sin(55.02^\circ)$.

2) For $N_t = 2$ and $N = 8$ ($B = 3$ feedback bits), the \mathbf{W} in [33] obtained by the Lloyd’s algorithm is:

$$\mathbf{W}^T = \begin{bmatrix} 0.3918 + 0.4725j & 0.7894 \\ 0.3086 - 0.2204j & 0.9253 \\ -0.2472 + 0.0029j & 0.9690 \\ 0.9932 & -0.0126 - 0.1156j \\ 0.8489 & 0.5065 + 0.1510j \\ 0.7915 & -0.5965 + 0.1328j \\ 0.7123 & -0.3405 - 0.6137j \\ 0.7580 & -0.0739 + 0.6480j \end{bmatrix}. \quad (9.95)$$

The achieved maximum correlation is $\max_{1 \leq i < j \leq N} |\mathbf{w}_i^H \mathbf{w}_j| = 0.82161$ and the achieved minimum chordal distance is $\min_{1 \leq i < j \leq N} d(\mathbf{w}_i, \mathbf{w}_j) = \sqrt{0.3250} = \sin(34.75^\circ)$. ■

Quantifying the power loss due to finite-rate feedback

For the finite-rate beamforming system, it is important to know how the system performance is affected by the number of feedback bits. To this end, we first need to evaluate the system

performance. We illustrate our derivation with s drawn from a PSK constellation; similar derivations can be carried out for other constellations.

Conditioned on the instantaneous SNR γ , the symbol error rate (SER) for PSK is available in (9.55) and replicated below for convenience:

$$\text{SER}(\gamma) = \frac{1}{\pi} \int_0^{\frac{(M-1)\pi}{M}} \exp\left(-\frac{g_{\text{PSK}}\gamma}{\sin^2 \theta}\right) d\theta. \quad (9.96)$$

Since \mathbf{h} is a random vector, the average SER is expressed as

$$\overline{\text{SER}} = E_{\mathbf{h}}\{\text{SER}(\gamma)\}. \quad (9.97)$$

Since γ in (9.87) depends on the specific beamformer design, the performance in (9.97) is also beamformer dependent. The exact expression for the average SER turns out to be difficult to find. However, with \mathbf{h} as in (9.90), a lower bound on $\overline{\text{SER}}$ is derived in [40]:

$$\begin{aligned} & \overline{\text{SER}}_{\text{lb}}(N_t, N, \bar{\gamma}) \\ &= \frac{1}{\pi} \int_0^{\frac{(M-1)\pi}{M}} \left(1 + \frac{g_{\text{PSK}}\bar{\gamma}}{\sin^2 \theta}\right)^{-1} \left[1 + \left[1 - \left(\frac{1}{N}\right)^{\frac{1}{N_t-1}}\right] \frac{g_{\text{PSK}}\bar{\gamma}}{\sin^2 \theta}\right]^{1-N_t} d\theta, \end{aligned} \quad (9.98)$$

where $\bar{\gamma} := E_s/N_0$ is the transmit SNR. This lower bound is a function of N_t , N , and $\bar{\gamma}$ but is independent of any particular beamformer design. A good beamformer should come as close as possible to this lower bound. This turns out to be consistent with the design guidelines in (9.91) and (9.93).

When N goes to infinity, the performance of beamformed transmissions with finite-rate feedback should approach the ideal case with perfect channel knowledge at the transmitter. With perfect CSI, the system is equivalent to a diversity system with maximum ratio combining (MRC) on N_t diversity branches, and its performance for PSK should be given by [28]:

$$\overline{\text{SER}}_{\text{perfect CSI}}(N_t, \bar{\gamma}) = \frac{1}{\pi} \int_0^{\frac{(M-1)\pi}{M}} \left(1 + \frac{g_{\text{PSK}}\bar{\gamma}}{\sin^2 \theta}\right)^{-N_t} d\theta. \quad (9.99)$$

Comparing (9.98) with (9.99), we first observe that the lower bound in (9.98) is tight with respect to N , since it coincides with (9.99) when $N = \infty$.

If the lower bound is achievable by some beamformer designs, then the distance between the two curves (9.98) and (9.99) quantifies the performance loss due to the finite-rate constraint, as elaborated in the following results proved in [40].

Result 6 Assume that the SER lower bound in (9.98) can be achieved by some good beamformer designs. To compensate for the performance loss due to the finite-rate constraint, let us increase the transmission power from $\bar{\gamma}$ to $\bar{\gamma}_{\text{new}}$, such that the performance with perfect CSI is achieved:

$$\overline{\text{SER}}_{\text{lb}}(N_t, N, \bar{\gamma}_{\text{new}}) = \overline{\text{SER}}_{\text{perfect CSI}}(N_t, \bar{\gamma}). \quad (9.100)$$

The difference between $\bar{\gamma}_{\text{new}}$ and $\bar{\gamma}$ expressing the power loss (in decibels) due to the finite-rate constraint is given by:

$$L(N_t, N, \bar{\gamma}) = 10 \log_{10} \bar{\gamma}_{\text{new}} - 10 \log_{10} \bar{\gamma}. \quad (9.101)$$

Table 9.1 The power loss (in decibels) due to the finite-rate constraint (B bits)

	$B = 1$	$B = 2$	$B = 3$	$B = 4$	$B = 5$	$B = 6$	$B = 7$
$N_t = 2$	1.51	0.62	0.29	0.14	0.07	0.03	0.02
$N_t = 3$	-	2.01	1.26	0.83	0.56	0.39	0.27
$N_t = 4$	-	3.24	2.26	1.65	1.23	0.94	0.72
$N_t = 6$	-	-	3.90	3.09	2.51	2.07	1.72
$N_t = 8$	-	-	5.16	4.25	3.57	3.05	2.63

Then, the power loss satisfies:

$$L(N_t, N, \bar{\gamma}) \leq L(N_t, N, \infty), \quad (9.102)$$

$$L(N_t, N, \infty) = 10 \log_{10} \left[1 - \left(\frac{1}{N} \right)^{\frac{1}{N_t-1}} \right]^{\frac{1}{N_t}-1}. \quad (9.103)$$

Although derived for PSK constellations, the power loss in (9.101) holds true for any arbitrary two-dimensional constellation [40]. Notice that the power loss $L(N_t, N, \bar{\gamma})$ is a function of $\bar{\gamma}$, and thus varies over the entire SNR range. However, Result 6 asserts that the power loss across the entire SNR range is bounded to be less than or equal to $L(N_t, N, \infty)$, which only depends on N and N_t .

Numerical results

We compute the power loss in (9.103) for various cases and list the results in Table 9.1, where we are interested in nontrivial configurations with $N \geq N_t$. We then compare the SER lower bound in (9.98) with the actual SER of (9.97), which is obtained via Monte Carlo simulations. We use QPSK constellations in all cases. Fig. 9.12 depicts the results with $N_t = 2$. The beamformer codebooks for $N = 4, 8$ are listed in Example 4. The codebook with $N = 2$ is $\mathbf{W} = \mathbf{I}_2$, which corresponds to the selection diversity scheme. As shown in Fig. 9.12, the SER lower bound for the $N_t = 2$ case is almost identical to the actual SER, even for small values of N .

We now test the SER lower bound with the actual SER for the $N_t = 4$ case. We use the beamformers listed in [33] (obtained by the Lloyd's algorithm) with $N = 16$ and 64 . The codebook with $N = 4$ is $\mathbf{W} = \mathbf{I}_4$, corresponding to selection combining. As shown in Fig. 9.13, the bound is also tight for the given beamformers. This suggests that the lower bound is a good performance indicator for carefully constructed beamformers.

Figs. 9.12 and 9.13 show that the distance between the SER lower bound and the SER with perfect CSI only slightly increases as the average SNR increases yet it stays always bounded by the maximum power loss listed in Table 9.1. This confirms (9.102).

9.4.3 Further results

Using error performance as a criterion, we have examined orthogonal STBC with statistical CSI in Section 9.4.1, and 1D beamforming with finite rate feedback in Section 9.4.2. Other

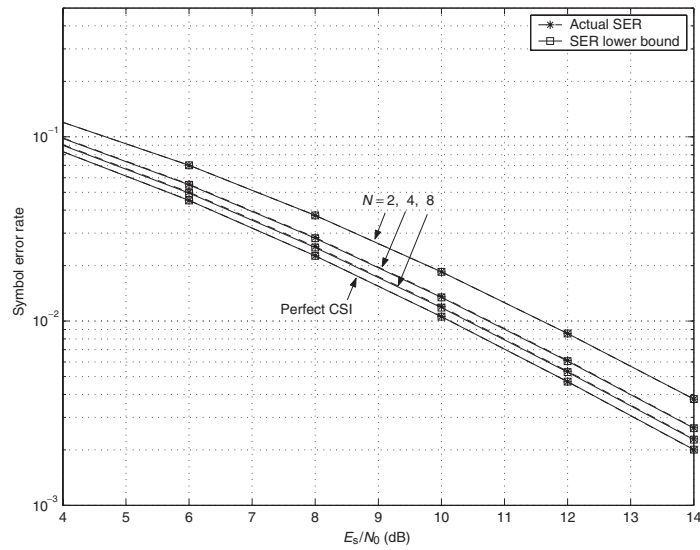


Figure 9.12 The actual SER versus the lower bound ($N_t = 2$)

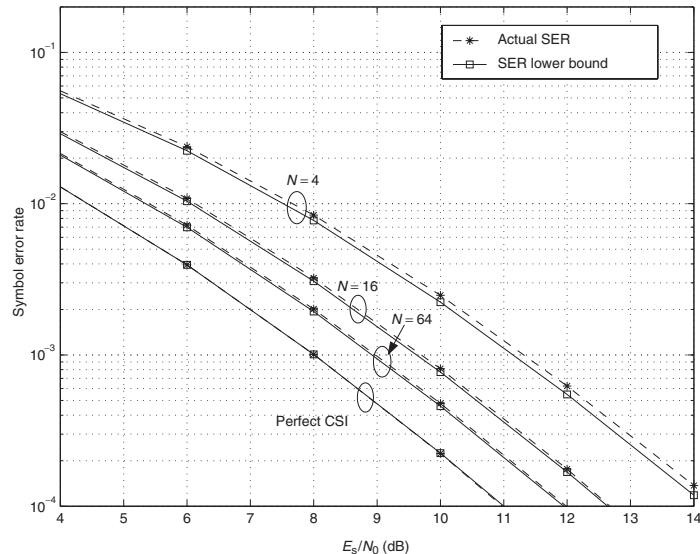


Figure 9.13 The actual SER versus the lower bound ($N_t = 4$)

combinations of existing space-time schemes with partial CSI are also possible. For example, one can improve the performance of STBC with finite-rate feedback, using a finite set of precoding matrices [21]; or, one can improve the performance of spatial multiplexers with either finite-rate feedback [20] or statistical CSI.

By casting the design of transmit-beamforming based on finite-rate feedback as an equivalent sphere vector quantization problem, [34] shows how to upper-bound the rate-distortion function of the vector source, and also lower-bound the operational rate-distortion performance achieved by the generalized Lloyd's algorithm. A simple relationship that emerges between the theoretical distortion limit and the achievable performance allows one to quantify the average signal-to noise-ratio performance. Building on designs for i.i.d. channels, [34] reports also beamformer codebook designs for correlated Rayleigh fading channels and derives a low-complexity codebook design that achieves near-optimal performance.

9.5 Adaptive Modulation with Partial CSI

In Section 9.4, the transmitter is exploiting partial CSI to improve the SER performance for a fixed modulation. On the other hand, the transmitter can dynamically change its modulation parameters to increase the data rate, subject to a predetermined error performance. This falls into the general framework of adaptive modulation [6]. In this section, we present two multiantenna transceivers with adaptive modulation based on partial CSI [39, 36].

9.5.1 Adaptive modulation based on 2D coder-beamformer

Fig. 9.14 depicts the multiantenna adaptive system put forth by [39], which is based on the 2D coder-beamformer in Fig. 9.6. Depending on channel feedback, the information bits are mapped to symbols drawn from a suitable constellation. The symbol stream is fed to the 2D coder-beamformer and transmitted through N_t antennas. For a fixed transmit-power, the adjustable transmitter parameters are the beam directions ($\mathbf{u}_{c,1}$ and $\mathbf{u}_{c,2}$), the power allocation ($\delta_{c,1}$ and $\delta_{c,2}$), and the constellation size M .

Since signal constellations are constantly adjusted in adaptive modulation, we need to adopt bit error rate (BER) as performance indicator rather than the SER we used in Section 9.4. Assuming Gray mapping on information bits, closed-form BER expressions can be

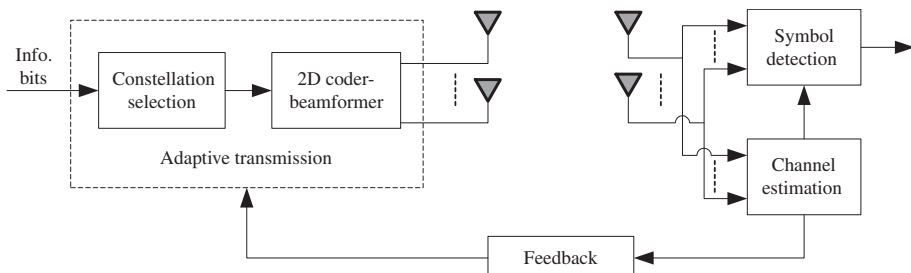


Figure 9.14 The system diagram for adaptive modulation-based 2D coder-beamformer

obtained, for example, QAM constellations. But in order to facilitate adaptive modulation, we rely on the following approximate BER expression that is very simple to compute and applicable to all constellations:

$$\text{BER}(\gamma) \approx 0.2 \exp(-g\gamma), \quad (9.104)$$

where g is the constellation-specific constant as listed in (9.58)–(9.60). The objective of the transmitter adaptation is to maximize the transmission rate while maintaining a target BER, denoted as $\text{BER}_{\text{target}}$.

We next describe the steps on transmitter adaptation with partial CSI in the form of mean feedback [39]. Suppose the transmitter has N different QAM constellations available with sizes

$$M_i = 2^i, \quad i = 1, 2, \dots, N. \quad (9.105)$$

For each constellation M_i , we denote the constant g as g_i . The value of g_i is evaluated from (9.59) or (9.60), depending on the constellation M_i . When the channel experiences deep fades, we will allow our adaptive design to suspend data transmission (this will correspond to setting $M_0 = 0$). The transmitter adapts its parameters as follows.

Transmitter adaptation to mean feedback

1. Collect the mean feedback parameters $(\bar{\mathbf{h}}, \sigma_\epsilon^2)$ and the system parameters (E_s, N_0) .
2. Fix the two beamforming vectors $\mathbf{u}_{c,1}$ and $\mathbf{u}_{c,2}$ as in (9.83).
3. For each constellation M_i , we first determine the associated optimal power-splitting factors $\delta_{c,1}$ and $\delta_{c,2}$. For notational convenience, we now denote them as $\delta_{i,1}$ and $\delta_{i,2}$ to signify the dependence on i , and calculate them as

$$\delta_{i,2} = [\delta_{i,2}^0]_+, \quad \delta_{i,1} = 1 - \delta_{i,2}, \quad (9.106)$$

$$\delta_{i,2}^0 := \frac{1 + \frac{N_r \sigma_\epsilon^2 + \lambda_1}{(N_r \sigma_\epsilon^2 + 2\lambda_1)\beta_i} + \frac{N_r \sigma_\epsilon^2 + \lambda_2}{(N_r \sigma_\epsilon^2 + 2\lambda_2)\beta_i}}{1 + \frac{(N_r \sigma_\epsilon^2 + 2\lambda_2)(N_r \sigma_\epsilon^2 + \lambda_1)^2}{(N_r \sigma_\epsilon^2 + 2\lambda_1)(N_r \sigma_\epsilon^2 + \lambda_2)^2}} - \frac{N_r \sigma_\epsilon^2 + \lambda_2}{(N_r \sigma_\epsilon^2 + 2\lambda_2)\beta_i}, \quad (9.107)$$

where $\beta_i = g_i \sigma_\epsilon^2 E_s / N_0$. The power computation of (9.106) is based on the approximate solution of [37]; see the details in [39]. For the MISO special case with $N_r = 1$, one can also use the exact computation in (9.75) with two virtual antennas.

With optimal $\delta_{i,\mu}$'s, we next compute the average BER for constellation M_i as

$$\overline{\text{BER}}(M_i) \approx 0.2 \prod_{\mu=1}^2 \left[\frac{1}{1 + \delta_{i,\mu}\beta_i} \exp\left(-\frac{\lambda_\mu \delta_{i,\mu}\beta_i}{N_r \sigma_\epsilon^2 (1 + \delta_{i,\mu}\beta_i)}\right) \right]^{N_r}. \quad (9.108)$$

The derivation of (9.108) is straightforward by averaging the instantaneous BER in (9.104) over the perceived random channels [c.f. (9.69)].

4. The transmitter finds the optimal constellation to be

$$M_{\text{opt}} = \arg \max_{M \in \{M_i\}_{i=0}^N} \overline{\text{BER}}(M) \leq \text{BER}_{\text{target}}. \quad (9.109)$$

Equation (9.109) can be simply solved by trial and error: we start with the largest constellation $M_i = M_N$ and then decrease i until we find the optimal M_i . With the optimal constellation chosen, the corresponding power splitting factors in step 3 are then chosen for transmission.

In this adaptation procedure, although $\bar{\mathbf{h}}$ has $N_t N_r$ entries, the constellation selection depends only on two eigenvalues: λ_1 and λ_2 . The two-dimensional space of (λ_1, λ_2) is thus split into $N + 1$ disjoint fading regions $\{D_i\}_{i=0}^N$, each one associated with one constellation. Specifically, we choose

$$M = M_i, \quad \text{when } (\lambda_1, \lambda_2) \in D_i, \forall i = 0, 1, \dots, N. \quad (9.110)$$

The rate achieved by the adaptive system in Fig 9.14 is given by

$$R = \sum_{i=1}^N \log_2(M_i) \iint_{D_i} p(\lambda_1, \lambda_2) d\lambda_1 d\lambda_2, \quad (9.111)$$

where $p(\lambda_1, \lambda_2)$ is the joint p.d.f. of λ_1 and λ_2 . The outage probability with no data transmission is thus:

$$P_{\text{out}} = \iint_{D_0} p(\lambda_1, \lambda_2) d\lambda_1 d\lambda_2. \quad (9.112)$$

In general, Monte Carlo simulations are needed to evaluate the rate in (9.111) and the outage probability in (9.112). Simple analytical expressions, however, are available for some special cases [39].

Numerical results

We now present numerical results for the adaptive system in Fig. 9.14. We adopt the channel setup of Example 1, with $\sigma_h^2 = 1$, and set $\text{BER}_{\text{target}} = 10^{-3}$. We recall that the feedback quality σ_ϵ^2 is related to the correlation coefficient $\rho = J_0(2\pi f_d \tau)$ via $\sigma_\epsilon^2 = 1 - |\rho|^2$.

Fig. 9.15 plots the rate achieved by the proposed adaptive transmitter with $N_t = 2$, $N_r = 1$, and $\rho = 1, 0.95, 0.9, 0.8, 0$. It is clear that the rate decreases relatively fast as the feedback quality drops.

For comparison, we also plot the average channel capacity with mean feedback, as summarized in Result 1. As shown in Fig. 9.15, the capacity is less sensitive to channel imperfections. With $\rho = 0.9$, the adaptive uncoded modulation is about 11 dB away from the capacity. The gap between capacity and transmission rate with uncoded modulation can be reduced considerably with coded modulation.

The adaptive system in Fig. 9.14 is for frequency-flat fading channels. The extension to adaptive MIMO-OFDM systems for frequency selective channels is carried out in [35], where joint power and bit loadings across OFDM subcarriers are combined with adaptive 2D coder-beamformer on a per subcarrier basis.

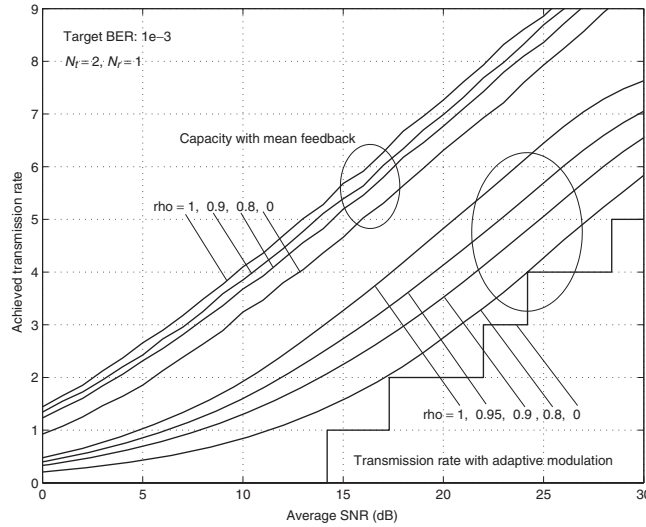


Figure 9.15 Transmission rates for variable feedback quality

9.5.2 Adaptive modulation/beamforming with finite-rate feedback

In Subsection 9.4.2, we were interested in the performance improvement of 1D beamforming in a MISO system with finite-rate feedback. In this subsection, we aim to improve the transmission rate via adaptive modulation in conjunction with the transmit beamforming, subject to a target BER performance. Different from Fig. 9.11, we now allow the transmission power and the signal constellation to vary, as depicted in Fig. 9.16.

With P denoting the transmit power, we assume that the information symbol s is drawn from an appropriate signal constellation of size M with average energy $E_s = 1$. With the beam-steering vector \mathbf{w} , the vector $\mathbf{w}^H \sqrt{P} s$ is transmitted through multiple antennas. The received signal is thus (c.f. (9.85)):

$$y = \mathbf{w}^H \mathbf{h} \sqrt{P} s + v, \quad (9.113)$$

where v is AWGN with zero mean and variance N_0 .

For adaptive modulation, we adopt rectangular and square QAM constellations with $M = 2^b$, where b is an integer. The transmission mode in our current setup is then characterized by the triplet of constellation size, transmission power, and beamforming vector, denoted as (M, P, \mathbf{w}) . With B feedback bits, the transmitter needs to construct $N = 2^B$ transmission modes, with each mode defined as

$$\mathcal{M}_n := (M_n, P_n, \mathbf{w}_n), \quad n \in \{1, 2, \dots, N\}.$$

Notice that different transmission modes may adopt the same signal constellation.

At the receiver side, the channel space is partitioned to N nonoverlapping regions, denoted as $\mathcal{H}_1, \dots, \mathcal{H}_N$. The design of the fading regions and transmission modes determines the achievable data rate. Our ultimate goal is to design $\{\mathcal{H}_n\}_{n=1}^N$ and $\{\mathcal{M}_n\}_{n=1}^N$ jointly

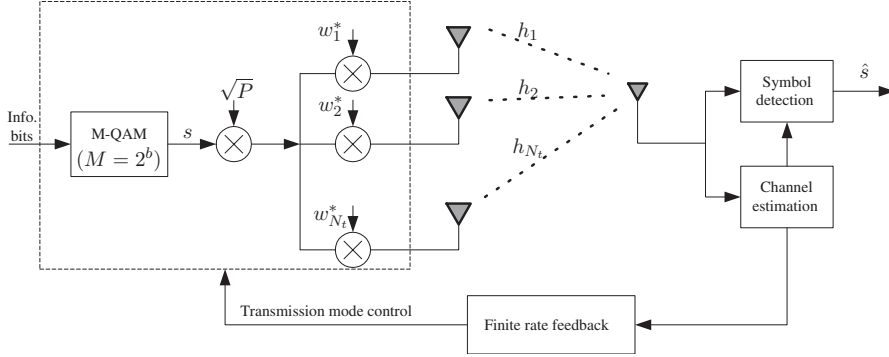


Figure 9.16 The system model with adaptive modulation/beamforming

to maximize the system transmission rate, subject to certain error performance and power constraints, as we formulate next.

To simplify the adaptive transceiver design, we rely on the approximate BER in (9.104). When the selected transmission mode is \mathcal{M}_n , we have from (9.113) that the output SNR is

$$\gamma_n = |\mathbf{w}_n^\mathcal{H} \mathbf{h}|^2 \cdot P_n / N_0. \quad (9.114)$$

The BER averaged over the channels in the region \mathcal{H}_n can then be written as

$$\overline{\text{BER}}_n = \text{E}_{\mathcal{H}_n} \left[0.2 \exp \left(-g_n |\mathbf{w}_n^\mathcal{H} \mathbf{h}|^2 P_n / N_0 \right) \right], \quad (9.115)$$

where g_n is the constellation-specific constant. Let $A_n := \Pr(\mathbf{h} \in \mathcal{H}_n)$ denote the probability that the channel vector \mathbf{h} lies in region \mathcal{H}_n , P_0 stand for the average power, and $\overline{\text{BER}}_0$ be the required BER performance. By jointly designing $\{\mathcal{H}_n\}_{n=1}^N$ and $\{\mathcal{M}_n\}_{n=1}^N$, the ultimate objective is to

$$\begin{aligned} & \text{maximize} && \sum_{n=1}^N A_n b_n, \\ & \text{subject to } 1) && \sum_{n=1}^N A_n P_n \leq P_0, \\ & && 2) \quad \|\mathbf{w}_n\| = 1, \quad \forall n, \\ & && 3) \quad b_n \in \{0, 1, 2, 3, \dots\}, \quad \forall n, \\ & && 4) \quad \overline{\text{BER}}_n \leq \overline{\text{BER}}_0, \quad \forall n. \end{aligned} \quad (9.116)$$

Equation (9.116) provides the general formulation for adaptive modulation on top of 1D beamforming with finite-rate feedback. However, solving (9.116) is difficult, which motivates suboptimal alternatives.

One possible approach is to rely on the finite-rate beamformer of Section 9.4.2. For example, one can divide the B feedback bits into two parts $B = B_1 + B_2$, with B_2 bits

dedicated to beamforming vectors, and the remaining B_1 bits conveying information about power loading and constellation selection. With the good beamformers of Section 9.4.2, the task is now to find power and constellation allocation utilizing finite-rate beamforming. The optimal distribution of B_1 and B_2 will also need to be specified in this approach.

Another approach is provided by [36], which simplifies the problem in (9.116) to a vector quantization problem through a series of approximations. The iterative algorithm described in Section 9.3.2 can be modified and used to find an approximate solution, as detailed in [36].

9.5.3 Other combinations

In subsection 9.5.1, adaptive modulation is combined with the 2D coder-beamformer on the basis of mean feedback to enhance the transmission rate. In subsection 9.5.2, adaptive modulation is combined with beamforming on the basis of finite-rate feedback. As one changes the basic modulation module, other adaptive systems can be constructed. For example, spatial multiplexers offer high rate transmitters that take full advantage of multiple antennas at both the transmitter and the receiver side. Combination of adaptive modulation with spatial multiplexing with either statistical CSI or finite rate feedback constitutes an interesting direction for future research.

9.6 Conclusions

This chapter highlights recent advances on multiinput multioutput (MIMO) communications based on partial CSI, from both information- and communication-theoretic perspectives. We first present two commonly used partial CSI models, one based on statistical modeling, and the other with rate constraints imposed on the feedback channel directly. On the basis of either statistical or finite-rate CSI, we presented optimal transmissions from different perspectives, which either maximize the mutual information between channel input and output or improve the error performance with fixed rate for a given space-time coding design or enhance the system throughput via adaptive modulation subject to a target error performance.

The schemes covered in this chapter are only representative of this specific research topic. Numerous possibilities on different configurations can be explored for future research.

Appendix

For convenience, we collect useful identities that have been used either explicitly or implicitly in the derivations of the main text in this chapter.

- Kronecker product properties:

$$(\mathbf{A}_1 \otimes \mathbf{A}_2)(\mathbf{A}_3 \otimes \mathbf{A}_4) = (\mathbf{A}_1 \mathbf{A}_3) \otimes (\mathbf{A}_2 \mathbf{A}_4) \quad (9.117)$$

$$(\mathbf{A} \otimes \mathbf{B})^T = \mathbf{A}^T \otimes \mathbf{B}^T \quad (9.118)$$

$$(\mathbf{A} \otimes \mathbf{B})^{-1} = \mathbf{A}^{-1} \otimes \mathbf{B}^{-1} \quad (9.119)$$

$$|\mathbf{I}_N \otimes \mathbf{A}| = |\mathbf{A}|^N \quad (9.120)$$

- Vec operator properties

$$\text{vec}(\mathbf{AB}) = (\mathbf{I} \otimes \mathbf{A})\text{vec}(\mathbf{B}) \quad (9.121)$$

$$\|\mathbf{AB}\|_F^2 = \text{vec}^H(\mathbf{B})[\mathbf{I} \otimes (\mathbf{A}^H \mathbf{A})]\text{vec}(\mathbf{B}) \quad (9.122)$$

- For a Gaussian vector $\mathbf{z} \sim \mathcal{CN}(\boldsymbol{\mu}, \boldsymbol{\Sigma})$ and a Hermitian matrix \mathbf{A} , the following identity holds true.

$$\begin{aligned} \mathbb{E}\{e^{-\mathbf{z}^H \mathbf{Az}}\} &= \frac{\exp(-\boldsymbol{\mu}^H \mathbf{A}(\mathbf{I} + \boldsymbol{\Sigma} \mathbf{A})^{-1} \boldsymbol{\mu})}{|\mathbf{I} + \boldsymbol{\Sigma} \mathbf{A}|} \\ &= \frac{\exp(-\boldsymbol{\mu}^H [\boldsymbol{\Sigma}^{-1} - (\boldsymbol{\Sigma} + \boldsymbol{\Sigma} \mathbf{A} \boldsymbol{\Sigma})^{-1}] \boldsymbol{\mu})}{|\mathbf{I} + \boldsymbol{\Sigma} \mathbf{A}|}. \end{aligned} \quad (9.123)$$

- Suppose $\boldsymbol{\Lambda}_Q$ is an $N \times N$ positive semi definite matrix with diagonal entries arranged in nonincreasing order, that is, $[\boldsymbol{\Lambda}_Q]_{1,1} \geq \dots \geq [\boldsymbol{\Lambda}_Q]_{N,N}$. Suppose $\boldsymbol{\Lambda}_A$ is an $N \times N$ positive definite matrix with diagonal entries arranged in nonincreasing order. If for arbitrary unitary matrix \mathbf{U}_Q , we define $\mathbf{Q} = \mathbf{U}_Q \boldsymbol{\Lambda}_Q \mathbf{U}_Q^H$, it follows that

$$\text{tr}\{\mathbf{Q} \boldsymbol{\Lambda}_A^{-1}\} \geq \text{tr}\{\boldsymbol{\Lambda}_Q \boldsymbol{\Lambda}_A^{-1}\}, \quad (9.124)$$

where the equality holds when $\mathbf{U}_Q = \mathbf{I}_N$ (the proof can be found in, for example, [13]).

References

- [1] S. M. Alamouti, "A simple transmit diversity technique for wireless communications," *IEEE Trans. Commun.*, vol. 16, no. 8, pp. 1451–1458, Oct. 1998.
- [2] R. S. Blum, "MIMO with limited feedback of channel state information," in *Proceedings of International Conference on ASSP*, Hong Kong, April 2003, pp. 89–92.
- [3] H. Boche and E. Jorswieck, "Optimum power allocation and complete characterization of the impact of correlation on the capacity of MISO systems with different CSI at the transmitter," in *Proceedings of International Symposium Information Theory*, Yokohama, Japan, Jul. 2003, pp. 353–353.
- [4] H. Boche and E. Jorswieck, "On the optimality-range of beamforming for MIMO systems with covariance feedback," *IEICE Trans. Fund. Electron., Commun. Comput. Sci.*, vol. E85-A, no. 11, pp. 2521–2528, Nov. 2002.
- [5] P. A. Chou, T. Lookabaugh, and R. M. Gray, "Entropy-constrained vector quantization," *IEEE Trans. Acoust., Speech, Signal Process.*, vol. 37, no. 1, pp. 31–42, Jan. 1989.
- [6] S. T. Chung and A. J. Goldsmith, "Degrees of freedom in adaptive modulation: a unified view," *IEEE Trans. Commun.*, vol. 49, no. 9, pp. 1561–1571, Sept. 2001.
- [7] J. H. Conway, R. H. Hardin, and N. J. A. Sloane, "Packing Lines, Planes, etc.: Packings in Grassmannian Space," *Exp. Math.*, vol. 5, pp. 139–159, 1996.
- [8] G. Ganesan and P. Stoica, "Space-time block codes: a maximum SNR approach," *IEEE Trans. Inf. Theory*, vol. 47, no. 4, pp. 1650–1656, May 2001.
- [9] A. Gersho and R. M. Gray, *Vector Quantization and Signal Compression*, Kluwer Academic Publishers, 1992.
- [10] D. Gesbert, H. Bolcskei, D. A. Gore, and A. J. Paulraj, "Outdoor MIMO wireless channels: models and performance prediction," *IEEE Trans. Commun.*, vol. 50, no. 12, pp. 1926–1934, Dec. 2002.

- [11] A. Goldsmith, S. A. Jafar, N. Jindal, and S. Vishwanath, "Capacity limits of MIMO channels," *IEEE J. Sel. Areas Commun.*, vol. 21, no. 5, pp. 684–702, Jun. 2003.
- [12] S. A. Jafar and A. J. Goldsmith, "Transmitter optimization and optimality of beamforming for multiple antenna systems with imperfect feedback," *IEEE Trans. Wireless Commun.*, vol. 3, no. 4, pp. 1165–1175, Jul. 2004.
- [13] S. A. Jafar, S. Vishwanath, and A. Goldsmith, "Channel capacity and beamforming for multiple transmit and receive antennas with covariance feedback," in *Proceedings of International Conference on Communications*, Helsinki, Finland, June 2001, vol. 7, pp. 2266–2270.
- [14] G. Jöngren, M. Skoglund, and B. Ottersten, "Combining beamforming and orthogonal space-time block coding," *IEEE Trans. Inf. Theory*, vol. 48, no. 3, pp. 611–627, Mar. 2002.
- [15] E. A. Jorswieck and H. Boche, "Optimal transmission with imperfect channel state information at the transmit antenna array," *Wireless Pers. Commun.*, vol. 4, pp. 33–56, Oct. 2003.
- [16] J. P. Kermoal, L. Schumacher, K. I. Pedersen, P. E. Mogensen, and F. Frederiksen, "A stochastic MIMO radio channel model with experimental validation," *IEEE J. Sel. Areas Commun.*, vol. 20, no. 6, pp. 1211–1226, Aug. 2002.
- [17] V. Lau, Y. Liu, and T.-A. Chen, "On the design of MIMO block-fading channels with feedback-link capacity constraint," *IEEE Trans. Commun.*, vol. 52, no. 1, pp. 62–70, Jan. 2004.
- [18] Y.-C. Liang and F. P. S. Chin, "Downlink channel covariance matrix (DCCM) estimation and its applications in wireless DS-CDMA systems," *IEEE J. Sel. Areas Commun.*, vol. 19, no. 2, pp. 222–232, Feb. 2001.
- [19] D. Love, *Personal Webpage on Grassmannian Subspace Packing*, Online at <http://dynamo.ecn.purdue.edu/~djlove/grass.html>, 2004.
- [20] D. J. Love and R. W. Heath Jr., "Limited feedback precoding for spatial multiplexing systems," in *Proceedings of Global Telecommunications Conference*, San Francisco, CA, Dec. 2003.
- [21] D. J. Love and R. W. Heath Jr., "Diversity performance of precoded orthogonal space-time block codes using limited feedback," *IEEE Commun. Lett.*, vol. 8, no. 5, pp. 305–307, May 2004.
- [22] D. J. Love, R. W. Heath Jr., and T. Strohmer, "Grassmannian beamforming for multiple-input multiple-output wireless systems," *IEEE Trans. Inf. Theory*, vol. 49, no. 10, pp. 2735–2747, Oct. 2003.
- [23] A. Moustakas and S. Simon, "Optimizing multiple-input single-output (MISO) communication systems with general Gaussian channels: nontrivial covariance and nonzero mean," *IEEE Trans. Inf. Theory*, vol. 49, no. 10, pp. 2770–2780, Oct. 2003.
- [24] K. K. Mukkavilli, A. Sabharwal, E. Erkip, and B. Aazhang, "On Beamforming with finite rate feedback in multiple antenna systems," *IEEE Trans. Inf. Theory*, vol. 49, no. 10, pp. 2562–2579, Oct. 2003.
- [25] A. Narula, M. J. Lopez, M. D. Trott, and G. W. Wornell, "Efficient use of side information in multiple-antenna data transmission over fading channels," *IEEE J. Sel. Areas Commun.*, vol. 16, no. 8, pp. 1423–1436, Oct. 1998.
- [26] H. Ozcelik, M. Herdin, W. Weichselberger, J. Wallace, and E. Bonek, "Deficiencies of 'Kronecker' MIMO radio channel model," *Electron. Lett.*, vol. 39, no. 16, pp. 1209–1210, Aug. 2003.
- [27] D.-S. Shiu, G. J. Foschini, M. J. Gans, and J. M. Kahn, "Fading correlation and its effect on the capacity of multi-element antenna systems," *IEEE Trans. Commun.*, vol. 48, no. 3, pp. 502–513, Mar. 2000.
- [28] M. K. Simon and M.-S. Alouini, *Digital Communication over Generalized Fading Channels: A Unified Approach to the Performance Analysis*, John Wiley & Sons, 2000.
- [29] S. Simon and A. Moustakas, "Optimizing MIMO antenna systems with channel covariance feedback," *IEEE J. Sel. Areas Commun.*, vol. 21, no. 3, pp. 406–417, Apr. 2003.

- [30] V. Tarokh, H. Jafarkhani, and A. R. Calderbank, "Space-time block codes from orthogonal designs," *IEEE Trans. Inf. Theory*, vol. 45, no. 5, pp. 1456–1467, Jul. 1999.
- [31] I. E. Telatar, "Capacity of multi-antenna Gaussian channels," *Eur. Trans. Telecommun.*, vol. 10, no. 6, pp. 585–595, Nov.–Dec. 1999.
- [32] E. Visotsky and U. Madhow, "Space-time transmit precoding with imperfect feedback," *IEEE Trans. Inf. Theory*, vol. 47, no. 6, pp. 2632–2639, Sept. 2001.
- [33] P. Xia, *Beamforming Codebooks Obtained by the Lloyd's Algorithm*, Online at <http://spincom.ece.umn.edu/pengfei/codebooks/> 2004.
- [34] P. Xia and G. B. Giannakis, "Design and analysis of transmit-beamforming based on limited-rate feedback," in *Proc. of the Vehicular Tech. Conf.*, Los Angeles, CA, September 16–19, 2004.
- [35] P. Xia, S. Zhou, and G. B. Giannakis, "Adaptive MIMO OFDM based on partial channel state information," *IEEE Trans. Signal Process.*, vol. 52, no. 1, pp. 202–213, Jan. 2004.
- [36] P. Xia, S. Zhou, and G. B. Giannakis, "Multi-antenna adaptive modulation with beamforming based on bandwidth-constrained feedback," *IEEE Trans. Commun.*, 2005 (to appear).
- [37] S. Zhou and G. B. Giannakis, "Optimal transmitter eigen-beamforming and space-time block coding based on channel mean feedback," *IEEE Trans. Signal Process.*, vol. 50, no. 10, pp. 2599–2613, Oct. 2002.
- [38] S. Zhou and G. B. Giannakis, "Optimal transmitter eigen-beamforming and space-time block coding based on channel correlations," *IEEE Trans. Inf. Theory*, vol. 49, no. 7, pp. 1673–1690, Jul. 2003.
- [39] S. Zhou and G. B. Giannakis, "Adaptive modulation for multi-antenna transmissions with channel mean feedback," *IEEE Trans. Wireless Commun.*, vol. 3, no. 5, pp. 1626–1636, Sept. 2004.
- [40] S. Zhou, Z. Wang, and G. B. Giannakis, "Quantifying the power-loss when transmit-beamforming relies on finite rate feedback," *IEEE Trans. Wireless Commun.*, 2005 (to appear).

Index

- algorithm
 - antenna selection, 251, 254, 259, 260
 - beamforming, 233
 - block-diagonalization, 228, 231
 - channel inversion, 211, 220
 - decremental selection, 262, 263
 - distributed primal-dual, 280
 - downlink, 222
 - ESPRIT, 43
 - Gauss-Seidel, 280
 - generalized Lloyd, 331
 - gradient projection, 280
 - incremental selection, 261, 263
 - integer least-squares, 225
 - interference-balancing, 211
 - interior-point, 304
 - iterative water-filling, 280
 - JAFE, 59
 - lattice reduction, 223
 - Lenstra-Lenstra-Lovász, 226, 234
 - Lloyd, 330, 345, 347
 - localized gradient, 58
 - low-complexity selection, 260
 - matrix pencil, 59
 - maximal ratio combining, 233
 - maximum norm based selection, 262
 - MMSE, 233
 - modulo precoding, 222, 223
 - multidimensional folding, 47, 53, 61
 - multiuser MIMO downlink, 217
 - MUSIC, 44, 53, 57
 - power control, 211
 - power control iterative, 280
 - precoding, 225
 - QR-based, 225
 - RARE, 61
 - scheduling, 235, 236
 - selection, 255, 262
 - SIMO/MISO selection, 251
 - sphere, 221
 - subset selection, 254
 - unitary ESPRIT, 55, 56
- amplifier, 25, 31–34
 - design, 32
 - gain, 34
 - input, 31
 - low noise, 245
 - matching, 33
 - noise characteristics, 33
 - noisy, 31
 - output, 31
 - performance, 32
 - power, 225, 245
 - receiver, 29, 30
 - uncoupled, 32
- angle
 - of arrival, 322, 328
 - spread, 322, 328
- angular spread, 27
- antenna
 - aperture, 12, 64, 66
 - array, 1, 15, 24, 62, 328
 - bandwidth, 12
 - base station, 25
 - calibration, 68
 - configurations, 3
 - correlation coefficients, 97
 - coupled, 29

- antenna (*Continued*)
coupling, 33, 68
decorrelation distance, 79
dipole, 27
dual-polarization, 28
element, 1, 5, 13, 17, 26, 63, 80,
82, 245, 246, 248, 252
high-gain, 12
impedance, 32
loop, 27
lossless, 29
multibeam, 25
multimode, 26
multipolarized, 27
mutual coupling, 1, 5, 25, 27, 28, 32
open-circuit, 29, 31
optimal selection, 256, 259, 264
optimal set, 259
optimally selected, 248, 249
polarization, 25
radiation pattern, 12, 25, 26, 29, 30
receive, 5–9, 12, 17–19, 24, 31, 63,
64, 67, 78–81, 98, 105, 108,
143, 149, 169, 170, 172, 188,
197, 201, 204, 211, 212, 214,
215, 227, 233, 245, 246, 248,
250–252, 254, 255, 259, 261,
262, 265, 301, 319, 322, 323,
338
receive selection, 251
selection, 245, 246, 248, 250, 251,
254–256, 259, 260, 262, 263,
266
selection gain, 248
separation, 15
spacing, 9, 10, 17, 23, 24, 34,
322
steered, 12
suboptimal selection, 259, 264
subset selection, 245, 254
switching, 66
system, 24
terminals, 3, 29–31
transmit, 5–9, 12, 17–19, 63, 64,
67, 78–81, 105, 128, 143, 169,
170, 172, 173, 187, 190, 193,
197, 198, 201, 204, 211–213,
215, 227, 231, 235, 245, 246,
248, 251, 252, 254, 255, 259,
264, 265, 301, 319, 320, 322,
323, 331, 338
vector field pattern, 24
vertically polarized patch, 22
array
aperture, 13
configurations, 5, 14, 25
coupled, 30
dual, 62
dual polarization, 25
element, 3
loss, 262
monopole, 11, 22
on the mobile, 25
output signal, 31
patch, 22, 28
processing, 106, 115, 146
radiation pattern, 3, 22
receive, 2, 3, 10, 41, 63, 65, 67
response, 68, 299
shape, 25
single polarization, 25
size, 11
switched, 5
system, 6
topology, 25
transmit, 2, 3, 10, 29, 30, 34, 41,
63–65, 231
uncertainties, 299
uniform circular, 66, 69
uniform linear, 64, 69
uniform rectangular, 65
virtual, 5
bandwidth, 3, 236, 279
antenna, 12
constraint, 322
efficiency, 153
frequency, 20
minimal, 235
power, 33
signal, 63, 66, 69
waveform, 4

- base station, 25, 62, 209, 212, 217, 231, 232, 234–236
antenna, 235
multiantenna, 278, 300
beam
 direction, 347
 optimal direction, 337
 random, 235
 steering, 350
beamforming, 13, 211, 270, 277, 278, 284, 302, 312, 342
 adaptive, 159, 350
 conventional, 340
 coordinated Tx/Rx, 231, 233
 finite-rate, 343, 351, 352
 joint transmit/receive, 236
 linear, 210, 213, 226
 linear transmit, 226
 matrix, 227, 329
MIMO, 78, 83, 84, 274
minimum variance distortionless response, 277
MMSE receive, 232
MMSE transmit, 211
multiple, 282
multiuser, 278
nonrobust, 309
one-dimensional, 329, 338–341, 345, 350, 351
opportunistic, 235
optimal directions, 337
optimal receive, 211, 232
optimal vector, 342
optimum, 83
power loaded, 333
receive, 211, 212, 231, 233, 234, 299
regularized transmit, 211
robust, 277, 279
robust worst-case, 277
single, 296, 301
transmit, 63, 211, 218, 232, 234, 331, 341, 342, 347, 350
transmit-receive, 231, 232, 234, 270, 284
two-dimensional, 338–340
vector, 338, 342, 348, 350, 352
zero-forcing receive, 211, 218
zero-forcing transmit, 211
bipolar junction transistor, 33
bit allocation, 285, 294
BLAST, 41, 169, 170, 209, 223, 225
 MMSE, 225
bound
 capacity, 211, 218, 256
 Chernoff, 178, 179, 181, 285
 Foschini's, 252
 pairwise error probability, 179
 sum capacity, 210
 symbol error rate, 334, 340, 345
 union, 134, 135
capacity, 11, 22, 23, 25, 26, 28, 32, 34, 35, 197, 210, 213–216, 218, 219, 228, 234, 236, 251, 255, 256, 326, 328
average, 324, 326, 329, 349
bound, 218
channel, 177, 248, 251, 252, 256, 260, 270, 279, 308, 328
dirty paper, 215
distribution function, 228, 233, 250
ergodic, 170, 174, 175, 328, 330
gain, 251
link, 279, 280
maximum, 213
MIMO, 169, 170, 247, 252, 253, 257, 319
MIMO broadcast, 215
multiuser, 219, 234
multiuser sum, 215
network, 210
optimization, 329–331
outage, 249, 250, 262, 329
region, 213, 214, 234
Shannon, 251, 259
sum, 210, 211, 213, 214, 219, 224, 233, 280
system, 105, 211, 215, 219
user, 41
worst-case, 80
capacity-optimal
 transmissions, 323, 324

- CDMA, 77, 157, 223, 291
 cellular radio, 63
 central limit theorem, 17
 channel
 AWGN, 118, 120, 122, 137, 140
 block-diagonalization, 227, 236
 broadcast, 209, 210, 215, 234, 235
 capacity, 5, 9, 10, 17, 22, 77, 177,
 197, 248, 251, 252, 255, 256,
 260, 270, 279, 308, 328, 349
 capacity bounds, 17
 characteristics, 322
 correlated, 79, 124
 correlated Rayleigh, 126
 correlated Rayleigh fading, 347
 correlation, 322
 covariance, 210
 delay profile, 66
 delay spread, 5
 diagonalization, 234
 diagonalizing, 211
 diversity, 251
 double-directional, 11, 13, 42, 64
 downlink, 210, 216
 downlink covariance, 322
 eigenmode, 270, 288, 290, 291, 297
 ergodic, 80
 estimate, 151, 152, 299
 estimation, 8, 13, 146, 147, 149,
 235, 299
 excess delay, 65
 fading, 77–80, 88, 101, 105, 124,
 169, 170, 216, 297, 301, 319
 feedback, 8, 212, 217, 299, 307,
 308, 320, 322, 329, 347, 352
 flat block fading, 106, 118, 143
 flat fading, 4, 108, 114, 118, 216,
 246, 299
 frequency-flat, 79, 349
 frequency nonselective, 4
 frequency-selective, 3, 4, 216, 269,
 299, 349
 frequency-flat fading, 319
 gain, 19
 Gaussian interference, 216
 identifiability, 150
 ill-conditioned, 218, 220
 impulse response, 3, 20, 30, 64, 65,
 67, 70
 indoor, 20
 inversion, 211, 217–219, 222, 223,
 228, 232, 236
 keyhole, 18
 line-of-sight, 79
 linear time invariant, 246
 low-rank, 211
 matrix, 3–5, 10, 11, 14, 17, 18, 22,
 30, 79, 81, 113–115, 119, 135,
 146, 159, 172, 174, 222, 223,
 255, 259, 265, 281, 282, 290,
 300, 323, 324, 329
 measured, 10, 11, 22
 measurement, 5, 11, 13, 17
 MIMO, 286, 295, 296, 300, 307
 ML estimate, 7
 ML inversion technique, 7
 model, 4, 13, 41, 42, 62, 63
 modeled, 11, 22
 modeling, 17, 29, 269
 multiantenna, 296, 299
 multipath, 11
 multiple access, 210, 235, 280
 multiuser, 211, 217
 multiuser downlink, 210
 mutual information rate, 77
 narrowband, 216
 non-line-of-sight, 79
 nonergodic, 80
 path loss, 5
 pinhole, 18
 power gain, 5
 precoding, 217
 probing, 6
 quasi-static, 216
 random fading, 254
 rank-deficient, 18, 218
 Rayleigh, 78–80, 89, 94, 96, 119,
 121, 122, 126–128, 131, 222,
 247, 251, 255
 reciprocity, 299, 307
 regularized inversion, 217–220,
 222, 236

- response, 64
- Rician, 78, 80, 88, 94, 95, 101, 119, 121–123, 128–131
- semicorrelated, 79, 96
- sounding, 42, 53, 65, 66
- state information, 81, 82, 119, 145, 154, 161, 178, 187, 210, 211, 216, 217, 226, 232, 234–236, 270, 298–301, 308, 309, 319–324, 326, 328, 331, 332, 334, 344, 345, 347, 348, 352
- stationarity, 18
- time-invariant, 18
- time-varying, 5, 65, 216, 235, 321
- tracking, 236
- transfer function, 4, 11
- transfer matrix, 3, 7, 12, 22
- uncorrelated, 79, 126
- uncorrelated Rayleigh, 119, 133
- uplink covariance, 322
- variation, 3, 8
- vector, 14, 82, 148, 149, 152, 153, 320
- wideband, 216
- code
 - Alamouti’s, 105, 128, 142–144, 149, 157, 161, 299, 337
 - amicable design, 105, 149
 - binary, 8
 - convolutional, 264
 - correlating, 6
 - cyclotomic diagonal linear space-time, 193
 - cyclotomic diagonal space-time, 171
 - cyclotomic linear dispersion, 197
 - diagonal space-time, 170, 193
 - dirty paper, 223
 - full diversity, 170, 171, 194, 200
 - full diversity linear dispersion, 171, 192, 194, 195
 - full diversity rectangular linear dispersion, 204
 - full diversity space-time, 197
 - full length, 6
 - full rate, 170, 171, 197, 200
- Gamal and Damen’s, 203
- Gaussian, 270
- generalized orthogonal design, 149
- information lossless, 170, 171
- length, 7, 8, 236
- linear cyclotomic, 197
- linear diagonal space-time block, 197
- linear dispersion, 134, 144, 145, 170, 172–174, 177, 179, 181, 184, 187, 188, 193, 195, 197, 200, 301
- linear dispersion space-time, 204
- linear space-time block, 170, 173, 181, 197, 204
- linear unitary, 134
- low density parity check, 234
- ML, 203
- nonsquare space-time, 171
- orthogonal design, 105
- orthogonal linear dispersion, 187
- orthogonal space-time block, 170, 183, 299
- rate, 143
- Rekaya, Belfiore and Viterbo’s, 203
- repeat-accumulate, 234
- space-time, 3, 171, 178
- space-time block, 170, 171
- space-time orthogonal, 105
- space-time trellis, 105, 170
- synchronization, 6, 7
- trace-orthogonal, 174, 182, 183, 191, 197, 204
- trace-orthogonal linear dispersion, 182, 187, 188, 190–192, 194
- trace-orthogonal linear triangular space-time block, 198
- trace-orthogonal space-time, 200, 203
- transmit, 6
- codebook, 330, 342
 - beamformer, 345, 347
 - design, 347
 - Gaussian, 81
 - of beamforming vectors, 342
 - size, 343

- codeword, 331
 - probability, 331
 - space-time, 331
 - STBC, 335, 336
- coding, 212, 216, 236
 - differential space-time, 146, 155
 - dirty paper, 211, 215, 219, 220, 223, 225, 234
 - gain, 197, 199, 200, 205
 - interference-depending, 220
 - multiantenna multiuser, 234
 - nested lattices, 234
 - orthogonal space-time block, 331
 - space-time, 13, 41, 105, 111, 146, 187, 270, 319, 323, 331, 352
 - space-time block, 105, 157
- coding-beamforming, 337, 338, 347
- constellation, 119–121, 123, 126, 130, 134–138, 142, 144–146, 149, 170, 171, 178, 179, 193, 198, 202, 204, 212, 216, 270, 285, 294, 333
 - M*-ary QAM, 283
 - 16-QAM, 223, 339
 - 2-PAM, 222
 - average energy, 123
 - biorthogonal, 128
 - BPSK, 143, 144, 149, 282, 294
 - constant modulus, 151, 152
 - design, 140
 - dimension-constrained, 135, 140
 - energy, 143
 - fixed, 294
 - GMSK, 282
 - large-size, 134
 - largest minimum distance, 139, 141
 - matrix, 134, 142
 - members, 134
 - MPSK, 152
 - multidimensional, 128
 - multidimensional OSTBC, 134
 - nonseparable, 111, 119, 128, 143
 - optimal, 133, 137, 138, 141–144, 349
 - PAM, 171
 - point, 140, 152, 159, 221
 - PSK, 344, 345
 - QAM, 171, 282, 295, 348, 350
 - QPSK, 126, 128, 149, 161, 294, 297, 339, 345
 - regular simplex, 134, 141, 142
 - scaling, 137
 - selection, 349
 - separable, 111, 116, 119
 - shape, 118, 147
 - simplex, 128, 132
 - size, 134, 144, 323, 335, 337, 347
 - small-size, 134, 141, 143
 - space invariance, 106, 111, 115, 116, 118, 119, 163
 - space-time, 133, 134, 144
 - two-dimensional, 345
 - unitary, 134
 - vector, 110
- convertor
 - analog-to-digital, 245
- correlation, 343
 - frequency, 296
 - matrix, 44, 119, 128, 322
 - receive, 9, 10, 17, 18, 25, 128
 - spatial, 296
 - transmit, 9, 10, 17, 18, 128, 336
- correlation matrix
 - channel, 337
 - receive, 322
 - transmit, 322
- covariance
 - channel, 210
 - full, 15
 - interference, 213
 - matrix, 14–18, 26, 81, 97, 147, 153, 159, 172, 174, 178, 214, 278, 281, 321, 322, 325, 327, 328
 - one-sided, 329
 - receive, 79
 - shift-invariant, 15
 - transmit, 79
- covariance matrix
 - array, 299
 - channel, 321, 328
 - data, 147
 - interference-plus-noise, 301

- noise, 280
- optimal, 329
- receive, 14, 15, 18
- sample, 151, 152, 161
- transmit, 14, 15, 18, 33, 280
- true, 151, 161
- Cramer-Rao bound, 59
- criterion
 - average capacity, 329
 - capacity, 256, 330
 - code design, 105
 - determinant, 179
 - maximum capacity, 255
 - minimum average BER, 294
 - MMSE, 218
 - orthogonality, 235
 - rank, 179
- decoder, 119
 - blind, 155
 - blind OSTBC, 106
 - coherent ML, 106, 110, 111, 115–117, 135, 155
 - differential, 106, 155
 - incoherent (blind), 115
 - incoherent ML, 155, 163
 - ML, 105, 111, 115, 116, 118, 119, 133, 135, 145, 163
 - nearest neighbor, 146
 - optimal ML, 145, 146
 - space-time, 3
 - symbol-by-symbol, 145
- decoding, 117, 152, 222, 234
 - algorithm, 146, 152
 - blind, 145, 152, 155–157
 - complexity, 105
 - equation, 117
 - formulae, 116
 - incoherent, 163
 - optimal linear, 332
 - optimal ML, 116, 130
 - OSTBC, 152
 - space-time, 157
 - symbol-by-symbol, 115, 116, 130
 - symbol-by-symbol ML, 106
 - unambiguous, 221
- degrees of freedom, 71, 121, 125, 161, 247, 253, 307
 - spatial, 26, 27
 - total, 169
- delay
 - channel excess, 65
 - feedback, 320
 - profile, 67
 - spread, 62
- demapper
 - soft, 264
- demultiplexing
 - spatial, 227
- detection
 - error, 177
 - ML, 119, 178, 283, 303
 - ML symbol, 153
 - multiuser, 159, 210
 - symbol, 153, 155
- detector
 - ML, 169, 170, 178, 179, 187, 197, 205, 300–302
 - MMSE, 184, 187, 203, 204
 - symbol-by-symbol, 160
- DFT, 291
- diagonal loading, 159, 278
- digital pattern generator, 6
- digital subscriber line, 223
 - wireline, 269
- dipole
 - coupled, 33
 - half-wave, 33
 - spacing, 34
- direction
 - of arrival, 12, 20, 42, 63, 64, 236
 - of departure, 12, 20, 42, 63
- diversity, 245, 249, 254, 257, 259
 - angle, 25, 26
 - benefit, 248
 - branch, 343, 344
 - channel, 251
 - combining, 41, 77, 101
 - frequency, 234, 236
 - full, 170, 179, 182, 192, 193, 195, 197, 198, 202, 225, 251, 254, 265, 331

- diversity (*Continued*)
 gain, 234, 245, 254–257, 259, 265
 maximum, 179
 multiuser, 234–236
 order, 132, 249, 250, 253
 pattern, 26
 polarization, 25, 26
 space, 169
 spatial, 25, 28, 234, 236, 269
 temporal, 234, 236
 downlink, 232
 training data, 217
 DTFT, 7
 duplex
 frequency-division, 210, 212, 217,
 235, 307, 312, 322
 time-division, 210, 212, 217, 231,
 235, 299, 307, 311, 322
 eigen-beamforming, 337, 340
 eigendecomposition, 176, 325, 332
 eigenvalue decomposition, 33, 50
 encoder
 space-time, 2, 113
 sphere, 219, 222, 223
 encoding, 234
 OSTBC, 112
 sphere, 217, 219, 221–223
 entropy
 constraint, 331
 environment
 dense urban, 21
 fading, 248, 250
 flat fading, 212
 forested, 19
 indoor, 8, 21, 27
 interference, 220
 lack-scattering, 79
 MIMO, 177
 multipath, 216
 outdoor, 25
 random fading, 249
 rich scattering, 79
 Rician fading, 14
 suburban, 69
 urban, 27, 66
 WLAN, 264
- equalizer
 linear, 281
 MMSE, 183, 187
 zero-forcing, 183
 error probability, 119, 122, 124, 130,
 134, 299
 analysis, 119, 124
 average pairwise, 134, 178
 averaged, 120, 130
 bit, 184, 204, 294
 pairwise, 119, 135, 169, 178, 179,
 198, 200
 pairwise worst-case, 179, 205
 symbol, 126, 187, 222, 283
 union bound, 134, 135
 error rate, 249
 bit, 183, 184, 187, 210, 229, 230,
 282–286, 294–297, 299, 300,
 312, 347, 348, 350, 351
 block, 132, 143
 minimum, 260
 packet, 264, 265
 symbol, 25, 121, 122, 124, 126,
 128, 129, 155, 163, 219, 333,
 334, 338–340, 344–347
 estimate
 capacity, 23
 channel, 8, 217, 299
 frequency, 7
 ML, 7
 MMSE Bayesian channel, 307
 phase, 7
 symbols, 3
 transfer matrix, 7
 estimation
 blind, 146, 147, 151, 155
 channel, 8, 13, 146, 147, 149, 151,
 153, 155, 235, 299
 DOA, 46
 frequency, 46
 semiblind, 149
 timing, 46
 estimator
 blind, 154
 blind ML, 153
 Capon, 153

- channel, 154
- ESPRIT, 13
- ML, 12, 154
- MMSE, 321
- MUSIC, 58, 153
- RARE, 53, 58
- subspace parametric, 13
- fading, 41, 62, 250, 291, 297
 - block, 109
 - correlated Rayleigh, 126, 347
 - correlation, 79, 97, 98
 - flat, 4, 105, 108, 212, 216, 246, 299
 - flat block, 106, 118, 163
 - flat Rayleigh, 255
 - frequency flat, 81, 319, 349
 - frequency-selective, 3, 62, 216, 256
 - Nakagami, 336
 - nonselective, 246
 - quasi-static, 216
 - random, 249, 254
 - Rayleigh, 14, 79, 81, 94, 119, 122, 127, 222, 247
 - Rayleigh flat, 133
 - Rician, 14, 79, 80, 88, 93–95, 121–123, 128–131, 336
 - slow, 319
 - spatial correlations, 322
 - time selective, 62
 - uncorrelated Rayleigh, 133
- FDMA, 235
- feedback, 210
 - bit, 322, 323, 342, 343, 350
 - channel, 8, 212, 299, 307, 308, 320, 322, 329, 347, 352
 - covariance, 321, 322, 325–328, 334, 336–338, 340
 - delay, 320
 - delayed, 321, 326
 - errors, 320
 - finite-rate, 322, 323, 331, 341–345, 350–352
 - imperfect, 234
 - information, 320
 - limited, 235
 - mean, 321, 325, 328, 334, 335, 337, 338, 348, 349
- MIMO covariance, 329
- MIMO mean, 329
- MISO covariance, 328, 329
- MISO mean, 325, 326, 329
- outdated, 234
- received, 321
- FFT, 6, 7, 60
- filter, 264
 - design, 277
 - FIR, 277
 - interpolation, 66
 - linear, 302
 - matched, 3, 4, 117, 145, 157, 247
 - MMSE, 265
 - moving average, 7
 - optimal MMSE, 264
 - pulse shaping, 2
 - Wiener, 284
 - zero-forcing, 218
- finite alphabet
 - constraint, 153–155
- forward-backward averaging, 49
- Fourier
 - discrete time transform, 7
 - discrete transform, 291
 - fast transform, 6, 7, 60
 - multidimensional transform, 53
 - resolution limit, 42
 - transform, 3, 64, 67, 70, 80
- frequency
 - band, 216
 - bandwidth, 20
 - calibration, 322
 - carrier, 4, 7, 63, 66, 69
 - center, 6
 - domain, 47, 65, 264
 - Doppler, 64, 321
 - Doppler shift, 63
 - hopping, 46
 - interleaving, 264
 - intermediate, 6, 7
 - reference, 66
 - response, 66
 - selectivity, 62
 - subcarrier, 264

- identifiability
 - bound, 47, 53
 - deterministic, 47
 - stochastic, 47, 51
 - sufficient conditions, 47
 - with probability one, 47
- impedance
 - characteristics, 29
 - matrix, 32
 - mutual, 29
 - self-impedance, 34
 - termination, 29
- inequality
 - Cauchy-Schwarz, 278
 - Fisher, 175
 - Hadamard, 180, 327, 337
 - Jensen, 176, 177, 184, 186
 - Minkovski, 199
 - triangle, 278
- interference
 - balancing, 210, 217
 - cochannel, 81
 - intersymbol, 216
 - interuser, 210, 211, 218, 227, 228
 - multiaccess, 159–161
 - self-interference, 160, 161, 163
 - semicorrelated Rayleigh, 81
 - spatial, 217, 227
- interleaving
 - frequency, 264
 - space-frequency, 264
- joint diagonalization, 13
- LAN, 216
 - wireless, 262
- line-of-sight, 69, 128
 - component, 14
- local area network, 216
- local oscillator, 6
- LOS, 128
- maximal ratio combining, 83–85, 94, 95, 232, 245, 247, 248, 250–252, 344
- measurements
 - angle of arrival, 22
 - channel, 11, 13, 17
 - channel sounding, 42
 - MIMO sounding, 62
 - MIMO system, 6
 - real-time, 65
 - transfer matrix, 22
 - transmit-receive, 66
 - urban, 17
- method
 - barrier, 277
 - bisection, 286
 - block-diagonalization, 228
 - Capon, 277
 - cutting-plane, 276
 - ellipsoid, 276
 - finite-difference time-domain, 33
 - gap-approximation, 285, 294
 - interior-point, 270, 276
 - primal-dual interior-point, 277
 - steepest descent, 304
- microcells, 24
- MIMO
 - antenna selection, 245, 251, 254, 259, 262, 265
 - beamforming, 83–85, 274
 - broadcast, 209, 210, 234, 235
 - capacity, 24, 28, 29, 32, 33, 169, 170, 247, 252, 253, 257, 319
 - channel, 2, 13, 14, 18, 41, 42, 62–64, 78, 170, 269, 284, 286, 295, 296, 300, 307
 - channel characteristics, 24
 - channel model, 63
 - channel sounding, 53, 65, 66, 70
 - downlink, 210, 216
 - eigenmodes, 18
 - measurements, 6
 - modeling, 15
 - multiaccess, 106, 157–159, 161, 163
 - multiantenna, 269
 - multiple access, 210, 235
 - multiuser, 213, 214, 216, 223

- multiuser channel, 149
- multiuser downlink, 209, 212, 217, 236
- multiuser network, 210
- narrowband system, 6
- noncoherent system, 171
- OFDM, 245, 262, 264, 349
- optimum combining, 85, 100
- orthogonally-coded system, 106
- performance, 6, 22, 24–26
- point-to-point, 106, 157, 209, 215, 280
- single-user, 210, 213, 216
- space-time adaptive links, 63
- system model, 2
- uplink, 210
- WLAN, 266
- minimum description length, 13
- minimum distance, 126, 221
- mobile station, 66, 67, 235
- model
 - array processing, 115
 - cluster, 20
 - double-directional, 42, 63
 - equivalent discrete-time, 172
 - fitting, 63
 - Jakes', 10, 17, 321
 - Kronecker-product, 79
 - parametric, 62
 - path-based, 14, 17, 30
 - plane-wave, 13
 - point-to-point MIMO, 106
 - Saleh-Valenzuela, 20–23, 34
 - two-ring, 19
- modulation
 - adaptive, 347, 348, 350, 352
 - BPSK, 6
 - coded, 349
 - constellation, 6
 - fixed, 347
 - multicarrier, 299
 - OFDM, 264
 - PAM, 222
 - PSK, 333
 - QPSK, 187, 204
 - rectangular QAM, 333
- square QAM, 333
- uncoded, 349
- multidimensional harmonic retrieval, 42, 43, 53, 57, 61
- identifiability, 46
- multiplexing, 212, 254, 259, 266, 269
 - frequency, 231
 - gain, 245, 254–256, 259, 265
 - MMSE, 265
 - orthogonal frequency division, 216
 - spatial, 209, 231, 235, 251, 254, 264, 352
 - time, 228
- mutual information, 33, 79, 80, 82, 94, 97, 100, 175, 299, 324, 326, 329, 352
 - averaged, 330
 - conditioned, 324
 - maximization, 293
 - upper bound, 176
- network, 29
 - ad hoc, 235, 236
 - ad hoc wireless, 280
 - analysis, 31
 - array combining, 32
 - cellular, 235
 - flow, 279
 - impedance transforming, 32
 - link, 280
 - matching, 30–32, 34
 - model, 4, 29
 - modeling, 28
 - multicommodity flow, 279
 - multihop, 280
 - multiport matching, 31
 - nodes, 236
 - optimal routing, 279
 - optimization, 279
 - performance, 279
 - resource allocation, 279
 - routing, 279
 - uncoupled, 32
 - utility, 280
 - wireless, 236, 278, 279

- NLOS, 79, 128
- non-line-of-sight, 128
- OFDM, 216, 245, 262, 264
 - subcarrier, 349
- OSTBC, 105, 106, 109, 110, 112–115, 118–120, 126, 134, 135, 140, 141, 144, 145, 149, 153, 154, 157, 161, 163, 299, 301–303, 309, 311, 312
 - decoder, 106
 - full-rate, 155
 - matrix, 112
 - optimality, 106, 133, 134, 140, 141, 144
 - suboptimality, 134
- outage, 300
 - BER, 296
 - capacity, 249, 250, 262, 329
 - probability, 77, 80, 101, 254, 329, 349
 - rate, 249, 250, 259, 262, 265
 - region, 250
- path loss, 63
 - time-varying, 63
 - variation, 24
- power allocation, 288, 290, 302, 305, 312, 347
 - equal, 340
 - maximin robust, 306
 - optimal, 287, 302, 312, 340
 - profile, 309
 - robust, 305, 312
 - uniform, 293
- power control, 217, 226, 228
 - downlink, 210
 - dual, 226
- power loading, 335
 - equal, 340
 - optimal, 228, 339, 340
- precoder, 173
 - linear, 150, 281
- precoding, 217, 223
 - linear, 331, 339, 340
 - matrix, 337, 347
- MMSE Tomlinson-Harashima, 228–231
- modulo, 222, 223
- nonlinear, 210, 222
- regularized vector, 223
- sphere, 221
- Tomlinson-Harashima, 223, 228
- unitary, 332
- vector, 220, 221, 223, 226, 234
- vector modulo, 211, 222
- propagation loss, 11
- QoS, 210, 211, 226, 307, 309
 - constraint, 210, 211, 285–287, 289, 295, 297, 303
- quality of service, 41, 210
- quantization
 - sphere vector, 347
 - vector, 323, 330, 331
- ray-tracing
 - predictions, 24
 - simulations, 20, 24, 322
 - techniques, 24
- receiver
 - Capon-type, 157
 - coherent, 119
 - coupling, 34
 - decision feedback, 281
 - decorrelator, 117, 157, 160
 - diagonal loading based, 159, 163
 - diagonally loaded minimum variance, 161
 - front-end, 3
 - informed, 154
 - linear multiuser, 157
 - matched filter, 117, 146, 157, 159, 160, 163
 - minimum output energy, 159
 - minimum variance, 106, 115, 159–161, 163
 - ML, 146, 151, 152, 154, 157, 281
 - MMSE, 183, 284, 297
 - multiantenna, 157, 158, 210, 227, 236
 - optimum linear, 298

- robust minimum variance, 161
- zero-forcing, 117, 284, 297
- reciprocity
 - transmitter-receiver, 120
 - transmitter–receiver, 126
- recovery
 - carrier, 6, 7
 - frequency, 264
 - timing, 6, 7, 264
- scattering, 41
 - cross-section, 19
 - diffuse, 13
 - discrete model, 19, 23
 - far-field, 12, 15
 - local, 23
 - long-range, 18
 - multipath, 17
 - non-line-of-sight, 79
 - rich, 79
- scheduling, 235
 - multiuser, 236
 - proportional fair, 235
- SDMA, 210, 235
- shadowing, 42
- Shur decomposition, 57, 59
- signal
 - analog-to-digital conversion, 6
 - despread, 7
 - downconversion, 6
 - filtering, 6
 - hopping, 236
 - matched filtering, 13
 - sampling, 6
 - self-nulling, 161
- signaling
 - 16-QAM, 219
 - capacity-achieving, 270
 - Gaussian, 270
 - PAM, 222
 - QPSK, 222
- singular value decomposition, 32, 50, 223
- spatial signature, 24
- spectrum
 - analog, 215
 - delay-Doppler, 67
- Doppler, 67
- efficiency, 41, 269
- time-frequency, 67
- STBC, 105, 109, 134, 182, 331, 332, 337, 339, 340, 345, 347
- codeword, 335, 336
- linear, 188
- linear dispersion, 199
- matrix, 331, 332
- trace-orthogonal, 183
- synchronization
 - carrier, 65
 - timing, 65
- TDMA, 235
- throughput, 249, 260
 - latency, 210
 - network, 211
 - penalty, 210
 - system, 319, 352
- transceiver, 264, 296
 - adaptive, 351
 - design, 323
 - linear, 280, 281
 - linear MIMO, 282, 296, 312
 - MIMO, 265, 270, 280, 282, 284
 - multiantenna, 347
- transmitter
 - adaptation, 348
 - adaptive, 349
 - array, 328
 - multiantenna, 157, 158, 209, 299
 - optimal design, 319
 - optimum linear, 298
 - robust, 300, 301
 - robust design, 298
- uplink
 - training data, 231
- water-filling, 10, 22, 33, 81, 228, 293, 296, 319, 327, 337
 - iterative, 274, 280
 - power profile, 270
- WLAN, 262, 264
- zero-forcing, 160, 163, 218, 284, 285